An experimental and numerical investigation of heat and mass movement in unsaturated clays

Rao Martand Singh

Geoenvironmental Research Centre

Cardiff School of Engineering

Cardiff University

Thesis submitted in candidature for the degree of Doctor of Philosophy at Cardiff University

August 2007

UMI Number: U584997

UMI U584997

Declarations

This work has not previously been accepted in substance for any degree and is not being concurrently submitted in candidature for any degree.

Signed ...*Rao Martand Singh* (Rao Martand Singh)

Date ....08/12/2007......

Statement One

This thesis is the result of my own investigations, except where otherwise stated. Other sources are acknowledged by the provision of references.

Signed ...*Rao Martand Singh*. (Rao Martand Singh)

Date ....08/12/2007........

Statement Two

I hereby give consent for my thesis, if accepted, to be available for photocopying and for inter-library loan, and for the title and summary to be made available to outside organisations.

Signed ...*Rao Martand Singh*.. (Rao Martand Singh)

Date...........18/12/2007....

Dedicated

To

My beloved mother Smt. Chandan Bala and father Sri. Prem Kumar

Acknowledgements

Summary

The study of heat transfer and moisture movement in liquid and vapour phase has attracted the attention of scientists from the beginning of 19th century. The study is very important to many geotechnical and geoenvironmental problems like diurnal heat mass movement in ground, performance assessment of nuclear waste disposal repositories, buried hot pipes, buried high voltage electric cables and landfill liners.

Significant experimental and theoretical development has been made in this field but still there is a lack of experimental data available specially for highly swelling clays. The heat transfer and liquid moisture movement theories for clays more or less are very well established but vapour transfer theory is still based upon rigid matrix granular soils. Therefore, this thesis presents an experimental, theoretical and numerical investigation of the heat and moisture movement in unsaturated clays.

A new apparatus termed a thermo-hydraulic (TH) cell has been designed, fabricated and calibrated in-house to perform thermal gradient, thermo-hydraulic gradient and isothermo-hydraulic gradient tests on two types of clays namely Speswhite kaolin and MX-80 bentonite. The TH cell is capable of measuring the transient temperature, relative humidity, volume flow rate of incoming water and swelling pressure. It also facilitates the determination of moisture content, dry density and chemical composition (anions and cations concentration) of the soil samples at the end of the tests.

In the thermal test, the clay sample is subjected to fixed temperatures of 85 °C at the bottom end and 25 °C at the top end. In the thermo-hydraulic test, same thermal gradient is used like the thermal test and in addition to this deionised and de-aired water was supplied at the top end under a pressure of 0.6 MPa. In the isothermal test, the clay sample is supplied deionised and de-aired water from the top end under a pressure of 0.6 MPa and the temperature kept at 25 °C at both ends of the clay sample.

The test results show that there is a cycle of vapour and liquid moisture movement within the clay sample, vapour moves from the hot end to the cold and condense to liquid at the cold end and liquid moisture moves to the hot end. The accumulation of chloride ions near the hot end indicate that liquid moisture moved from the cold end to the hot end. An empirical method has been developed to calculate the vapour fluxes using the variation of chloride ions concentration with time. The vapour fluxes calculated empirically found to be much lower than that determined by existing vapour theories. Therefore, the existing vapour theory has been modified to more closely predict the observed vapour fluxes. The new modified vapour transfer theory has been incorporated in transient finite element code and validated against the experimental work carried out in this study. The numerically simulated results match reasonably with the experimental heat and mass results. Further research is necessary to explore the new vapour theory application to large scale tests.

Contents

Chapter 3   Experimental design and methodology

Chapter 6   Thermal, thermo-hydraulic and isothermal tests on bentonite

Chapter 7   Assessment of vapour movement

Chapter 8   Conclusions and suggestions for further research

Appendix 1

Chapter 1

Introduction

Study of moisture transport in soils under thermal gradients has been a topic of great interest since the beginning of the 19th century. Initially water movement in subgrade material, which is a common cause of the structural failure of pavement surfaces, attracted the attention of highway engineers and scientists who found the wetting was attributed to a 'transpiration current' or an upward movement of moist air through the soil from the water table caused by a temperature gradient in the soil (Maclean and Gwatkin, 1946). The other problems of interest, where thermally induced moisture movement in unsaturated soils is an important phenomenon, are diurnal moisture movement in the ground, buried services (e.g. high voltage electric cables and hot water pipes), high level radioactive waste disposal, landfill liner performance, optimisation of geothermal energy utilisation (Rees et al., 2000) and thermally enhanced clean-up of contaminated land (Lee et al., 1999).

Knowledge of heat and mass transfer in soils is critical in the design and implementation of underground power transmission and distribution systems (Campbell and Bristow, 2002). Electricity flowing in a conductor generates heat. A resistance to heat flow between the cable and the ambient environment causes the cable temperature to rise. Moderate increases in temperature are within the range for which the cable was designed, but temperatures above the design temperature shorten cable life. Since the soil is in the heat flow path between the cable and the ambient environment, and therefore forms part of the thermal resistance, soil thermal and hydraulic properties are an important part of the overall design.

Compacted swelling clays are proposed as engineering barriers for the disposal of heat emitting nuclear waste (Bernier et al., 1997). Bottom barrier system consisting of clay is

commonly used to contain wastes in landfills in many countries (Katsumi et al., 2001). The engineering barriers are often subjected to high temperature and hydraulic pressure. Thermal drying at high temperature can cause cracks in the barrier and lead to escape of hazardous chemical into environment. The performance of nuclear waste repository and landfill depends in part upon the thermo-hydraulic properties of engineering barriers.

Geothermal energy is a sustainable energy derived from beneath the earth's surface and offers a number of advantages over traditional fossil fuel based sources. It is used to generate power and to keep the buildings warm during cold weather. Again to achieve optimum benefits from geothermal energy requires knowledge of heat and mass movement in soils.

The study of thermal induced moisture movement in soils has been of great interest since 19th century. Bouyoucos (1915) was the first to carry out a detailed experimental study on the effect of temperature on movement of water vapour and capillary moisture in cohesionless soils varying from sand to silt. He observed that moisture moved from the warm soil to the cold soil at different temperature ranges and that quantity increased regularly with increase in moisture content until particular moisture content termed as critical moisture content was reached. Lebedeff (1927) was also one of the earliest researchers to report movement of moisture in liquid and vapour phases in soils with and without a thermal gradient. He concluded that the upward movement of moisture took place in the vapour phase under a vapour pressure gradient. Smith (1939, 1943), Krischer and Rohnalter (1940) and Maclean and Gwatkin (1946) studied the movement of soil moisture under a thermal gradient and concluded that the mechanism causing the movement was vapour diffusion. Subsequently, Winterkorn (1947) enumerates four possible mechanism of moisture movement under a temperature gradient: (i) diffusion of water vapour through the pore space under a concentration or partial pressure gradient, (ii) diffusion of water in solid solutions as observed for hydrophilic membranes separating chambers of different water vapour pressure, (iii) movement as capillary water due to differences in surface tension at different temperatures and (iv) flow of moisture in the film phase along the internal surface of the porous system due to change in water affinity with change in temperature. The concept of film flow for moisture transport

under a temperature gradient was in contradiction to the vapour flow theory proposed by earlier researchers reported by Taylor and Cavazza (1954). Gurr et al. (1952) investigated the flow of moisture under a temperature gradient by using salts as a tracer and concluded that state of equilibrium can not be reached without a cyclic transfer of mass. They obtained a diffusion coefficient for the vapour using the vapour diffusion equation of Penman (1940) which greatly exceeded the expected value. Rollins et al. (1954) and Hadley and Eisenstadt (1955) confirmed the findings of Gurr et al. (1952) that water moving from the warm to the cold side in the vapour phase is returned to the warm side in the liquid phase. Rollins et al. (1954) developed the vapour diffusion equation based on molecular diffusion theory to predict the vapour movement in soils.

Philip and de Vries (1957) discussed the movement of liquid water and water vapour in porous media under the influence of gradients of temperature and moisture content. They developed simultaneous differential equations for the transfer of heat and moisture using numerical data for a coarse textured and a medium textured soil. Their vapour transfer theory is still in use all over the world.

Earlier researchers until 1960 used mostly natural soils sand, silt and loam and a maximum temperature of 40 °C because the aim of their studies was upward moisture movement in highway subgrade. Later studies aimed to investigate the heat and moisture transfer in surroundings of buried high voltage cables so a higher temperature was used. Preece (1975) used 70 °C temperature to predict the thermal behaviour of moisture dependent cable bedding sands.

In recent years a great deal of research has been conducted into the disposal of high level nuclear waste. This trend may be attributed to the increasing volume of nuclear waste produced by over 32 countries, operating over 400 nuclear power plants around the world (Mitchell, 2002). Swelling clays are the candidate material to be used as engineering barriers in nuclear waste repositories. Various researchers carried out experimental study of heat and mass transfer in swelling clays with applied maximum temperature up to 100 °C (Yong et al., 1997; Kanno et al., 1996; Villar et al., 1996; Börgesson et al., 2001; Pintado et al., 2002; Gatabin and Billaud, 2005).

Ewen and Thomas (1989) made changes in vapour transfer diffusivity terms of the numerical equations of Philip and de Vries (1957) based on a theoretical, experimental and numerical investigation of combined heat and mass transfer in unsaturated medium sand. This model was then applied to study the thermo-hydraulic behaviour of swelling clays with a certain degree of success. However, accurate prediction of thermo-hydraulic behaviour of such clays has remained an unresolved issue. Therefore, there is a clear need to develop an improved conceptual understanding of the thermo-hydraulic behaviour of swelling clays.

The principal aim of this study is to develop an experimental and theoretical understanding of heat and mass movement in unsaturated clays (either swelling or non-swelling) subjected to high temperature gradient and hydraulic gradient. Therefore, a detailed experimental programme was planned to carry out a large number of laboratory scale tests which included thermal, thermo-hydraulic and isothermal tests on swelling and non-swelling clays for various time intervals. Speswhite kaolin has been chosen as a non-swelling clay while MX-80 bentonite as swelling clay.

In the thermal test the clay samples are subjected to temperature gradient. In the thermo-hydraulic test the samples are subjected to temperature gradient and hydraulic gradient. The isothermal test is basically an isothermo-hydraulic gradient test in which the clay samples are subjected to a hydraulic gradient while the same temperature is maintained across the sample i.e. no temperature gradient.

After each and every test the soil samples are analysed for moisture content, dry density, degree of saturation, porosity and chemical (anion and cation) composition. The conservative ion (e.g. chloride ion) concentration is then used to determine the vapour amount and vapour fluxes within the clay samples at various time intervals. The experimentally determined vapour fluxes are compared with existing vapour theories like Philip and de Vries (1957) vapour theory and Ewen and Thomas (1989) theory.

The new vapour flux model is developed by modifying the existing vapour theories. The new vapour model is then introduced in existing transient finite element code to verify

against the tests i.e. thermal, thermo-hydraulic and isothermal tests performed on both swelling and non swelling clays in this study. Comparisons between experimental and numerical results are presented and discussed.

1.1   Research objectives

The main objectives of the present research may be summarised as follows:

1. Provide a state-of-the-art review of the development of theories and experimental work related to heat transfer and moisture movement in liquid and vapour phases in unsaturated soils from the beginning of 19th century to date.

2. Design and build new test apparatus to facilitate a large number of various combinations of thermal gradient and hydraulic gradient experiments. Create new laboratory facilities to provide operational support for the new cells. Conduct a preliminary experimental programme to demonstrate the working capacity and functionality of the new apparatus.

3. Establish a basic experimental methodology for sample preparation to obtain uniform homogenous samples and subsequent testing. Determine basic geotechnical properties that include physical and chemical properties and flow parameters i.e. hydraulic and thermal material parameters of testing clays.

4. Perform thermal gradient, thermo-hydraulic gradient and isothermo-hydraulic gradient tests to investigate the heat, liquid moisture and vapour moisture movement in clays with different initial degree of saturation but same dry density.

5. Develop an empirical method to calculate the vapour flux using the conservative ion (especially chloride ion) movement. Develop a new vapour flux model for swelling or non-swelling clays and integrate it within an existing transient finite element model.

Verify and validate the new vapour flux model against the results obtained from the heat and mass experiments performed in this study.

1.2 Research background

This section provides a brief review of the research work that has previously been conducted in this field at Cardiff University that includes experimental as well as numerical study.

At Cardiff University, research work has been primarily focused on the development of numerical models of coupled thermo/hydro/chemical/mechanical (THCM) behaviour. However, some experimental work has seen carried out in the past. Ewen (1987) investigated the thermo-hydraulic behaviour of unsaturated sand surrounding a heating rod. Rees (1990) determined the effect of moisture transfer on the volume change behaviour of Kimmeridge clay. More recently, Folly (2001) has investigated the THM behaviour of Speswhite kaolin clay and developed temperature and suction controlled oedometer. In order to extend the range of capabilities offered at Cardiff the current research work aims to develop new test apparatus to study heat and moisture movement especially vapour movement in swelling and non-swelling clays.

As stated earlier, at Cardiff, the primary focus was to develop numerical and computer based models to study the THM behaviour of unsaturated soils. First, a theoretical model of coupled transient heat and moisture transfer in unsaturated soil, including gravity effects was developed by Thomas (1985). Vapour flow was modelled by incorporating Philip and de Vries approach (1957), and the latent heat of vaporisation was also introduced (Luikov, 1966). Following an experimental investigation into the behaviour of unsaturated sand surrounding a heating rod (Ewen and Thomas, 1987), Ewen and Thomas (1989) amended the vapour transfer diffusivities of the numerical model to simulate coupled heat and moisture transfer processes in unsaturated soil. This numerical model was based on the variables of moisture content and temperature.

Thomas and King (1991) developed the previous approach, replacing the primary variable of moisture content with capillary potential. This was in order to make the theoretical model compatible with the current approach in unsaturated soil mechanics. The approach presented by Thomas and King (1991) was then extended to include the effect of elevated pore air pressure, deformation and movement of various chemical species by the various researchers with the time till now (Thomas and Rees, 1990, 1993; Thomas and He, 1994, 1995; Thomas and Sansom, 1995; Thomas and Li, 1997; Thomas and Cleall, 1997, 1999; Seetharam, 2003). Additionally, the aim of the current work is also to develop a new vapour flux model for swelling and non swelling clays and incorporate it into the existing numerical model to predict heat and moisture transfer in an efficient manner in unsaturated clays.

1.3 Scope and limitations

This section discusses the scope and the limitations of the experimental and numerical work pursued in this research study.

1. One of the principal assumptions of this study is that the soil is homogeneous though some heterogeneity (especially non-uniform dry density and water content) is observed during the experimental work.

2. The new test apparatus is designed for one dimensional thermo-hydraulic testing only.

3. The new test apparatus can work up to a maximum temperature of 100 °C and an applied hydraulic pressure of 1.5 MPa.

4. This study does not include the hysteresis effects that have been observed in the soil water characteristic curve (or water retention curve).

5. Approximate methods are employed for numerical analysis to solve the governing equations of heat and mass transfer.

6. The numerical modelling in this study does not include deformation behaviour and chemical species movement.

1.4 Thesis overview

A brief description of each chapter is presented below.

Chapter 2 presents the definition of unsaturated soil and explains non-swelling and swelling clay types, minerals and their internal structures with ion exchange chemistry. The theories of liquid moisture, vapour moisture movement and heat transfer in unsaturated soils are then presented. The hydraulic and thermal flow parameters required to determine the heat and mass fluxes using the theories are discussed in detail. A detailed review of thermo-hydraulic experiments is also presented.

Chapter 3 details the design and construction of the new test apparatus to facilitate heat and moisture movement study which is the main objective of the present research work. The overall design, fabrication and calibration of the new experimental set up are detailed. The various accessories to be used as the part of new apparatus and sensors required to measure temperature, relative humidity and pressure are also discussed. The experimental methodology and type of tests adopted to achieve the best possible results with the new apparatus are presented. The procedure and techniques employed to determine anion concentration using ion chromatography (IC) and cation concentration using inductively coupled plasma mass spectroscopy (ICP-MS) are detailed.

Chapter 4 describes the testing materials used for experimental investigation and details their physical, chemical and geotechnical properties and the determination technique used to obtain them. The aim of the chapter is to characterise the materials because their properties would be later used in subsequent chapters for analysis and validation. Physical properties including natural water content, specific gravity, particle size distribution, Atterberg limits, activity and linear shrinkage are covered. The compaction characteristic of the materials, which includes the development of compaction methodology to achieve the targeted uniform density and uniform water content, is

presented. Experimental determination of hydraulic flow parameters including the soil water characteristic curve and the saturated hydraulic conductivity is presented. Swelling properties that include swell index and swelling pressure are also discussed. Chemical properties including pH and cation exchange capacity are then considered. Subsequently, determination of specific surface area using ethylene glycol monoethyl ether (EGME) adsorption method is described. Finally, results of mineralogical analysis using X-ray diffraction (XRD) and microstructure analysis of the testing clays using Environmental Scanning Electron Microscope (ESEM) and Energy Dispersive X-ray Analyser (EDXA) are presented.

In chapter 5 the results of a series of thermal, thermo-hydraulic and isothermal tests performed on Speswhite kaolin are presented. The test results include the transient thermal distribution, transient relative humidity variation and moisture distribution, degree of saturation, dry density, porosity and chemical distribution which includes anion and cation concentration at the end of each test of different time duration. The aim of the tests is to use the tests results for a qualitative analysis of the liquid and vapour moisture.

In chapter 6 the results of a series of thermal, thermo-hydraulic and isothermal tests carried out on MX-80 bentonite are presented. The objective is to investigate both the heat transfer and mass movement in liquid and vapour phases in MX-80 bentonite. The test results again include the transient thermal distribution, transient relative humidity variation and moisture distribution, degree of saturation, dry density, porosity and chemical distribution that includes anion and cation at the end of each test of different time duration.

Chapter 7 presents the new vapour flux model and its validation to compare with the results of thermal, thermo-hydraulic and isothermal experiments carried out in this study. The empirical determination of vapour flux by using chloride ion is presented. The vapour flux calculated by the proposed empirical method is compared with the existing vapour flux theories. The development of new vapour flux model by modifying the existing vapour flux model and incorporating it into an existing transient finite element programme. Subsequently, the validation of the new vapour model and then verification

of it against the experimental results of thermal, thermo-hydraulic and isothermal tests for Speswhite kaolin and MX-80 bentonite is presented.

Chapter 8 presents the conclusions that can be drawn from this work, and suggestions are made for further research.

1.5 References

Bernier, F., Volckaert, G., Alonso, E. and Villar, M. (1997). Suction-controlled experiments on boom clay. Engineering Geology, 47, 325-338.

Börgesson, L., Chijimatsub, M., Fujitab, T., Nguyenc, T.S., Rutqvistd, J. and Jinge, L. (2001). Thermo-hydro-mechanical characterisation of a bentonite-based buffer material by laboratory tests and numerical back analyses. International Journal of Rock Mechanics & Mining Sciences, 38, 95-104.

Bouyoucos, G.J. (1915). Effect of temperature on movement of water vapour and capillary moisture in soil. U.S. Department of Agriculture, Journal of Agricultural Research Vol. V, No. 4, 141-172.

Campbell, G. and Bristow, K. (2002). Soil thermal resistivity. Australian Power Transmission and Distribution. Chapel Hill, Qld., PTD Publications, 46-48.

Ewen, J. (1987). Combined heat and mass transfer in unsaturated sand surrounding a heated cylinder. PhD thesis, School of Enginering, University of Wales, Cardiff.

Ewen, J. and Thomas, H.R. (1987). The thermal probe – a new method and its use on an unsaturated sand. Geotechnique, 37, No. 1, 91-105.

Ewen, J. and Thomas, H.R. (1989). Heating unsaturated medium sand. Geotechnique, 39, 455-470.

Folly, J.P.W. (2001). Thermo-hydro-mechanical behaviour of unsaturated soil: An experimental study. PhD thesis, School of Engineering, Cardiff University.

Gatabin, C. and Billaud, P. (2005). Bentonite THM mock up experiments. Sensors data report. CEA, Report NT-DPC/SCCME 05-300-A, Cedex.

Gurr, C.G., Marshall, T.J. and Hutton, J.T. (1952). Movement of water in soil due to a temperature gradient. Soil Sci., Vol. 74, No. 5, 335-345.

Hadley, W.A. and Eisenstadt, R. (1955). Thermally actuated moisture migration in granular media. Trans. American Geophysical Union, Vol. 36, No. 4, 615-623.

Kanno, T., Kato, K. and Yamagata, J. (1996). Moisture movement under a temperature gradient in highly compacted bentonite. Engineering Geology, 41, 287-300.

Katsumi, T., Benson, C.H., Foose, G.J. and Kamon, M. (2001). Performance-based design of landfill liners. Eng. Geol., 60, 139-148.

Krischer, D. and Rohnalter, H. (1940). Warmeleitung und dampfdiffusion in feutchen gutem. Verein Duet, Ing-Forschungsheft, 402.

Lebedeff, A.F. (1927). The movement of ground and soil waters. Proc. 1st Int. Congress of Soil Science, 1, 459-494.

Lee, G., Glascoe, N.M., Wright, S.J. and Abriola, L.M. (1999). Modelling the influence of heat/moisture exchange during bio-venting. J. Environ. Eng. ASCE, 125, 1093-1103.

Luikov, A.V. (1966). Heat and mass transfer in capillary porous bodies. Pergamon Press, Oxford.

Maclean, D.J. and Gwatkin P.M. (1946). Moisture movement occurring in soil due to the existence of a temperature gradient. Department of Scientific and Industrial Research England, Road Research laboratory Note RN/761.

Mitchell, H.P. (2002). A study of the thermo/hydro/mechanical behaviour of two large scale, in-situ experiments. PhD thesis, Cardiff School of Engineering, UK.

Penman, H.L. (1940). Gas and vapour movements in the soil. Int. Jour. Agr. Sci.30, 437-462.

Philip, J.R. and de Vries, D.A. (1957). Moisture movement in porous materials under temperature gradients. Trans. Amer. Geophys. Union, 38, 222-232.

Pintado, X., Ledesma, A. and Lloret, A. (2002). Backanalysis of thermohydraulic bentonite properties from laboratory tests. Eng. Geol., 64, 91-115.

Preece, R.J. (1975). The measurement and calculation of physical properties of cable bedding sands. Part 2: specific thermal capacity, thermal conductivity and temperature ratio across air filled pores. C.E.G.B. Laboratory Note No., RD/L/N 231/74.

Rees, S.W. (1990). Seasonal ground movement effects on buried moisture transfer in unsaturated soil. Ph.D. Thesis, School of Engineering, University of Wales, Cardiff.

Rees, S.W., Adjali, M.H., Zhou, Z., Davies, M. and Thomas, H.R. (2000). Ground heat transfer effects on the thermal performance of earth-contact structures. J. Renewable and Sustainable Energy Reviews, 4, 213-265.

Rollins, R.L., Spangler, M.G. and Kirkham, D. (1954). Movement of soil moisture under a thermal gradient. Proc. Highway Research Borad, Vol. 33, 492-508.

Seetharam, S.C. (2003). An investigation of the thermo/hydro/chemical/mechanical behaviour of unsaturated soils. PhD thesis, Cardiff School of Engineering, UK.

Smith, W.O. (1939). Thermal conductivities in moist soils. Proc. Soil Science Soc. Amer., 4, 32-40.

Smith, W.O. (1943). Thermal transfers of moisture in soils. Trans. Amer. Geophysical Union, 2, 511-523.

Taylor, S.A. and Cavazza, L. (1954). The movement of soil moisture in response to temperature gradients. Proc. Soil Science Soc. Amer., Vol. 18, No. 4, 351-358.

Thomas, H.R. (1985). Modelling two-dimensional heat and moisture transfer in unsaturated soils, including gravity effects. International Journal of Analytical Methods in Geomechanics, 9, 573-588.

Thomas, H.R. and Cleall, P.J. (1997). Chemico-osmotic effects on the behaviour of unsaturated expansive clays. Geoenvironmental engineering, Contaminated ground; fate of pollutants and remediation. Yong, R.N. and Thomas, H.R., eds., Thomas Telford, London, 272-277.

Thomas, H.R. and Cleall, P.J. (1999). Inclusion of expansive clay behaviour in coupled thermo hydraulic mechanical models. Engineering Geology, 54, 93-108.

Thomas, H.R. and He, Y. (1994). An elasto-plastic analysis of the thermo/hydraulic/mechanical behaviour of unsaturated soil. Proceedings of the 8th International Conference on Computer Methods and Advances in Geomechanics, Morgantown. Siriwardane, H.J. and Zaman, M.M. eds., Balkema, Rotterdam, 1171-1176.

Thomas, H.R. and He, Y. (1995). Analysis of coupled heat, moisture and air transfer in a deformable unsaturated soil. Geotechnique, 45, No. 4, 677-689.

Thomas, H.R. and King, S.D. (1991). Coupled temperature/capillary potential variations in unsaturated soil. Journal of Engineering Mechanics, American Society of Civil Engineers, 117, No. 11, 2475-2491.

Thomas, H.R. and Li, C.L.W. (1997). An assessment of a model of heat and moisture transfer in unsaturated soil. Geotechnique, 47, No. 1, 113-131.

Thomas, H.R. and Rees, S.W. (1990). An examination of the performance of a 3-level time stepping algorithm – Coupled heat and mass transfer computing. Proceedings of the 1st International Conference, Advances in Computer Methods in Heat Transfer, Southampton, U.K.

Thomas, H.R. and Rees, S.W. (1993). The numerical simulation of seasonal soil drying in an unsaturated clay soil. International Journal of Numerical and Analytical Methods in Geomechanics, 17, No. 1, 119-132.

Thomas, H.R. and Sansom, M.R. (1995). Fully coupled analysis of heat, moisture and air transfer in unsaturated soil. Journal of Engineering Mechanics, ASCE, 121, No. 3, 392-405.

Villar, M.V., Cuevas, J. and Martin, P.L. (1996). Effects of heat/water flow interaction on compacted bentonite: Preliminary results. Engineering Geology, 41, 257-267.

Winterkorn, H.F. (1947). Fundamental similarities between electro-osmotic and thermo-osmotic phenomena. Proc. Highway Research Board, Vol. 27, 443-455.

Yong, R.N., Mohammed, A.M.O., Shooshapasha, I. and Onofrei C. (1997). Hydro-thermal performance of unsaturated bentonite-sand buffer material. Engineering Geology, 47, 351-365.

Chapter 2

Literature review

2.1 Introduction

This chapter presents a review of the development of theories and experimental work related to heat transfer and moisture movement in liquid and vapour phase in unsaturated soils from the beginning of 19th century to the current day. A number of comprehensive reviews of the development of coupled heat and mass models have been carried out previously (Thomas, 1980; Ewen, 1987; Rees, 1990; King, 1991; Sansom, 1995; Cleall, 1998; Wang, 2000; Seetharam, 2003). This review focuses on the vapour transfer theories and the experimental advancement in the study of moisture movement under thermal influence in unsaturated clays.

The concept and definition of unsaturated soils is first reviewed in section 2.2. Section 2.3 deals with the non-swelling and swelling clay types, minerals and their internal structures with ion exchange chemistry. Section 2.4 details the theories of liquid moisture and vapour moisture movement in unsaturated soils. Theories related to heat in soils are presented in section 2.5. Section 2.6 details the hydraulic and thermal flow parameters required to determine the heat and mass fluxes using the theories presented in sections 2.5 and 2.6. A detailed review of thermo-hydraulic experiments is presented in section 2.7. Finally, overall conclusions are drawn from the above discussions in section 2.8.

2.2 Unsaturated soils

A soil mass consists of solid particles and pore spaces. In saturated and dry soils the pore spaces are filled with a single medium, either water or air. In unsaturated soils the pore spaces are filled with a mixture of two or more media, most commonly air and water

(Sivakumar, 1993). Wroth and Houlsby (1985) proposed three different categories of unsaturated soil on the basis of continuity of the fluid phases (air and water) as presented in Figure 2.1. The three categories are discussed briefly as below:

Category 1: Air phase discontinuous and water phase continuous as in Figure 2.1 (a). This type of structure is found in unsaturated soils having a very high degree of saturation. In such soils the air occurs in the form of discrete bubbles. This saturation probably occurs in a narrow transition zone in natural soil, above the saturated zone and below a zone with lower degree of saturation as shown in Figure 2.2.

Category 2: Air and water phases both continuous as in Figure 2.1 (b). This type of unsaturated soil is found in soil having an intermediate degree of saturation. This range of degree of saturation occurs in a transition zone in a natural soil deposit, above the previously mentioned zone in category 1 and below a dryer surface layer (Figure 2.2).

Category 3: Air phase continuous and water phase discontinuous as in Figure 2.1 (c). This type of unsaturated soil is found in soils having lower degree of saturation. This occurs in natural soils close to the surface as shown in Figure 2.2.

2.3 Non-swelling / swelling clays

McKeen (1992) proposed a classification system for swelling (expansive) clays. According to his classification, clays that swell less than 2.8 % on wetting are considered as non-swelling (non-expansive) clays, those which swell 2.8 to 5.3 % are moderately swelling clays, those which swell more than 5.3 to 10% are highly swelling clays and finally soils which swell more than 10 % are considered as special case of highly swelling clays. It is, however, a tentative classification because the amount of swelling of a soil is a function of the stress and suction histories of the soil (Sharma, 1998).

The amount of swelling in the soil depends upon the active clay mineral present. In these soils important physico-chemical interactions occur in the vicinity of the active clay minerals. Proper understanding of these interactions can explain some of the salient

features of clay behaviour. This helps in constructing a conceptual picture of the non-swelling or swelling processes in clays. Therefore, some fundamental aspects of clay behaviour at a micro-level such as unit layers and clay minerals (kaolinite and montmorillonite) are briefly reviewed.

2.3.1   Unit layers

A unit layer is a basic repeating structural element of a clay mineral. At the molecular level, clays are made up of two basic structural units: silica tetrahedral sheet and aluminium or magnesium octahedral sheet. The tetrahedral sheet consists of two dimensional arrays of silicon-oxygen tetrahedra and the octahedral sheet consists of two dimensional arrays of aluminium/magnesium-oxygen-hydroxyl octahedra as shown schematically in Figures 2.3 and 2.4. The tetrahedral sheet also known as silica sheet, has the oxygen atoms located on the four corners of a regular tetrahedron with the silicon atom in the centre. In the silica sheet, three of the four oxygen atoms of each tetrahedron are shared by three neighbouring tetrahedra. The fourth oxygen atom of each tetrahedron is pointed downward. This leads to a silica sheet of 4.63 Å thickness (Grim, 1962). The octahedral sheet also known as alumina (gibbsite) sheet or magnesia (brucite) sheet depending upon the type of central atom either aluminium or magnesium, has six oxygen or hydroxyl (OH) groups coordinated at the six corners of a regular octahedron. The oxygen atoms and hydroxyl groups lie in two parallel planes with aluminium or magnesium atoms between these planes. The octahedral sheet has a thickness of 5.05 Å (Grim, 1962). The analogous symmetry and the almost identical dimensions in the tetrahedral and the octahedral sheets allow the sharing of oxygen atoms between these sheets (van Olphen, 1963). The fourth oxygen atom protruding from the tetrahedral sheet is shared by the octahedral sheet. The most clay minerals are made up of tetrahedral and octahedral sheets superimposed in different fashions.

Unit layers are not electrically neutral, but carry an unbalanced electrical charge on the surfaces and edges (Grim, 1962). Possible sources of unbalanced electrical charge are:

1. In any unit layer positively charged ions are generally within the interior of the layer, whereas the oxygen or hydroxyl ions on the surface of the unit layer are negatively charged. This spatial distribution of the positive and negative charges results in a net negative charge on the surface of a unit layer.

2. Partial replacement of Si^{4+} by Al^{3+} in a tetrahedral sheet or of Al^{3+} by Mg^{2+} in an octahedral sheet (a process known as isomorphous substitution) results in a net negative charge on the unit layers.

3. At the edges of unit layers, tetrahedral silica sheets and octahedral sheets are disrupted, and primary bonds are broken. This leads to the hypothesis of positively charged edges of unit layers.

In this way, a unit layer can be conceptualised as a flake carrying negative charge on the surfaces and positive charge in the interior and on the edges.

2.3.2   Kaolinite mineral

The kaolinite mineral is the most common mineral of the kaolinite group of minerals. It is a representative non-swelling or slightly swelling mineral and its unit layer is formed by combination of one silica sheet and one alumina sheet sharing a layer of oxygen between them as shown in Figure 2.5. Therefore, a kaolinite mineral is called a 1:1 layer mineral. The kaolinite mineral is formed by the stacking of several unit layers one over the other. The extent of atom substitutions in the kaolinite structure is relatively small (van Olphen, 1963). The unit layers are held together by hydrogen bonding between hydroxyls from the alumina sheet on one face and oxygens from the silica sheet on the opposite face of the layer (Yong and Warkentin 1966). This type of bond is fairly strong to prevent swelling between unit layers in kaolinite. It has a low liquid limit and a low activity.

2.3.3 Montmorillonite mineral

The high degree of swelling in swelling clays is mainly due to the presence of active clay minerals such as montmorillonite. Montmorillonite is the mineral subgroup of the smectite group of minerals (Mitchell, 1993). It is the principal clay mineral of bentonite rock which originates from volcanic ash (van Olphen, 1963). It has repeating unit layers consisting of an alumina sheet sandwiched between two silica sheets with oxygens shared, as shown schematically in Figure 2.6. Bonding between successive unit layers is by van der Walls forces and by cations that are present to balance charge deficiency due to isomorphic substitution. These bonds are weak and easily separated or swell by adsorption of polar liquids like water. Montmorillonite can swell up to several times its dry volume when placed in contact with water. It has a high activity and high liquid limit.

2.3.4 Ion exchange

As discussed earlier the isomorphic substitution in the unit layers results in a deficit of positive charge or in other words an excess of negative charge on the unit layers. This excess of negative layer charge is compensated by the adsorption on the layer surfaces of cations which are too large to be accommodated in the interior of the crystal (van Olphen, 1963). In the presence of water, the compensating cations on the unit layer surfaces may be easily exchanged by other cations present in the solution, hence they are called exchangeable cations. The total amount of exchangeable cations is called cation exchange capacity (CEC) and expressed in miliequivalents per 100 g of dry soil. The CEC is a measure of the degree of substitution. The replaceability of one type of cation by another type depends upon valence and ion size. Ion exchange is primarily an electrostatic process; the more highly charged species are preferentially adsorbed (Deutsch, 1997). When present at equal solution concentrations, the affinity of the solid exchanger for solutes is as follows:

$$Al^{3+} > Ca^{2+} > Mg^{2+} > K^+ > Na^+$$

In addition to the charge on the ion, the smaller the radius of the ion, the closer it can approach the surface and the greater the affinity of the surface for the ion. However, ions in solutions are surrounded by water molecules; therefore their effective radius is the radius of the solvated ion and not the bare ion. The larger the bare ion, the smaller the solvated radius; thus for the monovalent ions the affinity of the solid exchange is as follows:

$$Cs^+ > Rb^+ > K^+ > Na^+ > Li^+$$
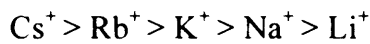
Although most of the cation exchange capacity of clay minerals is due to the permanent fixed charge at the clay surface, there is also a pH dependent charge that can contribute to exchange capacity. Details of exchange reactions of the clay minerals are discussed in length by several researchers, including van Olphen (1963), Sposito et al. (1983), Levy et al. (1983) and Rytwo et al. (1995). The CEC of montmorillonite is between 80-100 meq/100g and kaolinite between 3-15 meq/100g.

Anion exchange may also occur on clay minerals, but to a much lesser extent than cation exchange because of the dominant fixed negative charge on the clay mineral surface. In the acidic condition at low pH values (less than 6) hydrogen ions are strongly bonded to oxygen atoms at crystal edges and the loss of hydroxyl ion (OH^-) results in positive sites.

$$X\text{-}OH + H^+ = XOH_2^+ \text{ and } X\text{-}OH = X^+ + OH^-$$
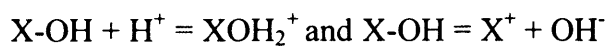
These above positive sites are available for anion exchange. Anion exchange capacity can be 10 % of the CEC for more heavily weathered soils where conditions are relatively acidic (Deutsch, 1997).

2.4 Moisture movement in unsaturated soil

Moisture transfer in unsaturated soil may be described as a two phase flow comprising, the flow of liquid moisture and the flow of vapour moisture. The following sections discuss the liquid flow mechanism and vapour flow mechanism in detail.

2.4.1 Liquid moisture flow mechanism

Several concepts have been used to explain the flow of liquid moisture through unsaturated soil. These have included, a moisture content gradient, a matric suction, and a hydraulic head gradient. Fredlund (1991) discounted the use of a moisture content gradient and the use of a matric suction gradient (Fredlund and Rahardjo, 1993). According to Fredlund and Rahardjo (1993), the liquid water can flow from a region of low water content to a region of high water content when there are variations in the soil type involved, hysteretic effects, or stress history variation are encountered. Similarly, the flow of liquid water does not fundamentally and exclusively depend upon the matric suction gradient. Fundamentally the most appropriate approach employs the hydraulic head gradient in conjunction with Darcy's law, to describe liquid water flow. In this study the following mechanisms are considered which cause the flow of water (Mitchell, 1993):

- Pressure head ($\frac{u_l}{\gamma_l}$)

- Elevation (or gravitational) head (z)

- Velocity head ($\frac{v_l^2}{g}$)

- Thermal gradient

- Chemical gradient

The first three of these mechanisms; pressure head, elevation (or gravitational) head and velocity head are combined to give the hydraulic head. The velocity head in a soil is negligible in comparison with the pressure head and the elevation head. The hydraulic head gradient is considered to be a driving potential for the water flow (Fredlund and Rahardjo, 1993). The hydraulic head, also known as total head or total potential, is basically the total energy of liquid water at a point and may be expressed as energy per unit weight in terms of pressure head and elevation head:

$$h_l = \frac{u_l}{\gamma_l} + z \qquad\qquad (2.1)$$

where h_l is the hydraulic head, u_l is the pore water pressure, γ_l is the unit weight of liquid water and z is the elevation.

Darcy (1856) postulated that the rate of water flow through a saturated soil mass was proportional to the hydraulic gradient. Later on various researchers including Buckingham (1907), Richards (1931), Childs and Collis-George (1950) and Nielson et al. (1986) stated that the Darcy's law can also be applied for the flow of liquid water through an unsaturated soil. Darcy's law for flow in unsaturated soil may be expressed as:

$$v_l = -k_l \nabla h_l \qquad\qquad (2.2)$$

where v_l is the liquid velocity, k_l is the unsaturated hydraulic conductivity and h_l is the hydraulic head. The negative sign in the equation indicates that water flows in the direction of a decreasing hydraulic head.

Substituting the value of h_l from equation (2.1) to (2.2) yields

$$v_l = -k_l \left[\nabla\left(\frac{u_l}{\gamma_l}\right) + \nabla z \right] \qquad\qquad (2.3)$$

Mitchell (1993) stated that the hydraulic conductivity is influenced by a number of factors, namely; fabric and pore fluid characteristics (density and viscosity), particle size and particle size distribution, void ratio, and mineralogical composition. Degree of saturation and turbulence of flow are also known to affect the hydraulic conductivity. However, the turbulence of flow may be neglected, as flow is slow. Unlike the saturated hydraulic conductivity, the unsaturated hydraulic conductivity is variable which is predominantly a function of the moisture content or matric suction of the unsaturated soil (Lloret and Alonso, 1980; Fredlund, 1991). Ewen and Thomas (1989) presented the expression of unsaturated hydraulic conductivity, k_l, as the function of volumetric moisture content, θ_l, and temperature, T,:

$$k_l(\theta_l, T) = \frac{\mu_r}{\mu(T)} k_{lr}(\theta_l)$$

(2.4)

where, μ is the dynamic viscosity and r is the subscript associated with room temperature. This incorporated the temperature effect into the liquid moisture movement.

Philip and de Vries (1957) were amongst the first who represented liquid moisture due to a thermal gradient. They employed Darcy's law for liquid movement and expressed the liquid moisture transfer equation into three components, that due to the temperature gradient, that due to volumetric moisture content gradient and that due to gravity. The equation may be written as:

$$v_l = -D_{Tl}\nabla T - D_{Ml}\nabla\theta_l - k_l\nabla z$$

(2.5)

here

$$D_{Tl} = k_l\gamma u_l$$

(2.6)

and

$$D_{MI} = k_I \frac{\partial u_I}{\partial \theta_I}$$ (2.7)

where v_I is the liquid velocity, D_{TI} is the thermal liquid diffusivity, D_{MI} is the isothermal liquid diffusivity, T is the temperature, θ_I is volumetric liquid moisture content, k_I is the unsaturated hydraulic conductivity, z is the elevation and γ is temperature coefficient of surface tension of water.

The soil liquid water also moves under the influence of physico-chemical forces associated with the interaction of the surface-active solids in the soil and water components. When the concentration of ions in a solution differs from that at another region or point, there is a tendency for the more dilute concentration liquid to diffuse into the region of higher concentration. This potential, existing specially in clay soils, will produce a gradient, which will induce moisture transfer to attain a more uniform ionic distribution, thereby creating a condition for osmotic flow (Seetharam, 2003).

Mitchell (1993) reported the significance of osmotically driven water flow relative to hydraulically driven water flow in heavily overconsolidated clays and clay shales, where the void ratio is low and the hydraulic conductivity is also very low. He proposed that the liquid velocity due to a chemical solute concentration gradient could be expressed as:

$$v_I^{c_d} = K_I^{c_d} \left(\nabla c_d \right)$$ (2.8)

where $K_I^{c_d}$ is the permeability with respect to chemical solute concentration gradient.

The combined effects of all the mechanisms, considered in equations (2.3) add (2.8), yield the total velocity of pore liquid moisture, which can be expressed as:

$$v_I = -D_{TI} \nabla T - D_{MI} \nabla \theta_I - k_I \nabla z + K_I^{c_d} \left(\nabla c_d \right)$$ (2.9)

2.4.2   Vapour moisture flow mechanism

Vapour transfer occurs as a result of two main mechanisms, namely; diffusive and pressure flows. The bulk air is considered to be a binary mixture of water vapour and dry air (Pollock, 1986) and can be dealt with via a generalised Darcy's law, following the approach of a number of researchers (Carman, 1956; Alonso et al, 1988).

Fick (1885) was the first who developed the steady state diffusion equation due to a concentration gradient. The formulation of Fick's law for diffusion in one dimension is as follows:

$$\frac{q}{t} = -D\frac{\partial c}{\partial x} \tag{2.10}$$

where q is the mass of substance diffusing across a unit area, t is the time, c is the concentration and D is the diffusion coefficient.

Later on researchers changed the concentration gradient into the pressure gradient to express the diffusion of water vapour. Penman (1940) used the findings of Buckingham (1904) that the rate of gas diffusion through a porous solid is approximately proportional to the square of the porosity. Penman studied the diffusion of carbon disulphide, acetone and carbon dioxide in porous material including soils. Penman (1940) expressed the diffusion equation in terms of pressure gradient for a steady state as follows:

$$\frac{dq}{dt} = -\frac{D}{B}A\frac{dP}{dl} \tag{2.11}$$

where q is the mass of gas, t is the time, D is the diffusion coefficient in porous material, A is the area, l is the length, and B = nP where n is the concentration of gas at pressure P.

Krischer and Rohnalter (1940) found the amount of water vapour diffusing through porous media under partial vapour pressure gradient as:

$$G_d = -\frac{K}{\mu R_d T} \frac{P_o}{P_o - P_a} \frac{dP_s}{dx}$$ (2.12)

where G_d is the vapour flux, K is the diffusion coefficient of water in air, μ is the dimensionless factor, R_d is the gas constant for water vapour, P_o is the total pressure and P_s is the partial water vapour pressure.

de Vries (1950) studied the effect of vapour diffusion under a thermal gradient on heat conductivity. He gave the following equation based on molecular diffusion of water vapour in soil pores:

$$q_v = -\alpha\phi D\gamma_w \frac{P}{P - P_v} \frac{dP_v}{dt}$$ (2.13)

where q_v is the vapour flux, α is the dimensionless factor depending on the soil structure, ϕ volume fraction of air filled pores, γ_w is the mass of 1 cm^3 water vapour, P is total pressure of moist air, P_v is the partial vapour pressure of water vapour.

Rollins et al. (1954) modified the above equation (2.13) of de Vries (1950) by inclusion of the Clapeyron gas equation and produced the following equation as:

$$q_v = -2.3 \times 10^{-6} \alpha\phi \frac{LP_v}{R(P - P_v)^{0.7}} \frac{dT}{dx}$$ (2.14)

where q_v is the vapour flux, α is the dimensionless factor depending on the soil structure, ϕ volume fraction of air filled pores, P is total pressure of moist air, P_v is the partial vapour pressure of water vapour, L is the latent heat of vaporation, R is the universal gas constant, dT/dx is the temperature gradient in the x direction.

In 1957, Philip and de Vries presented a vapour diffusion equation which is widely used. They presented a conceptual model of vapour flow under temperature gradients as a

series-parallel evaporation-condensation process. On a macroscopic scale water is assumed to evaporate from one soil water meniscus, diffuse across an air gap, and then condense back into the liquid phase at another meniscus. They suggested a simple mathematical model for this based on the expressions used to determine gas diffusion rates in Stefan's classic experiment, see Partington (1949) for details. They modified the then existing equations (Penman, 1940; Krischer and Rohnalter, 1940; van Bavel, 1952; Rollins et al., 1954) and expressed the velocity of vapour v_v as:

$$v_v = \frac{q_v}{\rho_l} = -\frac{D_{atms}v_v\tau_v\theta_a}{\rho_l}\nabla\rho_v \qquad (2.15)$$

where q_v is the vapour flux, ρ_l is the density of liquid moisture, D_{atms} is the molecular diffusivity of vapour through air, v_v is a mass flow factor, τ_v is the tortuosity factor, θ_a is the volumetric air content and $\nabla\rho_v$ is the vapour density gradient.

Philip and de Vries (1957) adopted an expression proposed by Krischer and Rohnalter (1940) for molecular diffusivity due to a temperature gradient as:

$$D_{atms} = 5.893 \times 10^{-6}\frac{T^{2.3}}{u_a} \qquad (2.16)$$

This equation is applicable in the temperature range of 293 – 343 K, (Philip and de Vries, 1957).

Phillip and de Vries (1957) introduced an expression for the mass flow factor v_v. It was incorporated to allow for the mass flow of vapour arising from the difference in boundary conditions governing the air and vapour components of the diffusion system. They adopted an expression proposed by Partington (1949), who showed that for steady state diffusion in a closed system between an evaporating source and a condensing sink:

$$v_v = \frac{u_a}{u_a - u_v} \qquad\qquad (2.17)$$

where u_a is the partial pressure of air and u_v is the partial pressure of vapour.

As stated previously, the air phase in soils can be considered to be a mixture of dry air and water vapour. Thomas and Sansom (1995) presented the following formulation to determine the density of dry air from the partial pressure of dry air and vapour. Applying Dalton's law of partial pressures yields:

$$u_a = u_{da} + u_v \qquad\qquad (2.18)$$

where u_{da} is the partial pressure of dry air. It has been found to obey the laws of a mixture of ideal gases to a sufficient degree of accuracy (Geraminegad and Saxena, 1986). The partial pressures of dry air and vapour can be expressed as:

$$u_{da} = \rho_{da} R_{da} T \qquad\qquad (2.19)$$

and

$$u_v = \rho_v R_v T \qquad\qquad (2.20)$$

where R_{da} is the specific gas constant of dry air, R_v is the specific gas constant for water vapour, ρ_{da} is the density of dry air, ρ_v is the vapour density and T is the temperature.

It was recognised by Philip and de Vries (1957) that the predicted value of the mass flow factor, v_v, from equation (2.15) may not be valid for non-stationary conditions, but that the expression was able to predict the correct order of magnitude. They also comment that the factor is close to 1 under normal soil temperatures.

Edlefsen and Anderson (1943) used the Kelvin's law of relative humidity and proposed the following relationship to determine the density of water vapour ρ_v:

$$\rho_v = \rho_0 h = \rho_0 \exp\left(\frac{\psi g}{R_v T}\right) \tag{2.21}$$

where ρ_0 is the density of saturated water vapour, h is the relative humidity, g is the gravitational constant and ψ is the capillary potential which is defined as:

$$\psi = \frac{u_l - u_a}{\gamma_l} \tag{2.22}$$

Ewen and Thomas (1989) presented a relationship fitted to standard data (Mayhew and Rogers, 1976) for the density of saturated water vapour:

$$\rho_0 = 1/\left\{194.4\exp\left(-0.06374(T-273)+0.1634\times10^{-3}(T-273)^2\right)\right\} \tag{2.23}$$

From equation (2.21) it can be observed that the density of water vapour, ρ_v, is dependent on the saturated soil water vapour, ρ_0, and the relative humidity, h. The gradient of vapour density may be expressed as:

$$\nabla\rho_v = h\nabla\rho_0 + \rho_0\nabla h \tag{2.24}$$

As ρ_0 is dependent on the absolute temperature, T, and the relative humidity is dependent on volumetric liquid moisture content, θ_l, the equation (2.24) can be expanded to give:

$$\nabla\rho_v = \left(h\frac{d\rho_0}{dT}\right)\nabla T + \left(\rho_0\frac{dh}{d\theta_l}\right)\nabla\theta_l \tag{2.25}$$

Substituting the vapour density gradient from equation (2.25) to (2.15) which gives

$$v_v = -\frac{D_{atms} v_v \tau_v \theta_a}{\rho_l}\left(h\frac{d\rho_0}{dT}\right)\nabla T - \frac{D_{atms} v_v \tau_v \theta_a}{\rho_l}\left(\rho_0 \frac{dh}{d\theta_l}\right)\nabla\theta_l \qquad (2.26)$$

Finally the above vapour velocity equation (2.26) is expressed by Philip and de Vries (1957) in the following form as:

$$v_v = -D_{TV}\nabla T - D_{MV}\nabla\theta_l \qquad (2.27)$$

where D_{TV} is the thermal vapour diffusivity and D_{MV} is the isothermal vapour diffusivity. They can be written as

$$D_{TV} = \frac{D_{atms} v_v \tau_v \theta_a}{\rho_l}\left(h\frac{d\rho_0}{dT}\right) \qquad (2.28)$$

and

$$D_{MV} = \frac{D_{atms} v_v \tau_v \theta_a}{\rho_l}\left(\rho_0 \frac{dh}{d\theta_l}\right) \qquad (2.29)$$

Experimental work carried out by Philip and de Vries (1957) suggested that the simple theory defined in equation (2.26) was not fully valid at increased temperature gradients. They proposed two refinements to the thermal vapour diffusivity term (D_{TV}). Firstly a flow area factor, f, was introduced to achieve a reduction of the vapour flow as the available flow area decreased at higher moisture contents. The air porosity was removed because factor f takes it into account. Secondly a microscopic pore temperature gradient factor, $(\nabla T)_a/(\nabla T)$, was introduced, which is the ratio of the average temperature gradient in the air filled pores to the overall temperature gradient. This factor takes account of the microscopic effect of heat flow paths being shared between sections of solid and fluid

paths, giving rise to microscopic temperature gradients in the fluid filled pores, which may be much higher than the macroscopic temperature gradients across the sample as a whole. Including these amendments into D_{TV} term (de Vries, 1958) yields:

$$D_{TV} = \frac{D_{atms} v_v}{\rho_l} f \frac{(\nabla T)_a}{(\nabla T)} \left(h \frac{d\rho_0}{dT} \right)$$

(2.30)

here

$$f = \begin{cases} \theta_a + \theta_l = n & \theta_l \leq \theta_{lk} \\ \theta_a + \dfrac{\theta_a \theta_l}{n - \theta_{lk}} & \theta_l > \theta_{lk} \end{cases}$$

(2.31)

where n is the porosity and θ_{lk} is the value of θ_l at which liquid continuity fails.

Preece (1975) proposed an expression to evaluate the microscopic pore temperature gradient factor, $(\nabla T)_a/(\nabla T)$, based on a proposed geometrical method (de Vries, 1966). The following expression was developed for a Washington Sand.

$$\frac{(\nabla T)_a}{\nabla T} = \frac{1}{3} \left[\frac{2}{1 + BG_v} + \frac{1}{1 + B(1 - 2G_v)} \right]$$

(2.32)

where

$$B = \frac{(\lambda_a + \lambda_v)}{\lambda_l} - 1$$

(2.33)

and

$$G_v = \begin{cases} 0.3333 - 0.325(n - \theta)_l/n & 0.09 < \theta_l < n \\ 0.0033 + 11.11(0.33 - 0.325(n - 0.09)/n)\theta_l & 0 < \theta_l < 0.09 \end{cases}$$

(2.34)

λ_a is the thermal conductivity of pore air, λ_l is the thermal conductivity of pore liquid and λ_v is the thermal conductivity of pore vapour, which can be defined as:

$$\lambda_v = D_{atms} v_v hL \frac{\partial \rho_0}{\partial t}$$
                                                                        (2.35)

where L is the latent heat of vaporisation.

Ewen and Thomas (1989) suggested two alterations to the extended vapour velocity equation proposed by Philip and de Vries (1957). These alterations affected the flow area factor f. The extended vapour velocity equation proposed by Philip and de Vries (1957) did not account for the flow area factor in the isothermal vapour diffusivity (D_{MV}) term and appear to show the choking of vapour flow at high moisture contents. Since it was assumed that the vapour velocity is proportional to the vapour density, Ewen and Thomas suggested that the vapour flow area factor should be present in both the thermal vapour diffusivity and isothermal vapour diffusivity terms. They also suggested that the form of flow area factor be modified to be equal to the porosity, and that no choking occurs. These suggestions yield the following expression for the thermal vapour diffusivity and isothermal vapour diffusivity as:

$$D_{TV} = \frac{D_{atms} v_v}{\rho_l} n \frac{(\nabla T)_a}{(\nabla T)} \left(h \frac{d\rho_0}{dT} \right)$$
                                                                        (2.36)

and

$$D_{MV} = \frac{D_{atms} v_v n}{\rho_l} \left(\rho_0 \frac{dh}{d\theta_l} \right)$$
                                                                        (2.37)

2.4.3   Limitations

The theories of liquid moisture and vapour moisture movement presented here are based on the experiments carried out on the porous and rigid media. The theories do not work with specially swelling clays where soils matrix change with moisture content. Hysteresis is not taken into account either. Also surface phenomenon at the interface between the matrix and the liquid is not considered. de Vries (1987) discussed the limitations and assumptions in the theory developed by Philip and de Vries in 1957. It should be noted however that in these mechanistic models some limitation are overcome via the experimental determination of some of the model parameters.

2.5   Heat transfer

Winterkorn and Eyring (1946) and Jakob (1949) stated that there are three mechanisms of heat flow in soils; conduction, in which the excitation of an atom or molecule is transmitted to its neighbour by direct contact, oscillation-like in solids and liquids and by impact and exchange of momentum in gases; convection, in liquids and gases, where a portion of matter at a higher temperature is mechanically mixed with matter at a lower temperature; radiation by means of waves traversing space from one body to another without affecting the interlying space. Generally heat flows through soils entirely by conduction, with radiation unimportant and convection important, only if there is high flow rate of water or air (Mitchell, 1993). Johansen (1975) considered thermal radiation across soil air spaces and concluded that it is only significant for very coarse material at low moisture contents. Heat transfer is also found to occur due to chemical concentration gradients. This effect is commonly referred to as the Dufour effect. Mitchell (1993) stated that the Dufour effect has not been found to be of significance in soils.

The fundamental equation for heat conduction as derived by Fourier (1822) is as follows:

$$Q = -\lambda_T \nabla T \qquad\qquad\qquad (2.38)$$

where, Q is the heat flux per unit area whereas in Darcy's equation it was the mass flux, λ_T is the thermal conductivity, ∇T is the temperature gradient.

The coefficient of thermal conductivity of unsaturated soil has been found to be a function of degree of saturation, typically exhibiting an increase with increasing degree of saturation, i.e.:

$$\lambda_T = \lambda_T(S_l)$$ (2.39)

de Vries (1958) presented heat flux equation that included the effect of conduction, latent heat of vaporisation and convection due to liquid and vapour moisture. The latent heat of vaporisation is the heat energy release when the vapour condenses and turns into liquid. Ewen and Thomas (1989) expressed the heat flux per unit area of unsaturated soil, Q, at reference temperature, Tr, as:

$$Q = -\lambda_T \nabla T + (v_v \rho_v + v_a \rho_v)L$$
$$+ (C_{pl} v_l \rho_l + C_{pv} v_v \rho_l + C_{pv} v_a \rho_v + C_{pda} v_a \rho_{da})(T - T_r)$$ (2.40)

where C_{ps}, C_{pl}, C_{pv}, and C_{pda} are the specific heat capacities of solid particles, liquid, vapour, and dry air, v_l, v_v, and v_a velocity of liquid, vapour and dry air , L is the latent heat of vaporisation and ρ_s, ρ_l, ρ_v and ρ_{da} is the density of solid particles, liquid, vapour, and dry air.

It can be seen from equation (2.40) that the heat flux accommodates heat transfer due to: conduction, convection, and latent heat flow associated with movement of vapour. The latent heat of vaporisation is also introduced (Luikov, 1966). Convection is considered to be the flow of heat due to movement of; the liquid phase, a vapour phase associated with a vapour pressure gradient, a vapour phase associated with the bulk flow of air, and the air phase. This form of representing the heat flux of an unsaturated soil is widely used (Milly, 1982; Olivella, et al., 1994; Thomas et al., 1996; Collin et al., 2002).

2.6   Determination of flow parameters

The heat and moisture movement equations presented above, required the correct values of hydraulic parameters and thermal parameters in order to predict the accurate heat and moisture transfer. The following sections describe these flow parameters and their determination methods.

2.6.1   Hydraulic parameters

Unsaturated hydraulic conductivity and suction are the important hydraulic parameters and their accurate measurement is the fundamental requirement of the moisture movement equations. The following sections discuss the suction, soil water characteristic curve and unsaturated hydraulic conductivity and their measurement in detail.

2.6.1.1   Soil suction

Soil suction was first defined by Schofield (1935) as pressure deficiency in the pore liquid within a soil. Due to this pressure deficiency, an unsaturated soil absorbs more water, if additional water is made available at atmospheric pressure (Sharma, 1998). The total suction can be divided into two components: matric and osmotic. The matric suction, which is a physically negative value of the pore water pressure, is due to the surface tension effects. The matric suction is defined as the difference in pore air and pore water pressures acting on the air-water interface in an unsaturated soil. The osmotic suction results from the dissolved ionic concentration in the pore liquid. The total suction, s, in a soil can be written as a function of matric suction, (u_a-u_l), and osmotic suction, π, i.e.

$$s = f\{(u_a - u_l), \pi\}$$ (2.41)

The measurement techniques of total suction, matric suction and osmotic suction is discussed in following sections.

2.6.1.1.1 Total suction

Edlefsen and Anderson (1943) stated that the total soil suction is commonly referred to the free energy state of soil water. The free energy of the soil water can be measured in terms of the partial vapour pressure of the soil water (Richards, 1965). According to Hillel (1980) the relationship between pore water potential and its partial vapour pressure described by Kelvin's equation, can be written in terms of total suction, s, as

$$s = -\frac{RT}{\upsilon\omega}\ln(RH) \tag{2.42}$$

where, R is the universal gas constant (8.314 J/mol K), T is the absolute temperature (K), υ is the specific volume of water (m^3/kg), ω is the molecular mass of water vapour (18.016 kg/kmol) and RH is the relative humidity. The total suction becomes zero at 100 % relative humidity. Hence, the total suction of an unsaturated soil sample can be determined by measuring the relative humidity.

There are various methods of measuring the total suction which are based upon the relative humidity measurement viz. thermocouple psychrometer, chilled-mirror hygrometer, polymer resistance/capacitance sensors, non-contact filter paper method and humidity control techniques.

The thermocouple psychrometer works on the principle of relating the temperature difference between non-evaporating surface (reference junction) of the psychrometer and the evaporating surface (measurement junction) of the soil to the relative humidity (Spanner, 1951). A typical psychrometer is the Peltier-type thermocouple psychrometer also called as Spanner psychrometer as shown in Figure 2.7. It consists of a thermocouple that is usually covered with a protective housing such as porous ceramic shield or stainless steel mesh. It is capable of measuring suction from 100 kPa to 8000 kPa under a constant temperature environment of ± 0.001 °C (Fredlund and Rahardjo, 1993). Krahn and Fredlund (1972) used thermocouple psychromters to determine the relationships between total suction and initial water content for compacted glacial till and compacted Regina clay, as presented in Figures 2.8 and 2.9. The curves indicate that the

total suction decreases with an increase in water content. The accuracy of results obtained from psychrometers depends upon the water vapour equilibration time and the need for a constant temperature environment (Folly, 2001).

Chilled-mirror sensing technology (Figure 2.10) has been used since the 1950s for determination of dew-point temperature in a closed, humid environment (Lu and Likos, 2004). Gee et al. (1992) describe the use of it for soils suction measurement. The basic operating principle of relative humidity measurement involves the thermoelectric chilling of a reflective surface, usually a metallic mirror, to a temperature at which condensation from ambient water vapour in the closed chamber forms on the mirror surface. When condensation occurs as the mirror is cooled to the dew-point temperature which is measured by a resistance thermometer embedded in the mirror. The dew-point temperature is then related to relative humidity and corresponding total suction by using Kelvin's law.

Lu and Likos (2004) described that polymer-based sensors consist of a porous probe containing two electrodes separated by thin polymer film or polymer-coated substrate that adsorbs or releases water as the relative humidity of the gas in equilibrium with the probe changes. As water is either adsorbed or desorbed onto or from the polymer surface, the resistance and capacitance of the electrode-polymer system changes. Capacitance sensors are less sensitive to temperature fluctuations compared to resistance sensors (Wiederhold, 1997). Sensors for rugged use are usually enclosed by a filtering element such as a plastic or stainless steel screen or sintered metal tube. In the present study relative humidity probes were used which are based on the principle of capacitance sensors.

The idea to use filter paper for soil suction measurement can be traced back to the work of Schull in 1916 (Leong et al., 2002). Gardener (1937) first reported the use of filter paper as a soil suction sensor. Since then filter paper has been used and investigated by numerous researchers (Fawcett and Collis-George, 1967; McQueen and Miller, 1968; Al-Khafaf and Hanks, 1974; McKeen, 1980; Hamblin, 1981; Chandler and Gutierrez, 1986; Houston et al., 1994; Swarbrick, 1995; Leong et al., 2002). The filter paper method has been recommended as a standard test method for measurement of soil suction in ASTM D

5298-94. The filter paper method is based on the assumption that a filter paper will come to equilibrium with respect to moisture flow with a soil having a specific suction. Equilibrium can be reached by either liquid moisture or vapour moisture exchange between the soil sample and filter paper (Thyagaraj, 2006). When a dry filter paper is suspended above a soil specimen, vapour flow of moisture will occur from the soil to filter paper until equilibrium is reached (Figure 2.11). Since filter paper is close to but out of contact with soil moisture, the vapour moisture transferred will effectively be distilled water and the measured suction will be total suction. The time required to achieve equilibrium for the filter paper is at least 7 days (Fawcett and Collis-George 1967; McQueen and Miller, 1968; Houston et al. 1994; ASTM D 5298-94). Having established the equilibrium conditions, the water content of the filter paper is measured. The water content of the filter paper is then related to suction through a suitable calibration. According to ASTM standard on filter paper method, the same calibration curve can be used for both matric and total suction measurements. The calibration curve exhibits bi-linearity as shown in Figure 2.12. The lower part of the curve represents high range of filter paper water contents where the water is held by the influence of capillary forces. On the other hand, the upper part of the calibration curve represents the lower water contents where the water is held as an adsorbed water film within the filter paper (Miller and McQueen, 1978; Fredlund and Rahardjo, 1993).

Fawcett and Collis-George (1967) and McQueen and Miller (1968) modified the standard technique by pre-treating the filter paper in order to prevent fungal and bacterial growth during the equilibration time. Furthermore, Sibley and Williams (1990) used other absorbent materials instead of filter paper to increase the sensitivity of this method over different range of suction. Experimental evidence has demonstrated that the filter paper method is simple to perform, inexpensive and capable of measuring the soil suction over the entire range. However, Totoev and Kleeman (1998) stated that the results of filter paper measurements have a tendency to underestimate the soil suction, they are unsuitable for areas of high humidity, and the long equilibration period may be disadvantageous in some situations.

Lu and Likos (2004) discuss that humidity control techniques rely on measurement of water content for soil samples of controlled total suction, unlike other methods (e.g. psychrometers, non-contact filter paper method) that rely on measurements of total suction for soil samples of controlled water content. Traditional methods for controlling relative humidity include isopiestic (or same pressure) methods which depend on attaining vapour pressure equilibrium for salt or acid solution in a closed thermodynamic environment and two pressure methods which rely on active manipulation of relative humidity, either by varying pressure or by mixing vapour-saturated gas with dry gas.

Most recently, several new innovative techniques have been developed to measure the total suction. Woodburn and Lucas (1995) described the use of a laboratory electronic humidity sensor for measuring high values of soil suction. Conciani et al. (1995) used the principle of X-ray computerised tomography to measure the soil suction. This method uses time domain reflectometry to determine the dielectric constant of the soil that is related to the volumetric water content. The volumetric water content is then related to suction through the independently established soil-moisture retention curve.

2.6.1.1.2 Matric suction

Matric suction arises from the combined effects of capillary and short-range adsorption (due to surface charge, van der Waals attraction and exchangeable cation hydration) in soils. The soil pores with small radii act as capillary tubes that cause the soil moisture to rise above the water table. The capillary has a negative pressure with respect to the atmospheric pressure. Capillary phenomenon produces curved water surface at the air-water interface in a soil. The radius of curvature is inversely proportional to the difference between the air and water pressure across the surface and is called matric suction (Fredlund and Rahardjo, 1993). Mathematically, matric suction ($u_a - u_l$), can be expressed as

$$u_a - u_l = \frac{2T}{r}\cos\alpha \qquad\qquad (2.43)$$

where, T is the surface tension of water, r is the radius of soil pore and α is the contact angle between menisci and wall of soil pore.

There are direct and indirect methods of measuring the matric suction. Direct methods include tensiometer and axis translation techniques while indirect methods use electrical/thermal conductivity sensors and contact filter paper method. Direct methods measure the negative pore-water pressure directly. The pore-air pressure which is atmospheric, minus the negative pore-water pressure gives the matric suction (Fredlund and Rahardjo, 1993).

Tensiometers and axis translation techniques depends upon the properties of high air entry (HAE) materials. A standard tensiometer is a water filled tube with an HAE ceramic tip at one end and some type of device for measuring negative water pressure at the other (Lu and Likos, 2004), as shown in Figure 2.13. The tensiometer is inserted into a pre-cored hole until there is good contact with the soil so that continuity can be established between the pore-water in the soil and the water in the tensiometer tube. Negative pressure is transmitted through the saturated pores of HAE ceramic tip such that water is withdrawn from the tensiometer until the internal pressure in the sensor body is equivalent to the matric potential of the soil water. Three types of commercial measuring systems for a tensiometer have been typically used for field measurements of matric suction (Figure 2.14), namely a mercury manometer, a vacuum gauge and an electronic pressure transducer (Folly, 2001).

Hilf (1956) proposed the axis translation technique of measuring the negative pore-water pressure. The axis translation techniques have two ways of matric suction measurement, first null and second extraction. An unsaturated soil sample is placed on HAE ceramic disk in a closed chamber. In null measurement the air pressure in the closed chamber is increased and flow of water between the soil and HAE disk is not allowed and matric suction is recorded at equilibrium. While in extraction method, the air pressure is elevated and drainage is allowed from the soil sample to HAE pores until equilibrium. The axis translation technique simply translates the origin of reference for the pore-water pressure from the standard atmospheric conditions to the final air pressure in the chamber.

There are three commercially available equipments that are based upon this technique namely pressure plate, Tempe cell and volumetric pressure plate extractor. Pressure plate is applicable for matric suction ranging from 0 to 1500 kPa, Tempe cell is applicable from 0 to 100 kPa and volumetric pressure plate extractor is applicable from 0 to 200 kPa. The volumetric pressure plate extractor in conjunction with hysteresis attachment can be used to study the hysteresis associated with drying and wetting of the soil. The axis translation technique is found to be reliable by many researchers (Olson and Langfelder, 1965; Mou and Chu, 1981). Theoretical studies on the technique suggest that it is best suited to soils with a continuous air-phase (Bocking and Fredlund, 1989). The presence of occluded air bubbles in the soil can result in an overestimation of matric suction (Thyagraj, 2006). Also, air diffusion through the HAE disk can cause an under estimation of the measured matric suction (Fredlund and Rahardjo, 1993).

Electrical/thermal conductivity sensors are made up of porous materials like ceramic, polymer synthetic, sintered metal or glass. The electrical and thermal conductivities of porous medium are the functions of moisture content. The sensors are embedded in a mass of unsaturated soil and matric suction is determined indirectly by correlation with a predetermined calibration curve.

The contact filter paper method is another indirect method of measuring the matric suction. The dry filter paper is placed in direct contact with a soil specimen and moisture transfer to the paper is controlled by capillary and particle adsorption forces comprising the matric suction (Figure 2.15). The moisture content of filter paper at equilibrium is measured gravimetrically and related to suction through a predetermined calibration curve for the particular type of paper. Commonly used types of filter papers include Whatman 42, Schleicher and Schuell 589, White Ribbon and Fisher 9-790A (Lu and Likos, 2004).

2.6.1.1.3 Osmotic suction

Osmotic suction, π, of an ionic solution in the soil sample is related to its dissolved salt concentration and is calculated from van't Hoff equation (Nelson and Miller, 1992; Mata et al., 2002) as:

$$\pi = iMRT \qquad\qquad\qquad (2.44)$$

where R is the universal gas constant (8.32 litre.kPa/moleK), T is the absolute temperature (K), M is the molarity of the dissolved ions in the soil solution (mole/litre) and i is the van't Hoff factor.

The osmotic suction can be measured indirectly using a pore fluid squeezer technique (Manheim, 1966). The apparatus consist of cylinder and piston squeezer that forces the pore water into a syringe shown in Figure 2.16. The electrical conductivity of the extracted pore-water is then measured to determine the total ion concentration of salts. The predetermined calibration curve is used to relate the electrical conductivity with osmotic suction. However, it is apparent that the magnitude of the applied extractor force affects the measurement of osmotic suction (Folly, 2001).

2.6.1.2 Soil water characteristic curve

The soil-water characteristic curve (SWCC) provides the relationship between matric suction and water content (volumetric or gravimetric or degree of saturation). The SWCC is more commonly referred as a soil-water retention curve (moisture retention curve) in soil sciences (Leong and Rahardjo, 1997). The SWCC is used to determine the unsaturated hydraulic conductivity indirectly; this would be discussed in section 2.7.1.3.2. Earlier, various suction measurement techniques have been discussed. These measurements often comprise only a small portion of the SWCC. Therefore, numerous approaches have been proposed for mathematical representation (i.e. fitting) or prediction of the SWCC (Lu and Likos, 2004).

Leong and Rahardjo (1997) stated that a number of equations have been suggested for the SWCC and almost all the equations suggested can be derived from the following generic form:

$$a_1\Theta^{b1} + a_2\exp(a_3\Theta^{b1}) = a_4 s^{b2} + a_5\exp(a_6 s^{b2}) + a_7 \qquad\qquad (2.45)$$

where

$$s = u_a - u_l \tag{2.46}$$

and

$$\Theta = \frac{\theta_l - \theta_{lr}}{\theta_{ls} - \theta_{lr}} \tag{2.47}$$

In the above equations a_1, a_2, a_3, a_4, a_5, a_6, a_7, b_1 and b_2 are constants, s is the matric suction $(u_a - u_l)$, Θ is the normalised water content which is dimensionless water content variable, θ_l is the volumetric liquid water content, θ_{lr} is the residual volumetric liquid water content and θ_{ls} is the saturated volumetric liquid water content.

There are various models including Brooks and Corey (1964), Gardner (1958), van Genuchten (1980) and Fredlund and Xing (1994) commonly used but only the van Genuchten (1980) model is presented here and later used in this study to plot SWCC.

van Genuchten (1980) proposed a smooth, closed form, three parameter model for the SWCC. van Genuchten model can be obtained from the equation (2.45), if $a_4/a_1 = \alpha^n$, $b_1 = m$ and $b_2 = n$. van Genuchten equation can be expressed as:

$$\Theta = \left[\frac{1}{1 + (\alpha s)^n} \right]^m \tag{2.48}$$

where α, n, m are constant fitting parameters.

The parameter n is related to the pore size distribution of the soil and the parameter m is related to overall symmetry of the SWCC. The parameter m is frequently constrained by direct relation to parameter n (Lu and Likos, 2004) as:

$$m = 1 - \frac{1}{n} \qquad\qquad (2.49)$$

or

$$m = 1 - \frac{1}{2n} \qquad\qquad (2.50)$$

2.6.1.3   Unsaturated hydraulic conductivity

In order to analyse liquid moisture movement in soil it is necessary to determine unsaturated hydraulic conductivity.   The unsaturated hydraulic conductivity can be determined using direct or indirect methods.

2.6.1.3.1   Direct methods

There are various direct laboratory methods to measure the unsaturated hydraulic conductivity. All the direct methods assume the validity of Darcy's law. The direct test methods can be divided into two primary groups, namely, steady-state methods where the quantity of flow is time independent, and unsteady-state methods where the quantity of flow is time dependent (Fredlund and Rahardjo, 1993).

The steady-state methods are performed by maintaining the hydraulic head gradient, matric suction and the water content constant across an unsaturated soil sample. Klute (1965) described an apparatus to measure the unsaturated hydraulic conductivity using a steady-state approach. The apparatus, shown in Figure 2.17, consists of a cylindrical soil sample placed between two high air entry ceramic plates. Two tensiometers are installed along the height of the specimen to measure the pore water pressure. The axis translation technique is employed to maintain a constant air pressure. The measured hydraulic gradient is used to calculate the hydraulic conductivity owing to uncertainties associated with the hydraulic head changes across the porous plates. The contact planes between the specimen and porous plate also produce uncertainties in predicting heads throughout the

specimen (Klute, 1972). Olson and Daniel (1981), Daniel (1983) and Fredlund and Rahardjo (1993) present several extensive reviews of the scope and limitations of this direct steady-state method of Klute.

Juca and Frydman (1995) reported various steady state experimental techniques to determine the unsaturated hydraulic conductivity. Folly (2001) also reviewed various steady-state experimental devices constructed by Uno et al. (1995) and Fleureau and Taibi (1995). All of them are based on Klute's approach.

The instantaneous profile method is an unsteady-state method. The method uses a cylindrical soil sample that is subjected to a continuous water flow in or out from one end of the specimen. When the water flows into the specimen it is a wetting process and when the water flows out it is a drying process. Richards and Weeks (1953) first described the instantaneous profile method for measuring the wetting and drying curve. Hamilton et al. (1981) used the apparatus shown in Figure 2.18 to measure the negative pore water pressure head distribution during the unsteady-state water flow and obtain the volumetric water contents from the soil water characteristic curve. The apparatus consists of a horizontal cylindrical cell with several ports available for thermocouple psychrometers or tensiometers to measure negative pore water pressure (or matric suction). The water is supplied from one end and it flows in a horizontal direction as a result of the pore water pressure head gradient. Therefore, gravitational head effects are negligible. The flow rate is computed from the volumetric water content. The ratio between the flow rate and hydraulic head gradient (computed from the pore water pressure gradient) gives the unsaturated hydraulic conductivity. Measurements at different locations along the sample at different time produce the series of unsaturated hydraulic conductivity corresponding to particular water content or matric suction.

The other unsteady-state methods include modified geotechnical equipments such as suction controlled oedometer and triaxial cells. Folly (2001) used the suction controlled oedometer in conjunction with the Gardner (1956) outflow method to determine the unsaturated hydraulic conductivity. Fourie and Papageorgiou (1995) used a standard

triaxial cell with a modified base to develop a rapid technique for determining the hydraulic conductivity of unsaturated soils.

2.6.1.3.2 Indirect methods

Indirect methods are basically predictive methods that use the soil water characteristic curve (SWCC), saturated hydraulic conductivity and soil pore size distribution to predict the unsaturated hydraulic conductivity. Various researchers including Richards (1931), Averjanov (1950), Burdine (1952), Gardner (1958), Brooks and Corey (1964), Arbhabhirama and Kridakorn (1968), Kunze et al. (1968), Green and Corey (1971) and Mualem (1976) presented various models to predict unsaturated hydraulic conductivity. Fredlund and Rahardjo (1993) and Lu and Likos (2004) provide the detailed reviews and analyses of several models. Mualem (1986) classified three types of approaches to model the hydraulic conductivity function namely, empirical model, macroscopic model and statistical model. Agus et al. (2003) provide a quantitative assessment of various statistical modelling approaches and suggest that the statistical models perform better for coarse-grained soils such as sand.

According to Brooks and Corey (1964) model, the unsaturated hydraulic conductivity, k_l, is determined by the following equations:

$$k_l = k_s \qquad\qquad \text{for } s \le s_b \qquad\qquad (2.52)$$

$$k_l = k_s \left[\frac{s_b}{s}\right]^{2+3\lambda} \qquad\qquad \text{for } s > s_b \qquad\qquad (2.53)$$

where k_s is the saturated hydraulic conductivity, s_b is the air entry value and s is the matric suction and λ is the pore size distribution index.

The air entry value is the matric suction value that must be exceeded before air recedes into soil pores. The unsaturated hydraulic conductivity values can be determined for various matric suction values.

Kunze et al. (1968) and Green and Corey (1971) models are based on Hagen-Poiseuielle's equation. Green and Corey (1971) presented a statistical model based on the work of Marshall (1958) and Millington and Quirk (1959). The approach of Green and Corey (1971) assumes that pore size can be related to a matric suction and volumetric moisture content relationship. The resulting model is often referred as a pore-size interaction model.

The central feature of the Green and Corey (1971) method is the subdivision of the SWCC into a number of zones. Each zone is related to the size of pores in the soil and can hence be evaluated from the amount of water the soil holds. Large pores are associated with the values of volumetric moisture content near saturation, whereas only the small pores retain water at lower moisture contents. Pore class subdivision is therefore accomplished by the subdivision of the volumetric moisture content range. The unsaturated hydraulic conductivity, k_l, can be written as:

$$(k_l)_i = \frac{k_s}{k_{sc}} \frac{30 T_s^2 \rho_l g}{\mu} \frac{\theta_{ls}^2}{N^2} \sum_{j=i}^{m} [(2j+1+2i)s_j^{-2}] \qquad (2.54)$$

where $i = 1, 2, 3, \ldots, m$

In the above expression, k_s is the saturated hydraulic conductivity, k_{sc} is the calculated saturated hydraulic conductivity, T_s is the surface tension of water, ρ_l is the liquid water density, g is the gravitational acceleration, μ is the absolute viscosity of liquid water, θ_{ls} is the volumetric moisture content at 100 % saturation, N is the total number of intervals computed between the saturated volumetric water content and zero volumetric water content, i is the interval number, m is the total number of intervals between the saturated volumetric water content and the lowest volumetric water content and s_j is the matric suction at the midpoint of the jth interval. The ratio k_s/k_{sc} is known as matching factor.

2.6.2   Thermal parameters

As heat transfer equation requires correct thermal parameters like thermal conductivity, specific heat capacity and latent heat of vaporisation to determine the accurate heat movement in the soil. The following sections present the method of measurement of these thermal parameters.

2.6.2.1   Thermal conductivity

Thermal conductivity is the property of a material that relates the heat flux (energy per unit area per unit time) to the temperature gradient (temperature difference per unit length) that exists over a material and can be expressed as:

$$\text{Thermal conductivity (W/mK)} = \frac{\text{Heat flux (W/m}^2)}{\text{Temperature gradient (K/m)}} \qquad (2.55)$$

Therefore, the measurement of thermal conductivity involves the measurement of the heat flux and temperature difference. The difficulty of the measurement is always associated with the heat flux measurement. Where the measurement of the heat flux is done directly (e.g. by measuring the electrical power going into the heater), the measurement method is termed absolute. Where the flux measurement is done indirectly (by comparison), the method is termed comparative. The measurement methods can be divided mainly into two categories namely steady state and non steady state.

2.6.2.1.1   Steady state method

The guarded hot plate method is the widely used steady state method for measuring thermal conductivity. The method is detailed in ASTM C 177-04. The apparatus takes two identical samples between the main heater and each auxiliary heater (Figure 2.19). The auxiliary heaters are controlled at the same temperature, whilst the main and guard heaters are controlled at a higher temperature. The guard heater surrounds the main heater minimising later heat loss. Thermocouples are installed within the soil and on the

heater surfaces to measure the temperature. It is assumed that the amount of heat energy flow through the sample is equal to power supplied to the main heater. Once the steady state equilibrium is achieved, the thermal conductivity is determined by the temperature drop across each sample, the thickness of each sample, the power supplied to main heater and the surface area of the main heater plate.

The test does not require any pre-test calibration by the user, but has the disadvantage that it takes long time to reach steady state thermal equilibrium. Table 2.1 shows the thermal conductivity values for typical soil components

2.6.2.1.2 Non-steady state method

Hot wire method is a non-steady state (transient) method to determine the thermal conductivity. This method is employed in thermal conductivity probes. The probe consists of a temperature sensor and a miniature heater housed in a ceramic block or tip (Figure 2.20). This is a quick method of measuring thermal conductivity unlike steady state method. Ewen and Thomas (1987) developed the thermal probe to determine thermal conductivity of unsaturated sand.

The accuracy of thermal conductivity probes is limited by installation and maintenance procedures (Folly, 2001). Common problems include poor contact between the porous block and soil, the air entrapment during installation, temperature and hysteretic effects and the deterioration of porous block. Ewen and Thomas (1992) stated that thermal probes are capable of measuring the thermal conductivity of a soil within a precision of about 10 % or less.

2.6.2.2   Specific heat capacity

Mayhew and Rogers (1976) have produced a range of quantities for the specific heat capacity of the constituent parts of soil. Several simple systems have been developed to measure heat capacity, however, they may not be applicable for measuring heat capacity

for all types of soils (Folly, 2001). Table 2.1 shows the specific heat capacity for various substances.

2.6.2.3 Latent heat of vaporisation

Latent heat or enthalpy of vaporisation is the heat energy that is required to transform a given quantity of liquid into vapour without an overall change of temperature. The latent heat of vaporisation is equal to latent heat of condensation but heat is absorbed during vaporisation and released during condensation. Folly (2001) explained that the latent heat of vaporisation is determined by enclosing a unit mass of ice below freezing point in a cylinder by a piston under a constant load and an atmospheric pressure. The ice is subjected to a temperature rise and consequently expands until a temperature of 0 °C is reached. Further heating results in a rise of a temperature of the liquid, a contraction in volume until the temperature is about 4 °C, and subsequent expansion until a temperature of 100 °C is reached. At this point a second phase change occurs at constant temperature with a large increase in volume until the liquid has been vaporised. The heat required in this case is called the latent heat of vaporisation. When vaporisation is complete the temperature rises once more. Mayhew and Rogers (1976) have determined a range of quantities to describe the latent heat of vaporisation for water at varying temperature as presented in Table 2.2

2.7 Review of thermo-hydraulic experimental setups

Bouyoucos (1915) was the first to develop an experimental apparatus to study the effect movement of water in sealed soil columns in the direction of high to low temperatures. He studied the movement of moisture from warm to cold soil in two different ways, first, when the column of soil lay horizontally and second, when it stood vertically. For the horizontal soil column case, the experimental setup consisted of two wooden boxes of size 22 inches long, 10 inches wide and 20 inches deep, having wooden partition in the centre which contained perforations to fit the brass tubes (8 inches long and 1.5 inches diameter) filled with soil to be tested, as shown in Figure 2.21. One compartment contained melting ice and the other hot water at the required temperature. To prevent any

exchange of water between the two compartments, the edges of the partition and the holes for the tubes were made water tight by means of paraffin. For the vertical soil column case, one box that contained melting ice was 24 inches long, 10 inches wide and 13 inches deep. The other box, that contained hot water was 13 inches long, 7 inches wide, 11 inches deep and was placed inside the first box (Figure 2.22). The bottom of the small box was supplied with holes to hold the brass tubes and again melted paraffin was used to make the small box leak proof. The investigation was carried out on five classes of soil: Miami light sandy loam, Miami heavy sandy loam, Miami silt loam, Clyde silt loam and Miami clay. There were only two amplitudes of temperature employed 0 °C to 20 °C and 0 °C to 40 °C. All the experiments were run for eight hours.

Bouyoucous (1915) investigated three different types of tests. First, the brass tubes were filled with soils of uniform moisture content and closing both ends of them with solid rubber stoppers. The half of the soil column kept at a high temperature either 20 °C or 40 °C and another half at a low temperature 0 °C for 8 hours, then determining the percentage of moisture of the two columns and attributing any difference in water content to thermal dislocation. Second, the brass tube was filled with moist and dry columns of soil with an air space of 0.25 inch between the two columns in the brass tube. The air space was created by placing a ring of cork between the two columns of soil, the two sides of the ring were closed with wire gauge that acted as supports of the two columns and prevented soil particles from coming into contact. The moist soil column was kept at a high temperature either 20 °C or 40 °C and another half at a low temperature 0 °C. Third, the tube was filled with a moist soil column in contact with a dry column and the former kept at 20 °C or 40 °C and the latter at 0 °C.

In the first type of test, it was found that the percentage of water moved from the warm to cold end increased in all types of soils with a rise in the initial moisture content until certain water content was reached and then it began to decrease again with further increase in initial moisture content. The percentage of moisture at which the maximum thermal dislocation occurred was designated as thermal critical moisture content. In the second test with the air gap, it was found that the amount of water lost from the soil by vapour was very small. Bouyoucous (1915) concluded that the capillary movement of

water in moist soils is not controlled entirely by the curvature of the capillary films, as is generally believed, but also by the unsatisfied attractive forces of the soil for water.

Smith and Byers (1938) designed an apparatus to study the thermal conductivities of soil but entered into moisture transfer complications. The apparatus consisted of a hard rubber container of 0.75 inches thickness with square faces 8 inches on side, as shown in Figure 2.23. The temperature gradient was applied across thickness. Heat was released at a hot face CH, transmitted across the soil, and picked up by a cold reservoir CC. The copper plates were used as hot face and cold reservoir. To determine soil moisture, samples were taken at SH of Figure 2.23 just next to the hot face and at SC of Figure 2.23 next to the cold face. Comparative studies were made of the Miami silty loam, Miami silty clay loam and Chester loam in the natural state and the fragmented state. The various initial moisture content and the thermal gradients that were used are detailed by Smith (1943). The important findings of the study was that moisture is transferred from a warm and moist soil to a cold and dry one only by the slow process of vapour diffusion and possibly convection.

Maclean and Gwatkin (1946) conducted a laboratory investigation on the movement of moisture when a temperature gradient exists in wet soil. The various factors, including soil type, initial soil moisture content, bulk density, mean soil temperature, and magnitude of thermal gradient, affecting the moisture movement were investigated. The soil specimens of size 4.5 inches long and 3.5 inches diameter were compacted in a cylindrical mould by compressing the soil with pistons situated at both ends of the cylinder. The soil specimens were then taken out from the mould and coated with Shellac varnish to prevent evaporation losses. The soil specimens were subjected to known thermal gradient in the apparatus shown in Figure 2.24. The apparatus consisted of two constant temperature baths between which 6 soil specimens were supported at the same time. Thermal contact between the soil specimen and the lower bath was obtained by Shellacing the base of the specimen into a metal cup which was immersed about 0.25 inches below the water surface in the constant temperature bath. In the case of the upper bath, thermal contact was obtained via a brass plate which covered the entire base of the bath and brass plates Shellaced to the top face of each soil specimen. The sides of

specimen were surrounded by cotton wool to prevent any loss or gain of heat. The temperature gradient in the soil specimen was determined by the means of thermo-junctions inserted near each end and at the middle of the soil specimen. The specimen took from 3 to 6 hours to reach steady temperature conditions, the shorter time being for the drier specimens and the longer time for the wetter ones. The specimen was cut into slices of 1 cm thick at the end of the test and the mean moisture content of each slice was determined. They used sand, sandy clay and clay as testing material. The maximum and minimum temperature used in the study was 42 °C and 14 °C with a wide range of temperature gradient from 0.8 to 2.4 °C/cm.

Maclean and Gwatkin (1946) found that moisture transfer takes place under a vapour pressure gradient and is associated with evaporation of moisture from the region of higher temperature and recondensation in the region of lower temperature. If the temperature gradient was maintained for a sufficient length of time, the movement of moisture ceased and an equilibrium moisture gradient was established. This time varied between 3 to 5 days.

Jennings et al. (1952) performed laboratory studies of the moisture migration in saturated and partially saturated soils under temperature gradients. Their objective was to investigate the effects of variations of mean moisture content, density or porosity of the system and general pressure in the system. They used Naboomspruit soil which had relatively low clay content. The soil was compacted in five layers in a Lucite tube with a piston type hammer compactor. The compacted soil samples of size 8 inches long and 2.25 inches diameter were placed between two baths as shown in Figure 2.25. At the centre of the cylindrical samples tapered nipple was fixed to allow the overall pressure in the system to be varied. At the end of the test samples were extruded and sliced to determine the moisture content. The tests were run for different time duration from 12 hours to 144 hours with temperature range of 20 °C to 40 °C.

Jennings et al. (1952) found that partial saturation in the soil is the necessary condition before flow of moisture under a temperature gradient can take place. They finally concluded that transfer of moisture in soils under temperature gradients is probably due,

primarily, to transfer of vapour under the vapour gradients caused by the differences in temperature.

Gurr et al. (1952) designed an apparatus to study the moisture movement due to a temperature gradient by measuring changes in the distribution of a small amount of soluble salt in the soil. The apparatus consisted of a Perspex cylinder, 10 cm long and 14 cm internal diameter, to hold the soil. On one end a heavy brass plate was bolted, on to which a flat circular heater was attached. On the other end another brass plate was bolted forming one face of a cylindrical water chamber through which cold water could be pumped. The joints were sealed by a rubber gasket and rubber cement. The temperature of these faces was measured by thermistors soldered to each face. Holes were drilled in the side of the Perspex cylinder to allow insertion of four thermistors at interval of 2 cm to measure the temperature gradient along the soil column. In each experiment the cold face was bolted to the cylinder first and then soil was compacted in several layers into the cylinder. The hot plate was attached after the whole cylinder had been filled with compacted soil. The test material used was loam soil and fine sand with a bulk density of 1.40 Mg/m^3 to 1.59 Mg/m^3. The cold end was kept at 10 °C and hot end at 25 °C resulted in a temperature gradient of 1.6 °C/cm. The tests were run for 5, 10 and 18 days. At the end of the test, the apparatus was dismantled and soil column was sampled in layers, each layer providing triplicate samples. The water contents of the triplicate samples were determined by oven-dry methods at 105 °C. The same samples were then transferred to 75 ml distilled water and shaken for 1 hour. The total soluble salts of the suspension was measured by the electric conductivity and chloride content was determined by the electrometric titration of Best (1929). The vapour flux was calculated by using the equation of Penman (1940).

Gurr et al. (1952) stated that the small amount of soluble salts acting as a tracer served to distinguish between liquid and vapour movement which is the basis of the present study. They observed the transfer of water toward the colder end and of salts towards the hotter end. They concluded that water evaporating from the hotter soil moves as a vapour into colder soil, where it condenses and returns as a liquid when a favourable gradient of pressure potential has been established.

Taylor and Cavazza (1954) used an air gap technique to study the moisture flow in the vapour phase. The experiments were carried out on Millville silt loam with initial moisture content of 49.9 % and 34.9 % in Lucite cylinders of size 10 cm long and 6.6 cm in diameter. The cylinders were set horizontally and vertically. Five thermistors were inserted at equal intervals to measure temperature. The soil was put in cylinders either continuously or five slices separated by four air gaps which were formed by wire screens and Lucite spacers. The test cylinders were placed between two water baths held at constant temperatures of 30 °C and 10 °C. At the end of each test, the soil sample was sliced and water content was determined by oven drying method. It was found that in the continuous soil the liquid water accumulated by condensation at the cold side. This produce a moisture tension gradient and liquid water flow back along this gradient. The equilibrium moisture distribution curve is reached when at every point the vapour flow and the liquid flow are equal in magnitude and opposite in direction. The return fluid flow is prevented where the soil column has air gaps, consequently moisture continued to move from warm to cold as vapour flow.

Rollins et al. (1954) designed an apparatus (Figure 2.26) for determining quantitatively the amount of water vapour in a steady state process. Water vapour moving through the soil system from the warm to the cold side was returned to the warm side through an external capillary tube, in which the rate of vapour movement was observed. The apparatus consisted of plexiglass soil tube of 10 cm long, 5 cm internal diameter and 0.25 inch wall thickness. At both ends the outside diameter was reduced by 0.25 inches for a distance of 0.25 inches from the ends of the tube. The porous disc was attached at the both ends of the tube. Another section of tubing about 1.25 inches long and 2.25 inches internal diameter was then cemented to the tube containing the porous disc. Two outlets were provided in each end cap; one for mercury manometer and another was attached to a tube consisting of a capillary tube to measure vapour pressure, which connected the two end caps, as shown in Figure (2.26). The temperature controlled tank consisted of two water baths at the ends. A refrigeration unit attached to the copper coil served as the temperature control in the cold unit. On the hot end side, a 750 watt heater operated by thermostat served to maintain the required temperature. The silty loam and fine sand was used with dry density varying from 1.23 Mg/m^3 to 1.33 Mg/m^3. The different end temperatures from 0 to 40 °C were applied. Durations of experiments varied from 60 to

100 hours. The vapour flow rate was calculated by the equation derived by Rollins et al. (1954) based on molecular diffusion. Finally it was found that the rate of vapour flow was a non linear function of the temperature gradient.

Hadley and Eisenstadt (1955) used radioactive tracers (cobaltous nitrate/chloride) to study thermally actuated moisture migration in granular media. The study was carried out in the specially built apparatus. Heating and refrigerating equipment were employed to produce the required thermal gradient along the tube connecting them. The connecting Lucite or Plexiglass tube was thermally insulated by a close fitting Dewar flask surrounded by a copper jacket and polystyrene foam, as shown in Figure 2.27. The liquid in the soil was water containing radioactive salt as a tracer of concentration of 0.1 g cobalt compound per litre. The presence of the radioactive salt can be detected by a Geiger tube and counter which can be moved along the sample length. If the moisture moves in liquid state the counts per minute would be registered by Geiger tube but if moisture moves in vapour phase there will be no change in radioactivity. It was found that there is critical moisture content about 4 % which determines the mode of moisture movement for both the hot end and the cold end. There is no circulation vapour away from the heat source and liquid toward it for soils above critical moisture content.

Preece (1975) investigated the thermal parameters of cable bedding sand in an apparatus (Figure 2.28) originally designed by Highgate and Mole (1966). The measurements were carried out on Washington sand with a porosity of 40 % and density of 1.6 Mg/m^3. Results cover the moisture range of 0 % to 19 % and the temperature range of 10 °C to 70 °C. The thermal conductivity, specific heat capacity and the ratio of temperature gradient, $(\nabla T)_a/(\nabla T)$, across air filled pores to that in the medium as a whole were determined.

Ewen and Thomas (1989) investigated combined heat and mass transfer in unsaturated Leighton Buzzard sand (trade name Garside grade 21). A sample of soil was formed inside a horizontal glass cylinder and heated by an embedded horizontal rod, running the entire length of the sample at its centre, as shown in Figure 2.29. The glass cylinder, of 219.6 mm internal diameter and 542 mm length, was sealed by two Perspex end pieces,

which were in turn, thermally insulated to restrict axial heat flow. The heating rod consisted of a 12.7 mm diameter, 16 gauge aluminium tube, sealed at both ends, containing a 10.16 Ω glass fibre coated electric resistance wire which ran the full internal length of the rod twice and completely surrounded by thermal transfer grease. The details of the apparatus are also presented elsewhere Thomas et al. (1996) and Thomas and Li (1997). The temperature distribution at the mid-section of the sample was recorded along a radial horizontal axis using eight 2.4 mm diameter 10 kΩ bead thermistors, fitted to a low thermal conductivity paxolin sensor holder (Figure 2.29). The initial temperature and volumetric liquid content for this experimental test were 20°C and 0.023 respectively. The sample was placed in an environmentally controlled laboratory at 20 ± 1.5 °C with a constant heating power input of 53.8 W/m for four weeks. Ewen and Tomas (1989) concluded that the best value for the effective specific area for vapour flow through soil is equal to the porosity and is not a function of air content.

Yong and Mohamed (1992) did infiltration experiments on unsaturated expansive soils. Yong and Mohamed (1996) and Yong et al (1997) used an apparatus (Figure 2.30), designed by Mohamed et al (1993), to determine temperature and moisture distributions in a clay based buffer material due to thermal gradients. The specimen prepared from the mixture of sodium bentonite and graded silica sand in equal proportion by dry weight with granitic ground water. The specimens of 110 mm height and 75 mm in diameter were statically compacted in equal lifts of 22 mm thickness inside the PVC sample tube with a known amount of soil to achieve a density of 1.67 Mg/m^3 (95% modified ASTM maximum dry density). In each test, water was allowed to infiltrate into a horizontal soil column under a constant hydrostatic head of 276 kPa. In one dimensional coupled heat and moisture flow tests performed on the clay-sand buffer material, three different heater skin temperatures were used i.e. 100, 80 and 60 °C (Yong et al. 1997). The PVC tube with compacted specimen was encased within a rigid support of concrete and steel around the perimeter and aluminium end plates. Each end of specimen is equipped with a controlled warming plate that provides a thermal source. A cooling system is installed inside the concrete and bottom end plates to control the temperature around the perimeter, and hence the temperature gradient. Yong et al. (1997) concluded that the diffusion

parameters can be expressed as a linear function of volumetric water content and temperature.

Kanno et al. (1996) designed an experiment device so that the coupled heat and water flow had a one-dimensional vertical movement. Figure 2.31 shows a schematic of the experimental apparatus. The compacted specimen was installed in a plexiglas cylindrical cell (inner diameter 51.1 mm, outer diameter 60 mm) and sandwiched between two water jackets of stainless steel. Each water jacket was connected to a thermostat, and temperatures of the upper and bottom ends of the specimen were kept at 30 ± 0.2 °C and 60 ± 0.2 °C, respectively. The annular gaps between the water jackets and the plexiglas cell were filled with a sealant to ensure impermeable boundaries for the water movement. The plexiglas cell was covered with heat insulating material to minimize the heat flux in the radial direction. Clay used in this study was a natural sodium bentonite Kunigel VI and specimens were compacted statically to dry density of 1.8 Mg/m^3 at a water content of 11.1 %. Two kinds of experiments were performed in their study. In the first kind, eleven thermocouples were installed in a specimen to obtain the time-dependent temperature distribution and water content distribution at different shut-down times. In the second kind, no thermocouple was used to obtain the water content distribution with different shut-down times. Finally, Kanno et al. (1996) found that the experimental results are qualitatively reproduced by the mechanistic model. The quantitative discrepancies between the experimental results of the water content distribution remain same in high water content region and the early time period. It was recommended that further studies on the vapour flow area factor and unsaturated hydraulic conductivity were required.

Villar et al. (1996) describe a laboratory experiment, where compacted clay (Boom clay) block is submitted to simultaneous heating and hydration. The clay sample was compacted into a stainless steel cell as presented in Figure 2.32. The cell had an inner diameter of 15 cm and a height of 14.6 cm. The bottom of the cell had two hydration ports leading to a porous plate. Hydration was induced in some of the samples by injecting water into the base of the sample at a pressure of 1 MPa. The heating element was inserted in the top of the cell along the axis of the cylinder. The element was 1.5 cm

long and 1 cm diameter for the first experimental setup, and 10 cm long and 2 cm diameter for the second experimental setup to provide an axial heat source. The heaters were powered to maintain a constant temperature of 100 °C (the maximum temperature of the canister walls in the Spanish concept). In addition, a thermal shower was applied maintaining a temperature of 30 °C on the outside of the cell. Thermocouples were used to record the temperatures within the cell throughout the experiment. At the end of the test the samples were analysed for final water content, dry density, and electric conductivity.

Villar et al. (1996) concluded that the temperature distribution seemed to depend mainly on the power and geometry of the heat source, and was relatively independent of the initial water content in the sample. The temperature distribution was also strongly influenced by the boundary conditions of the sample. However the hydration period was strongly influenced by the initial water content and the temperature distribution had little effect. The hydration was slower when the water content was higher. The final water content was influenced by the temperature profiles, and an influx of water produced an increase in water content and a decrease in density due to swelling.

Börgesson et al. (2001) reported thermal gradient tests in a twin apparatus called KID-BEN shown in Figure 2.33. The apparatus was made of bakelite and has insulating air layer. A compacted sodium bentonite (OT-9607, provided by Kunimine Ind. Japan) sample of dry density 1.65 Mg/m^3 and initial water content of 16 % with a diameter of 5 cm and height 10 cm was inserted in the bakelite cell. The end parts of the cell had temperature regulators consisting of a copper plate and a chamber, which was connected to a thermostat for circulating water with specified temperature. The temperature distribution was measured along the sample with 6 thermocouples installed in predrilled holes in the sample in one of the apparatus. The cold end temperature maintained at 25 °C while the hot end temperature varied from 35 °C to 70 °C. The numerical modelling was carried out and found to be reasonably matching with experimental results. They thought still much work required to improve these models of TH processed in bentonite.

Pintado et al. (2002) performed back analysis of thermo-hydraulic (TH) bentonite properties from laboratory tests conducted in the specially designed experimental apparatus (Figure 2.34) that allowed measuring the deformation during TH test. The material tested was a bentonite from the South-East of Spain (FEBEX bentonite). Bentonite was compacted at dry density of 1.63 Mg/m^3 and with a water content of 15.33 % (degree of saturation of 63 %). The objective of the test was to apply a controlled flux of heat on one of the ends of a cylindrical specimen (38 mm diameter, 76 mm height) and to maintain the other end at constant temperature. A latex membrane that allowed the deformation and kept constant the overall water content and a layer (5.5 cm thick) of heat insulating materials (deformable foam, expanded polystyrene and glass fibre) surround the specimen. All parts were located into a Perspex tube that gave stiffness to the whole equipment. In order to assure the knowledge of heat flux that crosses the sample, two specimens symmetrically placed with respect to the heater were used in the tests. The heater was a copper cylinder (38 mm diameter, 50 mm height) with five small electrical resistances inside. The resistances were connected to an adjustable feed source of direct current that allowed controlling the input power from 0 to 5 W. In the tests, a constant power of 2.17 W was used, reaching steady temperatures in the range of 70 °C – 80 °C in the hotter end of the specimen. In the cold end, a constant temperature of 30 °C was maintained by flowing water in a stainless steel head in contact with the soil. A temperature regulation system kept the temperature of the contact between the head and the soil, constant with variations smaller than 0.5 °C. In order to improve the sealing of the soil and the durability of the latex membrane, in the contact with the heater, the membrane was surrounded by liquid silicone that solidified in a few hours. In the whole specimen, the water loss during the test due to diffusion trough the membrane was about 0.1 g/day. In order to assure a good contact between the heads and the sample, a light stress (about 0.05 MPa) was applied on the upper zone of the equipment. During the tests, temperatures in both ends and in three internal points of the specimen, located at regular intervals, were monitored by means of a data acquisition system controlled by a personal computer. The system was also used to impose a constant temperature at the cold end of the sample. Temperature measurements were concentrated in one of the two specimens of each test, whereas in the other specimen the temperature was only measured at the central point, just to check the symmetry of heat flux. At the end of the tests, diameter change was measured in some points of the specimen with an accuracy of 0.01

mm. Finally, the soil samples were cut in six small cylinders and the water content of each one was determined. Finally, numerical back analysis was done to check the reliability of the model. The analysis indicated that the reliability of the identification is higher for the thermal parameters than for the hydraulic parameters. They concluded it is difficult to determine thermo-hydraulic parameters because of the highly non linear coupling of the processes involved.

Cuevas et al. (2002) performed thermo-hydraulic tests in hermetic cells in which a compacted block of bentonite was hydrated on the top while a thermal gradient was applied from the bottom. The body of the cell was made out of Teflon, although an external steel cylinder prevented its deformation swelling (Figure 2.35). A plane heater on stainless steel constituted the bottom of the cell and on the top of the cell, a chamber allowed the circulation of water at a controlled temperature, lower than that of the heater. A hydration channel crossed the upper chamber and allowed the hydration of the sample through a stainless steel sinter. The water was injected under a pressure of 1.1 MPa. The clay, with its water content at equilibrium with the laboratory conditions, was uniaxially compacted outside the cell to a dry density of 1.65 Mg/m^3. The specimen obtained was placed in the cell, where the dry density of the bentonite was of 1.59 Mg/m^3 due to the looseness between the specimen and the wall of the cell. The specimen was only 2.5 cm long and 5.0 cm diameter, which implies that saturation reached in a few days. This allowed the performance of a large number of tests of different duration and conditions. Two different thermal gradients were examined, in order to ascertain the effect of temperature in the observed processes: a high temperature gradient, between 100 and 60 °C (16 °C/cm) to simulate regions closer to the container, and a low-temperature gradient, between 60 and 35 °C (10 °C/cm), to simulate zones near the host rock.

Villar et al. (2005) carried out infiltration tests with isothermal and thermal gradient conditions on FEBEX bentonite. The tests were performed in a cell (size internal diameter 7 cm, inner length 40 cm and 1.5 cm thickness) with relative humidity probes to measure transient temperature and relative humidity at various locations along the sample height (Figure 2.36). The cell was made up of Teflon to minimise the heat losses and straightened by steel shells of 4 mm thickness. The O-rings were used to ensure water

tightness at the contacts between different pieces of the cell. The stainless steel heater was provided at the bottom of the cell with thermocouple and temperature control. The top part had hydration source with cooling system. The soil samples were statically compacted in blocks and inserted into the cell. The granitic water was injected from the top part at a pressure of 1.2 MPa. The highest temperature used at the bottom part of the sample was 100 °C and the top part was maintained at 20 - 30 °C. The water volume intake was monitored and relative humidity and temperature were measured by VAISALA HMP237 probes. It has been found that the permeability to water vapour of dry bentonite was very high, since a quick redistribution of water took place when the thermal gradient was applied compared to isothermal test.

Gatabin and Billaud (2005) conducted thermal gradient and thermo-hydraulic gradient test on MX-80 bentonite with initial dry density of 1.79 Mg/m^3 and degree of saturation of 75.5 % and 89.7 %. For this purpose, the experimental cell (Figure 2.37) was built which was capable of measuring transient pore water pressure, swelling pressure, temperature and relative humidity. The cell body is made up of polytetrafluoroethylene (PTFE) sleeve which is strengthened by steel tube outside. A heater was installed at the bottom of the cell and a hydration source at the top of it. Thirteen thermocouples and seven relative humidity sensors were installed in the cell. A force sensor was provided at top to measure the axial stress and eight total pressure sensors were used to measure radial stresses. The soil specimen was 202.7 mm in diameter and 203 mm height. The lower temperature at the top was maintained 20 °C and the heater temperature was increased from ambient temperature to 150 °C in steps of 10 °C/day up to 100 °C and then 5 °C/day. The experiments were run for 2706 hours. A leak was detected in one of the tests through one of the relative humidity sensors. Apart from it, the experiments were carried out successfully. It was found that de-saturated zone appear close to the heater, highlighting the water transfer from hot zone to cold one. Temperature and thermal gradient induced this water transfer process.

2.8 Conclusions

The theoretical and experimental developments in the field of heat and mass movement in unsaturated soils is presented. The concept and definition of unsaturated soils has been discussed. The swelling clay, its structure and mineralogy with ion exchange phenomenon is detailed.

The development of the theory of liquid moisture and vapour moisture movement from the beginning of 19th century is presented. The existing theories are based on rigid matrix and do not take into account the swelling and shrinking nature of expansive clays. Especially the vapour moisture flow has not been studied in past in same detail as liquid moisture flow and the relevant theories are not well developed. The microscopic pore temperature gradient factor, $(\nabla T)_a/(\nabla T)$, is still based upon sand. So the existing vapour flux theories do not capture the actual vapour in swelling soils. The heat transfer theories are more or less well established and predict the evolution of temperature in swelling clays quite accurately.

The flow parameters and their experimental determination are well presented. The flow parameters are the essential parameters to predict the heat and mass flow correctly. The accuracy of the theoretical models depends upon the accurate value of heat and moisture flow parameters.

The experimental development in the area of heat and moisture movement studies starting from 19th century till date is discussed. Earlier experiments (till 1950) were conducted on mostly loam and sandy soil i.e. non swelling soils. The aim of earlier experiments was to find the moisture movement in highway subgrade and so the temperatures applied to the soil samples were quite small in the range of 40 °C. Around 1975, higher temperatures were used in TH experiments because of the study of high temperature generated by high voltage buried cable. The most TH experimental setups have high heat losses and the soil samples were compacted outside the test cell which resulted in non homogeneity and a decrease in dry density of the soil specimen.

Overall, it is clear that vapour flow theories need to be re-developed or modified to be applied to swelling clays. However, in spite of the significant experimental work that has been done to date there is still a clear shortage of reliable experimental data.

2.9 References

Agus, S.S., Leong, E.C. and Schanz, T. (2003). Assessment of statistical models for indirect determination of permeability functions from soil-water characteristic curves. Geotechnique, 53(2), 279-282.

Alonso, E.E., Battle, F., Gens, A. and Lloret, A. (1988). Consolidation analysis of partially saturated soils - Application to earthdam construction. Numerical Methods in Geomechanics (Innsbruck 1988), 1303-1308.

Al-Khafaf, S. and Hanks, R.J. (1974). Evaluation of filter paper method for estimating soil watre potential. Soil Science, Vol. 117, No. 4, 194-199.

Arbhabhirama, A. and Kridakorn, C. (1968). Steady downward flow to a water table. Water Resources Res., Vol. 4.

ASTM C 177-04 (2004). Standard test method for steady-state heat flux measurements and thermal transmission properties by means of the guarded-hot-plate apparatus. Annual book of ASTM Standards.

ASTM D 5298-94 (1994). Standard test method for measurement of soil potential (suction) using filter paper. Annual book of ASTM Standards.

Averjanov, S.F. (1950). About permeability of subsurface soils in case of incomplete saturation. Eng. Collect., Vol. 7.

Best R.J. (1929). A rapid electrometric method for determining the chloride content of soils. Journal Agri. Sci., 19, 533-540.

Bocking, K.A. and Fredlund, D.G. (1989). Limitations of the axis translation technique. Proc. 4th Int Conf. on Expansive Soils, Denever, Colarado, Vol. 1, 117-135.

Börgesson, L., Chijimatsub, M., Fujitab, T., Nguyenc, T.S., Rutqvistd, J. and Jinge, L. (2001). Thermo-hydro-mechanical characterisation of a bentonite-based buffer material by laboratory tests and numerical back analyses. International Journal of Rock Mechanics & Mining Sciences, 38, 95-104

Bouyoucos, G.J. (1915). Effect of temperature on movement of water vapour and capillary moisture in soil. U.S. Department of Agriculture, Journal of Agricultural Research Vol. V, No. 4, 141-172.

Brooks, R.H. and Corey, A.T. (1964). Hydraulic properties of porous media. Colardo State Univ. Hydrol. Paper, No. 3, 27.

Buckingham, E. (1904). Studies of the movement of soil moisture. U.S.Dept.Agr. Bur. of Soils, Bulletin No. 38.

Buckingham, E. (1907). Studies of the movement of soil moisture. U.S.Dept.Agr. Bur. of Soils, Bulletin No. 38.

Burdine, N.T. (1952). Relative permeability calculations from pore size distribution data. Trans. AIME.

Carman, P.C. (1956). Flow of gases through porous media. Butterworths Scientific Publications, London.

Chandler, R.J. and Gutierrez, C.I. (1986). The filter paper method of suction measurement. Geotechnique, Vol. 36, No. 2, 265-268.

Childs, E.C. and Collis-George, N. (1950). The permeability of porous materials. Proc. Royal Soc., Vol. 201A, 392-405.

Cleall, P.J. (1998). An investigation of the thermo/hydraulic/mechanical behaviour of unsaturated soils, including expansive clays. Ph.D Thesis, Cardiff University, Wales.

Collin, F., Li, X.L., Radu, J.P. and Charlier, R. (2002). Thermo-hydro-mechanical coupling in clay barriers. Engineering Geology, 64, 179-193.

Conciani, W., Herrmann, P.S. and Soares, M.M. (1995). The time domain reflectometry to study matric suction. Proc. 1st Int. Conf. on Unsaturated Soils, Paris, France, 1481-1486.

Cuevas, J., Villar, M.V., Martyn, M., Cobena, J.C. and Leguey, S. (2002). Thermo-hydraulic gradients on bentonite: distribution of soluble salts, microstructure and modification of the hydraulic and mechanical behaviour. Applied Clay Science, 22, 25–38.

Daniel, D.E. (1983). Permeability test for unsaturated soil. Geotechnical Testing Journal, 6, 81-86.

Darcy, H. (1856). Les fontaines publiques de la ville de Dijon. V. Dalmont, Paris, 590-594.

Deutsch, W.J. (1997). Groundwater geochemistry, fundamentals and applications to contamination. Lewis Publishers, Boca Raton, NY.

de Vries, D.A. (1950). Some remarks on heat transfer by vapour movement in soils. Trans. 4th Int. Congress Soil Sci., Vol. II, 1950.

de Vries, D.A. (1958). Simultaneous transfer of heat and moisture in porous media. Trans. Amer. Geophys. Union, Vol. 39, No. 5, 909-916.

de Vries, D.A. (1963). Thermal properties of soils. In Physics of Plant Environment, Amsterdam, 210-235.

de Vries, D.A. (1966). Physics of plant environment. 2nd Edition, North Holland Publishing Company, 215-235.

de Vries, D.A. (1987). The theory of heat and moisture transfer in porous media revisited. Int. J. Heat Mass Tranfer, Vol. 30, No. 7, 1343-1350.

Edlefsen, N.E. and Andersen, A.B.C. (1943). Thermodynamics of soil moisture. Hiigardia, 15, No. 2, 31-298.

Ewen, J. (1987). Combined heat and mass transfer in unsaturated sand surrounding a heated cylinder. PhD thesis, School of Enginering, University of Wales, Cardiff.

Ewen, J. and Thomas, H.R. (1987). The thermal probe – a new method and its use on an unsaturated sand. Geotechnique, 37, No. 1, 91-105.

Ewen, J. and Thomas, H.R. (1989). Heating unsaturated medium sand. Geotechnique, 39, 455-470.

Ewen, J. and Thomas, H.R. (1992). Thermal probe – measurement of the thermal conductivity and drying rate of soil in the field. Geotech. Testing Journal, ASTM, 15, 256-263.

Fawcett, R.G. and Collis-George, N. (1967). A filter paper method for determining the moisture characteristics of soil. Australian Journal of Experimental Agriculture and Animal Husbandry, Vol. 7, No. 25, 162-167.

Fick, A. (1885). Ueber diffusion. Ann. Der Phys. (Leipzig), Vol. 94, 59-86.

Fleureau, J.M. and Taibi, S. (1995). Water-air permeabilities of unsaturated soils. Proc. 1st Int. Conf. Unsaturated Soils, Paris, 2, 479-484.

Folly J.P.W. (2001). Thermo-hydro-mechanical behaviour of unsaturated soil: An experimental study. PhD thesis, School of Engineering, Cardiff University.

Fourie, A.B. and Papagerorgiou, G. (1995). A technique for the rapid determination of the moisture retention relationship and hydraulic conductivity of unsaturated soils. Proc. 1st Int. Conf. Unsaturated Soils, Paris, 2, 485-490.

Fourier, J. (1822). Théorie analytique de la chaleur. Firmin Didot, Paris.

Fredlund, D.G. (1991). Seepage in saturated soils. Panel discussion: ground water and seepage problem. Proceedings 10th Int. Conf. Soil Mechanics and Foundation Engineering, Stockholm, 4, 629-642.

Fredlund, D.G. and Rahardjo, H. (1993). Soil mechanics for unsaturated soils. John Wiley & Sons, Inc., New York.

Fredlund, D. G. and Xing, A. (1994). Equations for the soil-water characteristic curve. Can. Geotech. J., 31, 533–546.

Gardener, R. (1937). A method of measuring the capillary tension of soil moisture over a wide moisture range. Soil Science, Vol. 43, No. 4, 277-283.

Gardner, W.R. (1956). Calculation of capillary conductivity from pressure plate outflow data. Soil Sci. Soc. Amer. Journal, 20, 317-320.

Gardner, W.R. (1958). Some steady state solutions of the unsaturated moisture flow equation with application to evaporation from a water-table. Soil Science, Vol. 85, No. 4.

Gatabin, C. and Billaud, P. (2005). Bentonite THM mock up experiments. Sensors data report. CEA, Report NT-DPC/SCCME 05-300-A, Cedex.

Gee, G., Campbell, M., Campbell G., and Campbell, J. (1992). Rapid measurement of low soil potentials using a water activity meter. Soil Science Society of American Journal, Vol. 56, 1068–1070.

Geraminegrad, M., and Saxena, S. (1986). Finite elements in plasticity: Theory and practice. Pineridge Press Ltd., Swansea.

Green, R.E. and Corey, J.C. (1971). Calculation of hydraulic conductivity: A further evaluation of some predictive methods. Proc. Soil Sci. Soc. Amer., Vol. 35, 3-8.

Grim, R.E. (1962). Applied clay mineralogy. McGraw-Hill, New York.

Gurr, C.G., Marshall, T.J. and Hutton, J.T. (1952). Movement of water in soil due to a temperature gradient. Soil Sci., Vol. 74, No. 5, 335-345.

Hadley, W.A. and Eisenstadt, R. (1955). Thermally actuated moisture migration in granular media. Trans. American Geophysical Union, Vol. 36, No. 4, 615-623.

Hamblin, A.P. (1981). Filter paper method for routine measurement of field water potential. Journal of Hydrology, Vol. 53, 355-360.

Hamilton, J.M., Daniel, D.E. and Olson, R.E. (1981). Measurement of hydraulic conductivity of partially saturated soils. Permeability and groundwater contaminant transport, ASTM, Special Tech. Publ. 746, 182-196.

Hilf, J.W. (1956). An investigation of pore-water pressure in compacted cohesive soils. Ph D Dissertation, Technical Memorandum No. 654, United States Department of the Interior Bureau of Reclamation, Design and Construction Division, Denever.

Highgate, D. and Mole, G. (1966). The electrical and research association, Report No. 4B/59.

Hillel, D. (1980). Fundamentals of soil physics, Academic Press, Inc.

Houston, S.L., Houston, W.N. and Wagner, A.M. (1994). Laboratory filter paper suction measurements. Geotechnical Testing Journal, Vol. 17, No. 2, 185-194.

Jakob, M. (1949). Heat transfer: Vol.1. Wiley.

Jennings, J.E., Heymann, P.R.B. and Wolpert, L. (1952). Some laboratory studies of the migration of moisture in soils under temperature gradients. South Africa Nat. Build. Res. Inst. Bul., 9, 29-46.

Johansen, O. (1975). Thermal conductivity of soils. Ph.D. thesis, University of Trondheim, Norway.

Juca, J.F.T. and Frydman, S. (1995). Experimental techniques. Proc. 1st Int. Conf. Unsaturated Soils, Paris, 3, 1257-1292.

Kanno, T., Kato, K. and Yamagata, J. (1996). Moisture movement under a temperature gradient in highly compacted bentonite. Eng. Geol., 41, 287-300.

King, S.D. (1991). A potential based model of coupled heat and moisture transfer in unsaturated soil. Ph.D. Thesis, School of Engineering, University of Wales, Cardiff.

Klute, A. (1965). The determination of the hydraulic conductivity and the diffusivity of unsaturated soils. Methods of Soil Analysis, Part 1, Amer. Soc. of Agronomy, Madisson, WI, 253-261.

Klute, A. (1972). The determination of the hydraulic conductivity and the diffusivity of unsaturated soils. Soil Science, Vol. 113, 264-276.

Krahn, J. and Fredlund, D.G. (1972). On total, matric and osmotic suction. Soil Science, Vol. 114, No. 5, 339-348.

Krischer, D. and Rohnalter, H. (1940). Warmeleitung und dampfdiffusion in feutchen gutern. Verein Duet, Ing-Forschungsheft, 402.

Kunze, R.J., Uehara, G. and Graham, K. (1968). Factors important in the calculation of hydraulic conductivity. Proc. Soil Sci. Soc. Amer., Vol. 32, 760-765.

Leong, E.C. and Rahardjo, H. (1997). Review of soil–water characteristic curve equations. Journal of Geotechnical and Geoenvironmental Engineering, ASCE, Vol. 123, No. 12, 1106–1117.

Leong, E.C., He, L. and Rahardjo, H. (2002). Factors affecting the filter paper method for total and matric suction measurements. Journal Geotechnical Testing, Vol. 25, No. 3, 322-333.

Levy, R., Tanji, J.K. and Whittig, L.D. (1983). Effect of precipitation of alkaline earth carbonates and magnesium hydroxide of Na-Ca-Mg exchange in Wyoming bentonite. Soil Science Scociety American Journal, Vol. 47, 906-912.

Lloret, A. and Alonso, E.E. (1980). Consolidation of unsaturated soils including swelling and collapse behaviour. Geotechnique, 30, No. 4, 449-477.

Lu, N. and Likos, W.J. (2004). Unsaturated soil mechanics. John Wiley & Sons, Inc., New York.

Luikov, A.V. (1966). Heat and mass transfer in capillary porous bodies. Pergamon Press, Oxford.

Maclean, D.J. and Gwatkin P.M. (1946). Moisture movement occurring in soil due to the existence of a temperature gradient. Department of Scientific and Industrial Research England, Road Research laboratory Note RN/761.

Manheim, F.T. (1966). A hydraulic squeezer for obtainng interstitial water from consolidated and unconsolidated sediment. U.S. Geological Survey Prof. Paper 550-C, 256-262.

Marshall, T.J. (1958). A relation between permeability and size distribution of pores. Journal Soil Sci., Vol. 9, 1-8.

Mata, C., Romero, E. and Ledesma, A. (2002). Hydro-chemical effects on water retention in bentonite-sand mixture. Proc. 3rd Int. Conf. on Unsaturated Soils, Vol. 1, Recife Brazil, 283-288.

Mayhew, Y.R. and Rogers, G.F.C., (1976). Thermodynamic and transport properties of fluids. 2nd Edition, Blackwell, Oxford.

McKeen, R.G. (1980) Field studies of airport pavements on expansive clay. Proc. 4th Int. Conf. on Expansive Soils, Denver, Colarado. Vol. 1, 242-262.

McKeen, R.G. (1992). A model for predicting expansive soil behaviour. Proc. 7th Int. Conf. on Expansive soils. Dallas, 1-6.

McQueen, I.S. and Miller, R.F. (1968). Calibration and evaluation of a wide range gravimetric method for measuring moisture stress. Soil Science, Vol. 106, No. 3, 225-232.

Miller, R.F. and McQueen, I.S. (1978). Moisture relations in rangelands, Western United States. Proc. 1st Int. Rangeland Congress, 318-322.

Millington, R.J. and Quirk, J.P. (1959). Permeability of porous media. Nature, Vol. 183, 387-388.

Milly, P.C.D. (1982). Moisture and heat transport in hysteretic, inhomogeneous porous media: a matric head-based formulation and a numerical model. Water Resour. Res., 18(3), 489-498.

Mitchell, J.K. (1993). Fundamental of soil behaviour. John Wiley & Sons, Inc., New York.

Mohammed, A.M.O., Yong, R.N. and Kjartanson, B. (1993). Temperature and moisture distributions in a clay based buffer material due to thermal gradients. Mat. Res. Soc. Symp. Proc., 294, 417-424.

Morrison, R.D. (1983). Ground water monitoring technology: Procedure, equipment and applications. Publisher Timco Mfg., Inc., Prairie Du Sac, WI.

Mou, C.H. and Chu, T.Y. (1981). Soil suction approach for swelling potential evaluation. Transportation Research Rec. 790, Washington, DC, 54-60.

Mualem, Y. (1976). A new model for predicting the hydraulic conductivity of unsaturated porous media. Water Resour. Res., 12, 513–522.

Mualem, Y. (1986). Hydraulic conductivity of unsaturated soils: Prediction and formulas. Methods of Soil Analysis, Part 1. Physical and Mineralogical Methods. 2nd ed., Agronomy Monograph No.9, American Society of Agronomy, Madison, WI, 799-823.

Nelson, J. D. and Miller, D.J. (1992). Expansive soils - problems and practice in foundation and pavement engineering. John Wiley & Sons, Inc., New York.

Nielson, D.R., Van Genuchten, M., and Biggar, J.W., (1986). Water flow and transport processes in the unsaturated zone. Water Resources Research, 22, No. 9, 89-108.

Olivella, S., Carrera, J., Gens, A. and Alonso, E.E. (1994). Non-isothermal multiphase flow of brine and gas through saline media. Transport in Porous Media, 15, 271-293.

Olson, R.E. and Daniel, D.E. (1981). Measurement of the hydraulic conductivity of fine grained soils. Permeability and groundwater contaminant transport, ASTM, Special Tech. Publ. 746, 18-46.

Olson, R.E. and Langfelder, L.J. (1965). Pore water pressures in unsaturated soils. Journal of Soil Mechanics and Foundation Division, Proc. ASCE, Vol. 91, 127-150.

Partington, J.R. (1949). Advanced treatise on physical chemistry. Vol. 1, Longmans, Green and Co., London, 943.

Penman, H.L. (1940). Gas and vapour movements in the soil. Int. Jour. Agr. Sci.30, 437-462.

Phene, C.J., Hoffman, G.J. and Rawlins S.L. (1971). Measuring soil matric potential in situ by sensing heat dissipation with a porous body: theory and sensor construction. Proc. Soil Sci. Soc. Amer., Vol. 35, 27-32.

Philip, J.R. and De Vries, D.A. (1957). Moisture movement in porous materials under temperature gradients. Trans. Amer. Geophys. Union, 38, 222-232.

Pintado, X., Ledesma, A. and Lloret, A. (2002). Backanalysis of thermohydraulic bentonite properties from laboratory tests. Engineering Geology, 64, 91-115.

Pollock, D.W. (1986). Simulation of fluid flow and energy transport processes associated with high-level radio active waste disposal in unsaturated alluvium. Water Resources Research, 22, No. 5, 765-775.

Preece, R.J. (1975). The measurement and calculation of physical properties of cable bedding sands. Part 2: specific thermal capacity, thermal conductivity and temperature ratio across air filled pores. C.E.G.B. Laboratory Note No., RD/L/N 231/74.

Rees, S.W. (1990). Seasonal ground movement effects on buried moisture transfer in unsaturated soil. Ph.D. Thesis, School of Engineering, University of Wales, Cardiff.

Richards, B.G. (1965). Thermistor Hygrometer for determining the free energy of moisture in unsaturated soils. Nature, Vol. 208, Issue 5010, 608-609.

Richards, L.A. (1931). Capillary conduction of liquids through porous medium. J. Physics, Vol. 37, 719-742.

Richards, S.J., and Weeks, L.V. (1953). Capillary conductivity from pressure plate outflow data with non-negligible membrane impedance. Netherlands Journal Agri. Sci., 7, 209-215.

Rollins, R.L., Spangler, M.G. and Kirkham, D. (1954). Movement of soil moisture under a thermal gradient. Proc. Highway Research Borad, Vol. 33, 492-508.

Rytwo, G., Nir, S. and Margulies, I. (1995). Interaction of monovalent organic cations with montmorillonite, adsorption and model calculations. Soil Science Scociety American Journal, Vol. 59, 554-564.

Sansom, M.R. (1995). A fully coupled numerical analysis of mass, air and heat transfer in unsaturated soil. Ph.D. Thesis, School of Engineering, University of Wales, Cardiff.

Schofield, R.K. (1935). The pF of the water in soil. Transactions of 3rd Int. Congress of Soil Science, Vol. 2, Plenary Session Papers, Oxford, 37–48.

Seetharam, S.C. (2003). An investigation of the thermo/hydro/chemical/mechanical behaviour of unsaturated soils. PhD thesis, Cardiff School of Engineering, UK.

Sharma, R.S. (1998). Mechanical behaviour of unsaturated highly expansive clays. PhD thesis, Keble College, University of Oxford.

Sibley, J.W. and Williams, D.J. (1990). A new filter material for measuring soil suction. Geotechnical Testing Journal, ASTM, 13, 375-380.

Sivakumar, V. (1993). A critical state framework for unsaturated soil. PhD Thesis, University of Sheffield.

Smith, W.O. (1943). Thermal transfers of moisture in soils. Trans. Amer. Geophysical Union, 2, 511-523.

Smith, W.O. and Byers, H.G. (1938). The thermal conductivity of dry soils of certain of the great soil groups. Proc. Soil. Sci. Soc. Amer., Vol. 3, 13-19.

Spanner, D.C. (1951). The Peltier effect and its use in the measurement of suction pressure. Journal exp. Bot. 2, 145-168.

Sposito, G., Jouany, C., Holtzclaw, K.M. and LeVesque, C.S. (1983). Calcium-magnesium exchange on Wyoming bentonite in the presence of adsorbed sodium. Soil Science Scociety American Journal, Vol. 47, 1081-1085.

Swarbrick, G.E. (1995). Measurement of soil suction using the filter paper method. Proc. 1st Int. Conf. on Unsaturated Soils, Paris, France, 653-658.

Taylor, S.A. and Cavazza, L. (1954). The movement of soil moisture in response to temperature gradients. Proc. Soil Science Soc. Amer., Vol. 18, No. 4, 351-358.

Thomas, H.R. (1980). Finite element analysis of shrinkage stresses in building materials. Ph.D. Thesis, University College, Swansea, U.K.

Thomas, H.R. and King, S.D. (1991). Coupled temperature/capillary potential variations in unsaturated soil. Journal of Engineering Mechanics, American Society of Civil Engineers, 117, No. 11, 2475-2491.

Thomas, H.R. and Sansom, M.R. (1995). A fully coupled analysis of heat, moisture and air transfer in unsaturated soil. Journal of Engineering Mechanics, American Society of Civil Engineering, 12, No.3, 392-405.

Thomas, H.R., He, Y., Sansom, M.R. and Li, C.L.W. (1996). On the development of a model of the thermo-mechanical-hydraulic behaviour of unsaturated soils. Engineering Geology, 41, 197-218.

Thomas, H.R. and Li, C.L.W. (1997). An assessment of a model of heat and moisture transfer in unsaturated soil. Geotechnique, 47(1), 113-131.

Thyagaraj, T. (2006). Influence of osmotic suction on the swell and compression behaviour of compacted expansive clays. PhD thesis, Indian Institute of Science, Bangalore.

Totoev, Y.Z. and Kleeman, P.W. (1998). An infilatration model to predict suction changes in the soil profile. Water Resources Research, 34, 1617-1622.

Uno, T., Sato, T. and Sugii, T. (1995). Laboratory permeability measurement of partially saturated soil. Proc. 1st Int. Conf. Unsaturated Soils, Paris, 2, 573-578.

van Bavel, C.H.M. (1952). Gaseous diffusion and porosity in porous media. Soil Sci., 73, 91-104.

van Genuchten, M. T. (1980). A closed-form equation for predicting the hydraulic conductivity of unsaturated soils. Soil Sci. Soc. Am. J., 44, 892–898.

van Olphen, H. (1963). Clay colloid chemistry. Interscience Publishers, John Wiley & Sons, Inc., New York.

Villar, M.V., Cuevas, J. and Martin, P.L. (1996). Effects of heat/water flow interaction on compacted bentonite: Preliminary results. Engineering Geology, 41, 257-267.

Villar, M.V., Martin, P.L. and Barcala, J.M. (2005). Infiltration tests at isothermal conditions and under thermal gradient. CIEMAT Technical report CIEMAT/DMA/M2140/1/05 Madrid.

Wang, J. (2000). Transient and dynamic thermo/hydraulic/mechanical behaviour of partially saturated soil. Ph.D. Thesis, Cardiff University, Wales.

Wiederhold, P.R. (1997). Water vapour measurement: Methods and Instrumentation. Marcel Dekker, Inc., New York.

Winterkorn, H.F. and Eyring, H. (1946). Theoretical aspects of water accumulation in cohesive subgrade soils. Proc. Highway Research Board, Vol. 25, 422-434.

Woodburn, J.A. and Lucas, B. (1995). New approaches to the laboratory and field measurement of soil suction. Proc. 1st Int. Conf. on Unsaturated Soils, Paris, France, 667-672.

Wroth, C.P. and Houlsby, G.T. (1985). Soil mechanics: Property characterisation and analysis procedure. Proc. 11th ICSMFE, San Francisco, Vol. 1, 1-55.

Yong, R.N. and Mohammed, A.M.O (1992). A study of particle interaction energies in wetting of unsaturated expansive clays. Can. Geotech. Journal, 29, 1060-1070.

Yong, R.N. and Mohammed, A.M.O (1996). Evaluation of coupled heat and moisture flow parameters in a bentonite-sand buffer material. Engineering Geology, 41, 269-286.

Yong, R.N., Mohammed, A.M.O., Shooshapasha, I. and Onofrei C. (1997). Hydrothermal performance of unsaturated bentonite-sand buffer material. Engineering Geology, 47, 351-365.

Yong, R.N. and Warkentin B.P. (1966). Introduction to soil behaviour. The Macmillan Company, New York.

Table 2.1 Some typical thermal properties of soils (de Vries, 1963)

Substance	Density (kg/m^3)	Thermal conductivity (W/mK)	Specific heat (W/m^{3}K)
Quartz	2660	8.79	2010
Clay minerals	2650	2.93	2010
Organic matter	1300	0.25	2512
Water	1000	0.57	4186
Ice	920	2.18	1884
Air	1.25	0.025	1.256

NB. These values have been converted to SI units from the original reference

Table 2.2 Some values of latent heat of vaporisation (Mayhew and Rogers, 1976)

Pressure (bar)	Temperature (°C)	Latent heat of vaporisation (J/kg) x 10^6
0.00612	0.01	2.375
0.010	7.0	2.385
0.023	20.0	2.401
0.043	30.0	2.416
0.075	40.0	2.430
0.130	50.0	2.444
0.200	60.0	2.456
0.310	70.0	2.469
0.480	80.0	2.482
0.700	90.0	2.494
1.013	100.0	2.507
220	373.7	2.097
221.2	374.15	2.014
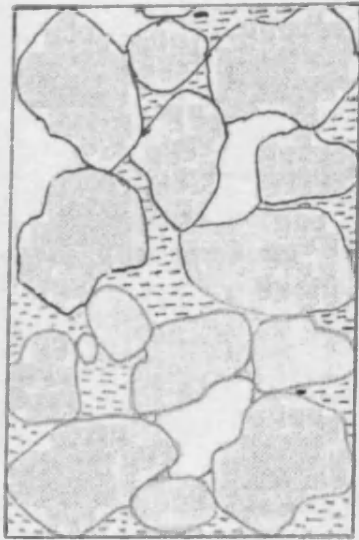
(a)
Continuous water,
discontinuous air
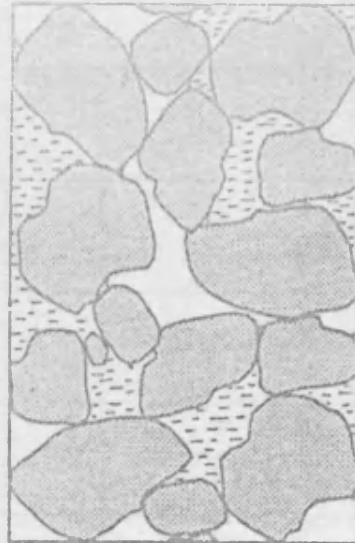
(b)
Continuous water,
continuous air

(c)
Discontinuous water,
continuous air

Key
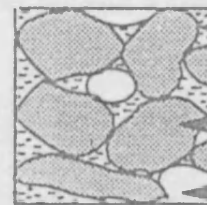
Water Phase

Solid Phase

Air Phase

Figure 2.1 Structure of unsaturated soils (Wroth and Houlsby, 1985)
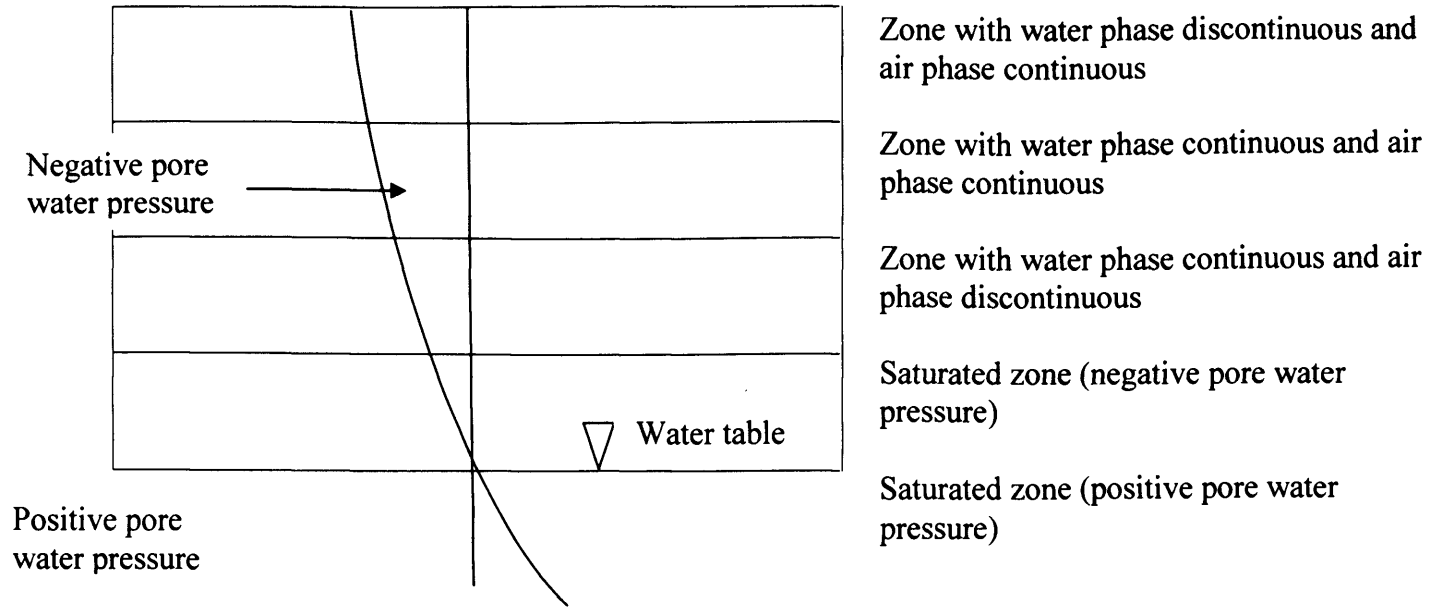
Figure 2.2 Continuous and discontinuous air and water phases in a soil stratum (Sivakumar, 1999)
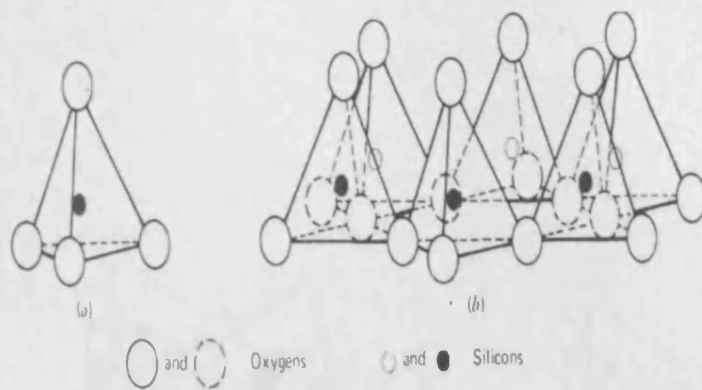
Figure 2.3 Tetrahedral unit and sheet (Mitchell, 1993)
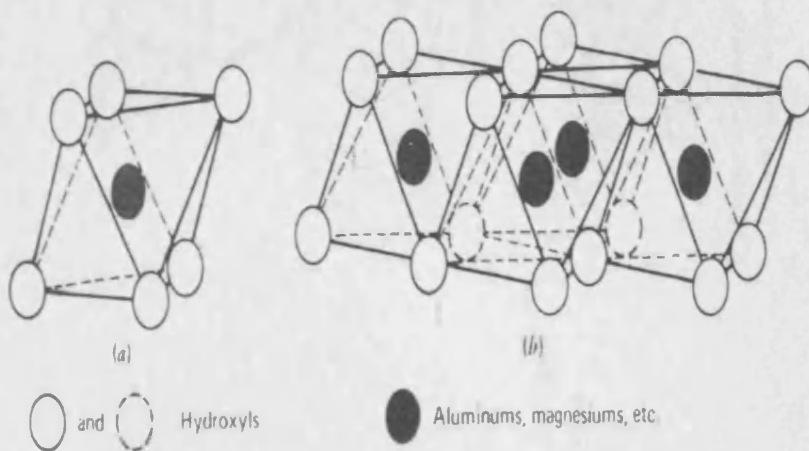
Figure 2.4 Octahedral unit and sheet (Mitchell, 1993)
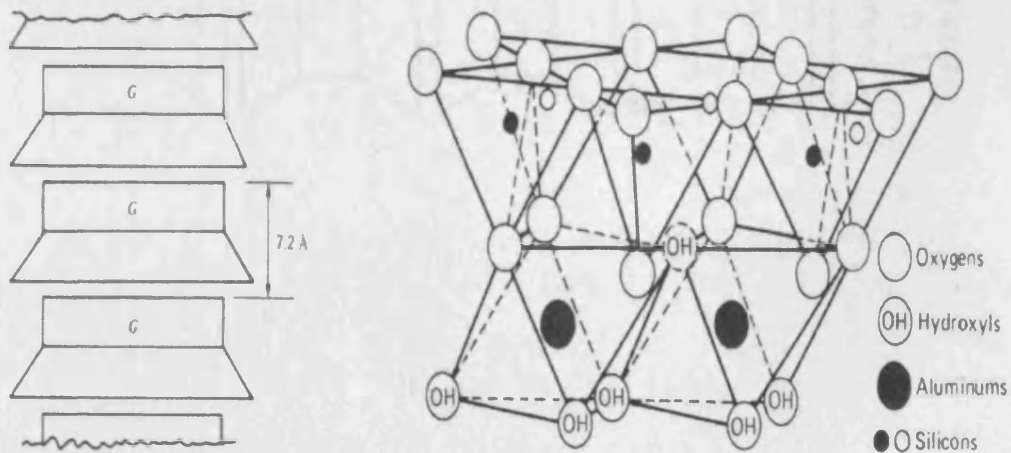
Figure 2.5 Schematic diagram of kaolinite structure (Mitchell, 1993)
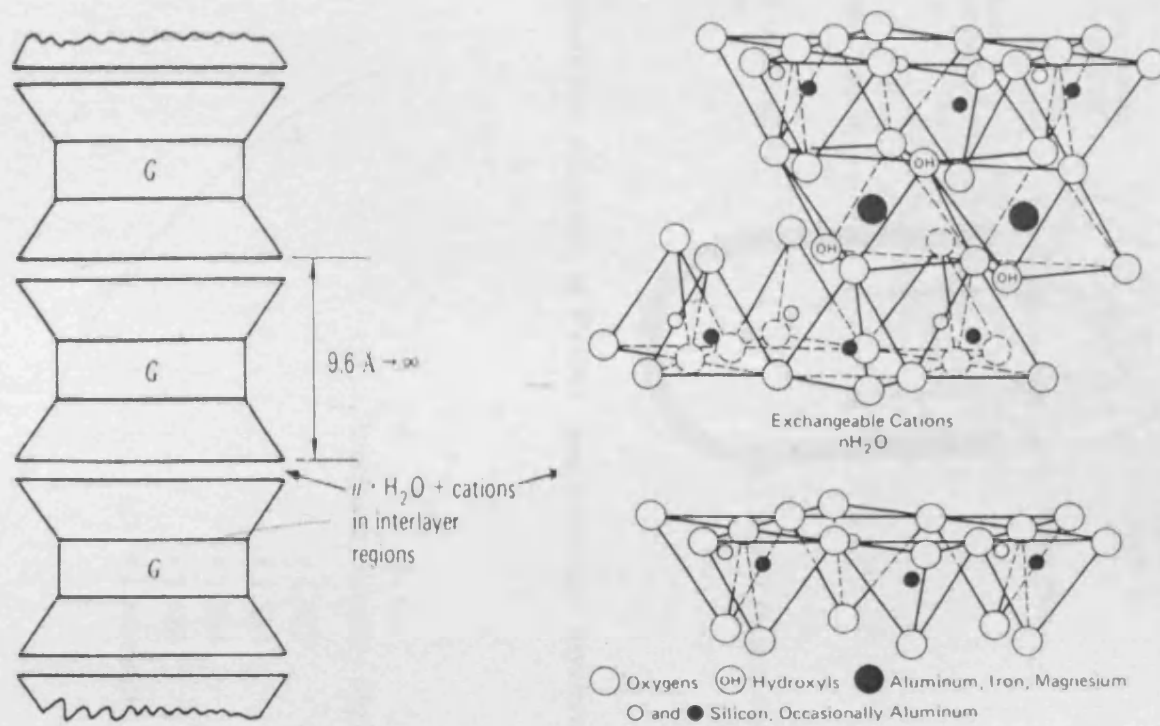
Figure 2.6 Schematic diagram of montmorillonite structure (Mitchell, 1993)
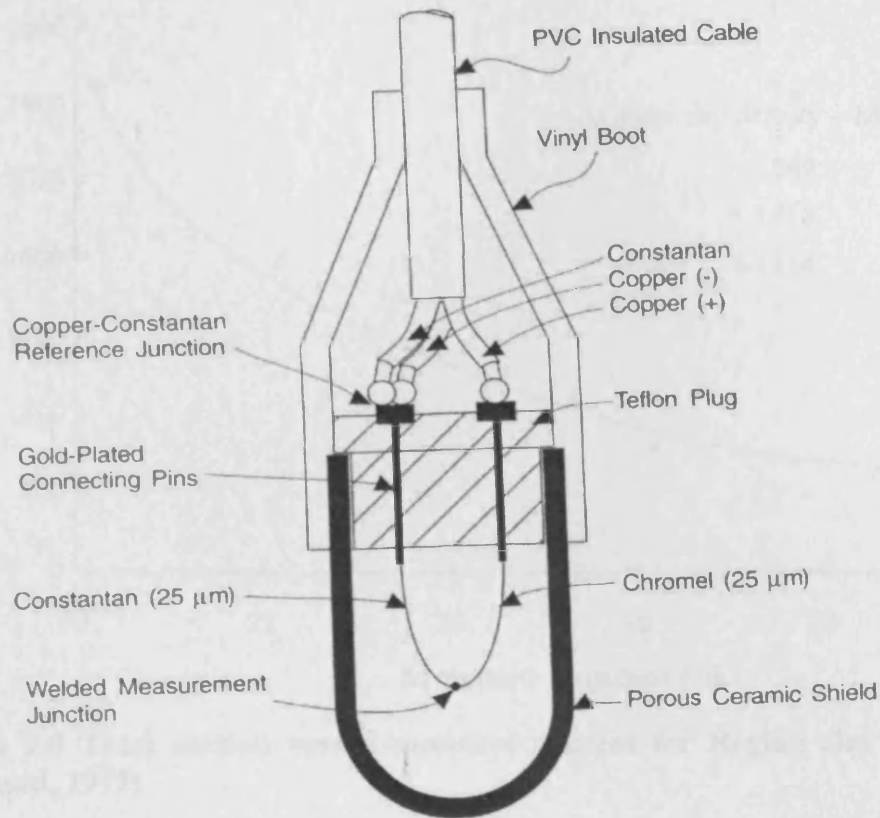
Figure 2.7 Schematic diagram of Peltier thermocouple psychrometer (Lu and Likos, 2004)
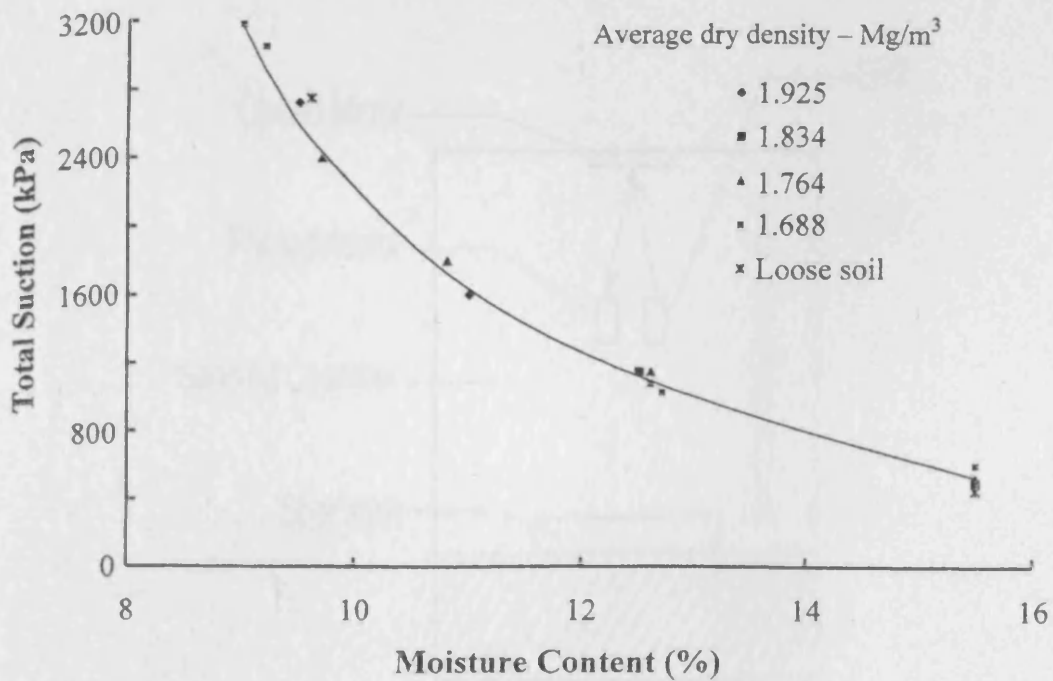
Figure 2.8 Total suction versus moisture content for glacial till (Krahn and Fredlund, 1972)
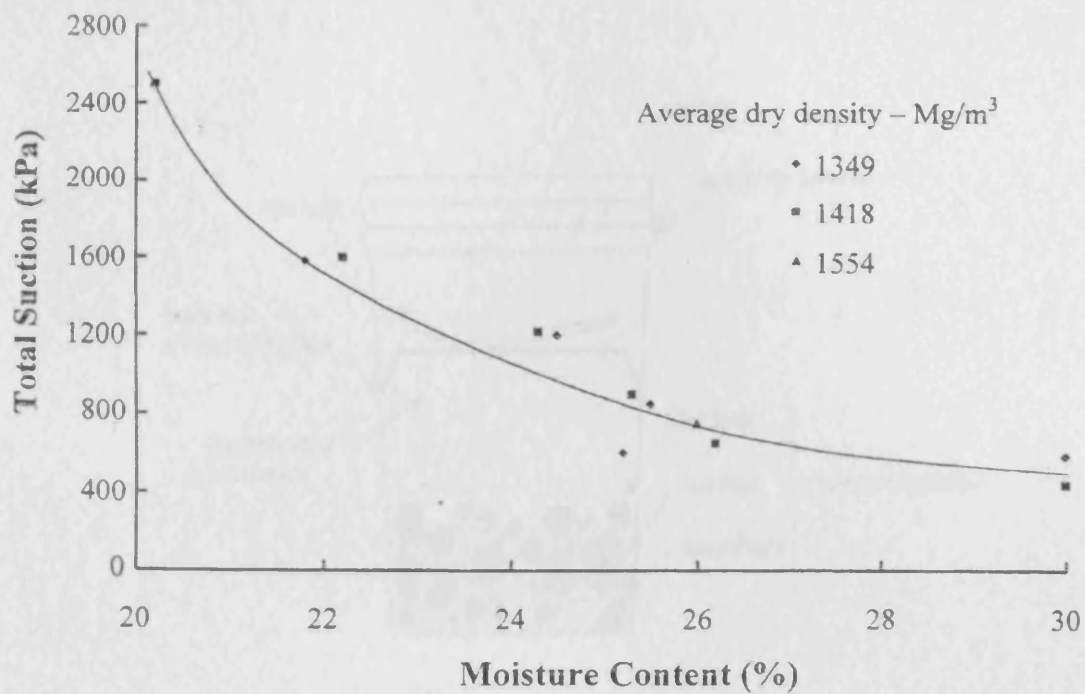
Figure 2.9 Total suction versus moisture content for Regina clay (Krahn and Fredlund, 1972)
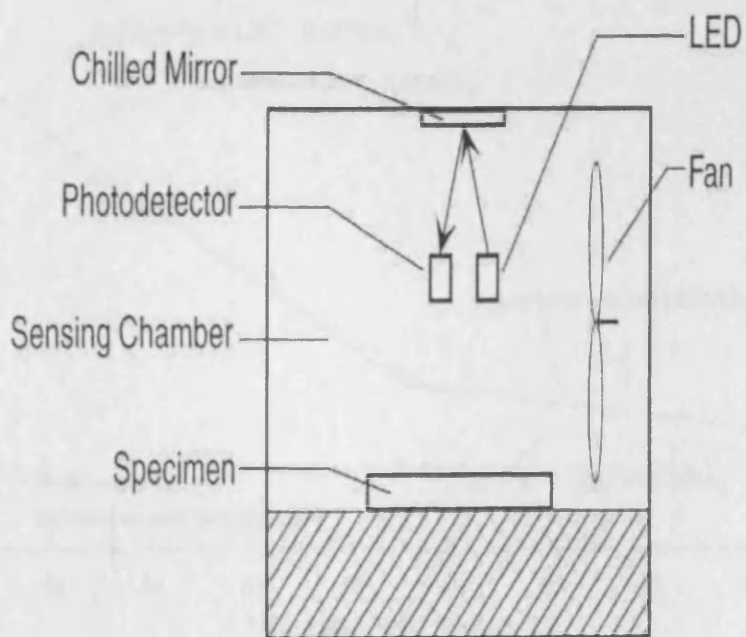
Figure 2.10 Schematic of chilled-mirror sensing technology (Lu and Likos, 2004)
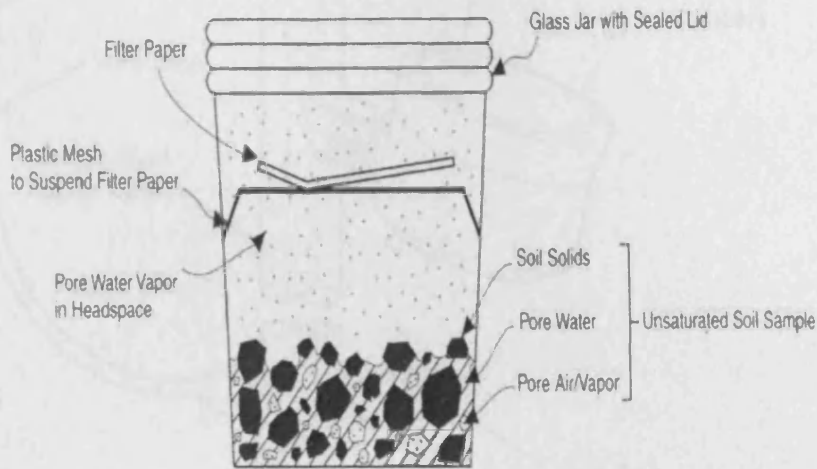
Figure 2.11 Non contact method for total suction (Lu and Likos, 2004)
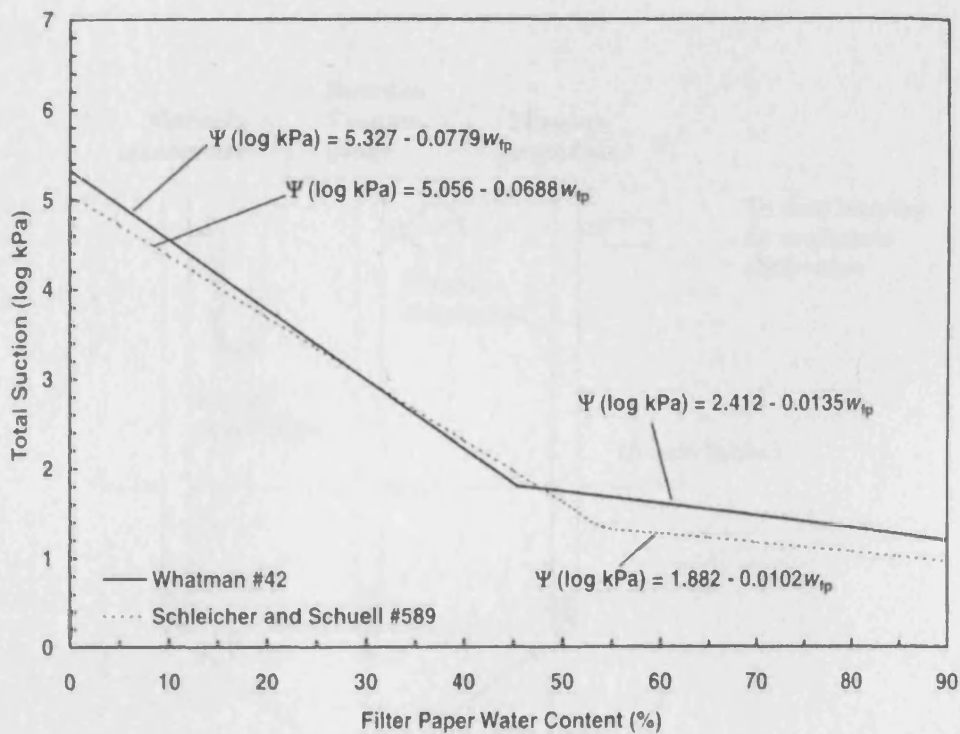
Figure 2.12 Calibration curve for filter paper (ASTM D 5298-94)
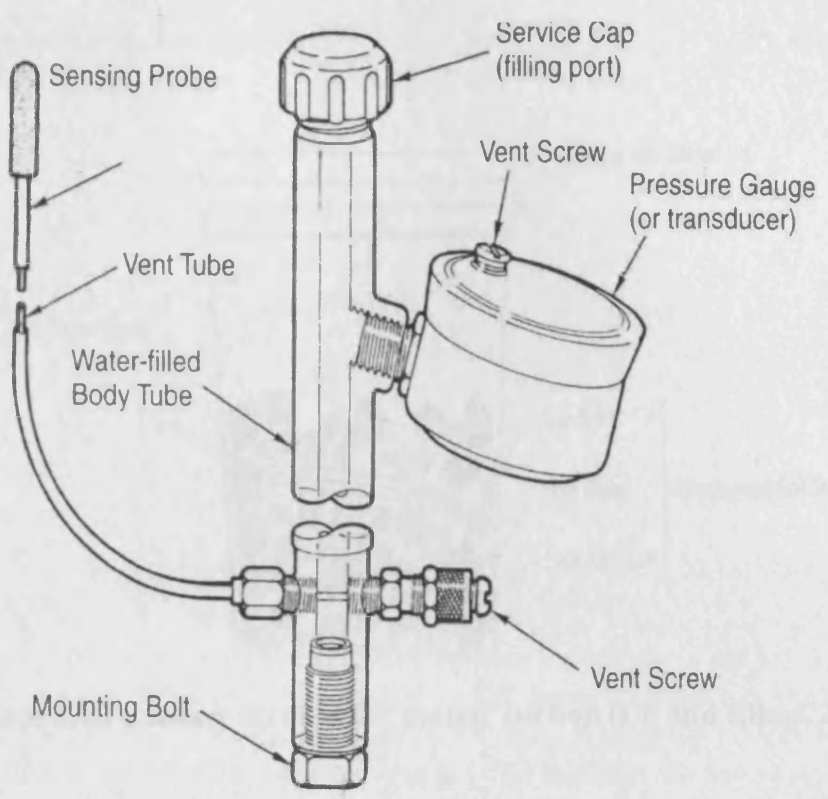
Figure 2.13 Schematic drawing of small tip laboratory tensiometer (Lu and Likos, 2004)
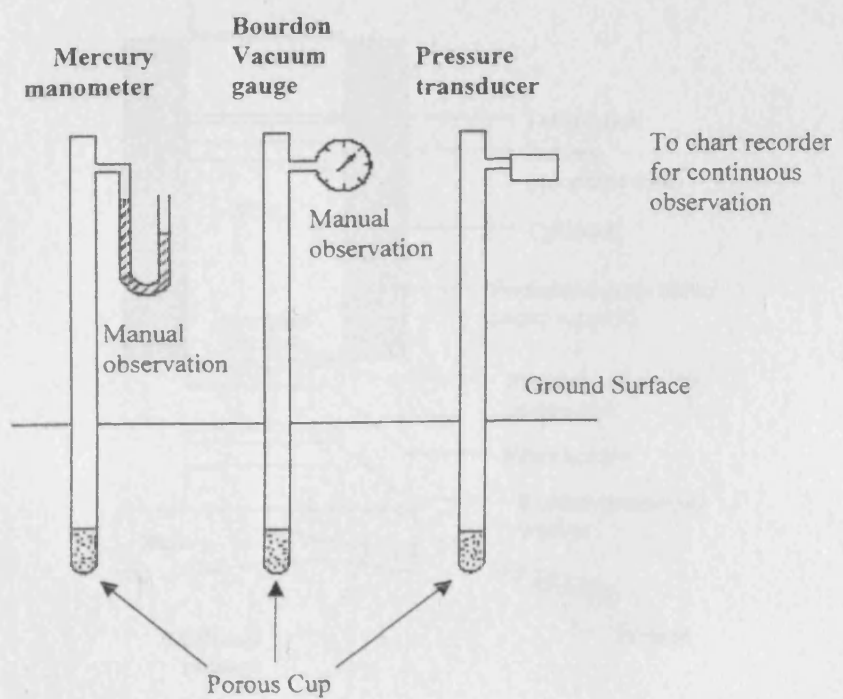
Figure 2.14 Various measuring systems for a tensiometer (Morrison, 1983)
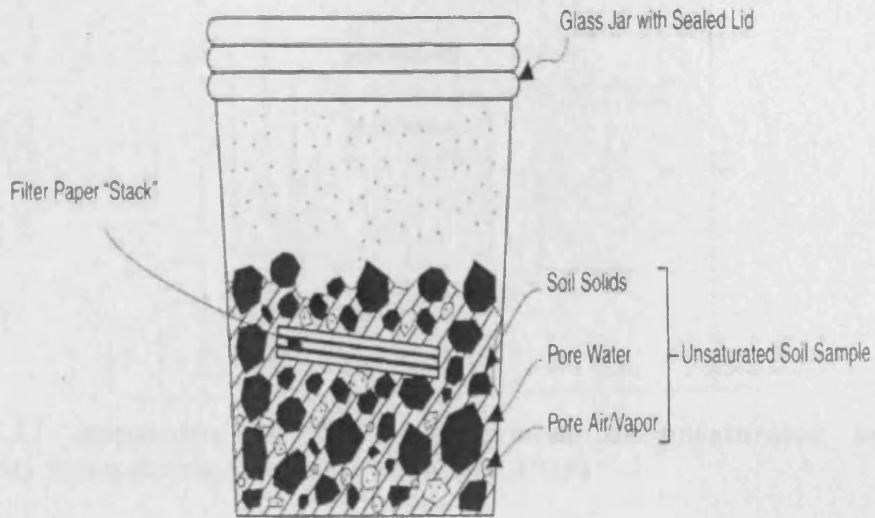
Figure 2.15 Contact method for matric suction (Lu and Likos, 2004)
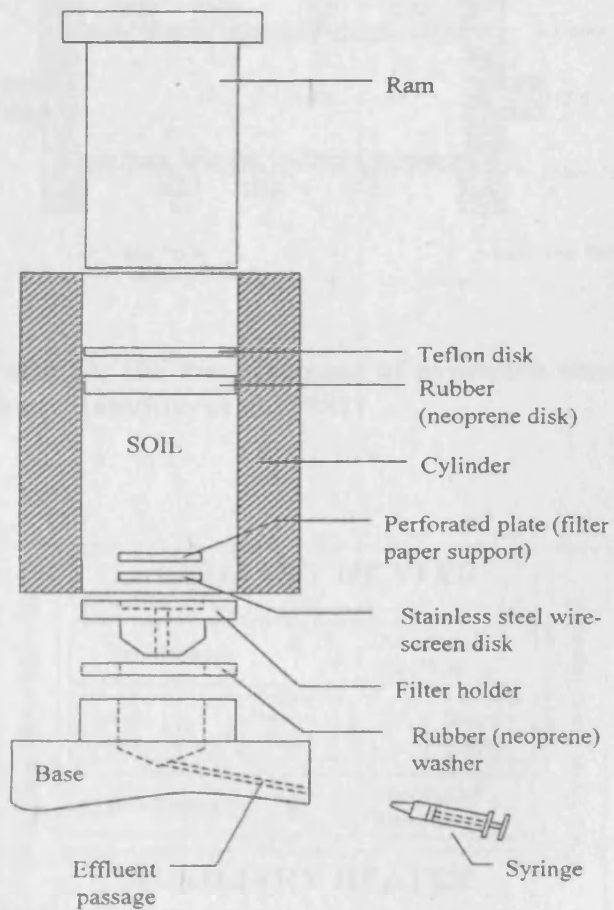
Figure 2.16 Design of the pore fluid squeezer (Manheim, 1966)
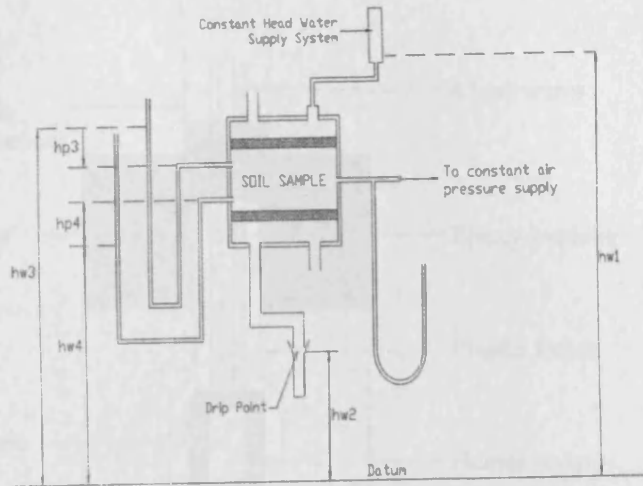
Figure 2.17 Apparatus for the measurement of unsaturated hydraulic conductivity using steady state method (Klute, 1965)
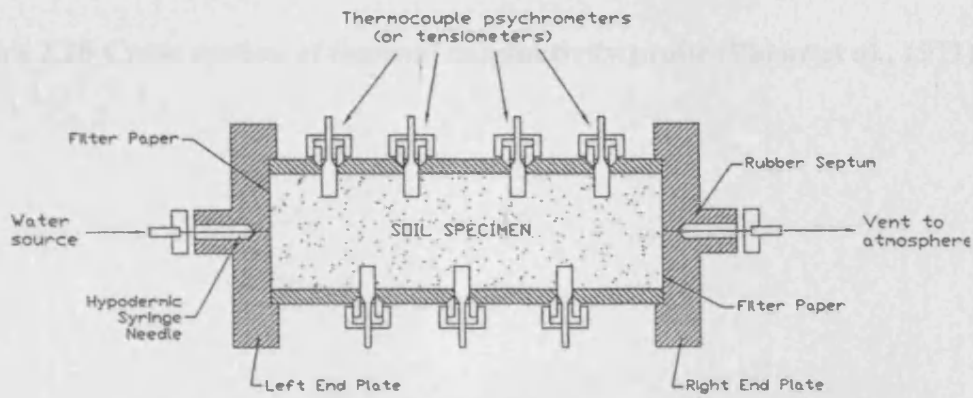
Figure 2.18 Apparatus for the measurement of hydraulic conductivity using the instantaneous method (Hamilton et al., 1981)
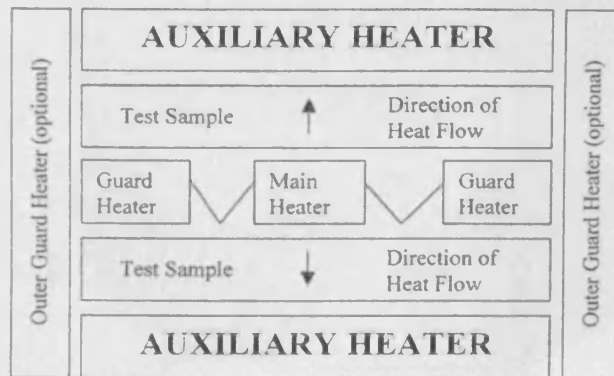
Figure 2.19 Schematic of guarded hot plate tests section (ASTM C 177-04)
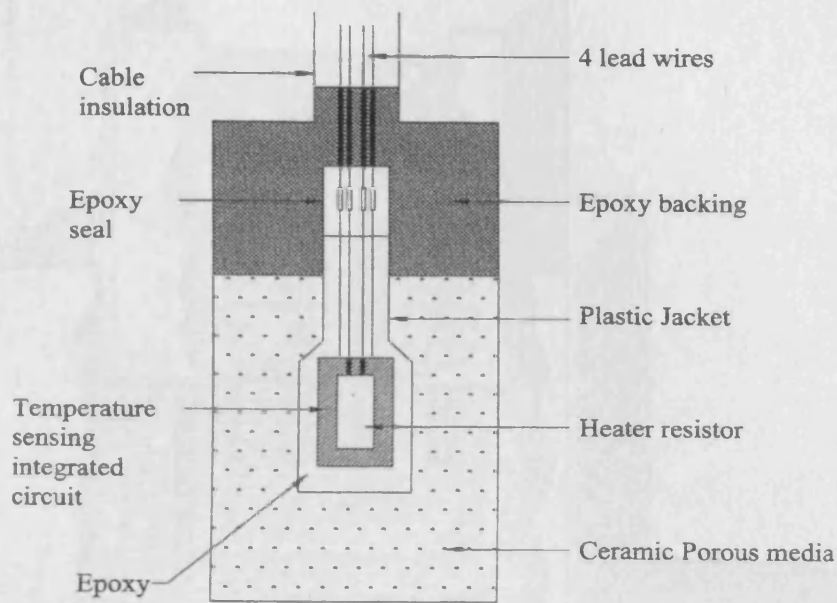
Figure 2.20 Cross section of thermal conductivity probe (Phene et al., 1971)

Cable insulation
4 lead wires
Epoxy seal
Epoxy backing
Plastic Jacket
Temperature sensing integrated circuit
Heater resistor
Ceramic Porous media
Epoxy
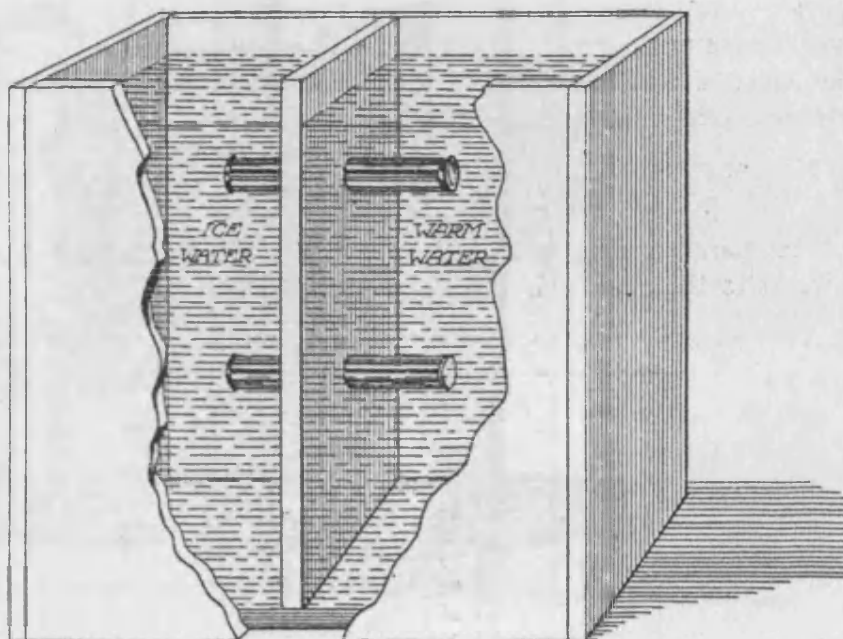
Figure 2.21 Apparatus for determining thermal dislocation of soil moisture when the soil column lay horizontally (Bouyoucos, 1915)

ICE WATER

WARM WATER
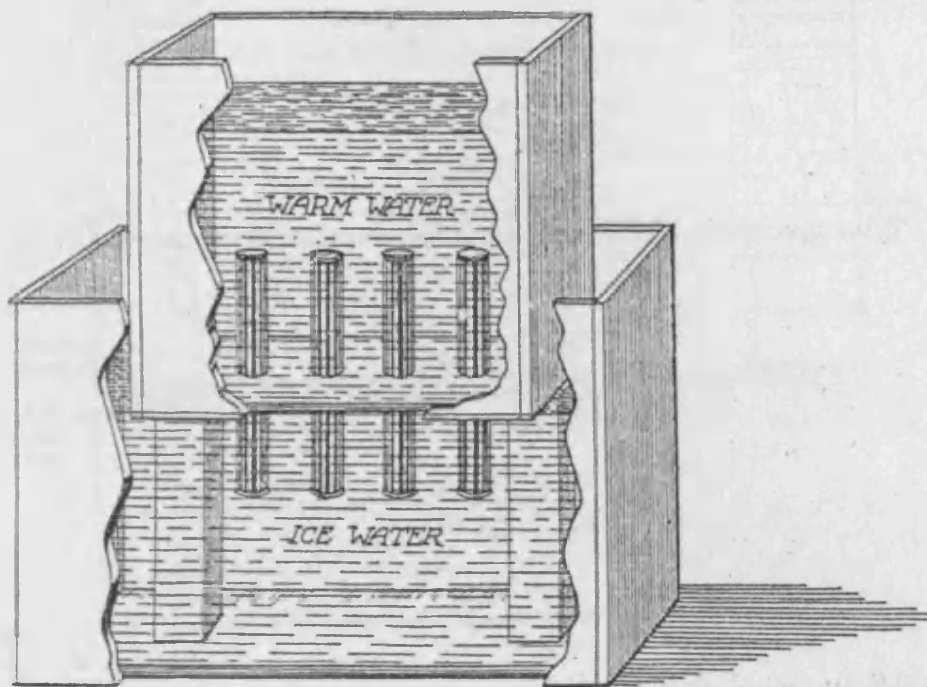
Figure 2.22 Apparatus for determining thermal dislocation of soil moisture when the soil column stood vertically (Bouyoucos, 1915)
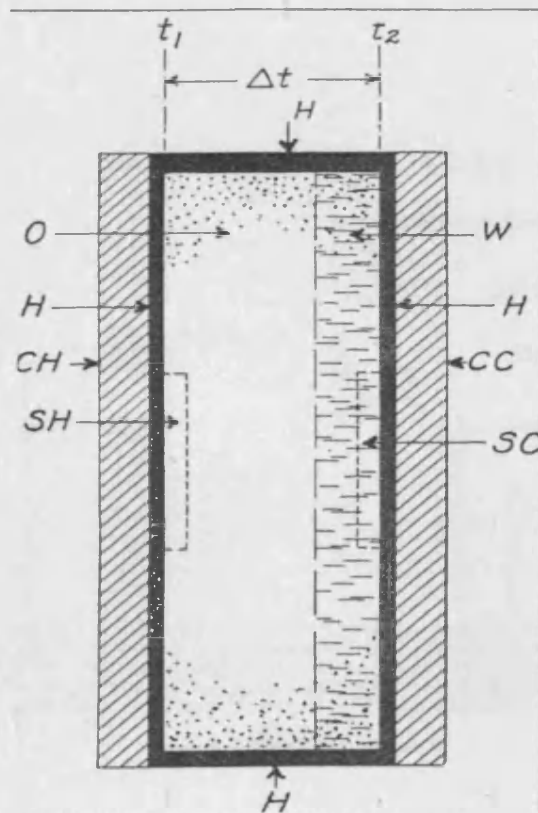
Figure 2.23 Apparatus for determining thermal tranfer (Smith and Byers, 1938)
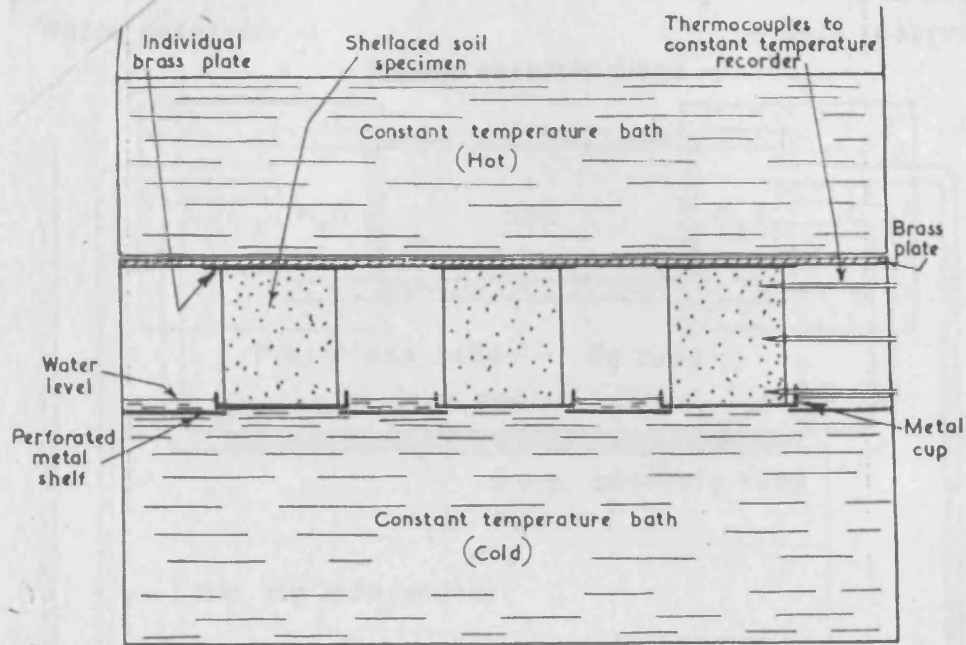
Figure 2.24 Constant temperature bath with specimens in position (Maclean and Gwatkin, 1946)
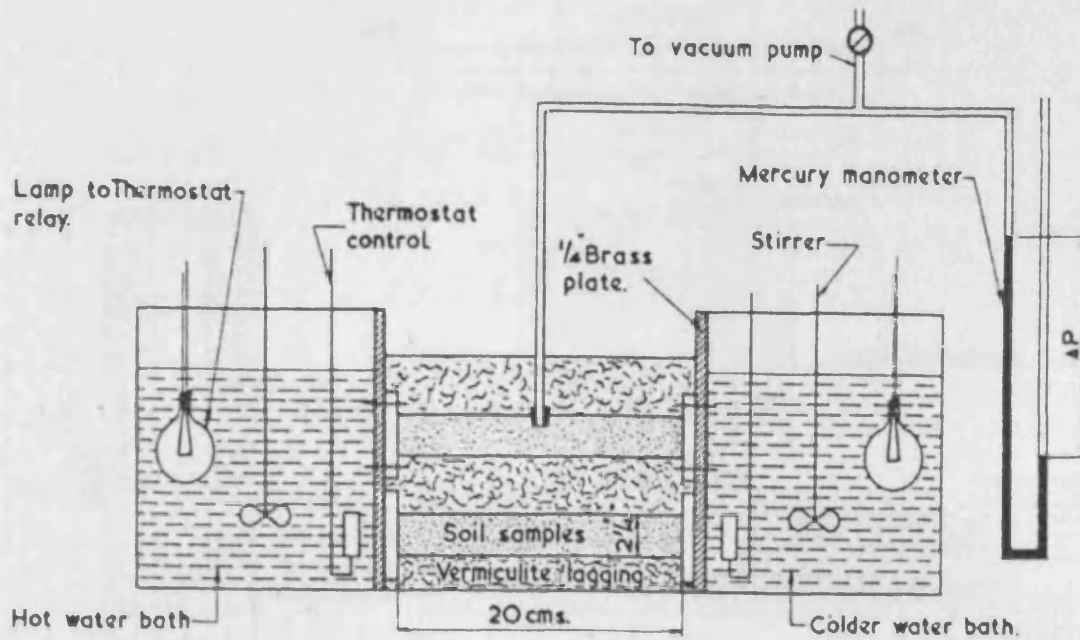
Figure 2.25 Experimental arrangements for studies of flow of moisture in unsaturated soil sample subjected to a temperature gradient (Jennings et al., 1952)
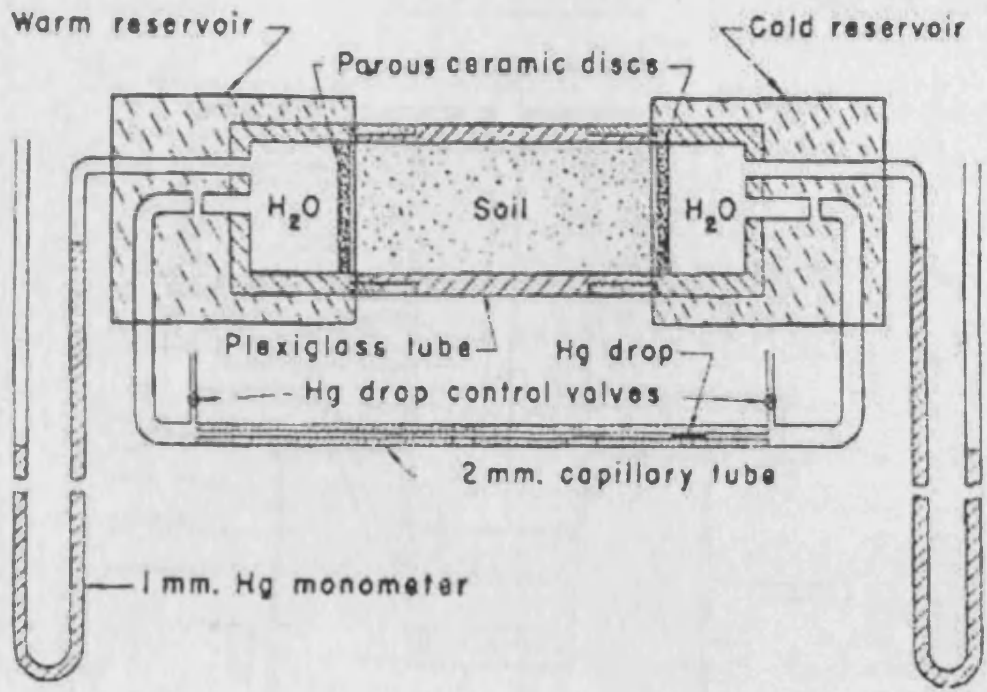
Figure 2.26 Schematic diagram of apparatus (Rollins et al., 1954)
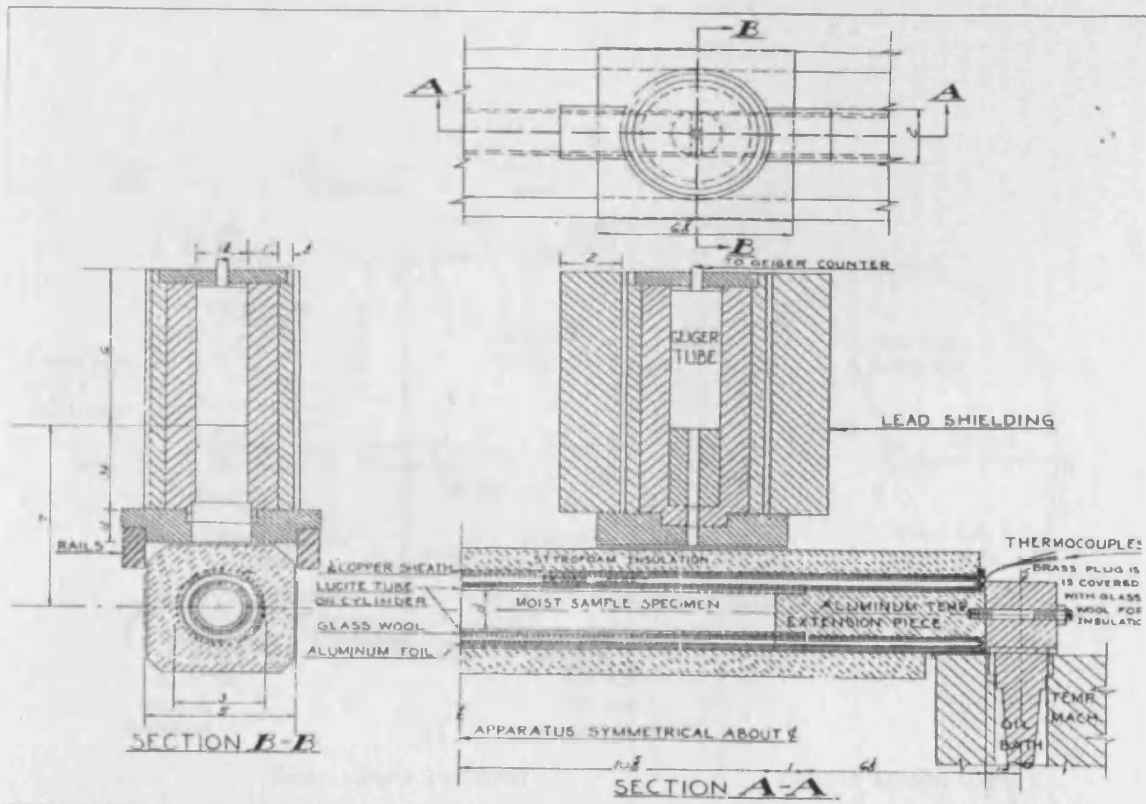
Figure 2.27 Details of the apparatus (Hadley and Eisenstadt, 1955)
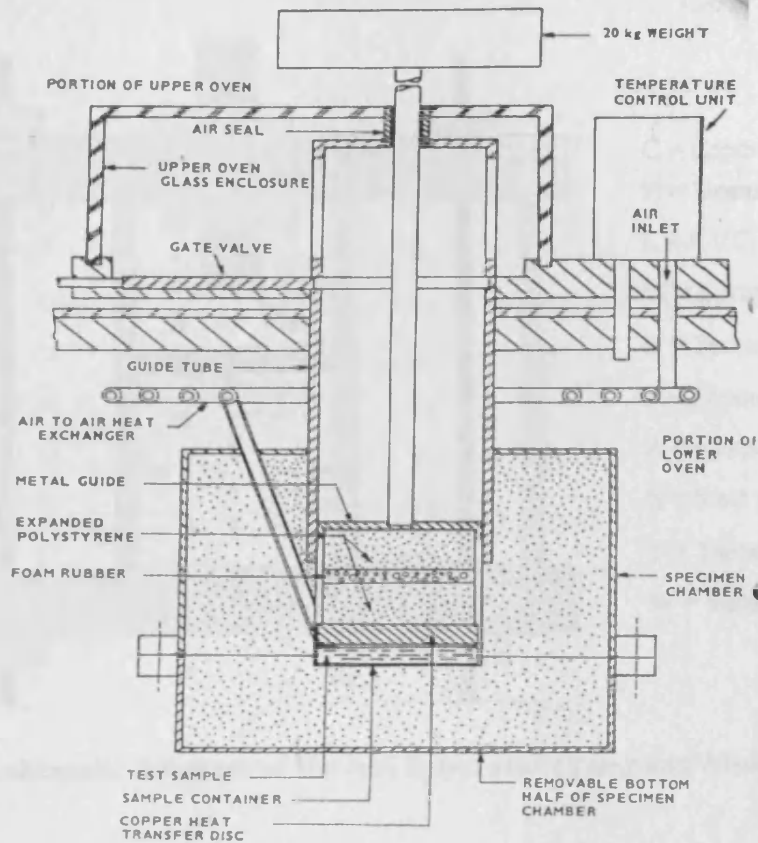
Figure 2.28 Diagrammatic arrangement of thermal diffusivity apparatus (Preece, 1975)
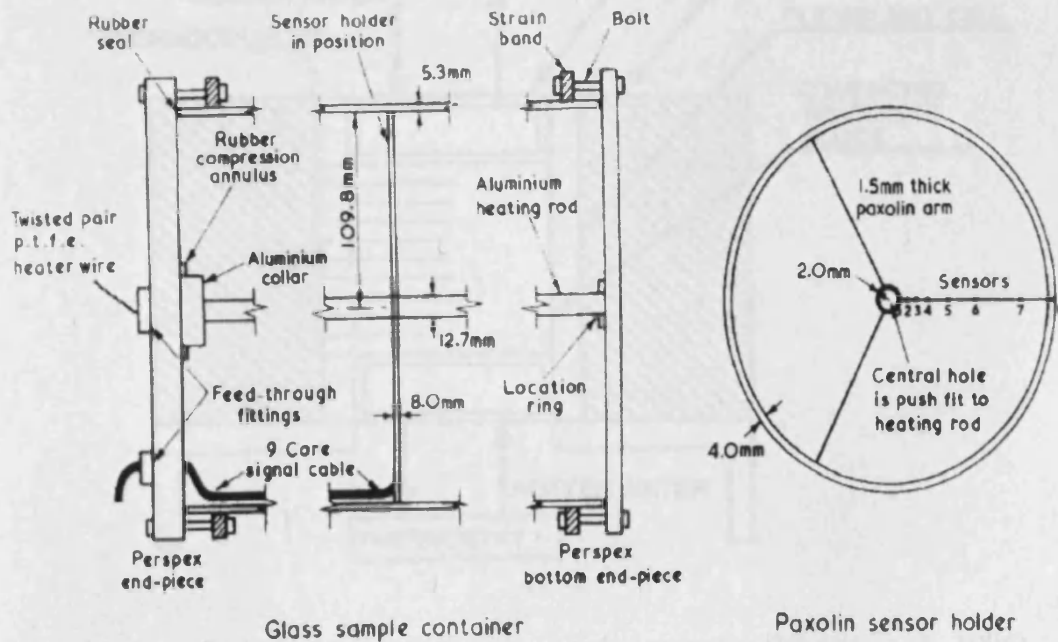
Figure 2.29 General layout of the experiment (Ewen and Thomas, 1989)

C = Concrete
H = Heater
L = P.V.C.
M = Compacted soil
N = Piston base plate
P = Pressure transducer
R = Copper cooling coil
S = Steel tube
T = Thermocouples
W = Water supply tube
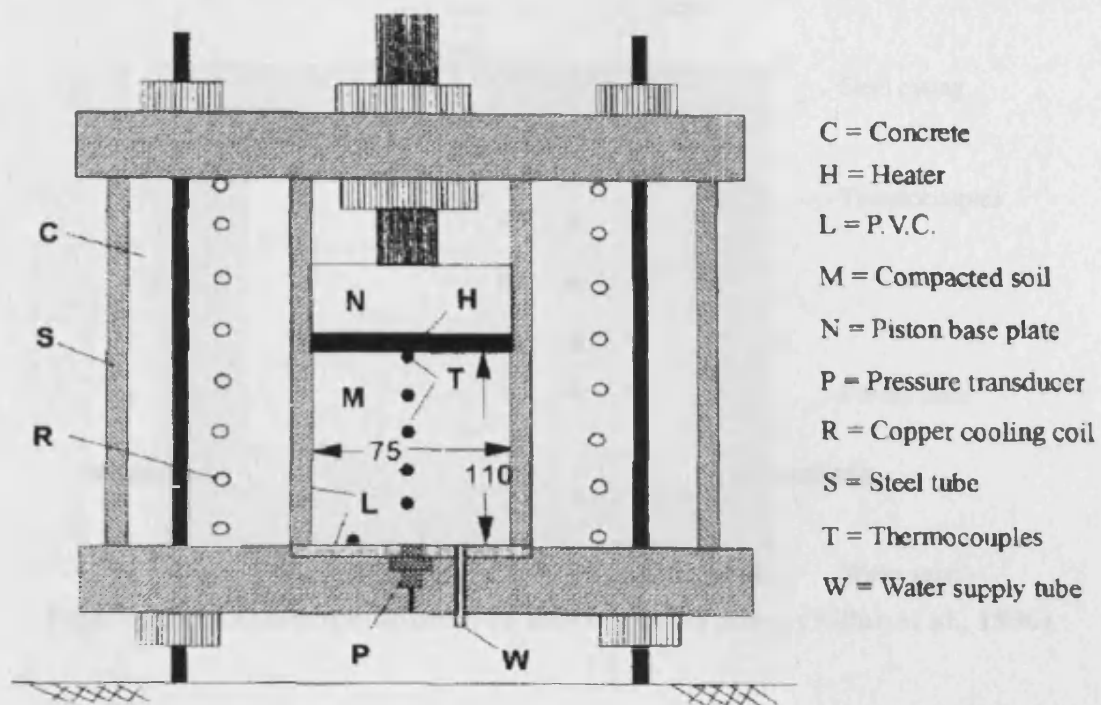
Figure 2.30 Schematic diagram of the test apparatus (Yong and Mohamed, 1996)
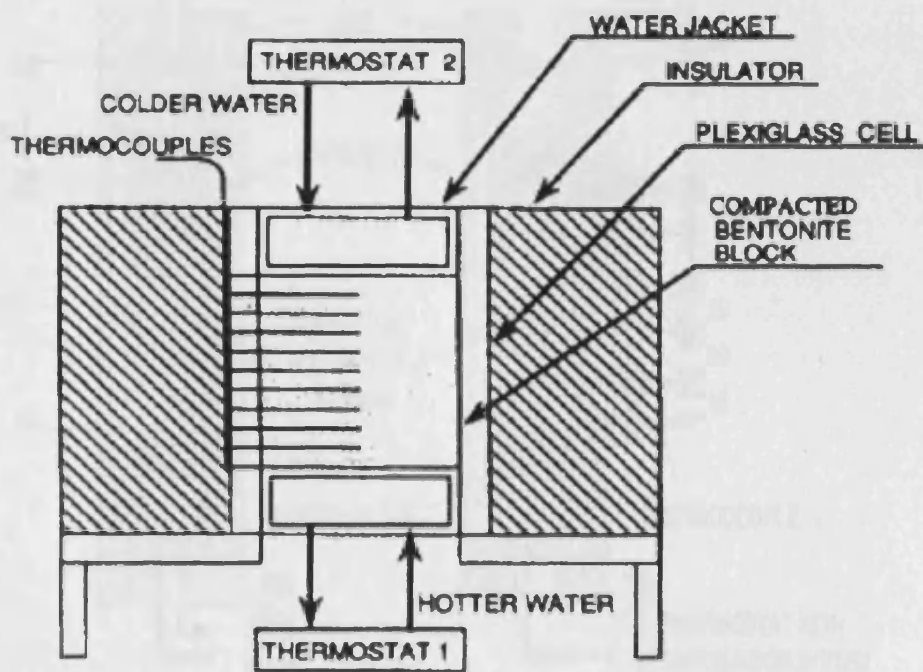
Figure 2.31 Schematic of experimental apparatus (Kanno et al., 1996)
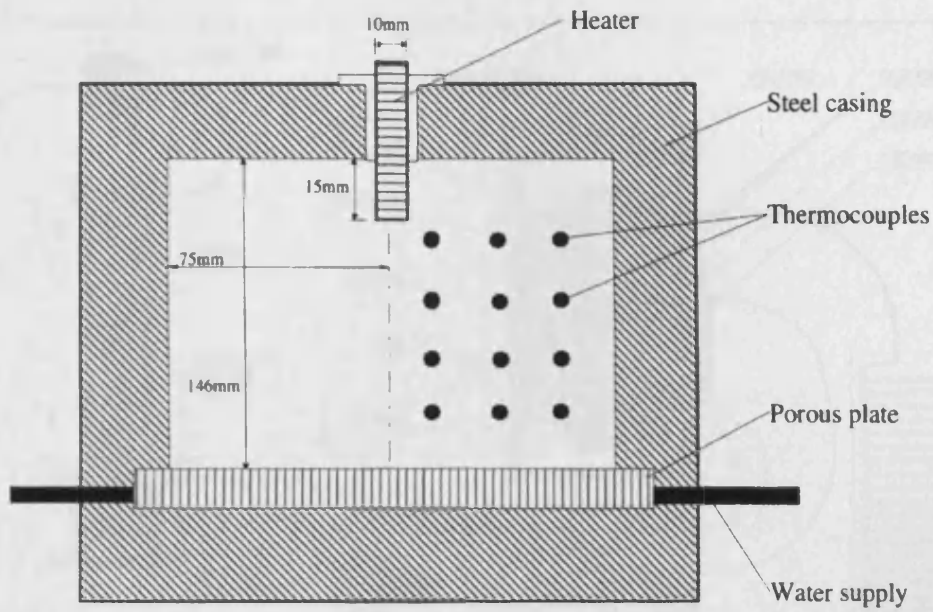
Figure 2.32 Experimental setup of heating experiment (Villar et al., 1996)
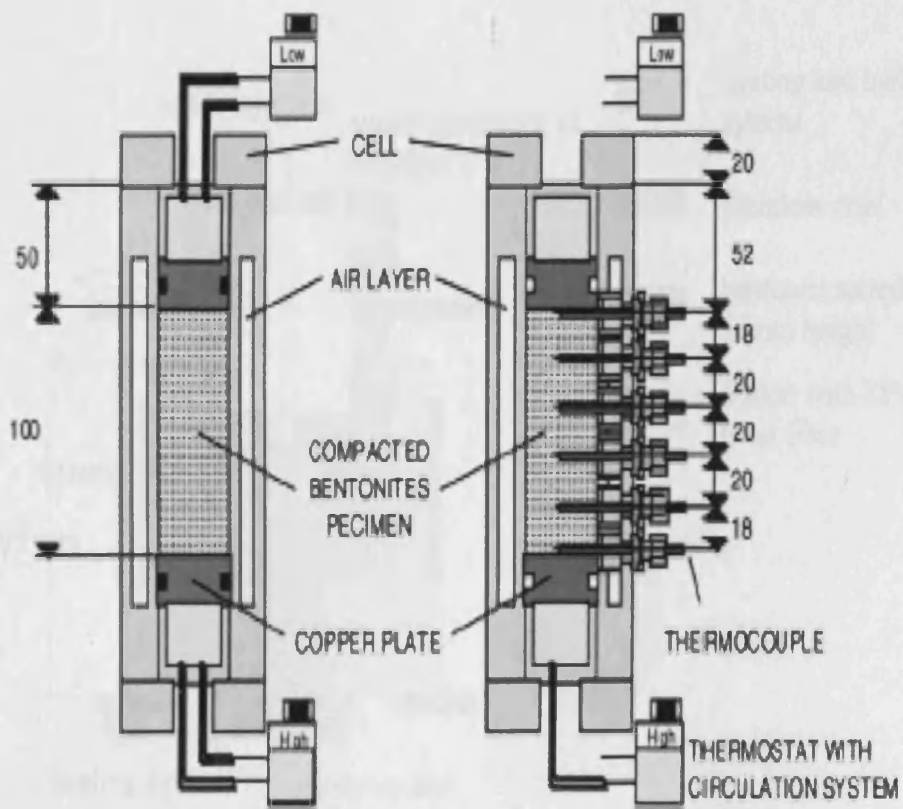
Figure 2.33 Thermal gradient tests in twin apparatus (Börgesson et al., 2001)
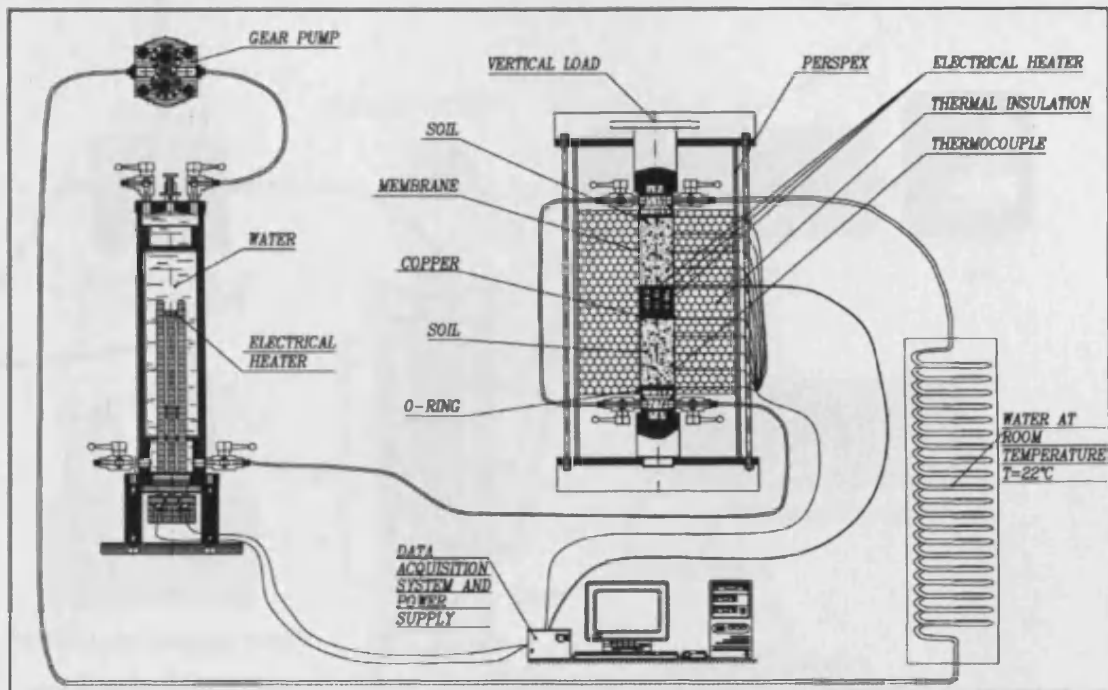
Figure 2.34 Schematic of the experimental device (Pintado et al., 2002)
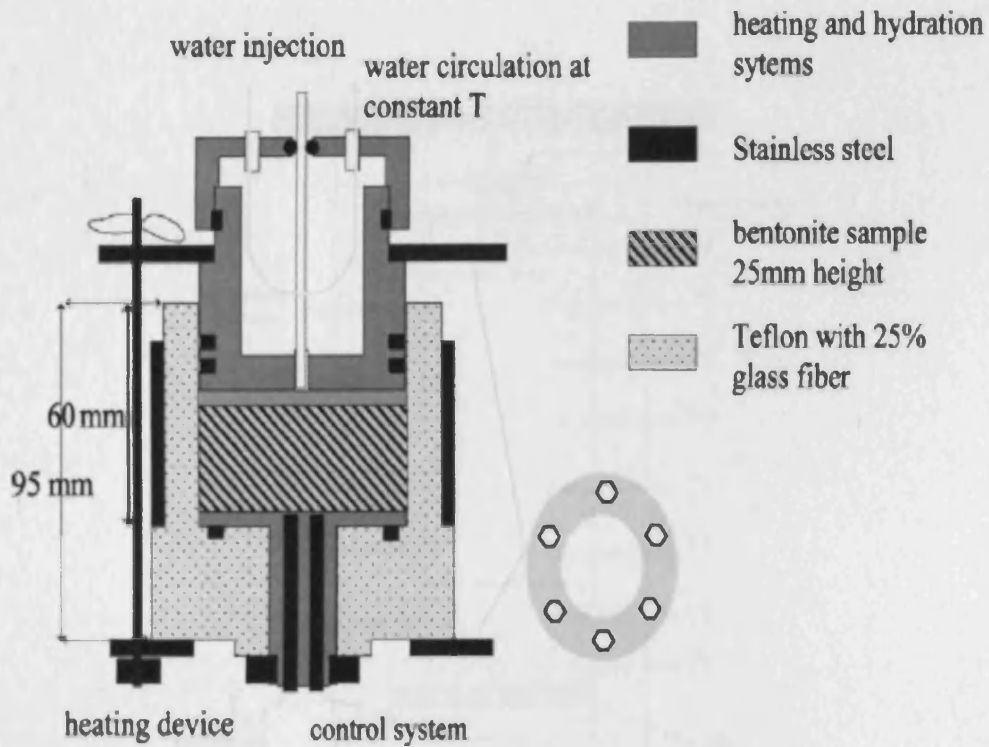
Figure 2.35 Schematic design of the small cells for thermo-hydraulic tests (Cuevas et al., 2002)
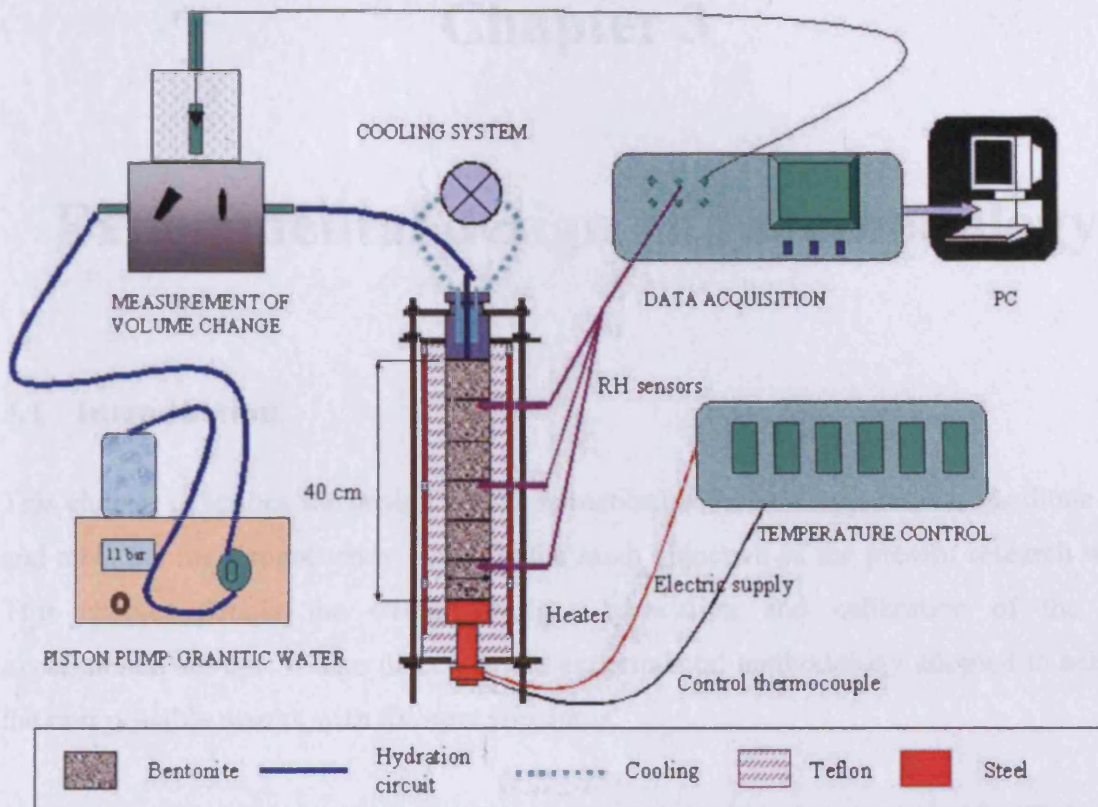
Figure 2.36 Experimental setup for the infiltration tests (Villar et al., 2005)
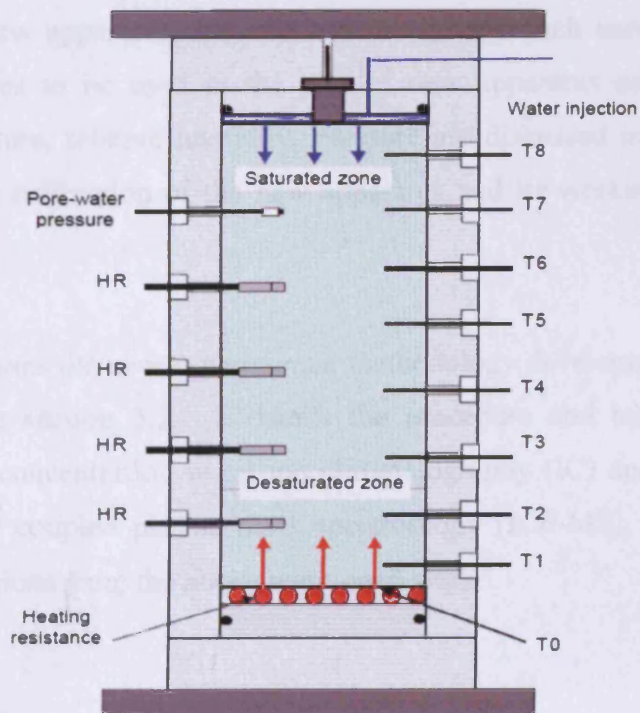
Figure 2.37 Schematic diagram of experiment (Gatabin and Billaud, 2005)

Chapter 3

Experimental design and methodology

3.1 Introduction

This chapter describes the design and construction of the new apparatus to facilitate heat and moisture movement study which is the main objective of the present research work. This chapter details the overall design, fabrication and calibration of the new experimental set up. It also discusses the experimental methodology adopted to achieve the best possible results with the new apparatus.

Section 3.2 discusses the type of tests required to be performed for the present study. Section 3.3 presents the necessity of new experimental apparatus to be built to carry out the tests mentioned in section 3.2. Sections 3.4 sets out the design criteria to be met for the construction of new apparatus. Subsequently, section 3.5 describes in detail the components of new apparatus, material and design approach used to make them. The various accessories to be used as the part of new apparatus and sensors required to measure temperature, relative humidity, pressure are discussed in sections 3.6 and 3.7. The integrity and calibration of the new apparatus and its working limits is covered in section 3.8.

Section 3.9 discusses the new experimental methodology developed to carry out the tests mentioned in the section 3.2. It details the procedure and techniques employed to determine anion concentration using ion chromatography (IC) and cation concentration using inductively coupled plasma mass spectroscopy (ICP-MS). Finally, section 3.10 draws the conclusions from the above mentioned work.

3.2 Testing programme

A detailed laboratory testing programme has been developed to investigate heat and moisture movement in clays. In particular three types of tests have been designed which apply different thermal and hydraulic boundary conditions to cylindrical clay samples. The following sections discuss each type of test carried out.

3.2.1 Thermal test

The thermal test (T-test) essentially applies a thermal gradient across a hydraulically sealed and confined clay sample. In the tests performed, 100 mm high samples were subjected to fixed temperatures of 85 °C at the bottom end and 25 °C at the top end. This resulted in a thermal gradient of 0.6 °C/mm along the length of the sample. In comparison Pintado et al. (2002) applied temperature of 80 °C at one end and 30 °C at the other of 76 mm high soil specimen. Whilst Cuevas et al. (2002) performed tests on 25 mm high bentonite samples with a higher thermal gradient of 1.6 °C/mm with applied temperatures between 100 °C and 60 °C and lower thermal gradient of 1.0 °C/mm with applied temperatures of 60 °C and 35 °C. The tests are to be performed on samples of two initial moisture contents termed the wet and dry. A series of tests will be undertaken at different time intervals to provide pseudo transient moisture content, dry density and chemical concentration data after dried sampling.

3.2.2 Thermo-hydraulic test

In the thermal-hydraulic test (TH-test) soil samples were again subjected to a thermal gradient of 0.6 °C/mm with temperatures of 25 °C and 85 °C applied at the top and bottom ends respectively, in addition to this deionised and de-aired water was supplied at the top end under a pressure of 0.6 MPa. In comparison in similar tests Yong et al. (1997) used a hydrostatic pressure of 0.276 MPa and Collin et al. (2002) used a constant water pressure of 1.1 MPa. Again a series of tests are to be performed on both wet and dry soil samples for different time intervals of 1, 2, 3, 4, 5, 7, 10, 15 and 30 days . Again this series of sub-tests, of different time durations, will provide pseudo transient data for

variables determined via invasive techniques such as moisture content, dry density and chemical concentration.

3.2.3   Isothermal test

In the isothermal test soil samples were only subjected to the application of a hydration source with the temperature kept at 25 °C at both ends of the soil samples. The resulting hydraulic gradient was obtained by supplying deionised and de-aired water from the top end under a pressure of 0.6 MPa. Again tests are to be performed on both wet and dry soil samples for a maximum 30 days. The tests performed will provide pseudo transient data for variables determined via invasive techniques such as moisture content, dry density and chemical concentration.

3.2.4   Summary of proposed testing programme

A summary of proposed testing programme is detailed in tabular form in Table 3.1. The tests are proposed to be performed on each of the two clays considered in this study. The initial condition of the wet and dry samples will be defined and discussed in more detail in chapters 4, 5 and 6.

3.3 Necessity of new experimental apparatus

There was a need to develop an experimental apparatus so that above mentioned tests could be carried out at laboratory scale. As the experimental apparatus required for this laboratory testing programme could not be adapted from available conventional soil testing equipment, a new apparatus was designed, fabricated and assembled. The purpose of the new apparatus was to measure following key parameters during the experiments:

- Transient temperature

- Transient relative humidity

- Transient volume flow rate of incoming water

- Transient swelling pressure

- End of test moisture content, dry density and chemical composition

3.4   Design criteria of apparatus

The experimental apparatus had to be designed to satisfy the following criteria so that the measurements of key parameters outlined in section 3.3 could be accomplished:

1- The clay sample can be properly compacted into the apparatus so that there is no air gap between the sample and the apparatus walls.

2- The internal dimension of the apparatus should be such to achieve the final sample size of 100 mm diameter and 100 mm height after compaction.

3- The apparatus has to be sufficiently strong to withstand the static compaction process and any hydraulic, vapour or swelling pressures developed during a test.

4- The sample can be subjected to a well regulated and stable temperature gradient via maintaining fixed temperature at each end of the soil sample.

5- An accurately measured and temperature controlled hydration source can be applied to one end of the compacted clay sample.

6- The apparatus can measure transient temperature, relative humidity and swelling pressure.

7- The clay sample can be removed intact from the apparatus to allow sampling of water content, dry density and chemical (anion / cation) concentration.

8- The apparatus can measure the volume of water induced by imposed hydraulic gradient.

9- The apparatus must be hydraulically sealed and thermally insulated.

10- The valves, fittings, pressure gauges and pressure lines should be high pressure resistant.

11- The apparatus must be both robust and easy to handle, assemble and dismantle.

12- The apparatus needs to be compatible with existing auxiliary equipment required for this laboratory testing programme.

13- The apparatus can be used for future research in thermal, hydraulic, mechanical and chemical studies of soils with minimal modifications.

3.5   Description of apparatus

An apparatus termed here as a thermo-hydraulic (TH) cell has been designed to fulfil the design criteria detailed above. A schematic diagram of the TH cell is shown in Figure 3.1. A total of three cells, shown in Figure 3.2, have been constructed and commissioned. Each of the cells consists of four main parts namely the top section, an interconnecting ring, a central section and a bottom section as shown in Figure 3.3. Material and design approach used to build the apparatus is dealt in following sections 3.5.1 – 3.5.2. Each of the components of the apparatus is detailed in the sections 3.5.3 – 3.5.6. Auxiliary devices used are described in section 3.6 and sensors used are described in section 3.7.

3.5.1   Material

An austenitic stainless steel of grade 316L was used to make the main components of the thermo-hydraulic cells. Type 316L austenitic stainless steel is low carbon molybdenum

bearing steel. It is more resistant to corrosion and pitting especially in chloride rich environments than conventional nickel chromium austenitic stainless steels such as 302-304. It also has excellent machining, forming, cutting and welding characteristics with good rupture and tensile strength at high temperature. The physical and mechanical properties of the austenitic stainless steel 316L are tabulated in Table 3.2. The stainless steel was supplied by CG Rees Ltd UK in tubes and plates close to the required size and machined to the actual size of various components of the TH cells. All outer surfaces of the TH cells were sand blasted to prevent slippage of cell during assembling and dismantling.

Viton® O-rings were used as sealant to inhibit moisture escape during experiments. The Viton® O-rings are made from a fluoroelastomer and can withstand a range of temperatures from -40 °C to +200 °C and have high chemical resistance with good compressibility. The O-rings were fitted at the interfaces of various components of the TH cell to provide flexible and moisture leak proof joints.

Polytetrafluoroethylene (PTFE) was used to reduce heat losses in the TH cells. PTFE has very low thermal conductivity, low coefficient of friction, high chemical resistance and good compressive strength. The compressibility characteristic of PTFE was measured in laboratory by simple compression test to verify the value provided by the supplier. Various engineering properties of the PTFE used are presented in Table 3.3.

3.5.2   Design approach

A detailed analysis of the stress distribution and deformation behaviour of the TH cell components was done prior to the fabrication using hand calculation. The components were designed to operate at twice the maximum soil swelling pressure of 1.67 MPa (i.e. factor of safety = 2). The swelling pressure of the soil sample was measured in laboratory and described in the next chapter. The hoop stresses and longitudinal stresses were calculated to determine the minimum thickness required. Full details of the design calculations are attached in Appendix 1.

3.5.3   Top section

The top section consists of a sand blasted austenitic stainless steel cylinder of outside diameter 142 mm, wall thickness 10 mm and height 100 mm with a stainless steel plate of diameter 250 mm and thickness 15 mm welded at its top end, shown in Figure 3.3. The top section has two primary functions; firstly, to maintain a constant temperature and secondly, to allow the supply of pressurised water (up to 0.6 MPa) to the top end of the soil sample.

Temperature control is achieved via the circulation of chilled or heated water within an internal copper coil as shown in Figures 3.1 and 3.4. This system is regulated by a thermocouple at the surface of the porous disc. Pressurised hydration water is supplied into the reservoir formed in the centre of the top section via a pressurised water supply system described in section 3.6.3. The top section has two watertight 1/4 inch BSP (British Standard Pipe) brass compression fittings specially adapted to take 1.5 mm diameter thermocouple and pressure transducer cables. The top section has one 1/4 inch BSP brass male elbow (also known as quick release fittings) for the pressurised water supply line and two 1/8 inch BSP brass male elbows to join external heating/refrigerating circulator (described in section 3.6.2) to the internal copper coil. The top section also has a manifold to which a pressure gauge, pressure relief valve and bleed valve are connected. The pressure gauge is used to monitor the pressure of water entering the soil sample and the pressure relief valve is fitted to ensure that the pressure does not exceed 1.0 MPa within the top section of the test cell.

3.5.4   Interconnecting ring

There is an interconnecting stainless steel ring between the top and central section. This ring is shown in Figure 3.5. The ring has one groove on the top and two grooves on the underside for the fitment of O-rings. The interconnecting ring also holds the porous steel plate in TH and isothermal tests or a solid steel plate for T-tests.

3.5.5   Central section

The central section holds the soil sample of size 100 mm diameter and 100 mm height. It consists of a PTFE (polytetrafluoroethylene) sleeve of outside diameter 124 mm, wall thickness 12 mm and height 140 mm. The PTFE sleeve is inserted tightly into a stainless steel cylinder of outside diameter 142, wall thickness 10 mm and height 140 mm as shown in Figure 3.3. The PTFE has very low friction that helps easier sample extrusion at the end of the experiments. In addition to the soil sample, the central section also houses the heater which is described below in section 3.6.1.

An insulating material is wrapped around the outside of the steel cylinder as shown in Figure 3.3 to minimise radial heat loss. The insulating material used is a Superwool 607 Max Blanket, supplied by RS Ltd UK. It has good thermal stability with excellent thermal insulating property and immune to any thermal shock. It has a thickness of 13 mm and has a very low thermal conductivity of 0.06 W/mK at 260 °C and a specific heat capacity of 1.13 kJ/kgK at 1090 °C. Its various physical and thermal properties are detailed in Table 3.4.

One cell has four access points staggered around the cell at every 2 cm in the central section to allow thermocouples or relative humidity probes to be inserted in to the soil sample as can be seen in Figure 3.3. The four watertight 1/4 inch brass compression fittings specially adapted were employed to take the thermocouple or relative humidity probes. Insertion of these probes requires drilling into the soil sample that causes inevitably disturbance in the vicinity of the measuring probes. To minimise these changes in the soil sample, the remaining two cells do not have any holes in the central section.

3.5.6   Bottom section

The bottom section, shown in Figure 3.3, is a solid austenitic stainless steel base of diameter 250 mm and thickness 30 mm and is designed to support the cell and allow access to the heater power supply and control cable and the duplex thermocouple wire. It

has two slots to take two O-rings, which ensure water tightness of the cell. The central section plus interconnecting ring and the top section sit on these O-rings. It also has five stainless steel tie rods with support nuts at their bottom end to connect it with the top section.

3.6   Accessories

The TH cells need a range of auxiliary devices related to temperature control and water supply. Equipment is also required to monitor the water intake during the tests. The following sections provide the detail of the approach adopted.

3.6.1   Heater and temperature controller

Ewen and Thomas (1989) and Mohamed et al. (1993) supplied heat to the system by using an electric heater. Considering the design criteria it was decided that the temperature control mechanism used in the TH cell should be capable of maintaining uniform temperatures from room temperature to at least 90 °C. To achieve this, a fully machined cast aluminium bronze heater was employed as a heating source at the bottom of soil sample. The heater has diameter of 99.9 mm and thickness of 20 mm and is shown in Figure 3.6. A Viton O-ring is fitted on the edge of the heater 2 mm down from its top surface to prevent vapour escape along the sides of the heater. The heater has one hole of 5 mm diameter in its centre for a duplex thermocouple. In addition, when the heater is inserted into the central section of the cell, air in the gap between the soil and heater is expelled through this hole. The heater is placed in contact with the bottom face of the soil sample within the central section. A PTFE disc of 20 mm thickness and 100 mm diameter is then pushed in below the heater to minimise heat loss through the bottom section of the cell, as shown in Figure 3.6. The PTFE disc has two holes to allow heater power supply cable and duplex thermocouple cables to pass through.

The stability of temperature supply within the heater depends upon the operating performance of temperature controller and sensor. A temperature controller, 2132 PID (Proportional, Integral and Derivative), is used to control the heater surface temperature

and can maintain the target heater temperature to within $\pm$ 0.25 °C without oscillation or overshoot. The duplex thermocouple in the centre of the heater was used as the sensor for the temperature controller.

3.6.2   Heating/refrigerating circulator

A heating/refrigerating (heater/cooler) water circulator, Fisherbrand® ET100-BC10 (Model reference: FB 51714), is used to control the temperature of hydration source of the TH-cell. As described above water is circulated at a constant temperature through an internal copper coil fitted inside the top section of the TH cell. The heating/refrigerating circulator is made of high-grade stainless steel and temperature resistant polymer. It has a PID controller and an adjustable over heating cut-out, the technical specification of the circulator is given in Table 3.5.

3.6.3   Pressurised water supply system

In the TH tests water is required to be supplied through the top section of the cell under a pressure of 0.6 MPa. A pressurised water supply system has been designed to serve this purpose as shown in Figure 3.7. It consists of an air water interface, compressed air line, water tank and vacuum pump. The air water interface comprises of a bladder in a Perspex cylinder constrained by tie bars between two end plates and has an operating pressure up to 1.0 MPa. The air line and water line are connected directly into the bladder and cylinder via the base plate. Compressed air inflates the bladder and pressurises the outside water in the cylinder. This pressurised water is then supplied to the cell via a pressure gauge. The vacuum pump has two functions firstly to supply the water to the water tank at top and secondly to de-air the water tank by applying a suction to remove any dissolved air.

3.6.4   Automatic volume change apparatus

An automatic volume change apparatus, WF17043 supplied by Wykeham Farrance UK, is used to measure the volume of water going into the soil sample in the TH tests. It consists of a calibrated chamber of 100 ml volume and a piston and allows precise measurement of the changing volume within the cylinder. Movement of the piston is recorded by an external linear strain transducer. If the change in volume exceeds 100 ml then a changeover valve allows the internal piston to move in the opposite direction. This can be repeated until the test has completed. The system has been calibrated with reference to direct accurate weighing measurements of the water. A balance capable of weighing 1 mg was used for this purpose. The calibration curve between volume of water and sensor (linear strain transducer) output is shown in Figure 3.8.

3.6.5   Compaction mould

A compaction mould was designed and made to allow compaction of the soil samples. The compaction mould consists of a base, a spacer, a collar and two wing nuts as shown in Figure 3.9. The base is made of aluminium bronze, the collar of austenitic stainless steel (grade 316L) and the spacer of aluminium. The soil sample was compacted in the central section of the TH cell with the spacer at the bottom and the collar at the top. The spacer has the same diameter as the heater and a thickness of 40 mm and provides the space to insert the heater and PTFE insulating disc in the TH cell after the compaction. The top surface of the spacer is covered with a thin plastic strip to prevent the soil adhering to its surface. The spacer has a screw hole at the bottom surface to pull it out of the central section of the TH cell after the compaction by screwing the rod into the hole. The collar screws the central section of the TH cell to the mould to provide stability during compaction. Figure 3.9 also shows the sequence of assembling the compaction mould.

3.6.6   Hydraulic extruder

An apparatus was required to push the soil sample out of the TH cell at the end of the experiment. The hydraulic extruder was designed, fabricated and assembled as shown in Figure 3.10. It consist of iron frame, plates, oil filled hydraulic jack with lever. It has a capacity to apply a 50 kN force.

3.7 Sensors

The various sensors that have been used to measure transient variation of temperature, relative humidity and swelling pressure during a test are detailed in this section. The data acquisition system consists of dataloggers and personal computer to collect the data from the sensors is also described in the following sections.

3.7.1   Temperature measurement

Three kinds of type K thermocouple have been used to measure temperature. Thermocouples are based on the principle that when two dissimilar metals (Chromel Ni-Cr alloy and alumel Ni-Al alloy in case of type K thermocouples) are joined, a voltage is generated that relates to the difference in temperature between the measuring junction and the reference junction (connected to the measuring device). All the thermocouples were connected to a datalogger to measure the transient temperature at various points in the soil sample. The three specific types of thermocouples employed are detailed below.

3.7.1.1   Mineral insulated metal sheathed thermocouple

Mineral insulated metal sheathed thermocouples type K with pot seal, (as shown in Figure 3.11), have been used to measure transient temperature variation in the soil sample. They have a 1.5 mm diameter and 150 mm long 310 stainless steel sheath to protect the insulated junction. A pot seal allows the transition to a 1m polyvinyl chloride (PVC) insulated lead. These thermocouples were used to measure the temperature within the soil sample at a distance of 20 mm, 40 mm, 60 mm and 80 mm from the heater surface.

They have been installed in the central section of the TH cell by using watertight 1/4 inch BSP brass compression fitting with a brass conical tubing sleeve (also known as an olive) fitted to the thermocouple stem.

3.7.1.2   Mineral insulated duplex thermocouple

A mineral insulated duplex thermocouple type K of 5mm diameter (as shown in Figure 3.11) was used to measure temperature at the heater and soil interface. The Duplex thermocouple has two outputs, one output is connected to the datalogger and another output goes to the temperature controller. The thermocouple is installed through the hole in the centre of the heater. The Viton O-ring fitted to the thermocouple and brass compression fitting was used for installation through the heater to ensure water tightness.

3.7.1.3   Welded tip teflon thermocouple

A welded tip teflon thermocouple type K (as shown in Figure 3.11) was used to measure temperature at top surface of the soil sample. It has 0.2 mm diameter twisted pair leads insulated with teflon and an operating range of -75 °C to +250 °C. This thermocouple has been installed on either the porous or solid steel plate, depending on whether a T or a TH test was being undertaken, in the interconnecting ring using epoxy resin as shown in Figure 3.11.

3.7.2   Relative humidity measurement

Relative humidity is the percentage ratio of actual amount of water vapour in the air to the saturated amount of water vapour the air can hold, in other words it is the percentage ratio of actual vapour pressure to saturated vapour pressure. Relative humidity is an important property and can be related to suction by the following equation proposed by Edlefsen and Anderson (1943):

$$h = \exp\left(\frac{\psi g}{R_v T}\right)$$ (3.1)

where h is the relative humidity, g is the gravitational constant, ψ is the capillary potential, R_v is the specific gas constant and T is the temperature.

Relative humidity could be measured by various methods and instruments like hygrometer and psychrometer but for the present study relative humidity probes were used because of their small size and advanced electronic technology. The relative humidity probes used in the present study have a capacitive electronic chip that sense water by applying an AC (alternating current) signal between two plates and measuring the change in capacitance caused by the amount of water vapour present. The following section discusses the relative humidity probe in detail.

3.7.2.1   Relative humidity probe

Hygroclip SC 05 relative humidity probes (as shown in Figure 3.12) have been used to measure relative humidity and temperature within the soil sample. These probes are supplied by Rotronic Instruments (UK) Ltd. The probe is made of a perforated stainless steel tube and it has a diameter of 5 mm and 52 mm length with 2 m long cable. The length of the probe was increased with an additional stainless steel tube. The probe can measure temperature from -40 °C to 100 °C and relative humidity from 0 to 100 %. The probe is very sensitive and its sensor is protected by a PTFE sleeve. The probes were calibrated by the manufacturer against chilled mirror hygrometer. A Hydrolog NT3 datalogger (shown in Figure 3.12) was used to collect data from the probes. This datalogger can directly take three probes at any time but also has a docking station, which has four additional access points for the probes. The datalogger is connected to a standard PC via a USB cable to allow data transfer and storage. A proprietary software package, HW4, is used to interact with the datalogger and store the observation data.

3.7.3   Pressure transducer

A miniature pressure transducer PS-20KB M260 has been employed to measure swelling pressure in TH tests. It is a strain gauge based transducer that converts pressure into an analog electronic signal. It consists of strain gauges bonded into the elastic diaphragm and wired into a wheatstone bridge configuration. Pressure applied to the pressure transducer produces a deformation of the elastic diaphragm which introduces strain to the gauges. The strain produces an electrical resistance change which changes the wheatstone bridge output voltage proportional to the pressure. The bridge output voltage is picked by datalogger and converted into the pressure by the following equation:

$$\text{Pressure (MPa)} = \frac{\text{Bridge output voltage (mV)} \times \text{Capacity (MPa)}}{\text{Bridge excitation voltage (V)} \times \text{Rated output voltage (mV/V)}} \quad (3.2)$$

where capacity of the pressure transducer is 2 MPa, bridge excitation voltage is 3 V and rated output voltage is 0.892 mV/V.

The pressure transducer has a maximum pressure capacity of 2 MPa that was selected on the basis of swelling pressure test conducted on the soil sample detailed in the next chapter. It is made by Kyowa Electronic Instruments Co. Ltd. and supplied by Sensors UK Ltd. It has a base diameter of 6 mm and mass of 0.5 g. The technical specifications are given in Table 3.6. The transducer is installed in the centre of the porous stainless steel disc as shown in Figure 3.5.

3.7.4   Data acquisition

As the tests are expected to be performed over a long duration, it will produce large quantities of transient data. Therefore, an automated data acquisition system is required. This has been achieved via a datalogging system consisting of junction box panels, amplifier rack, dataloggers and personal computer, which are placed on a mobile trolley. Figure 3.13 shows the front view of datalogger trolley with thermocouple sockets, junction box panel, two junction boxes and computer.

Two junction boxes are connected to two junction box panels respectively. Each junction box provides eight 5-pin DIN input locations for sensors. Pressure transducer and volume change measurement sensors were connected to the junction box. The junction box panel regulates the required excitation voltage for sensors connected to the junction box. The junction box panels are connected to a CR7 datalogger via an amplifier.

A CR7 datalogger was used to collect the data from temperature sensors, volume measurement sensor and pressure transducer. This datalogger was supplied by Campbell Scientific Ltd UK. The CR7 datalogger has a processor card and 7 slots for I/O cards namely; analogue input card (723), analogue input card with thermocouple (723-T), pulse counter card (724), excitation card (725), 50 volt analogue input card (726). The CR7 must be programmed before it makes any measurements. A program is created by keying it directly into the datalogger or on a personal computer using the PC208/PC208W datalogger support software program EDLOG. A hydrolog NT3 datalogger was used to collect readings from relative humidity probes. The flow diagram of data acquisition system is shown in Figure 3.14.

3.8   Testing of integrity/calibration of TH-cell

Whenever a new apparatus is designed and fabricated, the first step is to test its integrity and calibrate it. The strength of TH cell was tested under fluid pressure of 1.5 MPa to ensure the safety of the operator and equipment. Trial TH tests were then conducted to observe any faults and leaks during operation. During the trial tests, the heater temperature was varied from 0 °C to 110 °C; the temperature controller controlled the targeted temperature of the heater very precisely within ± 0.25 °C. The PTFE sleeve of the central section was softened and deformed slightly at higher temperature (110 °C) in the long run trial test of 30 days. The temperature and relative humidity probes, thermocouples and pressure transducer were tested in-situ with datalogger. It was observed that pressure transducer was not recording the response of swelling pressure smoothly because of its miniature size.

Apart from the small glitches mentioned above, it was found that new apparatus was working well and meeting all the design criteria stated in section 3.4. The following working limits of the apparatus were identified and can be summarised as:

- Maximum working temperature is 100 °C.

- Maximum swelling pressure measurement is 2 MPa.

- Maximum allowable water pressure is 1.5 MPa.

- Safe design pressure is 3.5 MPa.

3.9 Methodology developed

An experimental methodology was developed to carry out experiments efficiently. The following sections discuss the important steps including sample preparation, compaction technique, assembling and dismantling of the TH cell, sample sectioning and chemical analysis.

3.9.1 Sample preparation

The clays were dried for 24 hours in oven at 105 °C. Then, deionised water was mixed with dry soil by using a sprinkling bottle to ensure uniform moisture distribution. Then wet soil was mixed again thoroughly in a mechanical mixture for 5 minutes shown in Figure 3.15. The moist soil was then sieved through 1.18 mm sieve and kept in an air tight container in a temperature controlled laboratory for a day to achieve moisture equilibrium. Sivakumar and Wheeler (2000) suggested a similar method of mixing.

3.9.2   Compaction technique

The two options were considered to compact soil sample where either inside or outside the TH cell. Many of the researchers (for example Gatabin and Billaud, 2005; Villar et al., 2005) compacted the soil sample outside the test cell and then inserted the compacted sample into the test cell which resulted in disturbed and loose sample. In the present study the soil was compacted in the central section of the TH cell which results in good intimate contact of the undisturbed soil sample with the cell wall.

The three samples were taken from three different locations to measure initial moisture content of the soil in the air tight container to check uniformity of moisture distribution. The empty weight of the central section of the TH cell was measured on an electronic balance with an accuracy of 0.01 g. The compaction technique was established to achieve uniform density and homogeneous compacted sample. There were many trials attempted which are detailed in the compaction characteristic section of chapter 4. The static compaction method was finally selected in which the sample was compacted in 10 layers into the central section of the TH cell and each layer was compressed under a static load of 90 kN with a loading and unloading rate of 1.5 kN/s. A compaction mould, mentioned in section 3.6.5, was designed to allow compaction of the soil samples in the central section of the TH cell. After the compaction, the collar was removed and the excessive soil was trimmed off and levelled. The spacer was pulled out by screwing a rod into a hole provided at the bottom of the spacer. The resulting soil sample has diameter of 100 mm and height of 100 mm. The spacer leaves a space to be used for the heater and the PTFE disc. The weight of compacted sample with the central section of the TH cell was measured to find the overall initial dry density of compacted soil sample.

3.9.3   Assembling and test set up

The test set up depends upon type of test to be performed. After compaction the heater is pushed into the TH cell by keeping the central hole of the heater open so air can escape during insertion. Then, the duplex thermocouple is screwed in the central hole of the heater through air and vapour tight 1/4 inch BSP brass compression fitting. The PTFE

disc is pushed in afterwards which provides insulation at bottom of the heater and also allows heater power cables and duplex thermocouple cables to pass through. Then, the central section is placed on the bottom section of the TH cell. Depending upon the type of test, the interconnecting ring with solid plate or porous plate was placed on the central section. The solid plate fitted with O-ring on the edge is used for the thermal test to prevent moisture move out of the soil sample and the porous plate is used for thermo-hydraulic and isothermal tests to let water into the soil sample. The top section was then placed on the interconnecting ring and all the components were screwed tightly with five tie rods and nuts.

The holes were drilled with an automatic drill in the soil sample to install the temperature and relative humidity probes. The holes were drilled up to the centre of the soil sample and at the diameter required by the particular sensor to be placed. The heater was connected to temperature controller via the duplex thermocouple feed. The thermocouple and pressure transducer were installed in the top section. The relative humidity probes, thermocouples and pressure transducer were connected to data acquisition system which consisted of the datalogger and the personal computer. The top section was filled with deionised and de-aired water and connected to heat-refrigerated circulator. In the case of TH and isothermal tests, the top section was fed by pressurised deionised and de-aired water supply under 0.6 MPa pressure. The experiment was started by switching the heater and heat-refrigerated unit on.

3.9.4   Dismantling

After finishing the experiment, the TH cell is dismantled following the reverse order of assembling the components described above. First of all, the data is saved in the hard drive of personal computer and then the probes are disconnected from the datalogger and removed them from the cell one by one. The top section is then removed followed by interconnecting ring and central section. The soil sample and heater are extruded by mounting the central section on the hydraulic extruder so that the hydraulic piston could jack on the upstream end of the sample as shown in Figure 3.10. The extruded soil

sample was immediately placed into a plastic container to prevent moisture loss before the sample was sectioned into slices.

3.9.5   Sample sectioning

The soil sample was sectioned into 10 slices each of 10 mm thickness as soon as practicably possible after extrusion; this was typically no more than 30 minutes. Various methods were considered and tried for sectioning including hand saw, automatic machine saw, and cheese wire. The saw cutting gave a uniform thickness of slices but a lot of soil was lost during the cutting. The cheese wire was difficult to keep straight that resulted in non uniform thickness of slices. Eventually, it was found that use of a sharp spatula was the optimum method to cut the sample successfully. The thickness of each slice was measured at six points and the average thickness calculated. Then the slices were weighed and then oven dried.

3.9.6   Sample drying and storage

The soil sample slices were kept in the oven at 105 °C for 24 hours to determine the moisture content, dry density, degree of saturation and void ratio. The slices were then put inside airtight container and stored in a steel box in a humidity and temperature controlled environment.

3.9.7   Chemical analysis

The stored slices were later used for chemical analysis. The objective of chemical analyses was to find concentration of anions (negative ions) and cations (positive ions) present in the each slice of the soil sample. The following method was used to prepare the sample solution for anion and cation determination.

1- The slices were crushed to very fine powder by mortar and pestle. The mortar and pestle was cleaned by sand paper after crushing each and every slice to stop cross contamination between slices.

2- 2 g of soil sample was taken from the powder of crushed slice and diluted with 40 ml deionised water that gives a solid and water ratio of 1:20, in a 50 ml polypropylene centrifuge tube. US EPA 1312: 1994 recommends a soil and deionised water ratio of 1:20. The soil sample should be added slowly in the deionised water to stop soil clogging.

3- The sample solution in centrifuge tube was rotated on an end over end (tumbling) rotating agitator at 30 rpm for 23 hours (US EPA 1312: 1994).

4- The sample was then centrifuged at 3000 rpm until the solid part get precipitated at the bottom of the centrifuge tube. Non-swelling clays take about 5 minutes to precipitate but the highly swelling clays take about 60 minutes or more. The supernatant is then transferred into another 50 ml Whatman VectaSpin 20 centrifuge tube filter consisting of a 0.45 μm filter insert and outer tube with a screw-on cap.

5- The supernatant in centrifuge tube filter is then again centrifuged at 3000 rpm until enough liquid about 10 ml filtered through the filter insert and collected at the bottom of the centrifuge tube filter. Again highly swelling clays need more time (approximately 60 minutes or more) compared to other soils.

6- The filtered solution collected at the bottom of the centrifuge tube filter was sent for anion and cation determination as described below.

3.9.7.1   Anion determination using IC

Anion concentration was determined by ion chromatography (IC) also known as ion-exchange chromatography. The chromatography is a separation technique of components

in a mixture dissolved in a mobile phase passing through a stationary phase which separates the analyte to be measured. The IC is a column chromatography pioneered by Small et al (1975) which uses the principles of ion exchange and allows electrical conductance to be used for the identification and quantitative determination of ions at low levels after their separation.

The anion version of Dionex DX-80 Ion Analyser was used in this present study. It consists of a liquid eluent (mobile phase), high pressure pump, liquid injector, guard column, separator column (stationary phase), chemical suppressor, conductivity cell and data analysis system as shown in Figure 3.16. The eluent is a mobile liquid that carries the sample through the ion analyser. The eluent is made up of 0.6 mole sodium carbonate (Na_2CO_3) and 0.2 mole of sodium bicarbonate ($NaHCO_3$) diluted in deionised water to make 2 litres. A high pressure pump pushes the eluent and sample through the guard and separator column. The liquid sample is injected into the eluent stream through sample loop either manually or automatically. The guard column prevents the poisoning of the separator column by absorbing contaminants and particulates. The separator column is a chemically inert tube packed with a polymeric resin where the different sample ions migrate at different rate, depending upon their interaction with ion exchange sites. The suppressor acts to suppress the conductivity of the eluent that enhances the detection of the sample ions. A regenerant, a dilute 2 N sulphuric acid (H_2SO_4), is used to convert the suppressor back to its original form. The conductivity cell measures the conductance of the sample ion and produces the signal based upon chemical and physical property of the analyte (sample ion). After the conductivity cell, the eluent and sample ion go to the waste bottle. The data analysis system consists of a computer and a chromatography software programme, Peak Net IA, analyses the signal received from the conductivity cell by comparing the peaks in chromatogram to those produced by a standard solution during calibration. The results are displayed as a chromatogram. The ions are identified by their retention time and quantified by integrating the peak area of chromatogram.

In this study, the following steps were used to determine seven anions fluoride (F^-), chloride (Cl^-), nitrite (NO_2^-), bromide (Br^-), nitrate (NO_3^-), phosphate (PO_4^{3-}) and sulphate (SO_4^{2-}) present in the each soil slice:

1- In the beginning, the DX-80 Ion Analyser was calibrated with the Seven Anion Standard II as described in Table 3.7. The standard is the product of the Dionex the manufacturer of the DX-80 Ion Analyser.

2- The filtered solution of the each slice of the soil sample was filled into the 5 ml vial. Then the vial top was closed by the filter cap and placed in the automated sampler of the Dionex DX-80 Ion Analyser. The liquid sample was injected into the eluent stream automatically. The ion analyser identified and quantified the anions present in the solution, and thereby present in the soil slice by comparing the data obtained after calibration from the Seven Anion Standard II.

3.9.7.2   Cation determination using ICP-MS

Inductively coupled plasma mass spectroscopy (ICP-MS) was developed in the 1980 to combine the ICP technology that produces ions with the separation and detection technology of a mass spectrometer. The resulting instrument is capable of detecting multiple trace elements at the parts per trillion level. The ICP-MS has four main processes, sample introduction and aerosol generation, ionisation by an argon plasma source, mass discrimination, and detection system. The schematic diagram in Figure 3.17 illustrates the sequence of processes. The sample can be introduced in ICP-MS as solid or liquid form. The solid samples are introduced by a laser abalation system while liquid samples are introduced by a nebulizer which aspirates the sample with high velocity argon. The nebulizer generates the small droplets so they can be easily vaporised in the plasma torch. The high temperature (10,000K) argon plasma atomized (break into atoms) and ionised (atom loses electron) the droplets of the nebulised sample. The ions now enter into the mass spectrometer (MS) where they are removed from plasma by a quadrupole mass filter on the basis of their mass to charge ratio. The detector receives an ion signal proportional to the concentration. The concentration of ion is determined through calibration with elemental standards.

In this study cations including sodium (Na^+), magnesium (Mg^{2+}), aluminium (Al^{3+}), silicon (Si^{4+}), phosphorous (P^{4+}), potassium (K^+), calcium (Ca^{2+}) and iron (Fe^{3+}) concentrations present in soil slices were determined by the following steps:

1- The ICP-MS was calibrated by elemental standards.

2- 1 ml of the filtered solution of the each slice of the soil sample was mixed with 1ml of 10% nitric acid (HNO_3) and 8 ml of deionised water in the conical plastic tubes. The nitric acid preserves the sample for longer time and keeps the ions suspended in the solution (US EPA 1312: 1994). The tubes then placed in an automated sampler of ICP-MS that detects and quantifies the concentration of cations present by comparing the data obtained from standards.

3.10 Conclusions

This chapter has reported the successful design, fabrication and calibration of the three new TH cells with each of the defined design criteria met. Furthermore the accessories and sensors work in conjunction with the new cells. The new cell is capable of measuring the transient temperature, relative humidity and swelling pressure. It also facilitates the determination of moisture content, dry density and chemical composition of the soil samples at the end of the tests. However, safety constraints limit the maximum cell temperature 100 °C and working pressure 1.5 MPa.

The experimental approach was developed and defined that includes the soil preparation, compaction, assembling, dismantling, sectioning, and various soil properties determination with chemical composition. Also an experimental methodology has been developed to perform the thermal, thermo-hydraulic and isothermal tests. The trial tests included thermal and thermo-hydraulic tests calibration of the test cell and verification of the new experimental approach.

3.11 References

Campbell Scientific Inc. (1997). CR7 measurement and control system instruction manual.

Collin, F., Li, X.L., Radu, J.P. and Charlier, R. (2002). Thermo-hydro-mechanical coupling in clay barriers. Engineering Geology, 64, 179-193.

Cuevas, J., Villar, M., Martyn, M., Cobena, J.C. and Leguey, S. (2002). Thermo-hydraulic gradients on bentonite: distribution of soluble salts, microstructure and modification of the hydraulic and mechanical behaviour. Applied Clay Science, 22, 25–38.

Dionex Corp. (2002). DX-80 ion analyser operator's manual. Document No. 031675, Revision 02.

Edlefsen, N.E., and Andersen, A.B.C. (1943). Thermodynamics of soil moisture. Hiigardia, 15, No. 2, 31-298.

Ewen, J. and Thomas, H.R. (1989). Heating unsaturated medium sand. Geotechnique 39, No. 3, 455-470.

Gatabin, C. and Billaud, P. (2005). Bentonite THM mock up experiments. Sensors data report. CEA, Report NT-DPC/SCCME 05-300-A, Cedex.

Mohamed, A.M.O., Yong, R.N. and Kjartanson, B. (1993). Temperature and moisture distributions in a clay based buffer material due to thermal gradients. Mat. Res. Soc. Symp. Proc., 294, 417-424.

Pintado, X., Ledesma, A. and Loret, A. (2002). Backanalysis of thermohydraulic bentonite properties from laboratory tests. Engineering Geology, 64, 91-115.

Sivakumar, V. and Wheeler, S.J. (2000). Influence of compaction procedure on the mechanical behaviour of an unsaturated compacted clay. Part 1: Wetting and isotropic compression. Geotechnique 50, No. 4, 359-368.

Small, H., Stevens, T.S. and Bauman, W.C. (1975). Novel ion exchange chromatographic method using conductimetric detection. Anal. Chem. 47 (11), 1801-1809.

US EPA (United States Environmental Protection Agency) 1312 (1994). Test method for evaluating solid waste, physical/chemical methods (SW-846), 3rd edition, update 2B. EPA, National Centre for Environmental Publications, Cincinnati.

Villar, M.V., Martin, P.L. and Barcala, J.M. (2005). Infiltration tests at isothermal conditions and under thermal gradient. CIEMAT Technical report CIEMAT/DMA/M2140/1/05 Madrid.

Yong, R.N., Mohamed, A.M.O., Shooshapasha, I., and Onofrei, C. (1997). Hydro-thermal performance of unsaturated bentonite-sand buffer material. Engineering Geology, 47, 93-108.

Table 3.1 Testing programme
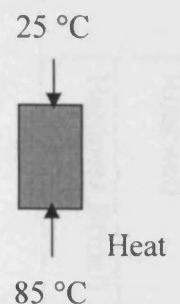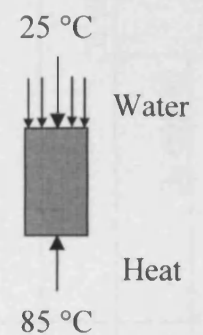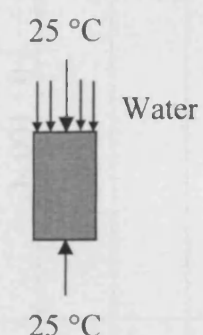
Type of test	Thermal gradient test (T-test)		Thermo-hydraulic gradient (TH-test)		Isothermal test	
	25 °C ↓ [heated block] ↑ Heat 85 °C		25 °C ↓↓↓↓ Water [block] ↑ Heat 85 °C		25 °C ↓↓↓↓ Water [block] ↑ 25 °C	
Initial water content (%)	Dry	Wet	Dry	Wet	Dry	Wet
Initial degree of saturation (%)	Lower	Higher	Lower	Higher	Lower	Higher
Experiment duration (Days)	1, 2, 3, 4, 5, 7, 10, 15 & 30	1, 2, 3, 4, 5, 7, 10, 15 & 30	1, 2, 3, 4, 5, 7, 10, 15 & 30	1, 2, 3, 4, 5, 7, 10, 15 & 30	30	30

Table 3.2 Physical and mechanical properties of stainless steel 316L

Property		Units	Value
Density		Kg/m^3	8000
Elastic modulus		GPa	193
Mean coefficient of thermal expansion	0 - 100 °C	μm/m/°C	15.9
	0 - 315 °C	μm/m/°C	16.2
	0 - 538 °C	μm/m/°C	17.5
Thermal conductivity	@ 100 °C	W/mK	16.3
	@ 500 °C	W/mK	21.5
Specific heat @ 0 - 100 °C		J/kgK	500
Electric resistivity		nΩm	740
Tensile strength		MPa	485
Yield strength 0.2 % proof stress		MPa	170
Elongation (% in 50 mm)		%	40
Hardness	Rockwell	HR B	95
	Hardness Brinell	HB	217

Table 3.3 Engineering properties of PTFE (provided by RS Ltd UK)

Property		Units	Value
Density		Mg/m^3	2.18
Tensile strength at yield		MPa	25
Elongation at break		%	500
Modulus of elasticity after tensile test		MPa	700
Hardness	Rockwell	-	M105
	Shore D	-	70
Melting point		°C	327
Max. service temperature long term		°C	260
Max. service temperature short term		°C	260
Min. service temperature		°C	-260
Thermal conductivity (23 °C)		W/Km	0.25
Specific heat (23 °C)		J/gK	1
Coefficient of thermal expansion (23 °C)		$10^{-5} K^{-1}$	12
Dielectric strength		KV/mm	48
Volume resistance		Ωcm	10^{18}

Table 3.4 Properties of Superwool 607 Max Blanket

Property		Units	Value
Density		Kg/m^3	128
Continuous temperature use limit		°C	1000
Classification temperature rating		°C	1260
Melting point		°C	1499
Thickness		mm	6.25 - 50
Width		mm	600, 1200
Length		m	4.5 - 7.5
Linear shrinkage (@ 1250 °C)		%	< 2
Specific heat (@ 1090 °C)		kJ/gK	1.13
Thermal conductivity	@ 260 °C	W/mK	0.08
	@ 538 °C	W/mK	0.13
	@ 816 °C	W/mK	0.22
	@ 982 °C	W/mK	0.28
Chemical composition	Silica, SiO$_2$	%	60 - 70
	Calcium oxide, CaO	%	16 - 22
	Magnesium oxide, MgO	%	12 - 19
	Alumina, Al$_2$O$_3$	%	trace

Table 3.5 Technical specification of the heat-refrigerated circulator

Specification	Units	Value
Temperature range	°C	-10 to +100
Temperature accuracy	°C	±0.02
Heater capacity	W	1500
Cooling capacity @ 20 °C	w	240
Pump pressure	mbar	300
Pump flow rate	L/min	15
Bath volume	L	3
Dimensions (w x d x h)	mm x mm x mm	195 x 360 x 540
Electric supply	V	-230
Electric supply	Hz	50/60

Table 3.6 Technical specification of miniature pressure transducer

Property	Units	Value
Rated capacity	MPa	2
Rate output (.002 strain)	mV/V	1 ± 20 %
Non-linearity	% RO	± 1
Hysteresis	% RO	± 1
Recommended excitation voltage (AC or DC)	V	1~2
Safe excitation voltage (AC or DC)	V	3
Bridge resistance	Ω	120 ± 10 %
Safe temperature range	°C	- 20 ~ 70
Thermal effect on balance	% RO/ °C	± 0.2
Thermal effect on output	± % / °C	0.2
Safe overloading rate	%	150

Table 3.7 Seven anion standard II

Components	Concentration	
	Labelled (mg/l)	Measured (mg/l)
Fluoride	20	20.1
Chloride	100	102
Nitrite	100	101
Bromide	100	100
Nitrate	100	100
Phosphate	200	200
Sulphate	100	99.4
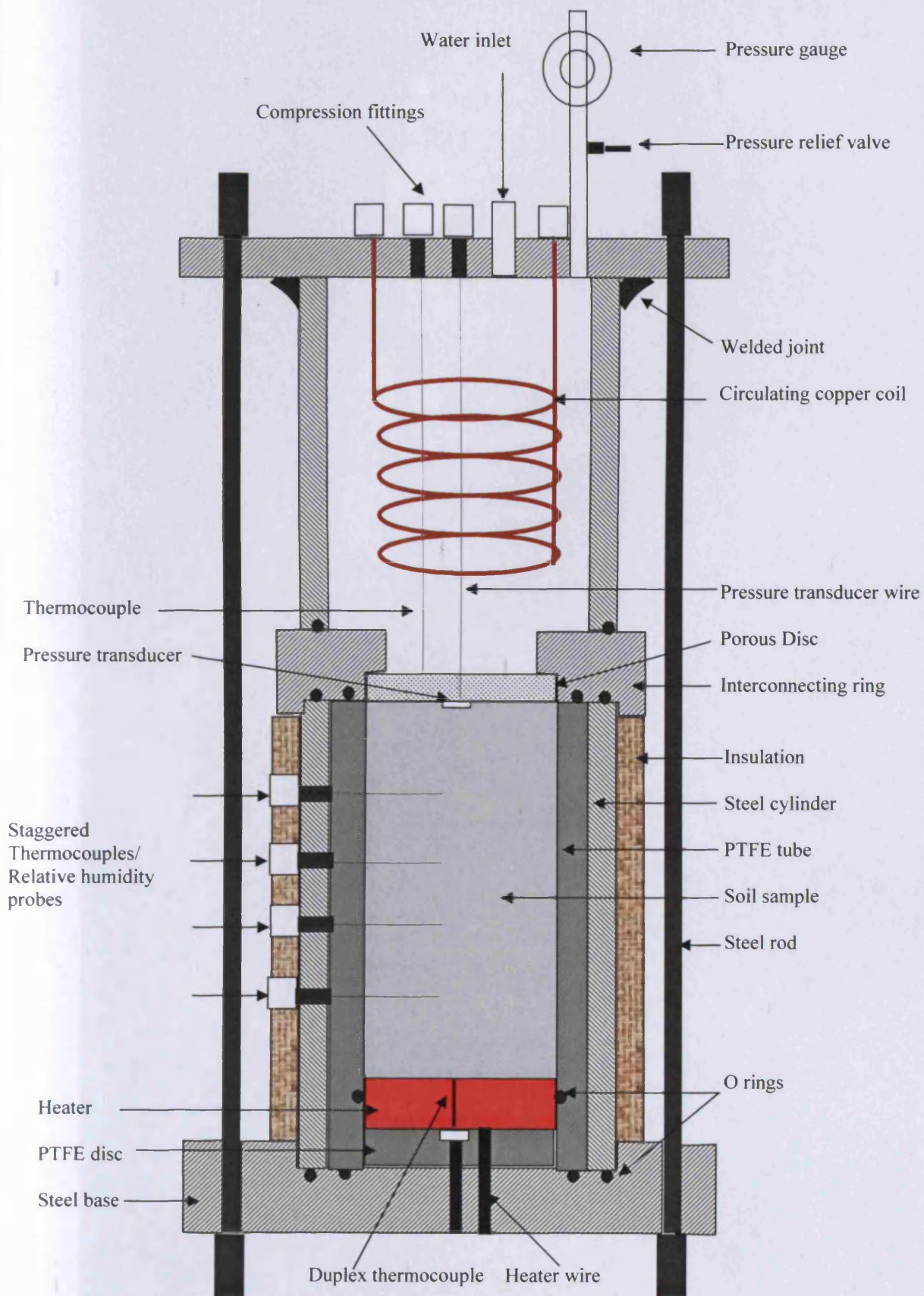
Figure 3.1 Schematic diagram of Thermo-Hydraulic cell
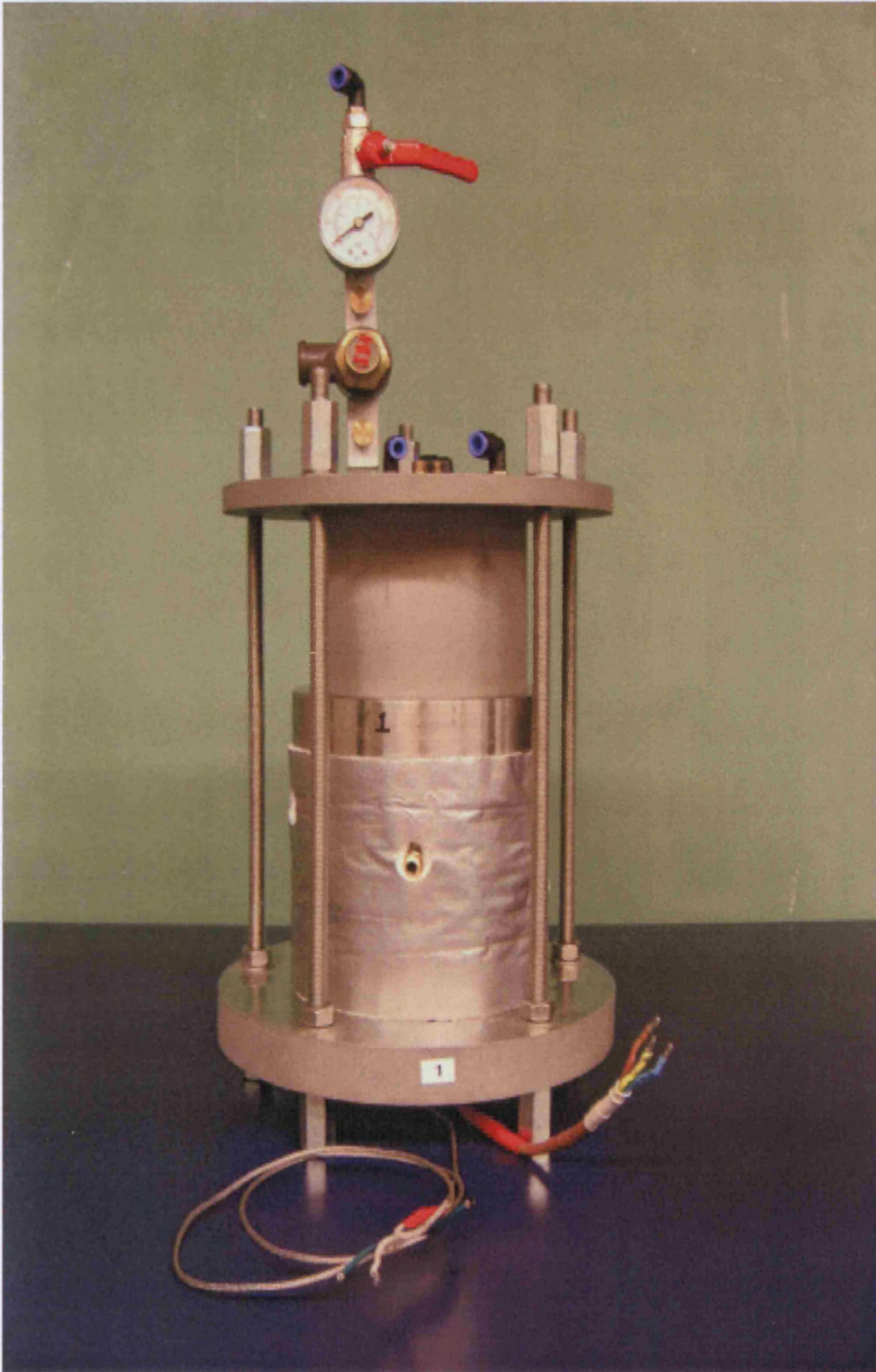
Figure 3.2 Assembled Thermo-hydraulic cell
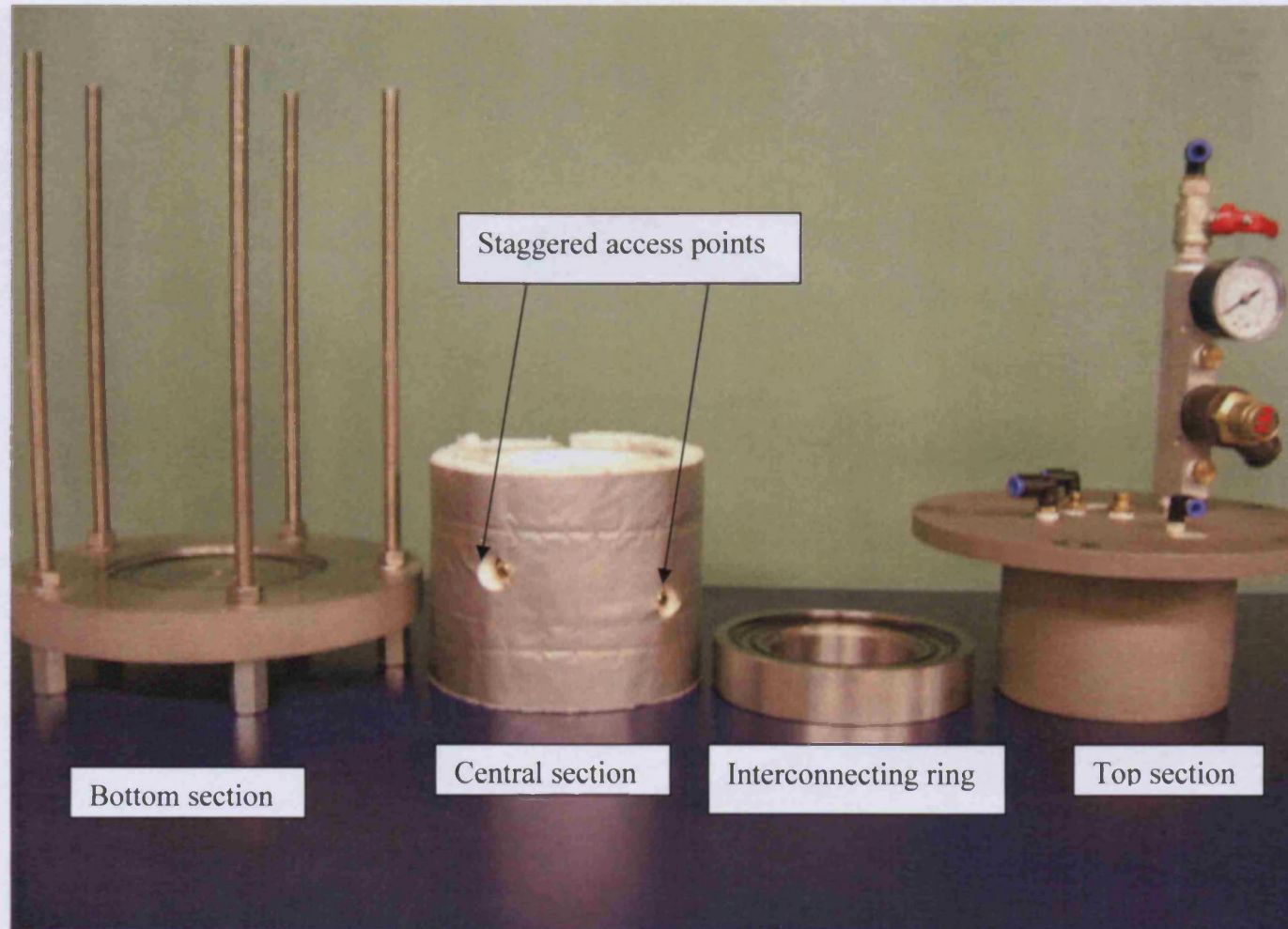
Figure 3.3 Individual components of thermo-hydraulic cell
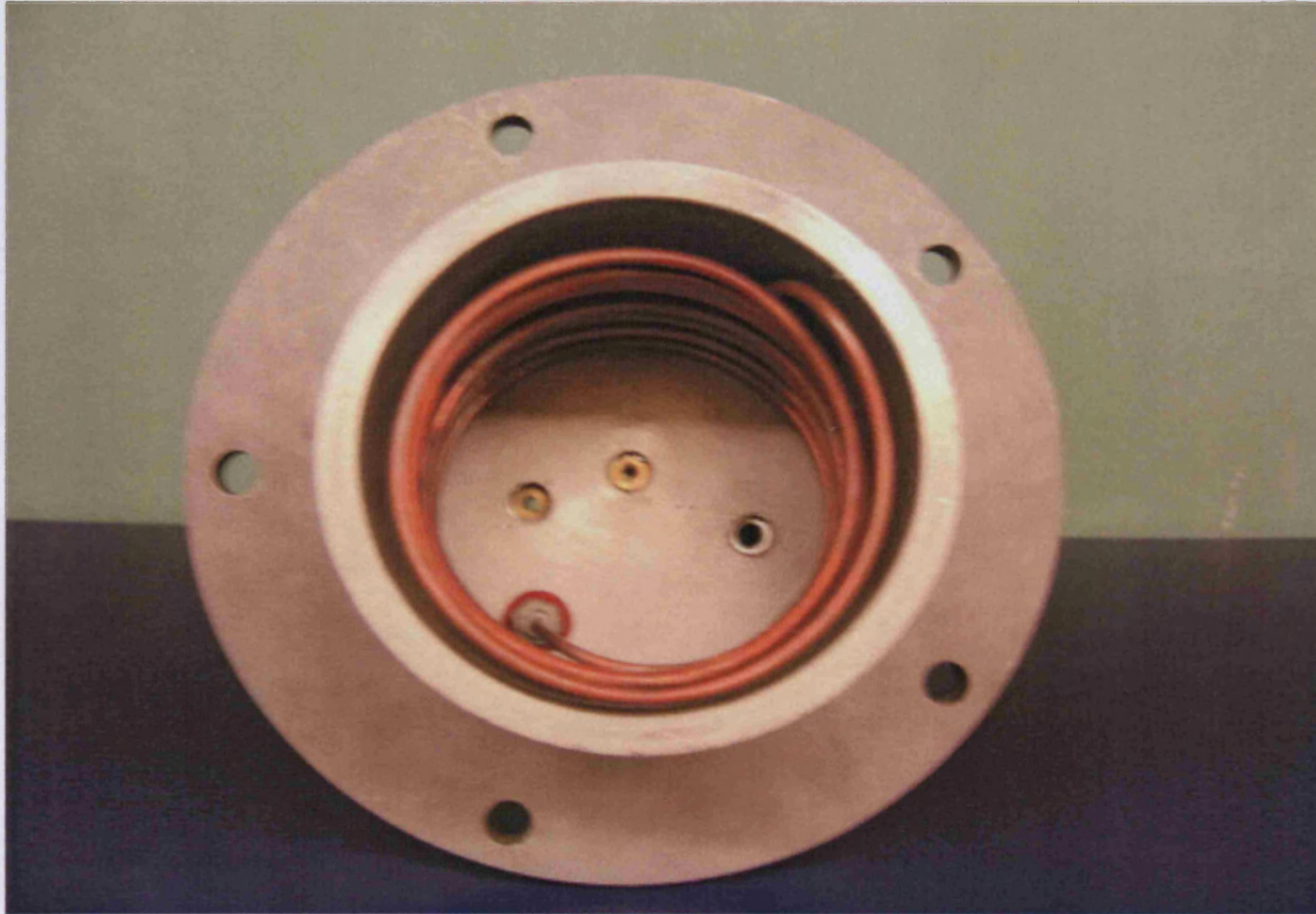
Figure 3.4 Inside view of top section
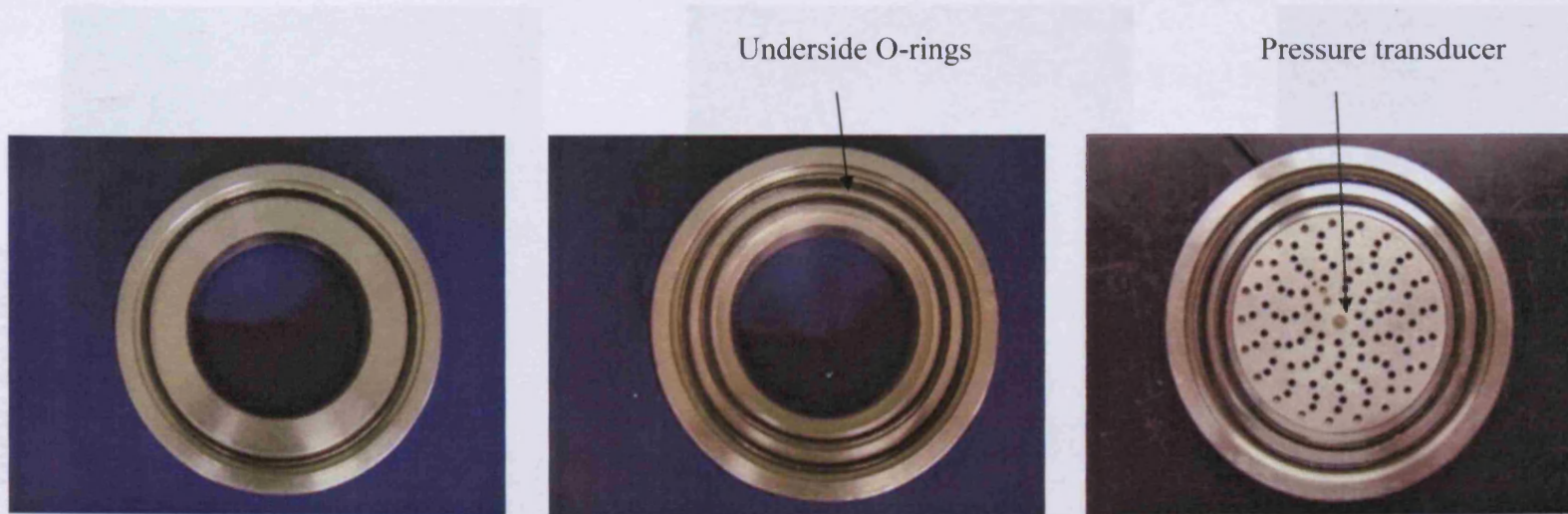
Figure 3.5 Interconnecting ring
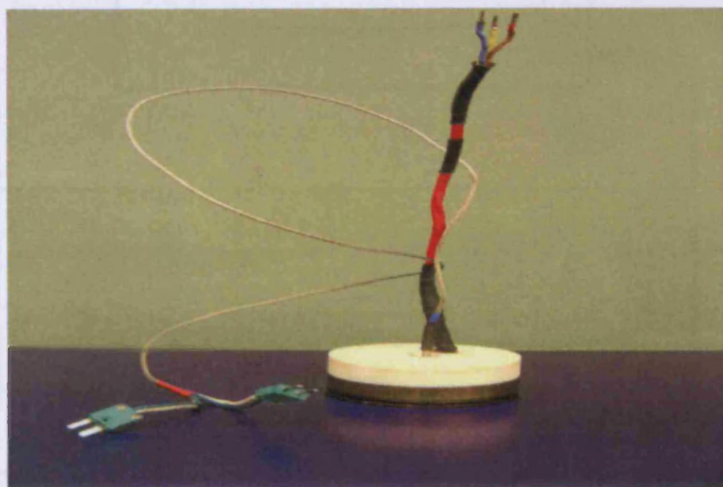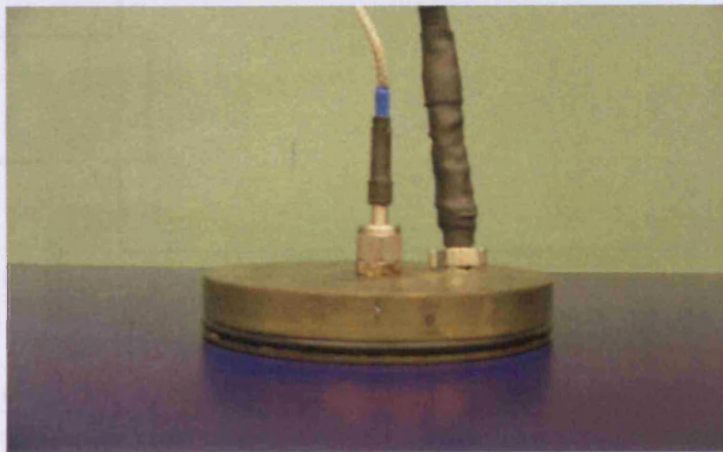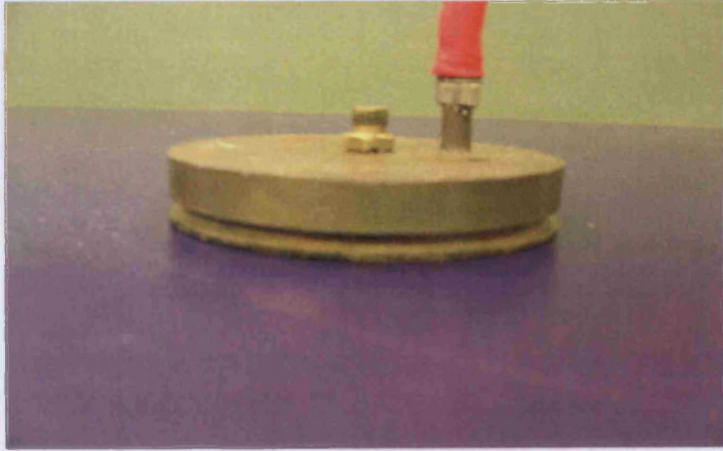
Figure 3.6 Heater
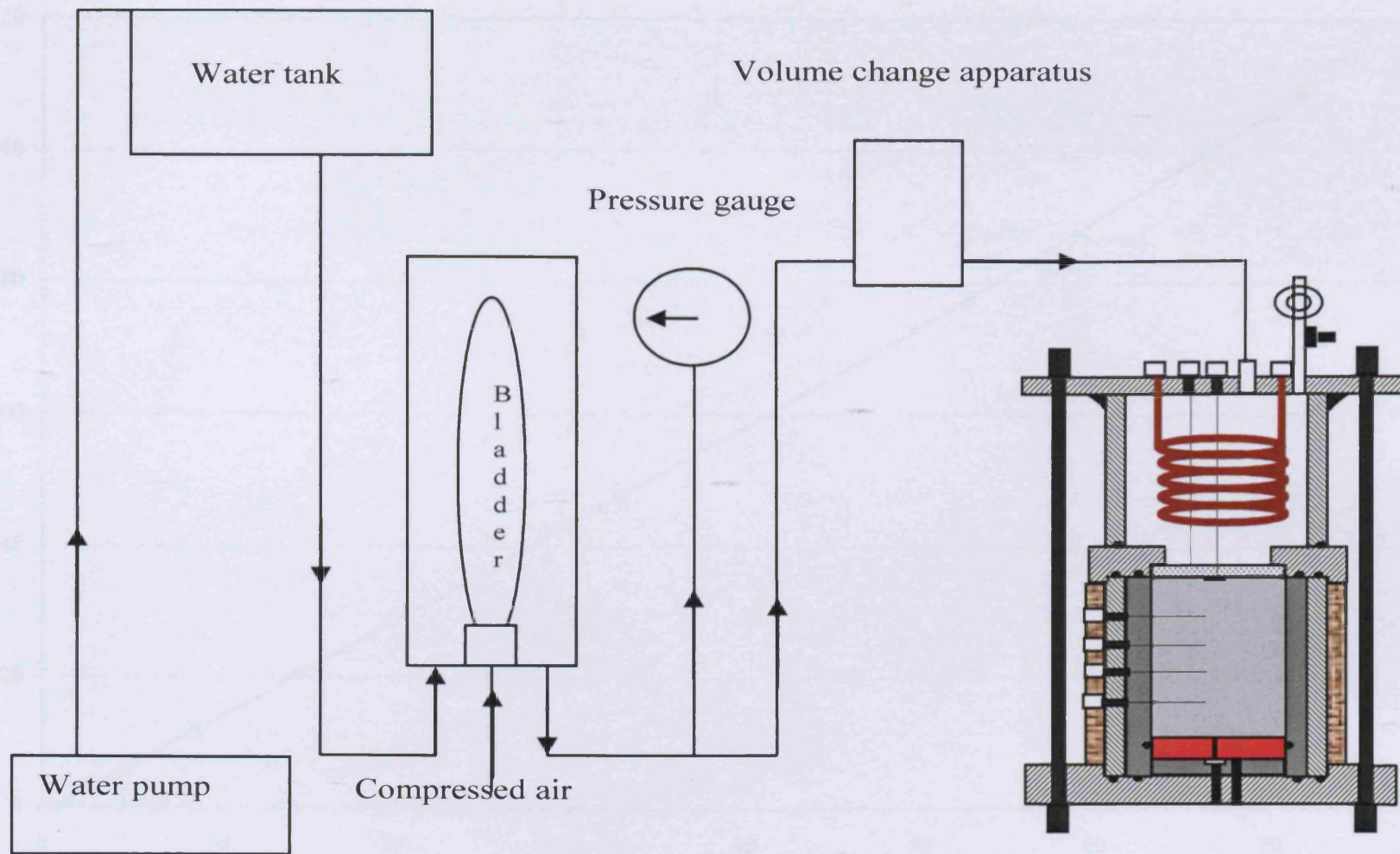
Figure 3.7 Pressurised water supply to TH-cell
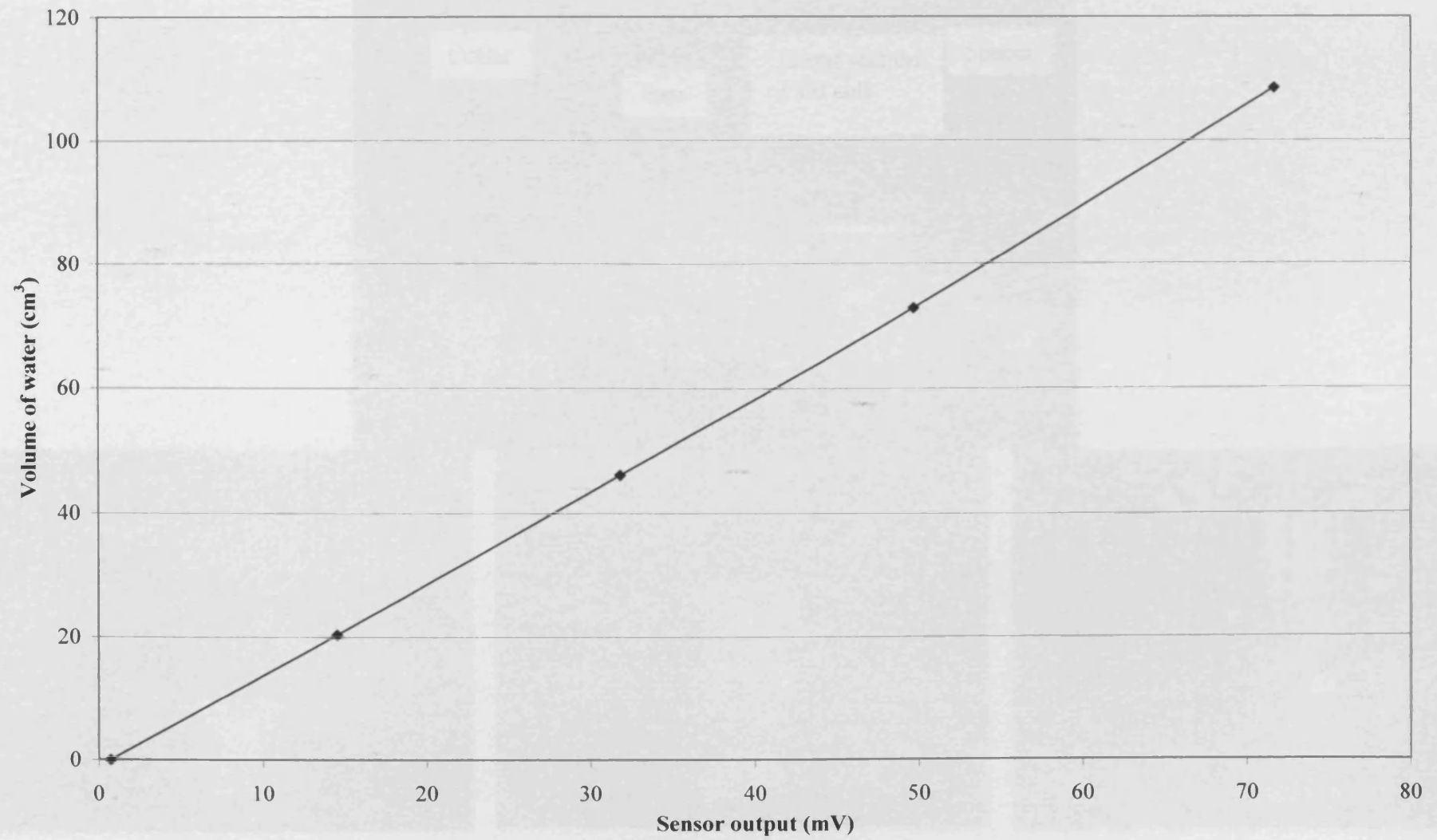
Figure 3.8 Calibration curve for volume change apparatus
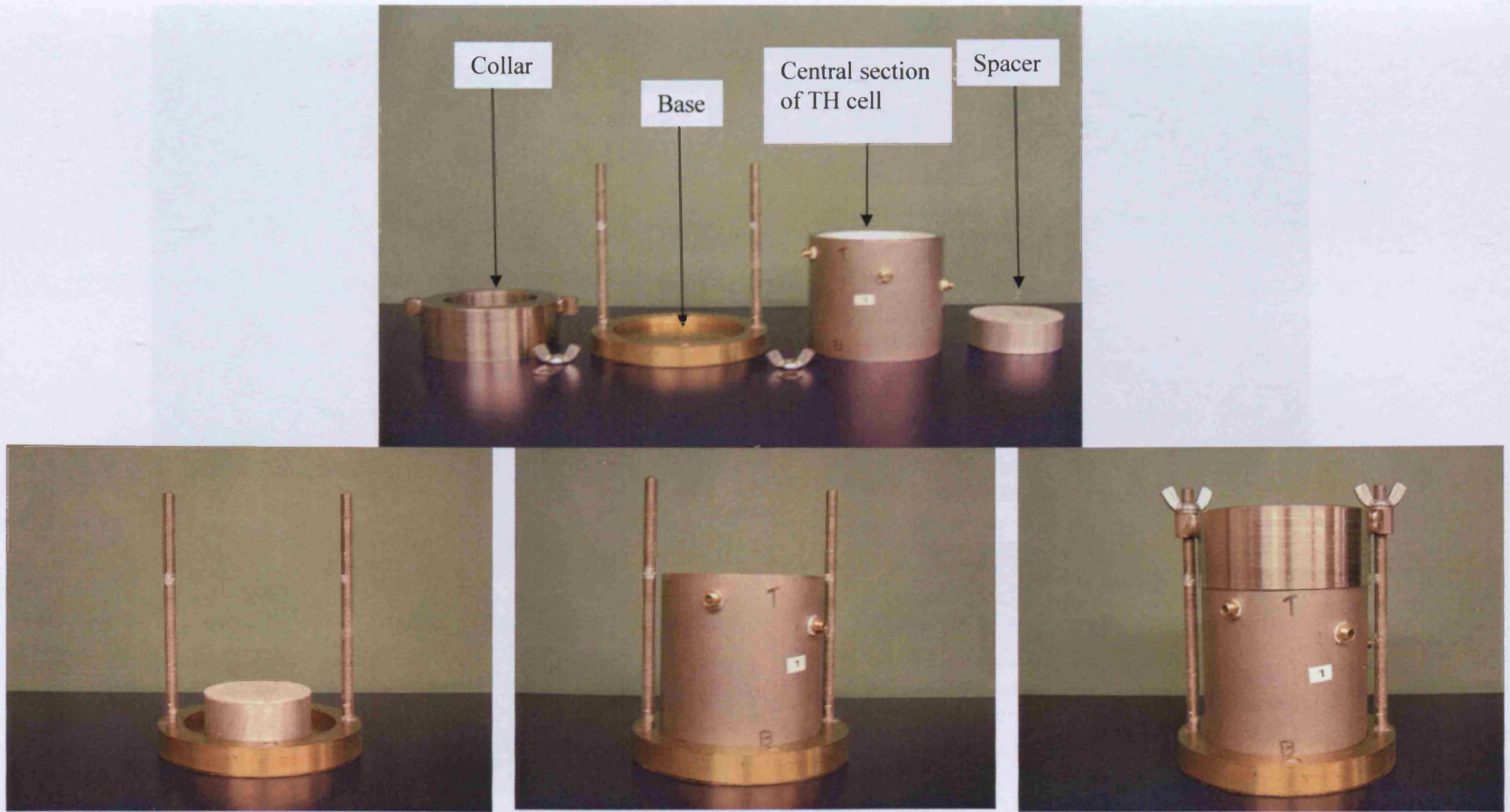
Figure 3.9 Compaction mould and its assembling
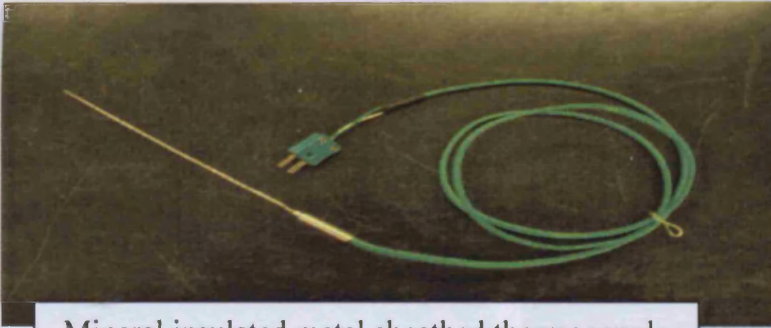
Reaction plate

Metal frame

Extruder plate

Cell support platen

Hydraulic jack

Hand lever

Base plate

Pressure release valve

Figure 3.10 Extruder

Mineral insulated metal sheathed thermocouple
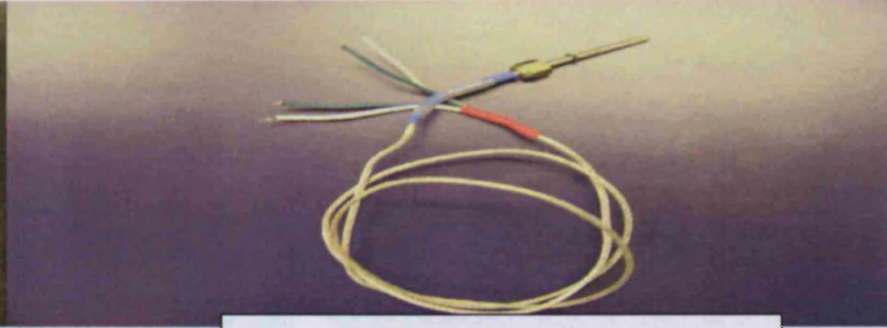
Mineral insulated duplex thermocouple
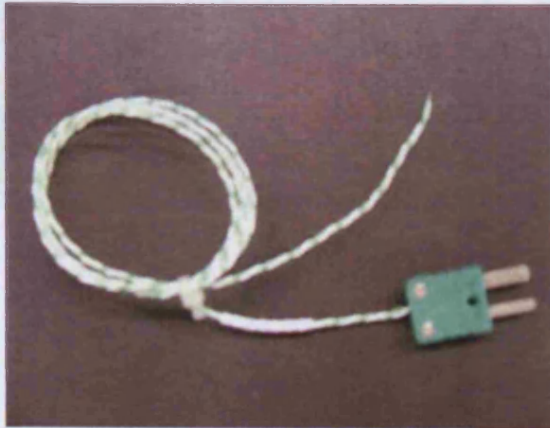
Welded tip teflon thermocouple

Figure 3.11 Thermocouples
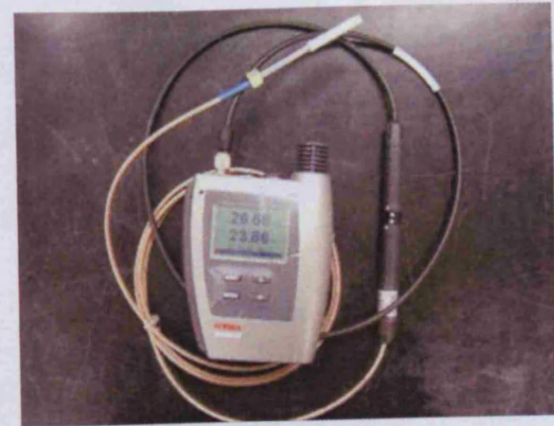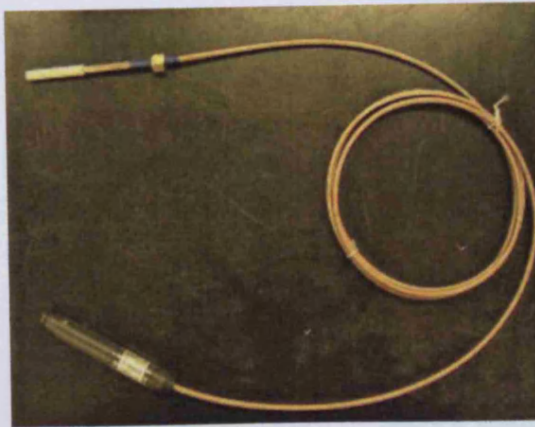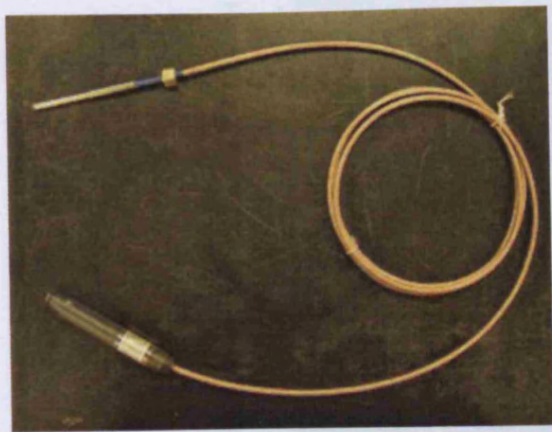
Figure 3.12 Relative humidity probe
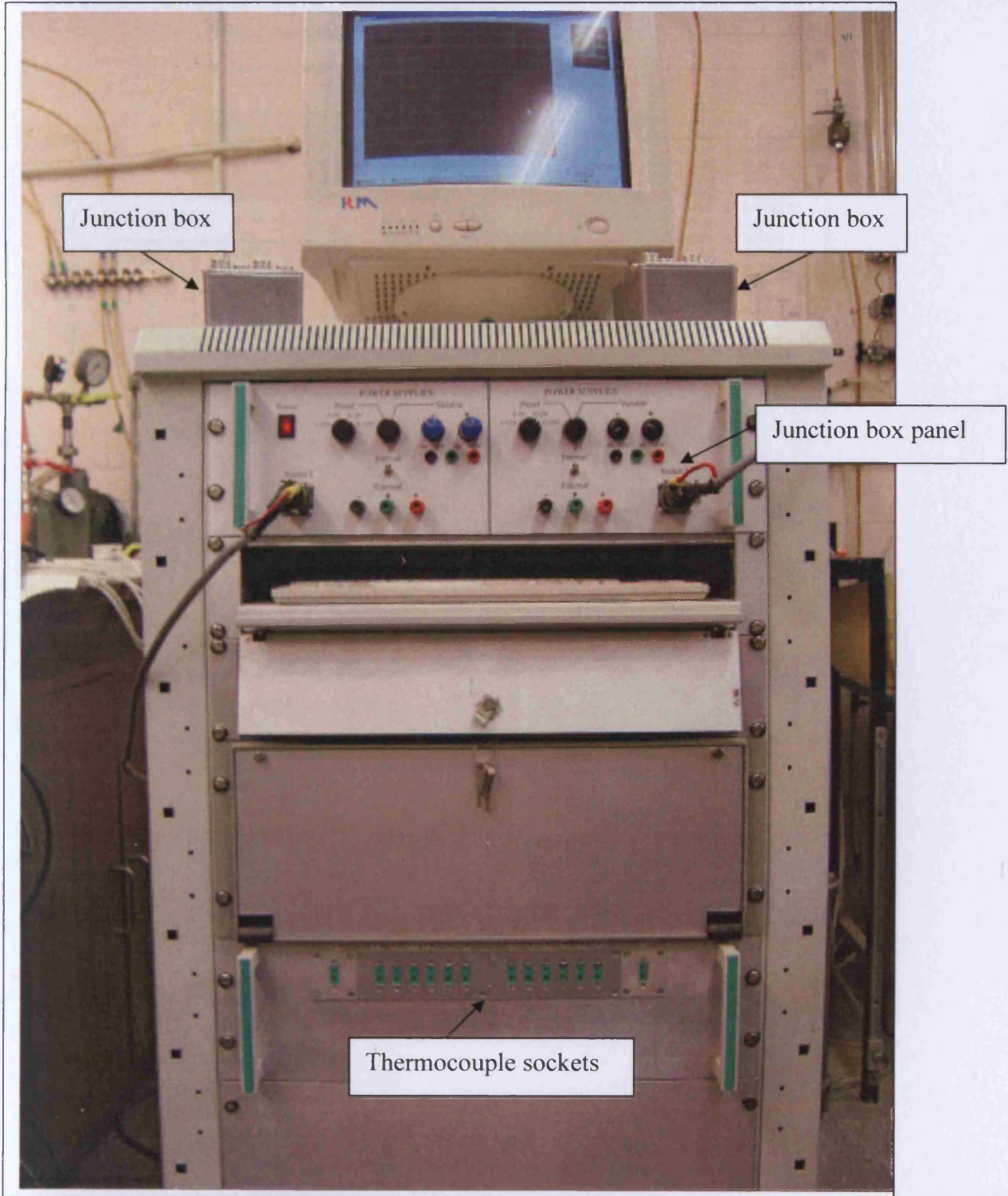
Figure 3.13 Front view of datalogger on a trolley

- - -▶ Fixed wiring signal flow   ——▶ Power supply flow

· · ·▶ Patch wiring signal flow

Data logger thermocouple socket front panel

1 2 3 4 5 6 7 8 9 10 11 12 13 14

Socket channel configuration

Socket 1	Ch 1	to Amp	1	to Board 3	Ch	1
	2	to Amp	2	to Board 3		2
	3	to Amp	3	to Board 3		3
	4	to Amp	4	to Board 3		4
	5	to Amp	5	to Board 3		5
	6	to Amp	6	to Board 3		6
	7	to Amp	7	to Board 3		7
	8	to Amp	8	to Board 3		8
Socket 2	Ch 1	to Amp	9	to Board 3		9
	2	to Amp	10	to Board 3		10
	3	to Amp	11	to Board 3		11
	4	to Amp	12	to Board 3		12
	5	to Amp	13	to Board 3		13
	6	to Amp	14	to Board 3		14
	7			to Board 4	Ch	1
	8			to Board 4		2

CR7

Board 1 — 723T Analog input / thermocouple

Board 2 — 725 Excitation

Board 3 — 723 Analog input

Board 4 — 723 Analog input

Board 5 — no board

Board 6 — no board

Board 7 — no board

▶ To PC running PC 208W

Data logger 5-pin DIN socket rear panel

Bank 2

Bank 1

1 2 3 4 5 6 7 8 9 10 11 12 13 14

Fylde 14 channel FE-351-UA universal amplifier rack

Output

Input

1 2 3 4 5 6 7 8 9 10 11 12 13 14

Note:

Attenuation switch gives 100 fold reduction in signal, which combined with amplifier gives gain x0.2 to x10,000

Data logger junction box front panel

Preset   Variable   Preset   Variable

Socket 1   Socket 2

Junction box   Junction box

1 2 3 4   1 2 3 4

5 6 7 8   5 6 7 8

Figure 3.14 Flow diagram of data acquisition system (Campbell Scientific Inc., 1997)

Figure 3.15 Mechanical mixture

4. Data Analysis

Suppressor

3. Detection

Conductivity
cell

**1. Eluent
delivery**

Injection

Separator
column

Sample

Guard
column

2. Separation

Waste

Sample loop

Pump
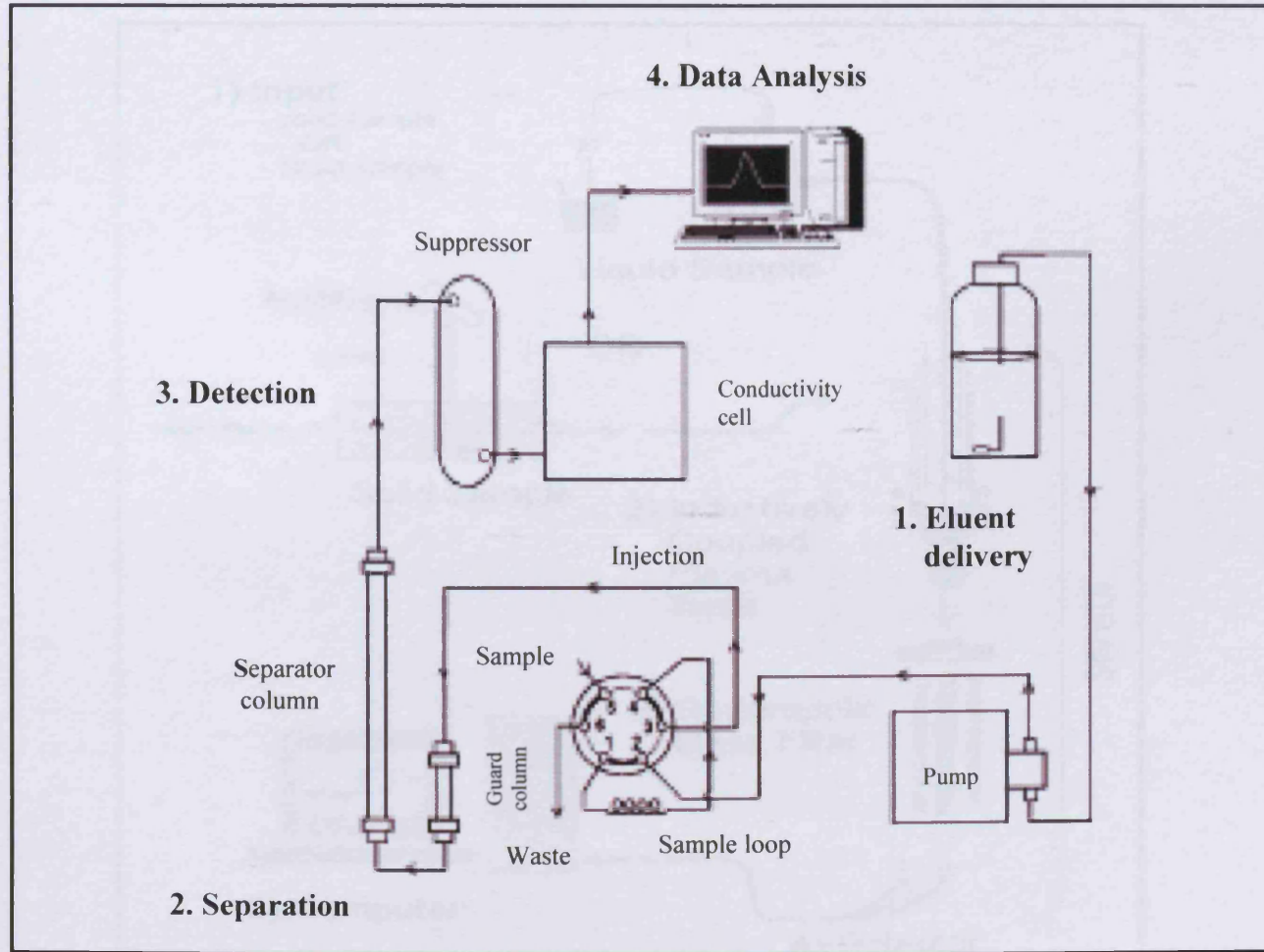
Figure 3.16 Flow diagram of DX-80 Ion Analyser (Dionex Corp., 2004)

1) Input
- solid sample
  OR
- liquid sample

Liquid Sample

Nd. YAG Laser

Laser

OR

Argon Gas

Sample

Solid Sample

2) Inductively Coupled Plasma Torch

ICP-MS

3) Quadropole Mass Filter

5) Computer

4) Detector
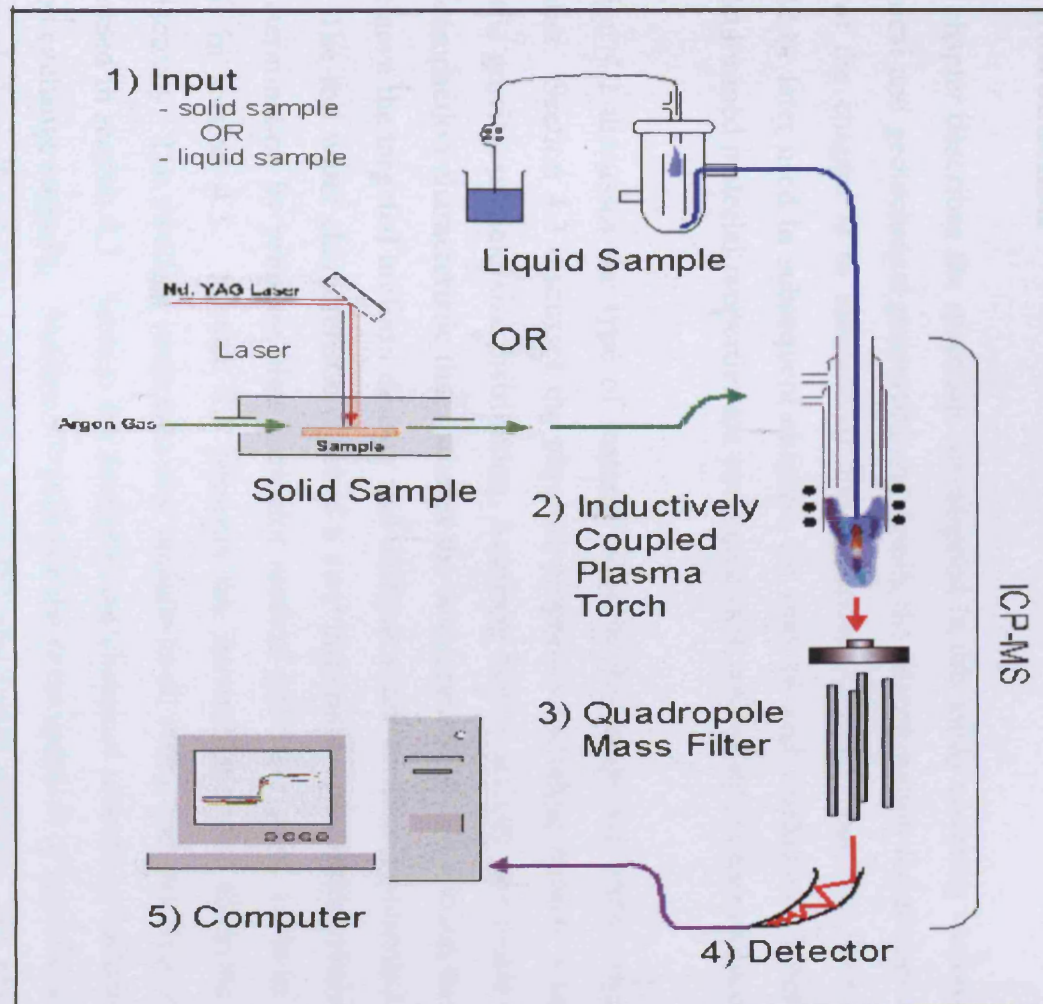
Figure 3.17 Schematic diagram of ICP-MS

Chapter 4

Material characterisation

4.1 Introduction

This chapter describes the materials investigated in this study covering various physical, chemical and geotechnical properties and details the determination techniques used. The aim of the chapter is to characterise the materials accurately because their properties would be later used in subsequent chapters for analysis and validation. Where possible the determined material properties are compared with past work of other researchers.

Section 4.2 discusses the type of material used in this study and their origin and the supplier. Section 4.3 discusses the physical properties including natural water content, specific gravity, particle size distribution, Atterberg limits, activity and linear shrinkage. The compaction characteristic that includes the development of compaction methodology to achieve the targeted uniform density and uniform water content is presented in section 4.4. The soil water characteristic curve is a very important constitutive relationship and its determination by pressure plate extractor method and filter paper method is dealt in detail in section 4.5. Section 4.6 presents the determination of saturated hydraulic conductivity. The swelling properties that include swell index and swelling pressure are discussed in section 4.7. Section 4.8 describes the chemical properties including pH and cation exchange capacity. Section 4.9 presents the determination of specific surface area using ethylene glycol monoethyl ether (EGME) adsorption method. The mineralogical analysis using X-ray diffraction (XRD) is described in section 4.10 to determine the minerals presents in the materials. Section 4.11 investigates the microstructure of the material using Environmental Scanning Electron Microscope (ESEM) and Energy Dispersive X-ray Analyser (EDXA). Finally section 4.12 draws the conclusions from the above work.

4.2 Material

The investigation has been carried out on two types of clays, a non-swelling clay Speswhite kaolin and highly swelling clay MX-80 bentonite. The following sections discuss about each of these materials.

4.2.1   Speswhite kaolin

Speswhite is highly refined kaolin of ultra fine particle size from Cornish deposits and is a product of IMERYS Mineral Ltd. It was supplied in packs of 25 kg each by WhitChem Limited, UK. The specification and properties given by the supplier are detailed in Table 4.1. Speswhite kaolin was chosen as a test material because it has been extensively used in research and many published data are available on its properties (Al-Tabba and Wood, 1987; Sivakumar, 1993; Wheeler and Sivakumar, 1995; Sivakumar and Wheeler, 2000; Folly, 2001). Kaolin is typically consists of 1:1 kaolinite mineral (for further detail see chapter 2). Its physical and chemical properties are described in length in this chapter.

4.2.2   MX-80 bentonite

Bentonite is highly swelling clay. Sodium bentonite was first found in Benton formation of Eastern Wyoming, USA. Bentonites typically consist of a large fraction of the 2:1 monmorillonite mineral (for further detail refer chapter 2). MX-80 bentonite has been selected for this investigation and has been subjected to a number of studies in the context of being a suitable engineering barrier material for a multi barrier high level nuclear waste disposal repository. MX-80 is mined in Wyoming USA and provided by SKB Sweden. Its various physico-chemical properties are presented in the following sections.

4.3 Physical properties

Physical characteristics like specific gravity, particle size distribution, Atterberg's limits (liquid limit and plastic limit) and activity are important properties of any soil. The following sections discuss their determination technique.

4.3.1   Natural water content

The natural water content was determined by oven drying method. The soils were supplied in 25 kg bags and contained some moisture. The soils were dried in oven at 105 °C as per method described in BS 1377-2:1990.

Speswhite kaolin was found to have a uniform natural water content of 1.2 %, this is consistent with the value provided by the supplier (Table 4.1).

The MX-80 bentonite was found to have a variable water content from 12 % to 14 %, this is consistent with the results presented by Bradbury and Baeyens (2002).

4.3.2   Specific gravity

The specific gravity or particle density of solid particles is defined as the ratio of the mass of a given volume of solids to the mass of an equal volume of water at 4 °C, in simple words; it is the ratio of the density of soil solids to the density of water (Arora, 1997). The specific gravity of the soils was found using the density bottle method described in BS 1377-2:1990.

Kaolin is a non-swelling soil and its specific gravity was determined as 2.61. This is similar to the results reported by the supplier Imerys Ltd (Table 4.1) and Folly (2001).

MX-80 bentonite exhibits swelling characteristic when mixed with water because the water is a polar liquid. Therefore, non-polar liquid propan-2-ol was used to determine the specific gravity of the MX-80 bentonite. The specific gravity of MX-80 was found to be 2.80. In comparison Bradbury and Baeyens (2002) and Tripathy et al. (2004) reported 2.76 specific gravity of MX-80 bentonite.

4.3.3   Particle size distribution

The particle size distribution was determined by two methods first, by using a hydrometer as per BS 1377-2:1990 and second by using a laser diffractometer. Figures 4.1 and 4.2 show the particle size distribution found by the hydrometer method for Speswhite kaolin and MX-80 bentonite respectively. Speswhite has 100 % finer than particle size 60 μm and 75 % finer than particle size 1 μm. MX-80 has 85 % finer than particle size 1 μm.

In particular the Malvern MasterSizer X laser diffractometer has been used to determine the particle size distribution. This approach works on the principle that particles scatter light at angles in inverse proportion to their size. It is basically a non imaging optical system due to the fact that sizing is accomplished without forming an image of the particle onto a detector. The MasterSizer X employs two forms of optical configuration first is the well known conventional Fourier optics and second is a reverse Fourier optics that allow to measure scattering at much higher angles thus measures very small particles down to 0.1 mm. It basically consists of a helium-neon red laser source, flow cell, optical lens and detector as shown in Figure 4.3. The helium neon laser source forms a collimated and monochromatic beam of light known as the analyser beam. The flow cell collects the sample mixed in a liquid (usually deionised water) from outside dispersion unit. The dispersion unit mixes the dry sample in the liquid by a mechanical stirrer and disperse the particles by ultra sound system to stop flocculation. The dispersion unit is basically a sample feeder that pumps the liquid sample into the flow cell where the analyser laser beam falls on the individual particle and gets diffracted. The optical lens which comes in different ranges depending upon the particle size to be analysed, collects the diffracted light and focus it onto the detector. The detector, which remains stationary and coaxial with the laser axis regardless of particle movement in the flow cell, analyses the diffracted light and sends information to a computer for processing.

1 g of dry Speswhite kaolin powder was first mixed in 50 ml deionised water and then introduced in the dispersion unit that is already full of deionised water. The sample is then mixed thoroughly in the dispersion unit and the particles are then allowed to disperse and fed into the flow cell of the MasterSizer. The optical lens of range 45 mm was used.

Figure 4.4 shows the particle size distribution curve between cumulative percentages of particle numbers versus particle diameter for kaolin.

In the case of MX-80 bentonite, methanol was used instead of water because MX-80 forms floc with water. MX-80 was also analysed by using the 45 mm optical lens. The particle size distribution curve for MX-80 is shown in Figure 4.5. MX-80 has 100 % particle size finer than 1 μm.

4.3.4   Liquid limit

The liquid limit is the water content at which a soil changes from the liquid state to the plastic state. In accordance with BS 1377-2:1990 two types of tests are suggested to determine the soil liquid limit, namely cone penetrometer and the Casagrande method. The cone penetrometer method is a static test that depends on the shear strength of the soil. It is a definitive method that is more consistent and less liable to experimental errors (Head, 1980). Alternatively, the Casagrande method is a dynamic test which is very susceptible to discrepancies between operators. Due to this reason the cone penetrometer method has been used in this study to measure the liquid limit.

In the cone penetrometer method, a stainless steel cone is released into a cup of soil for 5 seconds and its depth of penetration is measured. This procedure is repeated until the difference between consecutive penetrations is less than 0.5 mm. Subsequently, the sample water content is increased and further tests are repeated. The penetration values should cover the range of approximately 15 to 25 mm. The liquid limit is defined as the water content corresponds to 20 mm penetration. It is expressed as a percentage and reported to the nearest whole number.

Figure 4.6 shows that liquid limit of Speswhite kaolin corresponds to 20 mm penetration is 63 %. This is consistent with the liquid limit of Speswhite kaolin presented by Folly (2001).

Figure 4.7 shows that liquid limit of MX-80 bentonite corresponds to 20 mm penetration is 385 %.

4.3.5   Plastic limit

The plastic limit is the water content below which a soil stops behaving as a plastic material. The plastic limit of the both soils has been determined by standard thread-rolling method based on BS 1377-2:1990.

The standard thread-rolling method requires that a ball of soil be moulded in the palms of the hands until the heat of the palms has dried the soil sufficiently for slight cracks to appear on its surface. The sample is the rolled into a thread of 3 mm diameter by forward and backward movement of the hand. The procedure is repeated until the thread has developed shear cracks longitudinally and transversely. This water content of the thread is defined as the plastic limit of the soil. It is also expressed as a percentage and reported to the nearest whole number. It is an operator dependent method and depends upon the judgement of the operator. The plastic limit of Speswhite kaolin has been determined as 32 % and that of MX-80 bentonite as 39 % by this method. The similar results were reported by Stenke et al. (2006) and Folly (2001) for Spweshite kaolin and similar results for MX-80 were obtained by Tang and Cui (2005).

4.3.6   Plasticity index

The plasticity index is defined as water content range over which a soil exhibits plastic behaviour. It is equal to the difference between the liquid limit and the plastic limit. Thus

$$PI = LL - PL \qquad\qquad (4.1)$$

Where PI is the plasticity index, LL is the liquid limit and PL is the plastic limit.

Hence, the plasticity index for Speswhite kaolin found to be 31 %. Again, this result is consistent with Stenke et al. (2006) and Folly (2001). MX-80 bentonite determined to have a plasticity index of 346 %.

4.3.7   Activity

Activity is a measure of the water holding capacity of clayey soil (Arora, 1997). The changes in the volume of clayey soil during swelling or shrinkage depend upon the activity. The activity (A) of soil is defined as:-

$$A = \frac{PI}{C} \tag{4.2}$$

where PI is the plasticity index and C is the percentage of clay fraction finer than 2 μm in the soil.

Speswhite kaolin has 100 % fraction finer than 2 μm, resulting in an activity of 0.31 which is similar to that obtained by Folly (2001). MX-80 has activity of 3.46 that shows it is a highly active soil.

4.3.8   Linear shrinkage

The linear shrinkage is defined as change in length compared to initial length when the water content is reduced to the shrinkage limit. It is expressed as a percentage and reported to the nearest whole number. It has been determined in accordance with BS 1377-2:1990 to be for Speswhite kaolin as 7 % and for MX-80 bentonite as 42 %.

4.4   Compaction characteristic

The compaction characteristic is basically a relationship between water content and dry density. A number of studies of compacted clay (Pintado et al. 2002; Cuevas et al. 2002)

have used samples compacted to a dry density of 1.65 Mg/m^3, and this value was also selected as the target dry density. As discussed earlier in chapter 3, it was also decided to choose two water contents and same dry density. The main challenge was to achieve the same dry density and water content through out the sample. The followings sections discuss the method development to achieve the above outlined aims.

4.4.1 Dynamic compaction

The standard Proctor method was used in accordance with BS 1377-2:1990. The clay samples were compacted in the central section of the TH cell. The internal size of the central section is almost the same as the standard Proctor mould. An automatic compactor was used for compaction in which height of the rammer fall and number of blows could be set at the desired value. The maximum dry density achieved for both clays by this method was well below the aimed dry density (1.65 Mg/m^3). The weight of the rammer was then increased from 2.5 kg to 3.7 kg and again the Proctor method was repeated but this resulted in very slight increase in maximum dry density for both clays as shown in Figures 4.8 and 4.9. The number of blows was then increased this had little effect on the final densities. Also the samples did not have a uniform density after sectioning them, so a static compaction method was tried.

4.4.2 Static compaction

Following the trials using dynamic compaction, static compaction was attempted to achieve the desired high dry density. In the static compaction, the soil samples were basically compressed under a static load by a universal compression machine. The soil samples were statically compressed in layers in the central section by using a specifically designed and built rammer for this purpose as shown in Figure 4.10. Again different options were tried with the magnitude of static load, the loading rate and the number of layers being varied. Finally, a method was evolved by which the aimed uniform density could be achieved. The method involved compression of the soil samples in 10 layers under a maximum static load up to 90 kN with a loading and unloading rate of 1.5 kN/s. Then the compacted sample was sectioned in 10 slices of 10 mm thickness each to check

the uniform dry density and uniform water content along the sample length. Figures 4.11 - 4.12 show the static compaction curve between dry density versus water content (gravimetric) for kaolin and MX-80 respectively. For the present study two points were chosen as initial conditions on the static compaction curve with the same dry density but different water contents. One point was selected on dry side and another on wet side. A dry density of 1.63 Mg/m^3 was selected with 47 % and 84 % degree of saturation corresponds to 11 % and 19 % water contents respectively as initial conditions for Speswhite kaolin as shown in Figure 4.11. For MX-80, the dry density of 1.63 Mg/m^3 was chosen with 60 % and 88 % degree of saturation which relate to initial water contents of 16 % and 22 % respectively as initial conditions as presented in Figure 4.12. Figures 4.13 and 4.14 illustrate the achieved water content profiles with the depth of the soil sample for both clays. Figures 4.15 and 4.16 show the dry density profile achieved for the samples of each clay.

4.5 Hydraulic properties

The hydraulic parameters are important flow parameters which are used to determine the heat and mass transfer. The following sections present the various hydraulic properties experimental determination.

4.5.1 Soil-water characteristic curve

The soil-water characteristic curve (SWCC), also referred as the moisture retention curve, depicts the relationship between suction (or water potential) and volumetric (or gravimetric) water content (or degree of saturation). The SWCC over the entire suction range is often plotted using a logarithmic scale (Fredlund and Xing, 1994). There are various laboratory methods, presented in section 2.5.1.1 of chapter 2, available to determine the suction and water content relationship. For the present study, two methods were employed to measure suction, pressure plate extractor method and filter paper method.

4.5.1.1 Pressure plate extractor method

The pressure plate extractor method works on the principle of axis translation technique (Hilf, 1956) and measures the matric suction. This method has been used by many researchers (Olson and Langfelder, 1965; Mou and Chu, 1981) to induce matric suction. In the pressure plate apparatus, the soil specimen is placed on top of a saturated ceramic high air entry disk in an air chamber. The extractor can operate up to maximum pressure of 15 bar (1500 kPa). This is due to the fact that higher entry disks available commercially at present have maximum air entry value of up to 1500 kPa. This limits the use of the method for highly unsaturated soils as higher suction values (>1500 kPa) are often developed.

For the current investigation, ceramic pressure plate extractors manufactured by Soilmoisture Equipment Corp., California, USA, were used as shown in Figure 4.17. The pressure plate cell consists of a steel pressure vessel, a porous ceramic plate, covered on one side by a thin Neoprene diaphragm, sealed to the edge of the ceramic plate. An internal screen between the plate and the diaphragm provides a passage for water flow. An outlet stem running through the plate connects this passage to a burette via an outflow tube fitting, which connects to the atmosphere outside the extractor.

A saturated soil sample was prepared by mixing clay with deionised water and storing in air tight container for 24 hours so that the uniform equilibrium moisture could be achieved. The saturated soil sample was then placed and compacted in a stainless steel ring of size 45 mm diameter and 12 mm height. There are constraints on using the appropriate sample size, the manufacturer reports that it is desirable to keep sample height 10 mm to reach equilibrium within reasonable time because equilibration time varies with the square of the sample height. A further constraint on sample size is that the sample's lateral dimension should not be so large to make the sample fragile, to the extent that weighing or removal of the sample from the ceramic pressure plate becomes impracticable. The saturated and compacted soil sample rings were then placed on the saturated ceramic pressure plate which was submerged in deionised water for 24 hours. The ceramic plate with the sample rings were then placed in the steel pressure vessel and air pressure was applied through compresses air supply (up to 7 bars) available in the

laboratory or through nitrogen pressure tanks (>7 bars). The air pressure pushes the water very slowly out of the sample and ceramic plate into the burette. At equilibrium, the internal air pressure in the extractor is directly related to the suction in the soil (Rees, 1990; Fredlund and Rahardjo, 1993). The samples were taken out for mass and volume measurement. The soil tends to stick to the ceramic plate, so care is required to take out the soil samples. The sample volume was reduced because of drying and that is taken into account while working out volumetric water content. The electronic balance of accuracy up to 0.0001 g was used for mass measurement.

Figures 4.18 and 4.19 show the results obtained by this method for the Speswhite kaolin and MX-80 respectively.

4.5.1.2   Filter paper method

The idea to use filter paper for soil suction measurement can be traced back to the work of Schull in 1916 (Leong et al., 2002). Gardener (1937) first reported the use of the filter paper method as a soil suction sensor. The filter paper method is based on the assumption that a filter paper will come to equilibrium with respect to moisture flow with a soil having a specific suction. Equilibrium can be achieved by either liquid or vapour moisture exchange between the soil and the filter paper. When a dry filter is placed in direct contact with a soil sample, it is assumed that water flows from the soil to filter paper until equilibrium is achieved. Since the filter paper is in direct contact with the soil sample, matric suction was measured as soil moisture and moisture transferred to filter paper is identical and there will be no osmotic effects. This is known as the contact filter paper technique of matric suction measurement. When a dry filter paper is suspended in the headspace above a soil specimen, vapour flow of moisture will occur from the soil to the filter paper until equilibrium is achieved. The equilibrium amount of water adsorbed by the filter paper is a function of the pore air relative humidity and the corresponding total suction. This method is known as the non-contact filter paper technique of total suction measurement.

For the current work, the tests were conducted using Whatman No. 42 filter papers in accordance with ASTM D 5298-94. The experimental procedure can be outlined as follows:

1- The Whatman No. 42 filters of 55 mm diameter were oven dried at 105 °C in the aluminium cans with the lids half-open for overnight (16 hours) and then placed in a desiccator containing silica gel.

2- The soil sample was compacted in a stainless steel ring of size 45 mm diameter and 12 mm height.

3- One dry filter paper was cut to 50 mm diameter size and was sandwiched between two dry filter papers of 55 mm diameter. The outer filter papers protect the centre one from soil contamination. The mass of each filter paper was recorded before by an electronic balance of accuracy 0.0001 g.

4- The soil sample ring was then placed on the sandwiched filter papers to make sure an intimate contact between the filter papers and the soil sample.

5- The soil sample with filter papers was put into the 250 ml plastic container of 100 mm diameter.

6- A rubber O-ring of 40 mm diameter and 10 mm thickness was then placed on the top of the soil sample inside the plastic container, to provide a support for the non-contact filters.

7- Two weighed dry filter papers one on top of the other were inserted on the ring using tweezers. The filter papers should not touch the soil sample, the inside wall of the container and underneath the lid of the container.

8- The plastic container was then kept in temperature and humidity controlled conditions for 7 days.

9- After the 7 day equilibrating period, the top two filters were taken out by the tweezers and placed in the aluminium can of predetermined mass. The mass of can plus wet filter paper inside was taken very quickly to the nearest 0.0001 g accuracy. Then the centre filter was separated from the sandwiched filters and placed in the aluminium can for the mass measurement as well.

10- The cans were put into the oven at 105 °C with the lids half-open for 24 hours. Before taking mass measurement of dried filter papers, the cans were closed with their lids to equilibrate for 5 minutes.

11- The above steps were repeated with the soil samples of different initial water content.

12- The following calibration equations presented by Leong et al. (2002) were used to calculate the total and matric suction.

$$\text{Total suction} \begin{cases} \log\Psi = 8.778 - 0.222 w_f & w_f \geq 26 \\ \log\Psi = 5.31 - 0.0879 w_f & w_f < 26 \end{cases} \qquad (4.3)$$

$$\text{Matric suction} \begin{cases} \log\Psi = 2.909 - 0.0229 w_f & w_f \geq 47 \\ \log\Psi = 4.945 - 0.0673 w_f & w_f < 47 \end{cases} \qquad (4.4)$$

where ψ is respective suction and w_f is the water content percentage of the filter paper.

Figures 4.20 present the total suction and matric suction variation with volumetric water content for Speswhite kaolin. Figures 4.21 show the total suction and matric suction variation with volumetric water content for MX-80.

4.5.1.3 Curve fitting

The suction results obtained here comprise only a small portion of the SWCC. Therefore, van Genuchten (1980) numerical curve fitting approach has been used to predict the whole SWCC. The van Genuchten (1980) model is described in section 2.6.1.2 of chapter 2. Rewritting the van Genuchten equations which are employed in this study as:

$$\frac{\theta_l - \theta_{lr}}{\theta_{ls} - \theta_{lr}} = \left[\frac{1}{1 + (\alpha s)^n}\right]^m \tag{4.5}$$

and

$$m = 1 - \frac{1}{n} \tag{4.6}$$

where α, n, m are constant fitting parameters, θ_l is the volumetric liquid water content, θ_{lr} is the residual volumetric liquid water content, θ_{ls} is the saturated volumetric liquid water content and s is the matric suction.

Figure 4.22 presents the moisture retention curve (matric suction versus degree of saturation) obtained by fitting the van Genuchten model (1980) to experimental results for Speswhite kaolin. The volumetric water content is converted into degree of saturation by using the porosity corresponds to the reference dry density of 1.63 Mg/m^3. The following values of constant fitting parameters were used for kaolin:

$$\alpha = 0.015$$

$$n = 1.9$$

$$m = 0.474$$

$\theta_{lr} = 0.0001$

$\theta_{ls} = \text{porosity} = 0.38$

The moisture retention curve for MX-80 bentonite is shown in Figure 4.23 and the following values of constant fitting parameters were used:

$\alpha = 0.00075$

$n = 1.9$

$m = 0.474$

$\theta_{lr} = 0.0001$

$\theta_{ls} = \text{porosity} = 0.43$

4.5.2   Saturated hydraulic conductivity

Hydraulic conductivity is a property of the soil that describes the ease with which fluid can move through pore spaces. The hydraulic conductivity is the proportionality constant in Darcy' law that relates the water flow rate through a unit cross sectional area under a unit hydraulic gradient. It depends upon the intrinsic permeability and fluid properties like viscosity and unit weight. Saturated hydraulic conductivity describes the water movement through a saturated soil media. There are various direct laboratory methods based on Darcy' law to find the saturated hydraulic conductivity, in which a hydraulic gradient is applied between two points and flow rate is measured.

The saturated hydraulic conductivity was measured by triaxial permeability test as per BS 1377-6:1990. The test set up is shown in Figure 4.24. The soil was statically compacted

to dry density of 1.63 Mg/m^3 and 90 % degree of saturation in the TH cell and the sample core of size 40 mm diameter and 40 mm height was taken out. The sample core was set up on the pedestal of triaxial cell and saturated to 100 % before starting the test.

The saturated hydraulic conductivity of Speshwhite kaolin was determined as 1.02 x 10^{-10} m/s which is same as obtained by Folly (2001). MX-80 was determined to have a saturated hydraulic conductivity of 1.25 x 10^{-13} m/s, which is consistent with results reported by Engelhardt and Finsterle (2003) and Melhuish (2004).

4.5.3   Unsaturated hydraulic conductivity

Melhuish (2004) reported the unsaturated hydraulic conductivity relationship for the MX-80 bentonite which is based on the approach presented by Börgesson and Hernelind (1999). The unsaturated hydraulic conductivity, k_l, is a function of the void ratio, the degree of saturation and the temperature. In this approach k_l is associated with the hydraulic conductivity of saturated clay, k_{sat}, and the degree of saturation, S_l, by the following relationship:

$$k_l = (S_l)^\delta k_{sat}$$

where, δ is a parameter usually between 3 and 10. It was found that $\delta = 3$ was satisfactory for MX-80 bentonite according to the calibration and validation results performed by Börgesson and Hernelind (1999).

The same relationship has been used for Speswhite kaolin. It was found that $\delta = 2$ was satisfactory for kaolin according to the calibration and validation results performed by Folly (2001).

4.6 Thermal properties

The thermal parameters that include thermal conductivity and specific heat capacity were not determined in this study but their values were taken from the work of other researchers.

Melhuish (2004) reported the thermal conductivity of the MX-80 bentonite that has been measured as a function of the degree of saturation by Börgesson and Hernelind (1999). Figure 4.25 shows the laboratory results at a void ratio of 0.8. In order to find a relationship between the thermal conductivity and the degree of saturation Troy (2005) has performed the linear interpolation between the values. These results can be seen in Table 4.2 and Figure 4.25.

Winterkorn and Reno (1967) measured the thermal conductivity for kaolin clay as a function of moisture content at a porosity of 0.6. The moisture content values are converted into degree of saturation and the results are presented in tabular form in Table 4.3.

Melhuish (2004) reported the specific heat capacity of solids for MX-80 bentonite equals to 800 J/kg/K. The same value has been adopted for Speswhite kaolin in this study.

4.7 Swelling property

The swelling property of a soil are often characterised by the swell index and swelling pressure. The following sections discuss them in detail.

4.7.1 Swell index

The swell index test is an index method to quantify the swelling property of clay. In this study it has been determined as per ASTM D 5890-02. To perform the test, a 2 g sample of dried clay is dispersed into a 100 ml graduated cylinder in 0.1 g increments. A minimum of 10 minutes must pass between additions to allow for full hydration and

settlement of the clay to the bottom of the cylinder. The procedure is followed until the entire 2 g sample has been added to the cylinder. The sample is then covered and protected from disturbances for a period of 16 hours, at which time the level of the settled and swollen clay is recorded to the nearest 0.5 ml. The samples at the end of this test are shown in Figures 4.26 for Speswhite kaolin and MX-80 bentonite respectively. It was found that Speswhite kaolin has a swell index of 4 ml / 2 g and MX-80 a swell index of 32 ml / 2 g.

4.7.2   Swelling pressure

When swelling clays are not allowed to expand upon wetting, they exert a pressure called swelling pressure. There are three main methods available to measure swelling pressure, namely, free swell test, no swell test and load-swell test (Sridharan et al., 1986). In free swell test, the soil sample is allowed to freely swell on hydration and is then brought back to its original volume by applying pressure. In no swell test, also called constant volume test, the soil is not allowed to swell on hydration by continuously addition of load. The constant volume test requires careful applying of load increment otherwise it causes compression. In the load swell test (also known as swelling deformation test), the strain capacity of the soil is measured when it saturates under a previously established vertical pressure.

The present investigation used the free swell method to find out the swelling pressure. A modified oedometer was used to conduct the free swell test. The swelling pressure depends upon the initial water content, initial dry density and overburden pressure. The soil sample was compacted to a targeted density of 1.63 Mg/m^3 at water content of 22 % in the compaction mould and a modified oedometer ring of size 35 mm diameter and 10 mm height was pushed into the compacted sample. The ring was then taken out and excessive soil was trimmed off. The specimen inside the ring was then placed in the consolidation frame and an initial seating load of 6.5 kPa was applied. The initial seating load (or overburden pressure) of 6.5 kPa was recommended by Seed et al. (1962). The specimen was now saturated and allowed to swell freely. Once the swelling completed,

the loads were applied gradually to bring the soil specimen back to its original height (10 mm).

As might be expected Speswhite kaolin did not swell at all, resulting in a zero swelling pressure. MX-80 bentonite was found to have a final swelling pressure of 1.67 MPa after 4 days running the experiment. The swelling pressure was used to determine the range of pressure transducer needed for the TH cell.

4.8 Chemical properties

Determination of chemical properties like pH and cation exchange capacity and their measurement techniques are described below.

4.8.1 pH

The soil pH is an important chemical property that indicates the acidity or alkalinity of the soil sample. The pH test was done as per electrometric method described in BS 1377-3:1990. The pH value depends upon the soil and water ratio.

The pH value of Speswhite kaolin was found to be 5.0 for the soil water ratio of 1:10 and 5.2 for soil water ratio of 1:15. MX-80 has a pH of 9.20 for the soil water ratio of 1:10 and pH of 9.28 for the soil water ratio of 1:15.

4.8.2 Cation exchange capacity

Cation Exchange Capacity (CEC) is the quantity of exchangeable cations held by the soil which is a measure of the positively charged ions that could be held on the negatively charged sites on soil minerals (Yong et al., 2001). It is generally equal to the amount of negative charge and expressed as milliequivalent per 100 g of soil (meq/100g). Cations can be classified as either acidic (acid-forming) or basic. The common acidic cations are hydrogen and aluminium and the basic ones are calcium, magnesium, potassium and

sodium. The relative proportion of the acidic cation and the base cation on the exchange sites determines a soil's pH. CEC is sometimes also termed as the base exchange capacity when the basic cations are measured only. The ammonium acetate exchange method (Hesse, 1971; Lavkulich, 1981; Hashm, 1999) was used to measure the four basic cations sodium, potassium, calcium and magnesium and the procedure can be summarised as follows.

Extractable cations

Amonium acetate reagent is used to extract cations because ammonium ion replaces all the cations present in the soil. The following procedure was carried out to determine extractable cations.

1- 40 ml of ammonium acetate (CH_3COONH_4) reagent was taken into a 50 ml polypropylene centrifuge tube. The reagent is prepared by adding 57 ml of concentrated acetic acid (CH_3COOH) to 700 ml of deionised water in a fume cupboard. Then 68 ml of concentrated ammonium hydroxide (NH_4OH) is added to the solution and finally made up to 1 litre. The pH value of the solution was required to be 7 which was achieved by adding acetic acid when the pH was higher than this value and ammonium acetate when it was lower.

2- A 2 g sample of dry soil was accurately weighed and added slowly into the ammonium acetate reagent in the polypropylene centrifuge tube.

3- The centrifuge tubes were placed on an end over end (tumbling) rotating agitator at 30 rpm for 23 hours (US EPA 1312: 1994).

4- The sample was then centrifuged at 3000 rpm for 5 minutes. The solid part precipitated and the clear supernatant decanted into another 50 ml Whatman VectaSpin 20 centrifuge tube filter consist of a 0.45 μm filter insert and outer tube with a screw-on cap.

5- The supernatant in centrifuge tube filter was then again centrifuged. The samples were centrifuged at 3000 rpm for 5 minutes and most of the supernatant filtered through and collected at the bottom of filtered centrifuge tube.

6- 1 ml filtered solution from the filtered centrifuge tube was then transferred into conical tubes. 1 ml of 10 % HNO_3 (10 ml HNO_3 and 90 ml deionised water) and 8 ml of deionised water was added into conical tubes and gave the solution of ratio 1:10. Preservation of the samples for longer time (up to180 days) requires that sample should be acidified to pH < 1.5 with HNO_3 (US EPA 1312: 1994).

7- The samples in conical tubes were then analysed by induced coupled plasma mass spectrometer (ICP-MS) for basic cations sodium (Na^+), potassium (K^+), calcium (Ca^{+2}) and magnesium (Mg^{+2}).

8- The ICP-MS gives the amount of extractable cations in mg/l which is converted into meq/l00g using the equation below:

$$\text{Extractable cation (meq/100g)} = \frac{\text{Cation (mg/l)} \times \text{Amonium acetate (l)} \times 100}{\text{Equivalent weight of cation} \times \text{Mass of soil (g)}} \quad (4.7)$$

Here, the mass of soil is 2 g and the volume of ammonium acetate is 0.04 l (40 ml).

Soluble cations

The soluble amount of cations was found by adopting similar procedure mentioned above for extractable cations but deionised water was used instead of ammonium acetate reagent. The MX-80 samples needed to be centrifuged for about 60 minutes or more to filter most of the supernatant through.

Exchangeable cations

The amount of exchangeable cations was calculated by subtracting the amount of soluble cations from the amount of extractable cations. The amount of exchangeable cations represents the CEC.

The CEC results are tabulated in Tables 4.4 and 4.5, which shows the total CEC of Speshite kaolin found to be 3.74 meq/100g and that of MX-80 bentonite is 92.88 meq/100g.

4.9 Specific surface area

The specific surface area (SSA) is the surface area of the soil particles measured in m^2/g. It is also a strong indicator of the retention and sorption capacity of clays. The SSA was determined using the ethylene glycol monoethyl ether (EGME) adsorption method (Eltantawy and Arnold, 1973; Carter et al., 1986; Hashm, 1999; Yukselen and Kaya, 2006). EGME is a harmful substance and could be absorbed by body, so the SSA experiment was conducted in the fume cupboard. The EGME method used to find SSA is as follow:

1- 1 g of an oven dried soil sample (through 63 micron sieve) was weighed and placed in an aluminium tare. The sample was then placed in a sealed vacuum desiccator over silica gel in order to dry the sample to a constant mass. The weighing of the soil sample was repeated every hour until a constant mass was attained. The mass of soil was measured using an electronic analytical balance with an accuracy of 0.0001 g.

2- Approximately 3 ml EGME was added to the soil sample until all the soil particles were completely covered and the mixture was allowed to equilibrate in the desiccator for 1 hour in the fume cupboard.

3- Afterwards the silica gel was removed from the desiccator and replaced with a solvate of about 120 g of calcium chloride ($CaCl_2$) and EGME. This solvate was prepared by 100 g of hot anhydrous $CaCl_2$ oven dried (100° C) for 1 hour and mixed with 20 ml EGME

thoroughly in a fume cupboard. The solvate was allowed to cool and then placed in the base of the desiccator.

4- The aluminium tare containing soil plus EGME slurry was again placed in the desiccator. The aluminium tare was covered with another aluminium tare with some gap between them to prevent disturbance caused by the application of a vacuum. The experimental set up is shown in Figure 4.27. The desiccator was evacuated with a vacuum pump for 1 hour and the slurry allowed to equilibrate for another hour. The slurry was again weighed using electronic analytical balance. This is repeated until a constant mass was achieved.

5- The amount of EGME to cover 1 m^2 of surface of clay particles with a monolayer is 2.86×10^{-4} g. Therefore, the SSA of the soil can be calculated by the following equation:

$$SSA\ (m^2/g) = \frac{Mass\ of\ EGME\ retained\ (g)}{Mass\ of\ dry\ soil\ (g) \times 2.86 \times 10^{-4}} \tag{4.8}$$

The SSA of Speswhite kaolin was found to be 48 m^2/g and that of MX-80 to be 650 m^2/g. The results are consistent with those reported by other researchers (Cerato and Lutenegger, 2002).

4.10 Mineralogical analysis - XRD study

X-ray diffraction (XRD) is a non-destructive analytical technique to identify and quantify minerals in crystalline compounds within in a mixture or a pure phase. The results obtained from the XRD test are compound or mineral name opposed to element name determined by other analytical methods. The samples analysed with the XRD are solid and crystalline with a regular 3D distribution of atoms occupying a space with a particular arrangement to form a series of parallel planes or lattices which are separated from each other by distances d or d-spacings. The XRD identifies minerals by relating the angle of incidence of the X-rays to the d-spacings according to Bragg's law. The Bragg's law states, when a monochromatic X-ray beam with a known wavelength (λ) is incident on

the lattice plane in a crystal at an angle (θ) causes diffraction when the distance (d) travelled by the rays reflected from successive planes differs by a complete number (n) of wavelengths. It can be written in an equation form as

$$n \lambda = 2d \sin\theta \qquad\qquad (4.7)$$

By varying the angle (θ) the condition for Bragg's law is satisfied by different d-spacings within the crystalline structure. The different angular positions and intensities are then plotted and the plot is called diffractogram which is a fingerprint to identify the unknown mineral phase.

For the present study, a Philips automated powder diffractometer PW 1710 was used. The machine consists of a Goniometer (which houses the sample chamber and detector), a generator (a copper tube which generates X-rays by $CuK\alpha$ radiation at 35 kV and 40 mA) and a controller (which uses computer software PW1877APD version 3.6). The dry soil sample powder is packed into an aluminium holder. It is then placed in the Goniometer and bombarded with X-rays generated from the copper tube. The diffracted rays are collected by a detector and the information relayed to a computer where, using the Bragg's equation, it is converted to d-values of specific intensities. This information is plotted in the form of a diffraction pattern (diffractogram) and then matched against the database of 70,000 recorded phases, using the computer identification software (PW1876 PC-identify version 1.0b) and mineral powder diffraction file data book to identify the unknown mineral phases contained within the sample.

The intensity of a dominant X-ray diffraction peak on the diffractogram for each mineral can not be used directly as a measure of abundance because different atomic planes within a mineral do not generally have an equal ability to diffract the X-rays. Therefore, straightforward comparison of peak intensities does not give absolute quantitative information of the minerals present in the sample. Instead, semi-quantitative information is obtained from the diffractogram on the relative abundance of identified minerals. The integrated area under the dominant peak of the identified mineral gives the amount of that mineral. Measuring the integrated area under a peak has the advantage of minimising the

effect of crystallinity, non-uniform preferred orientation and heterogeneous composition. As atomic planes in minerals have varying ability to diffract X-rays it is necessary to employ a system of weighing factors (Table 4.6) that is inversely proportional to this ability (Biscaye, 1964).

Figure 4.28 presents the XRD results for speswhite kaolin and major peaks of kaolinite, illite and quartz mineral can be observed.   A semi-quantitive analysis gives the percentage of minerals viz kaolinite 95 %, illite 4 % and remaining 1 % quartz. The XRD result for the MX-80 bentonite shows montmorillonite, quartz and albite (feldspar family) mineral peaks, as in Figure 4.29. An XRD test was also performed on glycolated samples to confirm the presence of montmorillonite because the montmorillonite peak coincided with the chlorite peak. The sample in the aluminum holder was placed in the dessicator that has ethylene glycol solution at the bottom and kept in oven at 50 °C for 2 hours. Glycolation leads to an expansion of the lattice of the montmorillonite and the resulting change in the d-spacing results in shift of the montmorillonite peak but it does not affect the chlorite lattice (Figure 4.30).   A semi-quantitative analysis was done to find out approximate percentage of minerals and yielded values of montmorillonite 78 %, quartz 11 % and albite 10 %.

4.11 Microstructural analysis - ESEM study

Environmental Scanning Electron Microscope (ESEM) can be used to image objects, such as minerals, at a magnification far exceeding the capability of an optical microscope. The ESEM can operate under low vacuum condition which negates the requirement for the sample to be coated with conducting code of carbon or gold. The ESEM is capable of working in three conditions viz. conventional high vacuum, low vacuum and environmental or wet mode. Using a Peltier stage to cool the sample allows imaging of wet and possibly live samples.

The FEI XL30 FEG ESEM and Energy Dispersion X-ray Analyser (EDXA) (Oxford Instruments INCA) were used for the present research. The X-rays are generated when an electron beam hits the specimen can be collected by EDXA for elemental analysis. The

samples were mounted on 12.5 mm diameter pin stubs and coated with carbon. The pin stubs were then placed in high vacuum mode in the chamber of ESEM.

The ESEM images of kaolin are presented in Figure 4.31. The flaky structure of kaolin can be observed clearly from the magnified images. Figure 4.32 shows the ESEM results of MX-80 with micro structural inter layers being evident.

4.12 Conclusions

Both clays, Speswhite kaolin and Mx-80 bentonite, have been characterised successfully by determining their various geotechnical properties including physical and chemical properties. A summary of physico-chemical properties of Speswhite kaolin and MX-80 are presented in Table 4.4 and 4.5 respectively. The determination techniques of the properties have also been detailed. The properties are consistent with other reported observations of various researchers. The flow material parameters i.e. hydraulic and thermal parameters have also been determined for both clays.

A static compaction technique was established to achieve uniform high dry density and uniform water content along the length of the soil samples. The dry density of 1.63 Mg/m^3 was selected with 50 % and 85 % degree of saturation corresponding to 11 % and 19 % water contents respectively as initial conditions for the testing programme for Speswhite kaolin. For MX-80, the dry density of 1.63 Mg/m^3 was chosen with 60 % and 88 % degree of saturation which relate to initial water contents of 16 % and 22 % respectively as initial conditions.

4.13 References

Al-Tabbaa, A. and Wood, D.M. (1987). Some measurements of the permeability of kaolin. Geotechlique, 37, 499-503.

Arora, K.R. (1997). Soil mechanics and foundation engineering. 4th Ed. Standard Publishers Distributor, New Delhi.

ASTM D 5298-94 (1994). Standard test method for measurement of soil potential (suction) using filter paper. Annual book of ASTM Standards.

ASTM D 5890-02 (2002). Standard test method for swell index of clay mineral component of geosynthetic clay liners. Annual book of ASTM Standards.

Börgesson, L. and Hernelind, J. (1998). Preparatory modelling for the backfill and plug test – Scoping calculations of H-M processes. SKB, IPR-99-11.

Bradbury, M.H. and Baeyens, B. (2002). Porewater chemistry in compacted re-saturated MX-80 bentonite: Physico-chemical characterisation and geochemical modelling. PSI Bericht Nr Switzerland.

BS 1377-2 (1990). Soils for civil engineering purposes. Part 2: Classification tests. British Standards Instituition.

BS 1377-3 (1990). Soils for civil engineering purposes. Part 3: Chemical and electro-chemical tests. British Standards Instituition.

BS 1377-6 (1990). Soils for civil engineering purposes. Part 6: Consolidation and permeability test in hydraulic cells and with pore pressure measurement. British Standards Instituition.

Carter, D.L., Mortland, M.M. and Kemper, W.D. (1986). Specific surface. Methods of soil analysis. Part 1, 2nd Ed., A. Klute (Ed.), American Society of Agronomy, Madison, Wis., 413-423.

Cerato, A.B. and Lutenegger, A.J. (2002). Determination of surface area of fine grained soils by the ethylene glycol monoethyl ether (EGME) method. Geotechnical Testing Journal, Vol. 25, No. 3, 315-321.

Cuevas, J., Villar, M., Martyn, M., Cobena, J.C. and Leguey, S. (2002). Thermo-hydraulic gradients on bentonite: distribution of soluble salts, microstructure and modification of the hydraulic and mechanical behaviour. Applied Clay Science, 22, 25-38.

Eltantawy, I.N. and Arnold, P.W. (1973). Reappraisal of ethylene glycol mono-ethyl ether (EGME) method for surface area estimation of clays. Soil Sci. 24, 232-238.

Engelhardt, I. and Finsterle, S. (2003). Thermal-hydraulic experiments with bentonite/crushed rock mixtures and estimation of effective parameters by inverse modelling. Appl. Clay Sci. 23, 111-120.

Folly J.P.W. (2001). Thermo-hydro-mechanical behaviour of unsaturated soil: An experimental study. PhD thesis, School of Engineering, Cardiff University.

Fredlund, D.G. and Xing, A. (1994). Equations for the soil-water characteristic curve. Canadian Geotechnical Journal, Vol. 31, 521-532.

Gardener, R. (1937). A method of measuring the capillary tension of soil moisture over a wide moisture range. Soil Science, Vol. 43, No. 4, 277-283.

Hashm, A.A. (1999). A study of the transport pf a selection of heavy metals in unsaturated soil. Ph.D. Thesis, School of Engineering, University of Wales, Cardiff.

Head, K.H. (1992). Manual of soil laboratory testing, Vol. 1: Soil classification and compaction tests. Pentech press Ltd.

Hesse, P.R. (1971). A text book of soil chemical analysis. Chemical Publishing Co. Inc., New York.

Hilf, J.W. (1956). An investigation of pore-water pressure in compacted cohesive soils. Ph D Dissertation, Technical Memorandum No. 654, United States Department of the Interior Bureau of Reclamation, Design and Construction Division, Denever.

Lavkulich, L. (1981). Soil analysis manual. Pedology Laboratory, Department of Soil Science, University of British Columbia, Vancouver.

Leong, E.C., He, L. and Rahardjo, H. (2002). Factors affecting the filter paper method for total and matric suction measurements. Journal Geotechnical Testing, Vol. 25, No. 3, 322-33.

Melhuish, T.A. (2004). An investigation of the three-dimensional thermo / hydro / mechanical behaviour of large scale in-situ experiments. Ph.D. Thesis, School of Engineering, University of Wales, Cardiff.

Mou, C.H. and Chu, T.Y. (1981). Soil suction approach for swelling potential evaluation. Transportation Research Rec. 790, Washington, DC, 54-60.

Olson, R.E. and Llangfelder, L.J. (1965). Pore water pressure in unsaturated soils. Journal of the Soil Mechanics and Foundation Division, Proceedings of American Society of Civil Engineers, Vol. 91, 127-150.

Pintado, X., Ledesma, A. and Loret, A. (2002). Backanalysis of thermohydraulic bentonite properties from laboratory tests. Engineering Geology, 64: 91-115.

Rees, S.W. (1990). Seasonal ground movement effects on buried moisture transfer in unsaturated soil. Ph.D. Thesis, School of Engineering, University of Wales, Cardiff.

Seed, H.B. and Chan C.K. (1959). Structure and strength characteristics of compacted clays. Journal of the Soil Mechanics and Foundation Division, Proceedings of American Society of Civil Engineers, Vol. 85, 87-128.

Sivakumar, V. (1993). A critical state framework for unsaturated soil. PhD Thesis, University of Sheffield.

Sivakumar, V. and Wheeler, S.J. (2000). Influence of compaction procedure on the mechanical behaviour of an unsaturated compacted clay. Part 1: Wetting and isotropic compression. Geotechnique 50, No. 4, 359-368.

Sridharan, A., Rao, A.S. and Sivapullaiah, P.V. (1986). Swelling pressure of clays. Geotechnical Testing. ASTM, Vol. 9, No. 1, 23–33.

Stenke, F., Toll, D.G. and Gallipoli, D. (2006). Comparison of water retention curves for clayey soils using different measurement techniques. Proc. 4th International Conference on Unsaturated Soils, Phoenix, USA.

Tang, A.M. and Cui, Y.J. (2005). Controlling suction by the vapour equilibrium technique at different temperature and its application in determining the water retention properties of MX-80 clay. Canadian Geotechnical Journal, 42, 287-296.

Tripathy, S., Sridharan, A. and Schanz, T. (2004). Swelling pressures of compacted bentonites from diffuse double layer theory. Canadian Geotechnical Journal, Vol. 41, 437-450.

van Genuchten, M. T. (1980). A closed-form equation for predicting the hydraulic conductivity of unsaturated soils. Soil Sci. Soc. Am. J., 44, 892–898.

Wheeler, S.J. and Sivakumar, V. (1995). An elasto-plastic critical state framework for unsaturated soil. Geotechnique, 45, 35-53.

Winterkorn, H.F. and Reno, W.H. (1967). The thermal conductivity of kaolinite clay as a function of type of exchange ion, density and moisture content. Soil Science, Highway Research Board, Washington, USA, 79-85.

Yong, R.N., Yaacob, W.Z.W., Bentley, S.P., Harris, C. and Tan, B.K. (2001). Partitioning of heavy metals on soil samples from column tests. Engineering Geology, 60, 307- 322.

Yukselen, Y. and Kaya, A. (2006). Prediction of cation exchange capacity from soil index properties. Clay Minerals, Vol. 41, No. 4, 827-837.

US EPA (United States Environmental Protection Agency) 1312 (1994). Test method for evaluating solid waste, physical/chemical methods (SW-846), 3rd edition, update 2B. EPA, National Centre for Environmental Publications, Cincinnati.

Table 4.1 Specification and properties of Speswhite kaolin (Ref: IMERYS Ltd)

Property		Unit	Value
Brightness (ISO R457)		-	85.5 ± 1.0
Yellowness		-	4.7
+ 300 μm (mass % max)		%	0.02
+ 10 μm (mass % max)		%	0.5
-2 μm (mass % max)		%	80 ± 3
Moisture (mass % max)		%	1.5
Specific gravity		-	2.6
pH		-	5
Surface area (BET method)		m^2/g	14
Oil absorption		g/100g	42
Aerated powder density		kg/m^3	360
Tapped powder density		kg/m^3	620
Water soluble salt content (mass %)		%	0.2
Chemical analysis by X-ray Fluorescence (XRF)	SiO_2 (mass %)	%	47
	Al_2O_3 (mass %)	%	38

Table 4.2 Thermal conductivity of kaolinite clay (Winterkorn and Reno, 1967)

Moisture content ranges (%)	Degree of saturation (%)	Thermal conductivity (W/mK)
1.24 – 1.44	2.07 – 2.4	0.14 – 0.18
5.24 – 5.76	8.73 – 9.6	0.34 – 0.37
11.01 – 12.62	18.35 – 21.03	0.5 – 0.58
15.81 – 17.90	26.35 – 29.83	0.64 – 0.74
30.56 – 34.78	50.93 – 57.97	0.95 – 1.39

NB. These values have been converted to SI units from the original reference

Table 4.3 Thermal conductivity of MX-80 bentonite (Melhuish, 2005)

Degree of saturation (%)	Thermal conductivity (W/mK)
0	0.3
20	0.3
80	1.2
100	1.3

Table 4.4 Properties of Speswhite kaolin

Property		Unit	Value
Natural water content		%	1.2
Specific gravity		-	2.61
-1 µm (mass % max)		%	75%
Liquid limit		%	63
Plastic limit		%	32
Plasticity index		%	31
Activity		%	0.31
Linear shrinkage		%	7
Saturated hydraulic conductivity		m/s	1.27×10^{-9}
Swell index		ml/2g	4
pH	(soil water ratio 1:10)	-	5.0
	(soil water ratio 1:15)	-	5.2
Specific surface area (EGME method)		m^2/g	48
Cation exchange capacity	Sodium	meq/100g	1.53
	Magnesium	meq/100g	0.89
	Potassium	meq/100g	0.43
	Calcium	meq/100g	0.89
	Total	meq/100g	3.74
Mineral composition by X-ray diffraction (XRD)	Kaolinite	%	95
	Illite	%	4
	Quartz	%	1

Table 4.5 Properties of MX-80 bentonite

Property		Unit	Value
Natural water content		%	12 to 14
Specific gravity		-	2.80
-1 μm (mass % max)		%	85
Liquid limit		%	385
Plastic limit		%	39
Plasticity index		%	346
Activity		%	3.46
Linear shrinkage		%	42
Saturated hydraulic conductivity		m/s	1.25×10^{-11}
Swell index		ml/2g	32
pH	(soil water ratio 1:10)	-	9.20
	(soil water ratio 1:15)	-	9.28
Specific surface area (EGME method)		m^2/g	650
Cation exchange capacity	Sodium	meq/100g	53.08
	Magnesium	meq/100g	7.83
	Potassium	meq/100g	1.07
	Calcium	meq/100g	31.00
	Total	meq/100g	92.88
Mineral composition by X-ray diffraction (XRD)	Montmorillonite	%	78
	Albite	%	10
	Quartz	%	11

Table 4.6 Weighing factors (Biscaye, 1964)

Mineral	Weighing factor
Montmorillonite	1
Illite	4
Chlorite	2
Kaolinite	2
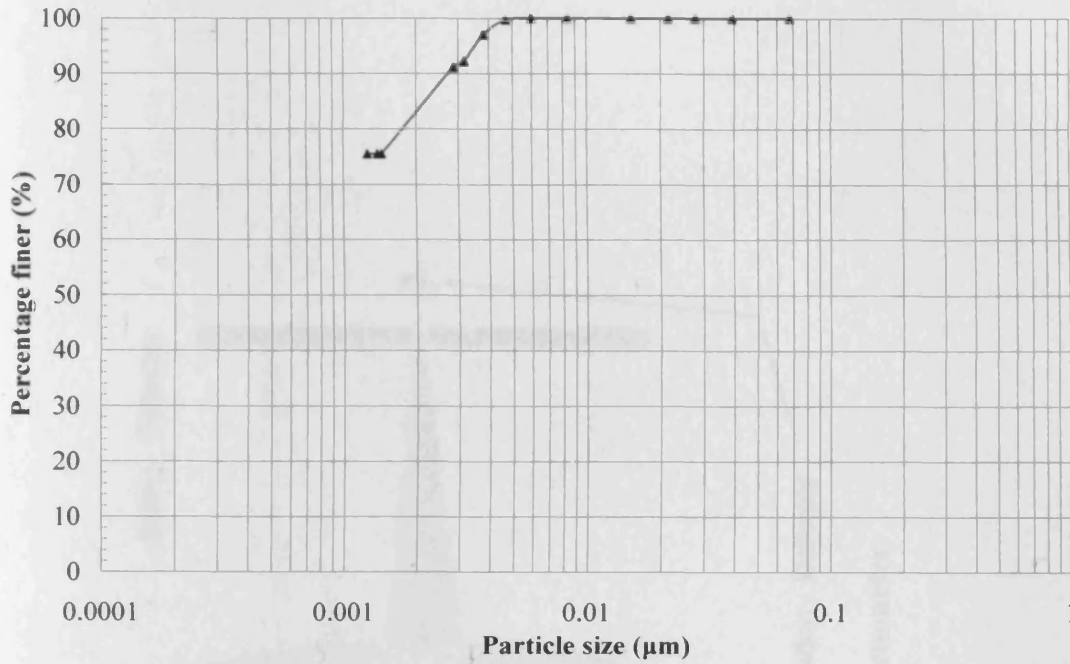
Figure 4.1 Particle size distribution curve for Speswhite kaolin by hydrometer method
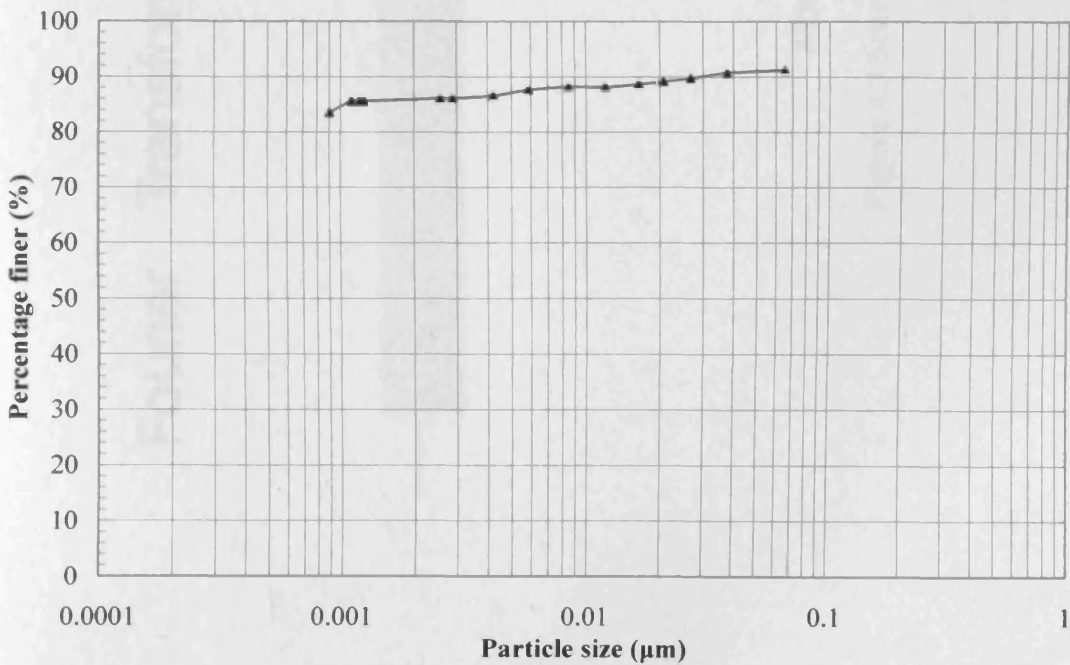
Figure 4.2 Particle size distribution curve for MX-80 bentonite by hydrometer method
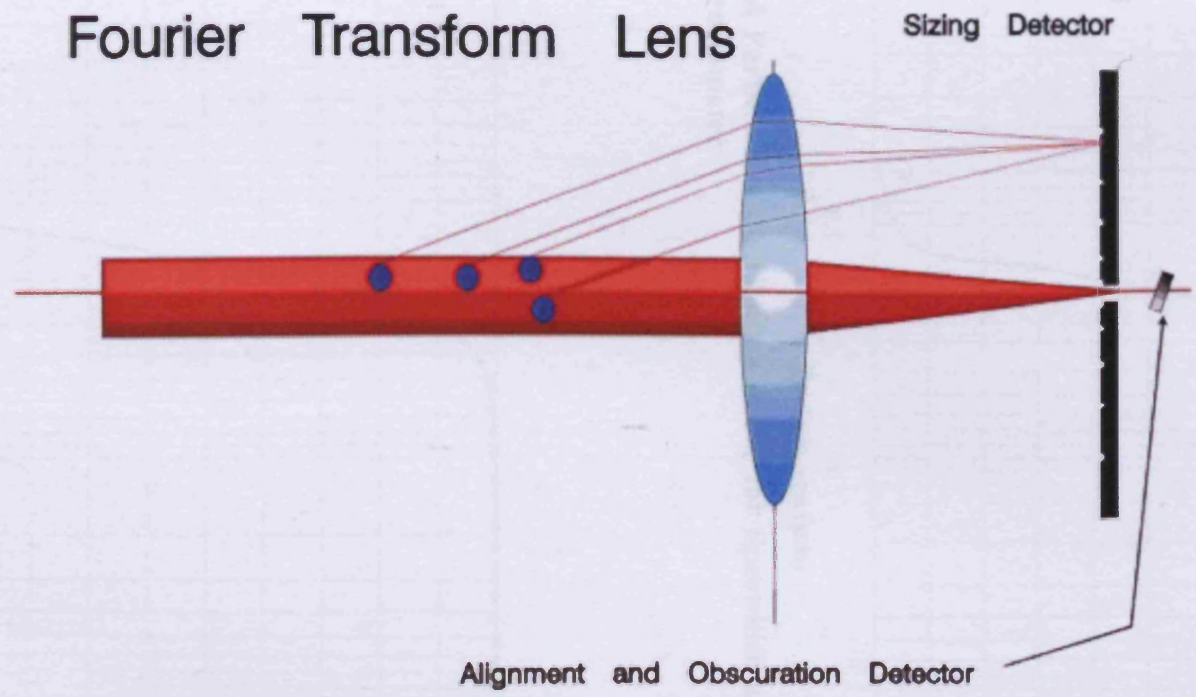
Figure 4.3 Schematic of laser diffractometer
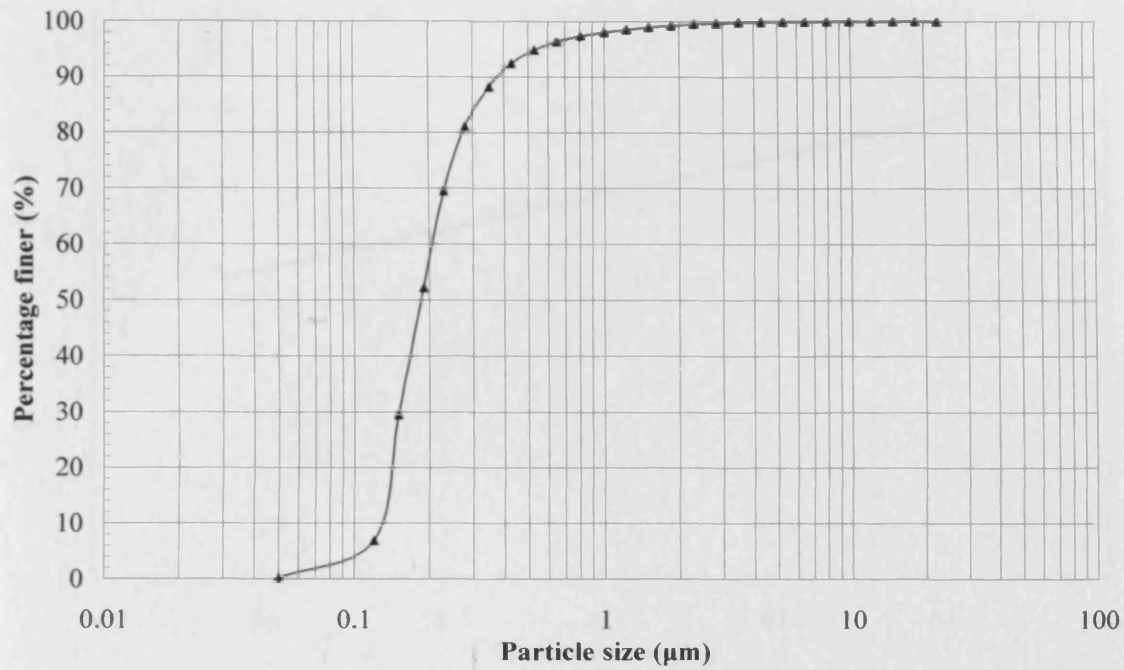
Figure 4.4 Particle size distribution curve for Speswhite kaolin by MasterSizer laser diffractometer
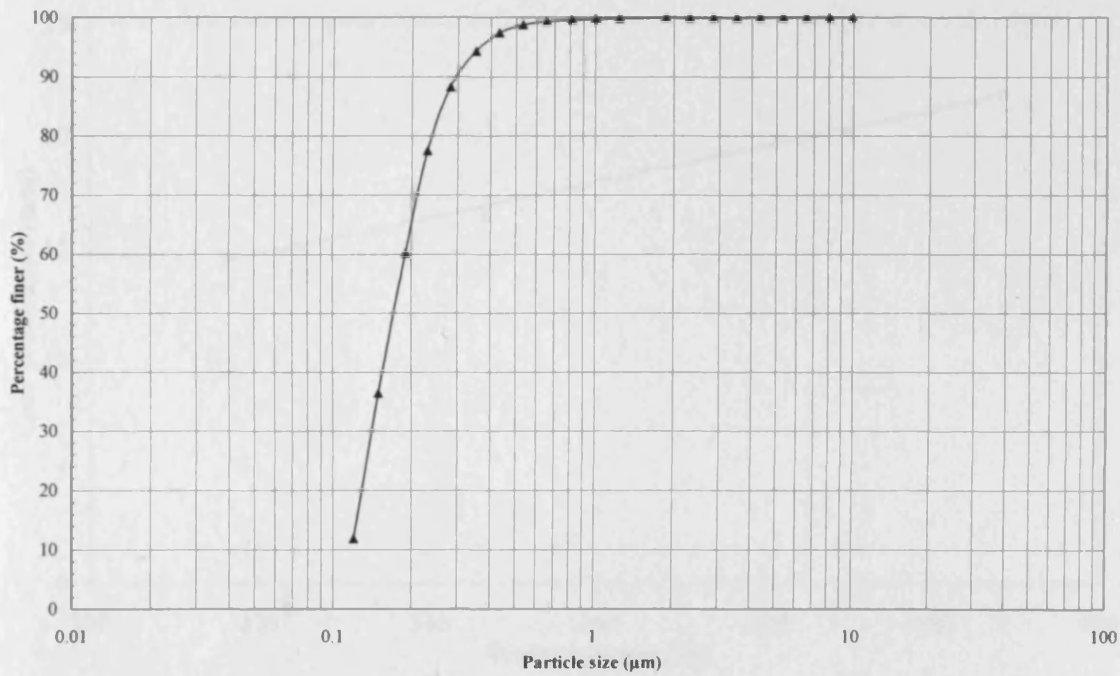
Figure 4.5 Particle size distribution curve for MX-80 bentonite by MasterSizer laser diffractometer
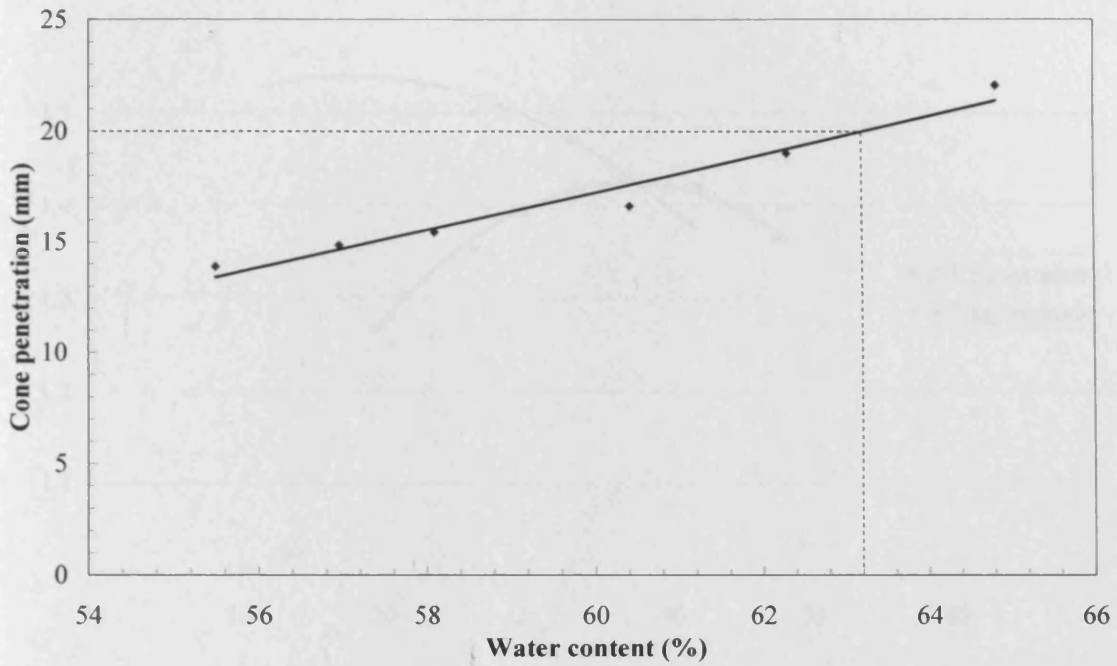
Figure 4.6 Liquid limit determination for Speswhite kaolin via the cone penetrometer method
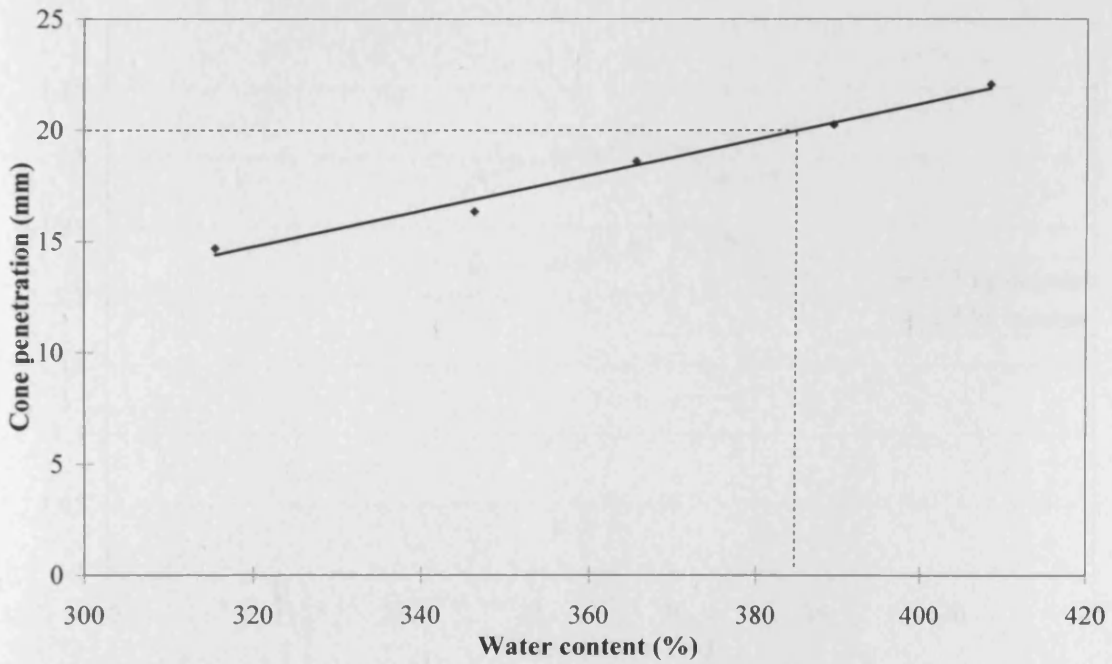
Figure 4.7 Liquid limit determination for MX-80 bentonite via the cone penetrometer method
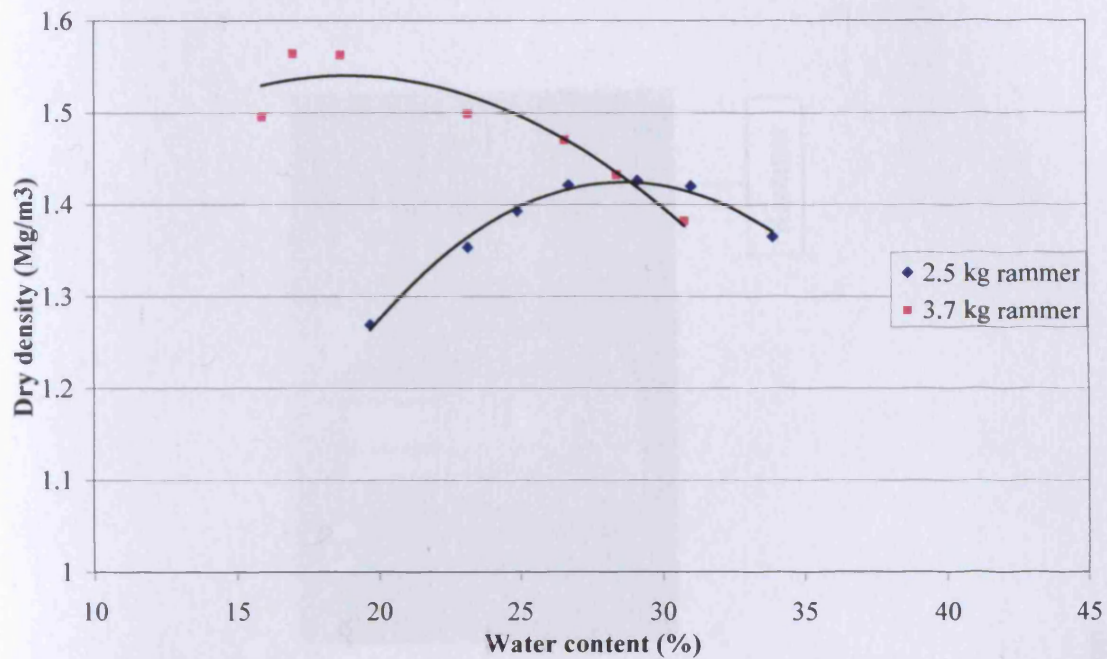
Figure 4.8 Dynamic compaction curve for Speswhite kaolin via standard Proctor method
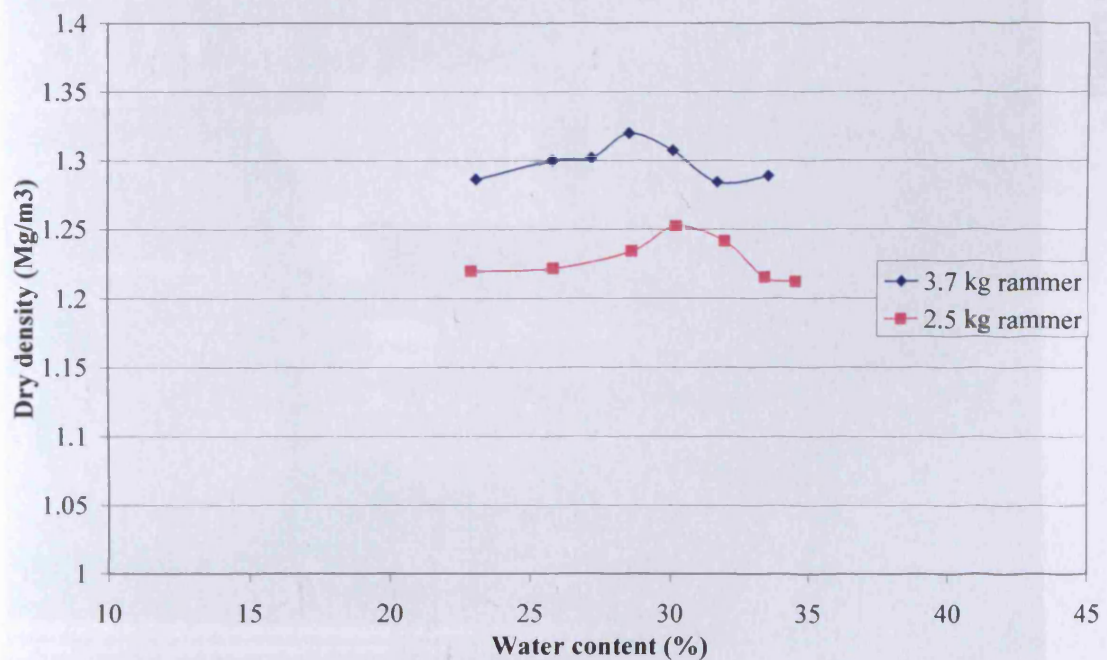
Figure 4.9 Dynamic compaction curve for MX-80 bentonite via standard Proctor method
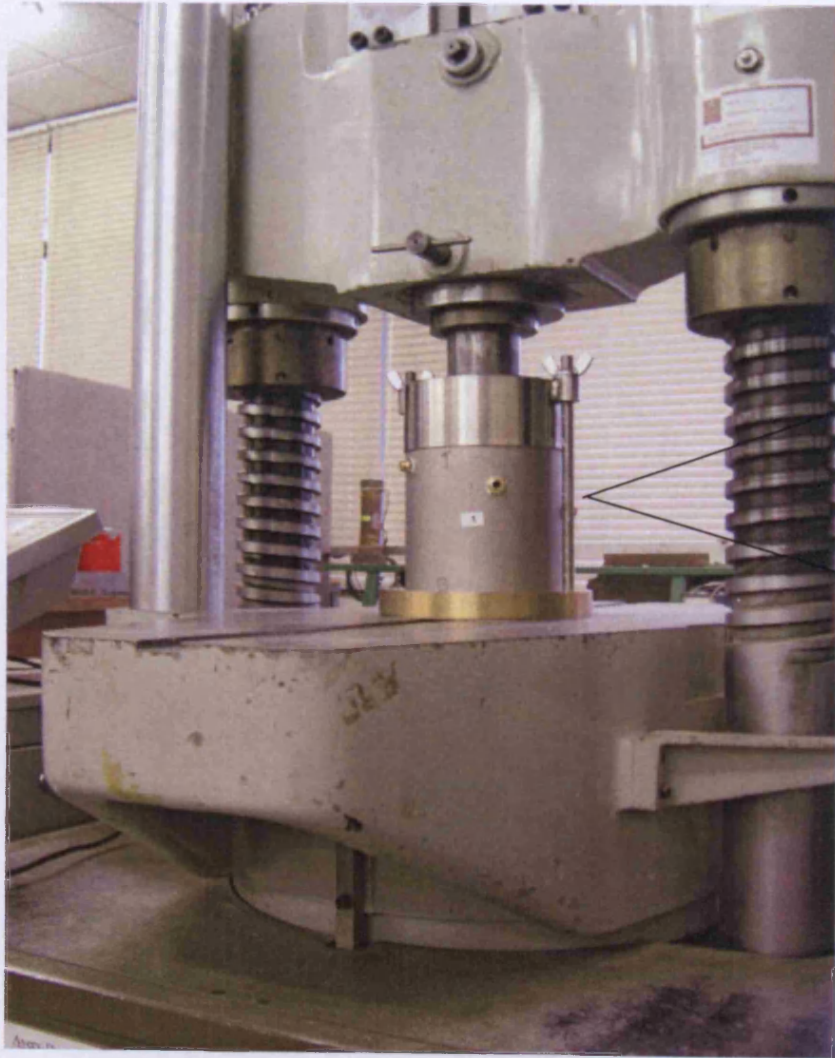
Figure 4.10 Static compaction

Rammer
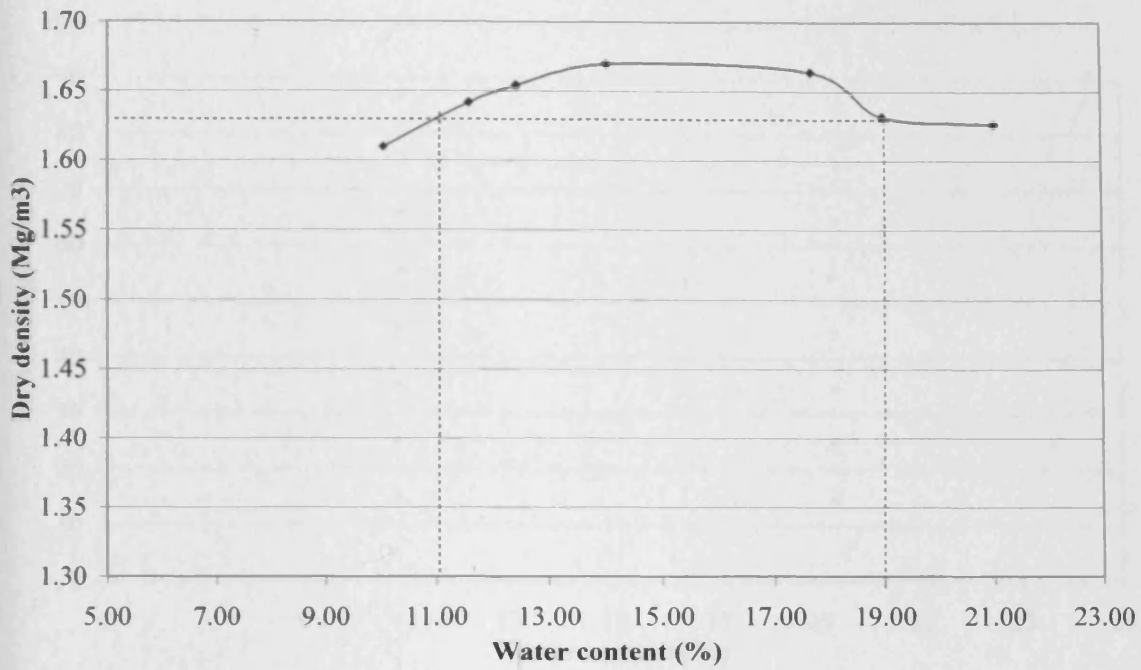
Figure 4.11 Static compaction curve for Speswhite kaolin
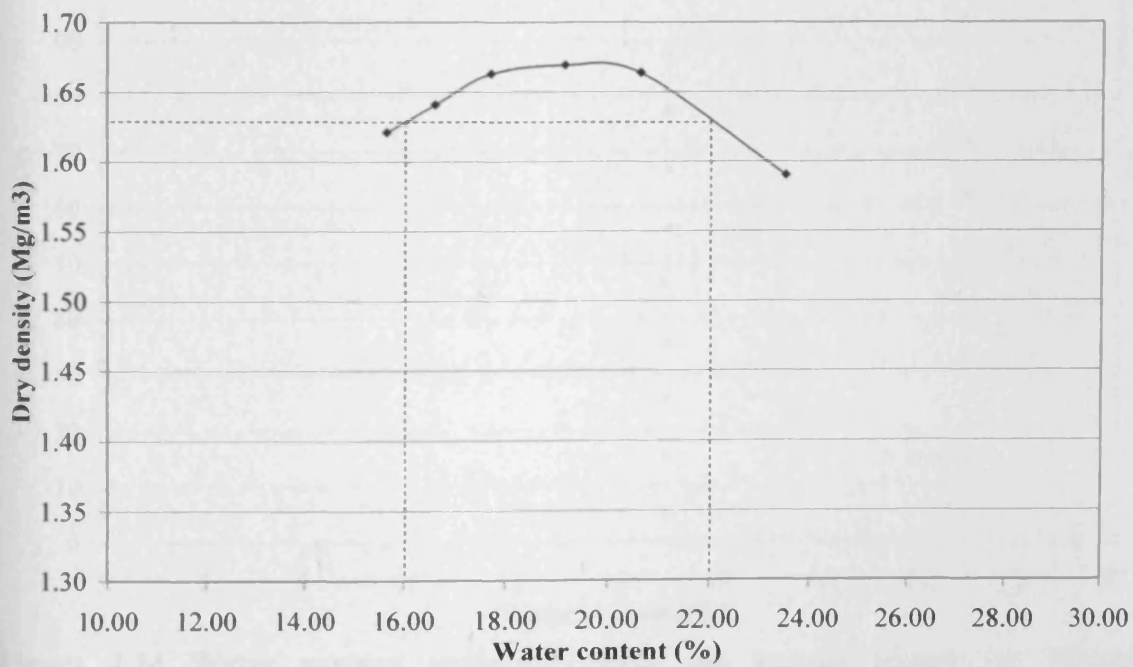
Figure 4.12 Static compaction curve for MX-80 bentonite
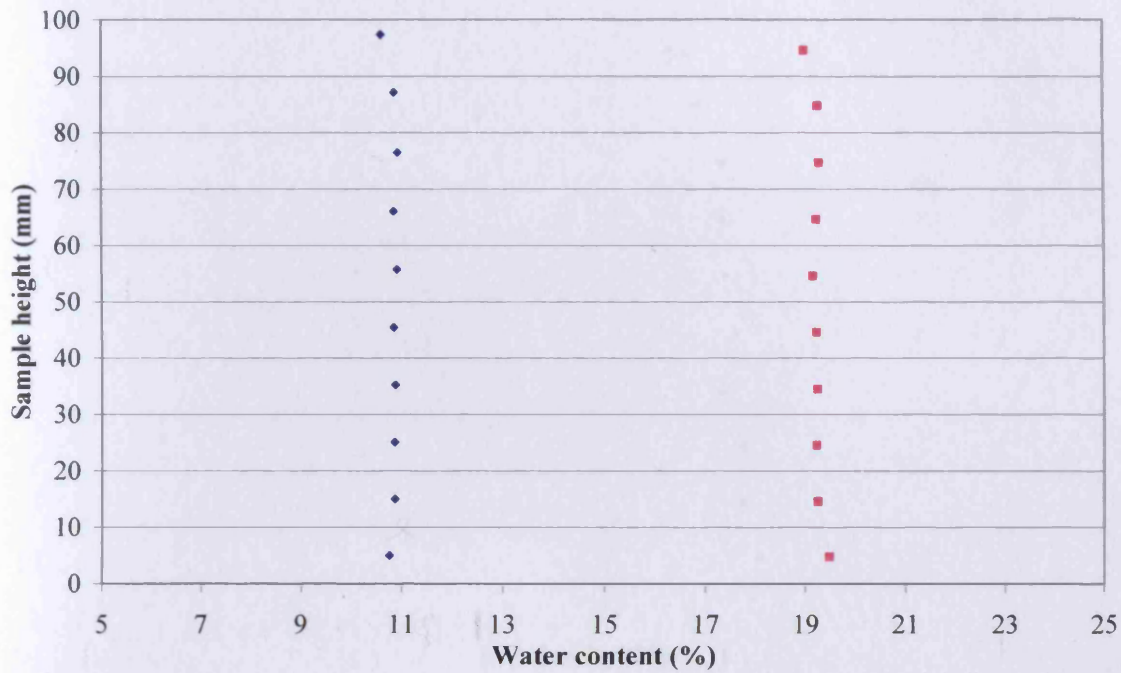
Figure 4.13 Water content variation along the sample length for Speswhite kaolin
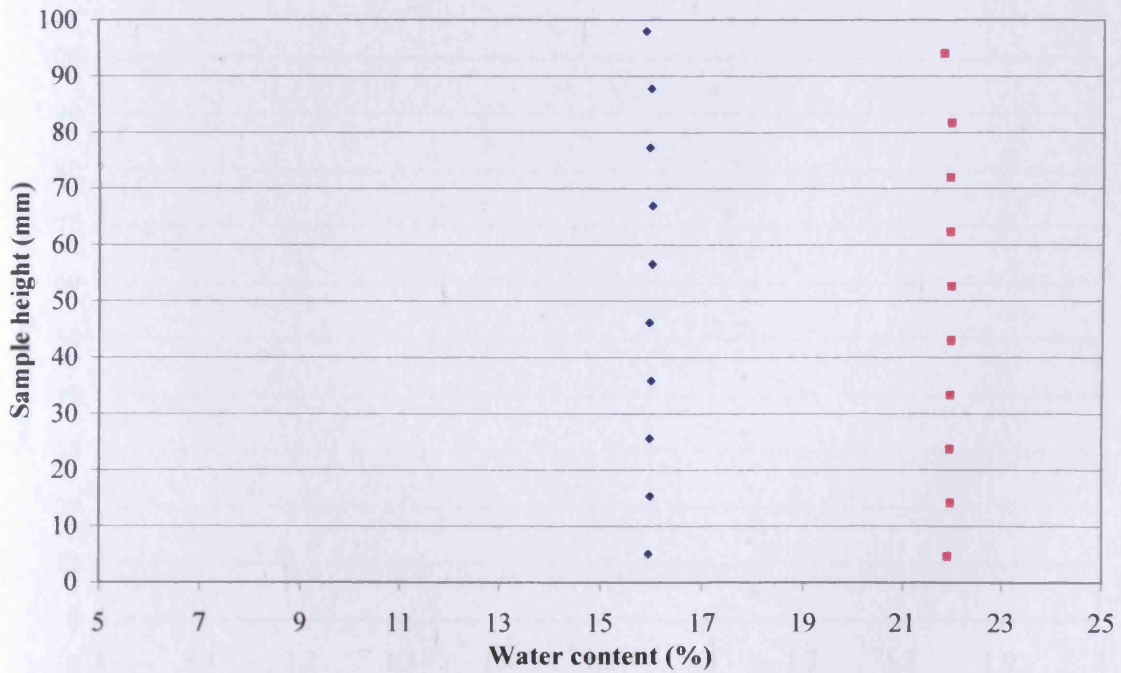
Figure 4.14 Water content variation along the sample length for MX-80 bentonite
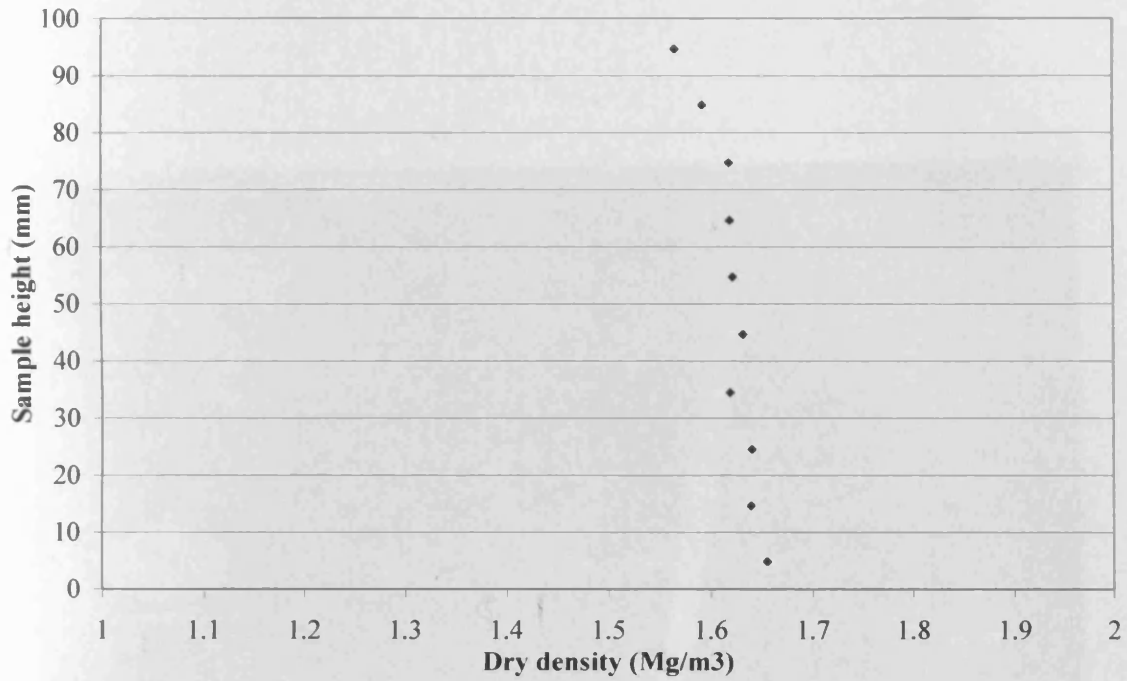
Figure 4.15 Dry density variation along the sample length for Speswhite kaolin
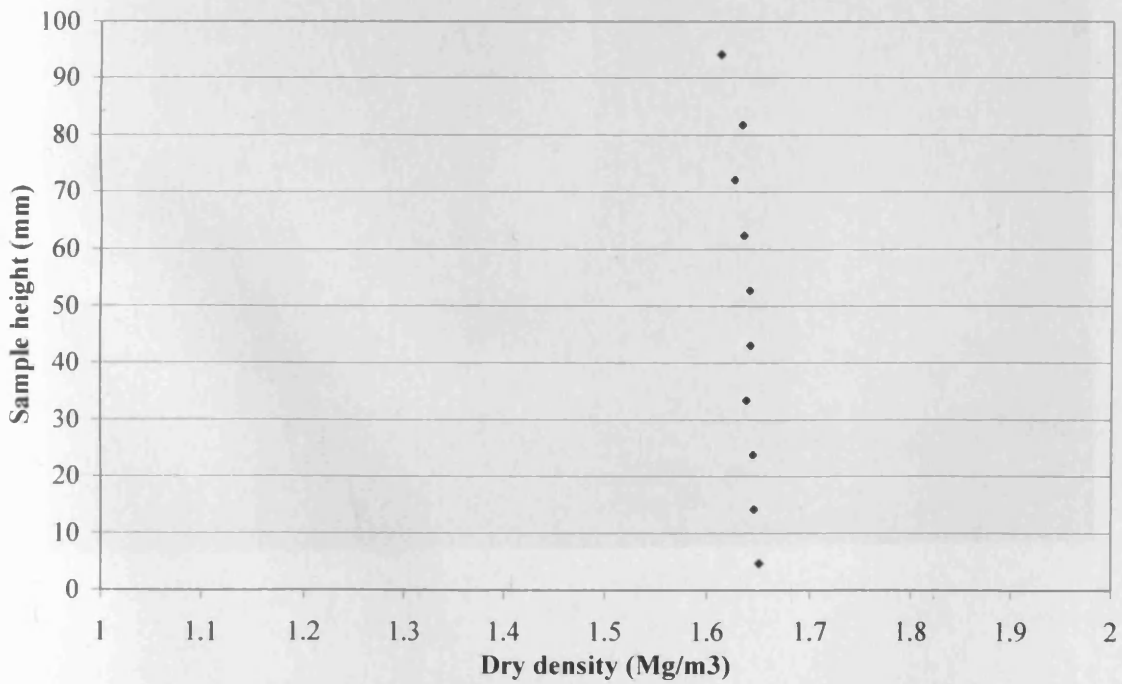
Figure 4.16 Dry density variation along the sample length for MX-80 bentonite
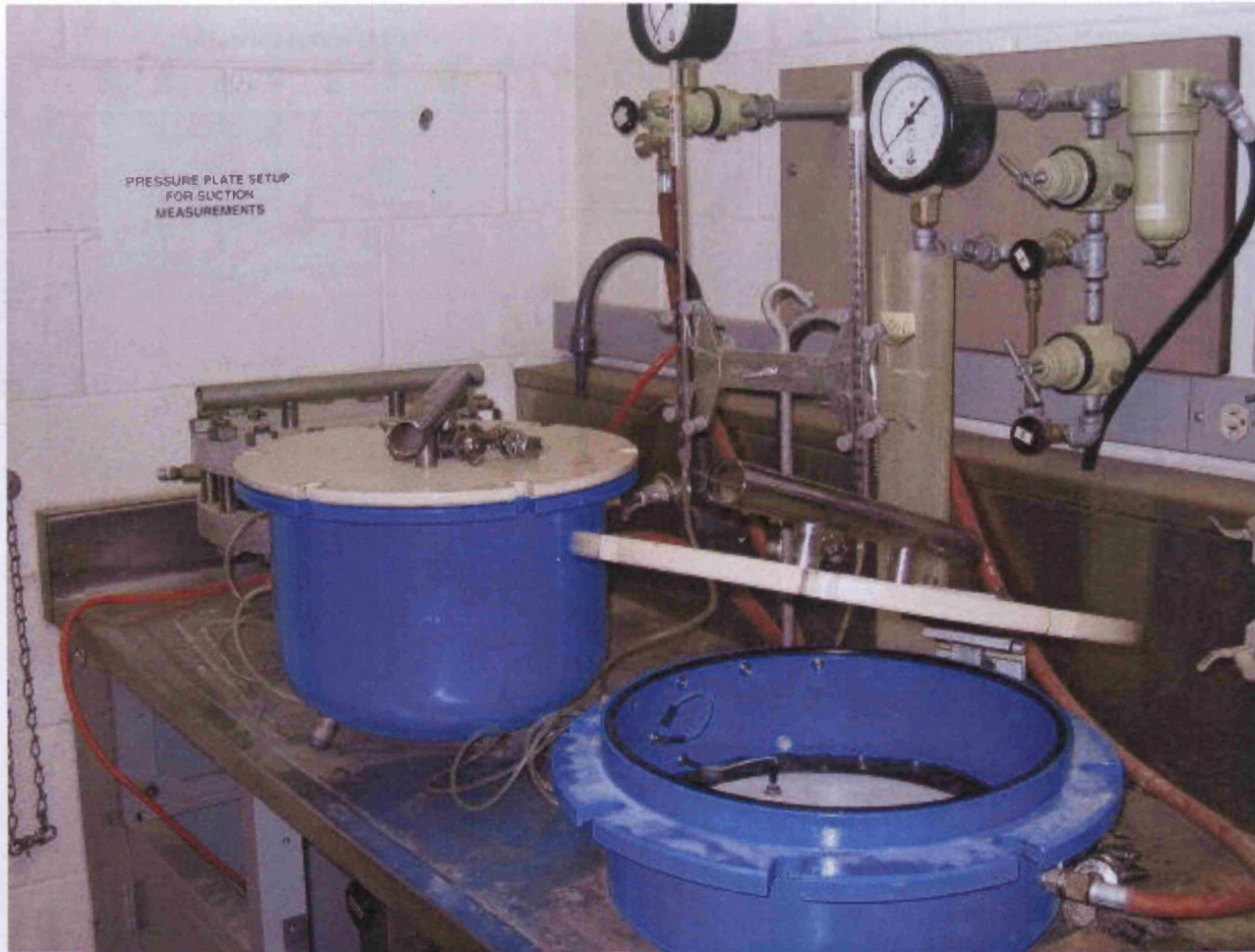
Figure 4.17 Pressure plate extractor
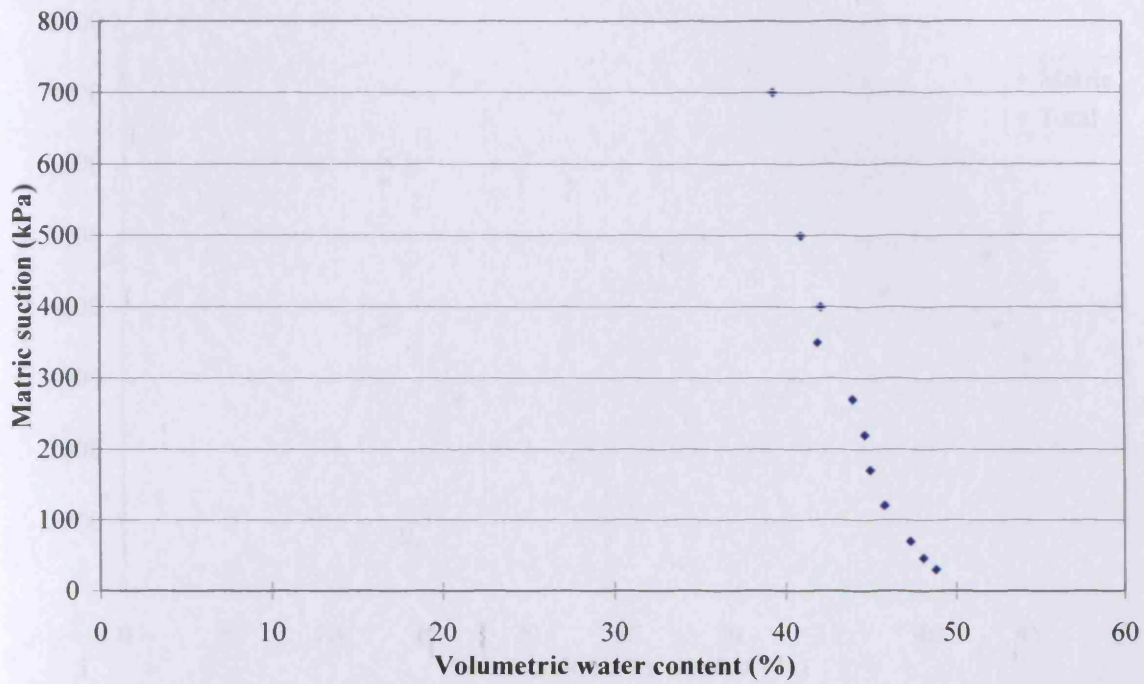
Figure 4.18 Matric suction for Speswhite kaolin by pressure plate extractor method
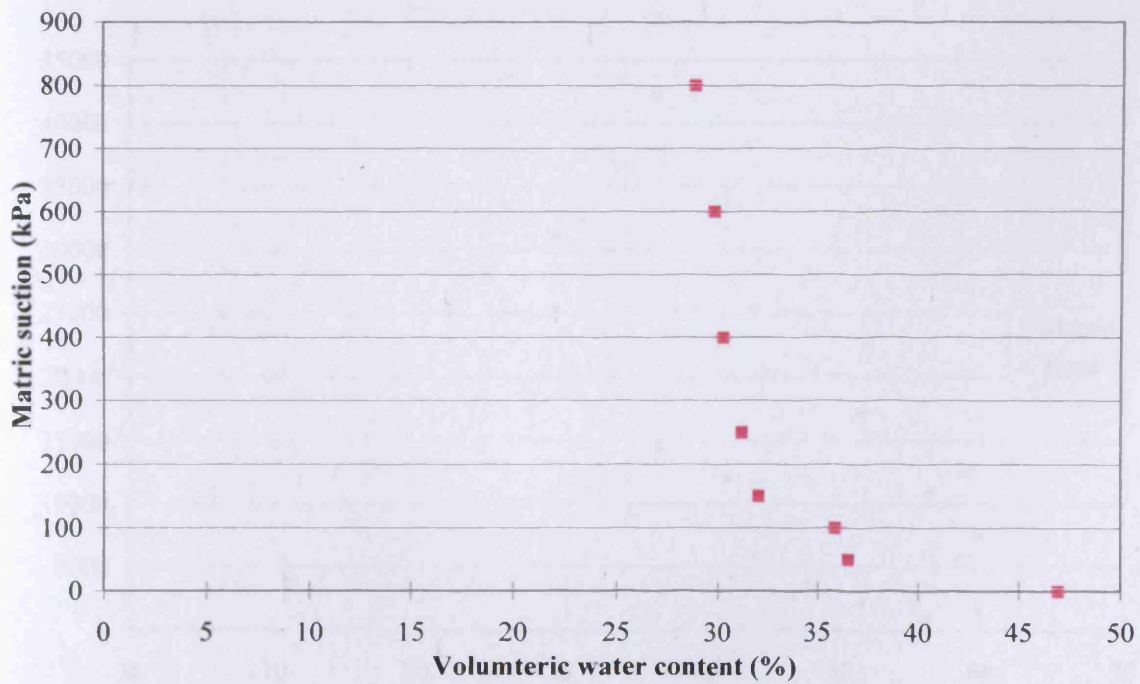
Figure 4.19 Matric suction for MX-80 bentonite by pressure plate extractor method
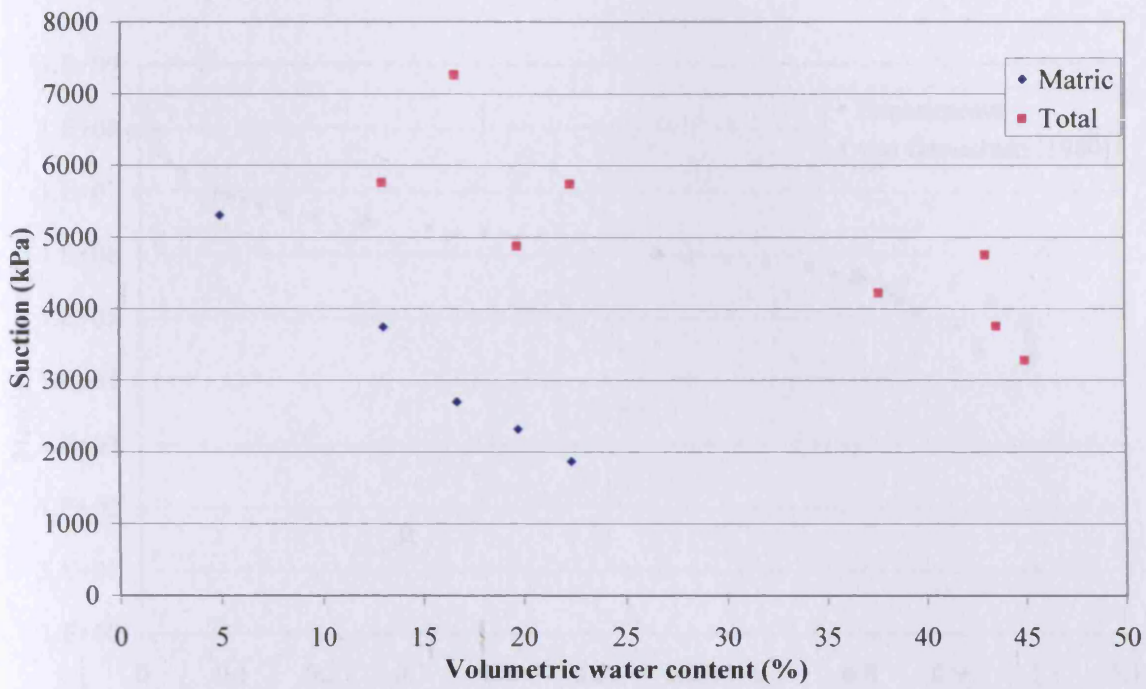
Figure 4.20 Matric and total suction for Speswhite kaolin by filter paper method
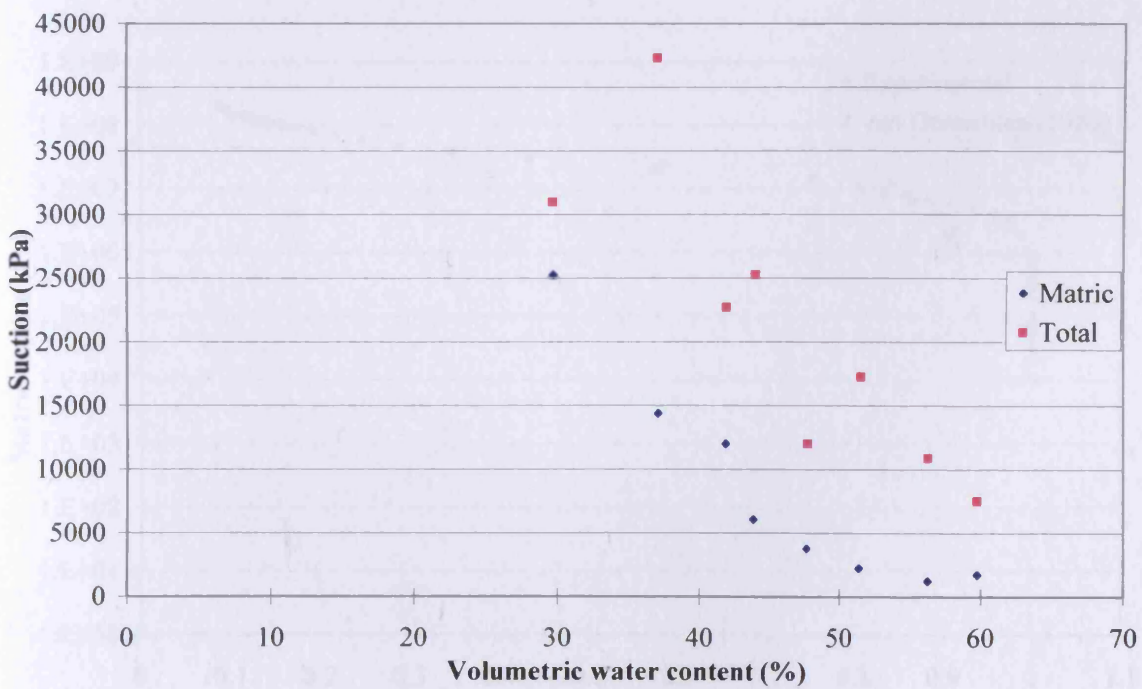
Figure 4.21 Matric and total suction for MX-80 bentonite by filter paper method
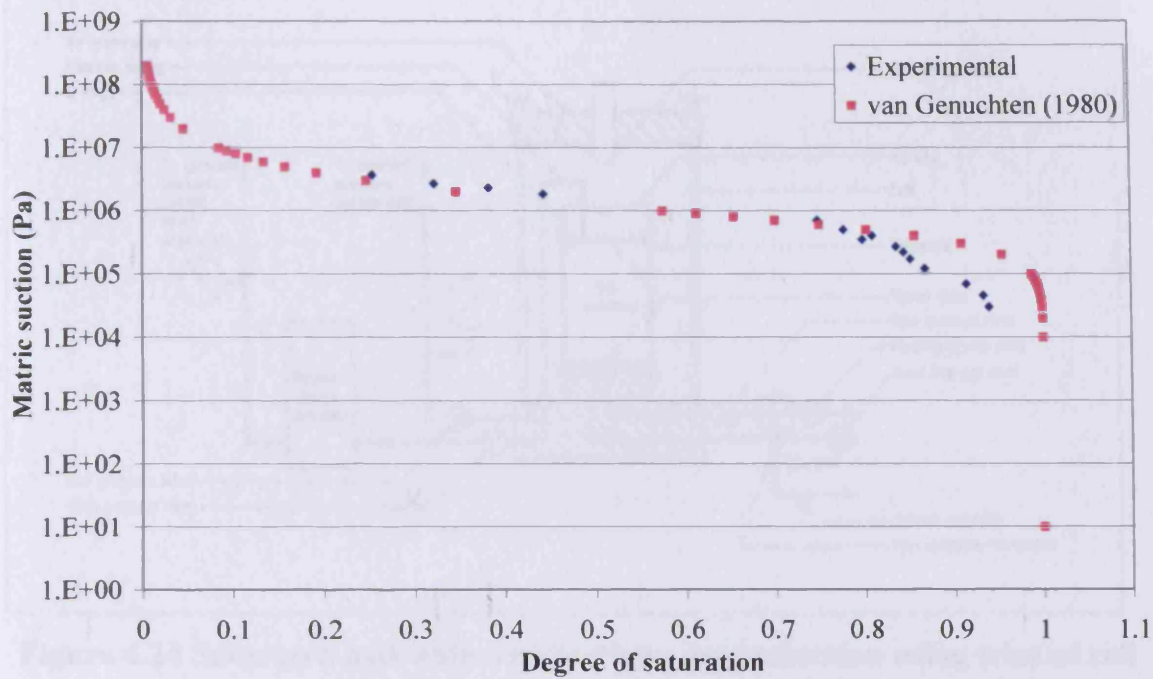
Figure 4.22 Moisture retention curve for Speswhite kaolin
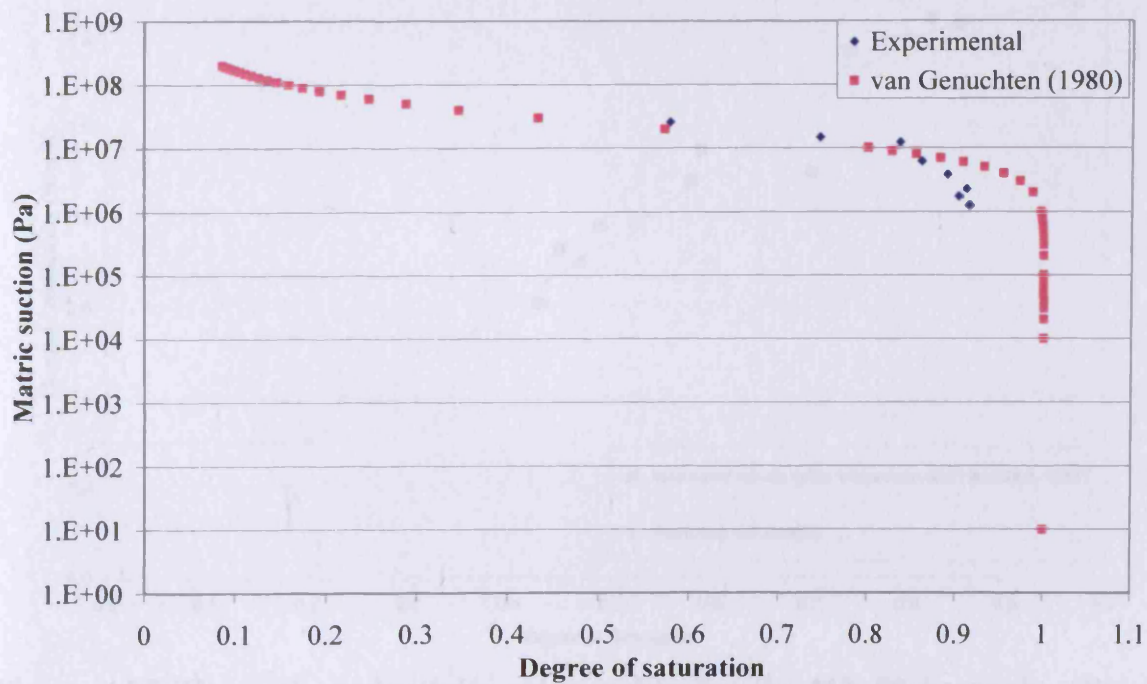
Figure 4.23 Moisture retention curve for MX-80 bentonite
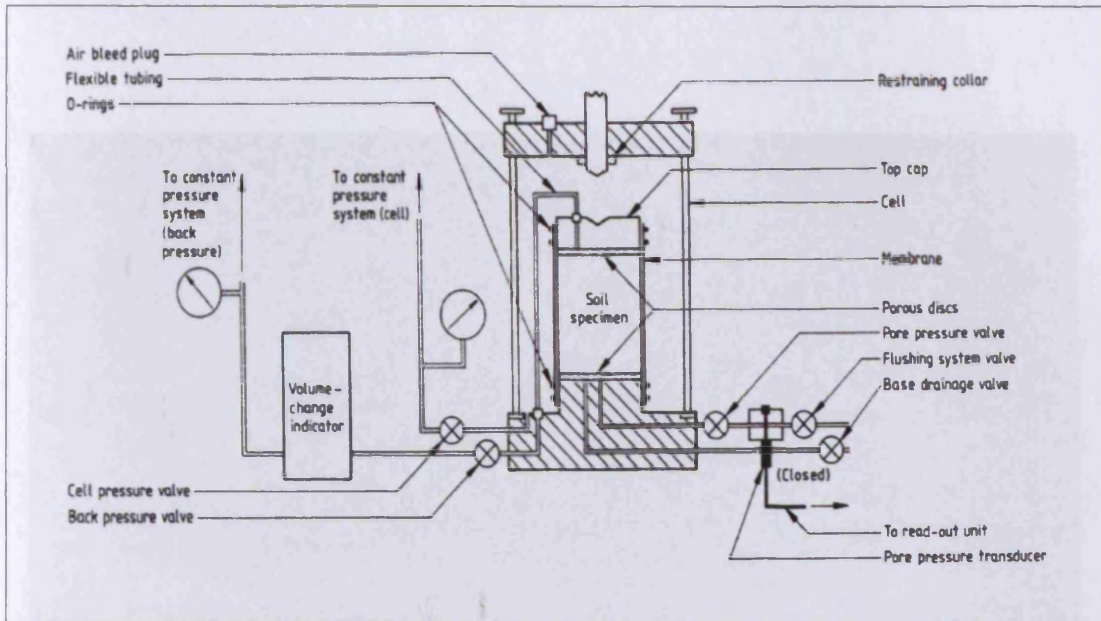
Figure 4.24 Saturated hydraulic conductivity determintaion using triaxial cell
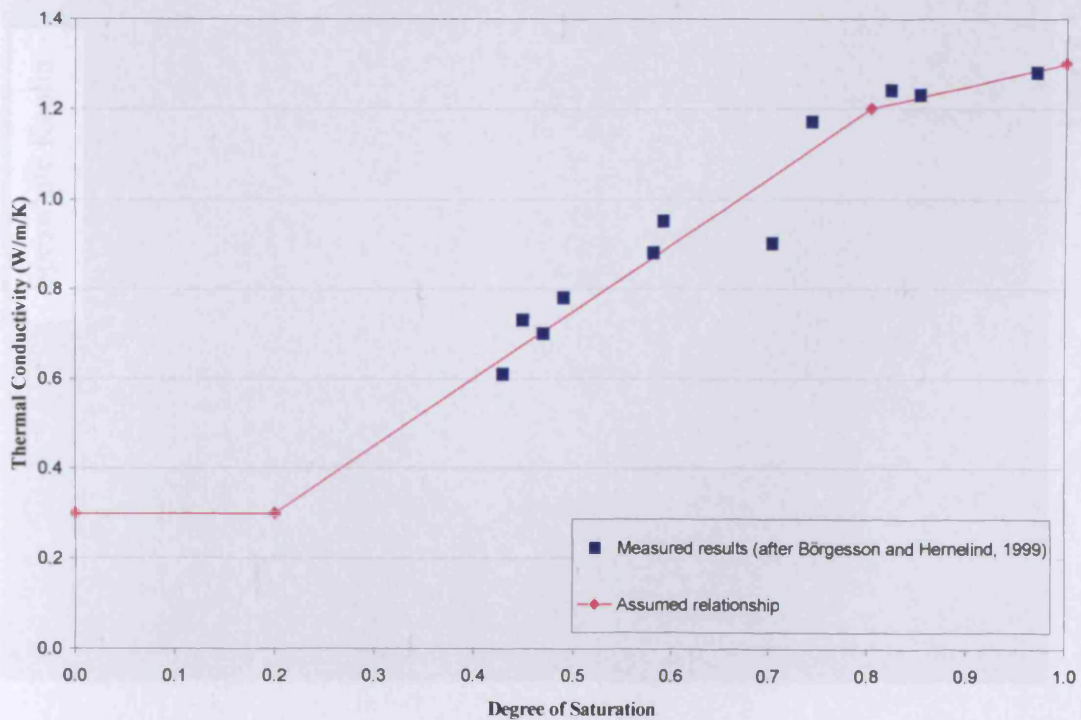
Figure 4.25 Thermal conductivity relationship for the MX-80 bentonite (Troy, 2005)

Speswhite Kaolin
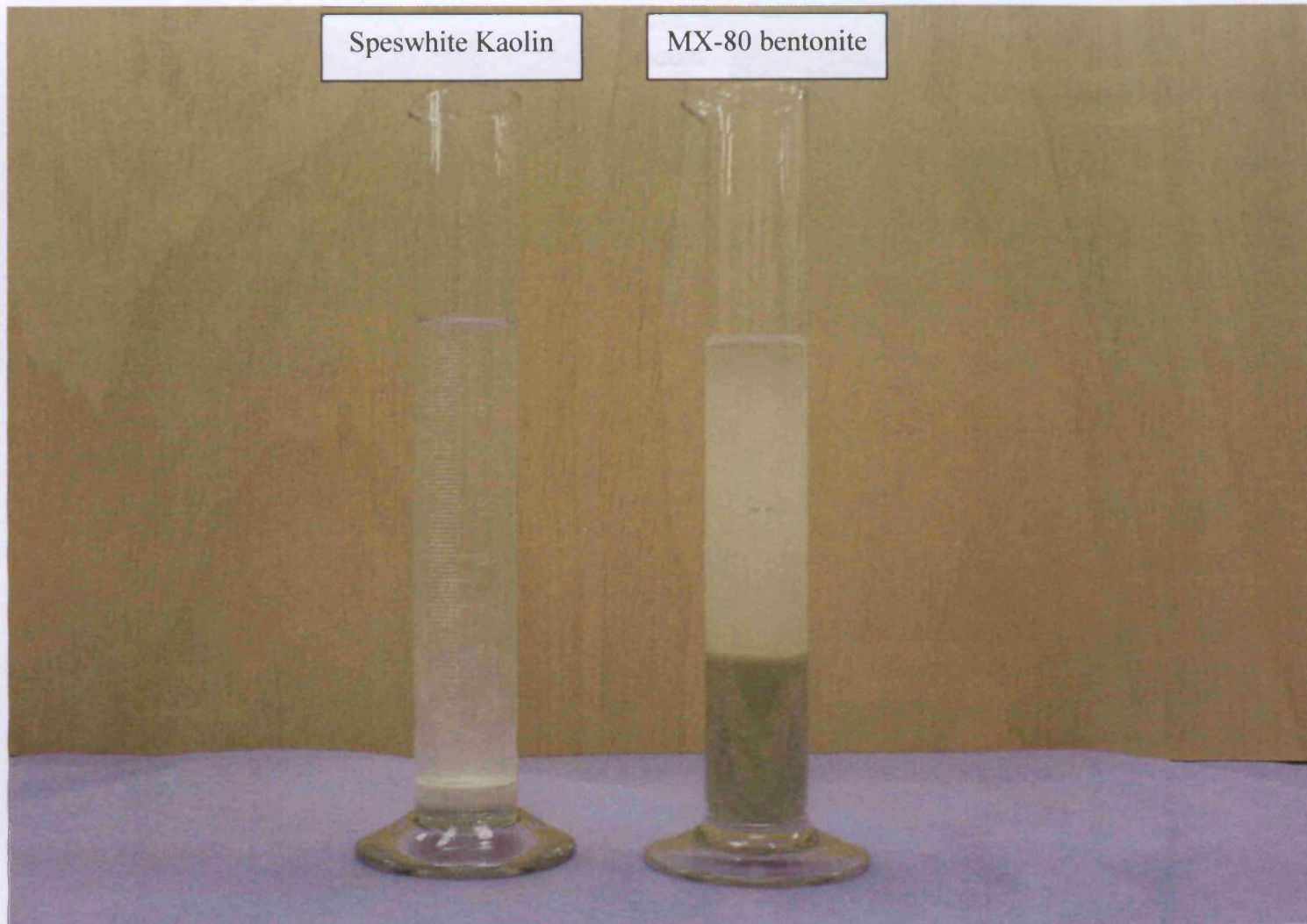
MX-80 bentonite

Figure 4.26 Swell index test
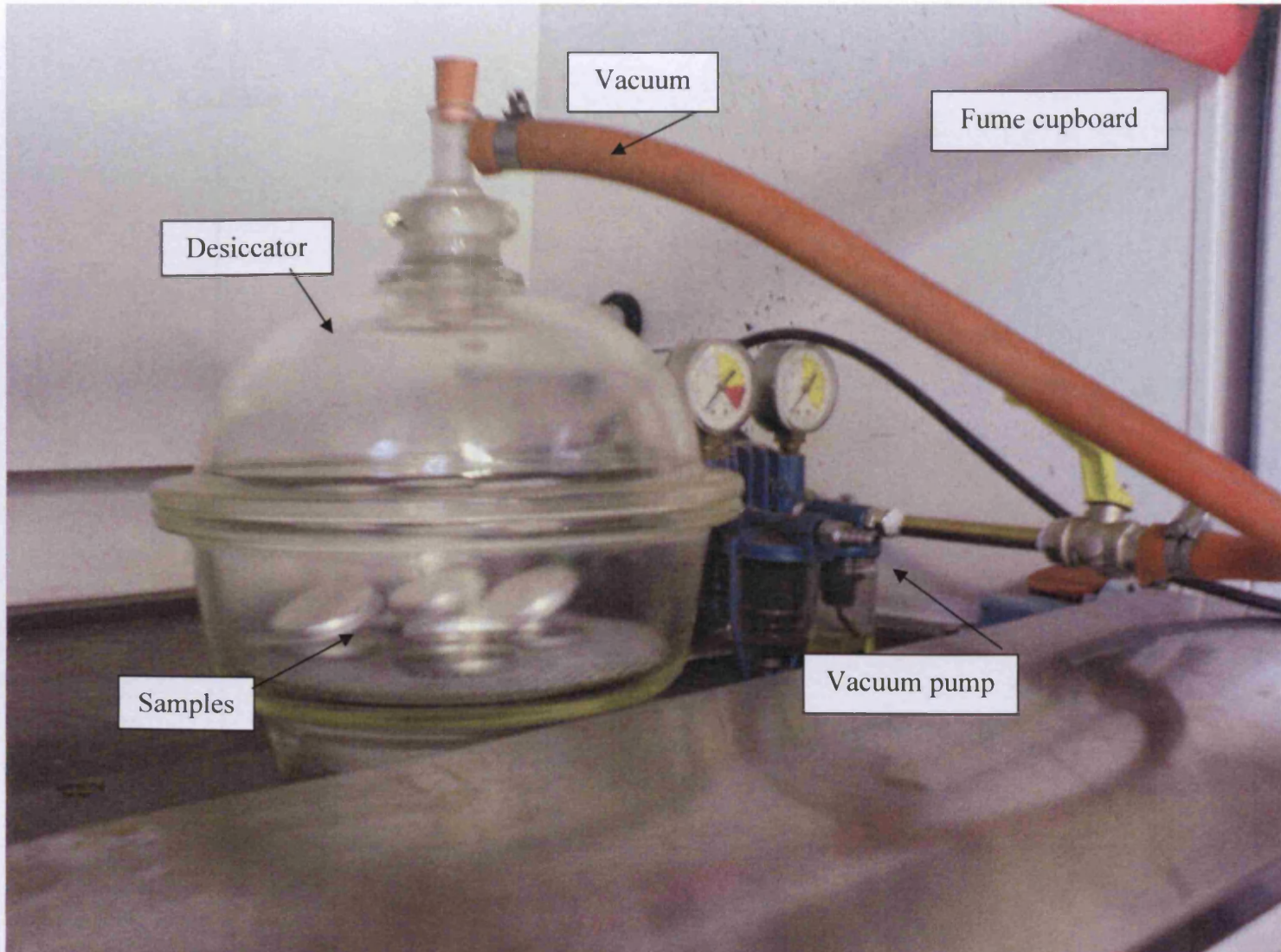
Figure 4.27 Specific surface area measurement using EGME method
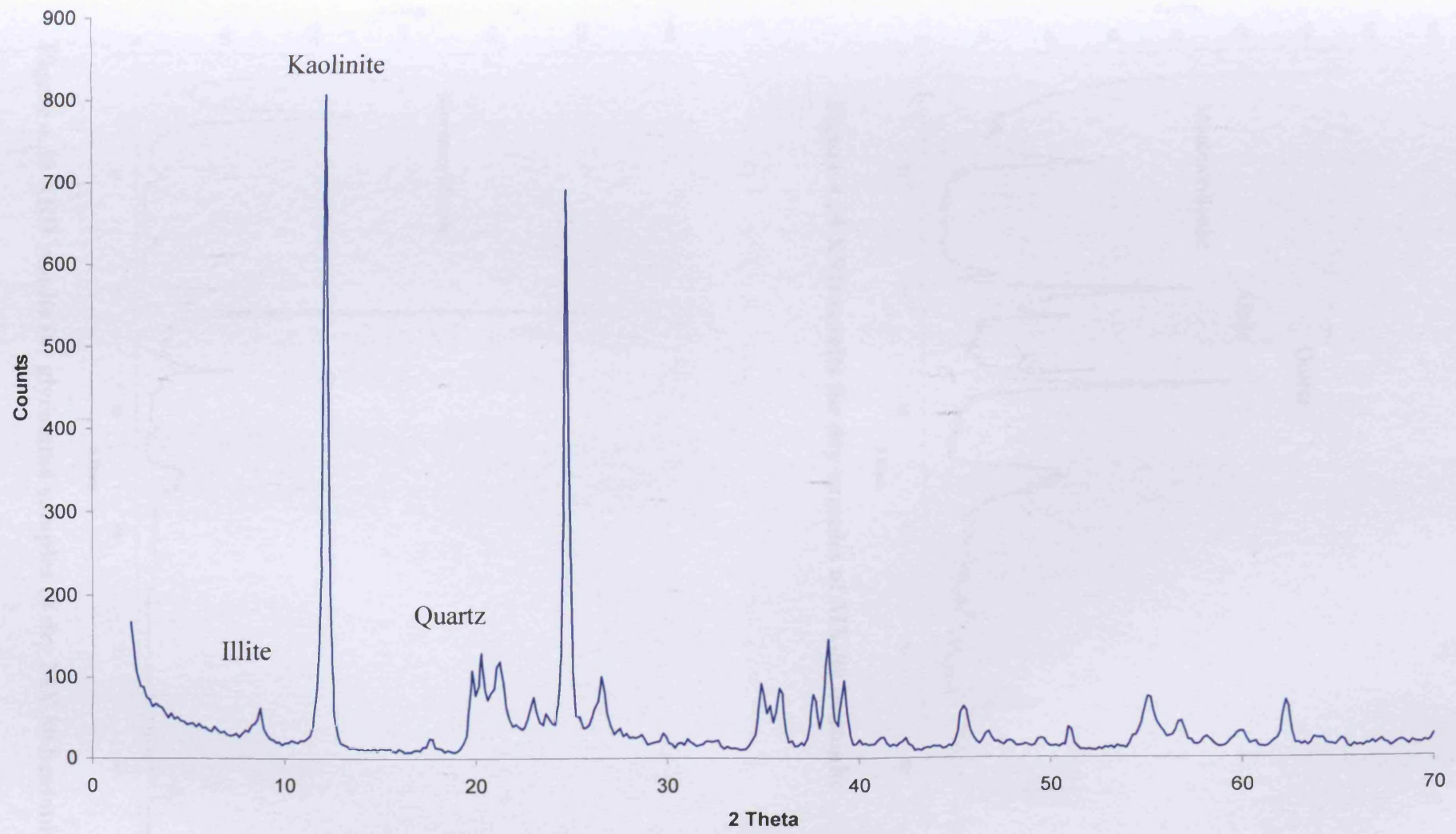
Figure 4.28 XRD results for Speswhite kaolin
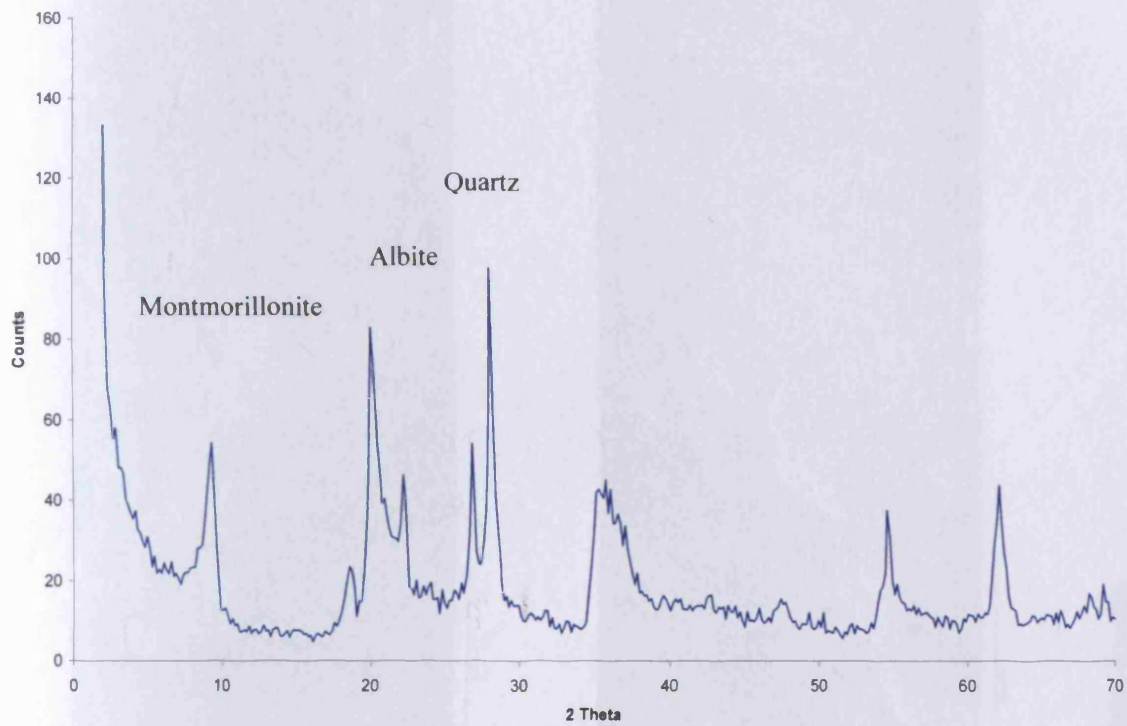
Figure 4.29 XRD results for dry samples of MX-80 bentonite
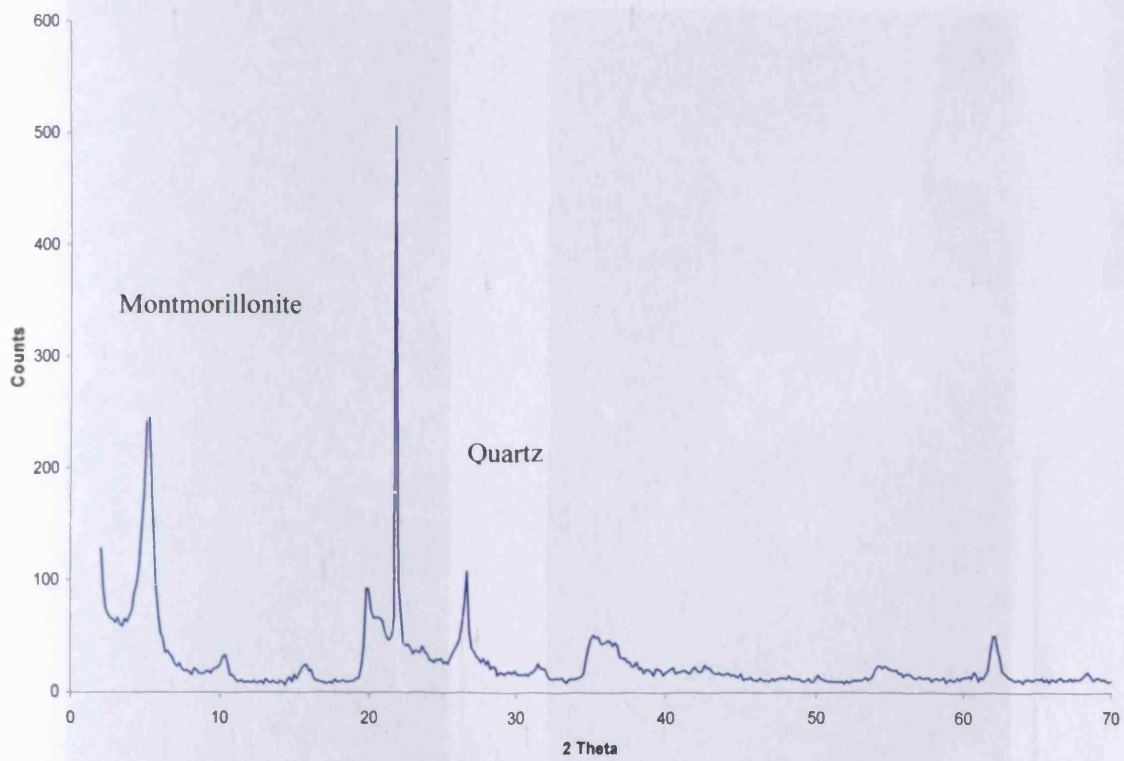
Figure 4.30 XRD results for glycolated samples of dry MX-80 bentonite
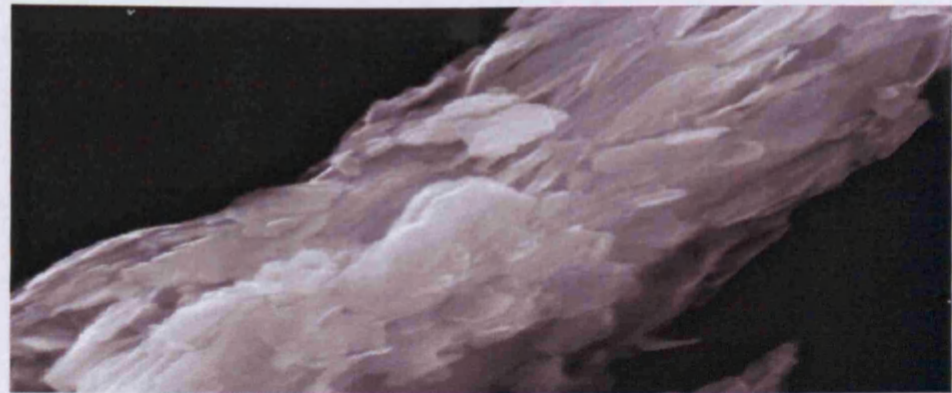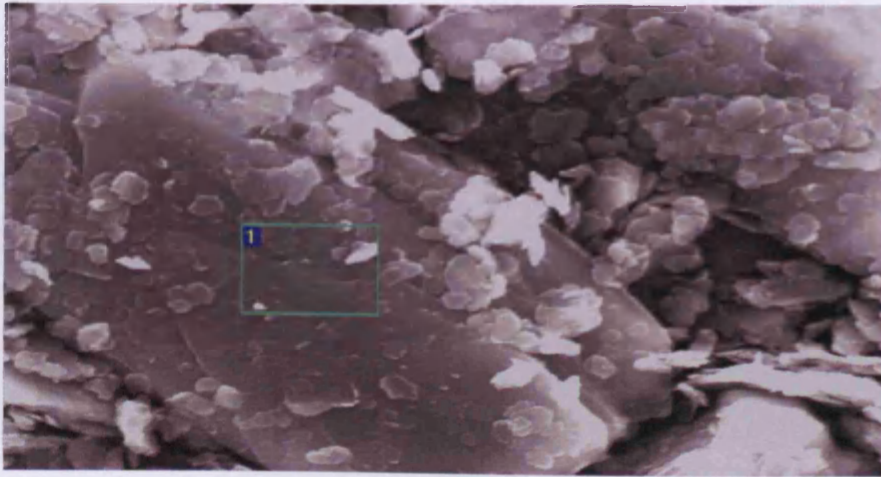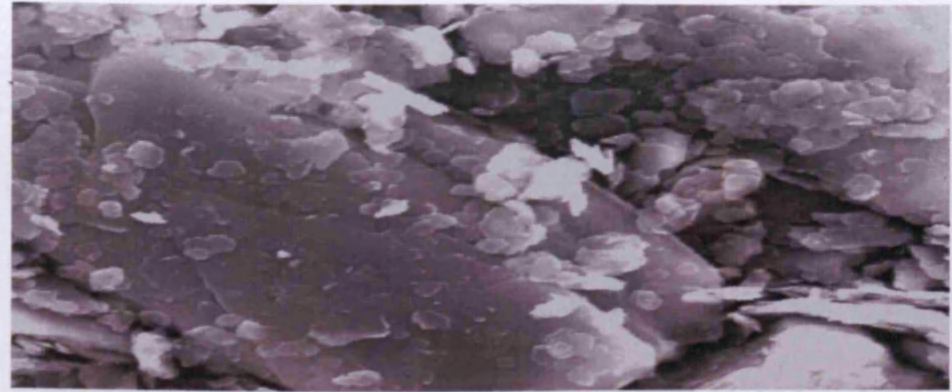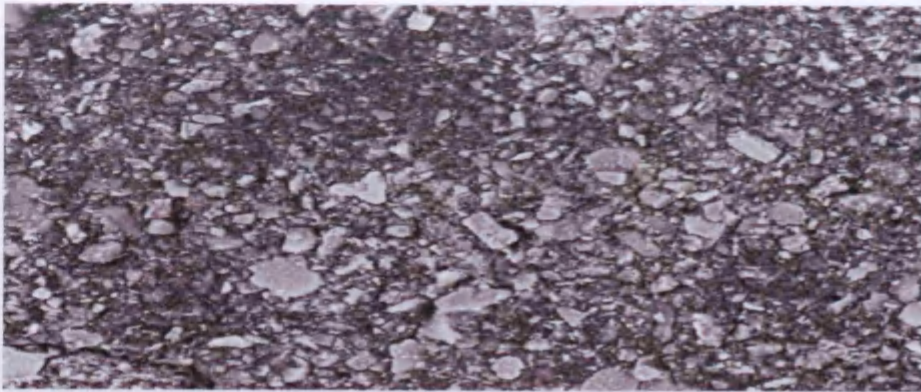
Figure 4.31 ESEM images for Speswhite kaolin
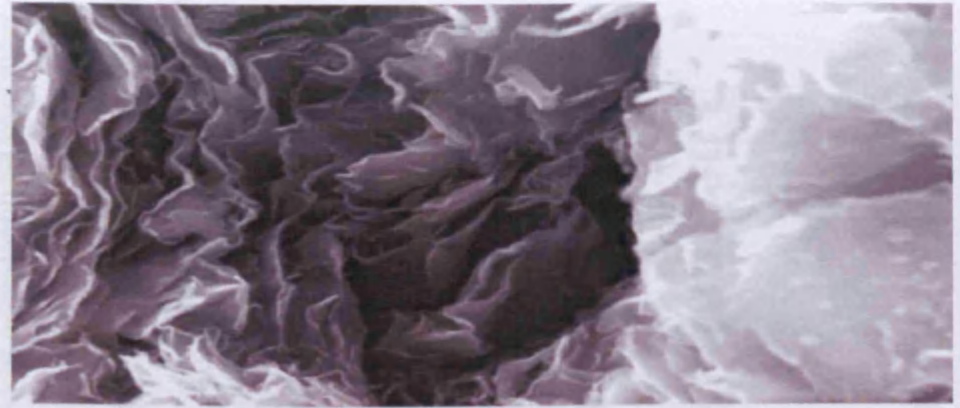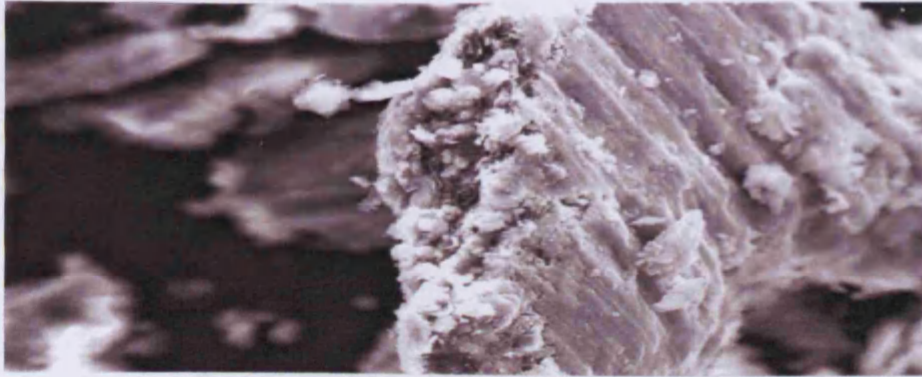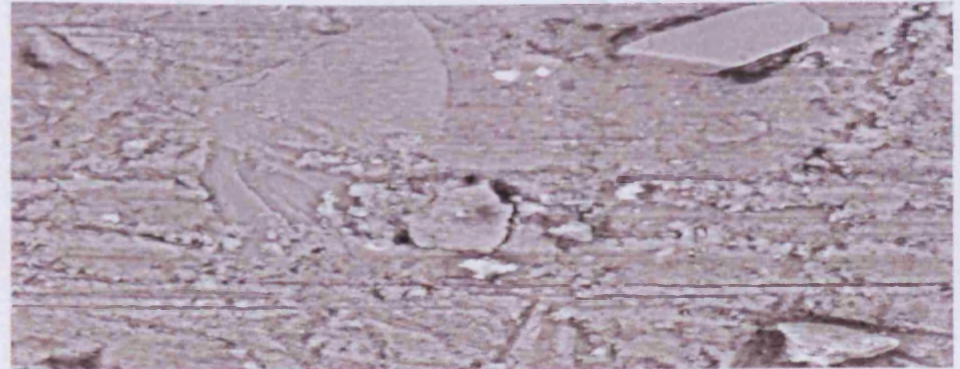
Figure 4.32 ESEM images for MX-80 bentonite

Chapter 5

Thermal, thermo-hydraulic and isothermal tests on kaolin

5.1 Introduction

This chapter presents the results of a series of thermal, thermo-hydraulic and isothermal tests performed on Speswhite kaolin. The aim of these tests is to investigate both the heat transfer and moisture movement in liquid and vapour phases in kaolin clay. The aim of the tests is for the test results to be used for a qualitative analysis of liquid and vapour moisture. The quantitive analysis to calculate the amount of liquid and vapour moisture movement will be undertaken in the chapter 7.

Section 5.2 describes the testing programme and testing conditions. Section 5.3 presents the thermal test results for the wet and dry samples. The thermal test (T test) results include the transient thermal distribution, transient relative humidity variation and moisture distribution, degree of saturation, dry density, porosity and chemical distribution that includes anion and cation at the end of each test of different time duration. Subsequently, similar sets of results are presented for the thermo-hydraulic tests (TH test) in section 5.4. Section 5.5 describes the isothermal test results. In the final section conclusions are drawn.

5.2 Testing programme

A detailed testing programme was designed to carry out T tests, TH tests and isothermal tests. A summary of testing programme is presented in Table 5.1. The testing programme in Table 5.1 describes the initial condition and experiment duration for each

type of test. As discussed in chapters 3 and 4 two different initial conditions were used for each type of test. The samples with an initial water content of 11 % and a degree of saturation of 50 % are termed as dry samples. The samples with an initial water content of 19 % and degree of saturation of 85 % are called wet samples. The 100 mm high and 100 mm diameter samples used are statically compacted to an average initial dry density of 1.63 Mg/m^3.

5.3 Thermal test

The thermal test is a temperature gradient test in which the 100 mm height sample is subjected to a bottom end temperature of 85 °C and the top end temperature is maintained at 25 °C. This resulted in a thermal gradient of 0.6 °C/mm along the length of the sample. The test duration and initial conditions are presented in Table 5.1.

5.3.1 Dry sample

In the following sections results from the thermal tests performed on the dry samples are presented.

5.3.1.1 Thermal distribution

The transient temperature distribution at every 20 mm distance from the heater surface is shown in Figure 5.1. The temperature at the heater surface reaches to its targeted constant value of 85 °C within 30 minutes and remains stable. The temperature at the other end (top end) is maintained at 25 °C by the circulation of water in the top section of the TH cell. Again the temperature reaches a stable value within 30 minutes of the start of the tests. The temperature at other depths within the soil sample takes a longer time, about 1 day, to reach stable value. The stable values are 66 ± 0.2 °C, 51.5 ± 0.2 °C, 41 ± 0.2 °C and 34 ± 0.2 °C at 20 mm, 40 mm, 60 mm and 80 mm distance from the heater surface respectively. It can also be noted that in the beginning temperature rises and later slightly drops to its stable value, with a higher drop observed near the heater surface.

This phenomenon can be explained by the drop in thermal conductivity because of moisture movement from the hot end to the other cool end. Similar results were obtained by Kanno et al. (1996) on comparable tests on Japanese sodium bentonite, Kunigel V1.

Figure 5.2 shows the thermal gradient variation with time along the sample length. The thermal gradient is changing until 1day and then reaches to steady state. After reaching steady state, the thermal gradient near the hot end is 0.95 °C/mm and near the cold end is 0.45 °C/mm compared to overall gradient of 0.6 °C /mm across the whole sample. It can be seen that the gradient is not constant along the sample length with the gradient decreasing with increasing distance from the heater surface. There are two potential reasons for this variation (i) a variation in thermal material parameters (thermal conductivity and specific heat capacity) with moisture content and (ii) a radial heat loss from the sample, which would be expected to be large at the hotter end of the sample, thereby explaining the steeper gradients in the region.

5.3.1.2   Moisture distribution

The gravimetric water content of each soil slice was determined by drying the soil slices in oven at 105 °C for 24 hours. Figure 5.3 presents the gravimetric water content distribution versus distance from the heater surface. The water content decreases near the hot region and increases at the colder region. Near the hot end, the water content drops to 1.26 %, 2.69 % and 1.91 % after 7, 10 and 15 days respectively. The water content near the heater surface progressively decreased up to 7 days but then a small increase could be observed after 10 and 15 days. In the colder region there is a progressive increase in water content with a final gravimetric moisture content of 14.32 %, 14.22 % and 13.83 % being reached after 3, 10 and 15 days respectively. Overall it can be seen that in this test the moisture content has changed from an initial value of 11 % to a minimum value of 1.26 % at the hot end and a maximum value of 14.32 % at the cold end. The overall mass balance of the each sample was checked and found to be within ± 0.35 % of the initial values. This indicates no moisture escape during the tests and that the TH cell remained sealed during the tests.

Profiles of the degree of saturation versus distance from the heater surface at various time intervals are shown in Figure 5.4. The degree of saturation for each soil slice is calculated by the following equation.

$$Sr = \frac{wG\rho_d}{G\rho_w - \rho_d}$$
(5.1)

where ρ_d is the experimentally measured dry density as presented in section 5.3.1.4, ρ_w is the density of water, w is the measured gravimetric water content, G is the measured specific gravity of the Speswhite kaolin and Sr is the degree of saturation.

In Figure 5.4, the initial degree of saturation is not constant and decreasing with the distance away from the heater surface. The degree of saturation depends upon the dry density, as in equation 5.1, higher dry density results in higher degree of saturation. The higher dry density is achieved at the bottom layers of the soil sample near the hot end as presented in section 5.3.14. This is the reason of higher initial degree of saturation near the hot end compared to the cold end. During the thermal test, the degree of saturation decreases near the heater surface up to the distance of 40 mm and increases thereafter. The degree of saturation continued to decrease near the heater surface up to 7 days and increased slightly afterwards. The degree of saturation near the heater surface is 5.32 %, 12.44 % and 7.91 % after the end of 7, 10 and 15 days T tests. The degree of saturation increased near the cold end as the moisture moved in from the heater surface. The maximum value of degree of saturation near the cold end is 56.26 % compare to 50 % initial degree of saturation. As would be expected the profiles of degree of saturation follow the trend of gravimetric moisture content profiles.

Figure 5.5 shows the transient relative humidity changes within the soil sample at 20 mm, 40 mm, 60 mm and 80 mm distance from the heater surface. At the beginning, the relative humidity values are not the same at every point because of non-homogeneity in the initial degree of saturation of the soil sample. There is a drop in relative humidity at 20 mm and 40 mm distance for a little time due to quick drying with the increase in temperature before steady state at the beginning of the test. The degree of saturation

decreases near the heater surface up to the distance of 40 mm and increases thereafter. The relative humidity, at the farthest point 80 mm from the heater surface, reaches 100 % in 150 minutes. The relative humidity at other points reaches to 100 % within 50 minutes. These observations illustrate the rapid vapour movement from the hot end to the cold end.

5.3.1.3   Dry density and porosity

The dry density of each slice was calculated by dividing the dry mass of the slice by its volume. The volume of each slice was calculated by multiplying the cross-section area of the slice to its average thickness. The average thickness of the soil slice was determined by measuring the thickness of the slice at 6 locations with digital callipers and taking the mean of them. Figure 5.6 presents the dry density variation along the sample height with the time. The initial dry density is not uniform along the sample height. There are two possible reasons for the non-uniformity of initial dry density; firstly the bottom layers get more compacted than the top layers of the soil specimen and secondly the measurement error in the volume of the soil slices. The overall average initial dry density of sample based upon the total sample size is 1.63 Mg/m^3. In the Figure 5.6 it can be observed that the dry density is decreasing along the sample height away from the heater surface due to increase in moisture content. Theoretically the dry density is inversely proportional to the gravimetric water content. The dry density and gravimetric water content has following relationship.

$$\rho_d = \frac{\rho}{1 + w} \tag{5.3}$$

where ρ_d is the dry density, ρ is the bulk density and w is the gravimetric water content.

In Figure 5.6, it can be noted that the dry density increases near the hot end and decreases near the cold end. This may be because of two reasons: First, the dry density increases with the decrease in water content which can be seen from equation (5.3) and second, the

kaolin shrinks near the hot end because of drying and swells slightly near the cold end because of incoming moisture.

The porosity is the ratio of volume of voids to total volume. The porosity of each slice was calculated by the following equation.

$$n = \frac{\theta}{Sr} \tag{5.4}$$

where n is the porosity, θ is the volumetric water content and Sr is the degree of saturation.

The porosity, n, can also be related to the dry density by the following equation.

$$n = 1 - \frac{\rho_d}{G\rho_w} \tag{5.5}$$

where ρ_d is the dry density, ρ_w is the density of water and G is the specific gravity of the Speswhite kaolin.

Figure 5.7 shows the porosity change with time along the sample height. The porosity is increasing with the time and the sample height. The porosity is increasing along the sample height with the time because the dry density is decreasing which is obvious from the equation (5.5).

5.3.1.4 Chemical distribution

Various anion and cation concentrations were measured at 1, 3, 7 and 15 days after chemical analysis of the 10 slices obtained from the each sample at the end of the experiments. The anion and cation variation along the sample height is discussed in the following sections.

5.3.1.4.1 Anion distribution

Figure 5.8 presents the chloride concentration variation along the sample height with the above mentioned time intervals. The chloride concentration at nearest point to the heater surface reaches to the value of 8.46E-04 mol/kg, 1.24E-03 mol/kg, 1.84E-03 mol/kg and 2.82E-03 mol/kg after 1, 3, 7 and 15 days compared to the initial value of 4.37E-04 mol/kg. The chloride concentration is increasing near the heater surface with time. This indicates that the moisture moves in liquid form towards the hot end and carries chloride ion with it. The chloride ions get accumulated near the hot end with the time as liquid moisture flows towards this dry region from the wetter region above. The progressive drying near the hot end indicates moisture moves away as vapour. It appears that a cycle of vapour and liquid moisture movement has become established. The mass balance of chloride ion was checked and found to be within ± 5 %.

Figure 5.9 and 5.10 show the nitrate and sulphate ion concentration versus distance from the heater surface with the time. The concentration of nitrate and sulphate ions also increases near the hot end with the time. The trend of nitrate and sulphate distribution is similar to that of chloride ion. The progressive increase in anions concentration near the hot end indicates again the liquid moisture movement towards the hot end. Gurr et al. (1952) also reported the accumulation of soluble salts near the hot zone for the thermal gradient test conducted on loam and sand.

5.3.1.4.2 Cation distribution

Figures 5.11 to 5.14 present the sodium, magnesium, potassium and calcium distribution in the soil sample with the time. The concentration of these ions is increasing near the heater surface with time but unlike the anions the trend is not regular. The cation movement in the clays is affected by the negative charge on the clay surface. The cations are attracted to the negative clay surface that makes it difficult to extract them. This may result in variable and irregular trend of cations concentration along the sample height with time. Though, the accumulation of cations towards the hot region indicates that they are also carried by liquid moisture.

5.3.2   Wet sample

The following sections discuss the results from the thermal tests carried out on the wet samples.

5.3.2.1   Thermal distribution

The transient temperature distribution at every 20 mm distance from the heater surface for wet kaolin samples is shown in Figure 5.15. The temperature reaches to its stable value at various points in the soil sample very quickly compare to the dry samples with the temperature reaching to stable value within 4 hours. The stable values are 72.9 ± 0.2 °C, 56.75 ± 0.2 °C, 44.25 ± 0.2 °C and 36.75 ± 0.2 °C at 20 mm, 40 mm, 60 mm and 80 mm from the heater surface respectively. The temperature is higher at corresponding points compared to the dry sample possibly because in the wet sample there are smaller variations in thermal conductivity, this is more evident in the thermal profiles discussed below.

Figure 5.16 presents the temperature gradient change with time. The temperature gradient keeps changing until 4 hours. In comparison with the dry samples, the temperature gradient for the wet samples reaches to steady state faster. Again, the temperature gradient is higher near the heater surface. At the steady state condition, the thermal gradient near the heater surface is 0.605 °C/mm and near the cold end is 0.587 °C/mm compare to the thermal gradient of 0.6 °C/mm across the total sample height. Compared to the dry sample the temperature gradient is much closer to linear profile i.e. 0.6 °C/mm. This indicates radial heat loss is minimal because for the wet sample there would be a much smaller variation in thermal conductivity compare to the dry sample.

5.3.2.2   Moisture distribution

The gravimetric water content distribution is shown in Figure 5.17. The overall trends of behaviour are as expected with significant drying in the hotter region of the sample and wetting in the cooler region. However closer inspection of the results indicates some

interesting pattern that are not immediately explainable by conventionally accepted models of drying and wetting phenomenon. It can be seen that the water content decreases near the heater surface till the end of 3 days and reaches to the value of 1.81 % from the initial value of 19 %. The water content is then observed to increase and reach to a value of 16.04 % at the end of 5 days test. This can happen only with the influx of liquid moisture towards the hot region. So the moisture moves away in vapour form causeing drying till the end of 3 days and then the moisture flows back in liquid form towards the heater surface. Then again moisture moves away from the heater surface resulting in decreasing water content to 2.11 % after 7 days. Again moisture comes back near the heater resulting in increasing water content to 7.96 % at the end of 10 days. Theoretically the sample should continuously dry at the hot region as in the case of dry samples. This unusual behaviour was verified by repeating the 5 and 10 days T tests. The results of repeated tests showed very similar patterns of behaviour. This indicates that the observed cycle of drying and wetting near the heater surface is real. This pattern of cyclic drying and wetting has not been reported elsewhere. Mass balance was again checked after the end of each test and found to be within approximately + 0.32 % which is acceptable.

Figure 5.18 shows the degree of saturation results with time for the wet Speswhite kaolin samples. The initial degree of saturation line is almost straight compare to the dry samples. The degree of saturation decreases near the hot end because of drying near the heater surface. The degree of saturation values near the hot end are 11.06 %, 78.83 %, 31.84 % at the end of 4, 5 and 10 days T tests. As with the water content results this indicates the sample initially drying then wetting and then again drying at the hot end. The degree of saturation increases near the cold end because the vapour comes in from the hot region and condenses. The degree of saturation reaches to 100 % near the cold end after 3 days and then decreases to 82.78 % at the end of 5 days.

Figure 5.19 shows the transient relative humidity variation at 4 locations 20 mm, 40 mm, 60 mm and 80 mm from the heater surface. The initial relative humidity (at time equals zero) is bit higher for the wet samples compare to the dry samples. Again the initial relative humidity is not same due to non homogeneity in the sample. The relative

humidity profiles for the wet sample have the same trend as the dry samples but reach to 100 % at the corresponding points much faster in the wet samples compared to dry samples. The drop in relative humidity at 20 mm and 40 mm in the beginning is due to drying near the hot end. The relative humidity reaches 100 % at every point with in the soil sample in 50 minutes. This indicates that the total suction should be zero and so there should not be any moisture flow but the relative humidity here represents the value at macroscopic level which might not hold true at microscopic level. The relative humidity probes used in this study are 5 mm diameter and thus they do not measure the relative humidity at microscopic level of the clay structure.

5.3.2.3 Dry density and porosity

The dry density variation with time is shown in Figure 5.20. The initial dry density is uniform compared to the dry sample. This indicates that the wet samples are more homogeneous than the dry samples. It can also be seen that the dry density is increasing near the hot end because of reduction in the water content and shrinking. The minimum value of dry density at the cold end is 1.45 Mg/m^3 after 3 days. The dry density is decreasing near the cold end because the water content is increasing near the cold end due to incoming moisture from the hot end and swelling of the soil.

Figure 5.21 presents the porosity change with time along the sample height. The initial porosity is quite uniform like initial dry density that indicates the homogeneity of the soil sample. The porosity is increasing away from the heater surface with the time. As discussed earlier in section 5.3.1.3 that the porosity increases with decrease in the dry density and vice versa.

5.3.2.4 Chemical distribution

The various anions and cations concentrations were measured with the time intervals of 1, 2, 3, 7 and 15 days and they are discussed in the following sections.

5.3.2.4.1 Anion distribution

The chloride ion distribution after 1, 3, 7 and 15 days thermal test is shown in Figure 5.22. It can be seen that the chloride ion concentration is increasing near the heater surface with the time. The chloride concentration near the heater surface is 8.37E-04 mol/kg, 8.98E-04 mol/kg, 1.09E-03 mol/kg and 1.49E-03 mol/kg after 1, 3, 7 and 15 days compare to initial value of 4.27E-04 mol/kg. This indicates that the liquid moisture is flowing towards the hot end from the beginning. The amount of chloride ion near to heater surface is less in the wet samples than the dry samples. This indicates that the less liquid moisture is moving towards the hot region in the case of wet samples compared to the dry samples. This could be due to fewer voids being available for vapour moisture movement in the wet samples and therefore lower fluxes of moisture being created; the cycle of vapour and liquid movement.

Figure 5.23 and 5.24 show the nitrate and sulphate ions concentration with the time along the distance from the heater surface. The trend of the both ions distribution is similar to chloride with different values of concentration.

5.3.2.4.2 Cation distribution

The sodium, magnesium, potassium and calcium ions concentration change with time within the soil sample is presented in Figures 5.25 – 5.28. The sodium, magnesium and potassium ions have a similar pattern where they are decreasing at the cold end and increasing near the heater surface because they are carried by liquid moisture from the colder region to the hotter region. But the calcium ion behaves in different way and its concentration is increasing at the cold end and decreasing at the other hot end. It could be due to interlayer cations like sodium, potassium and magnesium are exchanged by calcium ions. Hence, the calcium ions are attracted to interlayer surface strongly and precipitated during drying near the hot end.

5.3.3 Conclusions

The results of thermal gradient test for dry and wet samples are discussed. The temperature reaches to the stable value faster in the wet samples than the dry samples because of fewer voids available for moisture movement result in less change in the thermal material parameters namely, thermal conductivity and specific heat capacity. It is evident that radial heat loss is minimal in the tests from the results of the wet samples where reduced variations in thermal conductivity results in much more linear temperature profiles in the samples.

The results of gravimetric water content show that the moisture is moving away in vapour form from the hot end to the cold end. The dry sample has more voids compared to the wet samples result in more moisture movement from the hot end. The chemical analysis results show that the various anion and cations accumulating near the heater surface. This indicates that liquid moisture brought these ions from the cold end to the hot end. This means that the moisture moves in vapour phase away from the hot end to the cold end but liquid moisture comes back to the hot end. This forms a cycle of vapour and liquid moisture movement in the soil sample. The moisture and chemical species mass balance check indicates that no moisture or ions escape from the TH cell. The new apparatus, TH cell, is functioning correctly.

5.4 Thermo-hydraulic test

In the thermal-hydraulic test (TH-test) soil samples are subjected to a thermal gradient of 0.6 °C/mm with temperatures of 25 °C and 85 °C applied at the top and bottom ends respectively, in addition to this deionised and de-aired water was supplied at the top end under a pressure of 0.6 MPa.

5.4.1 Dry sample

In the following sections results from the thermo-hydraulic tests performed on the dry samples are presented.

5.4.1.1   Thermal distribution

The transient temperature distribution at every 20 mm distance from the heater surface is shown in Figure 5.29. The temperature reaches to a stable value after 500 minutes at every location within the soil sample. At the steady state condition after 500 minutes, the temperature attained the value of 67.1 ± 0.2 °C, 54.4 ± 0.2 °C, 43.8 ± 0.2 °C and 36.7 ± 0.2 °C at 20 mm, 40 mm, 60 mm and 80 mm from the heater surface respectively. It can be noted that the temperature does not decrease as in the thermal test for dry samples. This is due to the impact in this thermo-hydraulic test of the supply of water to the cold region resulting in a much higher material thermal conductivity in the samples.

Figure 5.30 shows the temperature profiles variation at various times. It can be observed that the temperature gradient progressively changing until 8 hours. After this time, the temperature gradients reach a stable value, with the temperature gradient steepest near the heater surface. The steady state thermal gradient is 0.9 °C/mm near the heater surface and 0.585 °C/mm near the cold end. As with the T tests this could be due to either thermal conductivity variation or heat loss from walls of the cell.

5.4.1.2   Moisture distribution

The gravimetric water content results for thermo-hydraulic tests are presented in Figure 5.31. The gravimetric water content is increasing with time along the sample height. The gravimetric water content near the heater surface increases even after 1 day due to water penetration, under high pressure, to the hot end from the hydration source at the cold end. As would be expected the gravimetric water content is higher near the hydration source compare to hot end due to moisture movement, in the vapour phase, away from the hot end. The maximum value of the moisture content is 22.99 % near the hot end and 29.66 % near the hydration source compare to the initial moisture content of 11 %.

The degree of saturation variation with time for the thermo-hydraulic tests is shown in Figure 5.32. The degree of saturation for each slice is calculated by using the equation (5.1). The degree of saturation is increasing with time as the water is supplied into the

soil sample from the cold end. The degree of saturation reaches more than 90 % even after 1 day. The highest degree of saturation value of 100 % has been reached at various points.

Figure 5.33 presents the transient relative humidity results at every 20 mm distance from the heater surface. The initial relative humidity is 97 % within the soil sample at the start of the test. The relative humidity reaches to 100 percent quickly at every point especially near the cold end compare to corresponding thermal test because water is supplied under pressure of 0.6 MPa from the cold end.

The transient water intake is measured via an automatic volume change apparatus. The water intake is shown in Figure 5.34. The rate of water intake is 0.67 cm^3/min, 0.54 cm^3/min, 0.42 cm^3/min, 0.28 cm^3/min and 6E-04cm^3/min at 50, 100, 200, 400 and 10000 minutes respectively. The rate of water intake is very high in the beginning and then reduces as the soil starts to approach saturation.

5.4.1.3 Dry density and porosity

Figure 5.35 shows the dry density at various time intervals of 1 to 15 days. The dry density is decreasing at all the locations with time as the water content is increasing. In such sealed tests the overall average dry density should remain constant; therefore such a trend of decrease in dry density throughout the sample must be due to some form of experimental error. The most likely cause is that regions close to the hydration source tend to swell and at the same time regions further from the hydration source are compressed. On sampling the restraining reactive force of the cell are removed allowing the compressed regions to recover, thereby resulting in an apparent decrease in the overall average dry density. This phenomenon is also observed in the other TH and isothermal tests reported later in both this chapter and chapter 6. The reduction in dry density is more near the hydration end than the hot end. The minimum dry density is 1.58 Mg/m^3 near the heater surface and 1.39 Mg/m^3 near the hydration source compare to initial value of 1.63 Mg/m^3. At various points the dry density does not follow this trend possibly because of errors involved in the volume measurement of the soil slice. The porosity

results for the thermo-hydraulic tests are shown in Figure 5.36. The porosity is increasing with time along the sample height as the dry density decreasing.

5.4.1.4 Chemical distribution

The anions and cations were determined at the end of the 1, 3, 7 and 15 day thermo-hydraulic tests. The following sections present the results of anion and cation distribution.

5.4.1.4.1 Anion distribution

The chloride ion distribution for thermo-hydraulic test after 1, 3, 7 and 15 days is shown in Figure 5.37. Near the heater surface, the chloride concentration is 7.70E-04 mol/kg, 7.20E-04 mol/kg, 6.92E-04 mol/kg and 4.80E-04 mol/kg at the end of 1, 3, 7 and 15 days compare to the initial concentration of 4.37E-04. It can be noted that the chloride ion concentration is decreasing near the heater surface with the time oppose to the thermal test in which chloride ion concentration increases with time near the hot end. In the beginning the chloride ions are carried by liquid moisture advectively to the hot end as 1 day results show but later the chloride ions diffuse away from the hot end because of concentration gradient and continuity of liquid moisture in voids. Near the cold end, the chloride concentration is 1.32E-04 mol/kg, 9.76E-05 mol/kg, 1.21E-04 mol/kg and 1.57E-04 mol/kg at the end of 1, 3, 7 and 15 days. The chloride concentration initially decreases at the hydration end due to the distilled water entering the sample diluting the system. After the rate of water influx into the system decreases the concentration near the cold end increase due to chloride ions diffusing away from the hot end under concentration gradient.

Figures 5.38 and 5.39 present the nitrate and sulphate ion concentration with time for TH tests. The nitrate and sulphate ions have similar concentration distribution but different amount within the soil sample. After the initial migration of ions towards the hot end and dilution of ions at the hydration end the ions are decreasing near the hot end and

increasing near the cold end with time due to diffusion of ions from the hot region to the cold region.

5.4.1.4.2 Cation distribution

Figures 5.40 – 43 show the concentration variation of sodium, magnesium, potassium and calcium with time. The sodium ion behaves similar to anion and concentration is decreasing near the hot region and increasing near the cold region with time due to diffusion. The other cations are decreasing with time almost every point within the soil sample. There is a possibility that these ions escaped to hydration source.

5.4.2 Wet sample

In the following sections results from the thermo-hydraulic tests performed on the wet samples are presented.

5.4.2.1 Thermal distribution

The transient thermal distribution for wet sample is shown in Figure 5.44. As with the dry sample, the temperature at all the locations within the soil sample reaches stable values within 500 minutes. At the steady state condition after 500 minutes, the temperature attained the value of 65.2 ± 0.2 °C, 56.4 ± 0.2 °C, 44.5 ± 0.2 °C and 36.7 ± 0.2 °C at 20 mm, 40 mm, 60 mm and 80 mm from the heater surface respectively. The temperature has increased slightly at all the points compare to the dry sample results because of higher thermal conductivity. Comparison of the temperature results from the thermal test shows that at 20 mm from the heater surface the TH test has a lower temperature. This is due to a combination of (a) different thermal conductivity due to different moisture content (b) the influence of cooler water entering the system.

Figure 5.45 shows the thermal gradient variation with time. The thermal gradient reaches a steady state at all the points in the soil sample after 8 hours. At the steady state the

temperature gradient is 0.99 °C/mm near the heater surface and 0.585 °C/mm. The thermal gradient response is similar to the dry sample except near the heart surface. Again the influence of variation in the material parameter and possible heat loss across the wall of the cell can be seen.

5.4.2.2 Moisture distribution

Figure 5.46 presents the gravimetric water content results for various time intervals from 1 to 15 days. The gravimetric water content is increasing with time at every point from the hot end to the cold end because the liquid moisture is supplied from the cold end. But the moisture content is higher at the cold region than the hot region. The maximum value of moisture content is near the cold end 32.75 % and 23.79 % near the heater surface. The maximum moisture content values are higher for the wet samples compare to the dry sample because of difference in the initial moisture content.

The degree of saturation variation with time along the sample height is shown in Figure 5.47. The degree of saturation reaches to 100 percent even after 1 day at the points near the hydration source at the cold end. The degree of saturation values are more than 95 % at almost every point. The degree of saturation values are higher at corresponding points similar to that for the dry sample results due to variation in initial conditions. The degree of saturation would be expected to increase with time as the water penetrates in but when this does not occur it could be due to error in volume measurement of the soil slice.

The transient relative humidity values at every 20 mm distance from the heater surface are shown in Figure 5.48. The relative humidity reaches to 100 % very quickly at every point. Compared to the T test the relative humidity at 80 mm from the heater surface increase at a faster rate due to the impact of the supply of water under pressure in the TH test and the variation in the initial conditions. Again the drop in relative humidity profiles happens due to rapid drying at the start of the test. Some evidence of drying is apparent in the region closer to the hot end (20, 40 mm) with an initial decrease in the relative humidity value.

The transient water intake into the soil sample from the hydration end is shown in Figure 5.49. The water intake rate is 0.34 cm^3/m, 0.24 cm^3/m, 0.15 cm^3/m, 0.09 cm^3/m and 3.5E-04 cm^3/m at 50, 100, 200, 400 and 10000 minutes. It can be seen that the water moves in faster in the beginning 400 minutes and then becomes slow as the soil saturates. The water intake quantity is less for the wet sample compare to the dry sample that is obvious because of difference of initial water content and degree of saturation.

5.4.2.3 Dry density and porosity

Figure 5.50 presents the dry density results with time for TH tests. The dry density is decreasing with time at every point from top to bottom end. This would be expected at the cold end but as discussed earlier in section 5.4.1.3 this is due to experimental error however the overall trends of variation are of interest. The reduction in dry density is higher near the hydration end compare to the hot end. The results are similar to those of the dry samples.

Figure 5.51 shows the porosity variation with time along the sample height. The porosity is increasing with time as the water supplied in and the dry density decreases. The maximum value of porosity is 0.383 near the heater surface and 0.461 near the hydration end compare to the initial value of 0.38. The increment in porosity is more near the hydration end. The initial porosity is same at every point. This indicates that the homogeneous samples were achieved.

5.4.2.4 Chemical distribution

The anion and cation concentration for wet sample after 1, 3, 7 and 15 days TH tests is described in the following sections.

5.4.2.4.1 Anion distribution

The chloride, nitrate and sulphate ions concentration after 1, 3, 7 and 15 days results are

shown in Figure 5.52 – 5.54. In Figure 5.52, the chloride concentration near the heater surface is 4.77E-04 mol/kg, 4.69E-04 mol/kg, 4.55E-04 mol/kg and 3.93E-04 mol/kg and near the hydration end is 7.65E-05 mol/kg, 1.94E-04 mol/kg, 1.83E-04 mol/kg and 1.73E-04 mol/kg at the end of 1, 3, 7 and 15 days compare to the initial concentration of 4.27E-04 mol/kg. It can be observed that the chloride concentration is decreasing with time at every point from the heater surface to the hydration end. The chloride ions move to hot end advectively in the beginning but once the sample saturates for its full height, the chloride ion starts to diffuse away from the hot end because of the concentration gradient. At the hydration end the incoming distilled water dilutes the chloride ions that cause reduction in chloride concentration. During the thermal test, drying occurs near the hot end and there is no continuity of moisture in voids resulting in precipitation and then accumulation of chloride ions near the heater surface and no back diffusion was observed. The results of nitrate and sulphate ions concentration follow the same trend as chloride ion.

5.4.2.4.2 Cation distribution

Figure 5.55 – 5.58 present the sodium, magnesium, potassium and calcium ions distribution with time. The sodium ion concentration profiles follow the similar trend as the chloride ion. The sodium concentration is decreasing with time at every point. The potassium ion is also decreasing at every point but the reduction is higher compare to the sodium ions. The magnesium and calcium ion results are variable because these ion replace sodium and potassium on the surface of kaolin particles that results in difficult extraction of them.

5.4.3   Conclusions

The thermo-hydraulic test result shows that the temperature reaches a stable value quicker than that for the equivalent T test. The wet sample has higher temperature at steady state condition due to higher thermal conductivity. It has also been observed that the higher heat loss through the walls of the TH cell result in higher value of temperature gradient.

The soil sample saturates within 1 day because of incoming liquid moisture from the cold end. The water intake rate is high in the beginning and then it slows down, with a higher water intake rate found in the dry samples. The moisture mass balance was cross checked with the amount of water intake and it found to be accurate. The variation of chemical concentration in the samples was dominated by three processes; firstly dilution due to the distilled water entering the sample and secondly advective movement of ions towards the hot region and thirdly diffusion of ions towards the hydration end after saturation is achieved. The chemical mass balance of few species was not achieved that indicates the ions escape to the hydration source.

5.5 Isothermal test

In the isothermal test soil samples were only subjected to the application of a hydration source with the temperature kept at 25 °C at both ends of the soil samples. The resulting hydraulic gradient was obtained by supplying deionised and de-aired water from the top end under a pressure of 0.6 MPa. In the isothermal tests, the temperature was kept the same 25 °C at both extremities of the sample that results in isothermal condition throughout the sample height. Therefore, the temperature field is not discussed further. The relative humidity reaches to 100 percent quickly during the T tests and TH tests, therefore the necessity of measuring relative humidity was not considered and the relative humidity was not measured during the isothermal tests.

5.5.1 Dry sample

The following section discusses the results of isothermal tests conducted on the dry samples.

5.5.1.1 Moisture distribution

The gravimetric water content variation after 15 days isothermal test is shown in Figure 5.59. The gravimetric water content is 28.89 % at the top end and 24.83 % at the bottom

end. The water content is increasing from the bottom end to the top end because the water is supplied in from the top end. Theoretically the gravimetric water content value should be same along the sample height. There are two possible reasons; firstly, air gets trapped at the bottom end of the sample that does not let the sample to achieve same gravimetric water content throughout the sample height and secondly, the bottom layers of the soil sample have a higher initial dry density resulting in more mass of soil solids and reduced gravimetric water content.

Figure 5.60 shows the degree of saturation variation after 15 days isothermal test. The degree of saturation increased at every point within the soil sample because water was supplied in from the top hydration end. The degree of saturation is not same at every point because of the error in measuring the volume of soil slice. A 5 % error in volume measurement can cause error of 10 % in the degree of saturation.

The water taken up by the soil sample during the isothermal test has been measured and presented in Figure 5.61. The water intake rate is 0.87 cm^3/min, 0.65 cm^3/min, 0.45 cm^3/min, 0.32 cm^3/min, 3.58E-04 cm^3/min at 50, 100, 200, 400 and 10000 minutes. It can be seen that water intake rate is higher at the beginning of the test till 500 minutes and then drop to very slow rate. The water intake rate for dry sample in the isothermal test is higher compare to the dry sample in the thermo-hydraulic test due to the difference in end temperature conditions. In the TH test, bottom end is maintained at 85 °C while during the isothermal test, it is maintained 25 °C.

5.5.1.2   Dry density and porosity

The dry density result after 15 days isothermal test is presented in Figure 5.62. As seen previously in the TH tests the average dry density should remain constant the results shown here indicate that the sample has expanded on removal from the confining cell. The dry density decreases because of incoming water from the hydration end. The reduction in dry density is more near the hydration source due to higher moisture content value.

Figure 5.63 presents the porosity results for the dry sample after 15 days isothermal test. The porosity increases from the bottom end to the hydration end due to decrease in the dry density. The porosity also increases after the compacted soil sample extruded out of the TH cell.

5.5.2   Wet sample

The results of isothermal test for the wet sample are presented in the following sections.

5.5.2.1   Moisture distribution

The gravimetric water content distribution for the wet sample is shown in Figure 5.64. The gravimetric water content value is 25.09 % at the bottom heater end and 31.64 % at the hydration end. The gravimetric water content is increasing from the heater end to the top end because the water is supplied into the soil sample from the top hydration end. The wet sample has almost same amount of final gravimetric water content after 15 days as the dry sample.

The degree of saturation variation for the wet sample after 15 days isothermal test is shown in Figure 5.65. It can be noted that the degree of saturation reaches to 100 percent at almost every point within the soil sample. The sample gets completely saturate after 15 days isothermal test.

The transient water intake rate for the wet sample during the isothermal test is presented in Figure 5.66. The water intake rate values are 0.41 cm^3/min, 0.30 cm^3/min, 0.21 cm^3/min, 0.13 cm^3/min and 4.7E-04 cm^3/min at 50, 100, 200, 400 and 10000 minutes. The water intake rate is higher at the start of the test and then slowing down. The water intake rate is lower compare to that of the dry sample due to the difference in the initial water content. The wet sample takes less water with a slower rate unlike the dry sample. In comparison with TH test, the water intake rate during the isothermal test is higher because of drying effect in the TH test at the heater end due to higher temperatures.

5.5.2.2 Dry density and porosity

Figure 5.67 presents the dry density change along the sample height after 15 days isothermal test. It can be observed that the dry density decreases at each and every point within the soil sample. The dry density decreases due to swelling by the incoming water from the hydration source.

Figure 5.68 shows the porosity variation for the wet sample after 15 days isothermal test. The porosity is increasing at every point within the soil sample. The porosity increases due to slight swelling of kaolin clay.

5.5.3 Conclusions

The isothermal 15 day test results are presented for the dry and wet samples. The moisture distribution is almost same for both types of samples. As would be expected there is no drying observed. The difference between TH test and isothermal test is that vapour moves away from the hot end even the water from the hydration source reaches to the hot end.

5.6 Overall conclusions

The results of thermal, thermo-hydraulic and isothermal tests are presented. The temperature distribution depends upon the initial conditions, the end conditions and the type of test. The different temperature values at steady state condition for the wet and dry samples indicates that the amount of variation of thermal material parameters (e.g. thermal conductivity and specific heat capacity) depend upon the initial amount of water.

The moisture distribution results show the moisture movement within the sample but the chemical analysis of the samples gives further insight in the actual process of liquid and vapour moisture movement. The accumulation of ions near the heater surface during the thermal test indicates that liquid moisture moved from the cold end to the hot end. This fact can not be observed solely from the moisture distribution results. Finally, T test

results show that there is a cycle of vapour and liquid moisture movement within the sample, vapour moves from the hot end to the cold and condense to liquid at the cold end and liquid moisture moves to the hot end.

The relative humidity results are almost same for the dry and wet samples irrespective of type of test. The relative humidity reaches to 100 % value very quickly and the total suction must reach to zero. The relative humidity values indicate the macroscopic level response but at microscopic level suction exists and causes moisture movement.

The moisture mass balance accuracy lies within ± 0.35 % for most of the test. This indicates the new test cell, TH cell, is working and functioning properly and does not allow any moisture escape. The chemical mass balance was achieved in the T test but not in the TH test possibly due to escape of ions to the hydration source during the TH tests.

5.7 References

Gurr, C.G., Marshall, T.J. and Hutton, J.T. (1952). Movement of water in soil due to a temperature gradient. Soil Sci., Vol. 74, No. 5, 335-345.

Kanno, T., Kato, K. and Yamagata, J. (1996). Moisture movement under a temperature gradient in highly compacted bentonite. Engineering Geology, 41, 287-300.

Table 5.1 Testing programme

Type of test	Thermal gradient test (T-test) 25 °C ↓ 85 °C		Thermo-hydraulic gradient (TH-test) 25 °C ↓↓↓↓ Water under 0.6 MPa 85 °C		Isothermal test 25 °C ↓↓↓↓↓ Water under 0.6 MPa 25 °C	
Sample type	Dry	Wet	Dry	Wet	Dry	Wet
Initial water content (%)	11	19	11	19	11	19
Initial degree of saturation (%)	50	85	50	85	50	85
Initial dry density (Mg/m^3)	1.63	1.63	1.63	1.63	1.63	1.63
Experiment duration (Days)	1, 2, 3, 4, 5, 7, 10 & 15	1, 2, 3, 4, 5, 7, 10 & 15	1, 2, 3, 4, 5, 7, 10 & 15	1, 2, 3, 4, 5, 7, 10 & 15	15	15
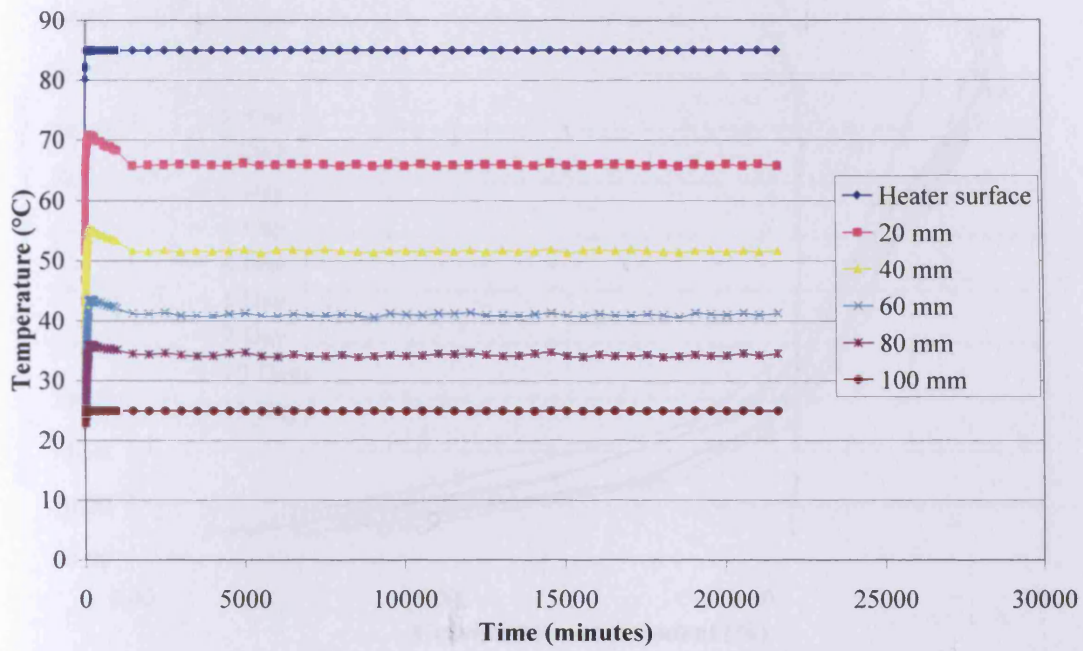
Figure 5.1 Temperature distribution of Speswhite kaolin dry sample for T test
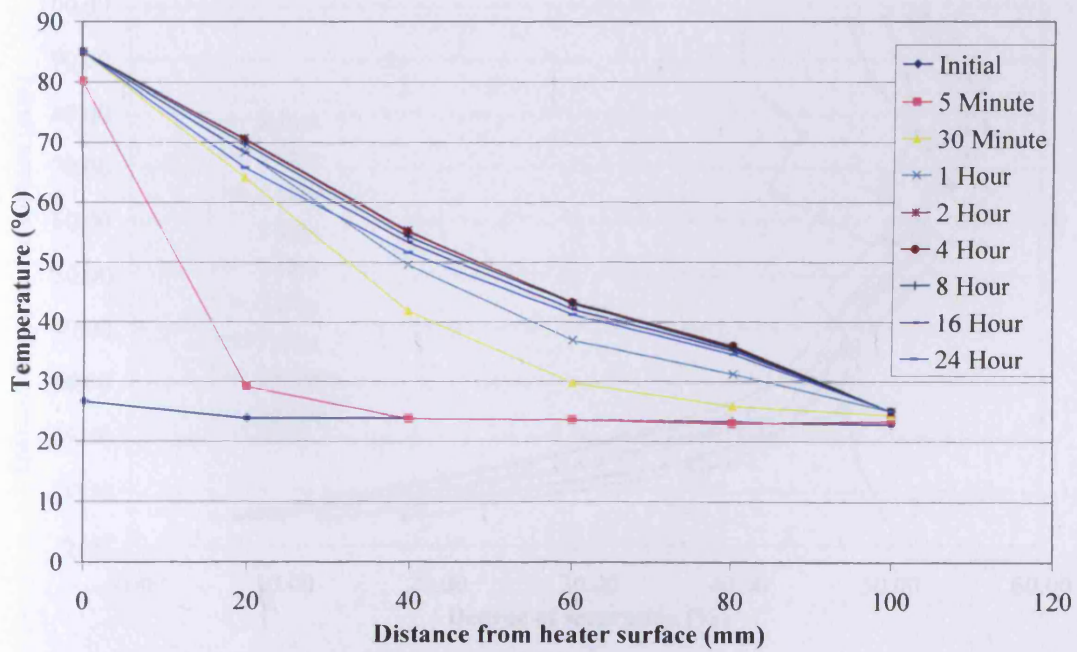
Figure 5.2 Temperature profile of Speswhite kaolin dry sample for T test
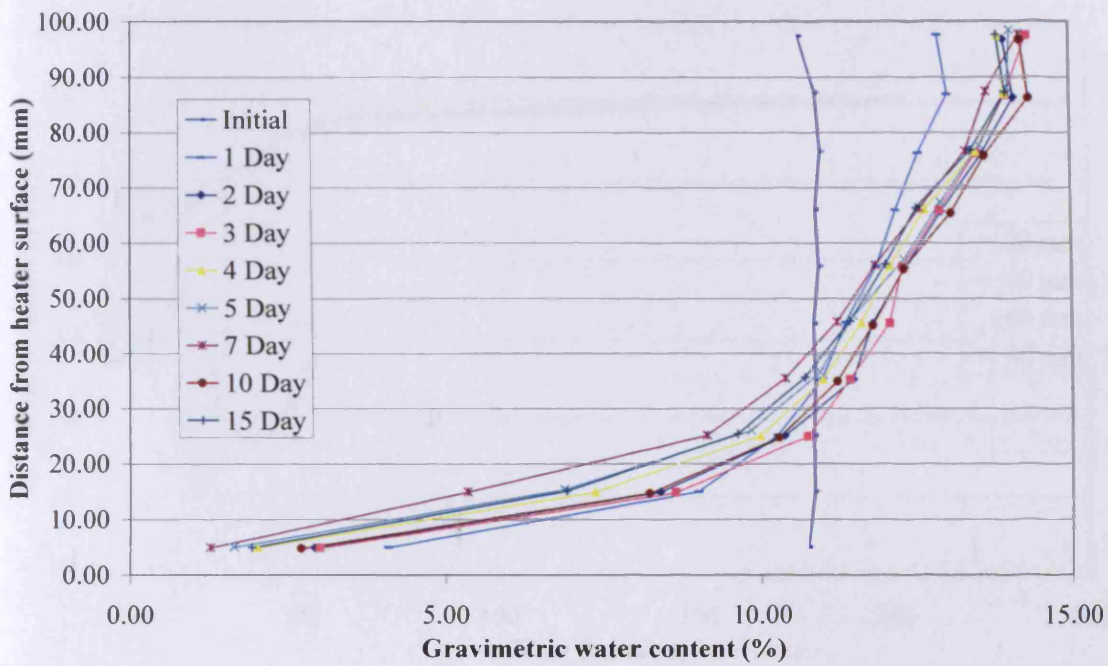
Figure 5.3 Gravimetric water content distribution of Speswhite kaolin dry sample for T test
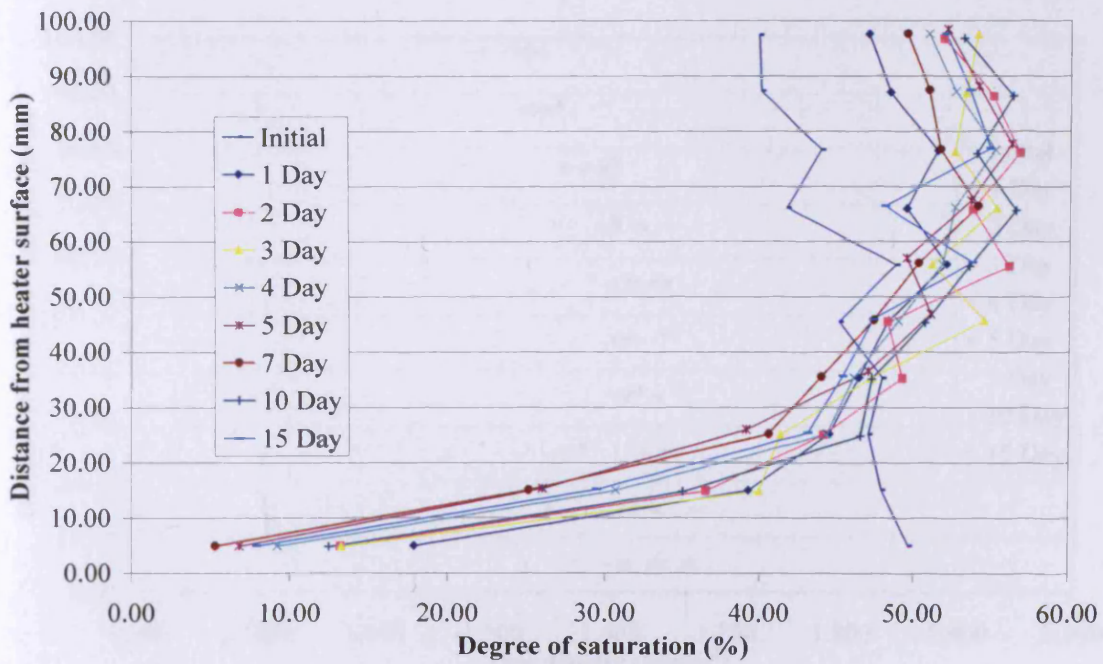
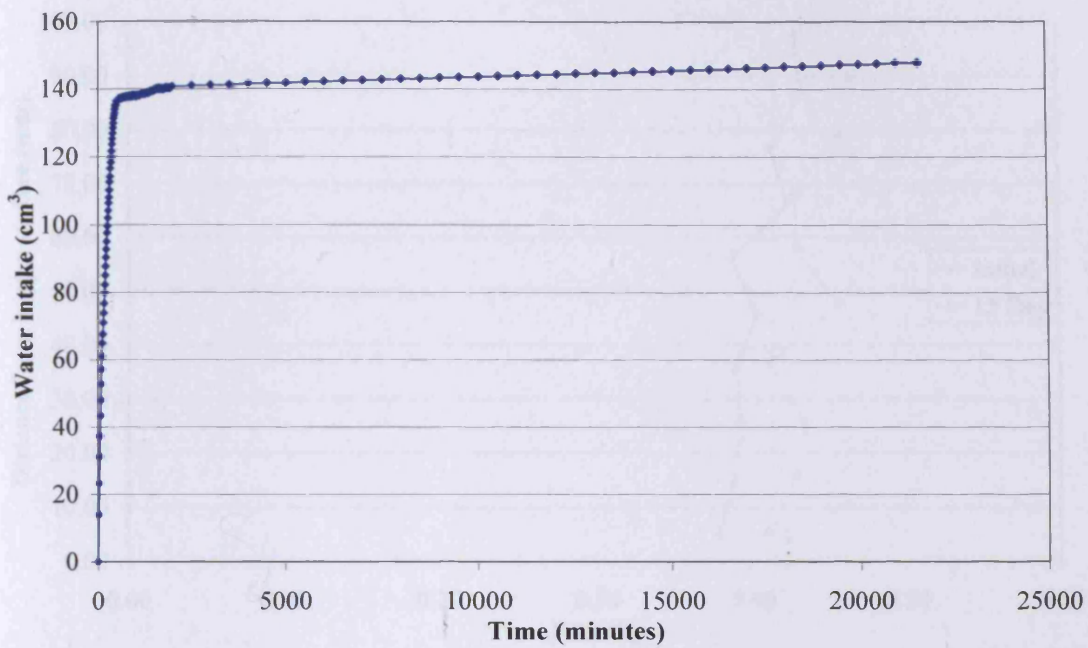**Figure 5.4 Degree of saturation of Speswhite kaolin dry sample for T test**
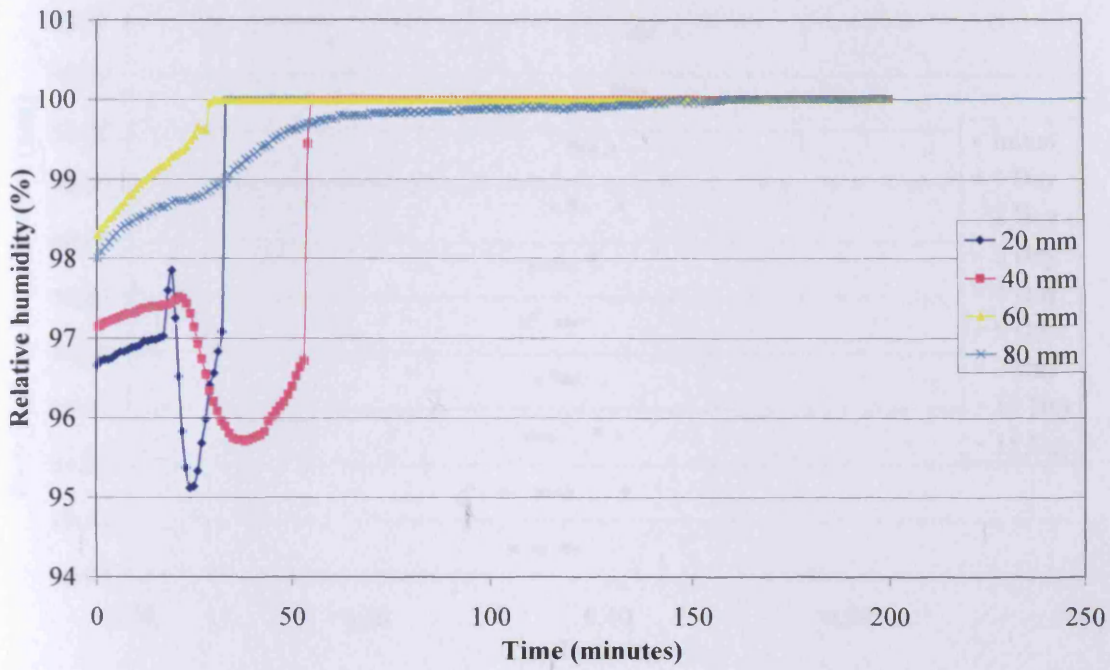
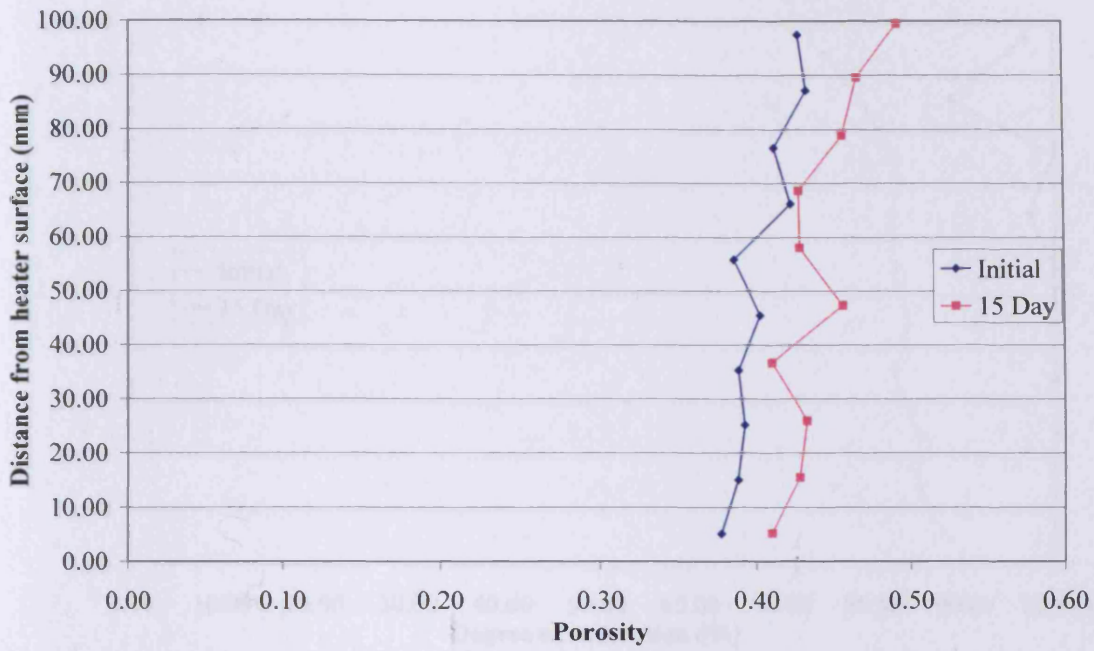**Figure 5.5 Relative humidity variation of Speswhite kaolin dry sample for T test**
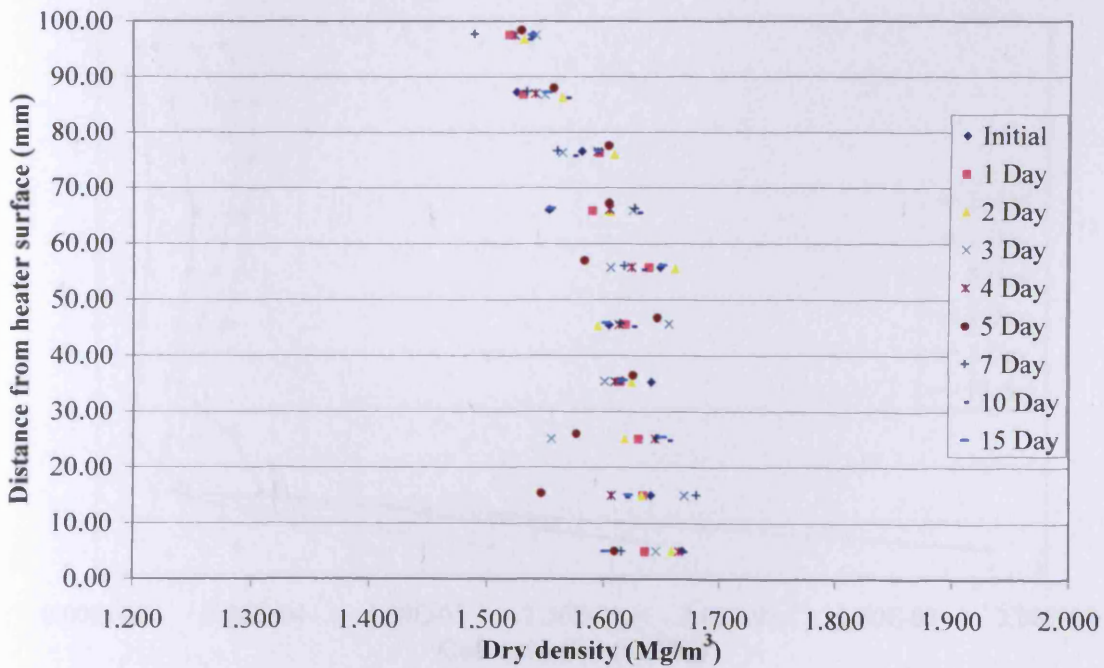
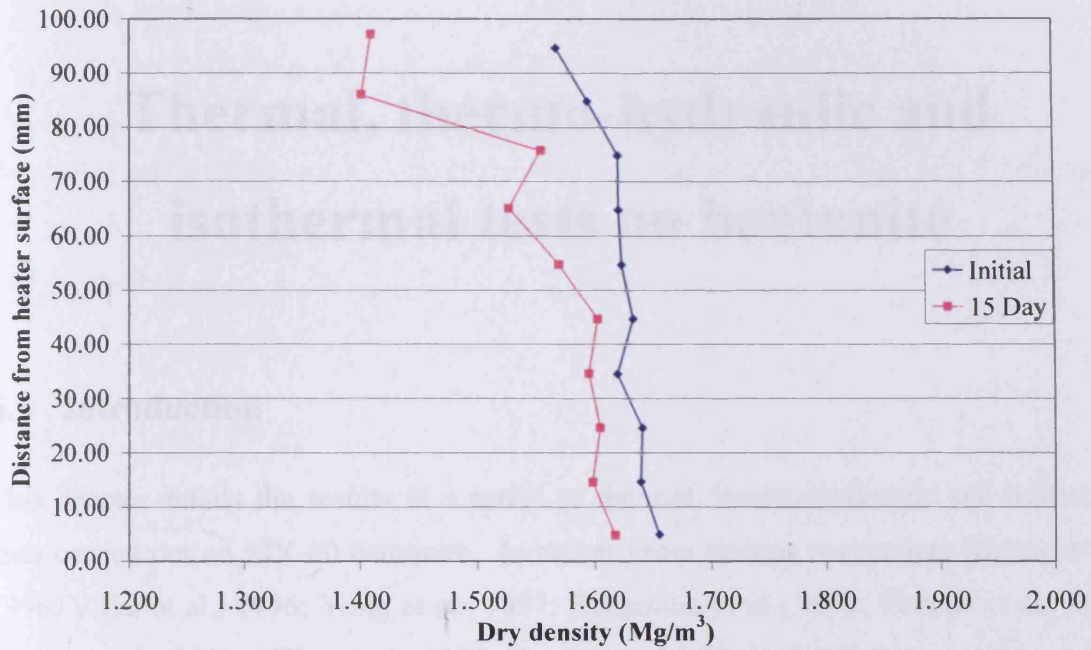**Figure 5.6 Dry density of Speswhite kaolin dry sample for T test**
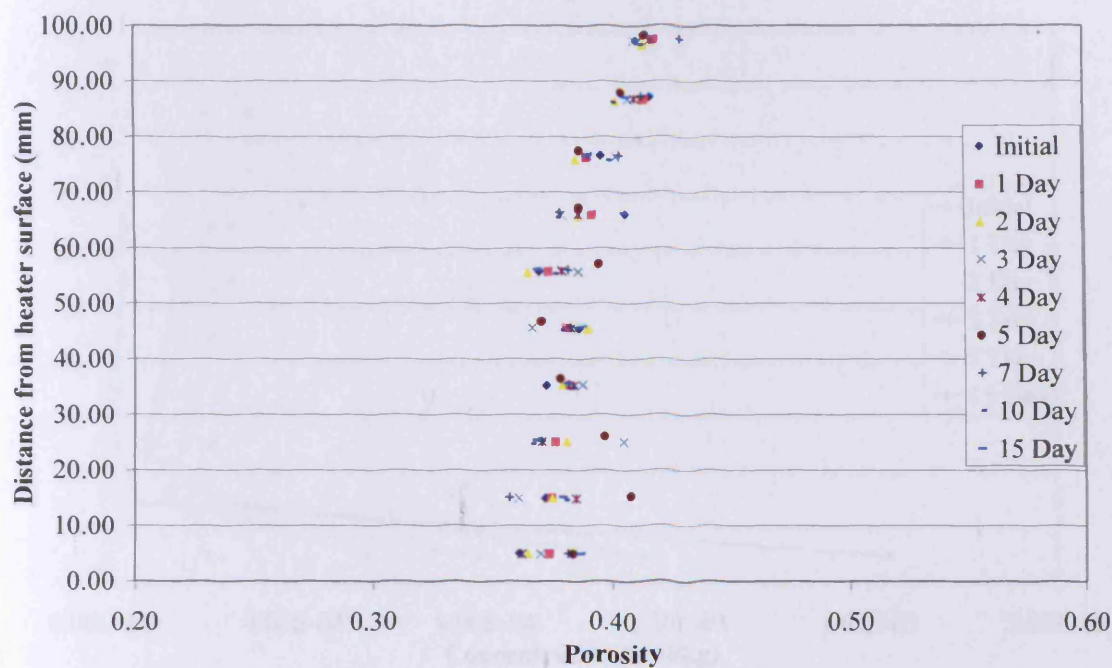
Figure 5.7 Porosity of Speswhite kaolin dry sample for T test
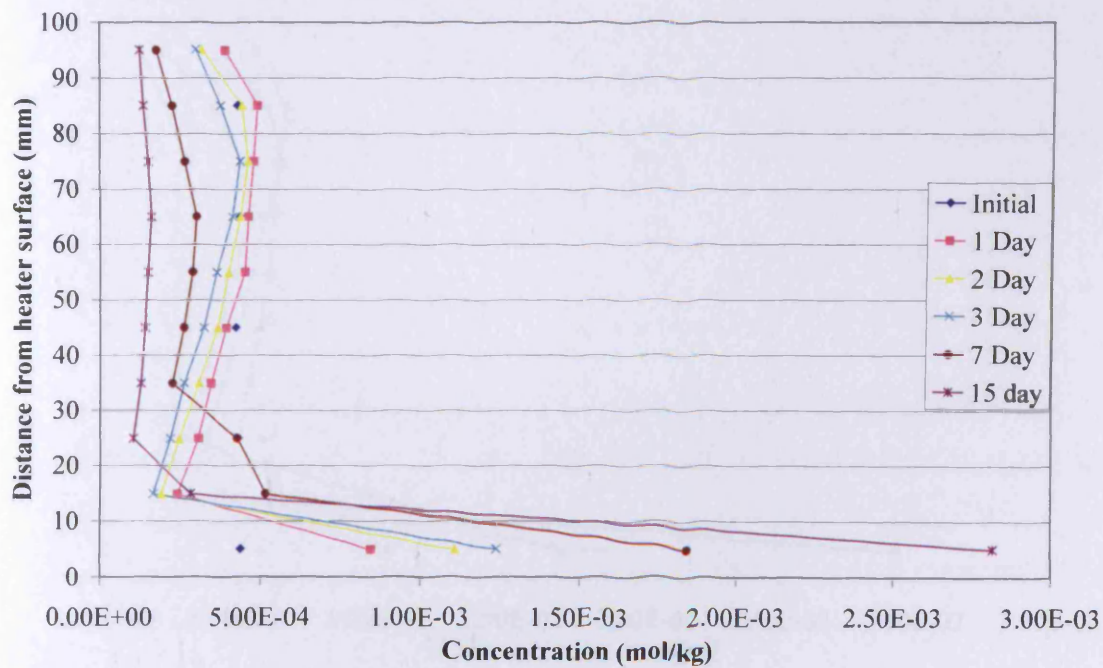
Figure 5.8 Chloride distribution of Speswhite kaolin dry sample for T test
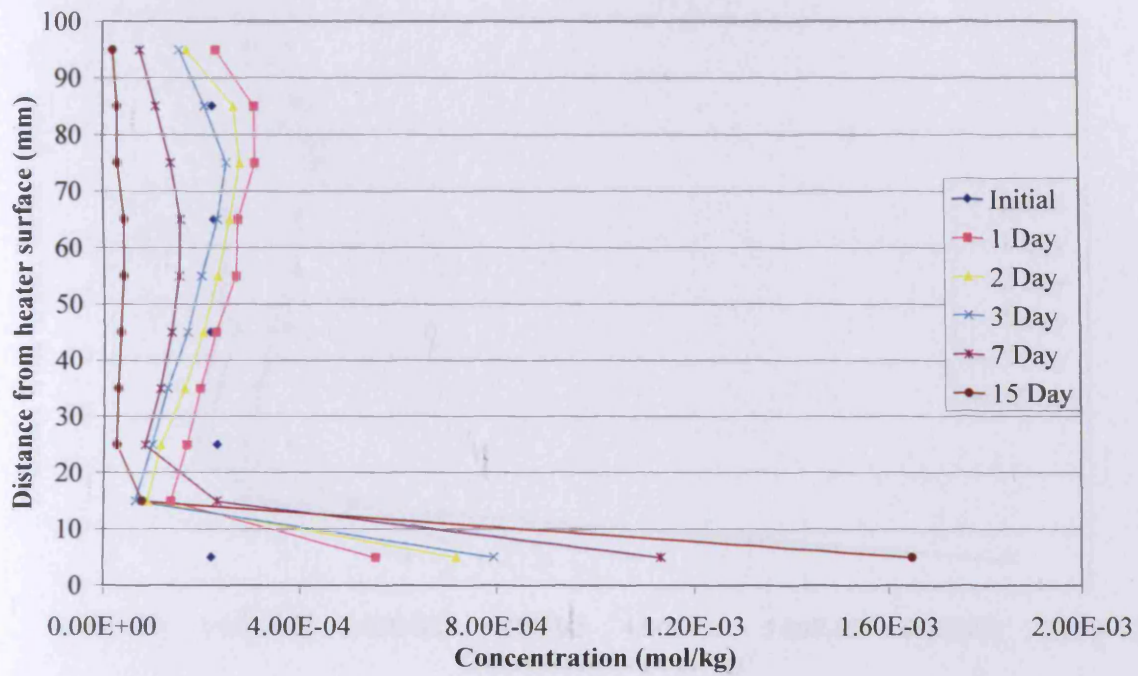
Figure 5.9 Nitrate distribution of Speswhite kaolin dry sample for T test
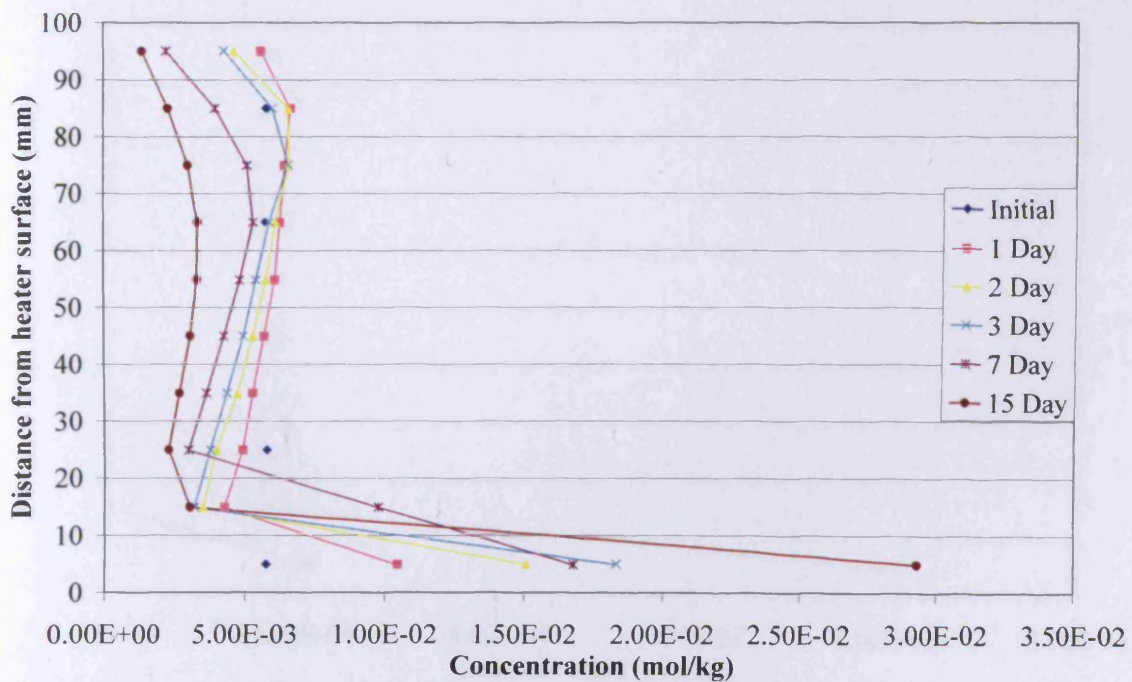
Figure 5.10 Sulphate distribution of Speswhite kaolin dry sample for T test
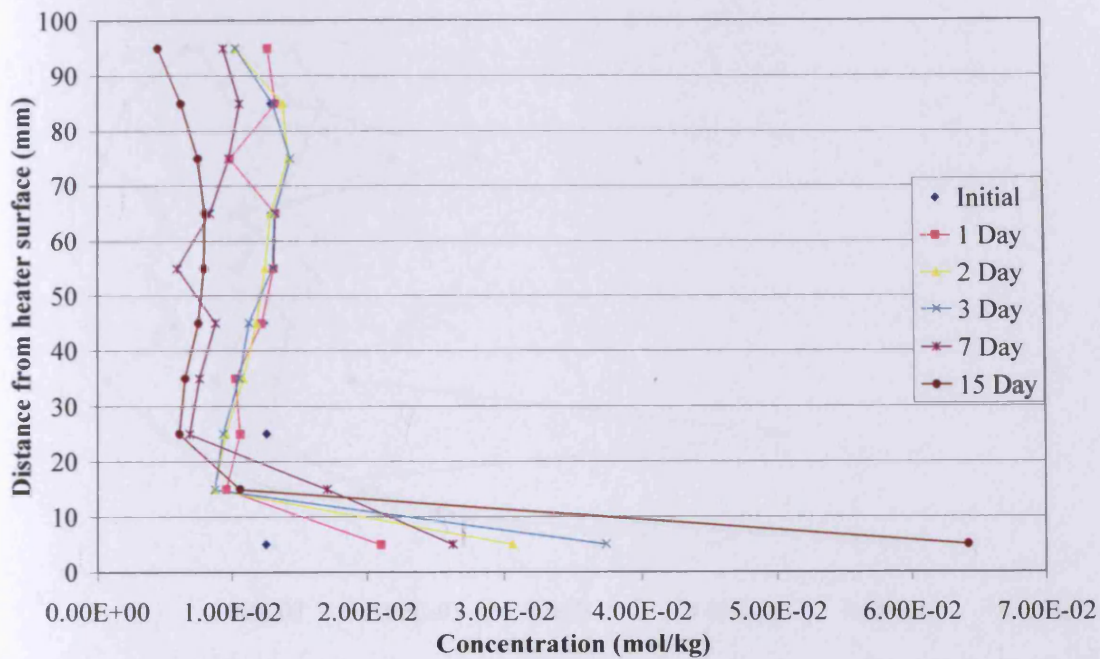
Figure 5.11 Sodium distribution of Speswhite kaolin dry sample for T test
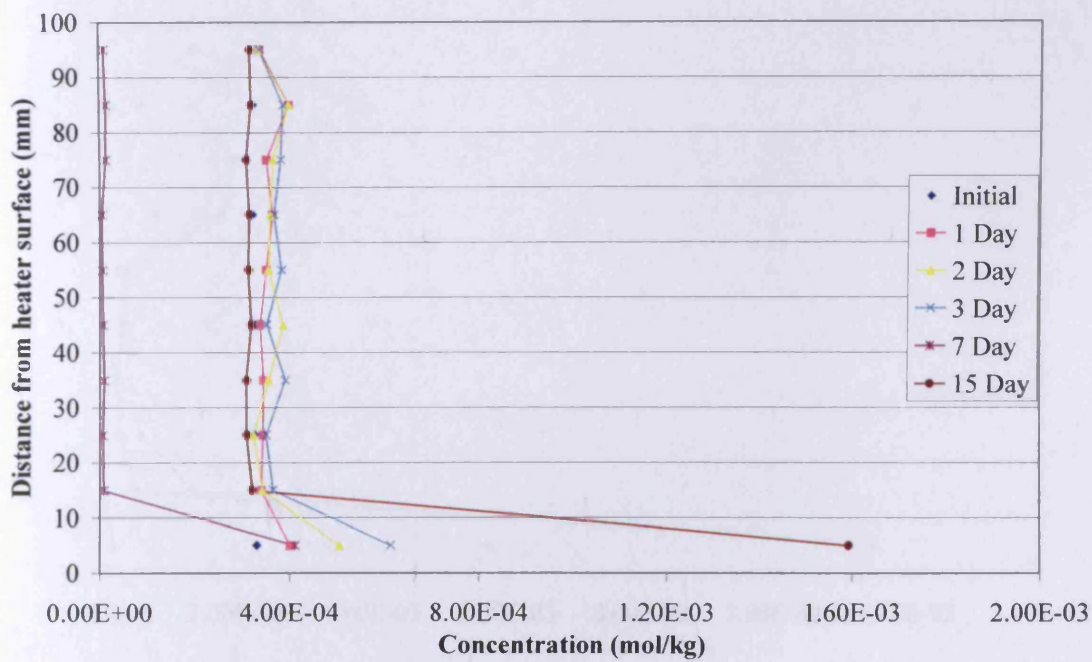
Figure 5.12 Magnesium distribution of Speswhite kaolin dry sample for T test
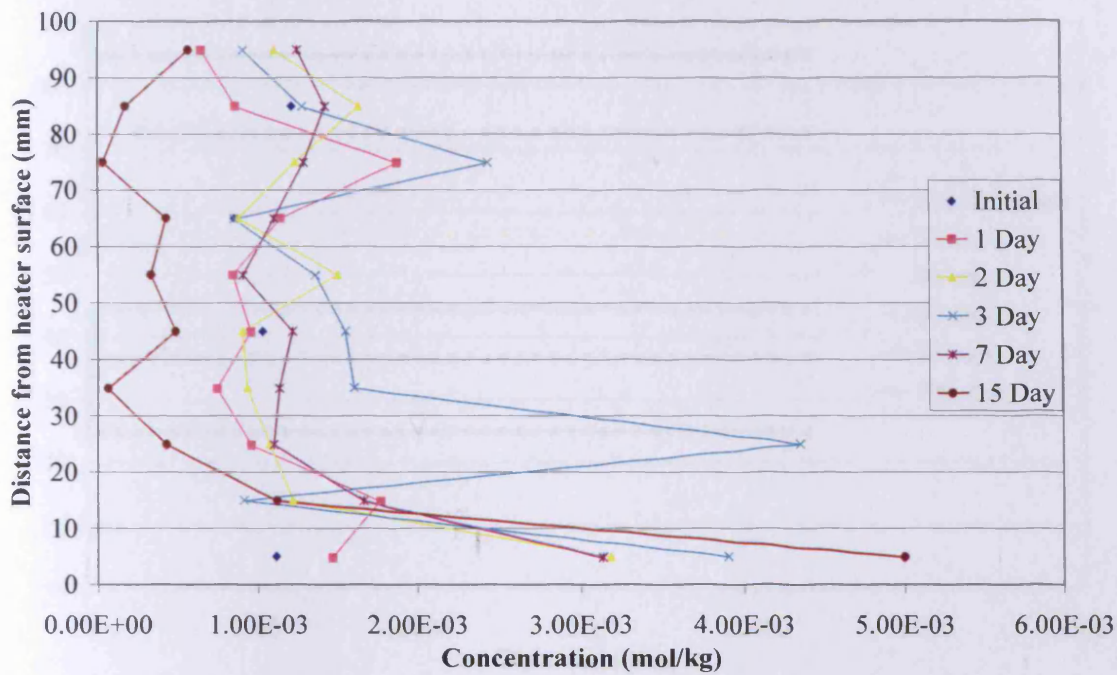
Figure 5.13 Potassium distribution of Speswhite kaolin dry sample for T test
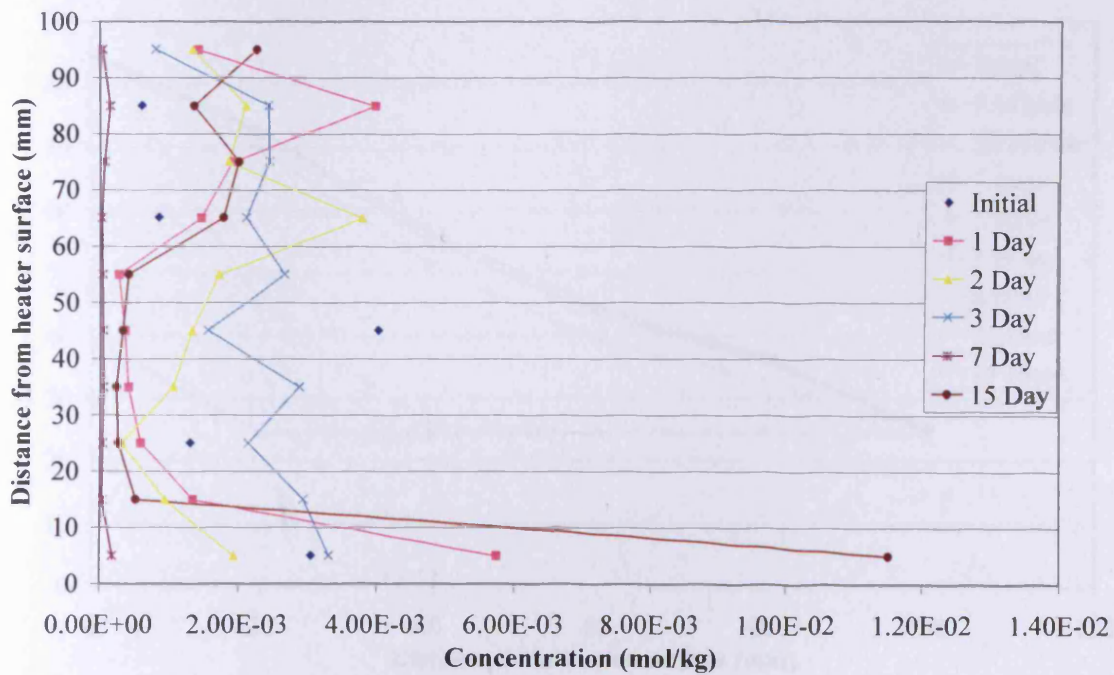
Figure 5.14 Calcium distribution of Speswhite kaolin dry sample for T test
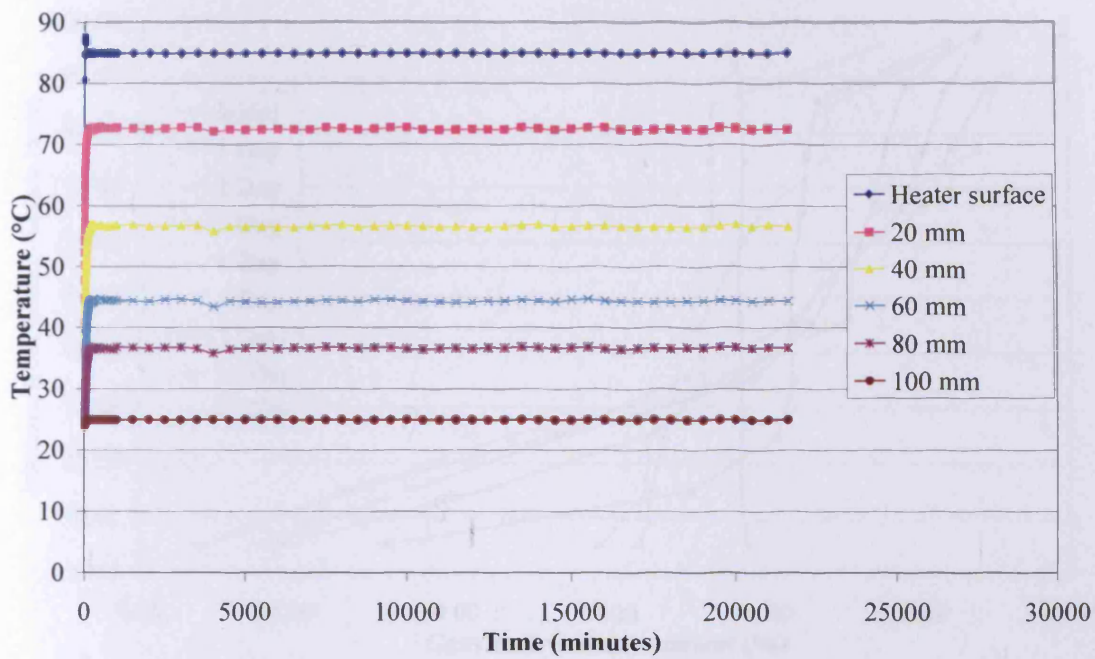
Figure 5.15 Temperature distribution of Speswhite kaolin wet sample for T test
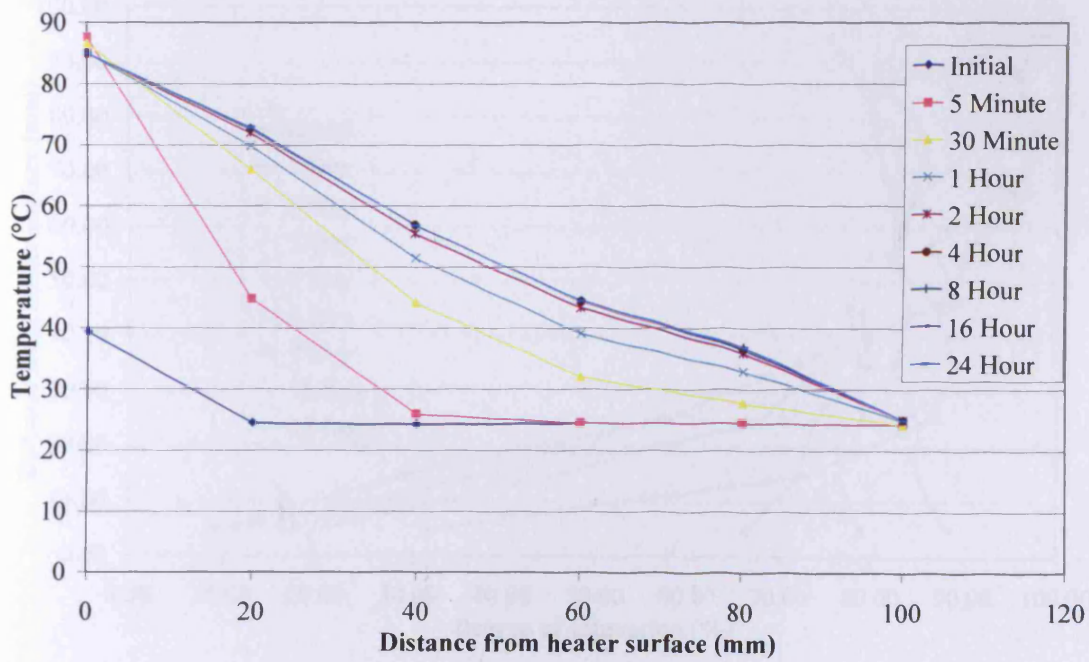
Figure 5.16 Temperature profile of Speswhite kaolin wet sample for T test
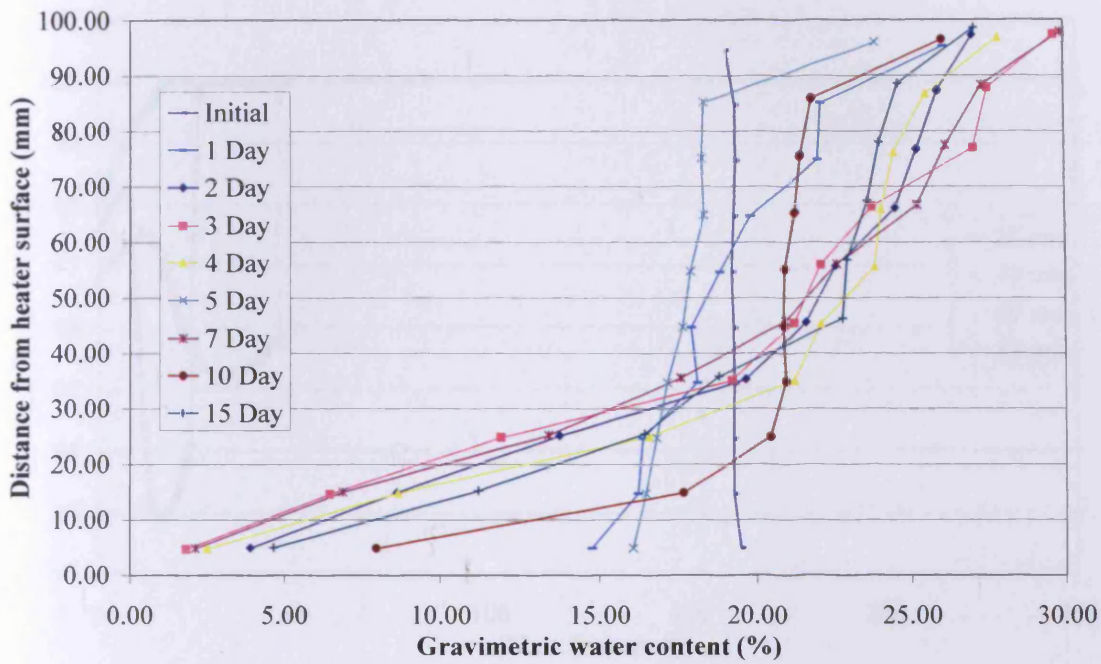
Figure 5.17 Gravimetric water content distribution of Speswhite kaolin wet sample for T test
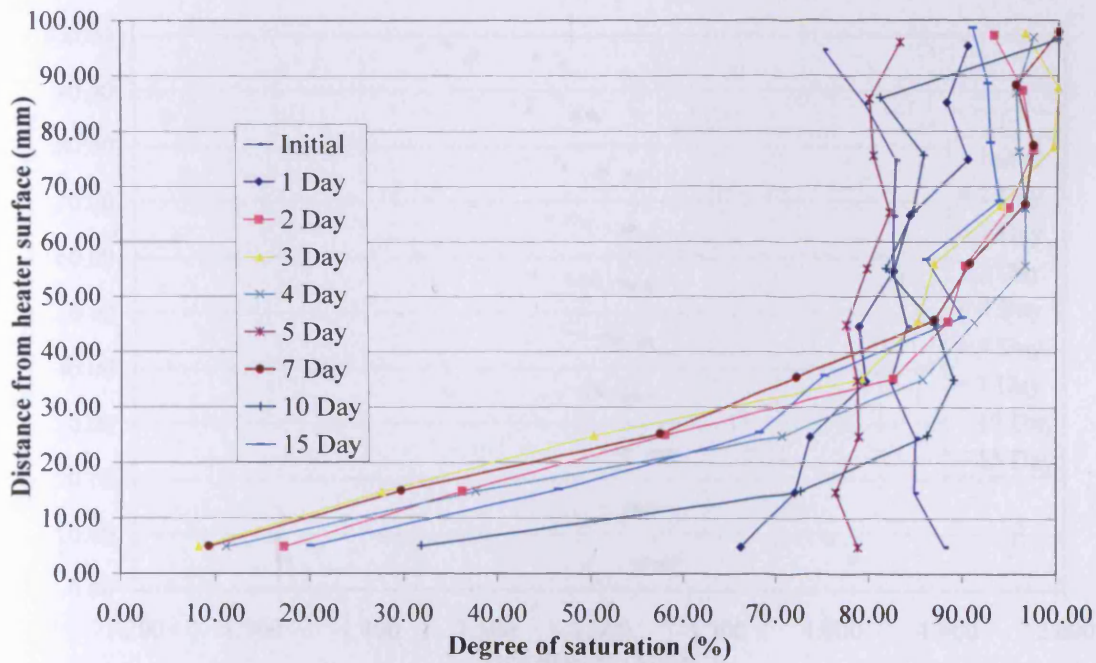
Figure 5.18 Degree of saturation of Speswhite kaolin wet sample for T test
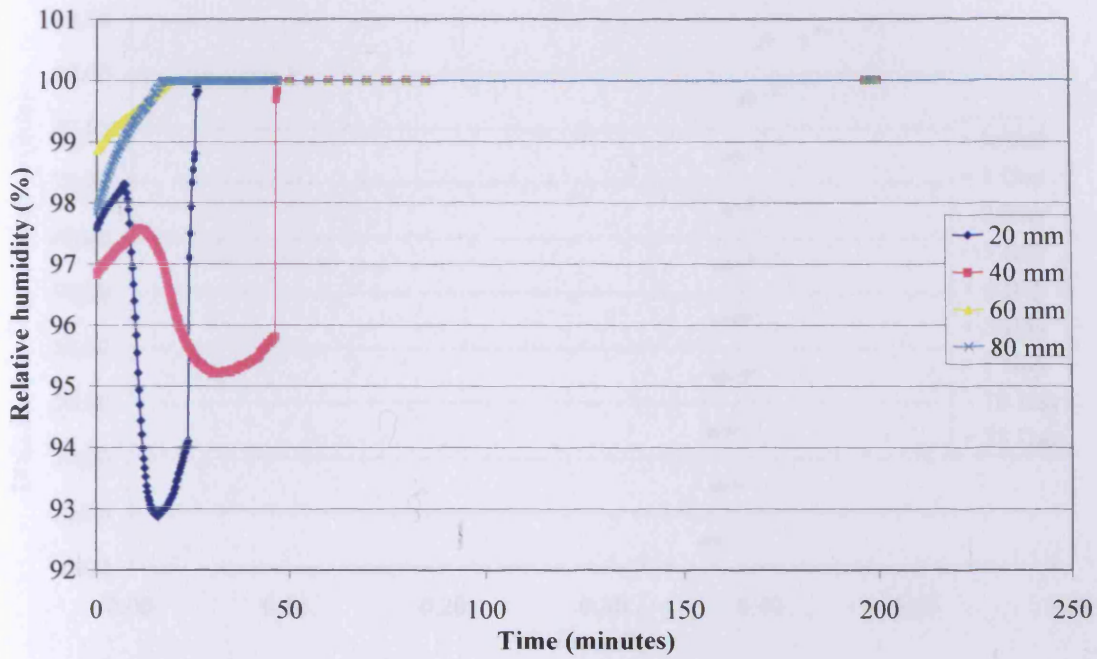
Figure 5.19 Relative humidity variation of Speswhite kaolin wet sample for T test
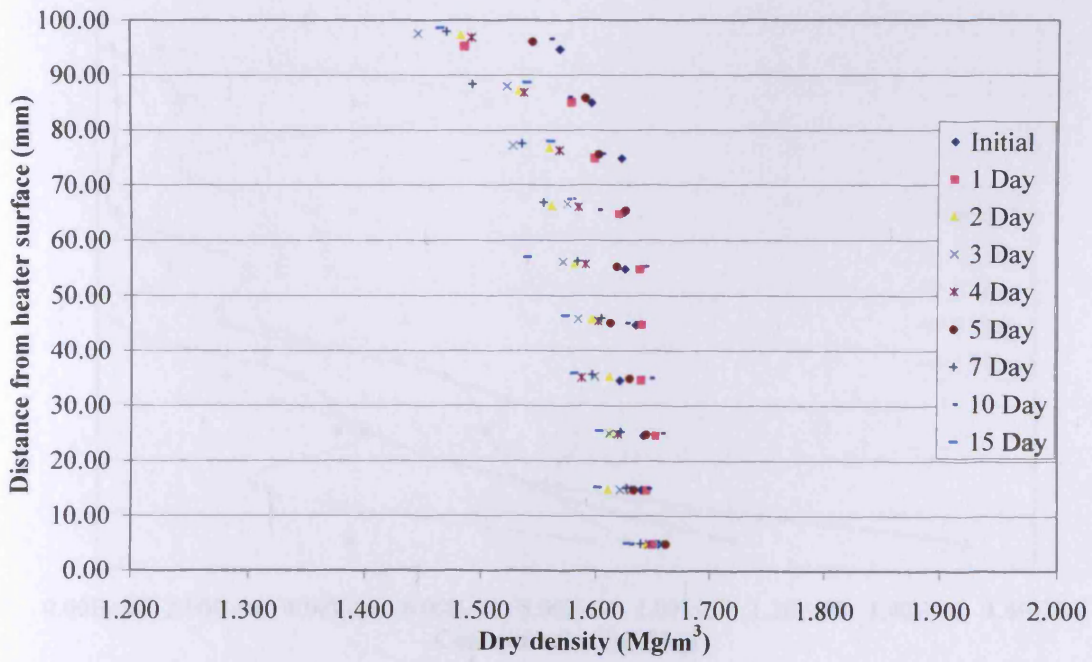
Figure 5.20 Dry density of Speswhite kaolin wet sample for T test
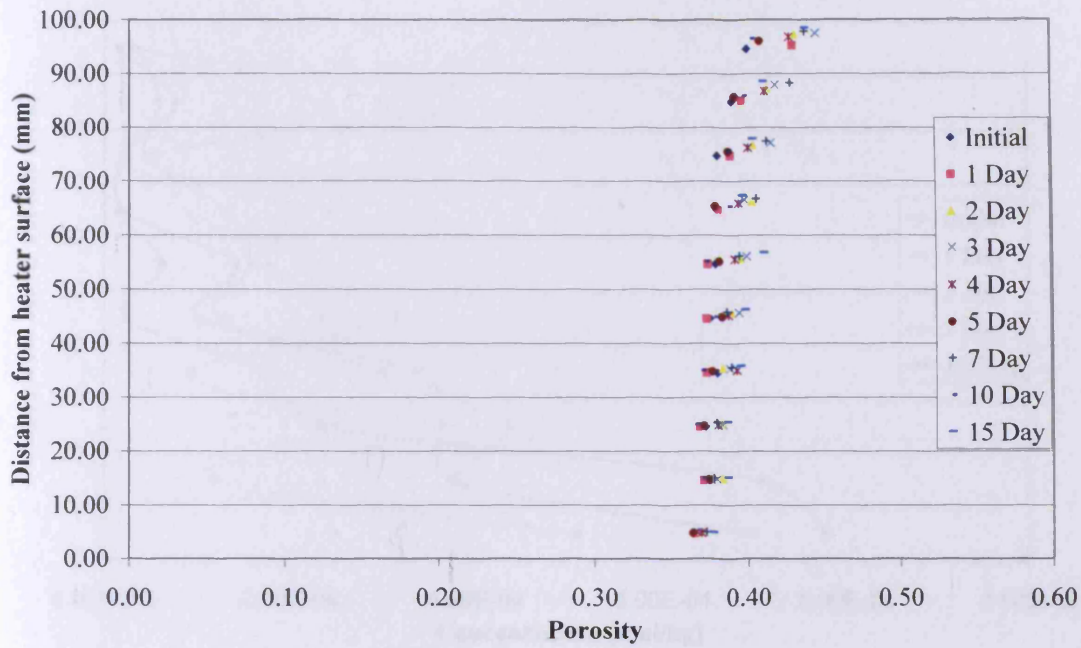
Figure 5.21 Porosity of Speswhite kaolin wet sample for T test
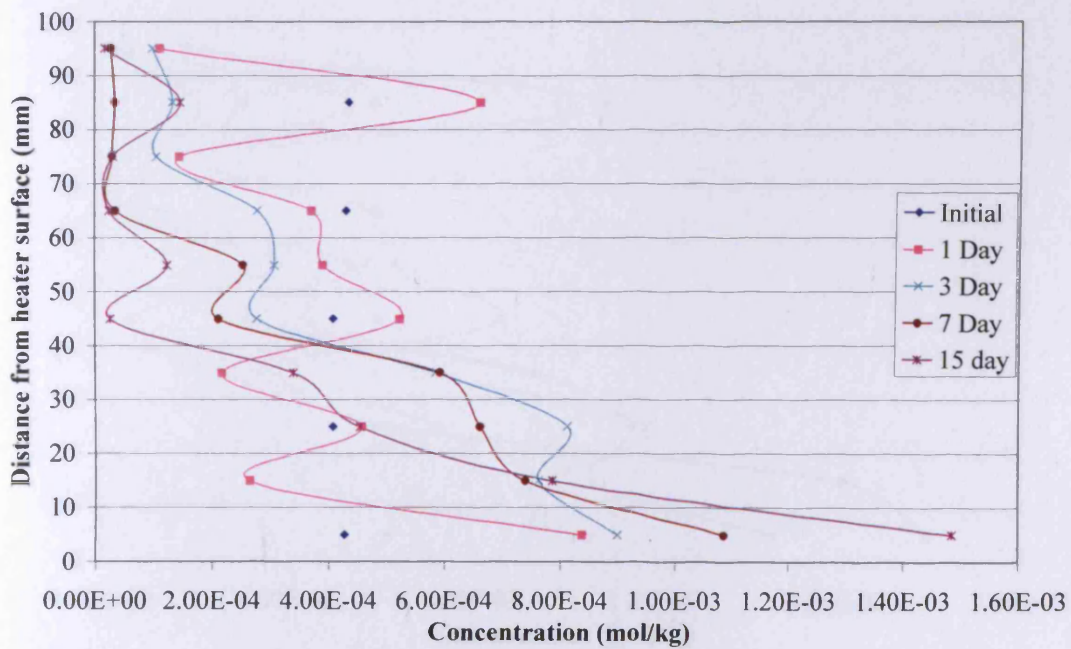
Figure 5.22 Chloride distribution of Speswhite kaolin wet sample for T test
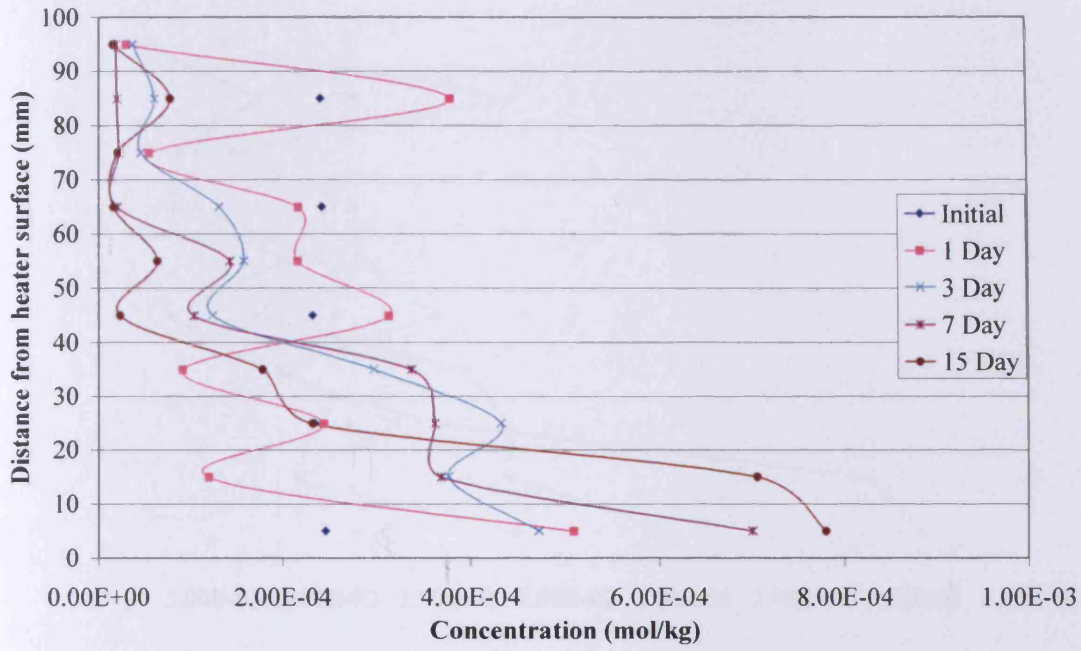
Figure 5.23 Nitrate distribution of Speswhite kaolin wet sample for T test
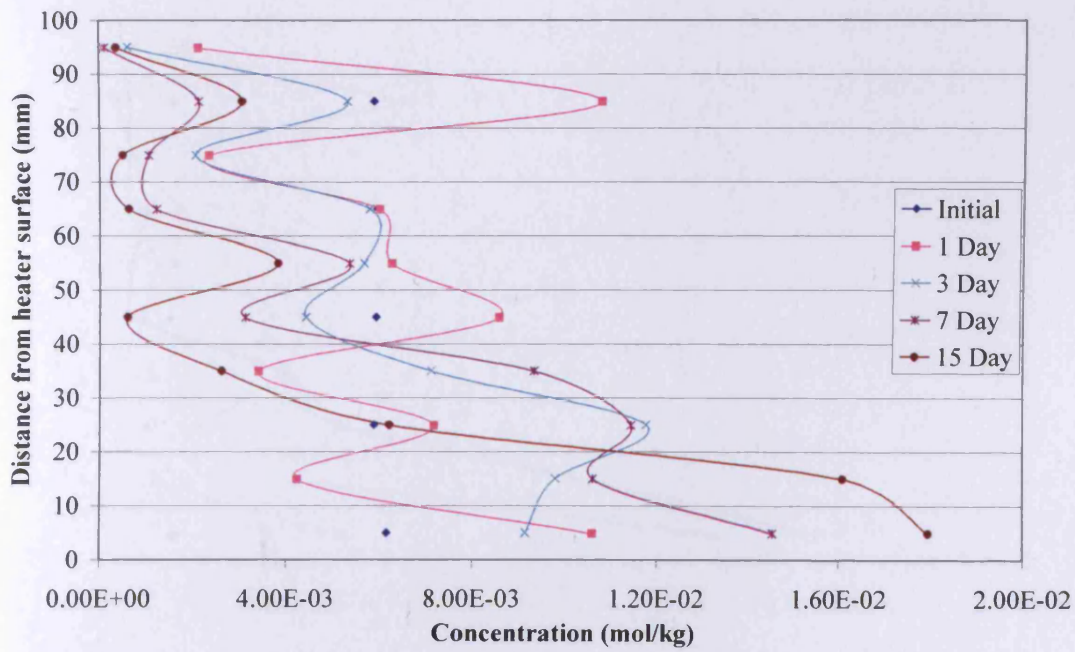
Figure 5.24 Sulphate distribution of Speswhite kaolin wet sample for T test
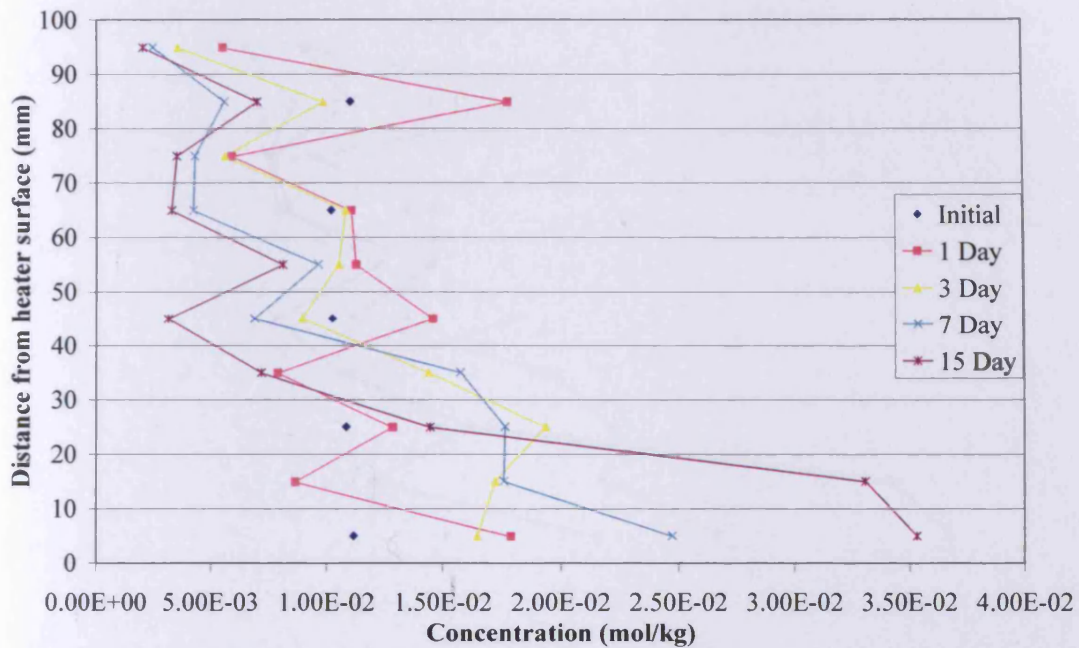
Figure 5.25 Sodium distribution of Speswhite kaolin wet sample for T test
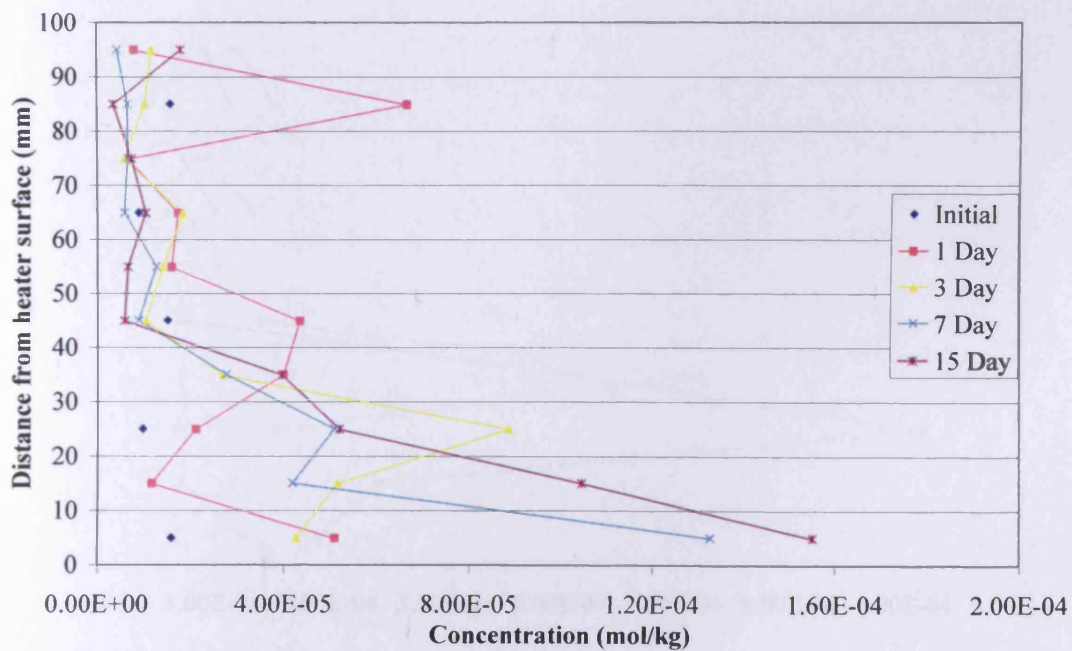
Figure 5.26 Magnesium distribution of Speswhite kaolin wet sample for T test
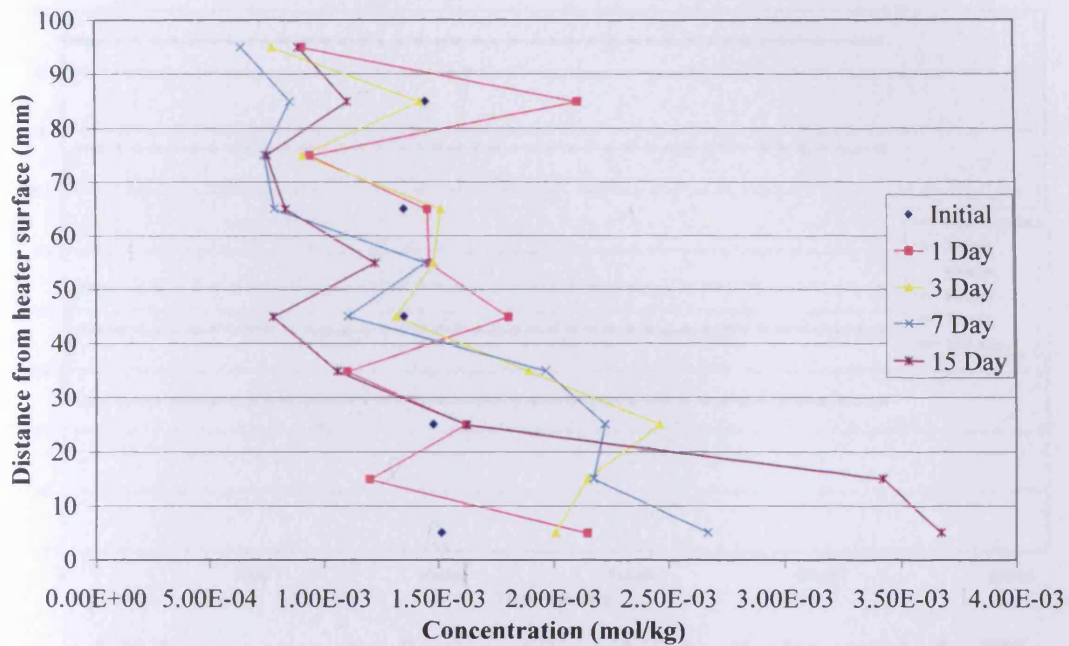
Figure 5.27 Potassium distribution of Speswhite kaolin wet sample for T test
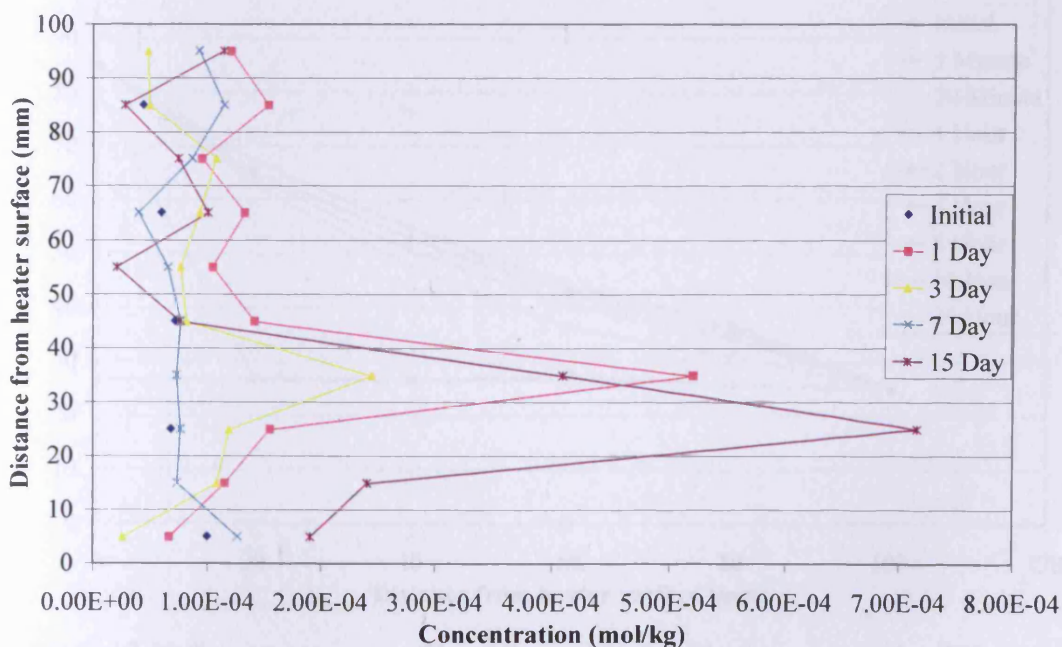
Figure 5.28 Calcium distribution of Speswhite kaolin wet sample for T test
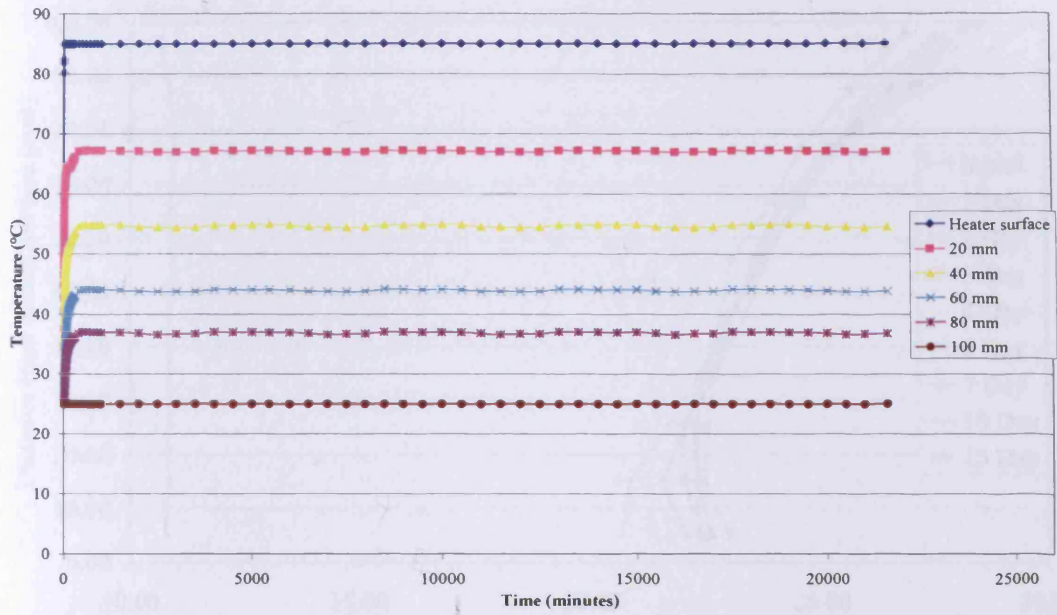
Figure 5.29 Temperature distribution of Speswhite kaolin dry sample for TH test
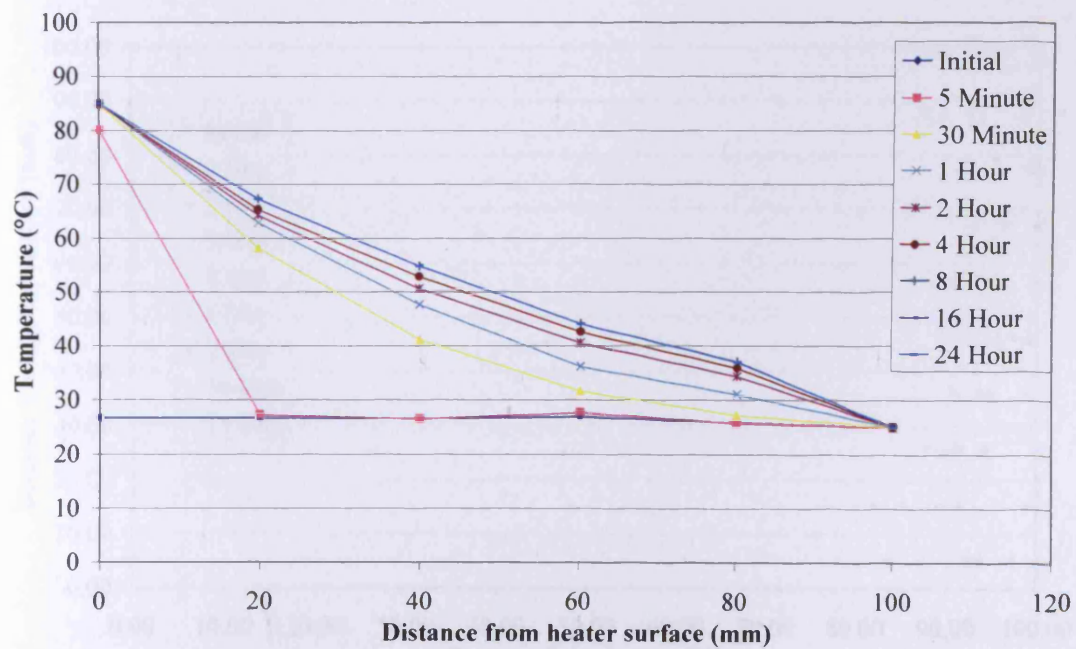
Figure 5.30 Temperature profile of Speswhite kaolin dry sample for TH test
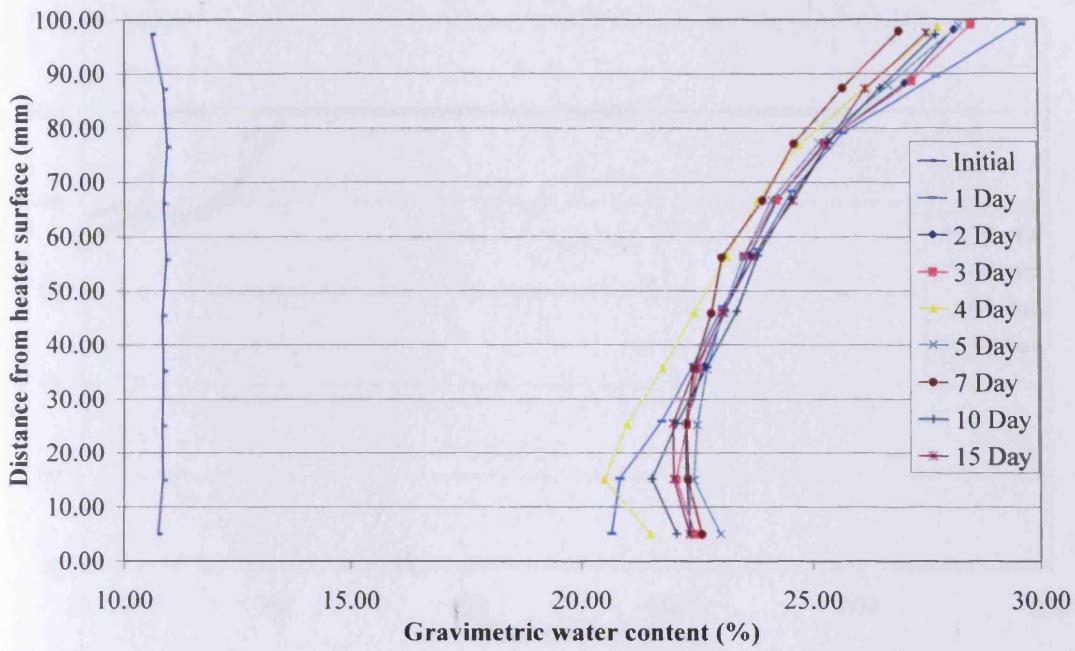
Figure 5.31 Gravimetric water content distribution of Speswhite kaolin dry sample for TH test
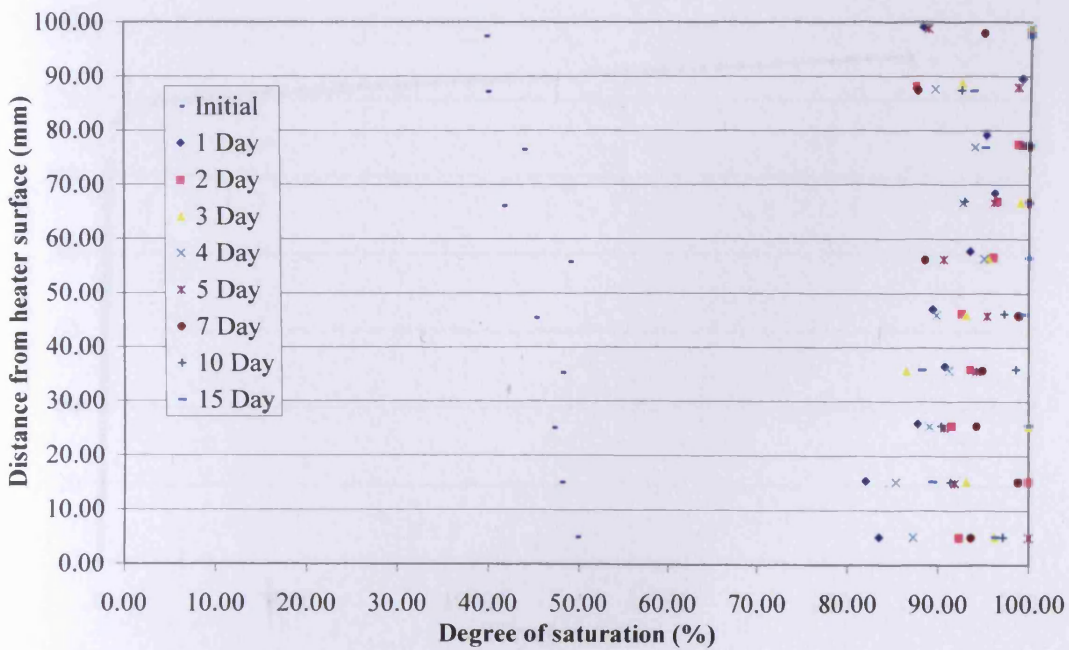
Figure 5.32 Degree of saturation of Speswhite kaolin dry sample for TH test
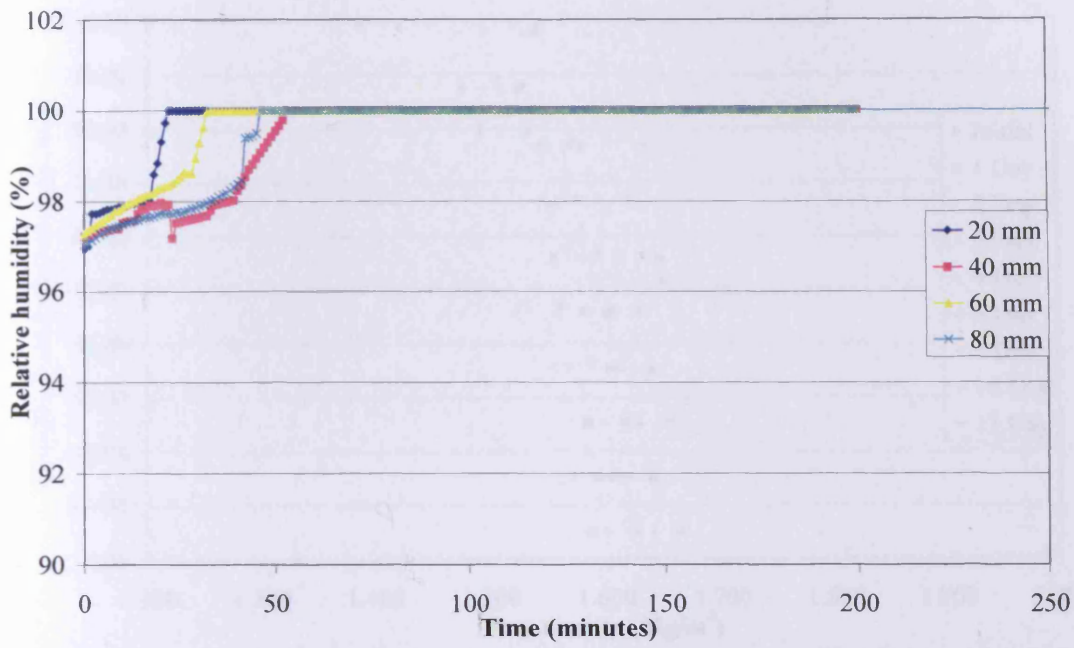
Figure 5.33 Relative humidity variation of Speswhite kaolin dry sample for TH test
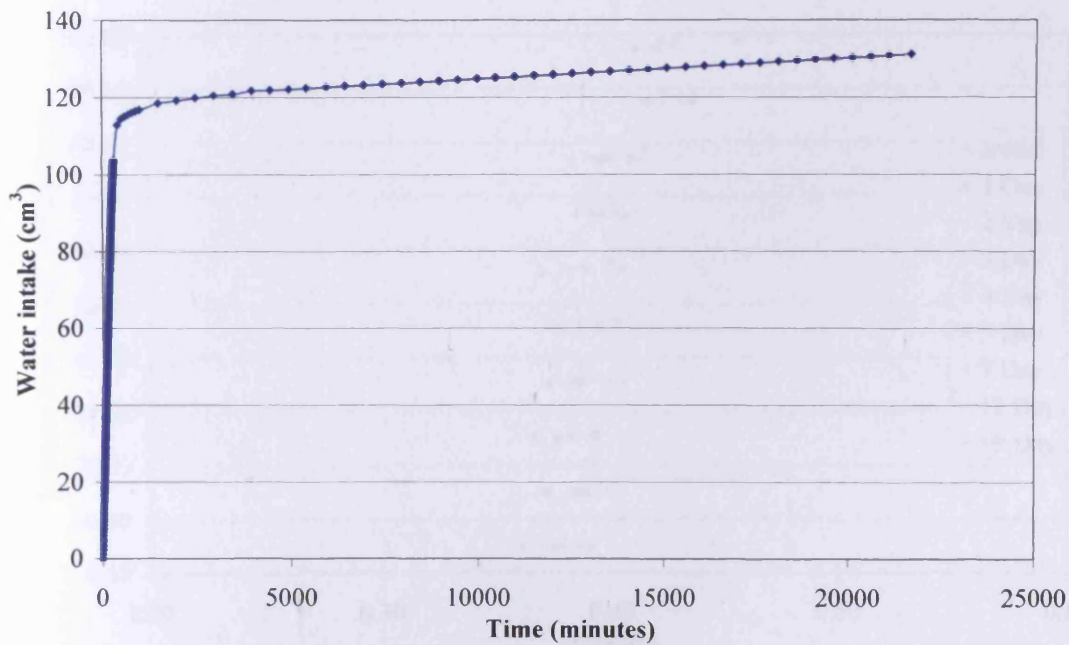
Figure 5.34 Water intake by Speswhite kaolin dry sample for TH test
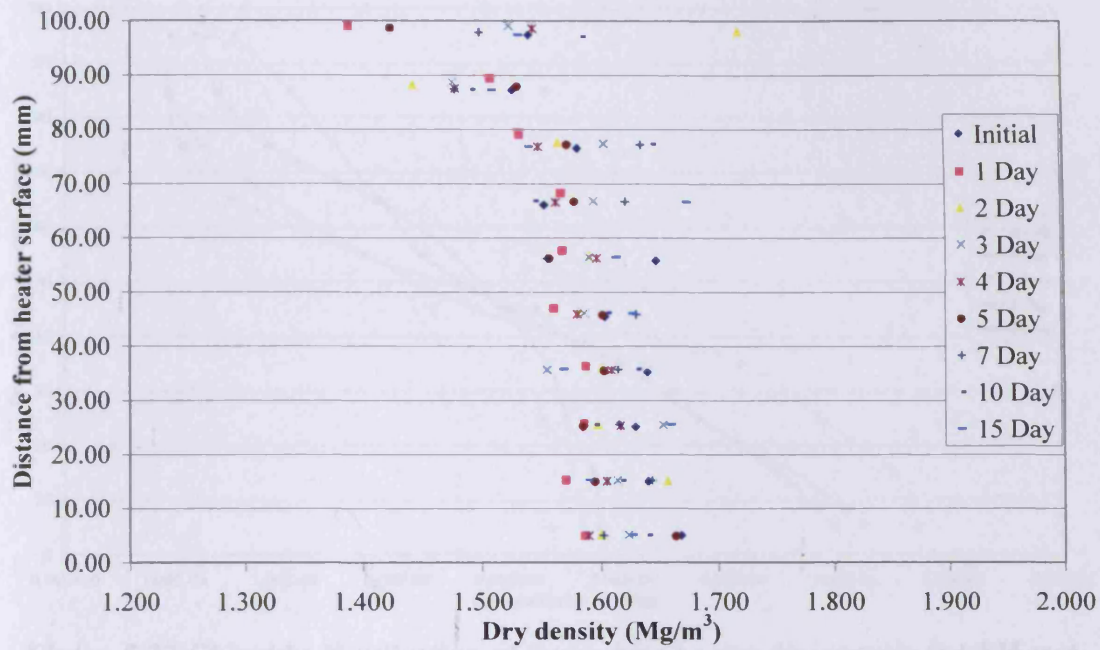
Figure 5.35 Dry density of Speswhite kaolin dry sample for TH test
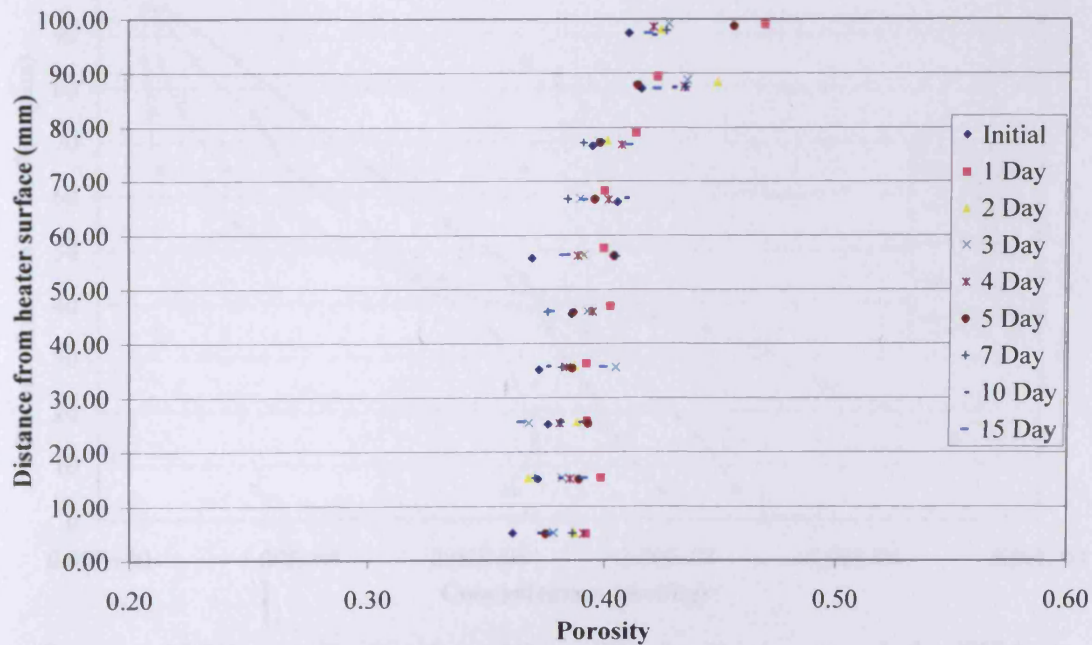
Figure 5.36 Porosity of Speswhite kaolin dry sample for TH test
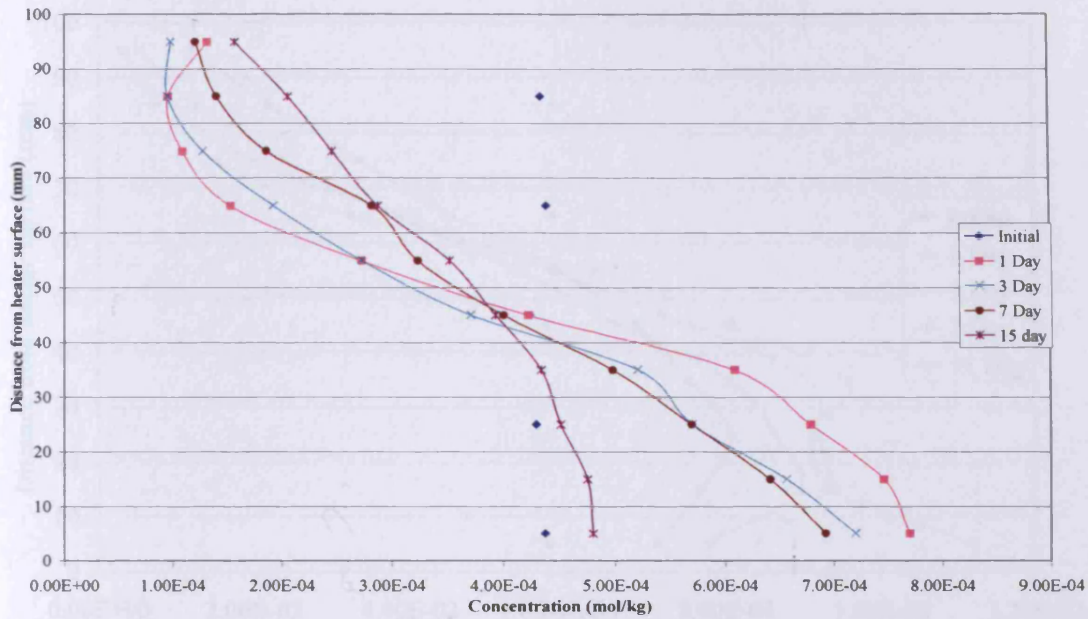
Figure 5.37 Chloride distribution of Speswhite kaolin dry sample for TH test
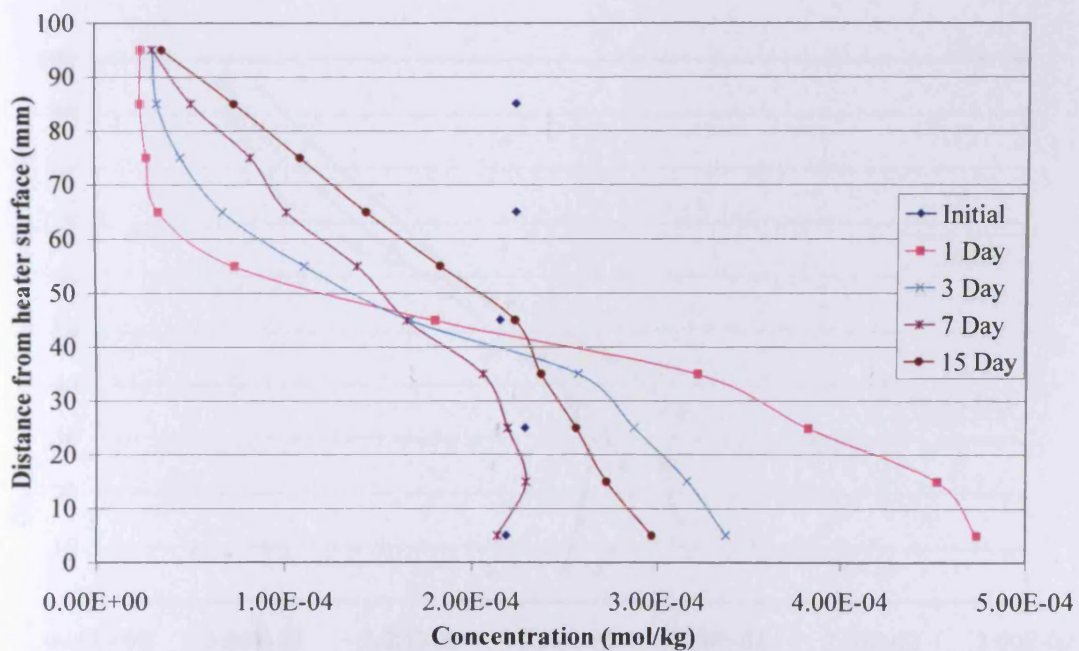
Figure 5.38 Nitrate distribution of Speswhite kaolin dry sample for TH test
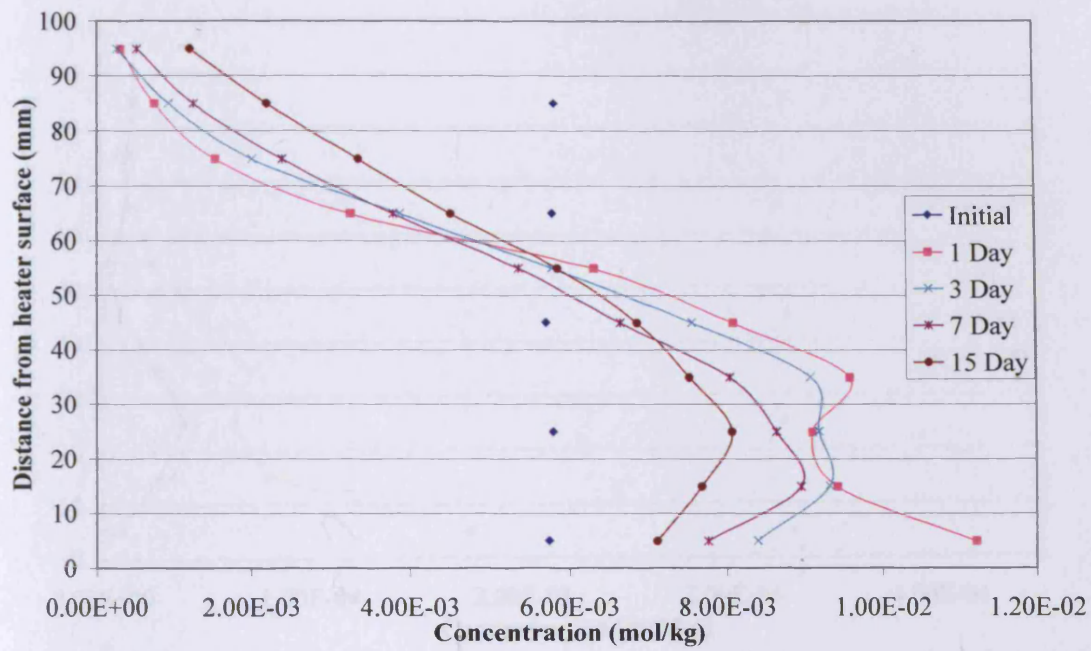
Figure 5.39 Sulphate distribution of Speswhite kaolin dry sample for TH test
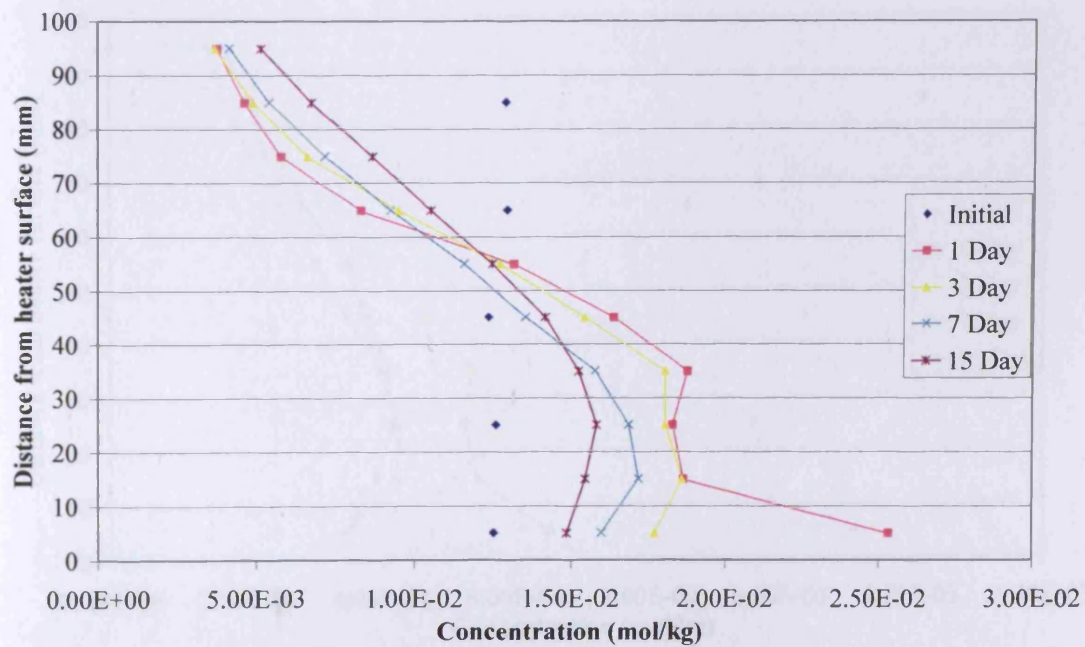
Figure 5.40 Sodium distribution of Speswhite kaolin dry sample for TH test
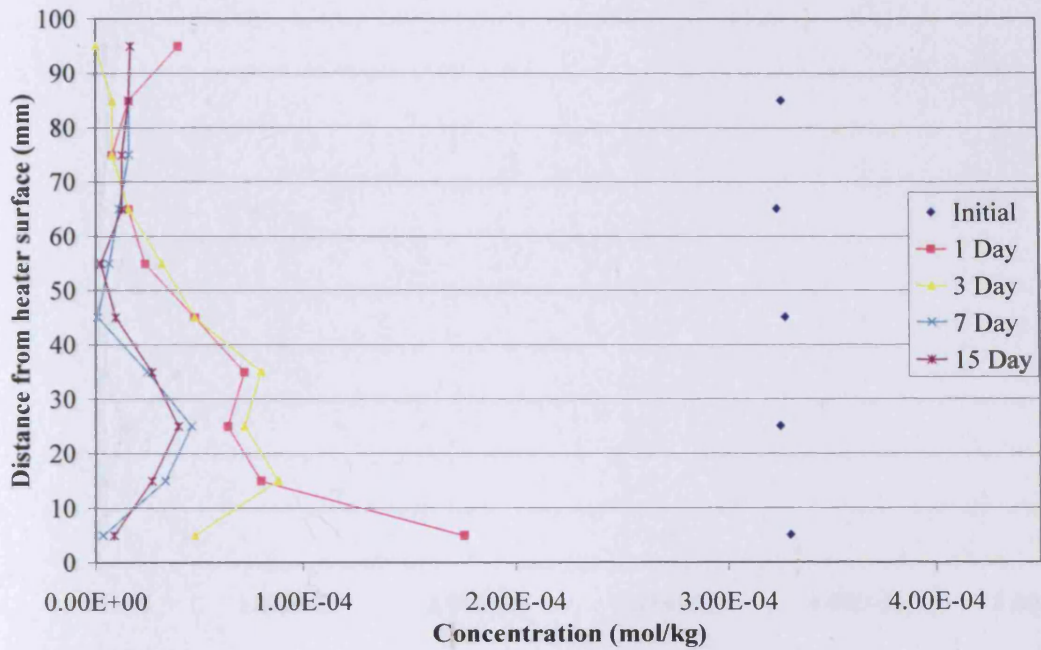
Figure 5.41 Magnesium distribution of Speswhite kaolin dry sample for TH test
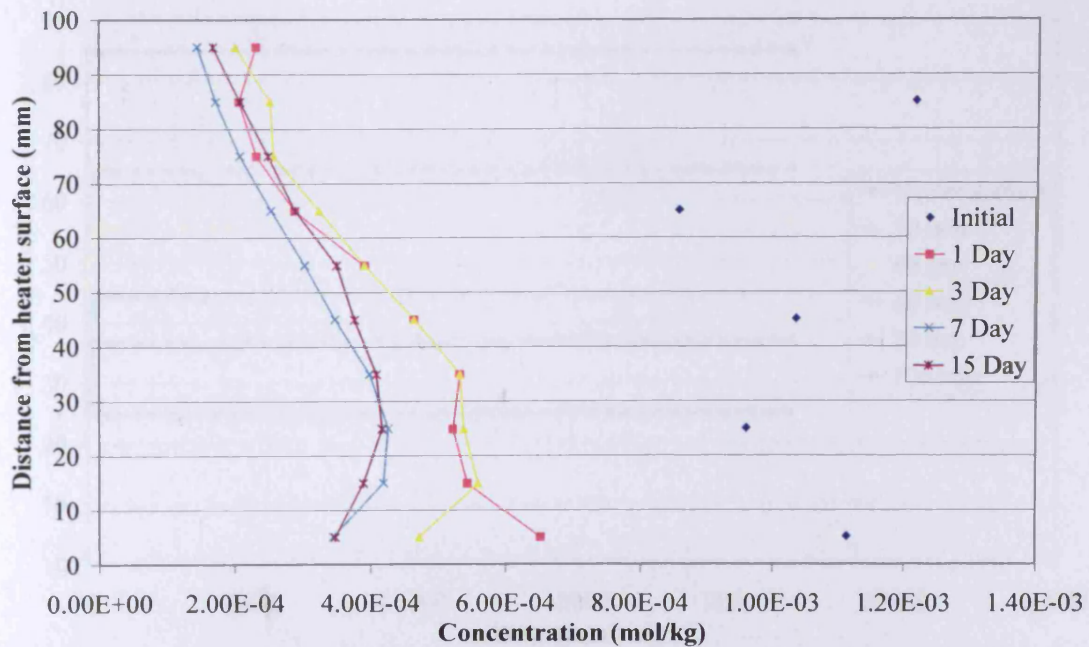
Figure 5.42 Potassium distribution of Speswhite kaolin dry sample for TH test
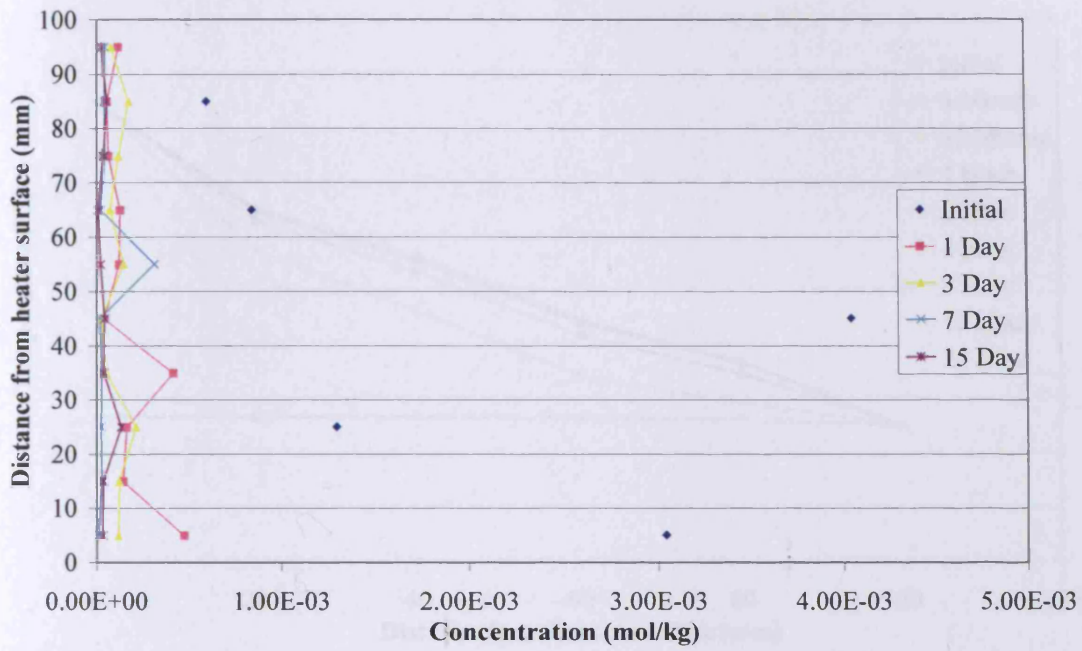
Figure 5.43 Calcium distribution of Speswhite kaolin dry sample for TH test
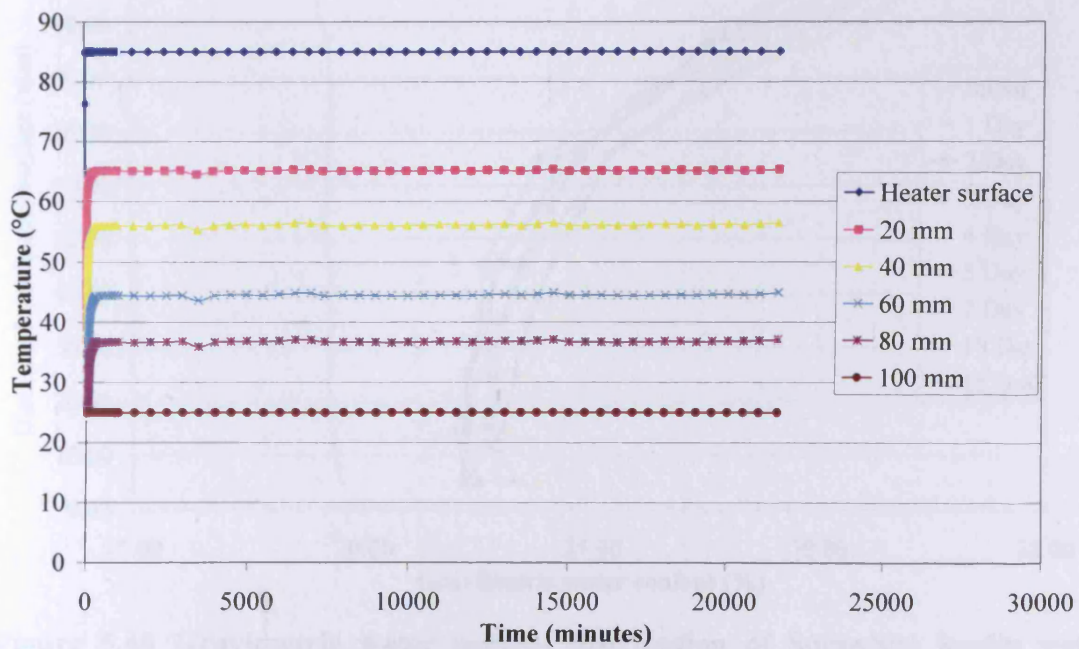
Figure 5.44 Temperature distribution of Speswhite kaolin wet sample for TH test
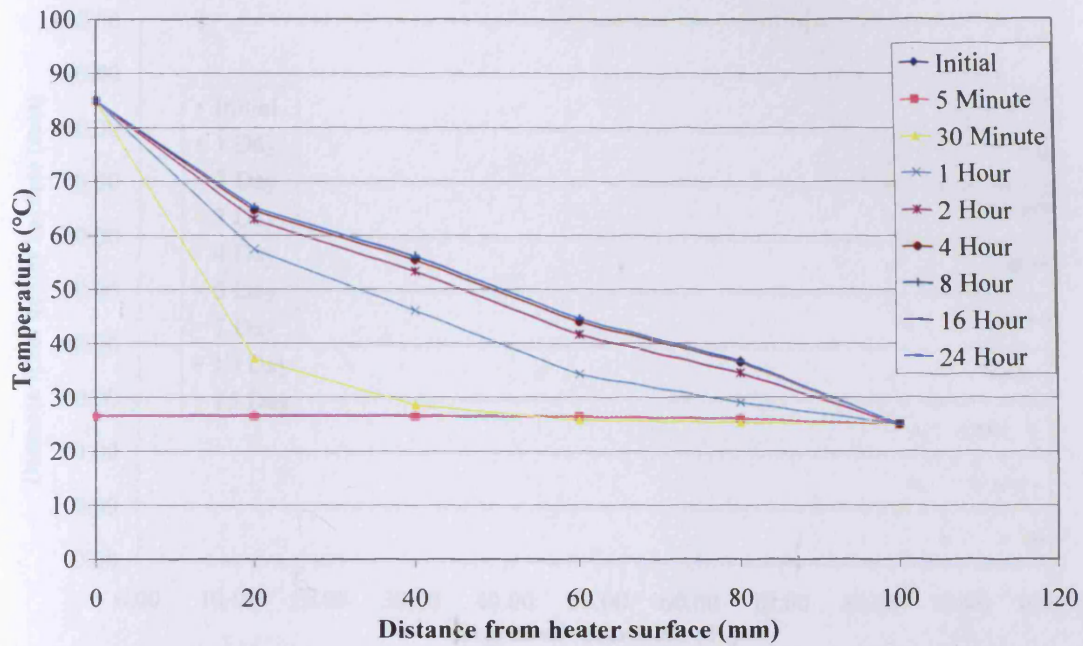
Figure 5.45 Temperature profile of Speswhite kaolin wet sample for TH test
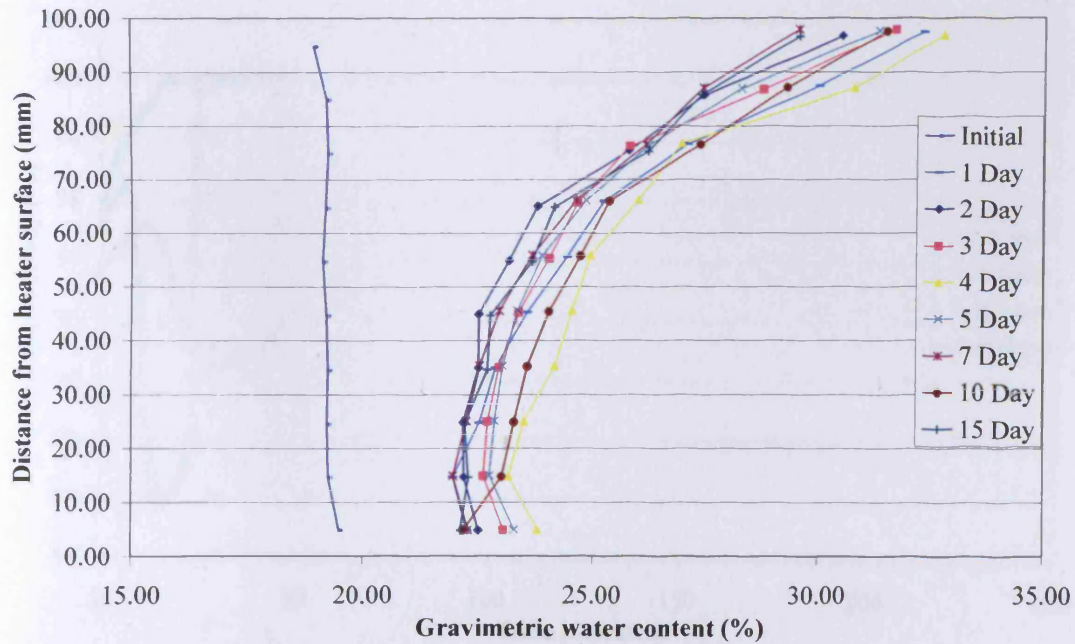
Figure 5.46 Gravimetric water content distribution of Speswhite kaolin wet sample for TH test
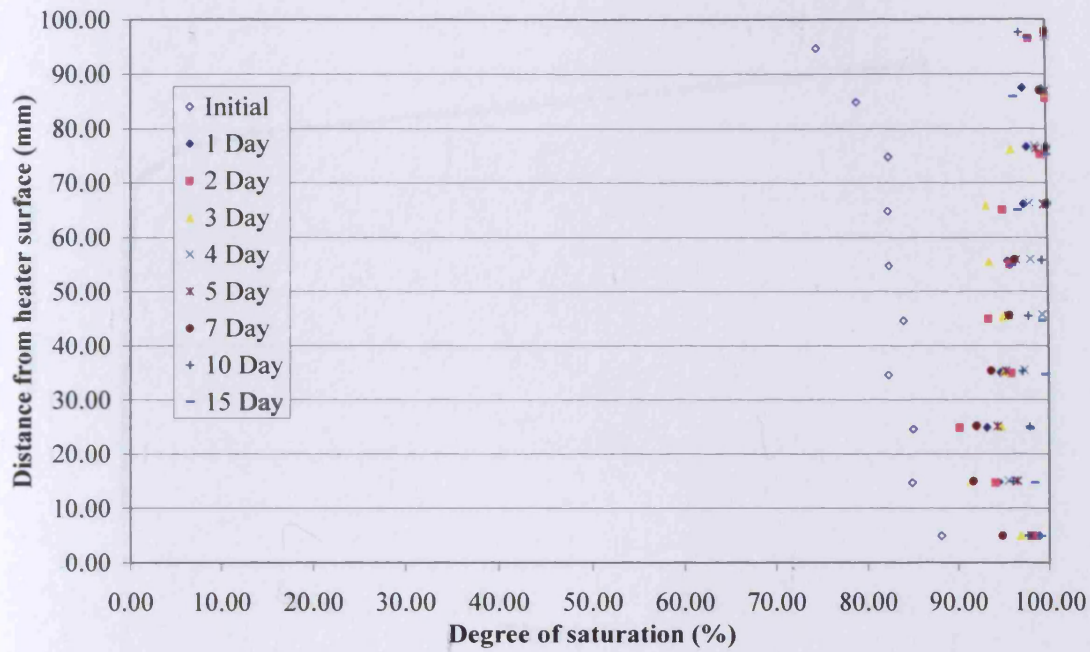
Figure 5.47 Degree of saturation of Speswhite kaolin wet sample for TH test
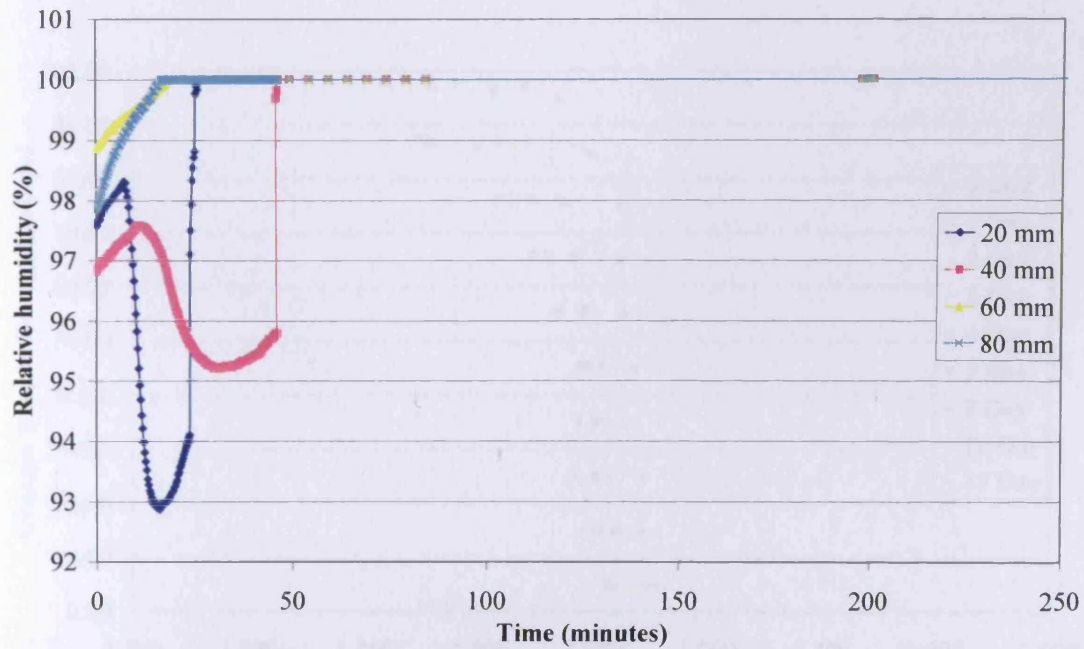
Figure 5.48 Relative humidity variation of Speswhite kaolin wet sample for TH test
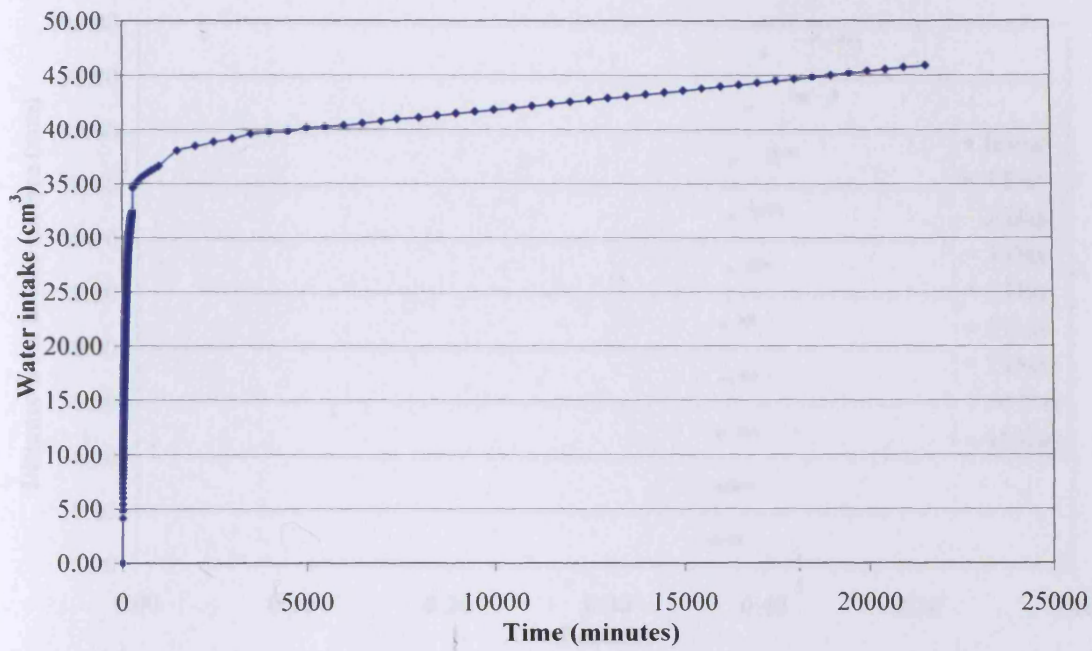
Figure 5.49 Water intake by Speswhite kaolin wet sample for TH test
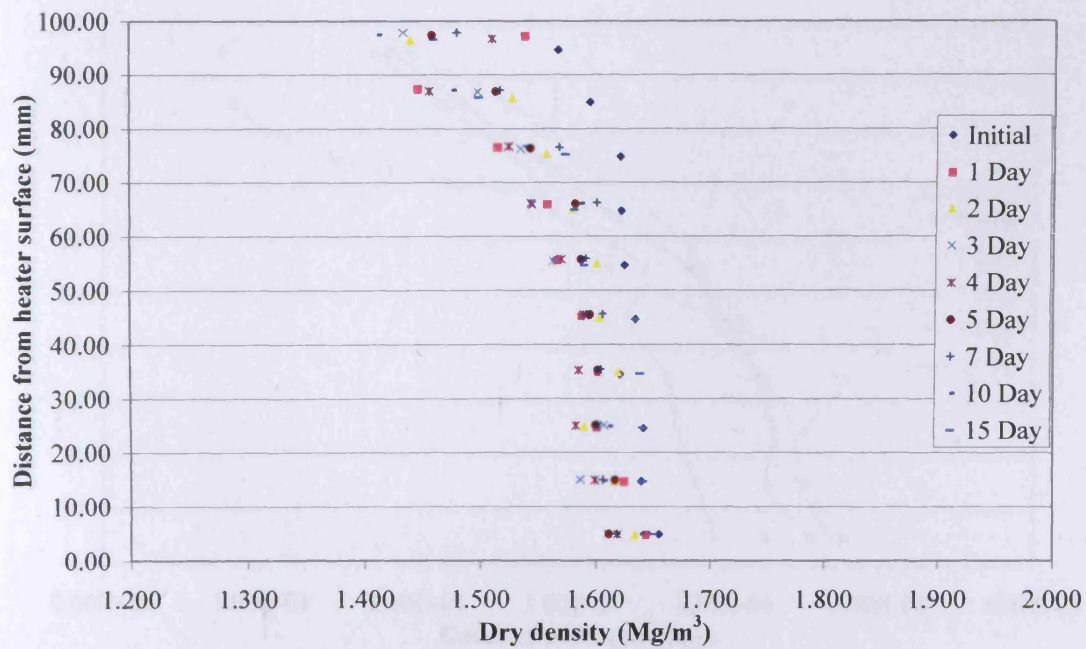
Figure 5.50 Dry density of Speswhite kaolin wet sample for TH test
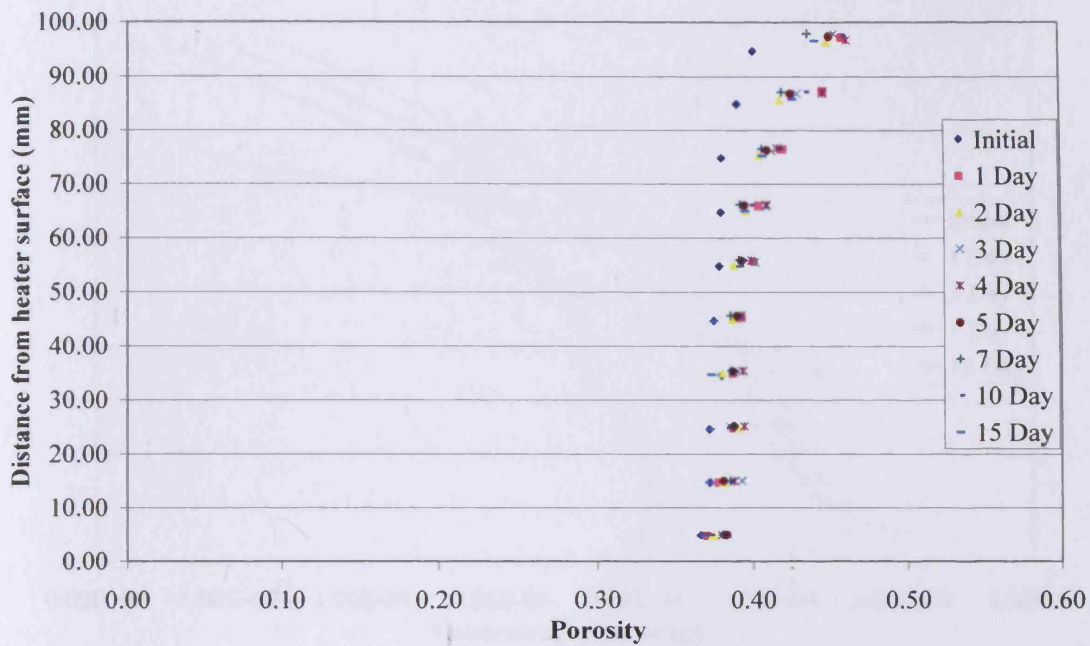
Figure 5.51 Porosity of Speswhite kaolin wet sample for TH test
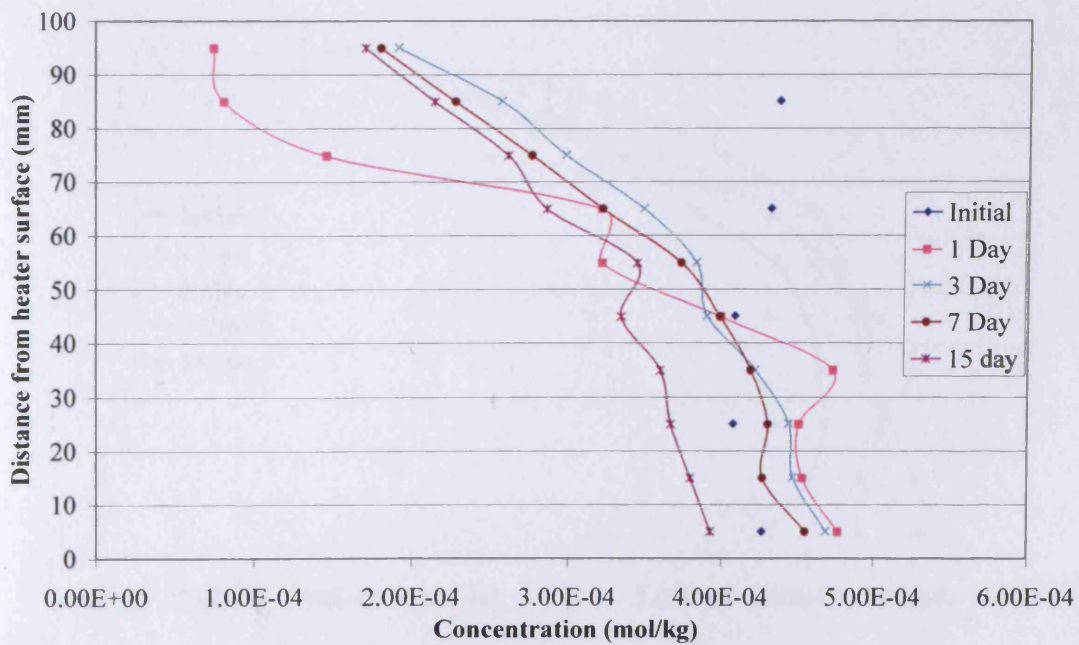
Figure 5.52 Chloride distribution of Speswhite kaolin wet sample for TH test
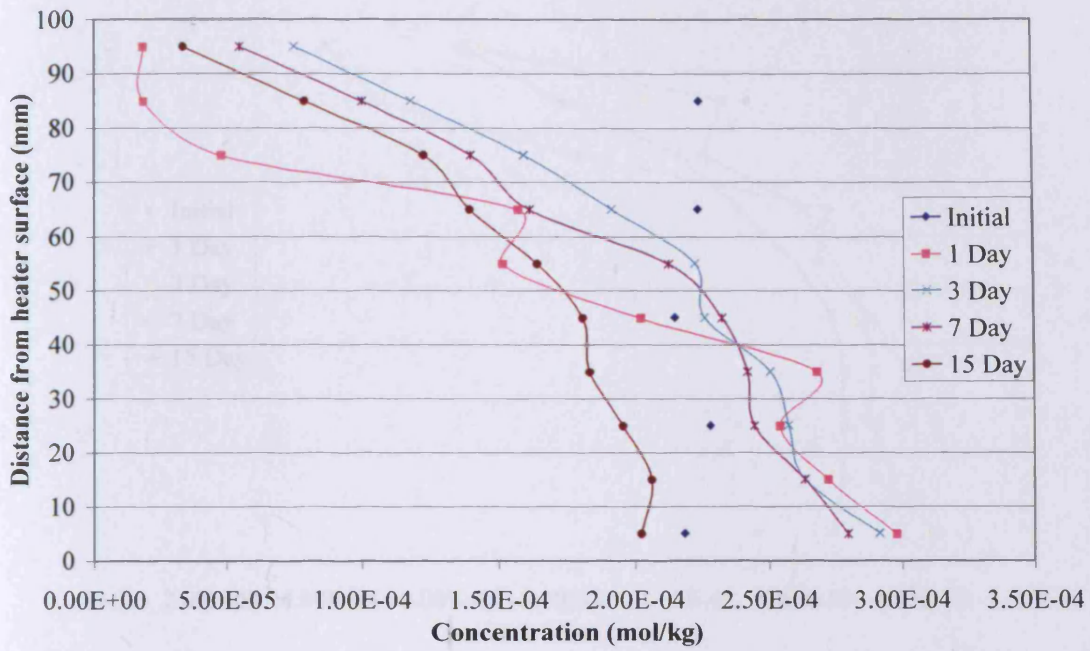
Figure 5.53 Nitrate distribution of Speswhite kaolin wet sample for TH test
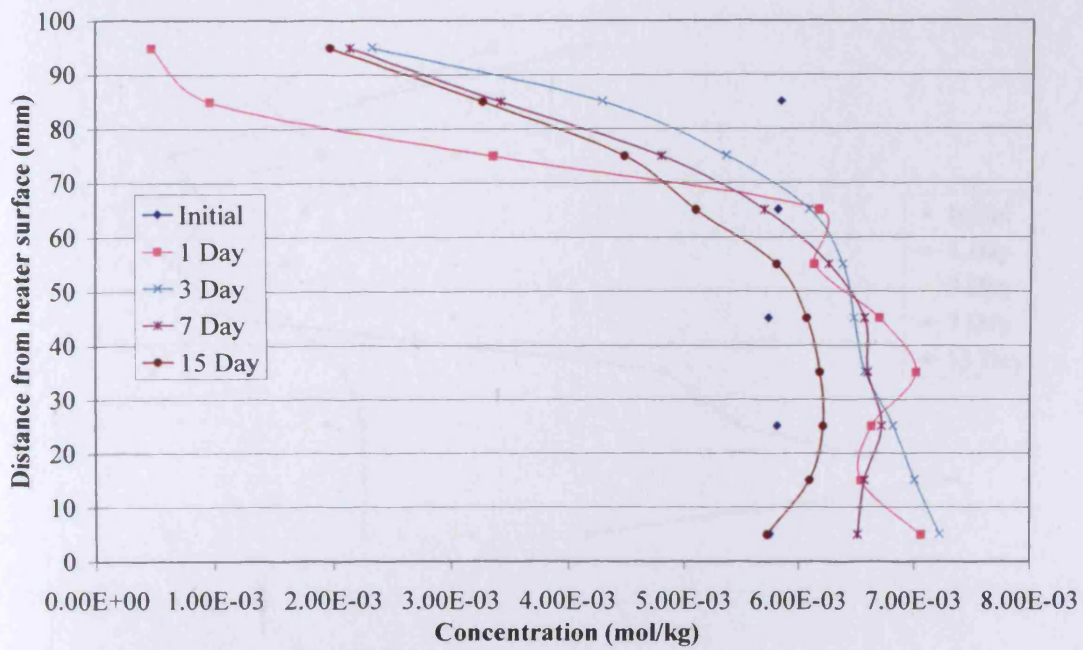
Figure 5.54 Sulphate distribution of Speswhite kaolin wet sample for TH test
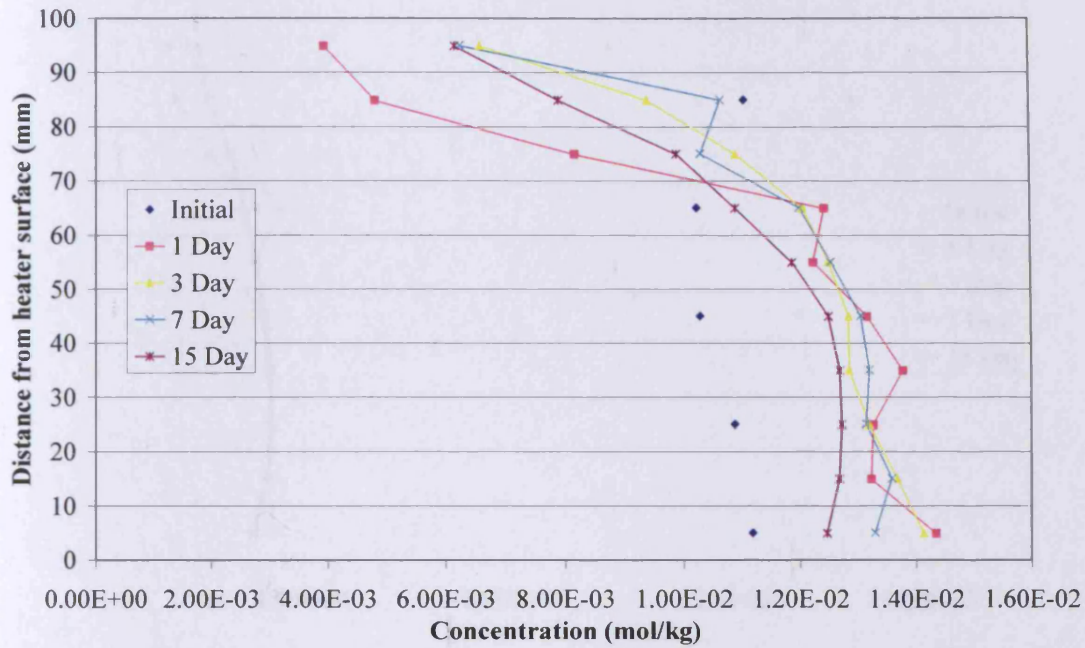
Figure 5.55 Sodium distribution of Speswhite kaolin wet sample for TH test
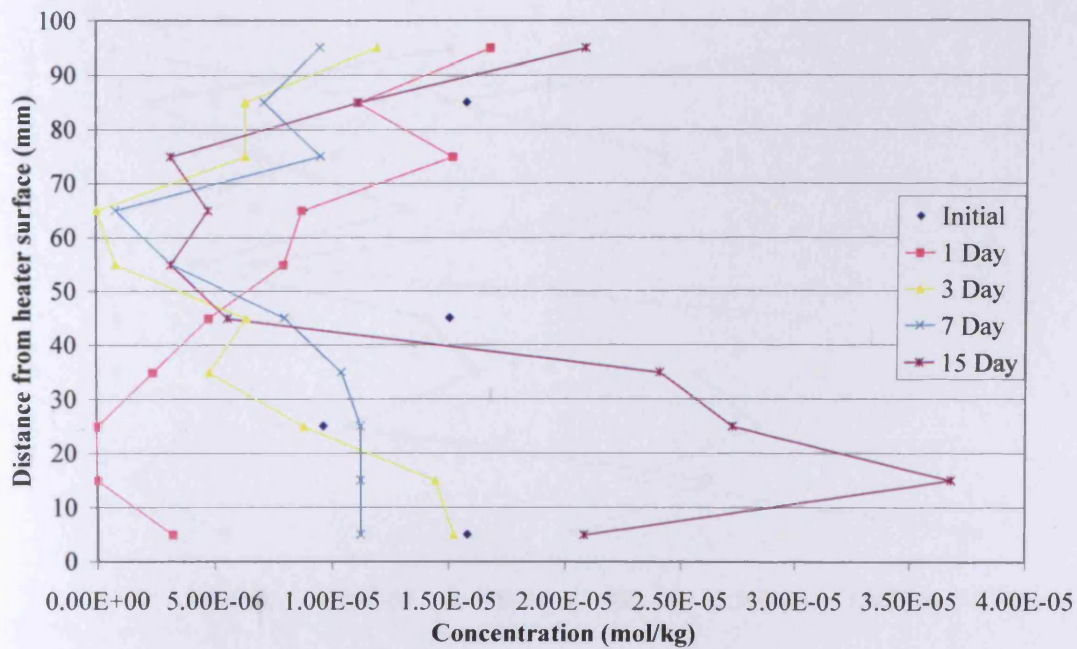
Figure 5.56 Magnesium distribution of Speswhite kaolin wet sample for TH test
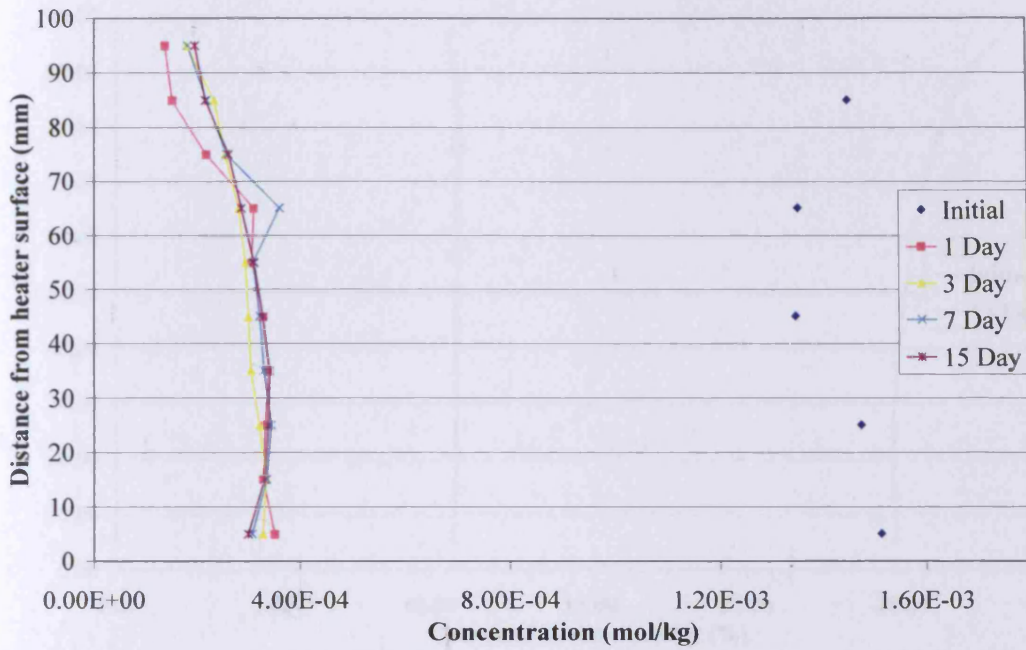
Figure 5.57 Potassium distribution of Speswhite kaolin wet sample for TH test
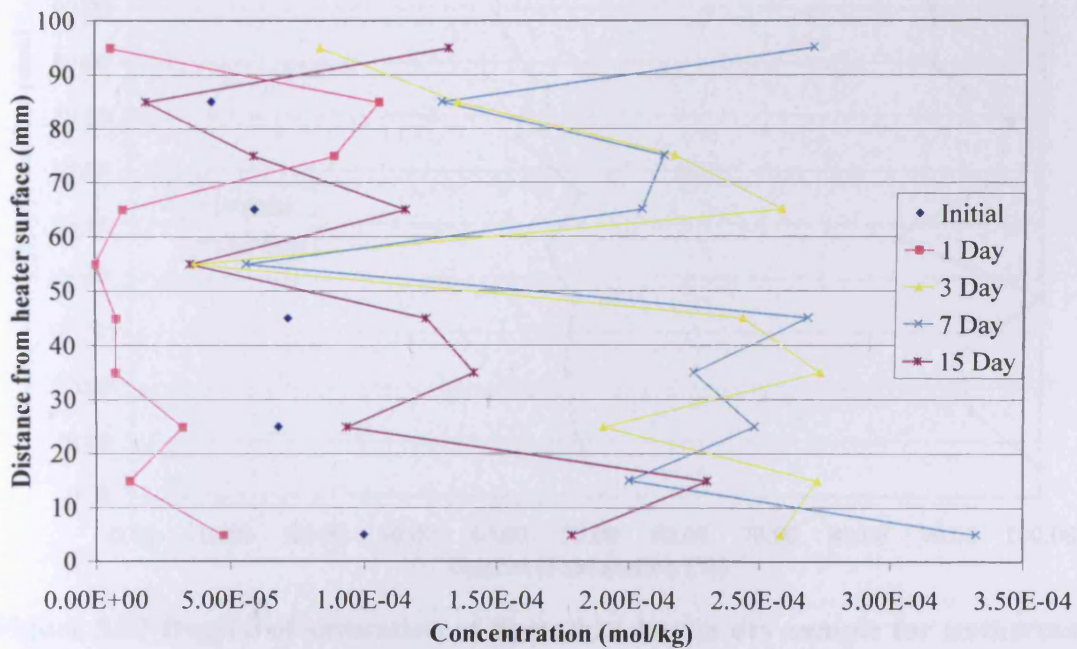
Figure 5.58 Calcium distribution of Speswhite kaolin wet sample for TH test
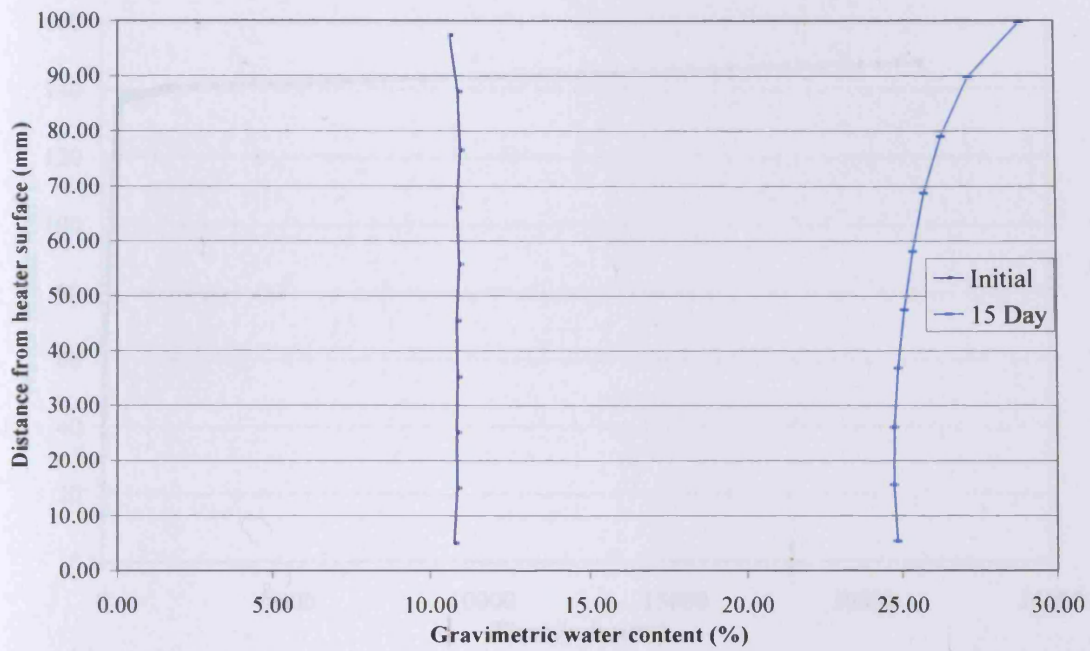
Figure 5.59 Gravimetric water content distribution of Speswhite kaolin dry sample isothermal test
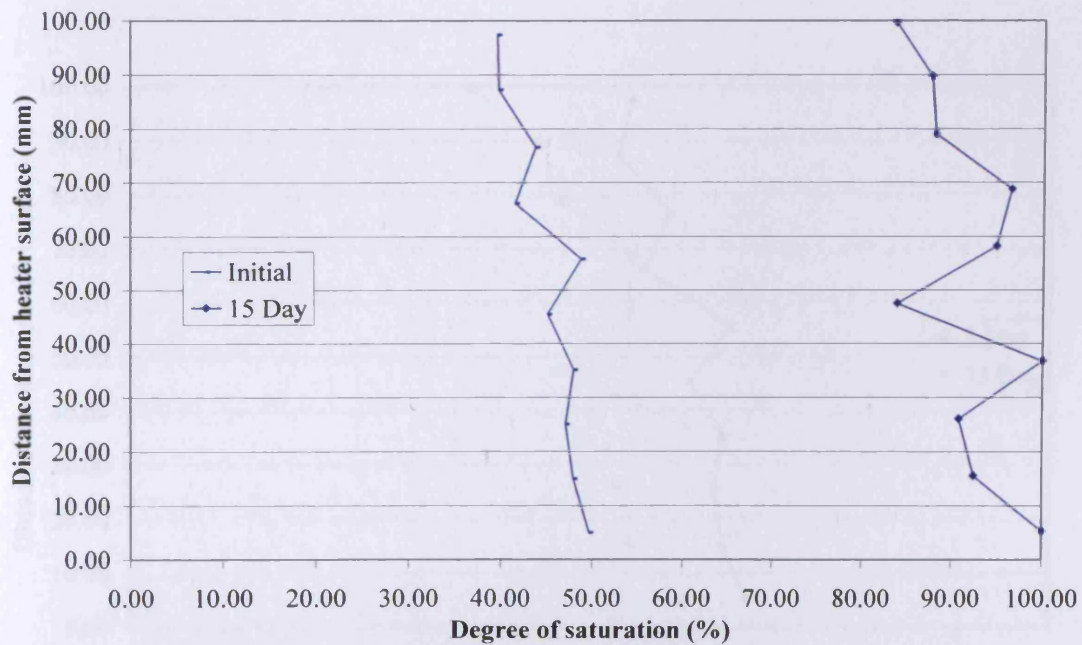
Figure 5.60 Degree of saturation of Speswhite kaolin dry sample for isothermal test

Figure 5.61 Water intake by Speswhite kaolin dry sample for isothermal test
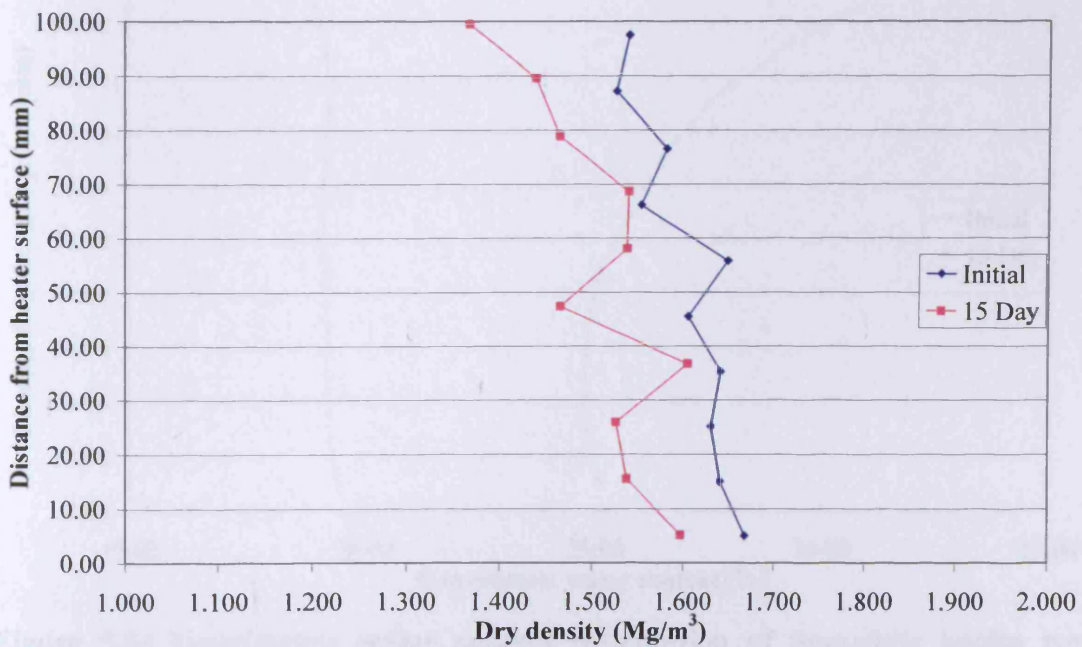
Figure 5.62 Dry density of Speswhite kaolin dry sample for isothermal test

Figure 5.63 Porosity of Speswhite kaolin dry sample for isothermal test
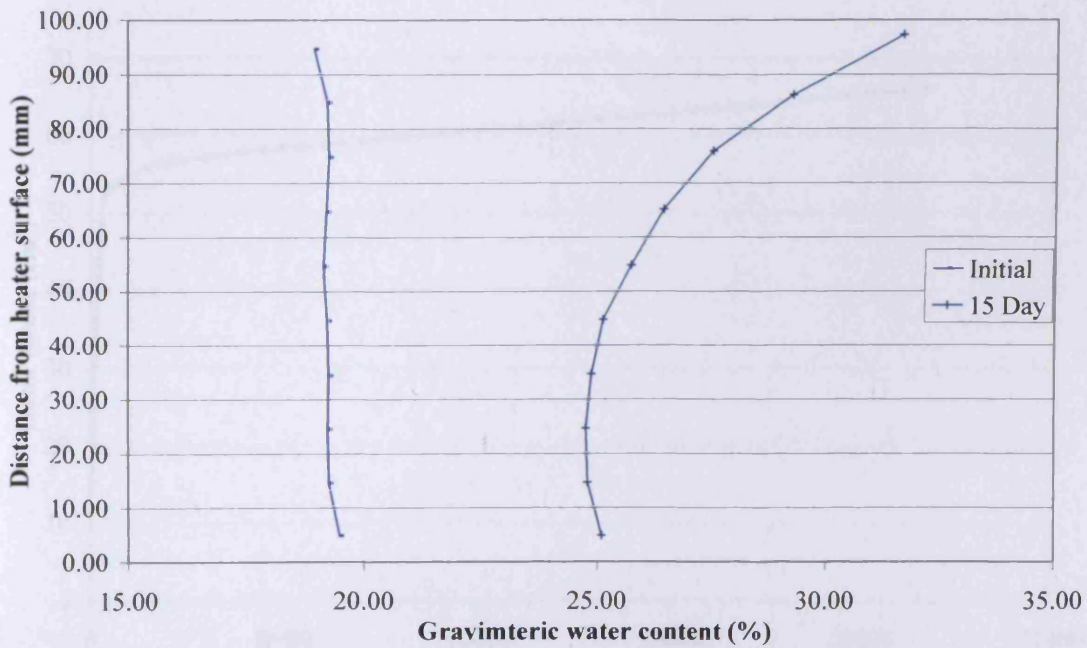
Figure 5.64 Gravimetric water content distribution of Speswhite kaolin wet sample for isothermal test
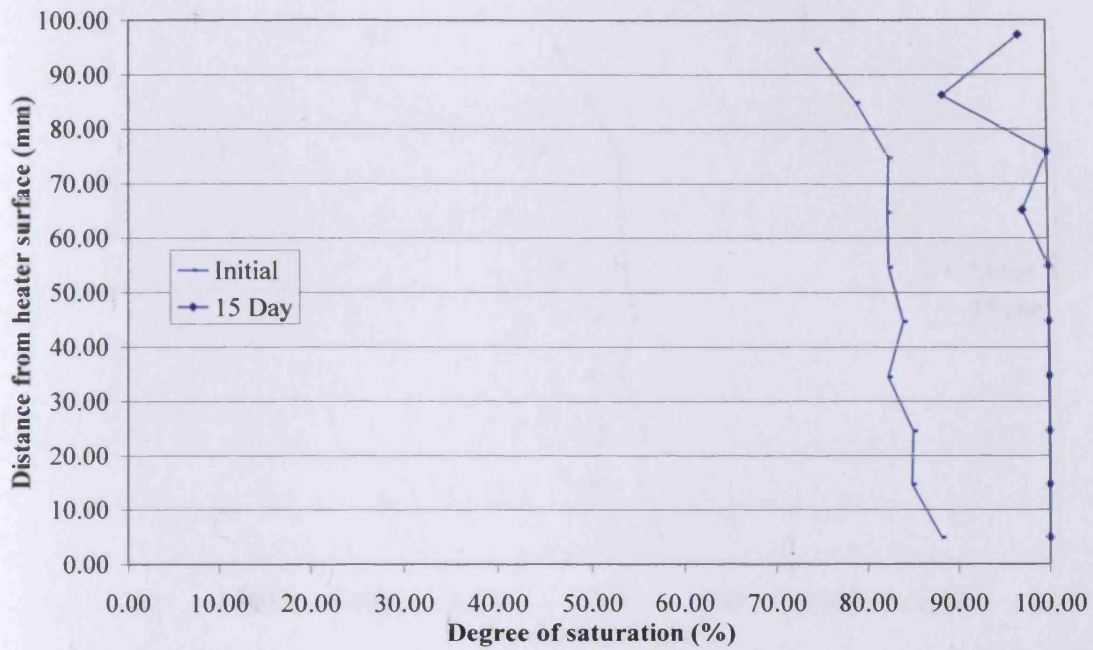
Figure 5.65 Degree of saturation of Speswhite kaolin wet sample for isothermal test
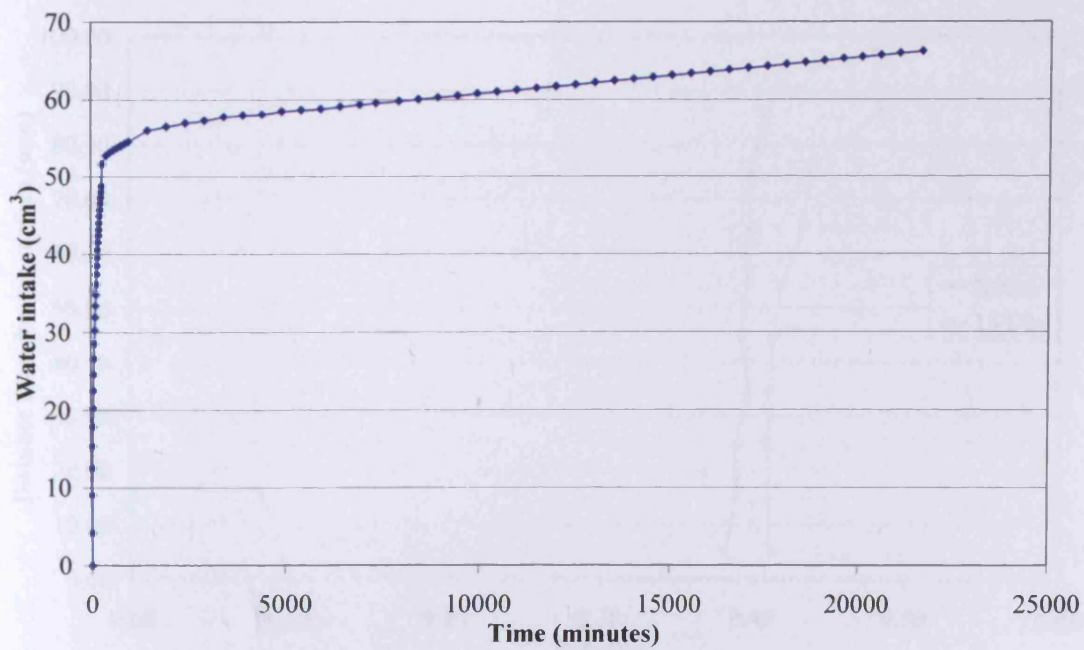
Figure 5.66 Water intake by Speswhite kaolin wet sample for isothermal test

Figure 5.67 Dry density of Speswhite kaolin wet sample for isothermal test
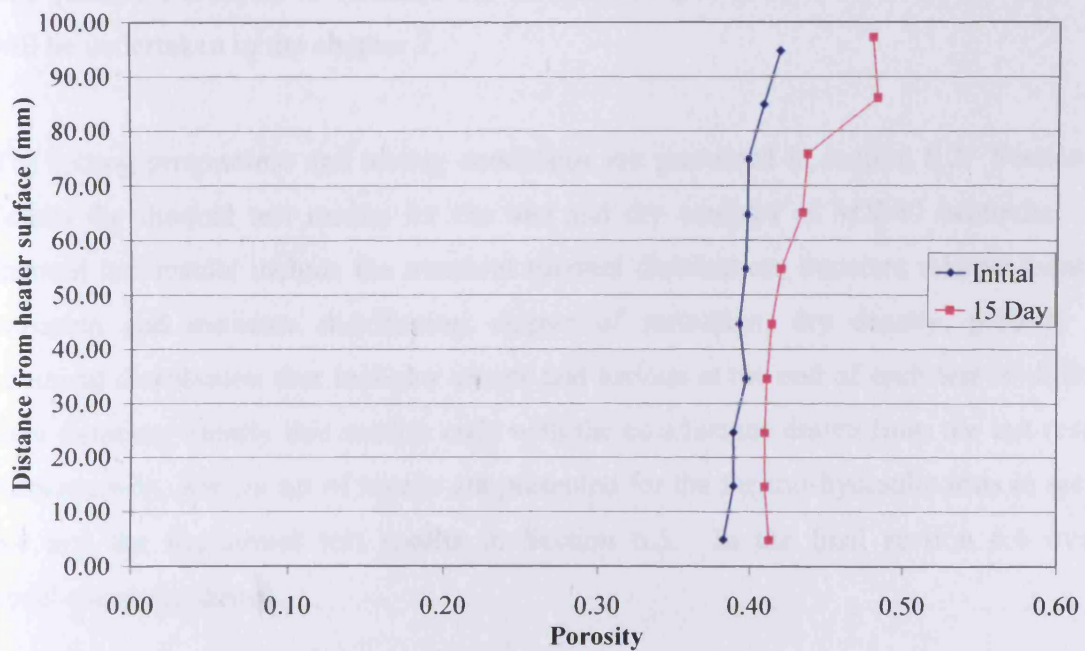
Figure 5.68 Porosity of Speswhite kaolin wet sample for isothermal test

Chapter 6

Thermal, thermo-hydraulic and isothermal tests on bentonite

6.1 Introduction

This chapter details the results of a series of thermal, thermo-hydraulic and isothermal tests carried out on MX-80 bentonite. In recent years various researchers (Kanno et al., 1996; Villar et al., 1996; Yong et al., 1997; Börgesson et al., 2001; Pintado et al., 2002; Cuevas et al., 2002; Villar et al., 2005; Gatabin and Billaud, 2005) have conducted such tests on various bentonite. The objecive of this chapter is to investigate both the heat transfer and mass movement in liquid and vapour phases in MX-80 bentonite. The aim of the tests is to use the tests results for a qualitative analysis of liquid and vapour moisture. The quantitive analysis to calculate the amount of liquid and vapour moisture movement will be undertaken in the chapter 7.

The testing programme and testing conditions are presented in section 6.2. Section 6.3 details the thermal test results for the wet and dry samples of MX-80 bentonite. The thermal test results include the transient thermal distribution, transient relative humidity variation and moisture distribution, degree of saturation, dry density, porosity and chemical distribution that includes anions and cations at the end of each test of different time duration. Finally this section ends with the conclusions drawn from the test results. Subsequently, similar set of results are presented for the thermo-hydraulic tests in section 6.4 and the isothermal test results in Section 6.5. In the final section 6.6 overall conclusions are drawn.

6.2 Testing programme

The summary of testing programme is tabulated in Table 6.1 that describes the initial condition and experiment duration for each type of test. The samples with an initial water content of 16 % and a degree of saturation of 60 % are termed as dry samples. The samples with an initial water content of 22 % and degree of saturation of 88 % are called wet samples. The samples used are statically compacted to an average initial dry density of 1.63 Mg/m^3.

6.3 Thermal test

The thermal test (T test) is basically a temperature gradient test in which the soil specimen is subjected to temperature of 85 °C at bottom end and the top end temperature is kept at 25 °C. This resulted in a thermal gradient of 0.6 °C/mm along the length of the sample. The experiments were run for two different initial conditions (dry and wet) and for different time intervals up to maximum of 30 days, as presented in Table 5.1.

6.3.1 Dry sample

The thermal test results for the dry sample with initial dry density of 1.63 Mg/m^3, initial water content of 16 % and initial degree of saturation of 60 % are presented in the following sections. The results discuss the temperature, moisture, dry density, porosity and chemical distribution

6.3.1.1 Thermal distribution

The transient temperature distribution for the dry samples of MX-80 bentonite is presented in Figure 6.1. It shows the transient temperature variation at every 20 mm distance from the heater surface. The temperature progressively rises at every point within the soil sample till 400 minutes and then slightly drops by 1 °C. The drop occurs due to change in thermal conductivity because of drying. Similar results were reported by Kanno et al (1996) for Japanese benotonite. The temperature reaches to steady state after

2000 minutes. The steady state temperature values are 69.8 ± 0.2 °C, 53.2 ± 0.2 °C, 41.5 ± 0.2 °C and 33.5 ± 0.2 °C at 20 mm, 40 mm, 60 mm and 80 mm distance from the heater surface respectively.

Figure 6.2 describes the temperature gradient changes with time. The temperature gradient keeps changing with time but reaches to stable value as the temperature achieves a constant value after 2000 minutes. At steady state, the temperature gradient is not same along the sample height; the thermal gradient value is 0.76 °C/mm near the heater surface and 0.425 °C/mm near the cold end. The temperature gradient is higher near the hot end and lower near the cold end. As with the tests reported in chapter 5 this variation in thermal gradient could be due to a combination of reasons; variation in thermal conductivity and heat loss through the walls of the TH cell.

6.3.1.2 Moisture distribution

The gravimetric water content variation at various time intervals for the dry samples is shown in Figure 6.3. The initial water content line is almost straight that indicates uniform water content and homogeneity throughout the sample length. It can be observed that the water content is 11.22 %, 7.95 %, 7.08 % and 4.68 % after 1, 5, 15 and 30 days near the heater surface compare to initial water content of 16 %. It can also be noted that near the cold end, the water content is 16.41 %, 19.34 %, 23.05 % and 26.15 % after 1, 5, 15 and 30 days respectively. It can be seen that the gravimetric water content is decreasing near the heater surface and increasing near the cold end with time. The high temperature at the heater surface causes moisture to moves away in vapour phase and then vapour get condense and turn into liquid near the cold end. The test results of 30 days (Figure 6.3) show that the bottom half of the sample height is subjected to drying and the remaining top half is wetting. The drying front is moving towards the middle height of the sample with the time. At the end of each experiment mass balance was checked and found to be within ± 0.2 % which is acceptable and indicates no mass loss from the TH cell.

Figure 6.4 shows the degree of saturation changes with time along the sample height for the thermal test conducted on the dry samples of MX-80 bentonite. The degree of saturation for each slice is calculated by the equation (5.2) in chapter 5. It can be noticed that near the heater surface, the degree of saturation attain the values of 43.65 %, 16.98 %, 29.72 % and 19.17 % after 1, 10, 15 and 30 days compare to the initial degree of saturation of 60 %. The degree of saturation is decreasing near the heater surface due to moisture moveing away in vapour phase from the hot region. The degree of saturation after 10 days test is lower compared to 15 and 30 days. There is a possibility that this is due to a measurement error in the dry density because the degree of saturation is calculated using the dry density (see equation (5.2) of chapter 5). Inspection of the dry density variation after 10 days, as presented in Figure 6.5, is abrupt and is possibly erroneous. In Figure 6.4, it can be seen that the degree of saturation is 55.29 %, 67.99 %, 75.60 % and 80.30% at 1, 10, 15 and 30 days respectively near the cold end. The degree of saturation is increasing near the cold end because moisture coming from the other hot end.

Relative humidity measurements were not taken for the thermal test because of fault with the relative humidity probes during the tests. Therefore, the relative humidity results are not presented here.

6.3.1.3 Dry density and porosity

The dry density variation with time for the dry samples is presented in Figure 6.5. The dry density for every slice of the soil sample was calculated by the method detailed in the section 5.3.1.3 of chapter 5. The dry density is increasing near the hot end due to drying and decreasing near the cold end because the gravimetric water content is increasing. The dry density is inversely proportion to the gravimetric water content according to the equation (5.2) presented in chapter 5. The maximum dry density is 1.679 Mg/m^3 near the heater surface and minimum dry density is 1.465 Mg/m^3 near the cold end. The initial dry density line is almost straight which indicates the uniform and homogenous samples were prepared.

The porosity distribution along the sample height for the dry samples is presented in Figure 6.6. The porosity for the each slice is calculated by using the equation (5.3) presented in chapter 5. It can be observed that the porosity is increasing with the time along the sample height due to the reduction in dry density. The porosity decreases with the increase in dry density according to the relationship between the porosity and the dry density presented in equation (5.4) of chapter 5.

6.3.1.4 Chemical distribution

The dried soil slices were crushed to the powder and the representative powdered sample was analysed for the chemical species. The following sections present various anions and cations concentration change with time intervals of 1, 3, 7, 15 and 30 days.

6.3.1.4.1 Anion distribution

The chloride concentration after 1, 3, 7, 15 and 30 days thermal test is described in Figure 6.7. The chloride concentration near to the heater surface reaches to the value of 2.63E-03 mol/kg, 3.64E-03 mol/kg, 5.59E-03 mol/kg and 6.54E-03 mol/kg after 1, 7, 15 and 30 days compared to the initial value of 3.00E-03 mol/kg. The chloride ion concentration near the cold end is 2.86E-03 mol/kg, 2.54E-03 mol/kg, 1.69E-03 mol/kg and 1.10E-03 mol/kg after 1, 7, 15 and 30 days respectively. It can be seen that the chloride ion concentration is increasing near the heater surface and decreasing away from the heater surface with time. The chloride ion can not be carried by vapour and can only be carried by liquid moisture. The increase in chloride ion concentration near the heater surface indicates liquid moisture moves towards hot end due to the higher suction developed because of drying near the heater surface. The chloride concentration does not change much, even after 7 days, from its initial value because MX-80 bentonite has very low permeability, resulting in very little liquid movement. The chloride ion gets accumulated near the hot end with time as more liquid moisture moves towards the hot end. Combining the outcomes of gravimetric water content and chloride ion results, it can be concluded that the moisture moves away in vapour phase from the hot end and then vapour condenses and turn into liquid near the cold end and the liquid moisture moves

towards the hot end. This sets up a cycle of vapour and liquid moisture movement within the soil sample.

Figures 6.8 and 6.9 present nitrate and sulphate ion concentration change with the time along the sample height. It can be noted that the both anions increasing near the heater surface like chloride ion. Gurr et al. (1952) also reported the accumulation of salts in the hot zone for the heating test conducted on loam and sand. This indicates that the liquid moisture brought them near the heater surface and they are building up with the time as more and more liquid is coming.

6.3.1.4.2 Cation distribution

The sodium, magnesium, potassium and calcium ions results are shown in Figures 6.10 – 6.13 respectively. The sodium ion has highest concentration compare to other cations because MX-80 is a sodium rich bentonite. The ions are decreasing with time at almost every point. The sodium and magnesium ions concentration results and the potassium and calcium ions concentration results have similar trend. The initial concentration results for magnesium and calcium are not consistent along the sample height because of difficulties in extracting divalent ions from the bentonite samples. The MX-80 bentonite which has montmorillonite mineral holds the positive ions (cations) strongly compare to kaolin. The divalent ions substitute monovalent ions in the interlayer that results in lower concentration of them compared to monovalent ions.

6.3.2 Wet sample

The following sections present the various results for the wet sample after performing the thermal test.

6.3.2.1 Thermal distribution

The transient temperature variation for the wet samples at every 20 mm distance from the

heater surface is shown in Figure 6.14. Initially, the temperature increases at each and every point within the soil sample till 1000 minute and then reaches to stable value. It can be noted that at the steady state, the temperature reaches to the value of 63.4 ± 0.2 °C, 51.0 ± 0.2 °C, 42.6 ± 0.2 °C and 36.2 ± 0.2 °C at 20 mm, 40 mm, 60 mm and 80 mm distance from the heater surface respectively. The steady state temperatures at each point within the wet samples are less compared to the dry samples due to an increased variation in temperature gradient as described in Figure 6.15. The temperature gradient is changing along the sample height. The temperature gradient is 1.08 °C/mm near the heater surface and 0.56 °C/mm near the cold end. The temperature gradient is higher close to the heater surface and then decreasing along the sample height to the cold end. The temperature gradient near the heater surface is higher than the overall temperature gradient of 0.6 °C/mm due to higher heat losses. Again the variations in thermal gradient are due to combination of reasons; change in thermal conductivity and heat loss from the cell.

6.3.2.2 Moisture distribution

The gravimetric moisture content results for the wet sample at various time intervals are presented in Figure 6.16. The moisture content near the heater surface is 20.86 %, 18.35 %, 15.66 % and 15.03 % at the end of 1, 7, 15 and 30 days T tests compare to the initial water content of 22 %. The water content near the cold end is 22.45 %, 23.71 %, 25.03 % and 27.67 % after 1, 7, 5 and 30 days respectively. It can be seen that the water content is progressively decreasing at the hot region and increasing at the cold region with time. The drying front is progressing with time and reaching to almost mid height of the sample after 15 days. It can also be noted that same amount of drying and wetting is achieved at both extreme ends after 30 days. The mass balance was checked at the end of each test and it was found that in the entire test series no or negligible moisture loss (less than 0.2 %) occurred.

Figure 6.17 shows the degree of saturation profiles for the wet sample at the end of various time intervals during the T tests. The degree of saturation is 81.76 %, 76.15 %, 64.75 % and 64.52 % after 1, 7, 15 and 30 days near the heater surface. The initial degree of saturation is 88 % at every point that indicates the uniformity and homogeneity of the

soil sample. It can be seen that the degree of saturation is decreasing near the heater surface with time due to drying. The degree of saturation near the cold end is 80.77 %, 85.08 % and 88.22 % at the end of 1, 7 and 30 days. The degree of saturation is increasing with time near the cold end due to vapour moisture coming from the hot region. The increment in degree of saturation near the cold end is not the same as the reduction near the heater surface due to strong changes in the porosity as shown in section 6.3.2.3.

The transient relative humidity results for the wet sample at every 20 mm distance from the heater surface are presented in Figure 6.18. The initial relative humidity at every point is almost equal to 91 % that indicates the homogeneity of the soil sample. The relative humidity starts to increase at every point within the soil sample as the thermal test sets off. The relative humidity reaches to 100 % very quickly at 20 mm distance from the heater surface. The relative humidity reaches to 100 % at the farthest point, 80 mm from the heater surface, very late due to slow moisture movement from the hot region to the cold region.

6.3.2.3 Dry density and porosity

The dry density changes for the wet samples with time and various distances from the heater surface are shown in Figure 6.19. The dry density is increasing near the heater surface due to drying and decreasing along the height with time due to wetting away from the heater surface. The maximum dry density near the heater surface reaches to 1.684 Mg/m^3 and the minimum value at the cold end reaches to 1.491 Mg/m^3. The initial dry density is almost same along the sample height that represents the uniform and homogeneous samples were achieved.

Figure 6.20 presents the porosity variation with time along the sample height for the wet sample at the end of T tests. The porosity follows the same trend like the dry density but with opposite changes. The porosity is decreasing near the heater surface and increasing along the sample height with time.

6.3.2.4 Chemical distribution

The soil slices were analysed to determine various anion and cations distribution within the sample. The following sections discuss the anion and cation concentration change for the wet samples with the time intervals of 1, 3, 7, 15 and 30 days during the T tests.

6.3.2.4.1 Anion distribution

Figure 6.21 presents the chloride ion concentration distribution along the sample height at the end of 1, 3, 7, 15 and 30 days T tests. The initial chloride concentration is 3.04E-03 mol/kg which is almost same at every point along the sample height. This indicates that the uniform soil samples were prepared. The chloride concentration near the heater surface is 3.32E-03 mol/kg, 4.24E-03 mol/kg, 5.79E-03 mol/kg, 8.21E-03 mol/kg and 1.19E-02 at the end of 1, 3, 7, 15 and 30 days. The chloride concentration near the cold end is 3.00E-03 mol/kg, 2.91E-03 mol/kg, 2.74E-03 mol/kg, 2.45E-03 mol/kg and 2.16E-03 mol/kg after 1, 3, 7, 15 and 30 days respectively. The chloride concentration is increasing near the heater surface and decreasing at the colder region with time like the dry samples results. This again indicates the chloride ions carried by the liquid moisture to the hot end. The liquid moisture is driven by the suction difference between the cold end and the hot end. In comparison with the dry sample results, the chloride ion concentration is higher near the heater surface for the wet samples that means more liquid moves in the case of the wet sample. This is quite expected as the wet samples have more liquid moisture compared to the dry samples.

Figure 6.22 and 6.23 show the nitrates and sulphate ions distribution with the time along the sample height. The both ions are increasing near the heater surface that confirms the liquid moisture movement towards the hot end. The nitrate ion results are quite similar to chloride ion distribution but different numerical values.

6.3.2.4.2 Cation distribution

Figures 6.24 – 6.27 present the sodium, magnesium, potassium and calcium ions variation

along the sample at the end of 1, 3, 7, 15 and 30 days during the T tests. The sodium ions concentration decreases with time except 7 days test results. The magnesium ions concentration does not change with the time along the sample height due to adsorption by the internal layers of bentonite though the magnesium concentration is quite low in MX-80. The concentration of potassium ions does not change from its initial value except for the 30 day results. The potassium concentration increases everywhere within the soil sample after 30 days due to release of the potassium ions in the soil solution. The calcium ions are decreasing with the time along the soil specimen height. The calcium is a divalent ion which substitutes the other low valence ions in the internal layers of bentonite. The calcium adsorption to the internal layers increases with time hence, the calcium ions reduce in the pore liquid.

6.3.3　Conclusions

The thermal gradient test results in terms of temperature distribution, moisture variation, dry density, porosity and chemical distribution are presented. The temperature reaches to the predefined values 85 °C and 25 °C at the bottom and top ends very quickly in all the tests. The temperature for the wet samples is less compared to the dry samples at corresponding points due to different thermal properties caused by different moisture content. Higher moisture content results in higher variations in thermal conductivity and possibly high heat loss from the cell wall. The moisture content is decreasing in the hot region and increasing in the cold region with time irrespective of different initial conditions. The higher moisture movement observed in the dry samples compared to the wet samples is due to more voids being available in the dry samples for vapour moisture to move away from the hot zone. The chloride ions accumulation near the heater surface proves that the liquid moisture is moving towards the hot region from the cold region. The cations movement is affected due to their adsorption on the interlayer surface of clay particles.

6.4　Thermo-hydraulic test

In the thermal-hydraulic test (TH test) soil samples were subjected to a thermal gradient

of 0.6 °C/mm with temperatures of 25 °C and 85 °C applied at the top and bottom ends respectively. In addition to this deionised and de-aired water was supplied at the top end under a pressure of 0.6 MPa.

6.4.1 Dry sample

In the following sections results from the thermo-hydraulic tests performed on the dry samples are presented.

6.4.1.1 Thermal distribution

Figure 6.28 presents the transient temperature distribution at every 20 mm distance from the heater surface. The temperature reaches to a stable value after 400 minutes at every location within the soil sample. At the steady state, the temperature reaches to the value of 71.2 ± 0.2 °C, 52.6 ± 0.2 °C, 42.0 ± 0.2 °C and 34.8 ± 0.2 °C at 20 mm, 40 mm, 60 mm and 80 mm distance from the heater surface respectively. It can be noted that the temperature values are the same as in the thermal test for dry samples.

The temperature profiles variation at various times is presented in Figure 6.29. The temperature gradient is progressively changing until 400 minutes. After this time, the temperature gradients reach a stable value, with the temperature gradient being steepest near the heater surface. It can be observed that at the steady state the temperature gradient value is 0.69 °C/mm near the heater surface and 0.49 °C/mm near the hydration end.

6.4.1.2 Moisture distribution

Figure 6.30 presents the gravimetric water content results of the wet samples for the thermo-hydraulic tests. The gravimetric water content values near the heater surface are 12.24 %, 7.55 %, 6.81 % and 6.58 % after 1, 7, 15 and 30 days TH tests compared to the initial water content of 16 %. The gravimetric water content is decreasing near the heater

surface with time due to drying. The water content is higher near the heater surface during TH tests compare to the thermal test due to reduction in voids by the incoming water from the hydration end. The water content values at the hydration end are 30.63 %, 32.07 %, 33.10 % and 34.22 % at the end of 1, 7, 15 and 30 days TH tests. The gravimetric water content is higher near the hydration source compared to the dry samples during T tests due to incoming water from the hydration end and the moisture movement, in the vapour phase, away from the hot end. The mass balance of each soil sample was verified with the quantity of incoming water from the hydration source and was found to be in agreement.

The degree of saturation profiles with time for the thermo-hydraulic tests is presented in Figure 6.31. The degree of saturation near the heater surface is 53.59 %, 34.36 %, 30.30 % and 25.95 % at the end of 1, 7, 15 and 30 days compare to initial degree of saturation of 60 %. The degree of saturation is decreasing with time near the hot end due to drying. The degrees of saturation at 5 and 10 days are lower than the 30 days due to error in volume measurement of the soil slices. As mentioned earlier the degree of saturation largely depends upon the volume of slice. The 5 % error in volume measurement can cause 10 % error in degree of saturation values. The degree of saturation near the hydration end within 10 mm distance is 89.7 % at 1 day and reaches to 100 % after 7 days. It happens obviously due to water supplied from the hydration end but complete saturation of the topmost part of soil sample still takes time because of low hydraulic conductivity of MX-80 bentonite. The soil sample beyond 10 mm distance from the hydration end is not saturated even after 30 days that indicates the soil has very low hydraulic conductivity.

The transient water intake is measured via an automatic volume change apparatus. The water intake with time is presented in Figure 6.32. The water intake rate is 16E-03 cm^3/min, 1.35E-03 cm^3/min, 0.78E-03 cm^3/min and 0.45E-03 cm^3/min at 1000, 5000, 30000 and 40000 minutes respectively. The rate of water intake is high at the start of the test. The rate of water intake then reduces as the soil start to approach saturation. It has been postulated that the hydraulic conductivity of bentonite decreases as the degree of

saturation increases because it swells that result in reduction in pores and the hydraulic conductivity (Thomas et al., 2001) and these results are consisted with that proposal.

6.4.1.3 Dry density and porosity

Figure 6.33 shows the dry density variation for the wet samples with the time. The initial dry density points lie in a straight line that indicates the uniform dry density and homogeneity of the samples. The dry density is decreasing with time along the sample height as the water content is increasing along the sample height. In such sealed tests the overall average dry density should remain constant; therefore such a trend of increase in dry density throughout the sample must be due to some form of experimental error. The most likely cause is that regions close to the hydration source tend to swell and at the same time regions further from the hydration source are compressed. On sampling the restraining reactive force of the cell is removed allowing the compressed regions to recover, thereby resulting in an apparent decrease in the overall average dry density. This phenomenon is also observed in the other TH and isothermal tests reported later in this chapter and earlier in chapter 5. The reduction in dry density is higher at the hydration end because of swelling due to wetting.

The porosity change with the time for the wet samples is presented in Figure 6.34. The porosity is increasing with time along the sample height as the dry density decreasing due to swelling caused by the incoming water from the hydration source. The porosity is decreasing at the hot region due to shrinkage caused by drying.

6.4.1.4 Chemical distribution

The various anions and cations were determined from the dry soil slices at the end of the 1, 3, 7 and 15 day thermo-hydraulic tests. The following sections present the results of anion and cation distribution.

6.4.1.4.1 Anion distribution

Figure 6.35 presents the chloride ion distribution with the time for the thermo-hydraulic test. The chloride ion concentration is 3.37E-03 mol/kg, 3.46E-03 mol/kg, 5.29E-03 mol/kg and 6.14E-03 mol/kg after 1, 3, 7 and 15 days near the heater surface compare to the initial concentration of 3.00E-03 mol/kg. The chloride concentration near the heater surface is increasing with the time due to the liquid moisture, coming to the hot region from the cold region, carrying the chloride ions. Compared to the T test results; the chloride concentration is higher in the TH test due to more liquid moisture coming in from the hydration end. The chloride ion concentration near the hydration end is 1.79E-03 mol/kg, 7.55E-04 mol/kg, 7.28E-04 mol/kg and 5.65E-04 mol/kg at the end of 1, 3, 7 and 15 days. The chloride ions amount is decreasing with time at the hydration end. It can happen due to various possible reasons, first the ions get diluted by the incoming water from the hydration end, second the ions carried by liquid moisture to the hotter region and third the ions diffuses to the hydration source but diffusion is a quite slow process.

The nitrate and sulphate ions variation with time is presented in Figures 6.36 and 6.37. The initial concentration of both ions lies on a straight line that indicates the uniformity and homogeneity of the soil sample. The both ions are increasing throughout the sample height with the time. The movement of these ions is not similar to that of conservative ions like chloride ions because their movement is affected by their larger size and the interaction with the cations available in the interlayers.

6.4.1.4.2 Cation distribution

The sodium, magnesium, potassium and calcium ions variation with the time is presented in Figures 6.38 – 6.41. The sodium ion concentration is decreasing with time at every location within the soil specimen until 3 days. Then the sodium ion increases but still less than the initial concentration (Figure 6.38) due to release of sodium ions in pore liquid with time. The magnesium ions do not have any trend even initial concentration is not same through out the sample height. The magnesium ion is not uniformly distributed

therefore results show irregular behaviour. The potassium ions behave similar to sodium ions, their concentration decreases till 3 days and then increases due to release of potassium ions into pore liquid with time. The calcium ions are decreasing with time because they get adsorbed to the interlayer of clay particle.

6.4.2   Wet sample

In the following sections results from the thermo-hydraulic tests performed on the wet samples are presented.

6.4.2.1   Thermal distribution

Figure 6.42 presents the transient thermal distribution for the wet samples subjected to the TH tests. It can be observed that at the steady state, the temperature is 61.5 ± 0.2 °C, 50.1 ± 0.2 °C, 42.5 ± 0.2 °C and 36.0 ± 0.2 °C at 20 mm, 40 mm, 60 mm and 80 mm distance from the heater surface respectively. The steady state temperature is slightly less compared to the same sample subjected to the T tests. Figure 6.43 shows the thermal gradient variation with the time for the TH tests. The temperature gradient near the heater surface is 1.175 °C/mm and near the hydration end is 0.55 °C/mm. This variation is due to different thermal conductivity due to different moisture content, possible heat loss from the cell and the influence of cooler water entering the system.

6.4.2.2   Moisture distribution

The gravimetric water content results for various time intervals from 1 to 30 days for the wet samples subjected to the TH tests is shown in Figure 6.44. The water content is 20.23 %, 19.62 %, 19.49 % and 18.19 % near the heater surface at the end of 1, 7, 15 and 30 days compared to the initial water content of 22 %. The gravimetric water content is decreasing with the time near the heater surface due to drying. The drying is slower compare to the same samples subjected to the thermal test because of different end conditions. The water is supplied in from the hydration end during the TH tests resulting

in reduction of suction at the hydration end that causes less moisture flow from the hot end. The gravimetric water content at the hydration end is 32.78 %, 32.72 %, 32.11 % and 33.93 % after 1, 7, 15 and 30 days. The water content is increasing largely within 1 day and then it is slightly increasing with time because of higher initial degree of saturation. The water content values are higher compared to the thermal tests due to the water supplied during the TH tests

The degree of saturation change with the time along the sample height is presented in Figure 6.45. The degree of saturation near the heater surface is 81.86 %, 82.80 %, 83.24 % and 79.03 % at the end of 1, 7, 15 and 30 days compare to the initial degree of saturation of 88 %. The degree of saturation is decreasing after 1 day but then slightly increasing at the end of 7 and 15 days. This could happen due to two reasons first the liquid moisture comes in from the cold end to the hot end and second any error in volume measurement. In comparison with the T tests, the degree of saturation is higher near the hot end for the TH tests due to slow drying. The degree of saturation at the hydration end is 97.38 %, 95.86 %, 96.41 %, 99.67 %. The degree of saturation is increasing till the end of 1day but then decreasing at the end of 7 and 15 days. This can happen due to the error in volume measurement of 1 day TH test. The degree of saturation is higher compare to the T test as would be expected due to the water supplied in from the top end during the TH tests.

Figure 6.46 shows the transient relative humidity values at every 20 mm distance from the heater surface. The relative humidity reaches to 100 % in 10 minutes, 213 minutes, 800 minutes and 2200 minutes at 20 mm, 40 mm, 60 mm and 80 mm distance from the heater surface respectively. The relative humidity reaches to 100 % quickly at every point except the 80 mm point. Compared to the T test the relative humidity at 80 mm reaches to 100 % quite faster due to the impact of the supply of water under pressure in the TH test.

Figure 6.47 presents the transient water intake into the MX-80 bentonite sample from the top cold end. The water intake rate is 3.00E-03 cm^3/min, 1.90E-03 cm^3/min and 0.74E-03 cm^3/min at 1000, 5000 and 30000 minutes respectively. It can be seen that the water

intake rate is varies and is very high at the start of the test and then become slow as the soil swells due to saturation. The water intake quantity is less for the wet sample compare to the dry sample due to different initial moisture contents. The water intake rate for the wet samples is less in the beginning compare to the dry samples but later on rate is almost similar as with the time both samples reach to similar degrees of saturation.

6.4.2.3   Dry density and porosity

The dry density profiles with the time for the wet samples along the sample height are shown in Figure 6.48. The dry density is decreasing with the time along the sample height that is obvious as the water content is increasing. This would be expected at the cold end, as discussed earlier in section 6.4.1.3, due to experimental error however the overall trends of variation are of interest. The dry density slightly increases near the heater surface due to shrinkage caused by drying.

Figure 6.49 presents the porosity variation with the time along the sample height for the wet samples. The porosity is increasing with time along the sample height as the soil swells due to water supplied in from the hydration end and the moisture coming from the hot end. It can also be noted that porosity decreases near the heater due to drying shrinkage.

6.4.2.4   Chemical distribution

The following section describes the anion and cation concentration change for the wet samples after the TH tests along the sample height with the time.

6.4.2.4.1 Anion distribution

Figure 6.50 presents the chloride ion concentration versus time profiles at the end of 1, 3, and 7 days in the TH tests. The chloride concentration near the heater surface is 3.54E-03 mol/kg, 4.03E03 mol/kg and 4.55E-03 and near the cold end is 1.70E-03 mol/kg, 1.15E-

03 mol/kg and 8.34E-04 mol/kg after 1, 3 and 7 days respectively. The chloride concentration is increasing with time near the heater surface and decreasing near the cold end. The chloride ion accumulates near the heater surface again due to liquid moisture movement towards the hot end. The chloride ion decreases near the cold end possibly due to back diffusion towards the hydration source and dilution.

The nitrate and sulphate ions concentration variation with time along the sample height is shown in Figures 6.51 and 6.52. The nitrate and sulphate ions both behave in a similar manner to the chloride ion. Their concentration is increasing at the hot end and decreasing at the cold end due to liquid moisture transfer towards the hot end and near the cold end dilution and diffusion through incoming water from the hydration source.

6.4.2.4.2 Cation distribution

Figures 6.53 – 6.56 presents the sodium, magnesium, potassium and calcium ions concentration change with time along the sample height. The sodium ions are decreasing with time due to adsorption to the clay surface. The magnesium ions are decreasing with time except in few layers within the soil sample. As mentioned earlier it may be due to non-uniform initial distribution of magnesium ions. The potassium ions are increasing with time due to release of ions into the solution. The calcium ion decreases with time till 3 days but then increases and their initial concentration is not uniform either. The calcium is a divalent ion and it substitutes the other monovalent ions, so its concentration decreases with time.

6.4.3 Conclusions

The thermo-hydraulic results are presented for the dry and wet samples of MX-80 bentonite. The temperature at the extreme ends reaches to predefined values quickly as in the thermal test. The steady state temperature for the dry samples is higher compared to the wet samples because the dry samples have less moisture resulting in low thermal conductivity and low heat dissipation. The initial moisture content affects the temperature results. The moisture content is decreasing with time in the hot region but

increasing in the cold region due to vapour condensing in the cold region and also the water being supplied from the top cold end. The porosity decreases near the hot end due to shrinkage and increases at the cold end due to swelling. The chloride, nitrate and sulphate ions increased at the hot end because they are carried with liquid moisture to the hot end from the colder region. The salts decreased near the cold end possibly due to back diffusion towards to the hydration source and dilution, though diffusion is a slow process.

6.5 Isothermal test

In the isothermal test soil samples were only subjected to the application of a hydration source with the temperature kept at 25 °C at both ends of the soil samples. The resulting hydraulic gradient was obtained by supplying deionised and de-aired water from the top end under a pressure of 0.6 MPa. In the isothermal tests, the temperature is kept same 25 °C at both extremities of the sample that results in isothermal condition throughout the sample height. Therefore, the temperature field is not discussed further.

6.5.1 Dry sample

The following section discusses the results of isothermal tests conducted on the dry samples.

6.5.1.1 Moisture distribution

Figure 6.57 presents the gravimetric water content variation at the end of 30 days isothermal test. The gravimetric water content at the bottom end (i.e. near the heater surface) is 15.87 % and at the top hydration end is 33.39 % compared to the initial water content of 16 %. The gravimetric water content is increasing gradually from the bottom end to the top hydration end because the water is supplied in from the top end. The water content at the bottom end is almost equal to the initial water content. This indicates that

the water from the top end does not reach to the bottom end due to the low permeability of the material.

The degree of saturation results after 30 days are shown in Figure 6.58. The degree of saturation is increasing in the top part of the soil sample due to water supplied from the top end. The highest degree of saturation is 96.69 % at the top end. The degree of saturation does not change from its initial value at the bottom part of the soil sample because the water from the hydration end does not reach to the bottom part of the soil sample due to the low hydraulic conductivity of the MX-80 bentonite.

The transient water intake by the dry samples of MX-80 bentonite during the isothermal test is presented in Figure 6.59. The water intake rate is 28.98E-03 cm^3/min, 5.79E-03 cm^3/min, 1.91E-03 cm^3/min and 1.45E-03 cm^3/min at the end of 100 minutes, 1000 minutes, 10000 minutes and 40000 minutes respectively. The water intake rate is decreasing with time. At the beginning of the test, the water intake rate is very high because of higher suction but as the sample start to reach saturation, the water intake rate decreases.

6.5.1.2 Dry density and porosity

Figure 6.60 presents the dry density results for the dry sample subjected to the isothermal test. The dry density is decreasing along the sample height due to the swelling caused by the incoming water from the hydration end. The minimum dry density near the hydration end is 1.306 Mg/m^3. As seen previously in the TH tests the average dry density should remain constant the results shown here indicate that the sample has expanded on removal from the confining cell.

The porosity variation for the dry sample along the sample height is presented in Figure 6.61. The porosity is increasing along the sample height. Again, it happens due to the swelling caused by the penetrating water from the hydration end. The porosity also increases after the compacted soil sample extruded out of the TH cell due to release of stresses.

6.5.2   Wet sample

The results of isothermal test for the wet sample are presented in the following sections.

6.5.2.1   Moisture distribution

The gravimetric water content distribution for the wet sample subjected to the isothermal test is presented in Figure 6.62. The gravimetric water content is 21.98 % near the bottom end and 32.02 % near the top end compare to initial water content of 22 %. The gravimetric water content is increasing from the heater end to the top hydration end because the water is supplied into the soil sample from the top end. The water content at the bottom end is equal to its initial value. The water content is increasing in the soil sample due to water coming from the hydration end.

The degree of saturation variation profile after 30 days isothermal test is shown in Figure 6.63. The degree of saturation reaches to 100 % near the hydration end. The degree of saturation more or less remains same as its initial value for the bottom half of the soil sample. This indicates the water from the hydration does not reach to the bottom part of the soil sample.

Figure 6.64 presents the transient water intake by the wet samples subjected to the isothermal test. The water intake rate is 3.06E-03 cm^3/min, 2.91E-03 cm^3/min, 1.16E-03 cm^3/min and 0.74E-03 cm^3/min after 100 minutes, 1000 minutes, 10000 minutes and 40000 minutes respectively. The water intake rate is higher in the beginning and then decreases as the soil sample swells upon saturation results in less permeability. The water intake rate is low compared to the dry samples subjected to the same test due to the different initial conditions. The wet sample has lower suction due to higher initial degree of saturation compared to the dry samples.

6.5.2.2   Dry density and porosity

Figure 6.65 shows the dry density change along the sample height after 30 days subjected

to the isothermal test. The dry density decreases along the sample height due to the incoming water from the hydration source. The maximum reduction in dry density occurs near the hydration end due to maximum swelling and 100 % degree of saturation.

The porosity variation for the wet sample subjected to the isothermal test is shown in Figure 6.66. The porosity increases along the sample height due to the water supplied into the soil sample results in swelling and increased pore size. Again, the maximum change in porosity occurs at the top end due to maximum swelling at that end caused by highest degree of saturation. As discussed previously the another reason of increase in porosity is the expansion of the soil sample after extruding it out of the TH cell due to release of stresses.

6.5.3   Conclusions

The isothermal test results are presented for the dry and wet samples of MX-80 bentonite. The moisture distribution is almost same for both types of samples. The both type of samples has similar water content at the top end after 30 days. The degree of saturation does not change for the bottom half of the soil specimen because the moisture does not reach to bottom half of the sample due to very low permeability of bentonite. The dry density decreases due to swelling near the top hydration end.

6.6   Overall conclusions

The thermal, thermo-hydraulic and isothermal test results on MX-80 bentonite have been presented. The temperature distribution depends upon the initial conditions. The different temperature values at steady state condition for the wet and dry samples indicates that the amount of variation of thermal material parameters (e.g. thermal conductivity and specific heat capacity) is dependent upon the initial amount of water.

The gravimetric moisture content is decreasing near the hot end when the temperature gradient is applied due to moisture movement in vapour phase away from the hot region

to the cold region. The amount of drying depends upon the initial moisture content. The dry sample has higher drying compared to the wet sample. The accumulation of salts (like chloride, nitrate and sulphate) near the hot end indicates that the liquid moisture moves towards the hot end from the colder region. The salts specially chloride ions are a good indicator of the liquid moisture movement and will be used in chapter 7 to calculate the quantities of liquid and vapour movement.
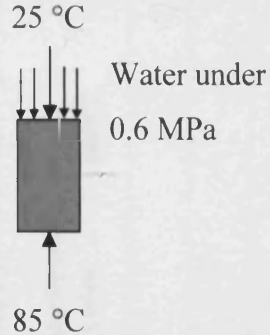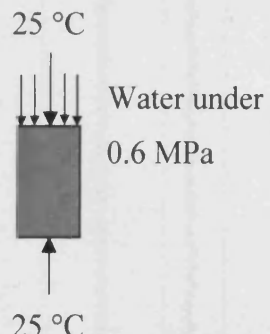
6.7 References

Börgesson, L., Chijimatsub, M., Fujitab, T., Nguyenc, T.S., Rutqvistd, J. and Jinge, L. (2001). Thermo-hydro-mechanical characterisation of a bentonite-based buffer material by laboratory tests and numerical back analyses. International Journal of Rock Mechanics & Mining Sciences, 38, 95-104

Cuevas, J., Villar, M.V., Martyn, M., Cobena, J.C. and Leguey, S. (2002). Thermo-hydraulic gradients on bentonite: distribution of soluble salts, microstructure and modification of the hydraulic and mechanical behaviour. Applied Clay Science, 22, 25–38.

Gatabin, C. and Billaud, P. (2005). Bentonite THM mock up experiments. Sensors data report. CEA, Report NT-DPC/SCCME 05-300-A, Cedex.

Gurr, C.G., Marshall, T.J. and Hutton, J.T. (1952). Movement of water in soil due to a temperature gradient. Soil Sci., Vol. 74, No. 5, 335-345.

Kanno, T., Kato, K. and Yamagata, J. (1996). Moisture movement under a temperature gradient in highly compacted bentonite. Engineering Geology, 41, 287-300.

Pintado, X., Ledesma, A. and Lloret, A. (2002). Backanalysis of thermohydraulic bentonite properties from laboratory tests. Engineering Geology, 64, 91-115.

Thomas, H.R., Cleall, P.J., Mitchell, H.P., Chandler, N.A. and Dixon, D.A. (2001). An assessment of the thermal and hydraulic interaction between a clay buffer and host rock. Proc. 3rd British Geotechnical Society Geoenvironmental Engineering Conference, Edinburgh, 374-379.

Villar, M.V., Cuevas, J. and Martin, P.L. (1996). Effects of heat/water flow interaction on compacted bentonite: Preliminary results. Engineering Geology, 41, 257-267.

Villar, M.V., Martin, P.L. and Barcala, J.M. (2005). Infiltration tests at isothermal conditions and under thermal gradient. CIEMAT Technical report CIEMAT/DMA/M2140/1/05 Madrid.

Yong, R.N., Mohammed, A.M.O., Shooshapasha, I. and Onofrei C. (1997). Hydro-thermal performance of unsaturated bentonite-sand buffer material. Engineering Geology, 47, 351-365.

Table 6.1 Testing programme

Type of test	Thermal gradient test (T-test)		Thermo-hydraulic gradient (TH-test)		Isothermal test	
	25 °C ⬇ 🟫 ⬆ 85 °C		25 °C ⬇⬇⬇⬇ 🟫 ⬆ 85 °C — Water under 0.6 MPa		25 °C ⬇⬇⬇⬇ 🟫 ⬆ 25 °C — Water under 0.6 MPa	
Sample type	Dry	Wet	Dry	Wet	Dry	Wet
Initial water content (%)	15	22	15	22	15	22
Initial degree of saturation (%)	60	88	60	88	60	88
Initial dry density (Mg/m^3)	1.63	1.63	1.63	1.63	1.63	1.63
Experiment duration (Days)	1, 2, 3, 4, 5, 7, 10, 15 & 30	1, 2, 3, 4, 5, 7, 10, 15 & 30	1, 2, 3, 4, 5, 7, 10, 15 & 30	1, 2, 3, 4, 5, 7, 10, 15 & 30	30	30

Figure 6.1 Temperature distribution of MX-80 bentonite dry sample for T test
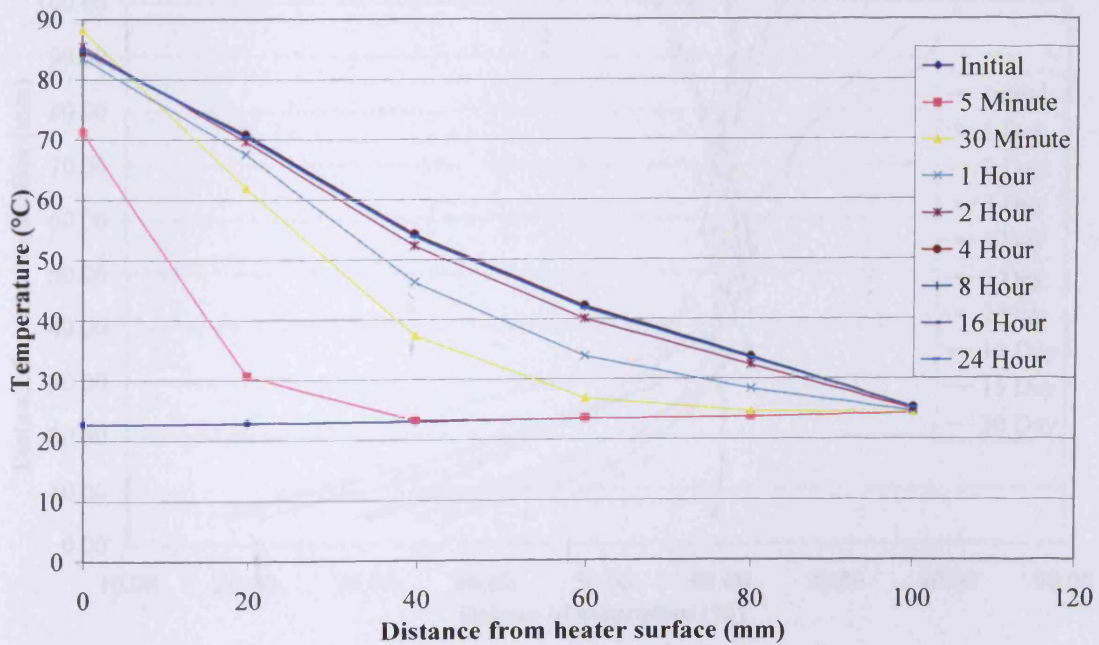
Figure 6.2 Temperature profile of MX-80 bentonite dry sample for T test
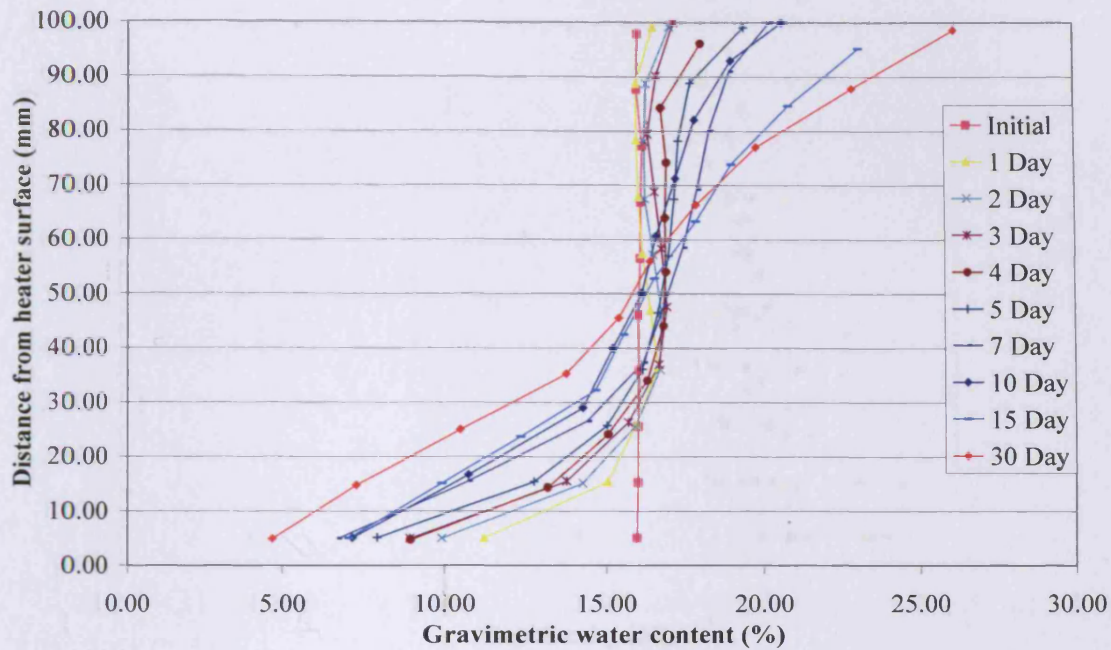
Figure 6.3 Gravimetric water content distribution of MX-80 bentonite dry sample for T test
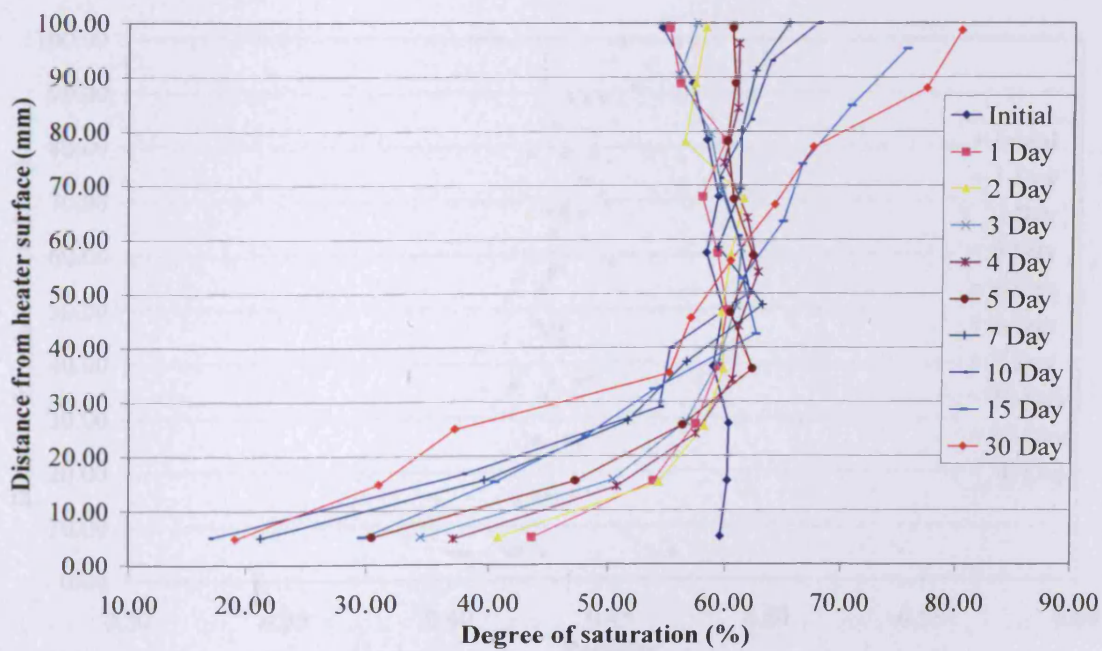
Figure 6.4 Degree of saturation of MX-80 bentonite dry sample for T test
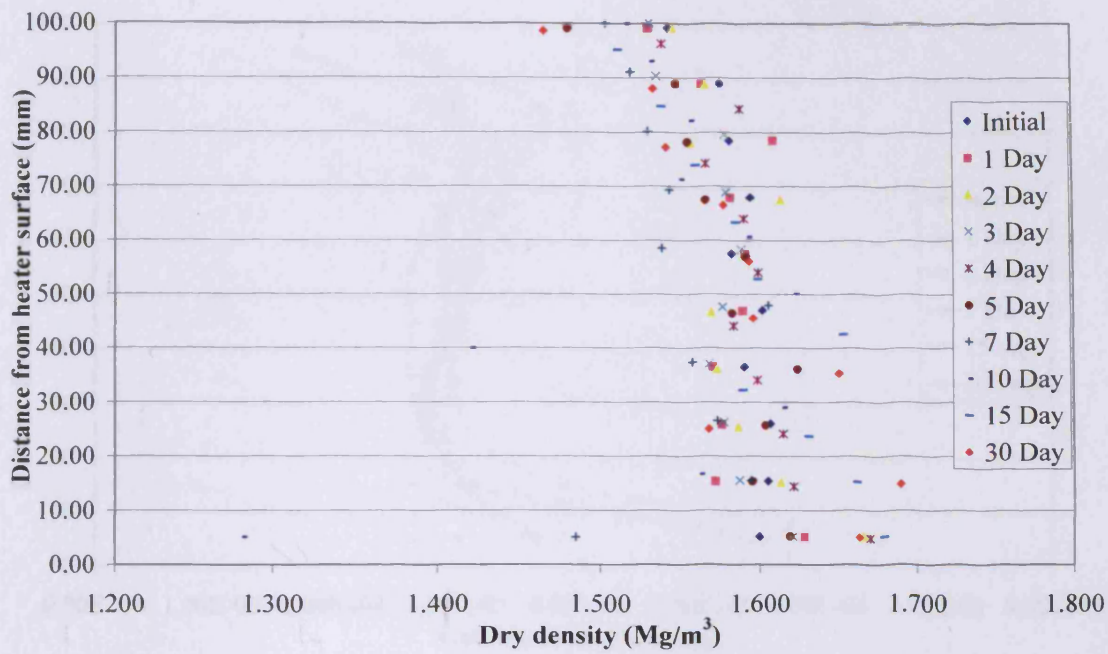
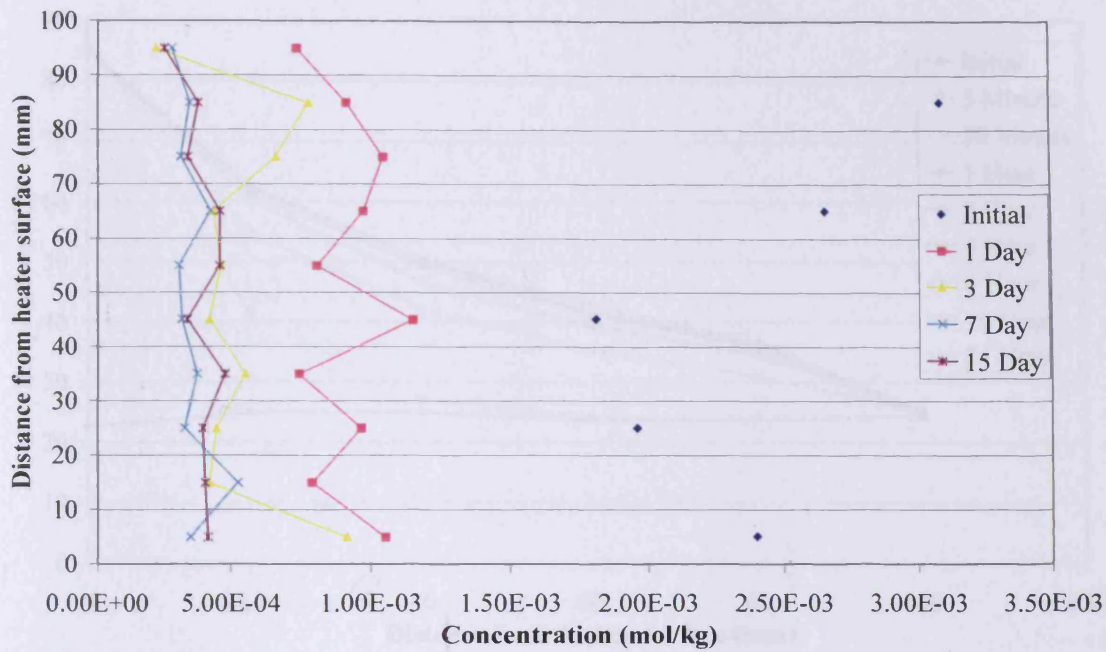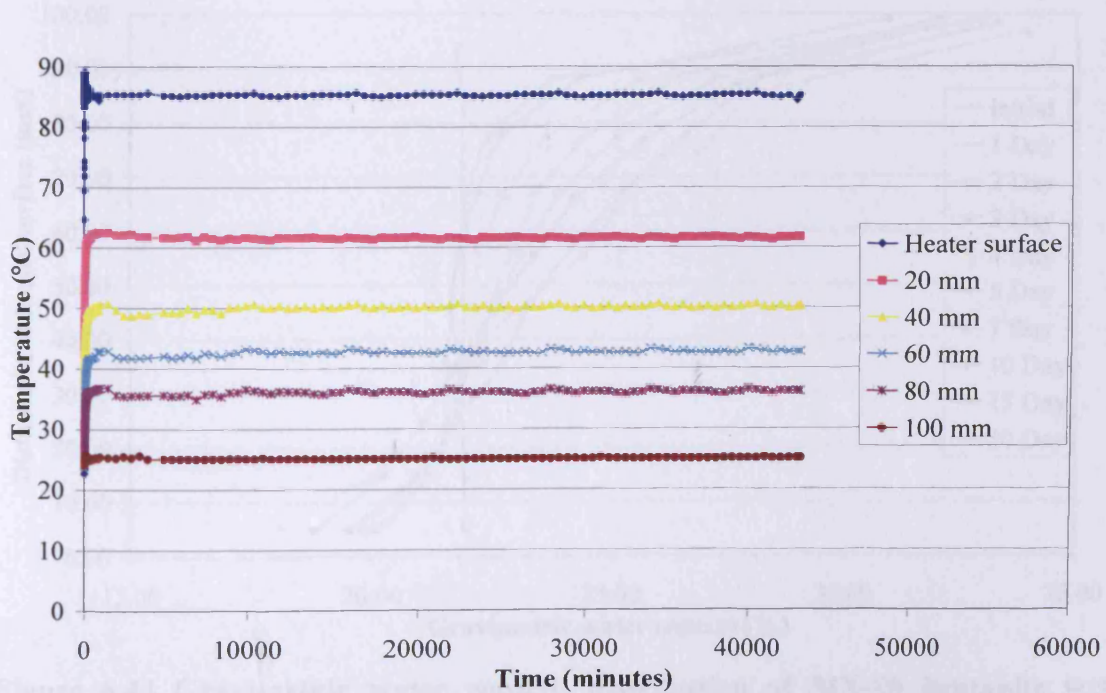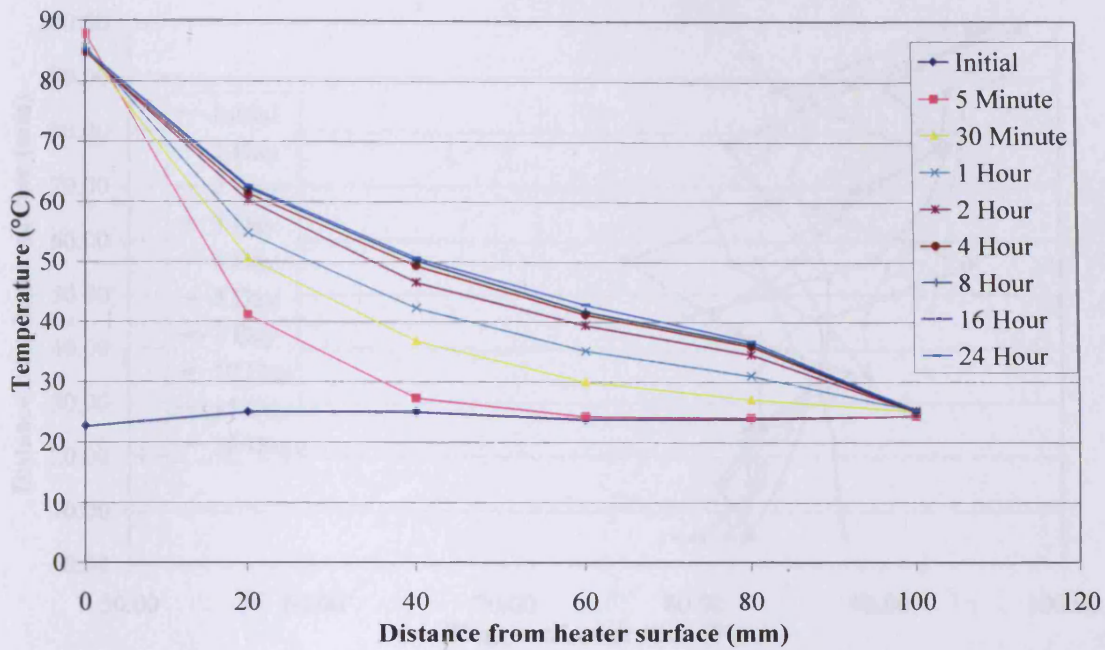**Figure 6.5 Dry density of MX-80 bentonite dry sample for T test**
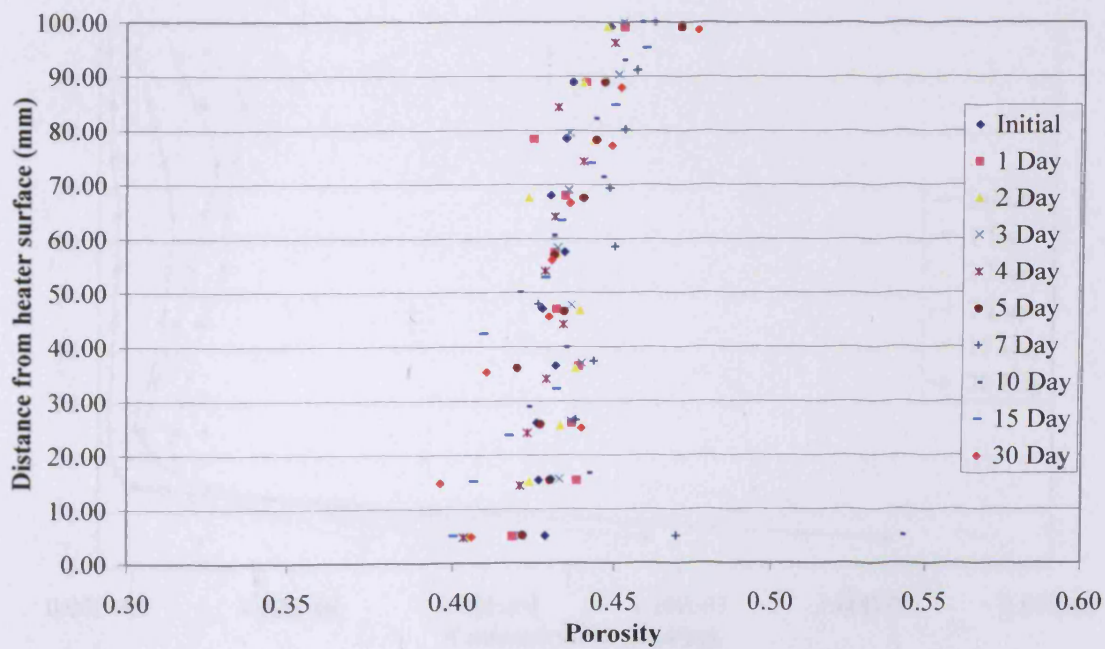
Figure 6.6 Porosity of MX-80 bentonite dry sample for T test
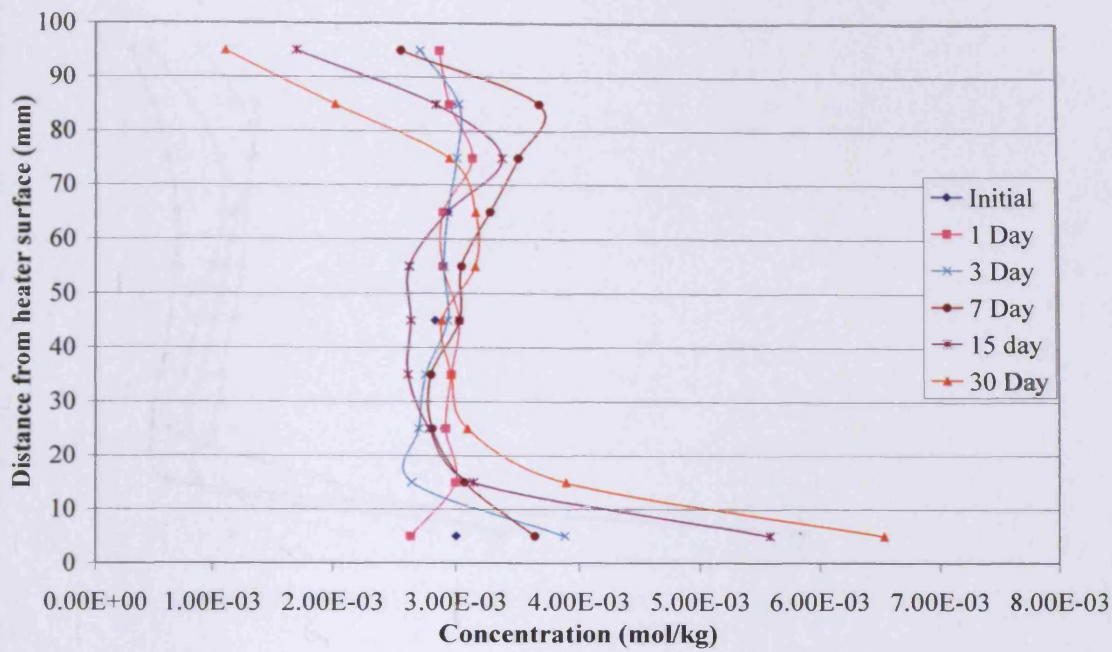
Figure 6.7 Chloride distribution of MX-80 bentonite dry sample for T test
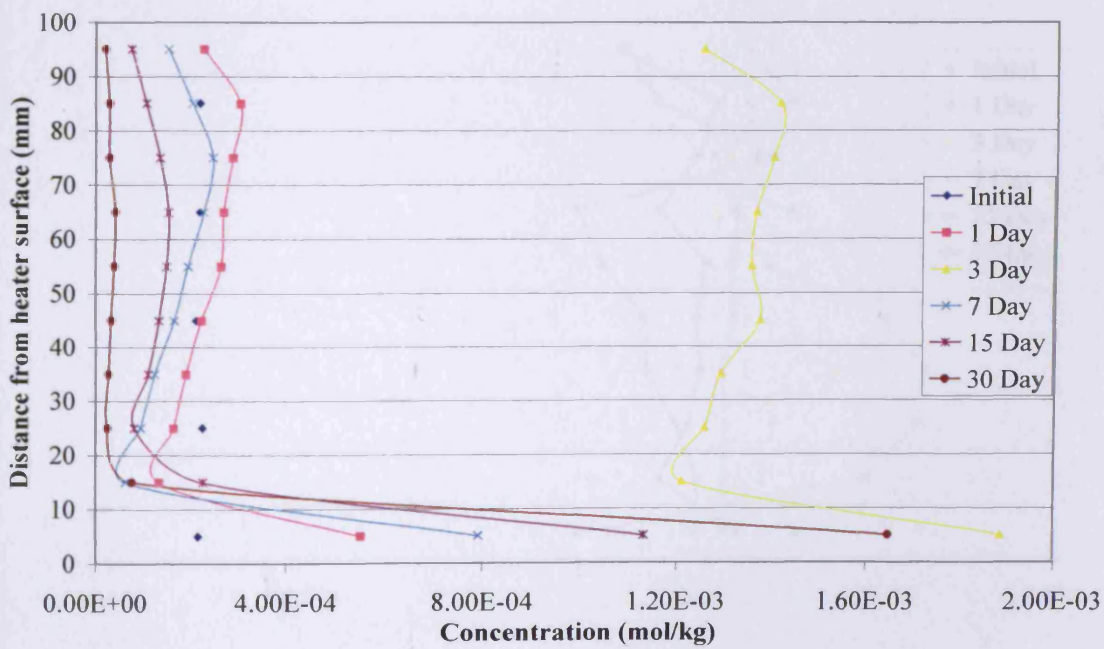
Figure 6.8 Nitrate distribution of MX-80 bentonite dry sample for T test
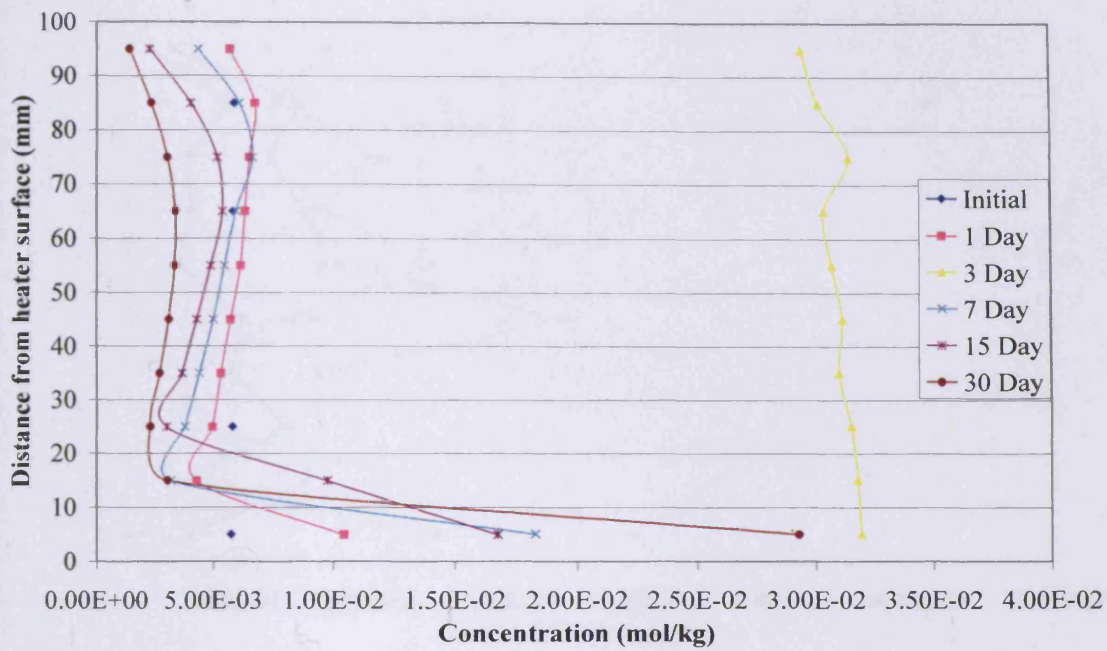
Figure 6.9 Sulphate distribution of MX-80 bentonite dry sample for T test
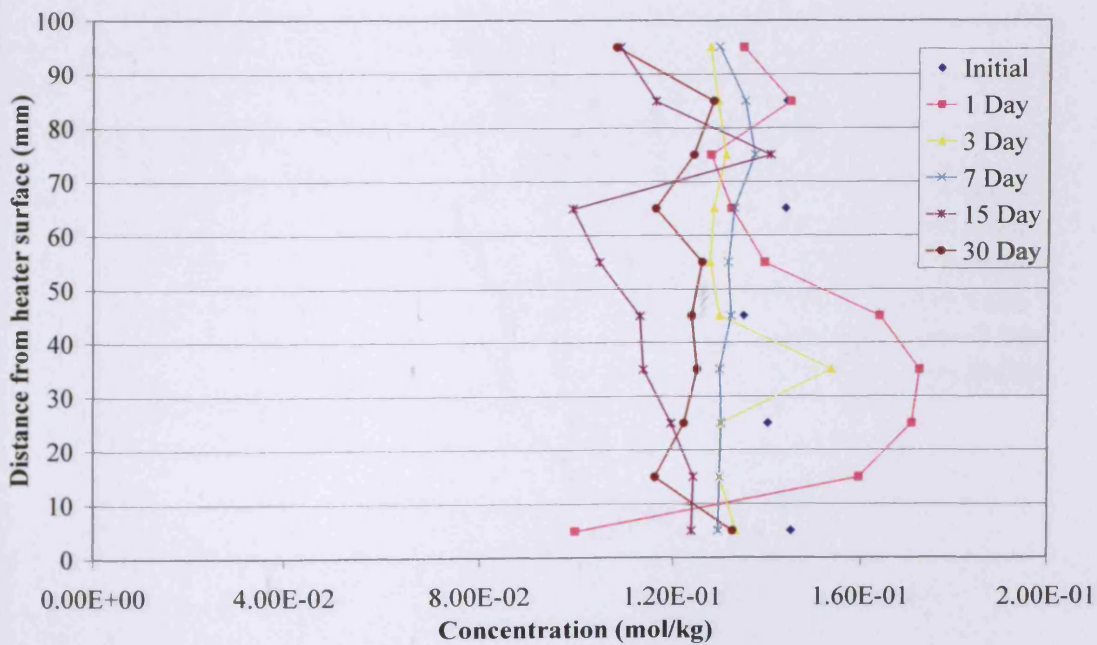
Figure 6.10 Sodium distribution of MX-80 bentonite dry sample for T test
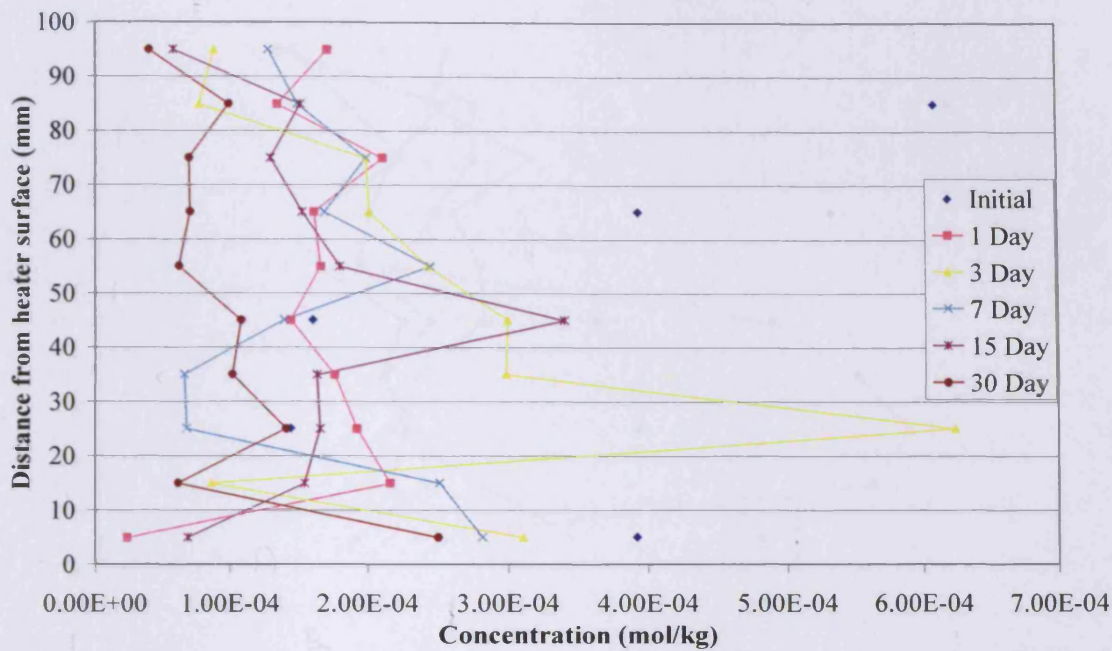
Figure 6.11 Magnesium distribution of MX-80 bentonite dry sample for T test
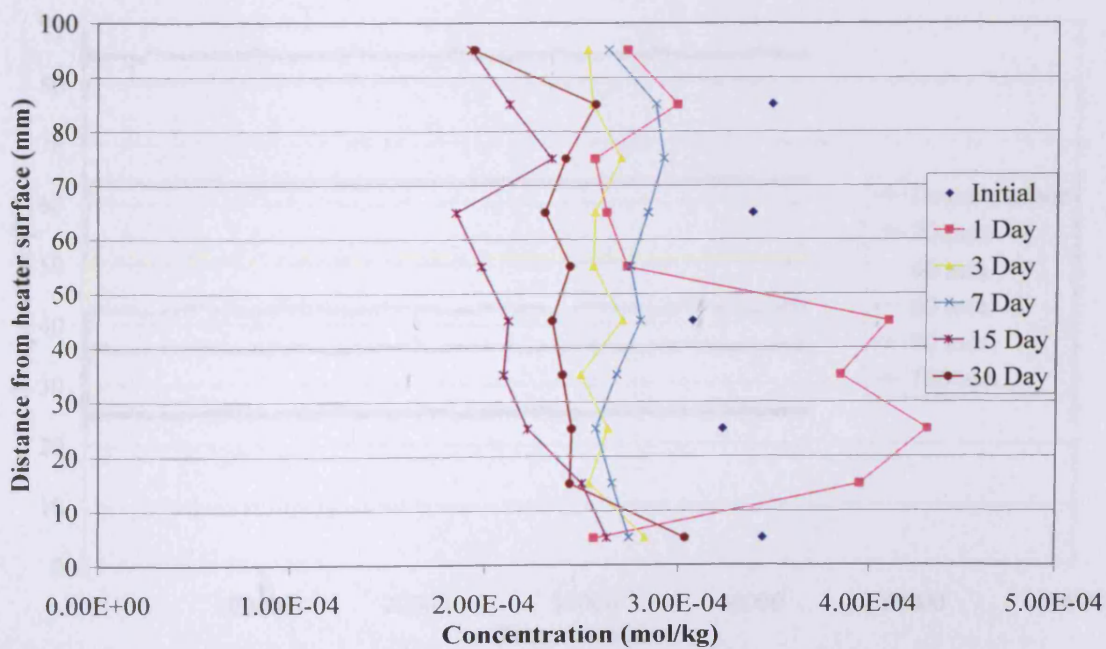
Figure 6.12 Potassium distribution of MX-80 bentonite dry sample for T test
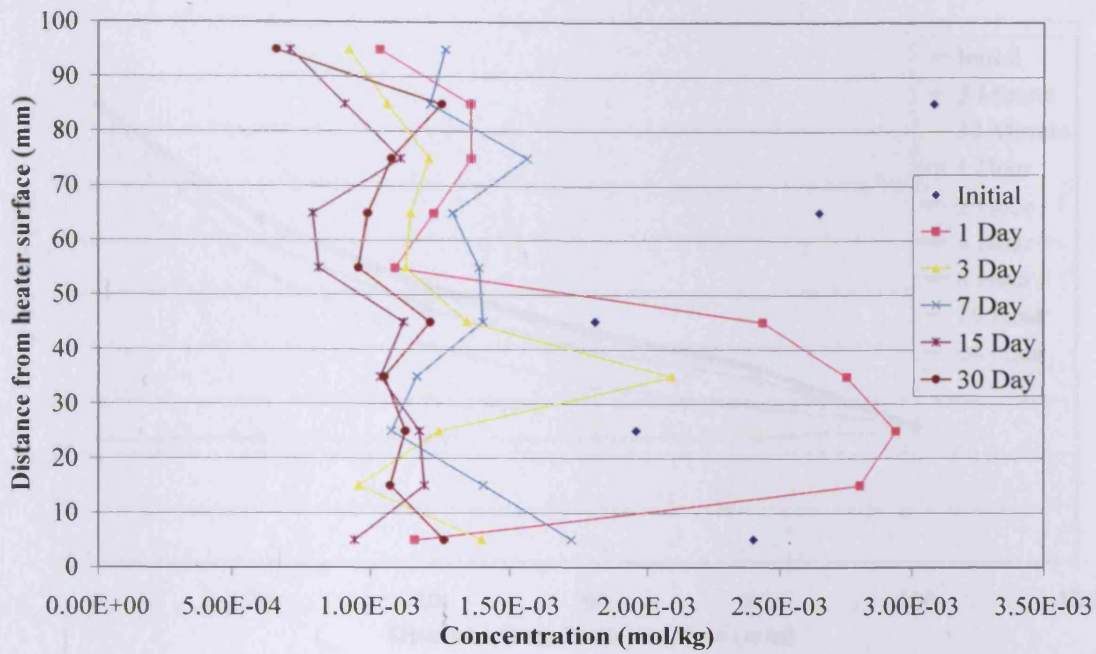
Figure 6.13 Calcium distribution of MX-80 bentonite dry sample for T test
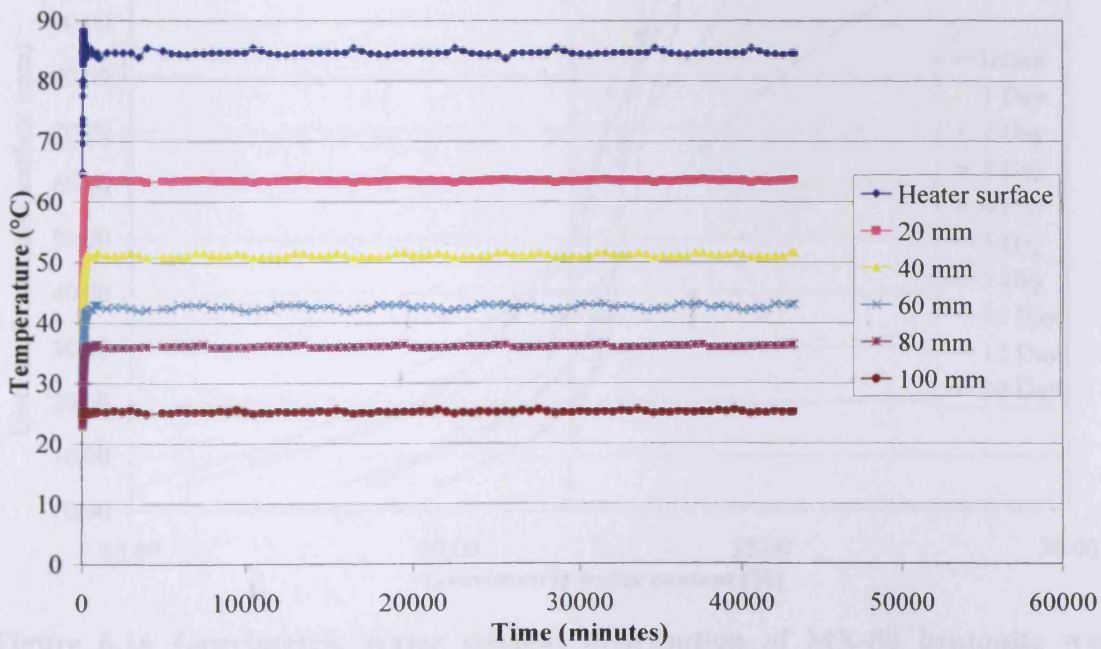
Figure 6.14 Temperature distribution of MX-80 bentonite wet sample for T test
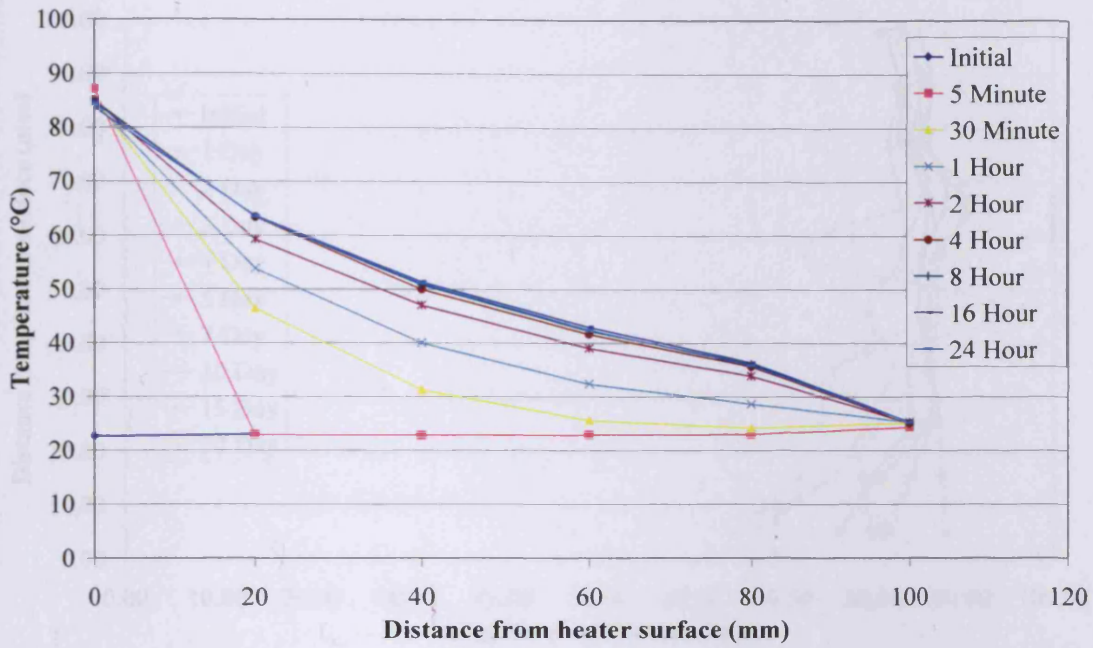
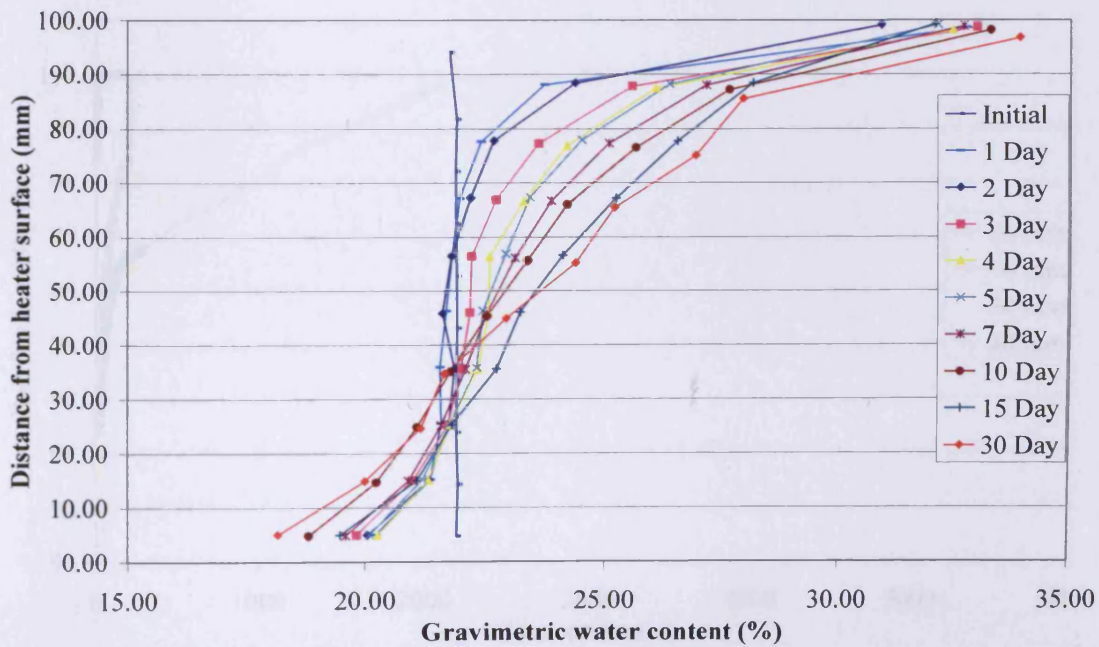**Figure 6.15 Temperature profile of MX-80 bentonite wet sample for T test**
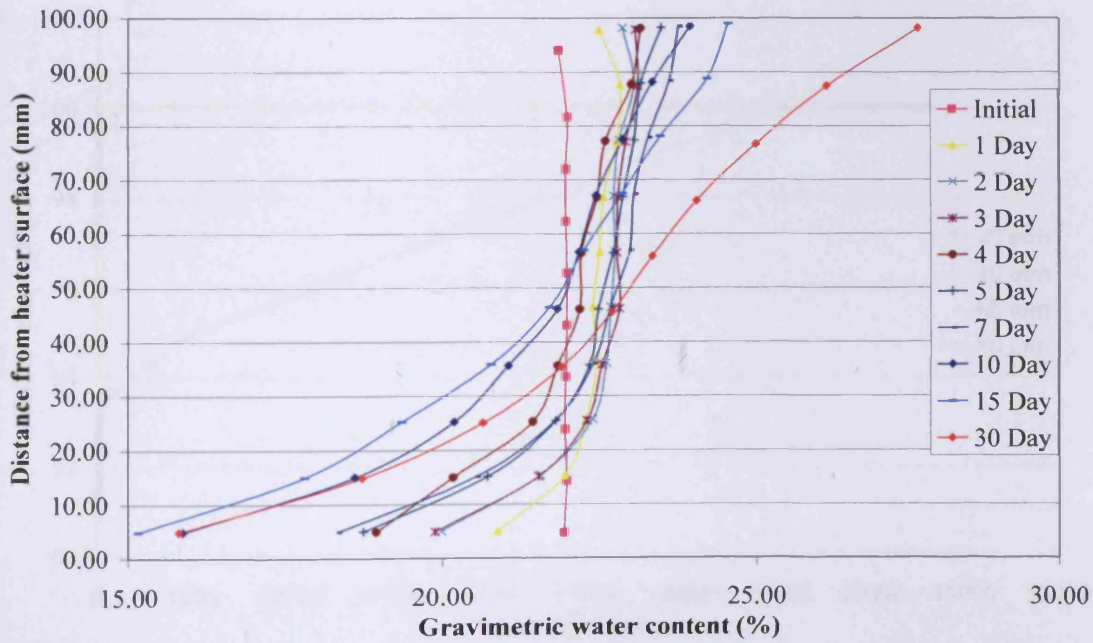
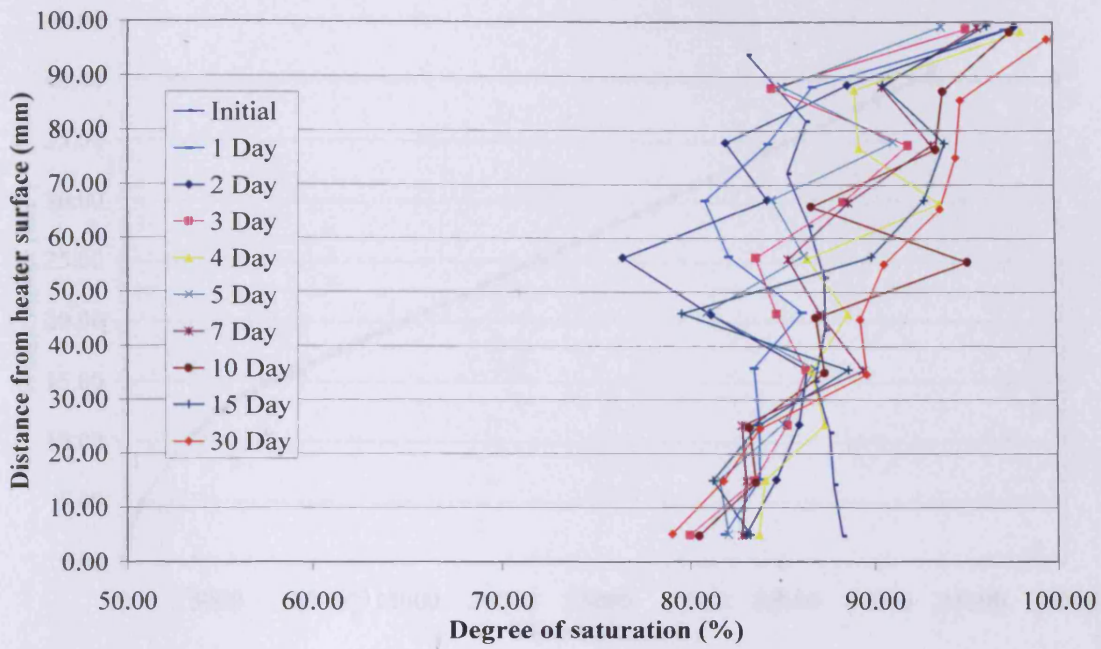**Figure 6.16 Gravimetric water content distribution of MX-80 bentonite wet sample for T test**
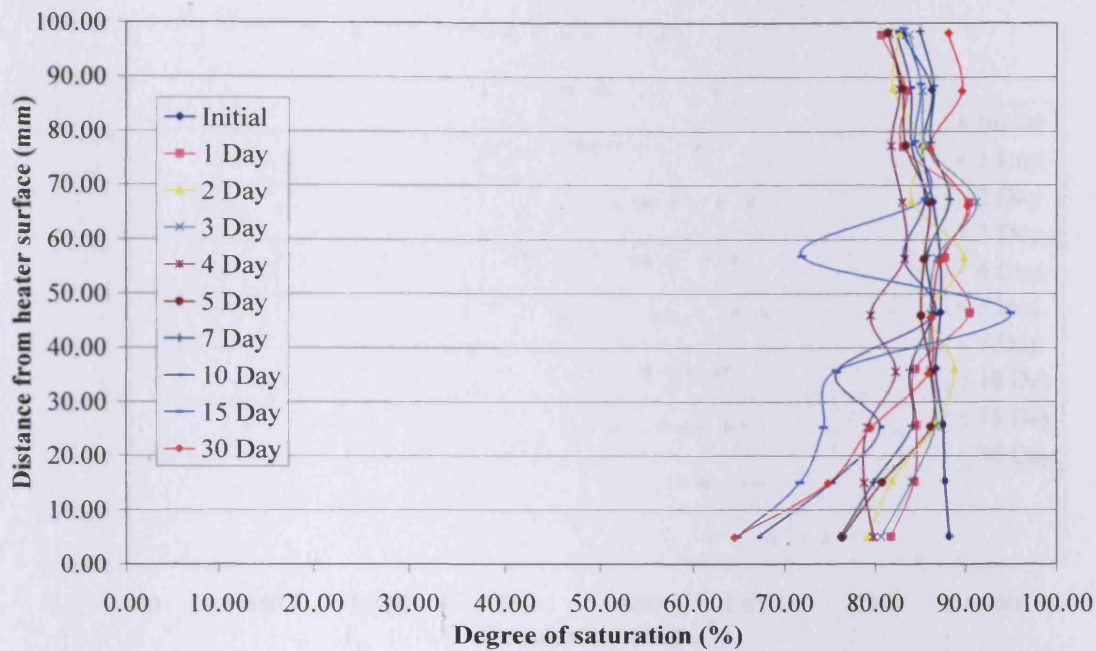
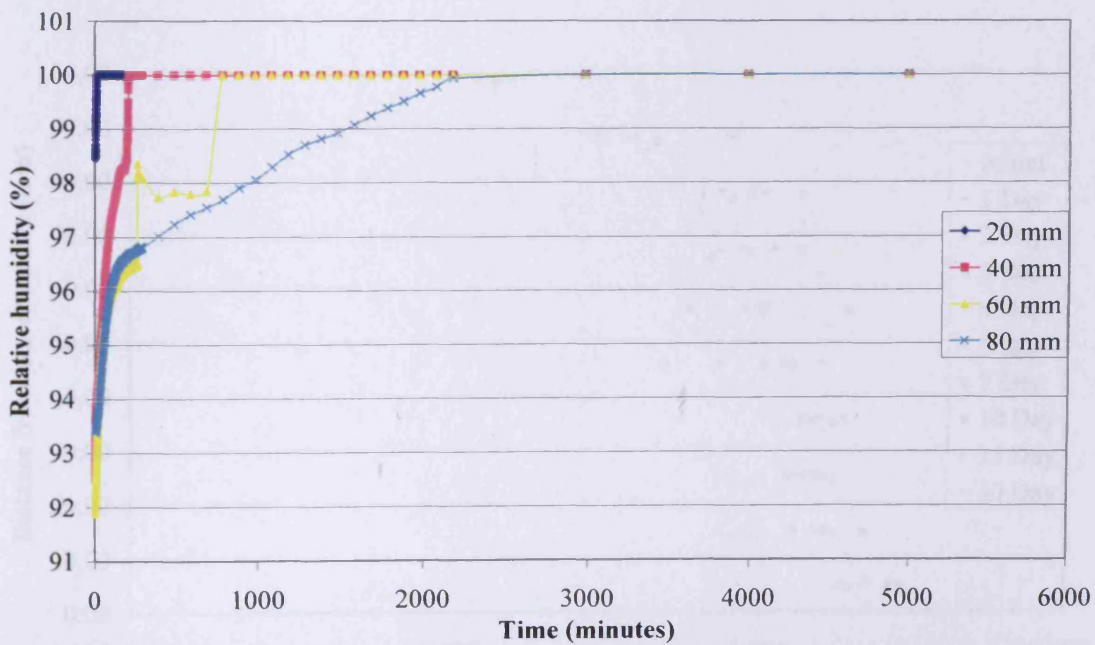**Figure 6.17 Degree of saturation of MX-80 bentonite wet sample for T test**
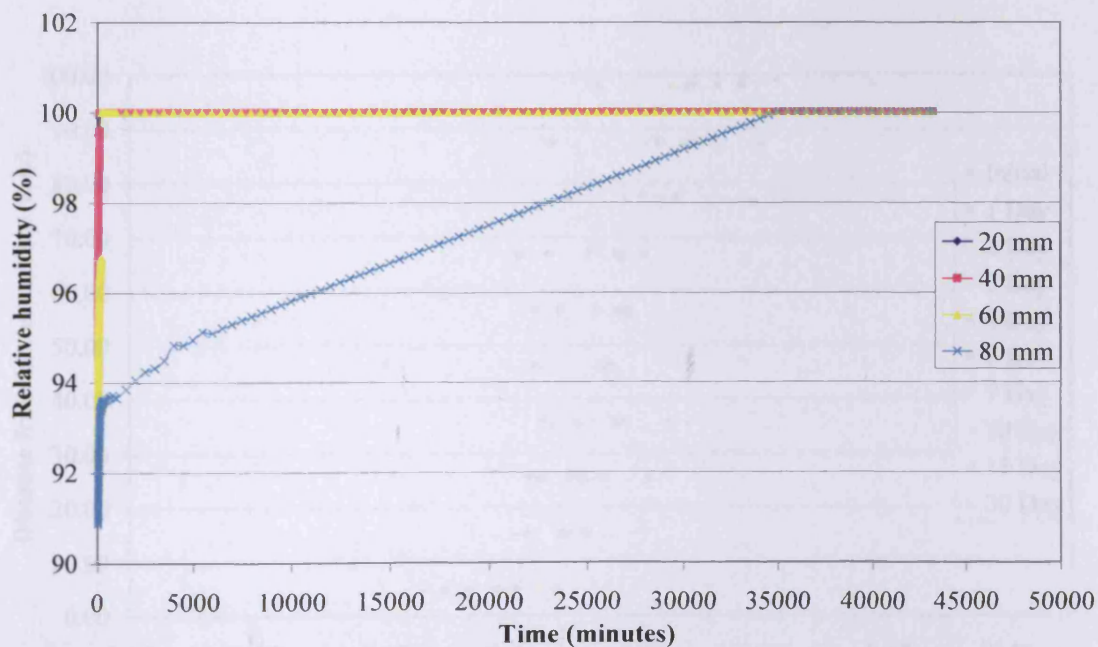
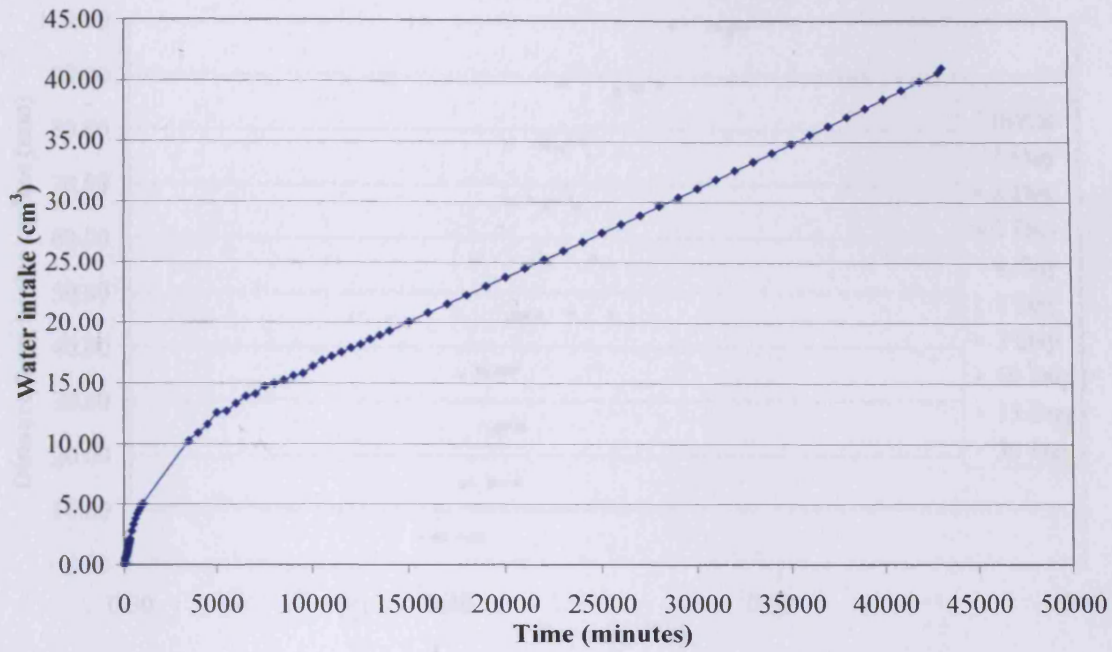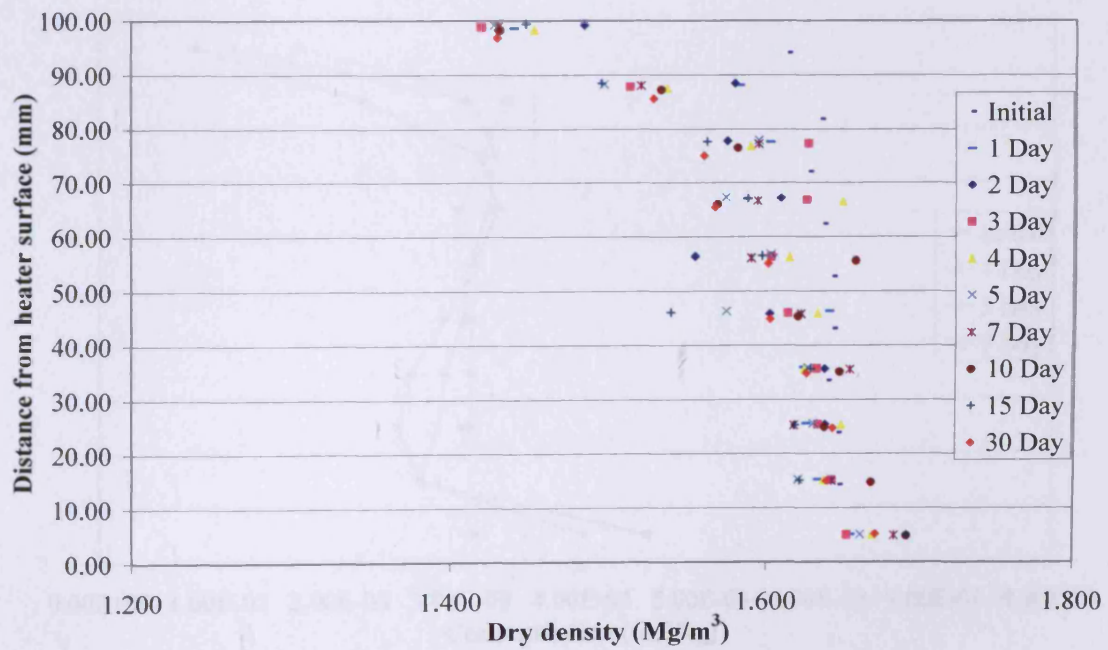**Figure 6.18 Relative humidity variation of MX-80 bentonite wet sample for T test**
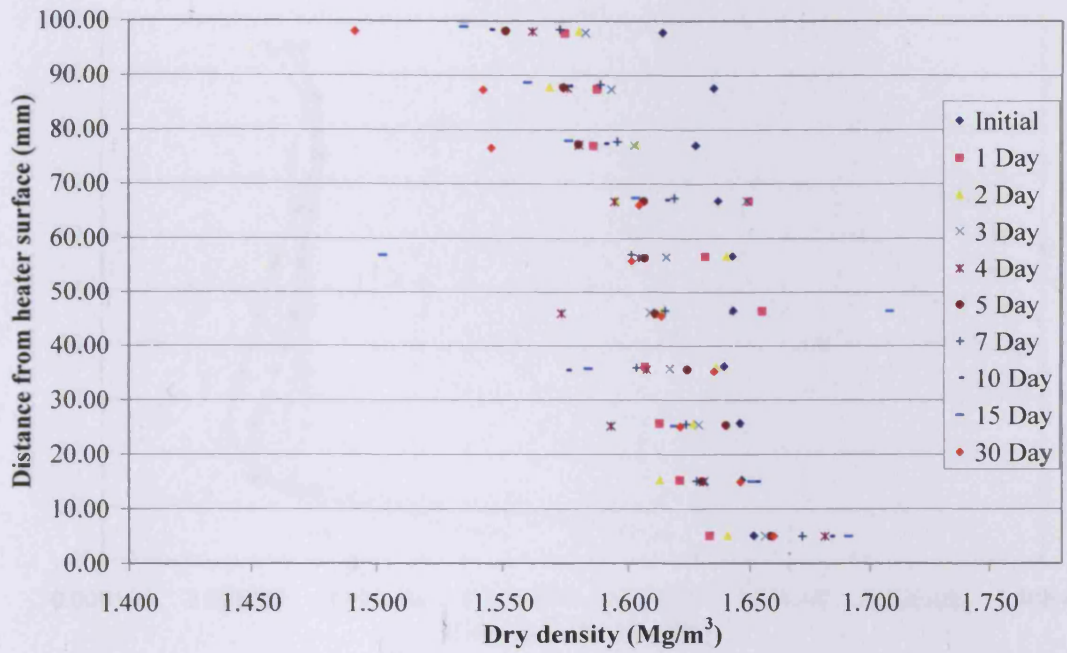
Figure 6.19 Dry density of MX-80 bentonite wet sample for T test
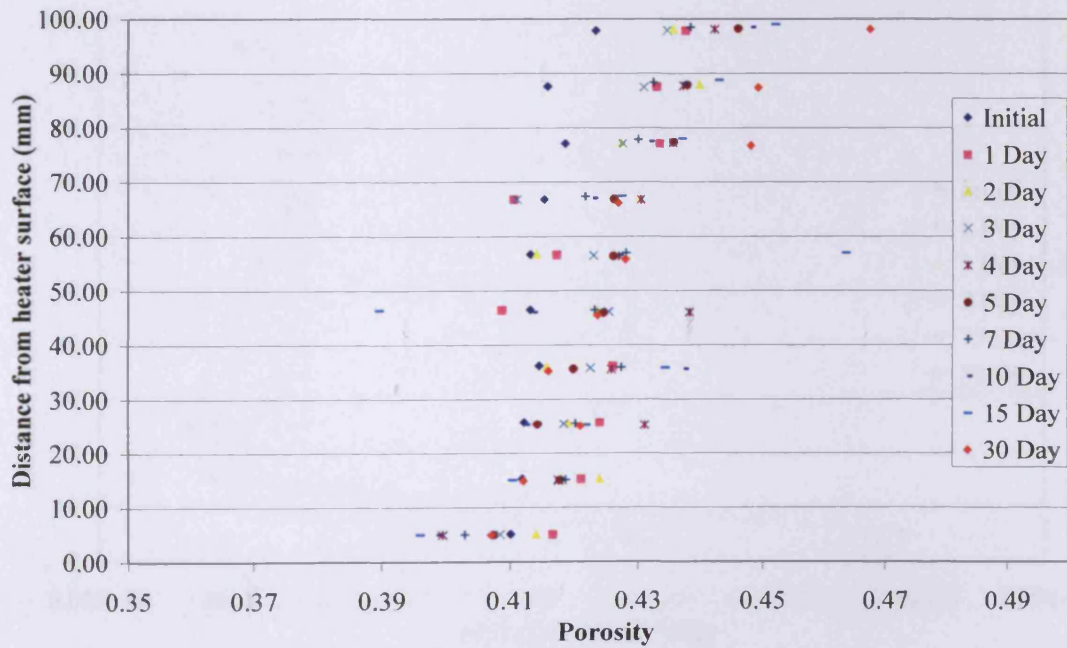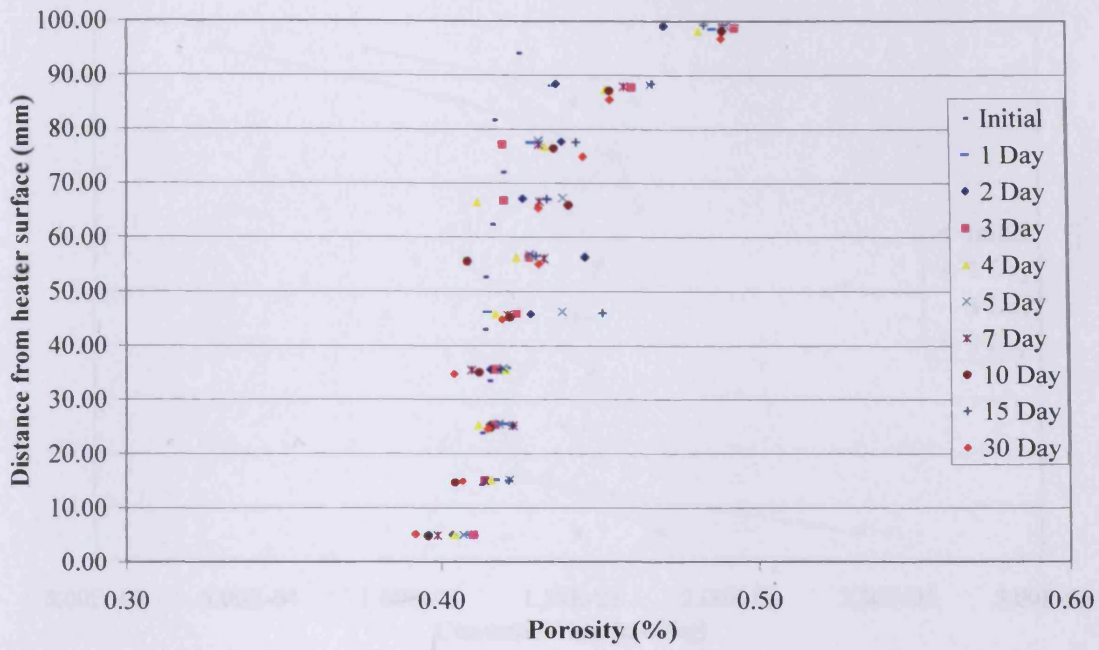

Figure 6.20 Porosity of MX-80 bentonite wet sample for T test
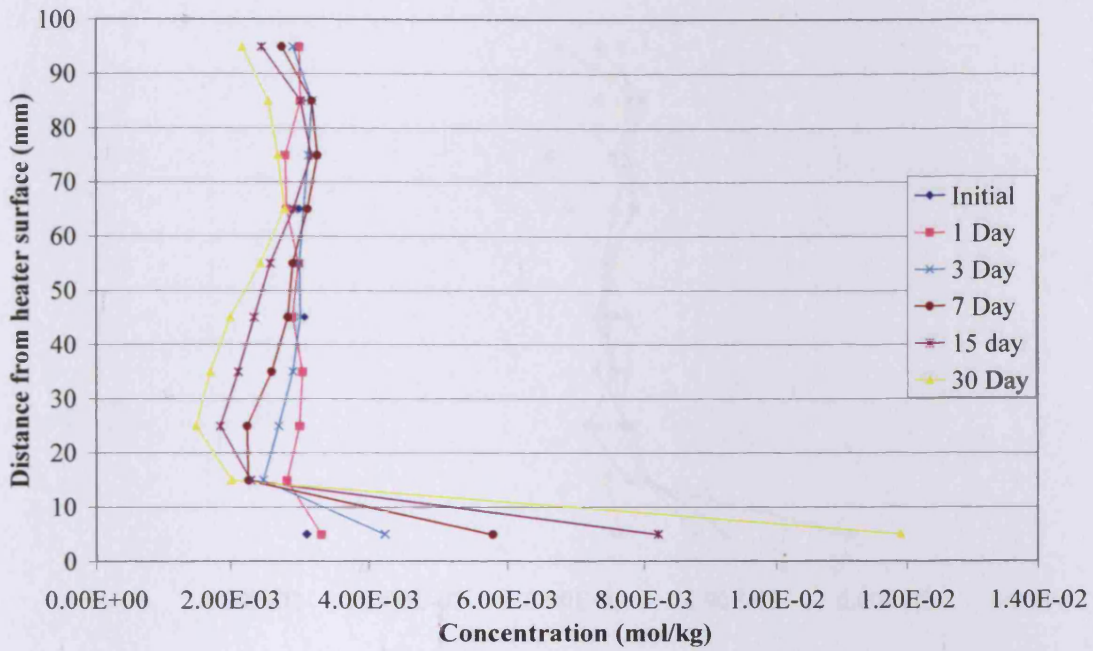
Figure 6.21 Chloride distribution of MX-80 bentonite wet sample for T test
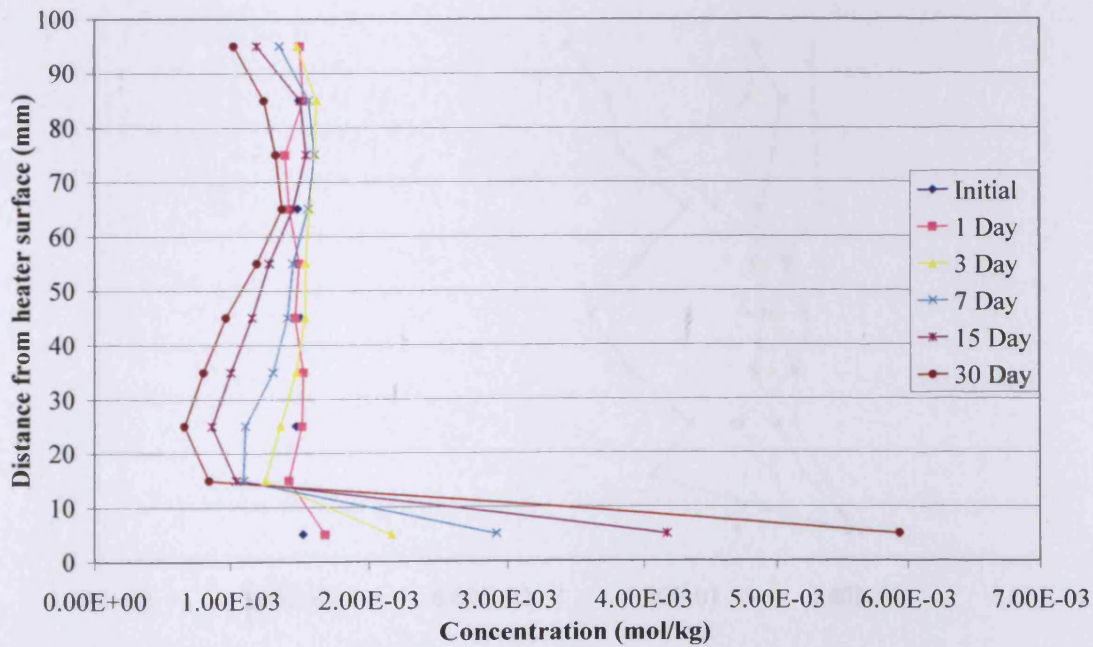
Figure 6.22 Nitrate distribution of MX-80 bentonite wet sample for T test
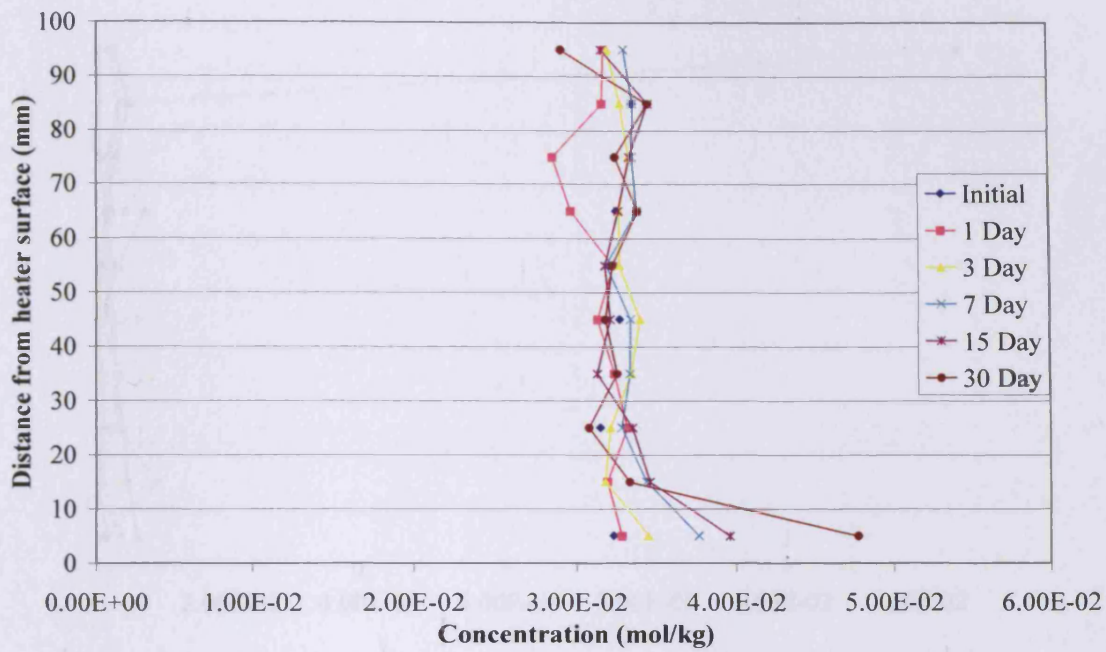
Figure 6.23 Sulphate distribution of MX-80 bentonite wet sample for T test
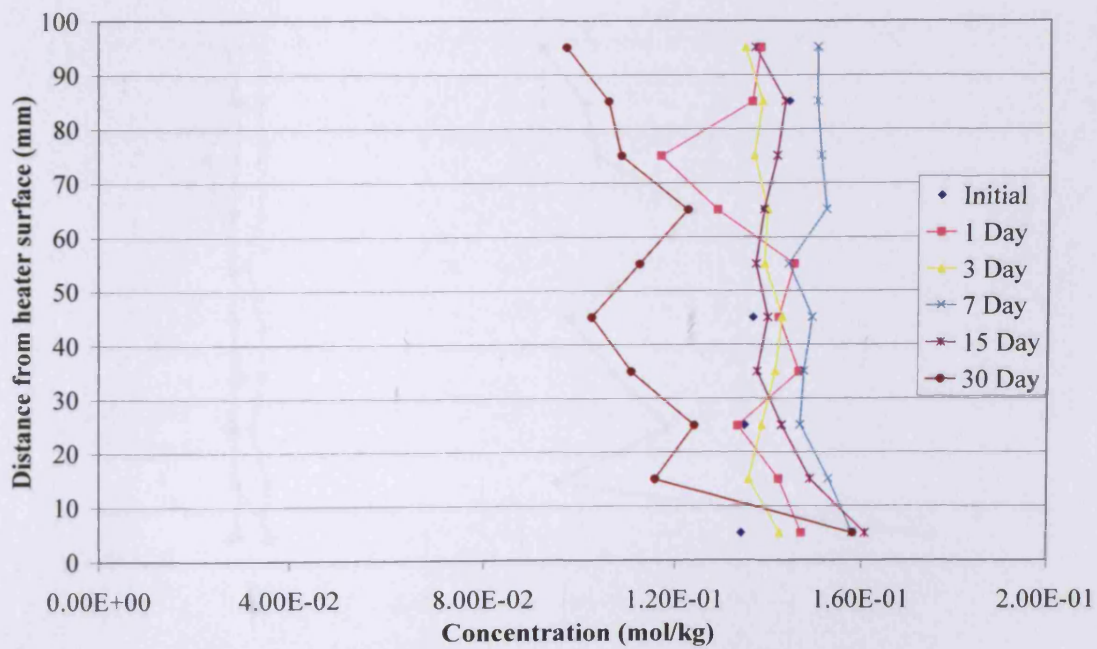
Figure 6.24 Sodium distribution of MX-80 bentonite wet sample for T test
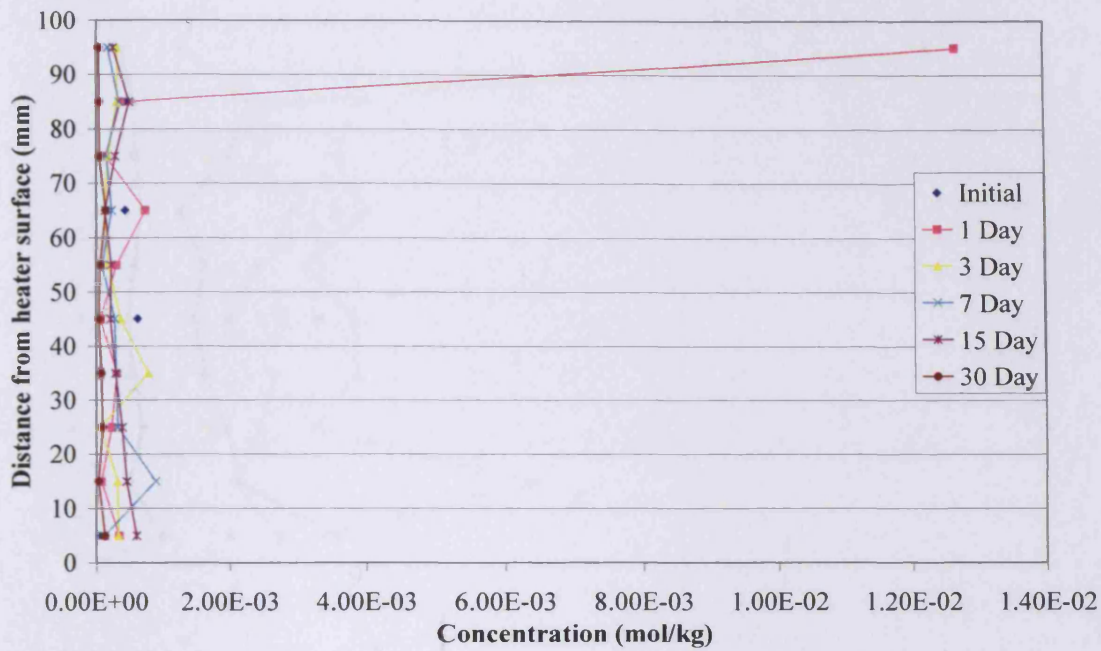
Figure 6.25 Magnesium distribution of MX-80 bentonite wet sample for T test
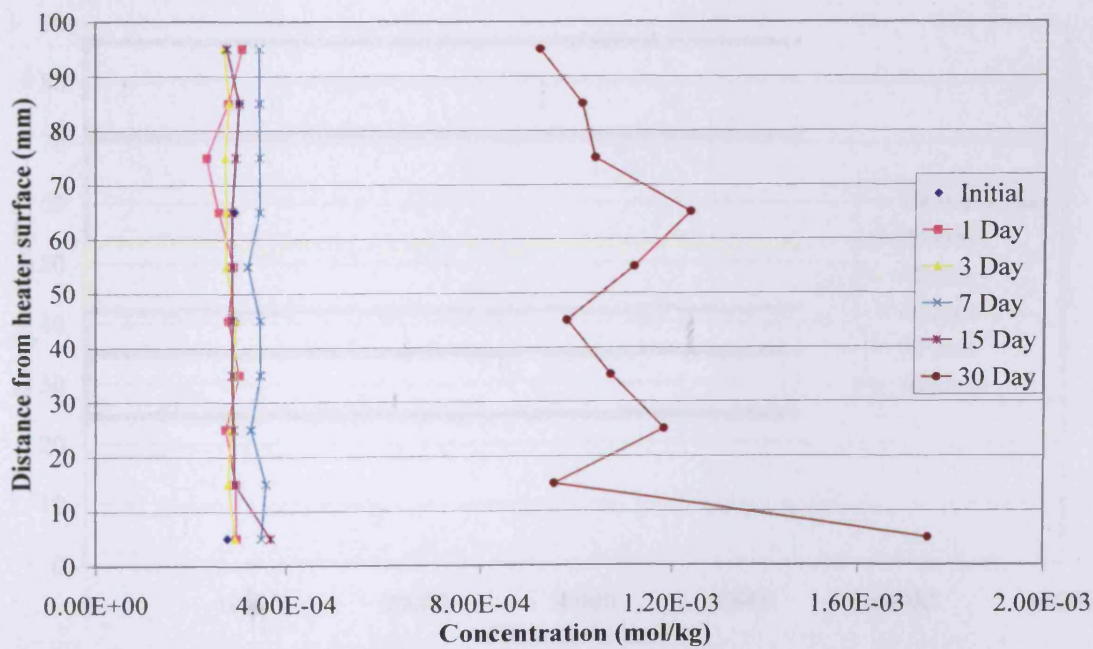
Figure 6.26 Potassium distribution of MX-80 bentonite wet sample for T test
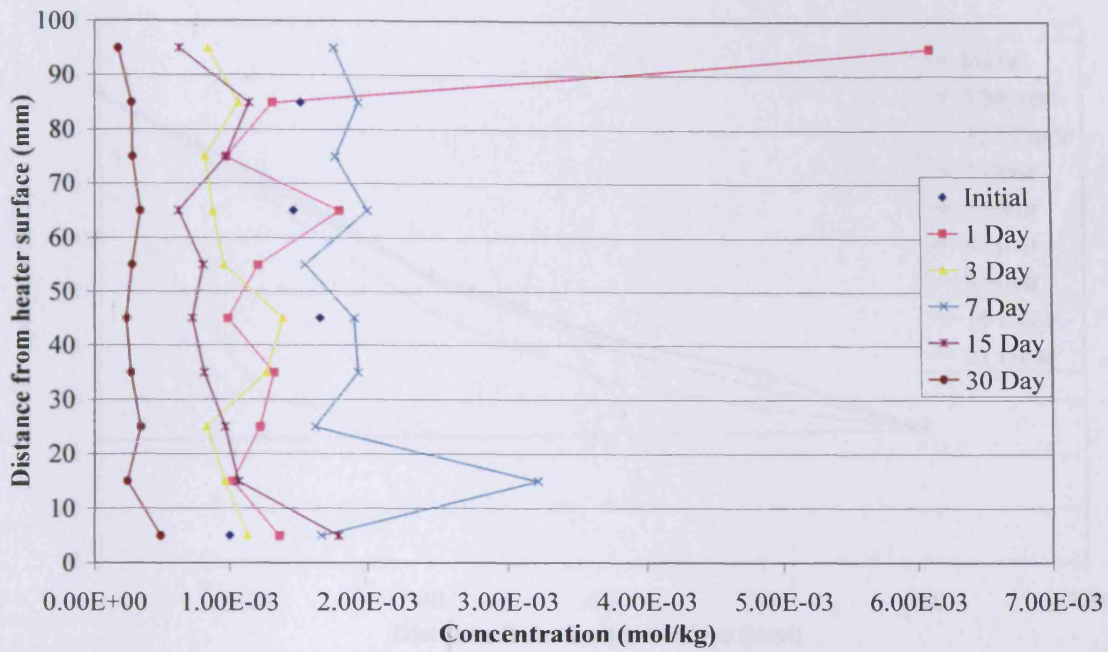
Figure 6.27 Calcium distribution of MX-80 bentonite wet sample for T test
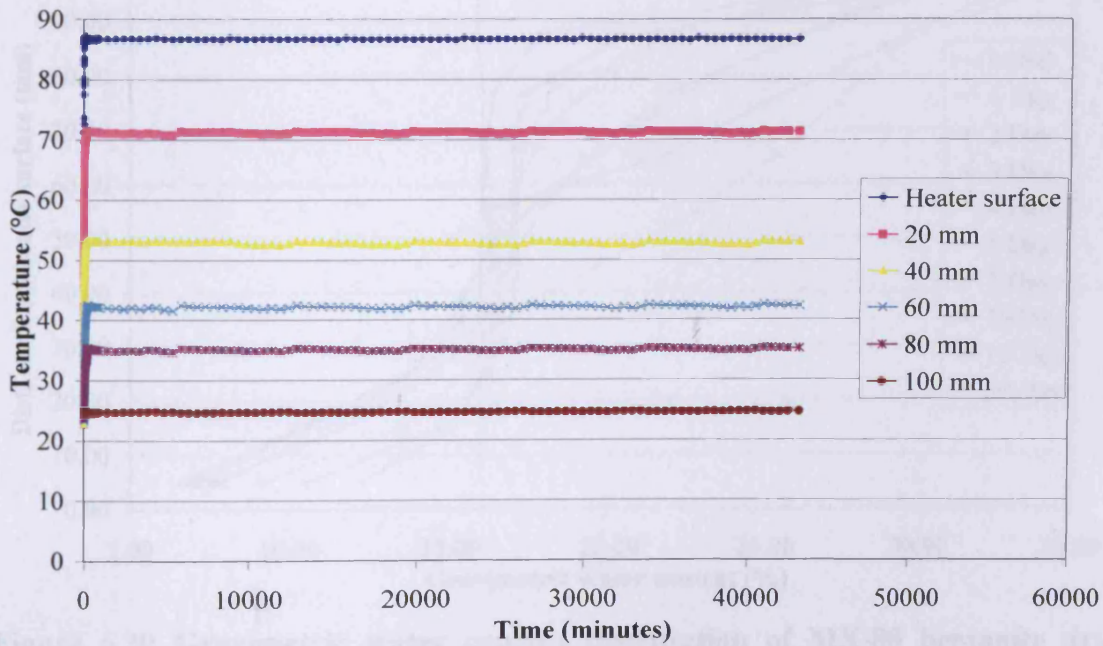
Figure 6.28 Temperature distribution of MX-80 bentonite dry sample for TH test
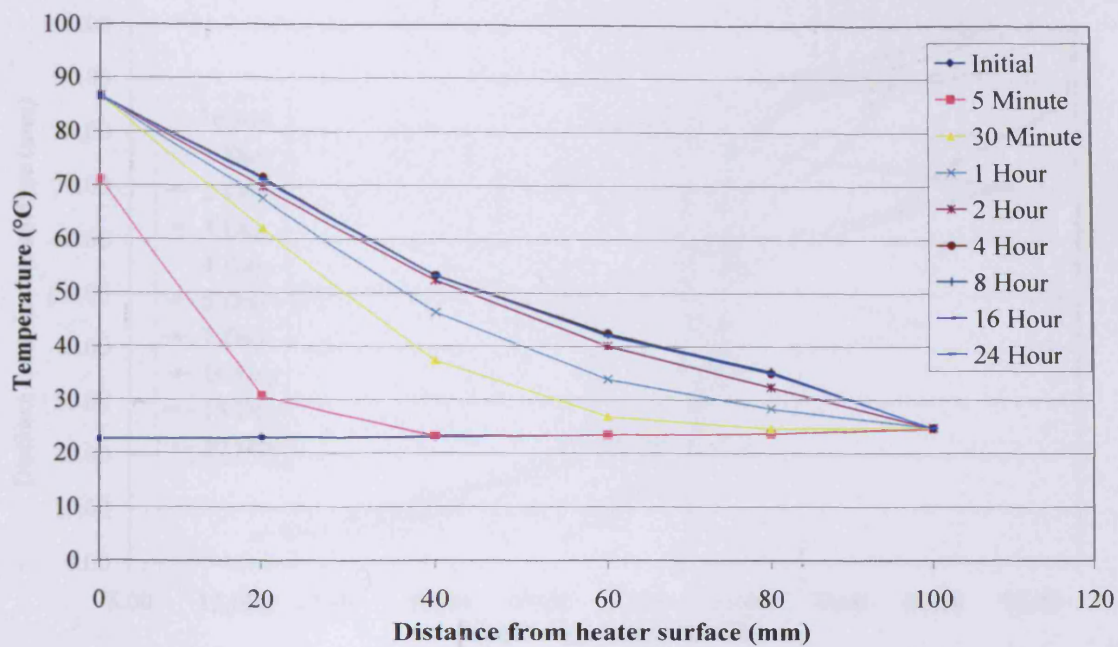
Figure 6.29 Temperature profile of MX-80 bentonite dry sample for TH test
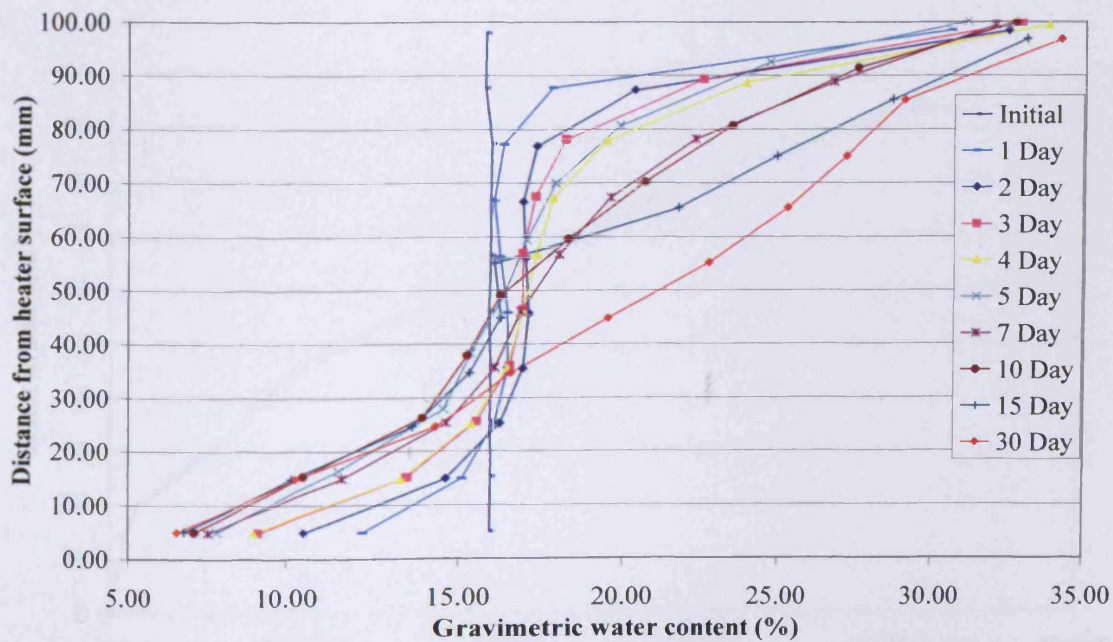
Figure 6.30 Gravimetric water content distribution of MX-80 bentonite dry sample for TH test
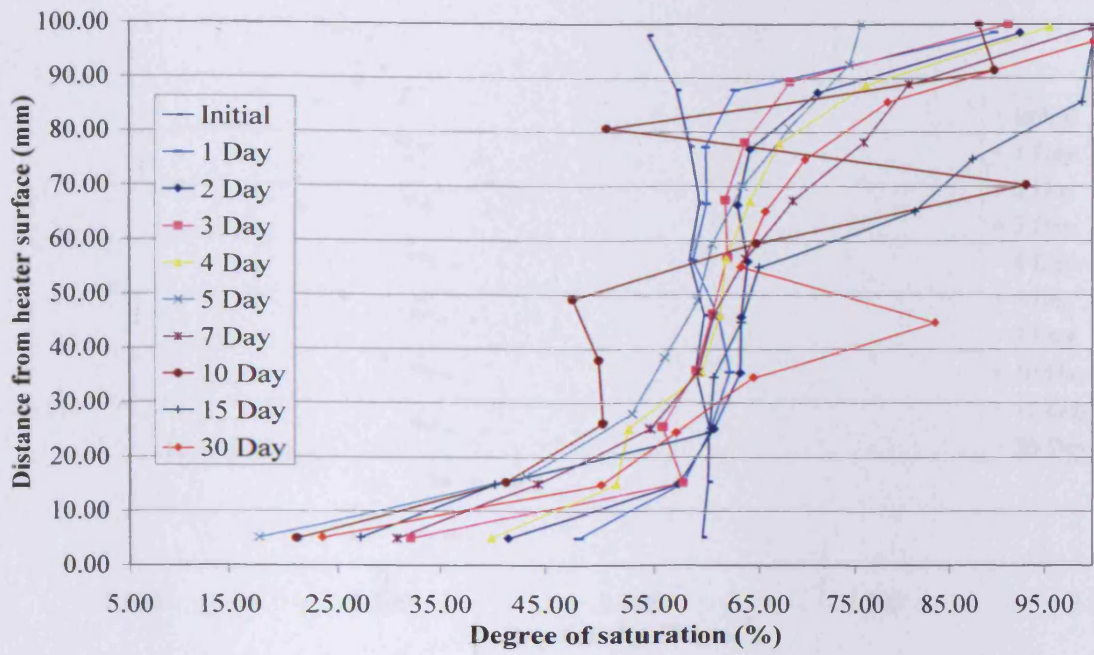
Figure 6.31 Degree of saturation of MX-80 bentonite dry sample for TH test
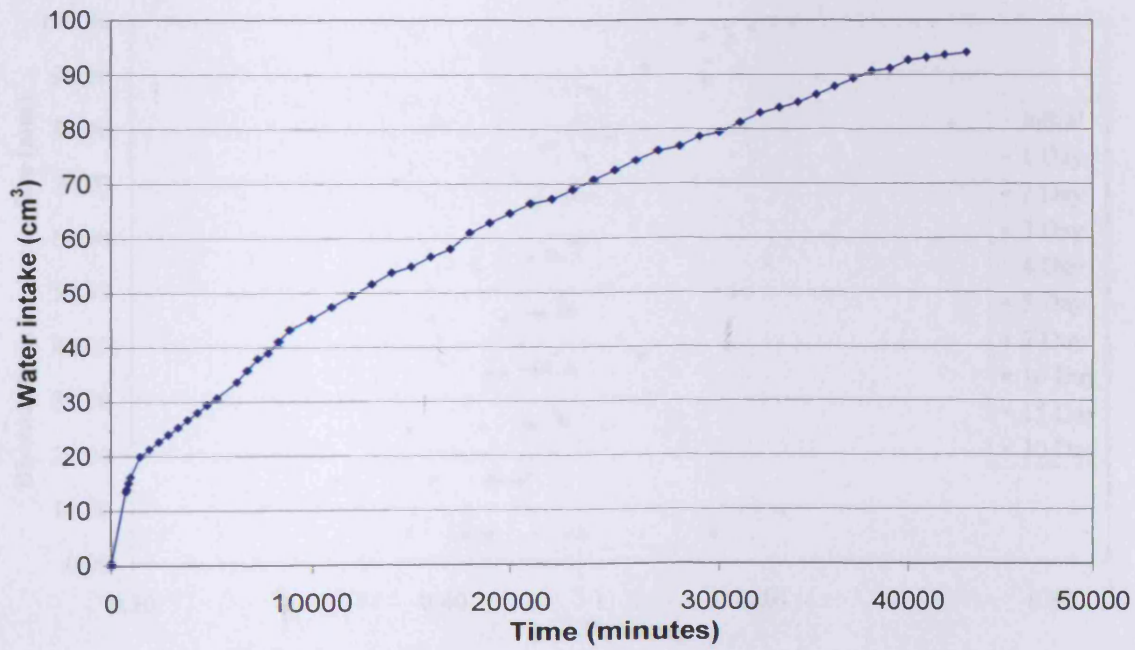
Figure 6.32 Water intake by MX-80 bentonite dry sample for TH test
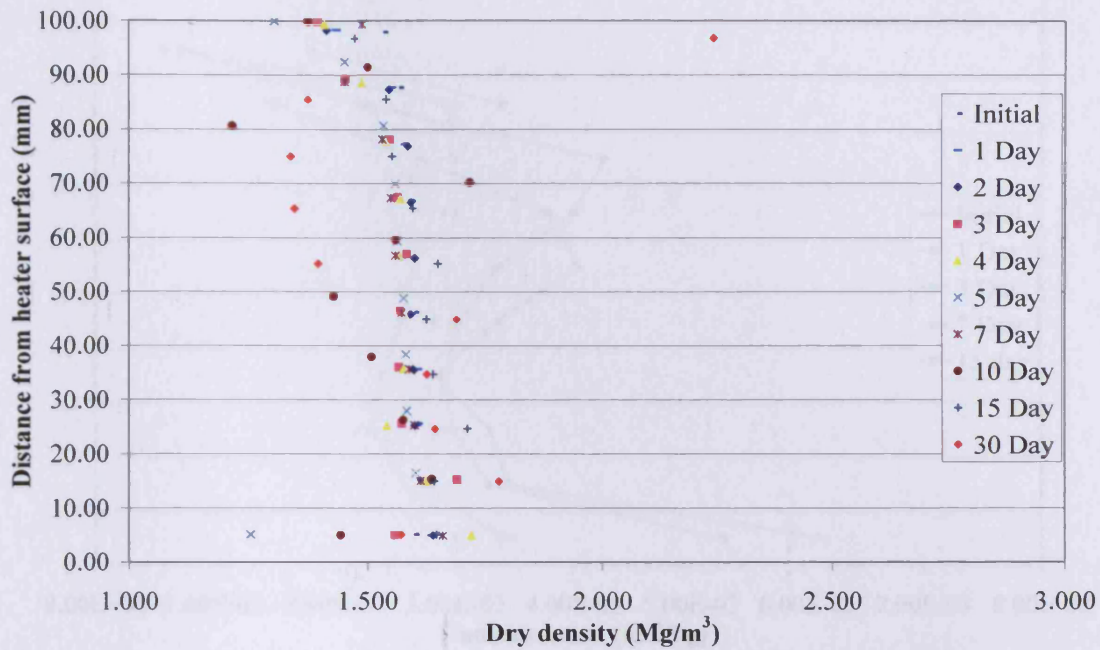
Figure 6.33 Dry density of MX-80 bentonite dry sample for TH test
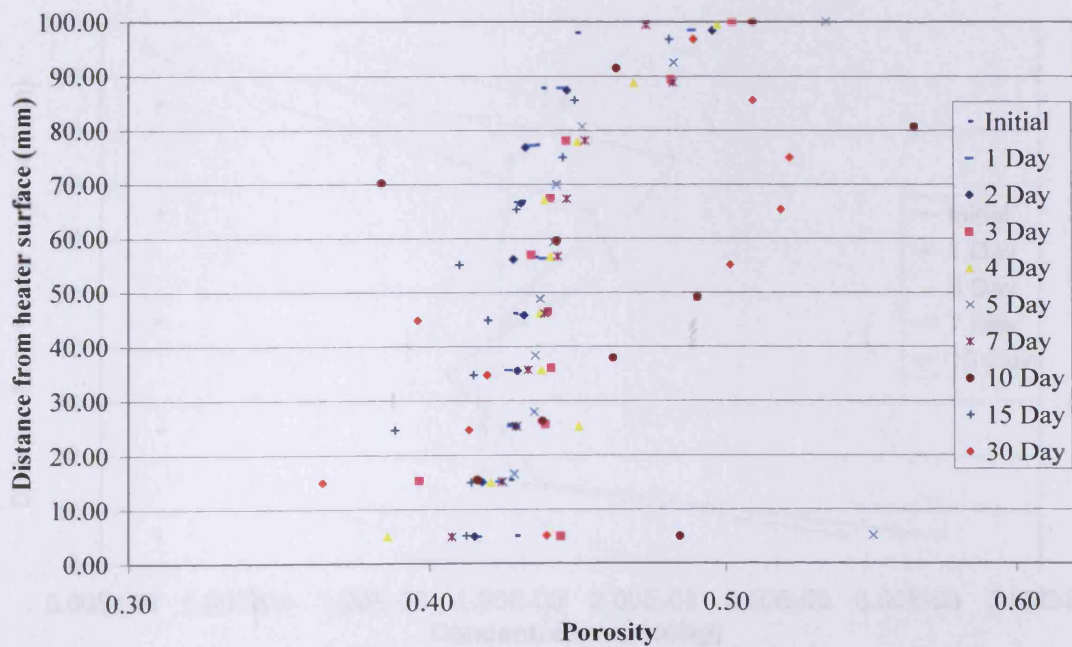
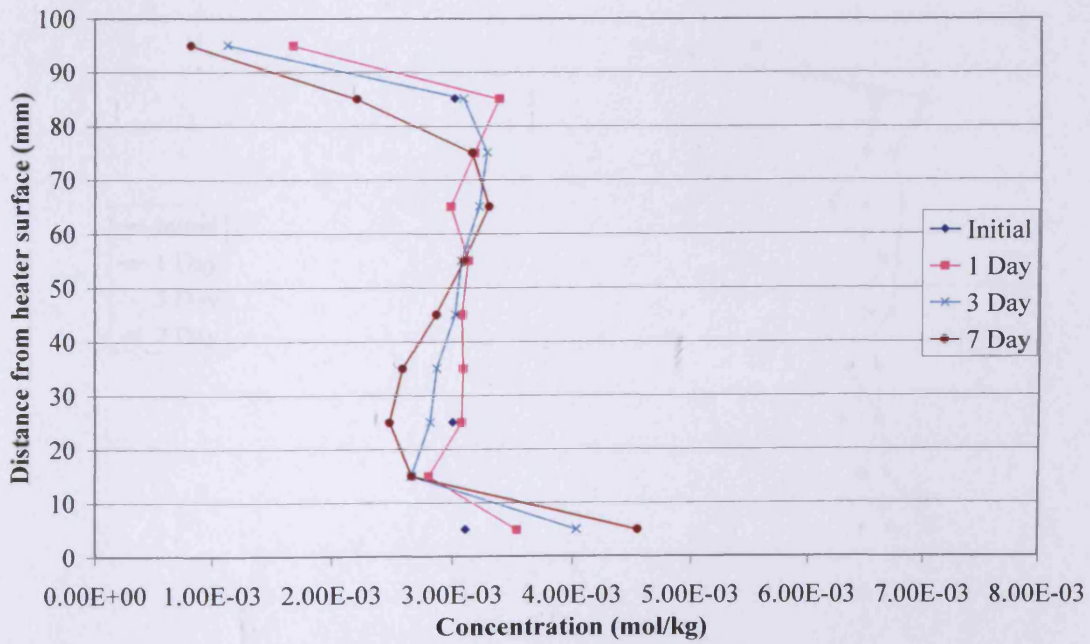
Figure 6.34 Porosity of MX-80 bentonite dry sample for TH test
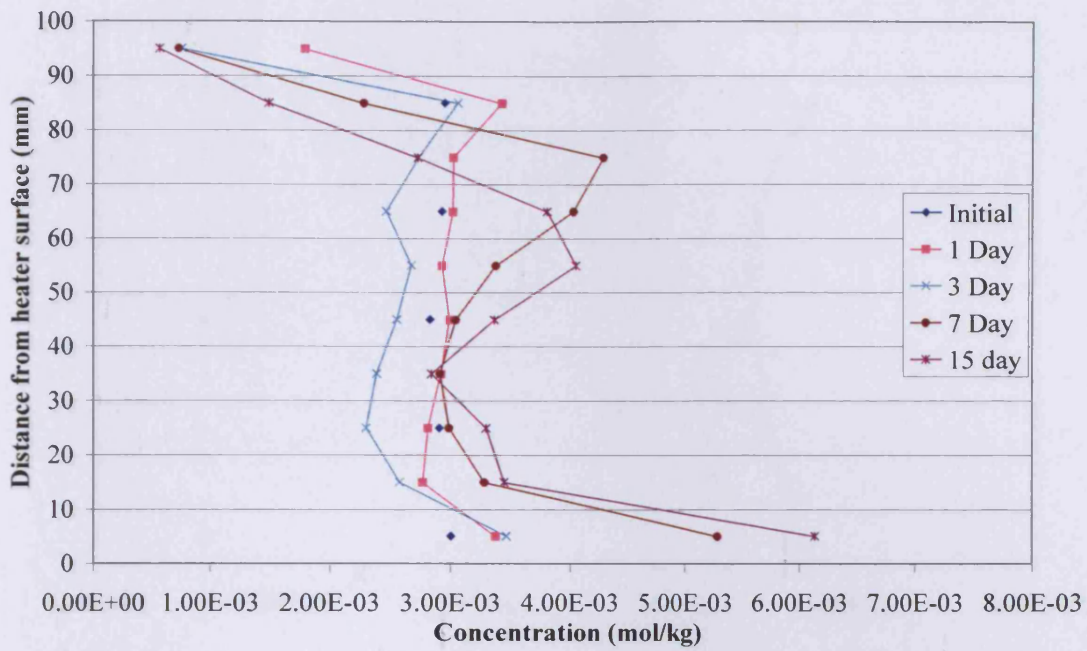
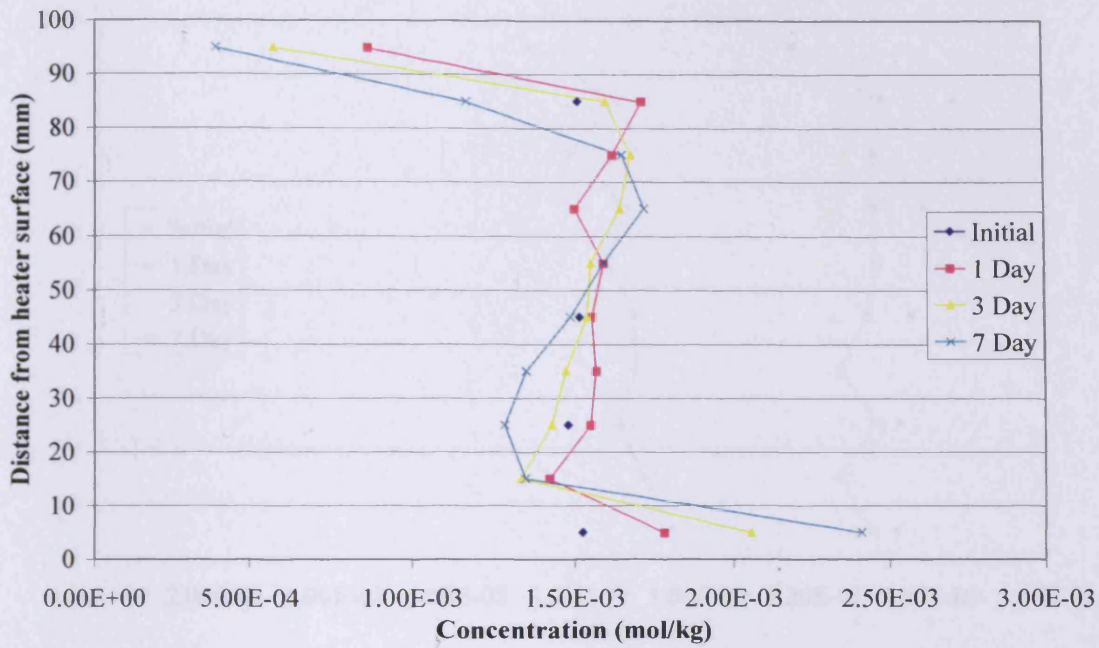**Figure 6.35 Chloride distribution of MX-80 bentonite dry sample for TH test**
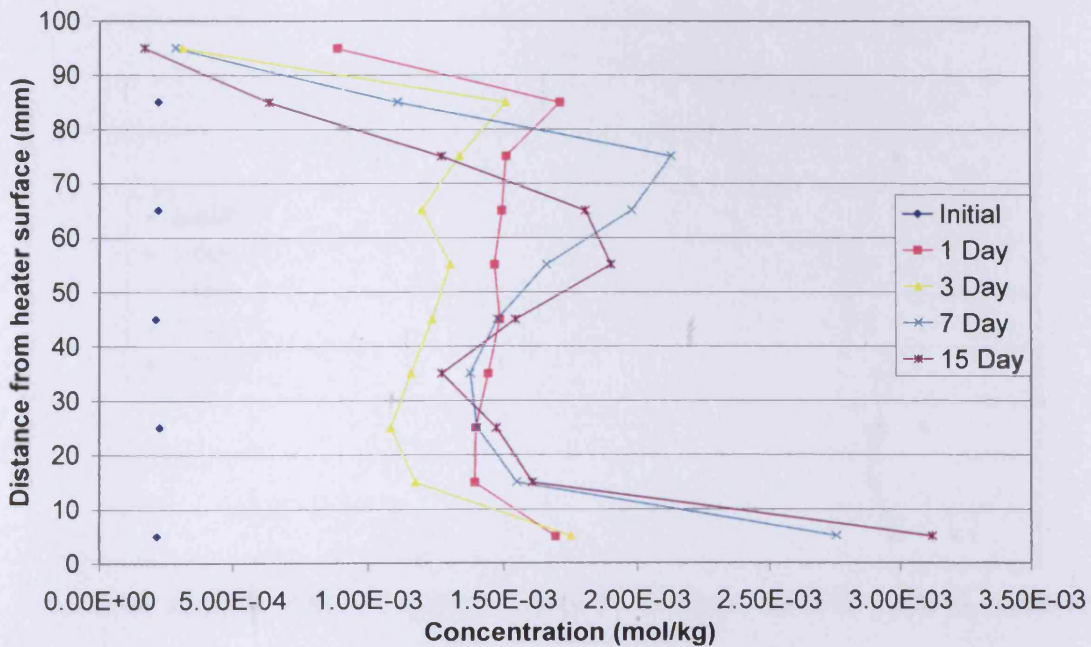
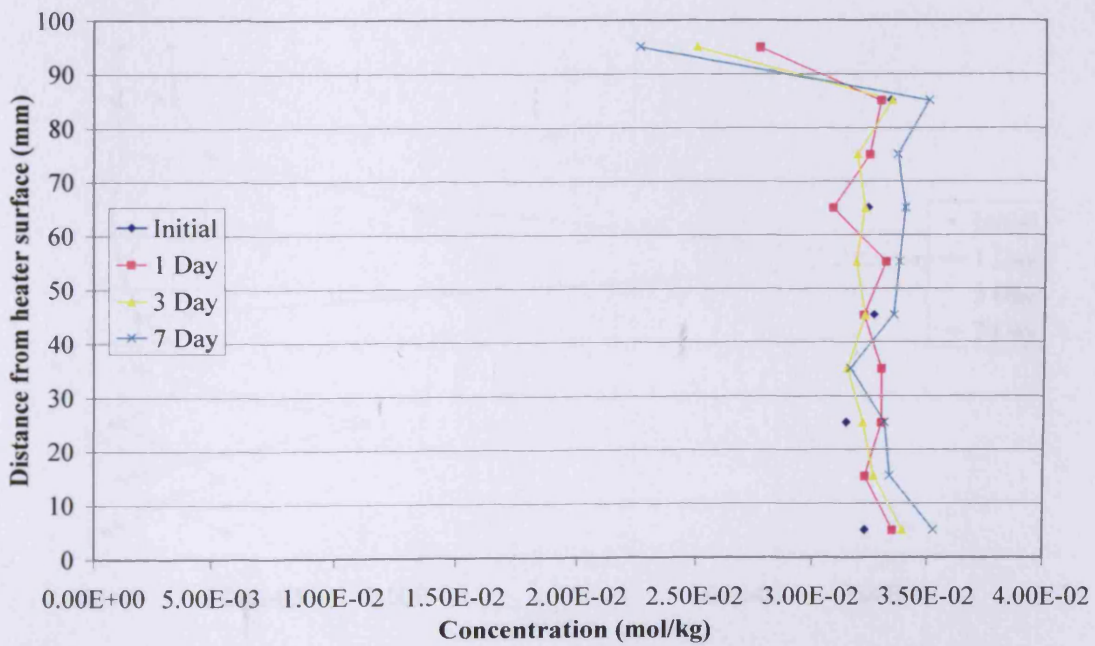**Figure 6.36 Nitrate distribution of MX-80 bentonite dry sample for TH test**
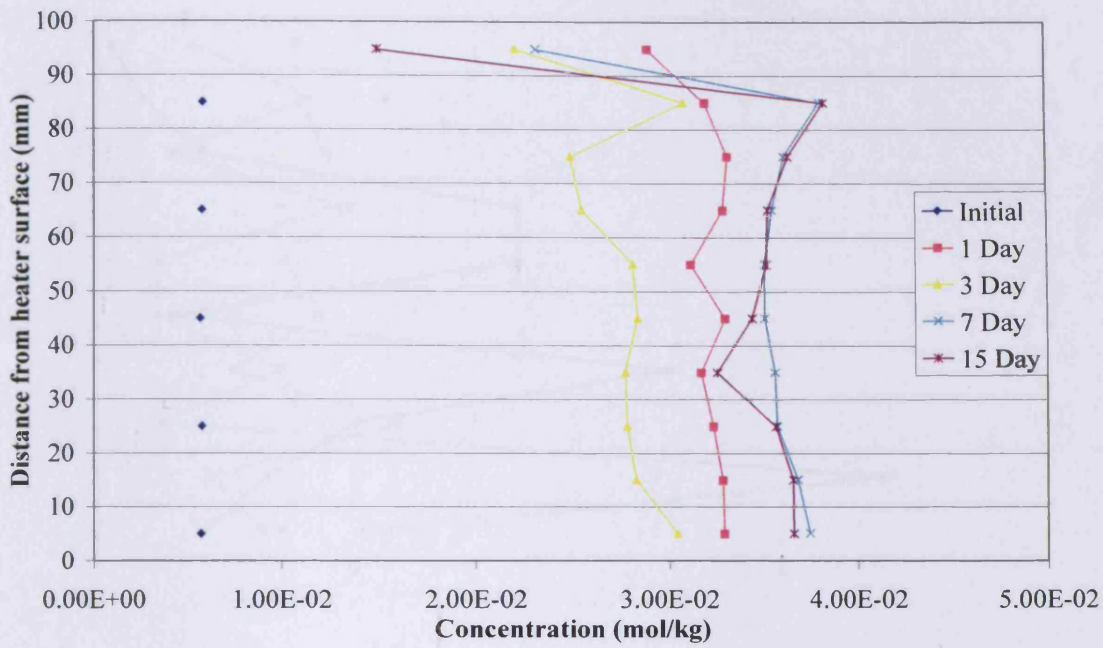
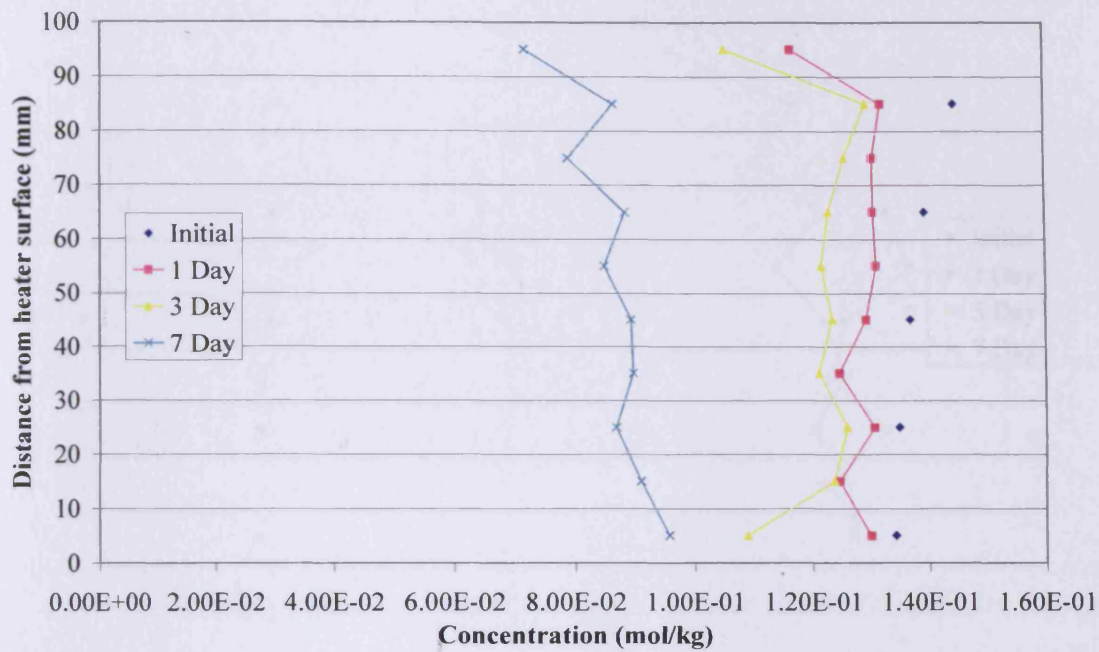**Figure 6.37 Sulphate distribution of MX-80 bentonite dry sample for TH test**
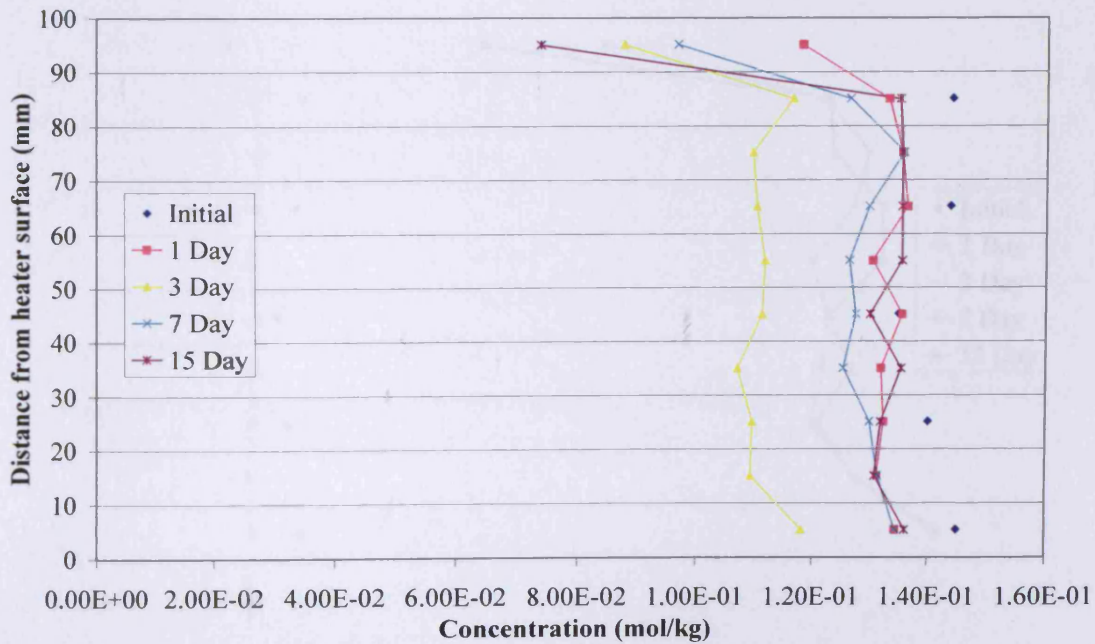
Figure 6.38 Sodium distribution of MX-80 bentonite dry sample for TH test
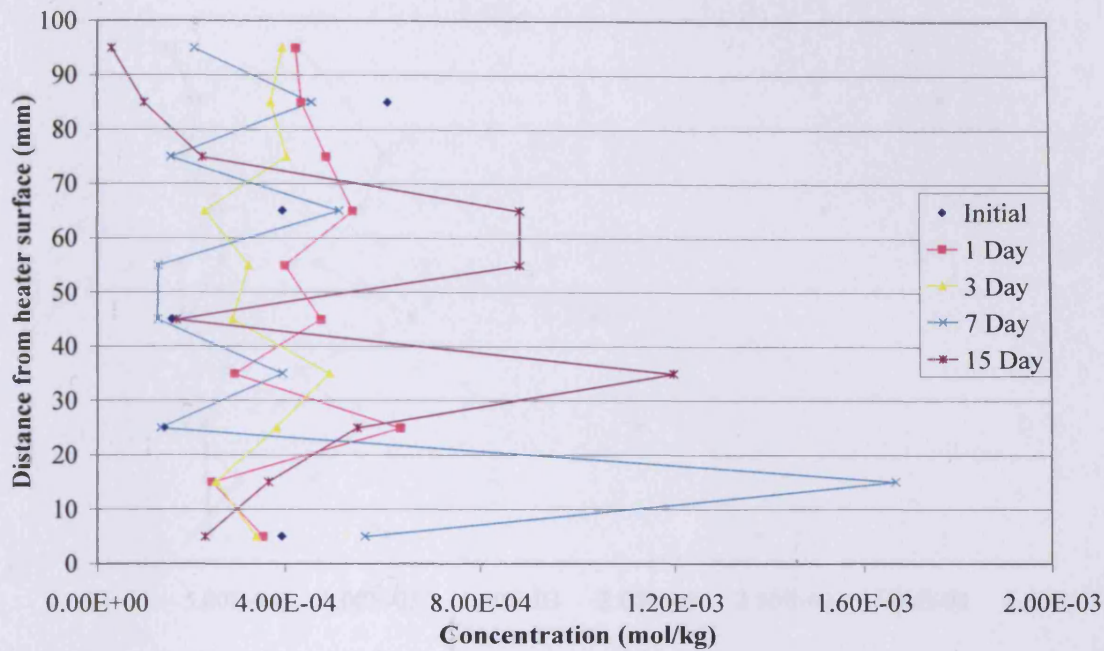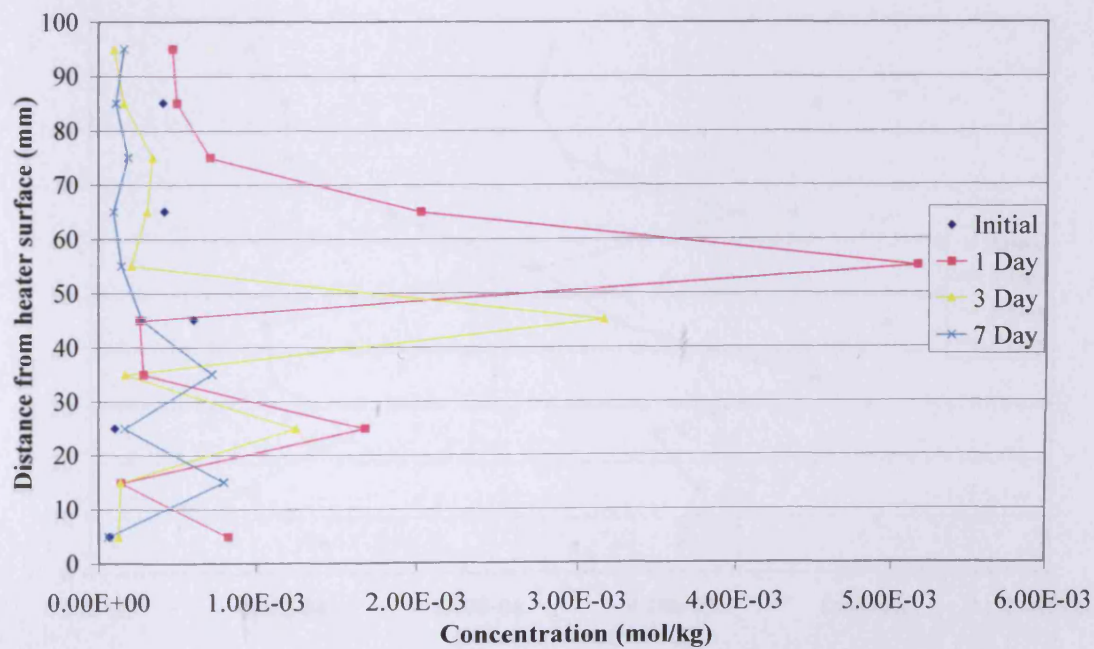
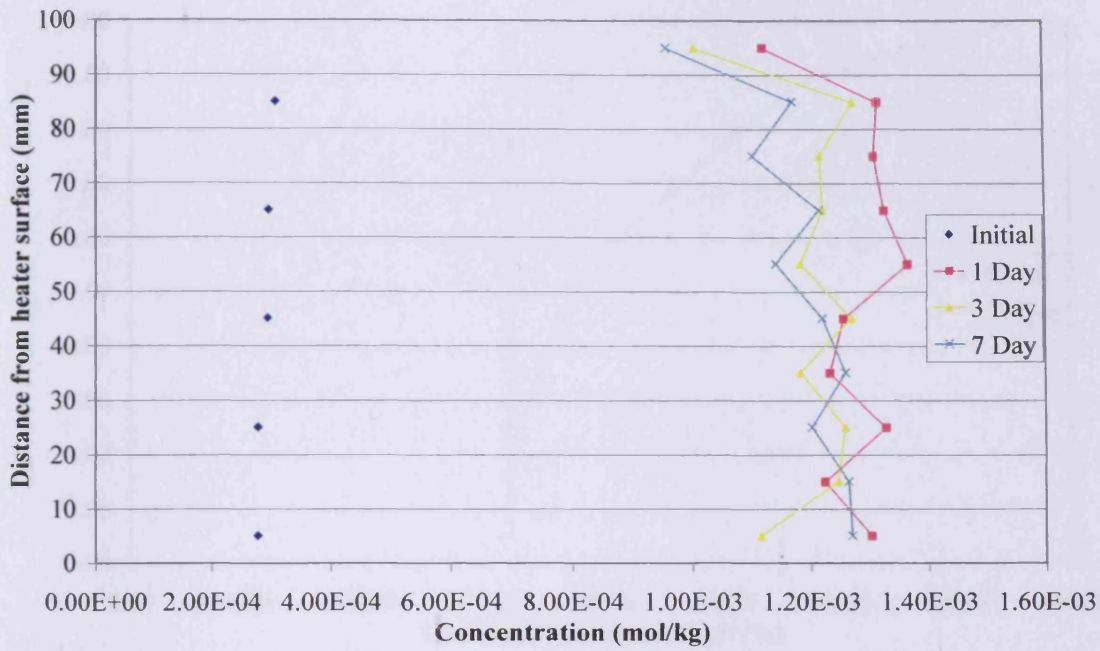**Figure 6.39 Magnesium distribution of MX-80 bentonite dry sample for TH test**
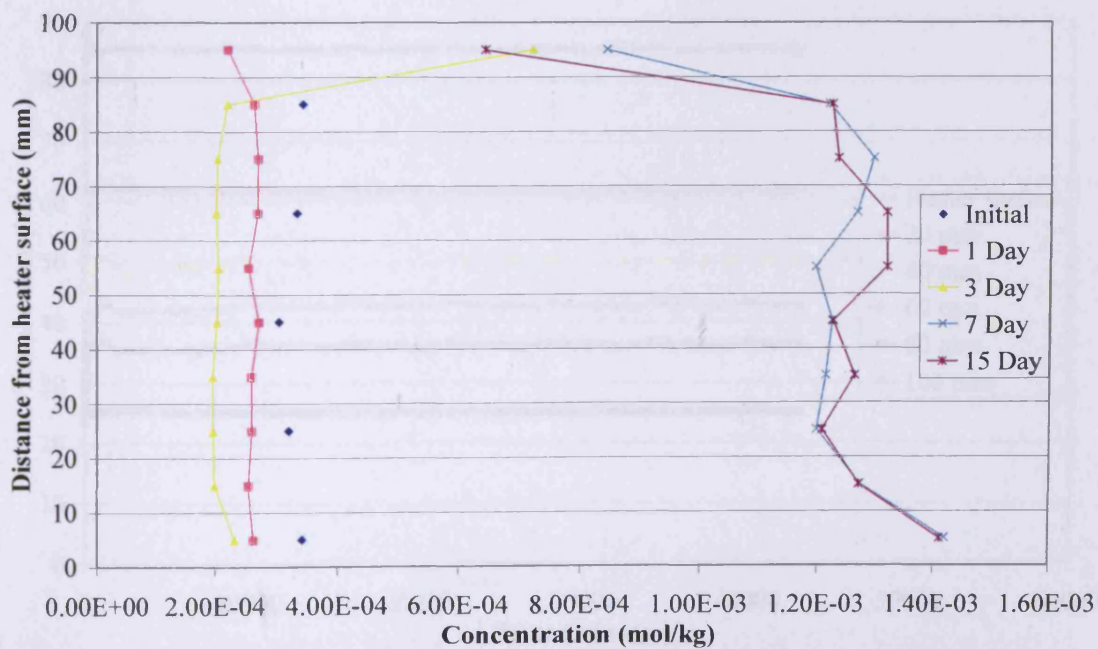
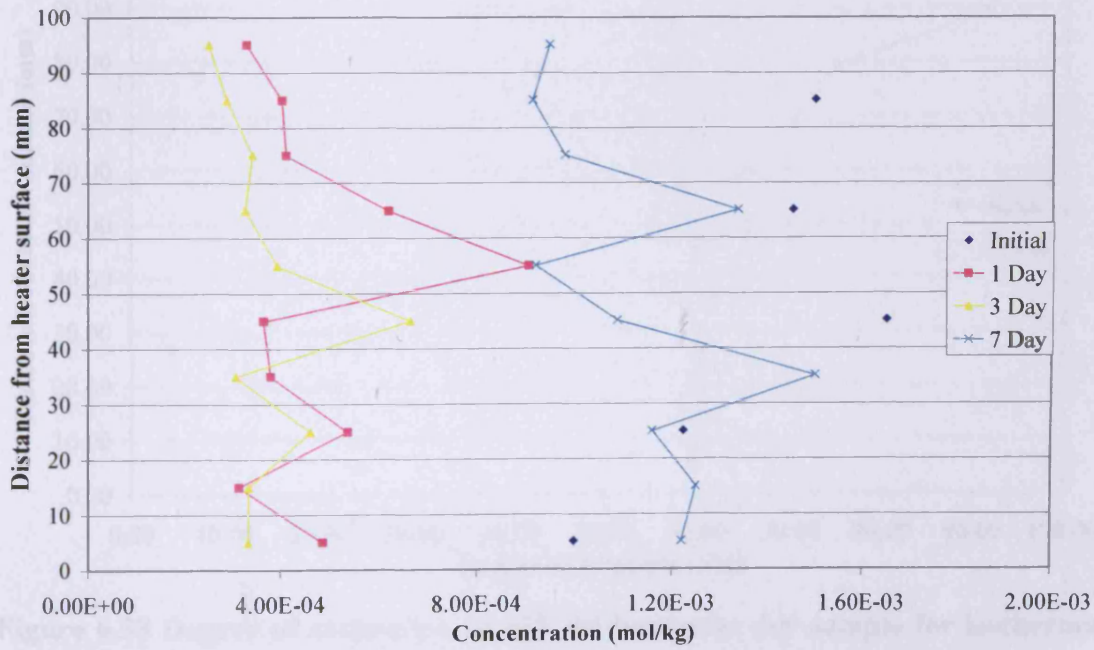**Figure 6.40 Potassium distribution of MX-80 bentonite dry sample for TH test**

Figure 6.41 Calcium distribution of MX-80 bentonite dry sample for TH test

Figure 6.42 Temperature distribution of MX-80 bentonite wet sample for TH test

Figure 6.43 Temperature profile of MX-80 bentonite wet sample for TH test
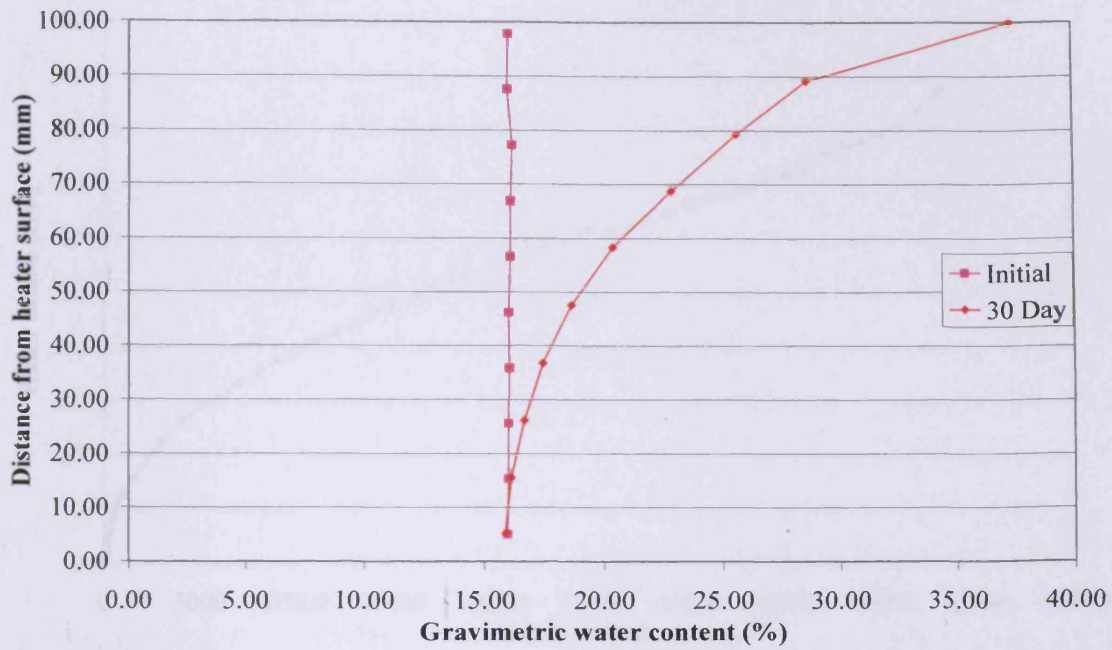

Figure 6.44 Gravimetric water content distribution of MX-80 bentonite wet sample for TH test

Figure 6.45 Degree of saturation of MX-80 bentonite wet sample for TH test

Figure 6.46 Relative humidity variation of MX-80 bentonite wet sample for TH test

Figure 6.47 Water intake by MX-80 bentonite wet sample for TH test

Figure 6.48 Dry density of MX-80 bentonite wet sample for TH test

Figure 6.49 Porosity of MX-80 bentonite wet sample for TH test

Figure 6.50 Chloride distribution of MX-80 bentonite wet sample for TH test

Figure 6.51 Nitrate distribution of MX-80 bentonite wet sample for TH test

Figure 6.52 Sulphate distribution of MX-80 bentonite wet sample for TH test

Figure 6.53 Sodium distribution of MX-80 bentonite wet sample for TH test

Figure 6.54 Magnesium distribution of MX-80 bentonite wet sample for TH test

Figure 6.55 Potassium distribution of MX-80 bentonite wet sample for TH test

Figure 6.56 Calcium distribution of MX-80 bentonite wet sample for TH test

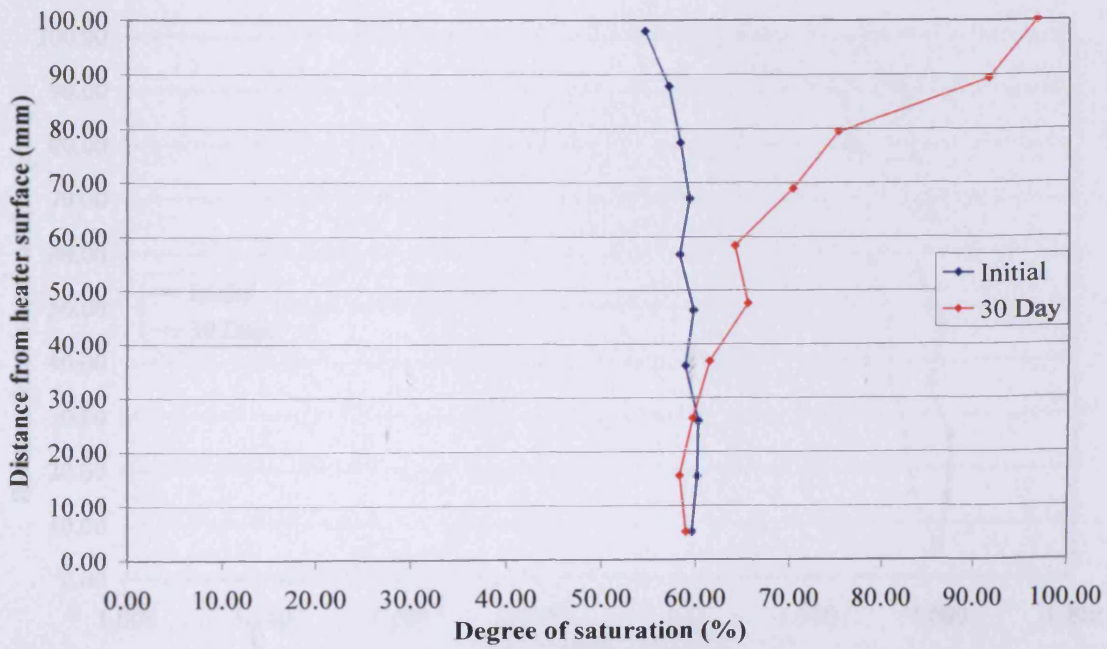**Figure 6.57 Gravimetric water content distribution of MX-80 bentonite dry sample isothermal test**

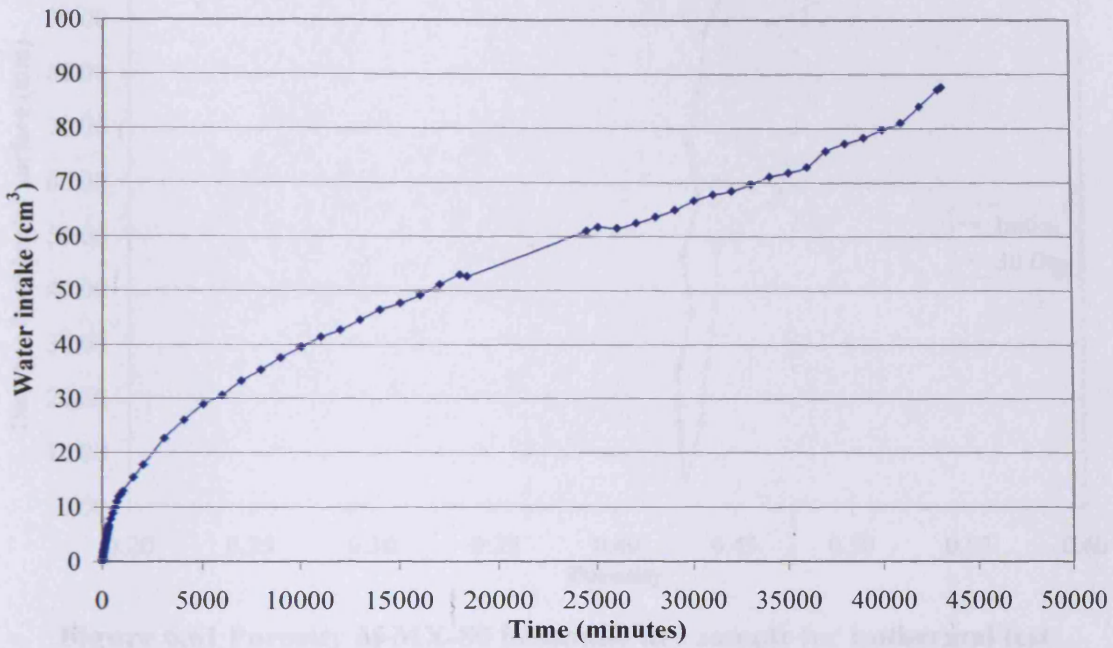**Figure 6.58 Degree of saturation of MX-80 bentonite dry sample for isothermal test**

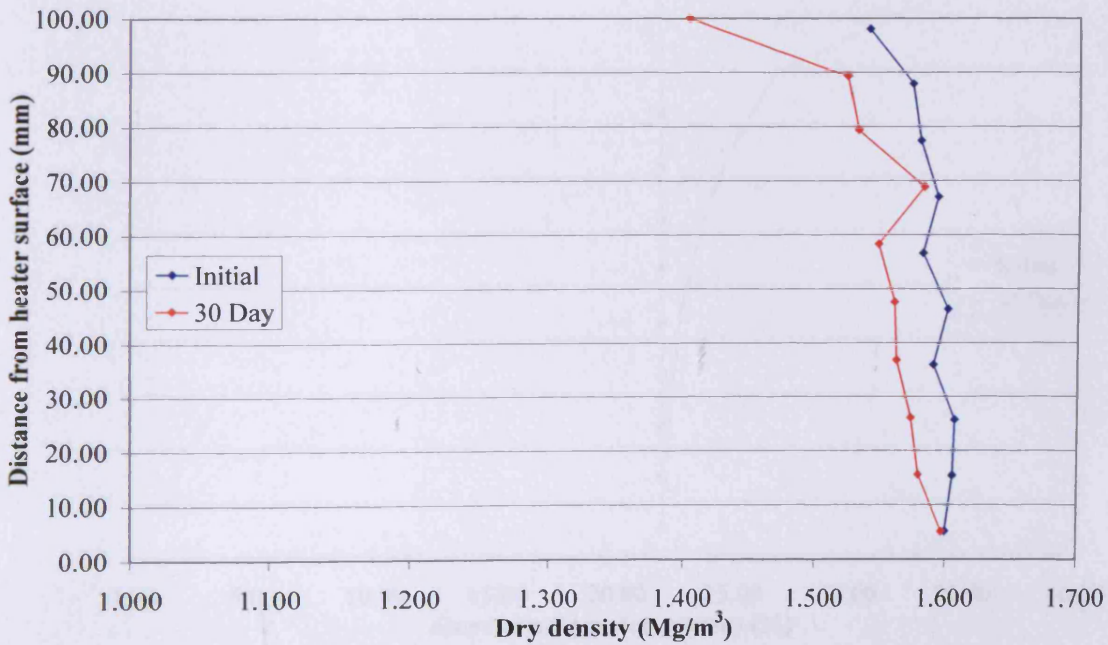**Figure 6.59 Water intake by MX-80 bentonite dry sample for isothermal test**

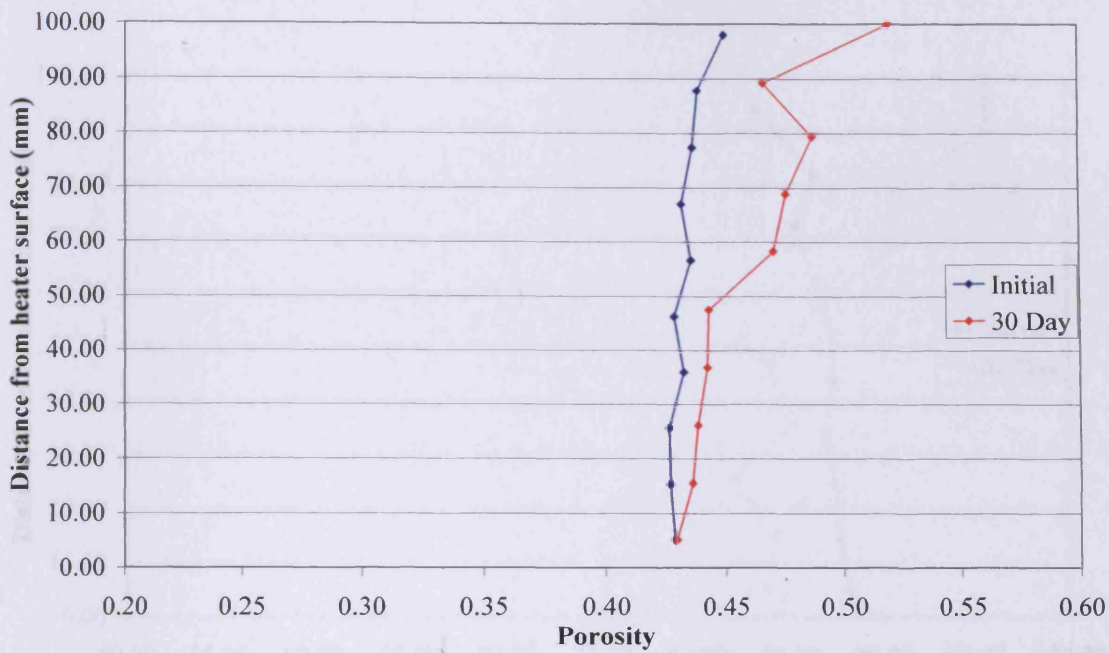**Figure 6.60 Dry density of MX-80 bentonite dry sample for isothermal test**

Figure 6.61 Porosity of MX-80 bentonite dry sample for isothermal test
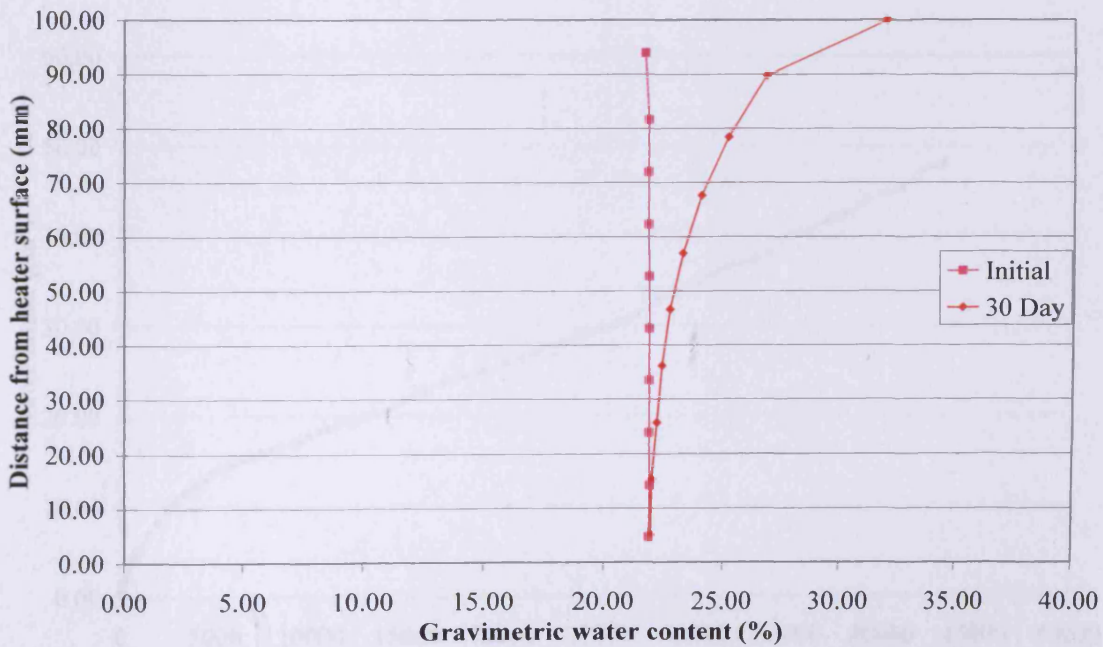

Figure 6.62 Gravimetric water content distribution of MX-80 bentonite wet sample for isothermal test
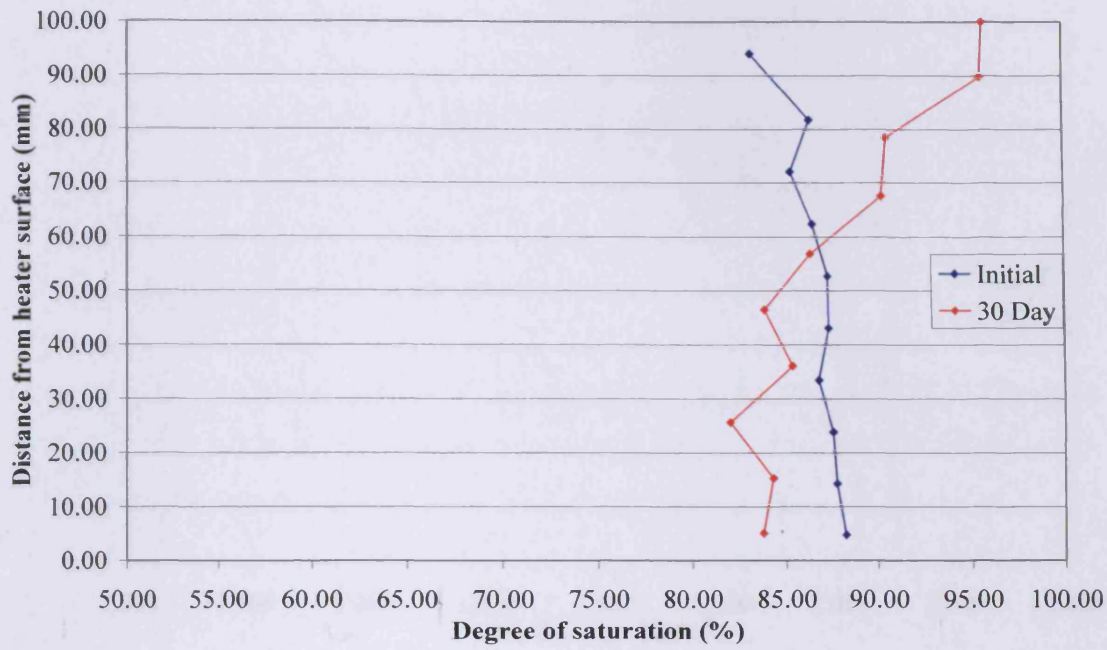
Figure 6.63 Degree of saturation of MX-80 bentonite wet sample for isothermal test
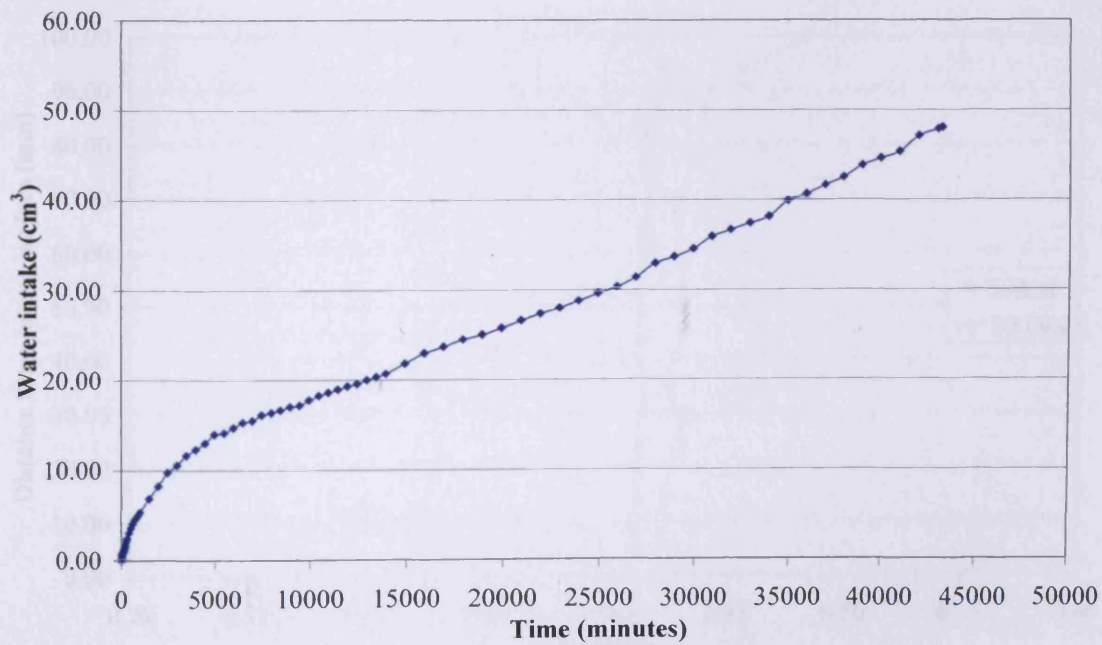

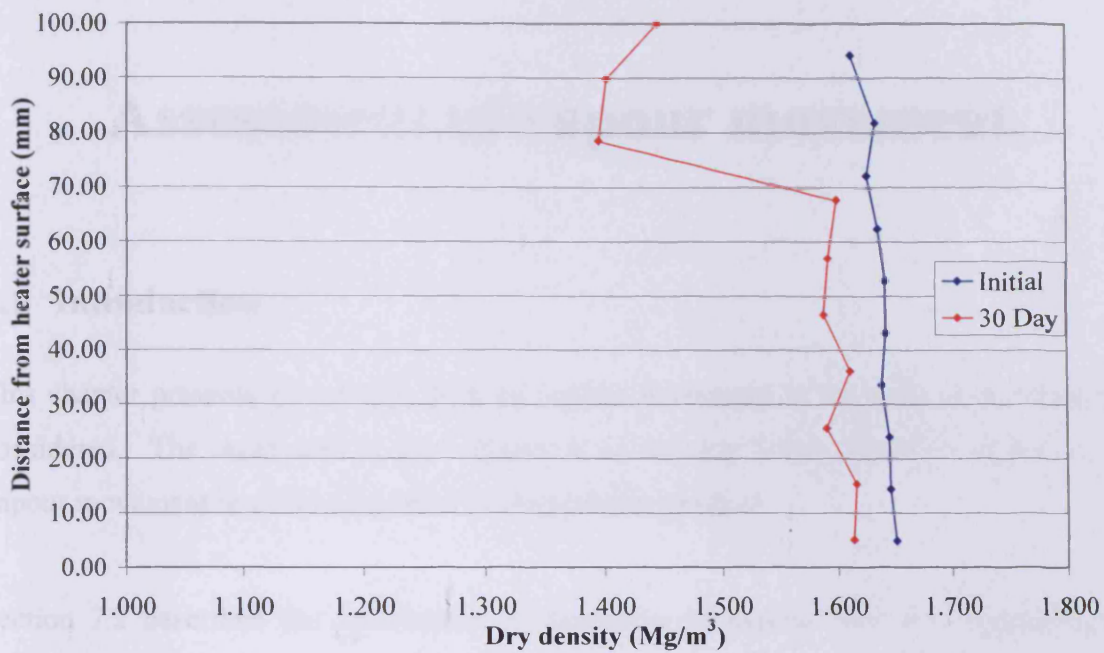**Figure 6.64 Water intake by MX-80 bentonite wet sample for isothermal test**

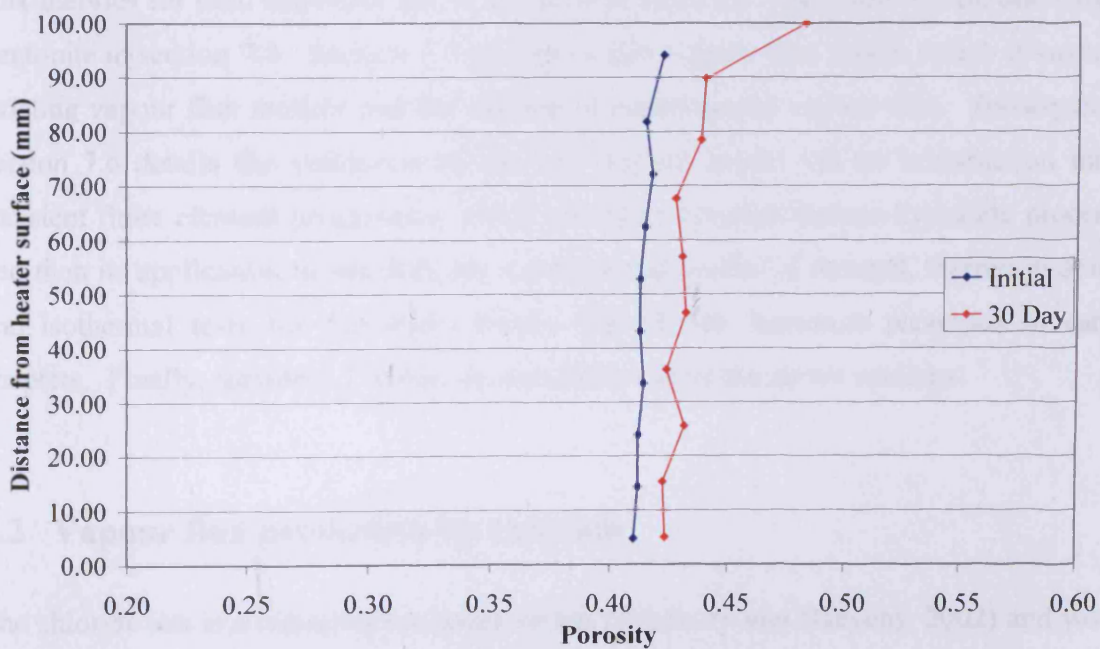**Figure 6.65 Dry density of MX-80 bentonite wet sample for isothermal test**

Figure 6.66 Porosity of MX-80 bentonite wet sample for isothermal test

Chapter 7

Assessment of vapour movement

7.1 Introduction

This chapter presents an investigation of vapour movement in the each of the materials considered. The main aim of this chapter is to develop a new model to represent the vapour movement in clays subjected to temperature gradient.

Section 7.2 describes the assessment of quantities of vapour flux by considering the movement of chloride ions. It explains the reason of choosing chloride ion as an indicator. The proposed empirical model to calculate the vapour flux based on the experimental measurement of the movement of chloride ions is presented in section 7.2. The vapour flux calculated by the empirical method is compared with the existing vapour flux theories for both materials use in the present study i.e. Speswhite kaolin and MX-80 bentonite in section 7.4. Section 7.5 presents a new vapour flux model which is based on existing vapour flux models and the calculated experimental vapour flux. Subsequently, section 7.6 details the validation of the new vapour model via its introduction into a transient finite element programme which considers coupled thermo-hydraulic processes and then its application to simulate the experimental results of thermal, thermo-hydraulic and isothermal tests for Speswhite kaolin and MX-80 bentonite presented in earlier chapters. Finally, section 7.7 draws the conclusion from the above sections.

7.2 Vapour flux prediction by chloride

The chloride ion is a conservative negative ion (Bradbury and Baeyens, 2002) and would be expected to move advectively with bulk liquid moisture. As the chloride movement is not affected by the negative charge of the clay particles little or no retardation will occur.

Gurr et al. (1952) found that the small amount of soluble salts acting as a tracer served to distinguish between liquid and vapour movement. They also found accumulation of chloride ions in the hotter regions of a soil. They worked out the vapour flux using the vapour diffusion equation of Penman (1940). This study investigates and proposes an empirical model for vapour flux determination based on vapour fluxes calculated from chloride ions movement.

7.3 Proposed empirical method of vapour flux calculation

As mentioned in earlier chapters, the soil samples were sliced and dried after each T test and TH test, and then chemically analysed to determine the various anions and cations. The chloride ions were measured for each slice and expressed as mol/kg of dry mass of soil slice.

The proposed empirical calculation determines the vapour flux using chloride ion concentration for each slice and is based on the assumption that advection is the dominant process occurring in the soil at this time and that diffusion processes are small and can be ignored. Considering the quantities of moisture movement this is not unreasonable. The proposed empirical model assumes that the soil sample consists of stack of layers on top of each other, as shown in Figure 7.1. A thermal gradient is applied across the soil sample with the higher temperature at the bottom end and the lower temperature at the top end. The bottom layer (first layer) initially (at time t = 0) has mass of chloride ions m_1^0. After the start of the test the first layer has an influx of chloride ions carried by liquid moisture from the next layer (layer two). At any time (t = t), the mass of chloride ions in first layer is m_1^t. The change in mass of chloride ion, Δm_1, in first layer can be determined as:

$$\Delta m_1 = m_1^t - m_1^0 \qquad (7.1)$$

Δm_1 is the mass of chloride that has entered into the first layer from the second layer with liquid moisture. The concentration of chloride ion in the second layer is known. The

chloride ion will move with liquid moisture to the first layer from the second layer with the existing concentration in second layer. Therefore, the amount of liquid moisture, ΔV_{liq1-2}, coming with chloride ions from the second layer to the first layer can be calculated as:

$$\Delta V_{liq1-2} = \frac{\Delta m_1}{C_{2m}}$$ (7.2)

where

$$C_{2m} = \frac{C_2^0 + C_2^t}{2}$$ (7.3)

C_{2m} is the average chloride concentration (in mg/l) in the second layer, C_2^0 is the initial chloride concentration (in mg/l) in second layer at time (t = 0), C_2^t is the chloride concentration (in mg/l) in second layer at any time (t = t).

The liquid moisture, ΔV_{liq1-2}, comes in from the second layer to the first layer and adds to the existing initial liquid moisture, $(V_{liq1}^0)_{exp}$, of the first layer. Therefore, the new liquid moisture, $(V_{liq1}^t)_{cal}$, in the first layer at any time (t = t) should be as:

$$(V_{liq1}^t)_{cal} = (V_{liq1}^0)_{exp} + \Delta V_{liq1-2}$$ (7.4)

It is likely that the moisture will move away in the vapour phase from the first layer to the top layers due to the thermal gradient. The amount of vapour movement, V_{v1-2}, from the first layer can be determined by the difference between the liquid moisture calculated by the above equation (7.4) and the liquid moisture, $(V_{liq1}^t)_{exp}$, measured by oven drying method for the first slice as:

$$V_{vl-2} = (V_{liq1}^{t})_{cal} - (V_{liq1}^{t})_{exp} \qquad (7.5)$$

Therefore, the vapour flux, q_{1-2}, across the interface between the first and the second layer can be determined by dividing the amount of vapour, V_{vl-2}, found from the equation (7.5), by total time, t, and cross sectional area, A, of the soil sample as:

$$q_{1-2} = \frac{V_{vl-2}}{A.t} \qquad (7.6)$$

This calculation can then be repeated for each interface moving up through the sample slice by slice. An example of vapour flux calculation is presented in Table 7.1. It should be noted that this method can only be applied to the sealed thermal tests.

7.4 Comparison with existing theories

In this section the vapour fluxes calculated by the above method in section 7.3 for each of the thermal tests, are compared against existing vapour flux theories. As mentioned in literature review chapter 2, the Philip and de Vries (1957) theory and Ewen and Thomas (1989) theory are often used and these are considered here.

According to Philip and de Vries (1957) the vapour flux can be determined by the equation 2.27 in chapter 2. Rewriting the equation 2.27 here:

$$v_v = -D_{TV}\nabla T - D_{MV}\nabla \theta_l \qquad (7.6)$$

where D_{TV} is the thermal vapour diffusivity and D_{MV} is the isothermal vapour diffusivity. They can be written as

$$D_{TV} = \frac{D_{atms}v_v}{\rho_l} f \frac{(\nabla T)_a}{(\nabla T)} \left(h \frac{d\rho_0}{dT} \right) \qquad (7.7)$$

and

$$D_{MV} = \frac{D_{atms} v_v \tau_v \theta_a}{\rho_l} \left(\rho_0 \frac{dh}{d\theta_l} \right) \qquad (7.8)$$

Ewen and Thomas (1989) modified the Philip and de Vries (1957) theory and proposed new D_{TV} and D_{MV} terms. According to Ewen and Thomas (1989) the thermal vapour diffusivity D_{TV} and the isothermal vapour diffusivity D_{MV} can be written as (for detail see chapter 2):

$$D_{TV} = \frac{D_{atms} v_v}{\rho_l} n \frac{(\nabla T)_a}{(\nabla T)} \left(h \frac{d\rho_0}{dT} \right) \qquad (7.9)$$

and

$$D_{MV} = \frac{D_{atms} v_v n}{\rho_l} \left(\rho_0 \frac{dh}{d\theta_l} \right) \qquad (7.10)$$

In the following sections the vapour flux calculated from the experimental results as described in section 7.3 is compared with the vapour flux calculated by the above two theories for both test materials used in this study.

7.4.1   Speswhite kaolin

Figures 7.2 - 7.5 present the vapour flux comparisons for the dry sample of Speswhite kaolin subjected to the 1, 3, 7 and 15 days thermal test. The vapour fluxes presented are average fluxes during 0 - 1, 1 - 3, 3 - 7 and 7 - 15 days. The vapour fluxes calculated from the experimental results by the proposed empirical method are considerably lower than the vapour fluxes calculated by Philip and de Vries (1957) and Ewen and Thomas (1989) theories. The reason for this is most likely that both theories are based on vapour movement in granular soils. The vapour flux would be less in the case of clays, as

although kaolin exhibits negligible swelling but its pore size is small compared to the granular soils. The vapour fluxes are reducing with time as would be expected due to less vapour available with the time near the hot end.

The vapour flux comparisons during 0 - 1, 1 - 3, 3 - 7 and 7 - 15 days, for the wet samples of Speswhite kaolin subjected to the thermal test, are shown in Figures 7.6 - 7.9. Again the vapour fluxes by the proposed empirical method are much lower than calculated by the theoretical approaches and also vapour fluxes are reducing with time.

7.4.2   MX-80 bentonite

Vapour flux comparisons during 0 - 1, 1 - 3, 3 – 7, 7 - 15 and 15 -30 days, for the dry samples of MX-80 bentonite subjected to the thermal test, are shown in Figures 7.10 - 7.14. The vapour flux determined experimentally is again much lower than calculated by both theories and vapour flux reducing with time. The fluxes are probably lower due to the swelling nature, small pore structure and less free water available in the benonite. The fluxes are smaller compared to Speswhite kaolin which is expected due to different interlayer structure and swelling properties of the two materials.

Figures 7.15 - 7.19 present the vapour flux comparisons during 0 - 1, 1 - 3, 3 – 7, 7 - 15 and 15 -30 days for the wet sample of MX-80 bentonite subjected to the 1, 3, 7, 15 and 30 days thermal test. Again the vapour fluxes calculated by proposed empirical method are less than the both existing theories and also vapour fluxes reducing with time.

7.5   New modified vapour model

As it can be seen the existing theories do not capture the vapour flux in the clays considered. A sensitivity analysis was carried out to modify the existing Philip and de Vries (1957) model so that the new modified model can represent the vapour flux observed empirically via consideration of movement of the chloride ions. New thermal vapour diffusivity and isothermal vapour diffusivity terms were obtained by applying the

factors η_1 and η_2 to the terms in equations (7.7 and 7.8) proposed by Philip and de Vries (1957). The new modified diffusivity terms are:

$$D_{TV} = \eta_1 \frac{D_{atms} V_v}{\rho_l} f \frac{(\nabla T)_a}{(\nabla T)} \left(h \frac{d\rho_0}{dT} \right)$$

(7.11)

and

$$D_{MV} = \eta_2 \frac{D_{atms} V_v \tau_v \theta_a}{\rho_l} \left(\rho_0 \frac{dh}{d\theta_l} \right)$$

(7.12)

The factors η_1 and η_2 are determined for both soil types by sensitivity analysis and introducing them into Philip and de Vries (1957) brings vapour flux values close to the empirical fluxes. The factors for Speswhite kaolin are found to be:

$\eta_1 = 0.22$ and $\eta_2 = 1.00$

The thermal vapour diffusivity, D_{TV}, is reduced but isothermal vapour diffusivity, D_{MV}, is kept same as in Philp de Vries (1957) theory. So the vapour fluxes are reduced by considerable amount after applying the above factors for the Speswhite kaolin which is evident from the Figures 7.20 and 7.21.

After a similar sensitivity analysis was carried out for MX-80 bentonite and the factors were found to be:

$\eta_1 = 0.17$ and $\eta_2 = 0.60$

In case of MX-80 bentonite, both the thermal vapour diffusivity, D_{TV}, and the isothermal vapour diffusivity, D_{MV}, are reduced more than that for Speswhite kaolin. This is done because the vapour fluxes in MX-80 are less compared to Speswhite kaolin. Figure 7.22

and 7.23 show the results from the new vapour flux model are almost equal to the vapour fluxes obtained experimentally.

7.6   New modified vapour model validation

The thermal - hydraulic gradient tests performed on each of the materials offer the posiblity of new vapour flux model being validated against the experimental results of the tests conducted on Speswhite kaolin and MX-80 bentonite. The new vapour diffusivity terms are introduced in to a finite element code (COMPASS, Code for Modelling *Partial* Saturated Soil) which is based on a mechanistic approach. COMPASS has been developed in Cardiff University and this development has been detailed by various researchers (Thomas and King, 1991; Thomas and He, 1995; Thomas and Sansom, 1995; Thomas et al. 1996; Thomas and Li, 1997; Thomas and Cleall, 1999; Wang, 2000; Seetharam, 2003). The code uses the same approach for heat and mass transfer that has been presented in sections 2.4 and 2.5 of chapter 2. A summary of theoretical development of the code is briefly discussed here but full details can be found in Thomas and King (1991), Thomas and He (1995) and Thomas and Sansom (1995). A numerical solution of the coupled equations is achieved via utilisation of the finite element method for spatial discretisation and the finite difference method for temporal discretisation, again full details can be found in Thomas and King (1991), Thomas and He (1995) and Thomas and Sansom (1995).

7.6.1   Theoretical formulation

The theoretical formulation is based on the consideration that an unsaturated soil is a three phase porous medium consisting of solid, liquid and gas. A set of coupled governing equations can be developed to describe the flow and deformation behaviour of the soil, although deformation behaviour is not considered in this study. The development of heat and mass flow equations is dealt with below. The primary variables considered are pore water pressure, pore air pressure, temperature and dsiplacement.

Heat transfer

Heat transfer is defined by conservation of heat energy via a classical conservation equation:

$$\frac{\partial \Omega}{\partial t} = -\nabla . Q$$

where, Ω is the heat content of unsaturated soil per unit volume that includes latent heat of vaporisation and the classical components of heat capacity and Q is the heat flux per unit area. The heat flux and its expression which includes conduction, convection and transfer of latent heat of vaporisation have been detailed in section 2.5 of chapter 2.

Moisture transfer

The governing equation for moisture transfer in an unsaturated soil can be expressed as:

$$\frac{\partial(\rho_l n S_l)}{\partial t} + \frac{\partial(\rho_v n(S_l - 1))}{\partial t} = -\rho_l \nabla . v_l - \rho_l \nabla . v_v$$

where, n is the porosity. The velocity of pore liquid is based on generalised Darcy's law which has been presented in section 2.4 of chapter 2. In the original model (Thomas and He, 1995; Thomas et al. 1996; Thomas and Cleall, 1999; Wang, 2000; Seetharam, 2003) the definition of vapour velocity is based on the flow laws proposed by Philip and de Vries (1957) and Ewen and Thomas (1989) as discussed earlier. But for this study, the vapour velocity is based on the new vapour model as presented in section 7.5.

7.6.2 Numerical simulation

A number of numerical analyses have been performed using the model described above which includes the new vapour model. The results of numerical analysis are compared

with the experimental results for both test materials presented in earlier chapters. Details of the analyses undertaken including definition of domain and its discretisation and defining the initial and boundary conditions are presented in the following sections.

7.6.2.1 Geometry and discretisation

The soil sample used in this study was cylindrical in shape of size 100 mm diameter and 100 mm height. An axisymmetric domain geometry has been considered. The boundary conditions applied to the sample results in an effectively pseudo 1D axisymmetric analyses being performed to investigate the validation of new vapour flux model. A uniform mesh of 50 and 8 noded isoparametric elements, as shown in Figure 7.24, and a time step of 3600 seconds has been found to yield converged results.

7.6.2.2 Initial conditions

The initial conditions applied depend upon the type of testing soil (i.e Speswhite kaolin and MX-80 bentonite) and the type of sample (i.e. dry and wet). The initial temperature is 25 °C as the both soils were prepared, mixed and stored in humidity and temperature controlled laboratories where the temperature is fixed at 25 ± 0.2 °C. Based on the initial degree of saturation the initial suction of the material was determined from the moisture retention curve based on the van Genuchten model (1980) presented in chapter 4. The initial conditions used in the analyses for both soils are detailed in Table 7.2.

7.6.2.3 Boundary conditions

Various boundary conditions have been used in the analyses depending upon the type of test i.e. thermal, thermo-hydraulic and isothermal. In all cases a zero heat flux insulating condition was applied to the side of the domain, to represent the insulation system used in experiments. The following additional boundary conditions, depending upon the type of test, are also applied.

Thermal test

In the present study, during the thermal gradient test the soil sample is subjected to bottom end temperature of 85 °C whilst the top end temperature is maintained at 25 °C. The same fixed boundary conditions were applied at both ends of the sample for numerical analyses. A zero flux hydraulic boundary condition was applied on all the surfaces.

Thermo-hydraulic test

In the present study, during thermal-hydraulic test (TH-test) soil samples were subjected to a thermal gradient of 0.6 °C/mm with temperatures of 25 °C and 85 °C applied at the top and bottom ends respectively, in addition to this deionised and de-aired water was supplied at the top end under a pressure of 0.6 MPa. Similarly, in the numerical analysis a fixed temperature boundary condition of 85 °C and 25 °C was applied at the base and the top respectively. A fixed pore water pressure of 0.6 MPa was applied at the top surface and a zero flux hydraulic boundary condition was applied on all other surfaces.

Isothermal test

A fixed boundary temperature of 25 °C was applied at both top and bottom ends of the sample. Similar to the TH test, a fixed pore water pressure of 0.6 MPa was applied at the top surface and with a zero flux hydraulic boundary condition applied on all the other surfaces.

7.6.2.4   Material parameters

The material parameters used in these analyses are based on the experimental results reported in chapter 2 and are summarised in Tables 7.3 and 7.4 for Speswhite kaolin and MX-80 bentonite respectively. It is to be noted that the tortuosity factor was adopted as 1 throughout the numerical analyses due to the lack of available data for the tested clays.

7.6.3 Numerical simulation results

The following sections discuss and compare the results obtained from the experimental and numerical analyses for both types of clays used in this study.

7.6.3.1 Speswhite kaolin

The comparison of experimental and numerical results for the dry and wet samples of Speswhite kaolin is presented in the following sections.

7.6.3.1.1 Dry sample

The comparison of experimental and numerical results for the dry sample of Speswhite kaolin is presented first.

Thermal test

The temperature profile results of the numerical analysis for the dry sample of Speswhite kaolin subjected to the thermal gradient for various time intervals are shown in Figure 7.25 alongside the experimental values. It can be seen that the numerical and experimental values are very close except for the 1 day results. At 1 day, numerical values are slightly higher than that obtained experimentally possibly due to some heat energy being taken by the cell and insulation materials.

The degree of saturation results of the numerical analysis are presented in Figure 7.26 alongside the experimental values for the dry samples of kaolin. The numerical analysis results and experimental values are quite similar at the hot end but at the cold end numerical values are showing more wetting compared to experimental results though with the time the difference between numerical and experimental values reduces. At the mid height of the sample both results follow the same trend.

Thermo-hydraulic test

The temperature profile results of both numerical and experimental methods for the TH tests are shown in Figure 7.27. It can be noted that the numerical analyses predict the temperature results considerably well. The degree of saturation results are presented in Figure 7.28. The numerical results predict that the sample saturates along its height within 3 days while the experimental results are not consistent. It is mentioned earlier in chapters 5 and 6 that there is about 5 % error in the measurement of degree of saturation. The difference between experimental and numerical results is not more that 5 % at various points hence it can be said that the numerical results predict the mass movement reasonably well.

Isothermal test

Figure 7.29 present the degree of saturation profile determined numerically and compared against experimental values for the isothermal test. The numerical results show the 100 % degree of saturation at every point within the sol sample after 15 days. The experimental values reach to 100 % saturation at some points near the bottom end, so the sample should have achieved complete saturation at the top end too because the water was supplied from the top end. Again, this can happen due to the measurement error in degree of saturation values. However, the numerical results are reasonable and predicting the moisture field quite well.

Figure 7.30 show the transient water intake profiles determined numerically and measured experimentally for the Speswhite kaolin subjected to the isothermal condition. The numerical water intake values are little higher than the experimental values. This is thought to be due to the measurement error in automatic volume change apparatus. At the start of the test, the soil sample takes in the water very quickly and the volume change apparatus response is not quick enough to record the faster rate.

7.6.3.1.2 Wet sample

The following paragraphs describe the numerical results and compare them against experimental values for the wet samples of Speswhite kaolin.

Thermal test

The thermal gradient profile results obtained numerically and experimentally are presented in Figure 7.31 for the wet samples of kaolin clay. It can be noted that the numerical results and experimental results are in reasonable agreement. Both results are changing simultaneously with time due to change in thermal properties of the material. This indicates that the numerical model predicts the temperature field accurately.

Figure 7.32 present the degree of saturation results of numerical analysis alongside the experimental values for the wet samples of kaolin subjected to thermal gradient test. It can be seen that near the hot end, the numerical results are showing more wetting and more drying near the cold end compare to the experimental values though 1 day and 5 days results are very close. Near the hot end the difference between the numerical and experimental results is quite high. This can happen due to the fast cyclic movement of moisture within the wet sample of kaolin clay which is mentioned in section 5.3.2.2 of chapter 5. This kind of fast cyclic behaviour could not be predicted by the numerical model used. Therefore, there is a need to investigate this behaviour further and possibly incorporate it in the numerical model.

Thermo-hydraulic test

Figures 7.33 show the temperature profile and degree of saturation along the sample height at various time intervals for the wet samples of kaolin determined by numerical and experimental methods. Again, the numerical model captures the thermal field quite precisely. The numerical results follow the experimental trend quite well.

The degree of saturation results for both numerical and experimental methods are shown in Figure 7.34. The numerical results show that sample reaches to 100 % saturation within 1 day at all the points. The experimental results are also very close to 100 % degree of saturation values almost every point. The inconsistency in experimental results is thought to be due the measurement error as mentioned earlier.

Isothermal test

The degree of saturation profiles for the wet sample of kaolin subjected to 15 days isothermal test is shown in Figures 7.35. The numerical results reach to 100 % degree of saturation at all the points and the experimental results are also showing 100 % degree of saturation almost all the points. Figure 7.36 compares the transient numerical and experimental results for water intake in the kaolin samples subjected to the isothermal test. It can be noted that in the beginning the numerical water intake rate is quite similar to experimental one. The numerical analysis predicts less total water intake amount at the end of 15 days compared to the experimental value. This is a result of the average porosity used in numerical analysis which has been given a constant value for all of the analysis presented here not representing the actual experimental values which are variable along the sample height.

7.6.3.1.3 Conclusions

The thermal profile of numerical analysis matches closely with the experimental values for both dry and wet samples of Speswhite kaolin subjected to various end conditions. The small differences between numerical and experimental results are attributed to the assumption of no heat loss across the boundaries of the soil sample in the numerical analysis.

The moisture results are presented in terms of degree of saturation and water intake. The degree of saturation results obtained by both numerical and experimental methods is quite close except for the wet sample subjected to the TH test. During the TH test, the wet samples show quick cyclic movement of moisture that can not be predicted numerically

and further investigation is required. The numerically simulated water intake values do not match exactly with experimental measurements. This is due to the error in volume measurements and the average porosity used for numerical analysis not fully matching the experimental conditions.

7.6.3.2   MX-80 bentonite

The numerical and experimental results for the dry and wet samples of MX-80 bentonite are presented in the following sections.

7.6.3.2.1 Dry sample

The following sections present the comparison of experimental and numerical results for the dry sample of MX-80 bentonite.

Thermal test

The temperature profile results of the numerical analysis for the dry sample of MX-80 bentonite subjected to the thermal gradient tests for various time intervals are shown in Figure 7.37 alongside the experimental values. It can be noted that numerical results are similar to the experimental values. At one day, there is a little difference between numerical and experimental values but the difference reduces with time. Overall the numerical results follow the experimental trend considerably well.

Figure 7.38 presents the degree of saturation results of the numerical analysis alongside the experimental values for the dry samples of bentonite subjected to the thermal tests. It can be seen that the numerical results show higher drying near the heater surface and higher wetting near the cold end. Near the hot end, the numerical values for 1, 3 and 7 days lie very close to the experimental values and then there is a little difference between the values after 15 and 30 days. Near the cold end, there is a little difference between the numerical and experimental results. Overall the numerical results follow the

experimental trend well and the difference between the values can be due to the measurement error in experimental values.

Thermo-hydraulic test

Figures 7.39 present the temperature profile results determined numerically and measured experimentally for the dry samples of bentonite subjected the thermo-hydraulic gradient. It can be seen that there is a little difference between numerical and experimental results but still numerical results the capture the thermal field very well. The difference between the both results could be due to the assumption of no heat loss across the boundaries of soil sample in the numerical analysis.

Figure 7.40 presents the degree of saturation results obtained numerically as well as experimentally for the MX-80 bentonite samples subjected to the TH test. It can be seen that again numerical results are quantitatively matching very well to the experimental values along the sample height.

Isothermal test

The degree of saturation results determined numerically and compared against the experimental values for the dry samples of MX-80 bentonite subjected to 30 days isothermal test are shown in Figure 7.41. The numerical results are very close to the experimental values for the bottom half of the bentonite sample but for the top half there is a little difference between both results. The difference can be due the measurement error in degree of saturation during experiments. However the numerical analysis captures the experimental trend reasonably well.

Figure 7.42 presents the transient water intake profiles determined numerically and measured experimentally for the dry samples of bentonite subjected to the isothermal condition. The numerical water intake rate is less compared to that obtained experimentally. The total water intake amount predicted numerically is also quite less compared to the measured experimental value at the end of 30 days. This can be largely

attributed to the non uniform initial moisture content in the soil sample as shown in Figure 7.41.

7.6.3.2.2 Wet sample

The following sections present the numerical results and compare them against experimental values for the wet samples of MX-80 bentonite.

Thermal test

The thermal gradient profile results obtained numerically and experimentally are presented in Figure 7.43 for the wet samples of bentonite subjected to the thermal tests. It can be seen that numerical and experimental results are similar except little difference between the values at the mid height of the soil sample. The difference could be due to radial heat loss not being considered in the numerical analysis.

The degree of saturation results of numerical analysis alongside the experimental values for the wet samples of bentonite subjected to thermal gradient test are shown in Figure 7.44. The numerical results show the higher drying near the hot end and higher wetting near the cold end. Initially both results are quite close but the difference increases with the time. However, overall the numerical results are predicting the trends of the experimental results well.

Thermo-hydraulic test

The temperature profile results along the sample height at various time intervals for the wet samples of bentonite determined by numerical and experimental methods are presented in Figures 7.45. The numerical analysis show the higher temperature values compared to the experimental one. This is happening again due to the assumption of no heat loss across the boundaries of the soil sample during numerical analysis. The degree of saturation results obtained both numerically and experimentally is shown in Figure

7.46. The numerical results capture the moisture field well except slightly higher drying with the time at the hot end.

Isothermal test

The degree of saturation for the wet sample of bentonite subjected to the 30 days isothermal test are presented in Figures 7.47. The numerical results predicting higher degree of saturation at every point compared to the experimental results. The experimental results are indicating lower degree of saturation for the bottom half of the sample which is down to variation in the sample preparation and experimental error in the measurement of the degree of saturation. Figure 7.48 presents the water intake results obtained numerically and measured experimentally. Again the numerical results are not matching with the experimental results. This happens due to the constant average porosity used in the numerical analysis.

7.6.3.2.3 Conclusions

The thermal profiles results for MX-80 bentonite are well captured by numerical analysis. The little difference between the results can be due to neglecting the heat loss in numerical analysis. The degree of saturation results predicted by new modified model vapour model is close to the experimental values except higher drying near the hot end predicted by the numerical model. Overall, the numerical analysis captures the moisture field well. The water intake determined numerically does not match with the experimental values for MX-80 bentonite as happened with Speswhite kaolin. As mentioned earlier the reasons are same that the average porosity used in numerical analysis is not same throughout the sample height and possibly the volume measurement error.

7.7 Overall conclusions

The new empirical method of predicting and calculating the vapour flux by using the chloride ions concentration distribution is presented. The empirical vapour flux values for both kaolin and bentonite clays are quite small compared to that calculated by Philip and de Vries (1957) theory and Ewen and Thomas (1989) theory. The existing theories are applicable to rigid matrix and needed to be changed. Hence, the new vapour flux model has been developed by introducing the factors to thermal diffusivity and isothermal diffusivity terms of Philp and de Vries (1957). The new vapour flux model has been introduced in the finite element code COMPASS and numerical analyses have been carried out.

The thermal and moisture regime is generally well captured by numerical analysis for both clays subjected to various end conditions. The water intake profiles determined numerically are not matching exactly due to the volume measurement error in the automatic volume change apparatus and the uniform average porosity used for numerical analysis not always reflecting the experiment condition. Overall the introduction of new vapour flux model improves the numerical analysis capability of finite element code.

The numerical results are very sensitive to hydraulic and thermal material parameters. There is a need to determine the material parameters in the same conditions as used in the numerical analysis. The factors applied to the diffusivity terms in the vapour flux equation are constant but the vapour flux reduces with the time. It would be interesting to investigate the dependency of the factors on the rates of drying and wetting. It is recognised that due to the time constraints in this study the new modified vapour model was applied to only for heat and mass problem. Further investigation is required to include the deformation and chemical species movement.

7.8 References

Bradbury, M.H. and Baeyens, B. (2002). Porewater chemistry in compacted re-saturated MX-80 bentonite: Physico-chemical characterisation and geochemical modelling. PSI Bericht Nr Switzerland.

Cleall, P.J. (1998). An investigation of the thermo/hydraulic/mechanical behaviour of unsaturated soils, including expansive clays. Ph.D Thesis, Cardiff University, Wales.

Ewen, J. and Thomas, H.R. (1989). Heating unsaturated medium sand. Geotechnique, 39, 455-470.

Gurr, C.G., Marshall, T.J. and Hutton, J.T. (1952). Movement of water in soil due to a temperature gradient. Soil Sci., Vol. 74, No. 5, 335-345.

Penman, H.L. (1940). Gas and vapour movements in the soil. Int. Jour. Agr. Sci.30, 437-462.

Philip, J.R. and De Vries, D.A. (1957). Moisture movement in porous materials under temperature gradients. Trans. Amer. Geophys. Union, 38, 222-232.

Seetharam, S.C. (2003). An investigation of the thermo/hydro/chemical/mechanical behaviour of unsaturated soils. PhD thesis, Cardiff School of Engineering, UK.

Thomas, H.R. and Cleall, P.J. (1999). Inclusion of expansive clay behaviour in coupled thermo hydraulic mechanical models. Engineering Geology, 54, 93-108.

Thomas, H.R. and He, Y. (1995). Analysis of coupled heat, moisture and air transfer in a deformable unsaturated soil. Geotechnique, 45, No. 4, 677-689.

Thomas, H.R., He, Y., Sansom, M.R. and Li, C.L.W. (1996). On the development of a model of the thermo-mechanical-hydraulic behaviour of unsaturated soils. Engineering Geology, 41, 197-218.

Thomas, H.R. and King, S.D. (1991). Coupled temperature/capillary potential variations in unsaturated soil. Journal of Engineering Mechanics, American Society of Civil Engineers, 117, No. 11, 2475-2491.

Thomas, H.R. and Li, C.L.W. (1997). An assessment of a model of heat and moisture transfer in unsaturated soil. Geotechnique, 47, No. 1, 113-131.

Thomas, H.R. and Sansom, M.R. (1995). Fully coupled analysis of heat, moisture and air transfer in unsaturated soil. Journal of Engineering Mechanics, ASCE, 121, No. 3, 392-405.

van Genuchten, M. T. (1980). A closed-form equation for predicting the hydraulic conductivity of unsaturated soils. Soil Sci. Soc. Am. J., 44, 892–898.

Wang, J. (2000). Transient and dynamic thermo/hydraulic/mechanical behaviour of partially saturated soil. Ph.D. Thesis, Cardiff University, Wales.

Table 7.1 Empirical method of vapour flux calculation

Slice no	Initial (t=0) water content (g)	At any time (t=t) water content (g)	Initial (t=0) chloride conc. (mg/l)	At any time (t=t) chloride conc. (mg/l)	Initial (t=0) chloride mass (mg)	At any time (t=t) chloride mass (mg)	Chloride moved in (mg)	Liquid moisture moved in (g)	Liquid moisture (g)	Vapour amount (g)	Vapour flux (kg/m²s)
10	12.29	16.08	144.77	109.06	1.78	1.75	-0.03	0	0	0	0
9	14.14	16.89	141.22	134.93	2.00	2.28	0.28	2.22	16.36	0.53	7.76E-07
8	14.22	16.24	141.17	136.57	2.01	2.22	0.21	1.52	15.74	0.50	7.30E-07
7	13.75	15.61	143.12	136.04	1.97	2.12	0.16	1.12	14.87	0.74	1.09E-06
6	14.54	15.35	140.08	136.24	2.04	2.09	0.05	0.39	14.93	0.42	6.18E-07
5	14.12	14.84	138.78	123.52	1.96	1.83	-0.13	-0.92	13.20	1.64	2.41E-06
4	14.11	14.27	139.41	112.36	1.97	1.60	-0.36	-2.77	11.34	2.93	4.32E-06
3	14.05	13.28	140.60	106.12	1.98	1.41	-0.57	-4.50	9.55	3.73	5.49E-06
2	$(V_{liq2}^0)_{exp}$ =14.01	$(V_{liq2}^t)_{exp}$ =11.61	C_2^0 =141.71	C_2^t =95.51	m_2^0 =1.99	m_2^t =1.11	Δm_2 =-0.88	$\Delta V_{liq2\text{-}3}$ =-7.11	$(V_{liq2}^t)_{cal}$ =6.90	$V_{v2\text{-}3}$ =4.71	$q_{2\text{-}3}$ =6.93E-06
1	$(V_{liq1}^0)_{exp}$ =14.05	$(V_{liq1}^t)_{exp}$ =5.21	C_1^0 =144.31	C_1^t =736.89	m_1^0 =2.03	m_1^t =3.84	Δm_1 =1.81	$\Delta V_{liq1\text{-}2}$ =15.27	$(V_{liq1}^t)_{cal}$ =29.32	$V_{v1\text{-}2}$ =-24.11	$q_{1\text{-}2}$ =3.55E-05

Table 7.2 Initial conditions of both kaolin and bentonite for numerical analysis

Conditions	Speswhite kaolin		MX-80 bentonite	
	Dry	Wet	Dry	Wet
Specific gravity	2.61	2.61	2.80	2.80
Porosity	0.38	0.38	0.43	0.43
Dry density (Mg/m^3)	1.63	1.63	1.63	1.63
Temperature (K)	298	298	298	298
Degree of saturation (%)	47 %	84 %	60 %	88 %
Pore water pressure (MPa)	-1.40	-0.32	-18.4	-6.95

Table 7.3 Material parameters used for Speswhite kaolin for numerical analysis

Parameters	Function / constant	Reference
Absolute reference temperature (K)	298	-
Hydraulic parameters Saturated hydraulic conductivity, k_{sat} (m/s) Unsaturated hydraulic conductivity, k_l, (m/s) Moisture retention curve	1.02×10^{-10} $k_l = (S_l)^\delta k_{sat}$ and $\delta = 3$ $\dfrac{\theta_l - \theta_{lr}}{\theta_{ls} - \theta_{lr}} = \left[\dfrac{1}{1 + (\alpha s)^n} \right]^m$ Where $\alpha = 0.015, n = 1.9$ $m = 0.474, \theta_{lr} = 0.0001$ $\theta_{ls} = $ porosity $ = 0.38$	Section 4.5 of Chapter 4 Section 4.5 of Chapter 4 Section 4.5 of Chapter 4
Thermal soil parameters Thermal conductivity, λ, (W/mK) Specific heat capacity, C_{ps}, (J/kgK)	$\lambda = f(\theta_l)$ 800	Section 4.6 of Chapter 4 Section 4.6 of Chapter 4
Soil liquid moisture Density, ρ_l, (kg/m^3) Thermal conductivity, λ_l, (W/mK) Latent heat of vaporisation, L, (J/kg)	1000 0.6 2.4×10^6	Thomas, et al (1996) Thomas, et al (1996) Thomas, et al (1996)
Soil vapour moisture Specific heat capacity, C_{pv}, (J/kgK) Specific gas constant, R_v, (J/kgK)	1870 461.5	Thomas, et al (1996) Thomas, et al (1996)

Table 7.4 Material parameters used for MX-80 bentonite for numerical analysis

Parameters	Function / constant	Reference
Absolute reference temperature (K)	298	-
Hydraulic soil parameters Saturated hydraulic conductivity, k_{sat}, (m/s) Unsaturated hydraulic conductivity, k_l, (m/s) Moisture retention curve	 1.25×10^{-13} $k_l = (S_l)^{\delta} k_{sat}$ and $\delta = 3$ $\dfrac{\theta_l - \theta_{lr}}{\theta_{ls} - \theta_{lr}} = \left[\dfrac{1}{1 + (\alpha s)^n} \right]^m$ Where $\alpha = 0.00075 , n = 1.9$ $m = 0.474 , \theta_{lr} = 0.0001$ $\theta_{ls} = $ porosity $ = 0.43$	 Section 4.5 of Chapter 4 Section 4.5 of Chapter 4 Section 4.5 of Chapter 4
Thermal soil parameters Thermal conductivity, λ, (W/mK) Specific heat capacity, C_{ps}, (J/kgK)	 $\lambda = f(S_l)$ 800	 Section 4.6 of Chapter 4 Section 4.6 of Chapter 4
Soil liquid moisture Density, ρ_l, (kg/m^3) Thermal conductivity, λ_l, (W/mK) Latent heat of vaporisation, L, (J/kg)	 1000 0.6 2.4×10^6	 Thomas, et al (1996) Thomas, et al (1996) Thomas, et al (1996)
Soil vapour moisture Specific heat capacity, C_{pv}, (J/kgK) Specific gas constant, R_v, (J/kgK)	 1870 461.5	 Thomas, et al (1996) Thomas, et al (1996)

At time t=0

Cold end

10
9
8
7
6
5
4
3
2
1

Hot end

At time t=t

Cold end

10
9
8
7
6
5
4
3
2
1

Hot end

Liquid + Chloride ions

Vapour

Figure 7.1 Soil sample consists of layers for empirical method of vapour flux calculation
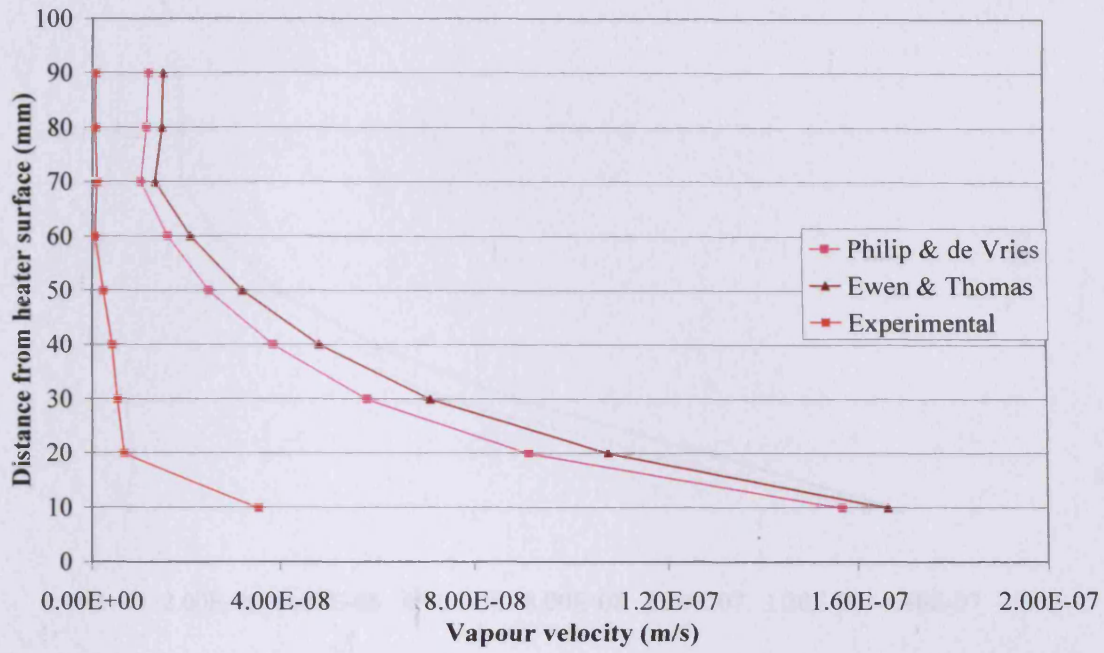
Figure 7.2 Vapour flux for the dry sample of Speswhite kaolin during 1 day thermal test
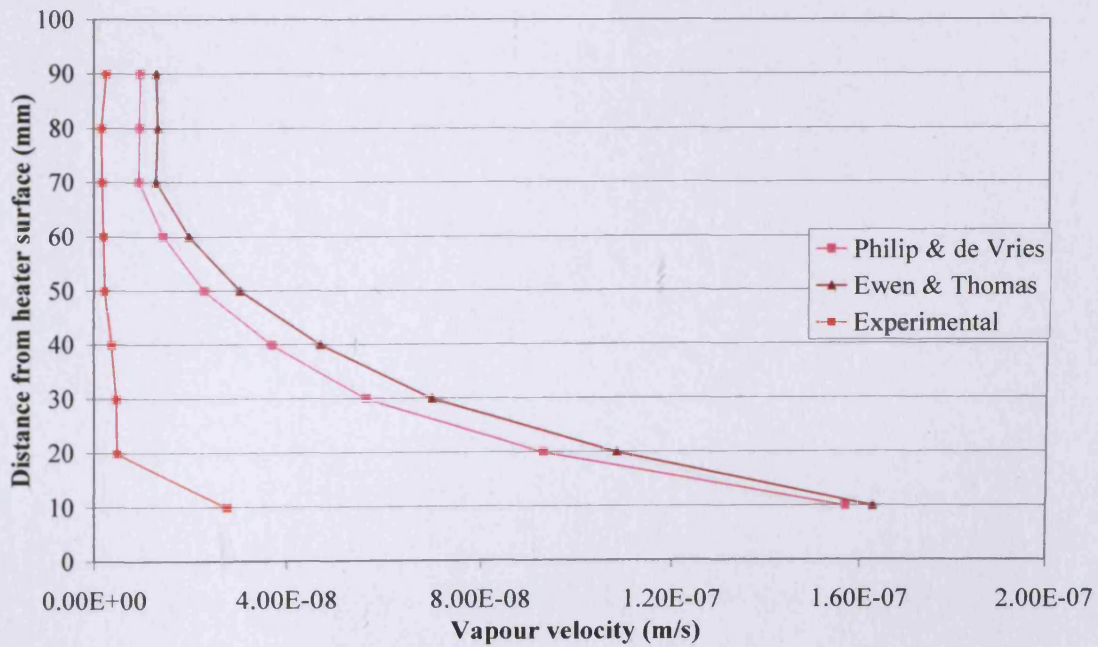
Figure 7.3 Vapour flux for the dry sample of Speswhite kaolin during 1 to 3 day thermal test
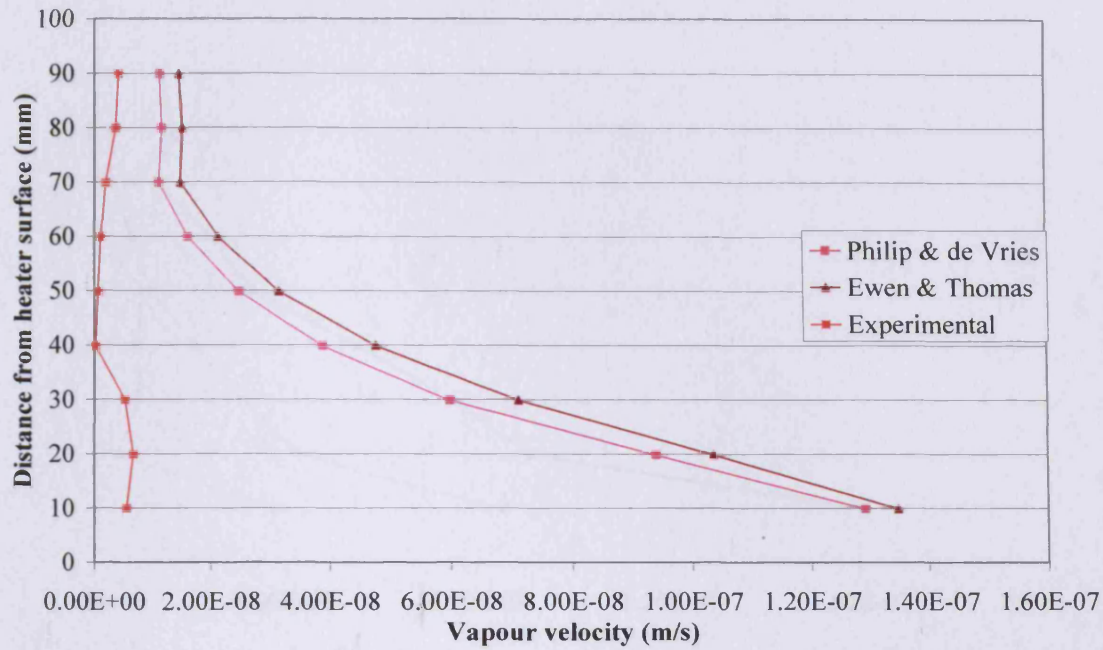
Figure 7.4 Vapour flux for the dry sample of Speswhite kaolin during 3 to 7 day thermal test
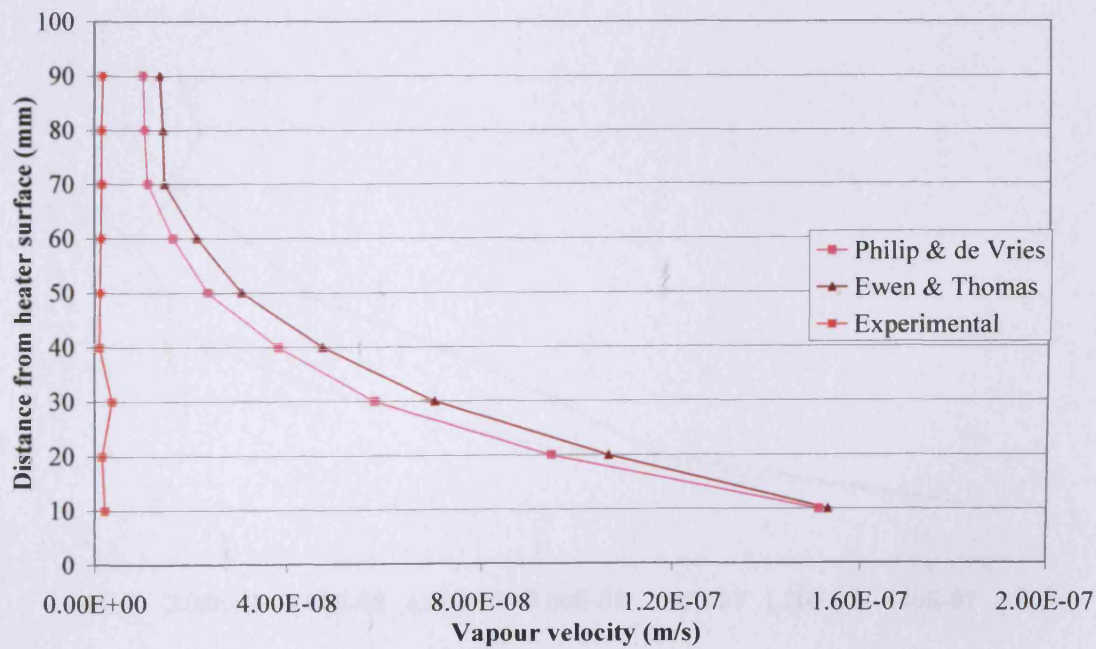
Figure 7.5 Vapour flux for the dry sample of Speswhite kaolin during 7 to 15 day thermal test
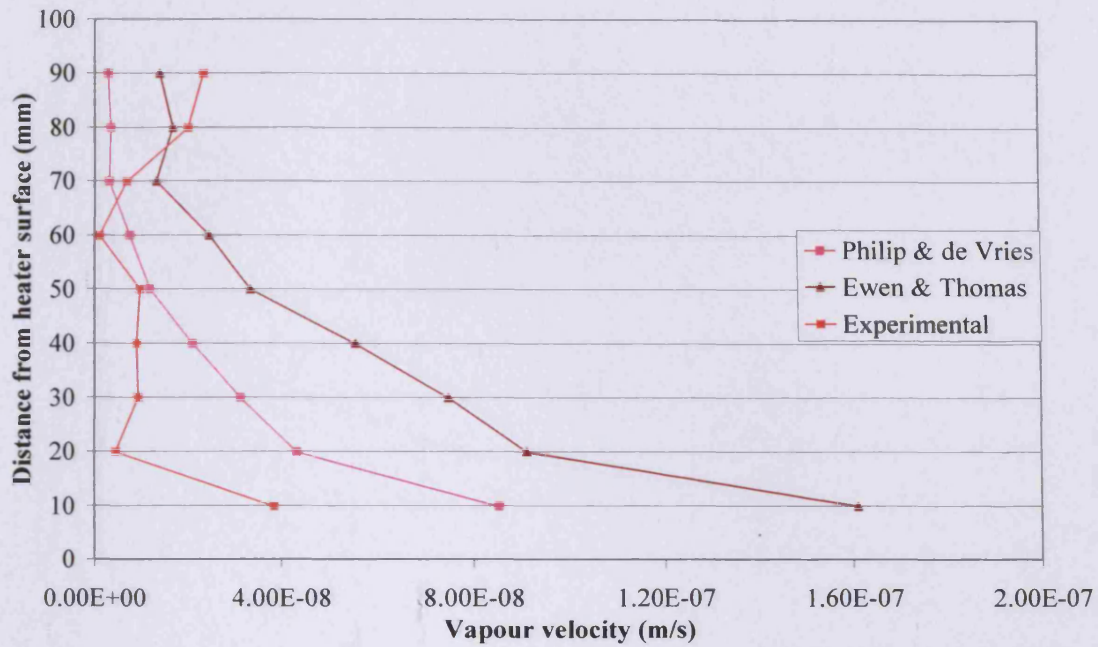
Figure 7.6 Vapour flux for the wet sample of Speswhite kaolin during 1 day thermal test
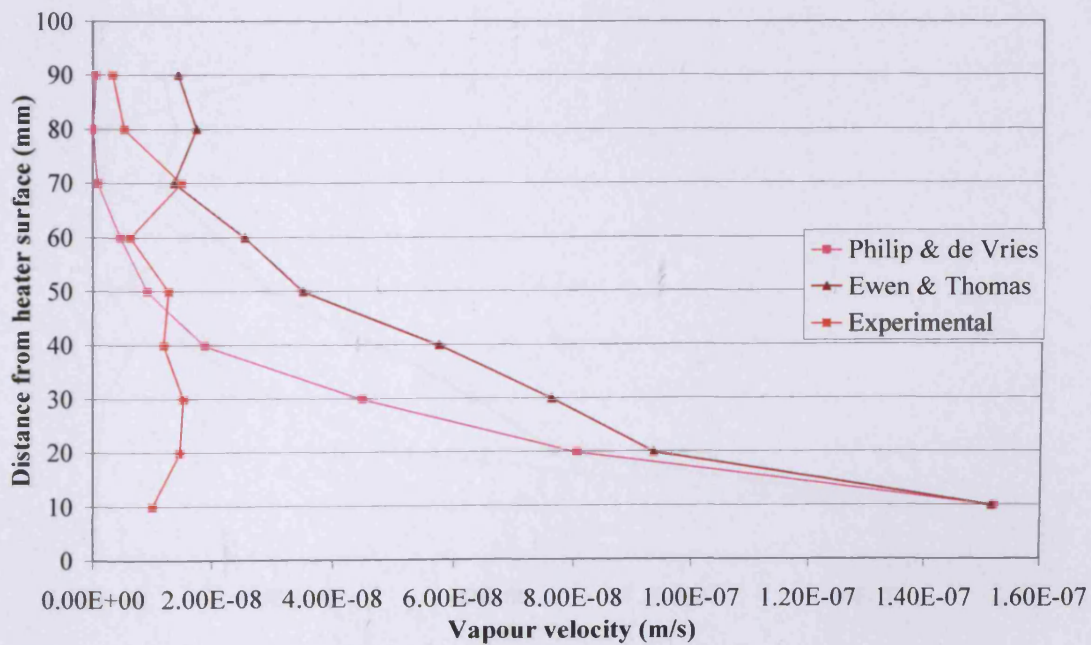
Figure 7.7 Vapour flux for the wet sample of Speswhite kaolin during 1 to 3 day thermal test
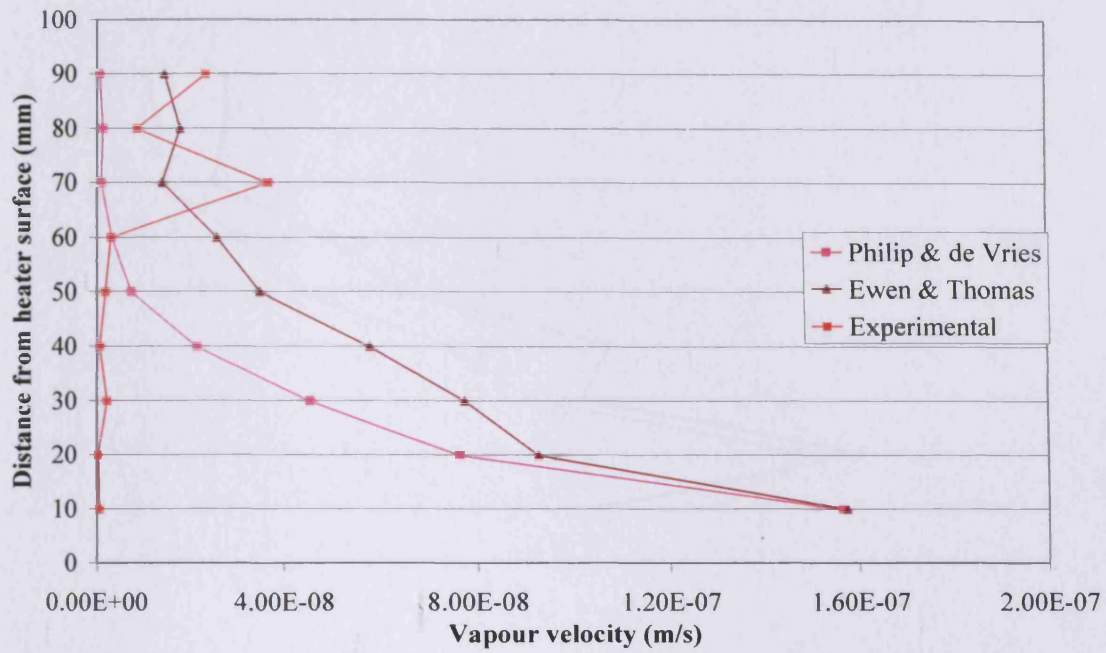
Figure 7.8 Vapour flux for the wet sample of Speswhite kaolin during 3 to 7 day thermal test
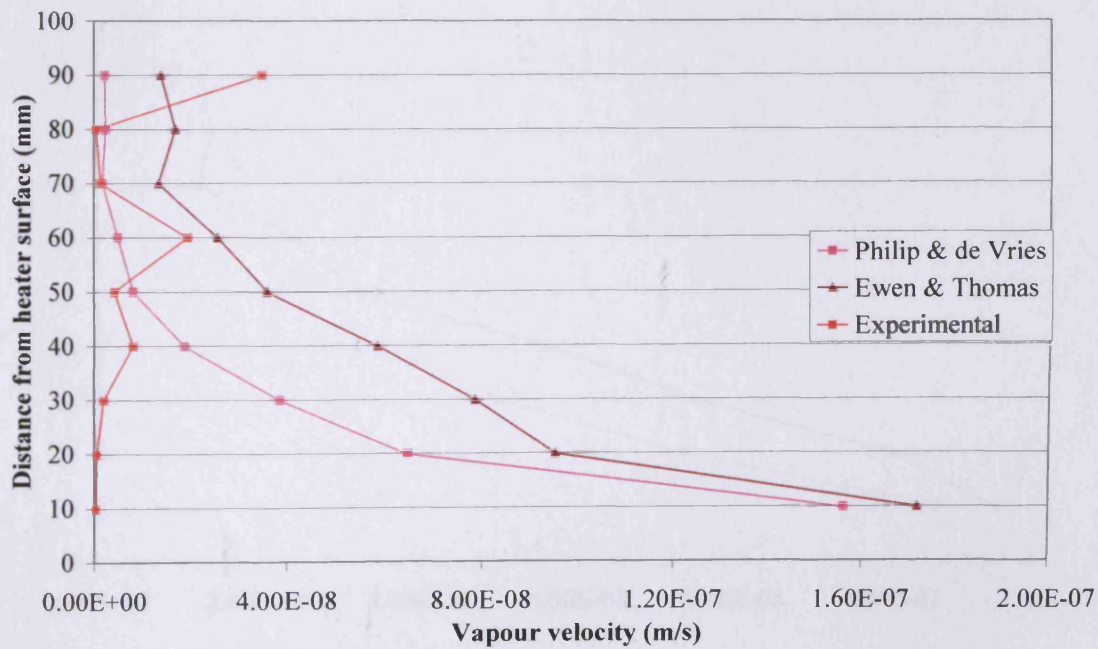
Figure 7.9 Vapour flux for the wet sample of Speswhite kaolin during 7 to 15 day thermal test
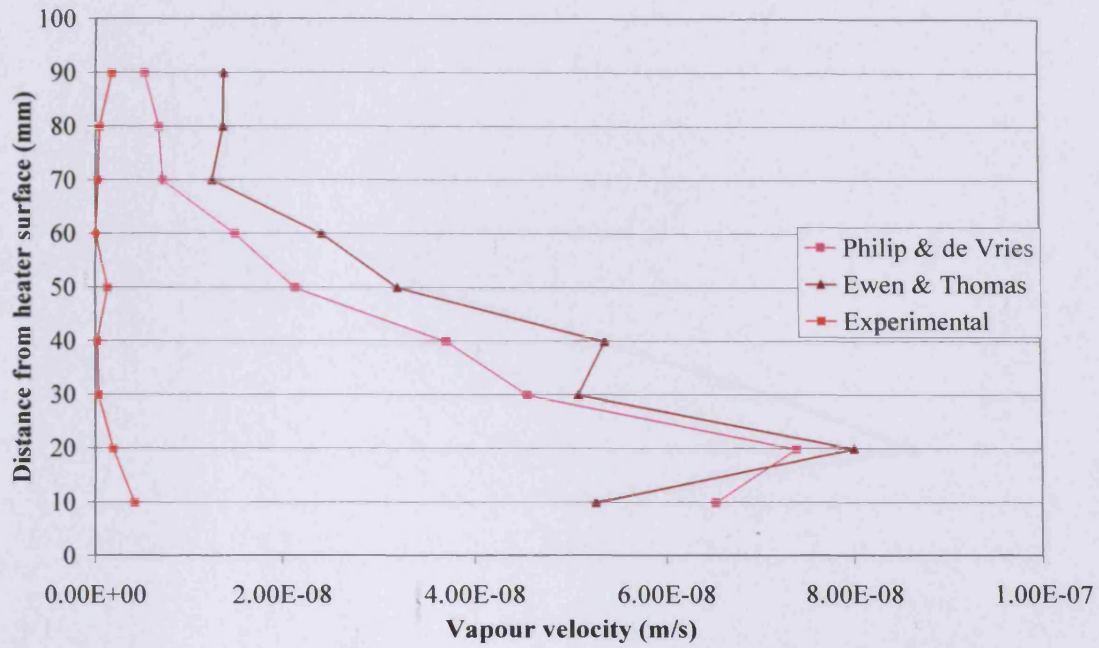
Figure 7.10 Vapour flux for the dry sample of MX-80 bentonite during 1 day thermal test
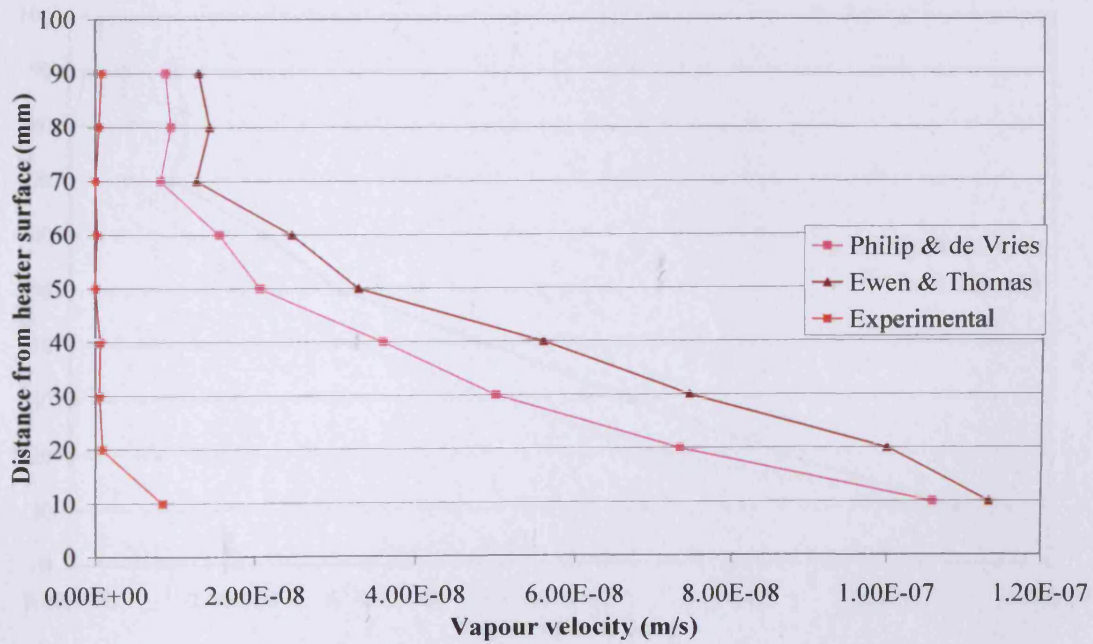
Figure 7.11 Vapour flux for the dry sample of MX-80 bentonite during 1 to 3 day thermal test
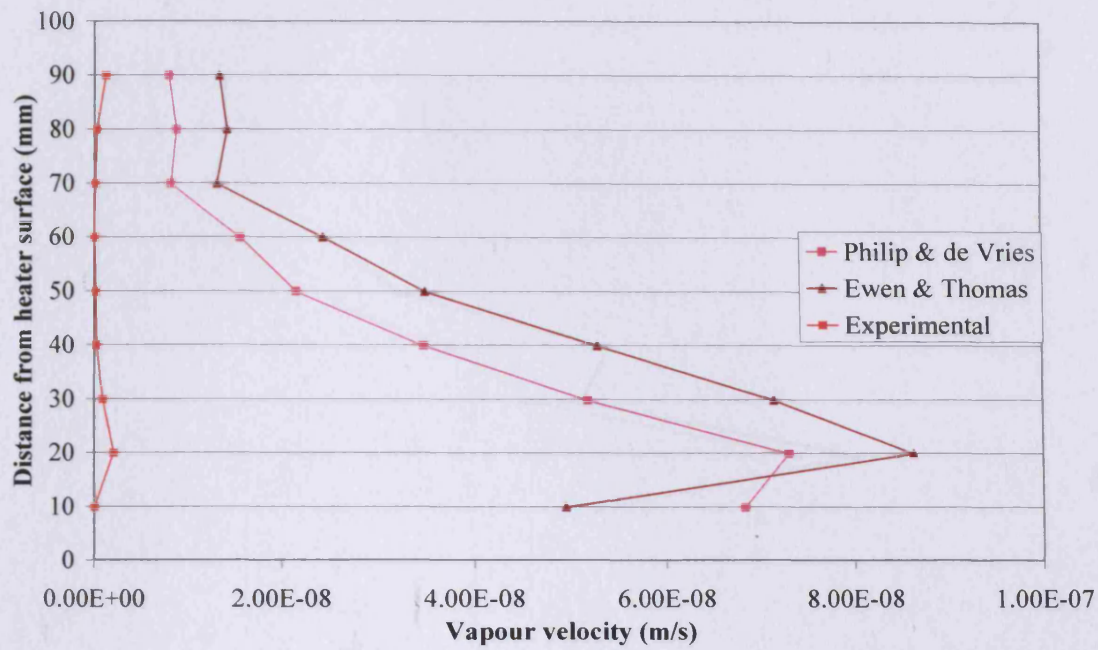
Figure 7.12 Vapour flux for the dry sample of MX-80 bentonite during 3 to 7 day thermal test
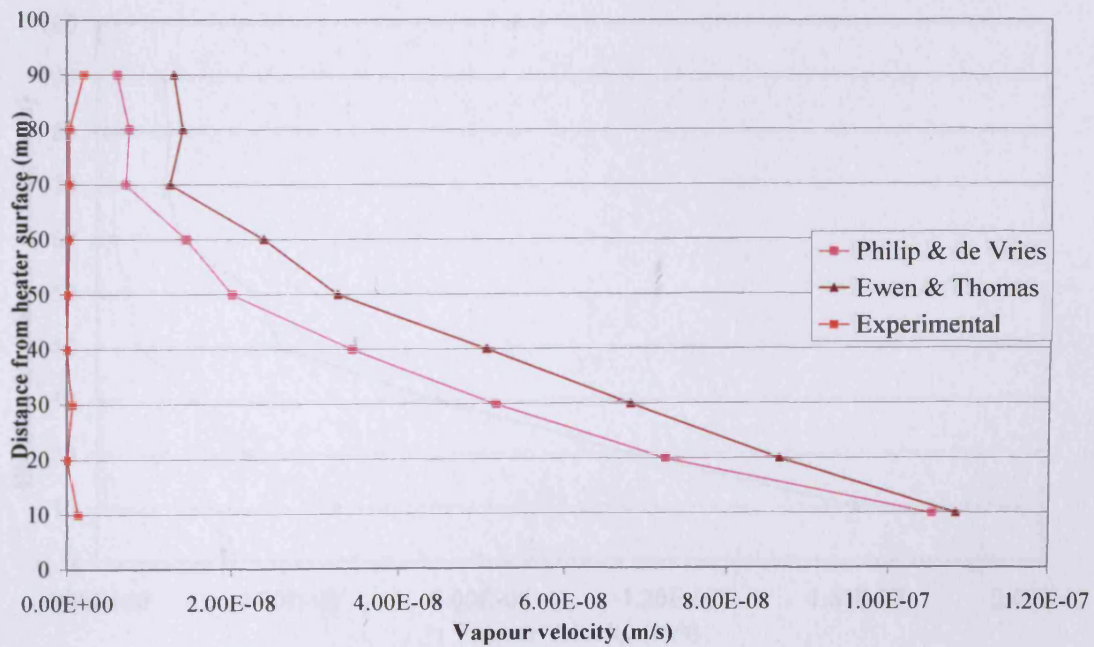
Figure 7.13 Vapour flux for the dry sample of MX-80 bentonite during 7 to 15 day thermal test
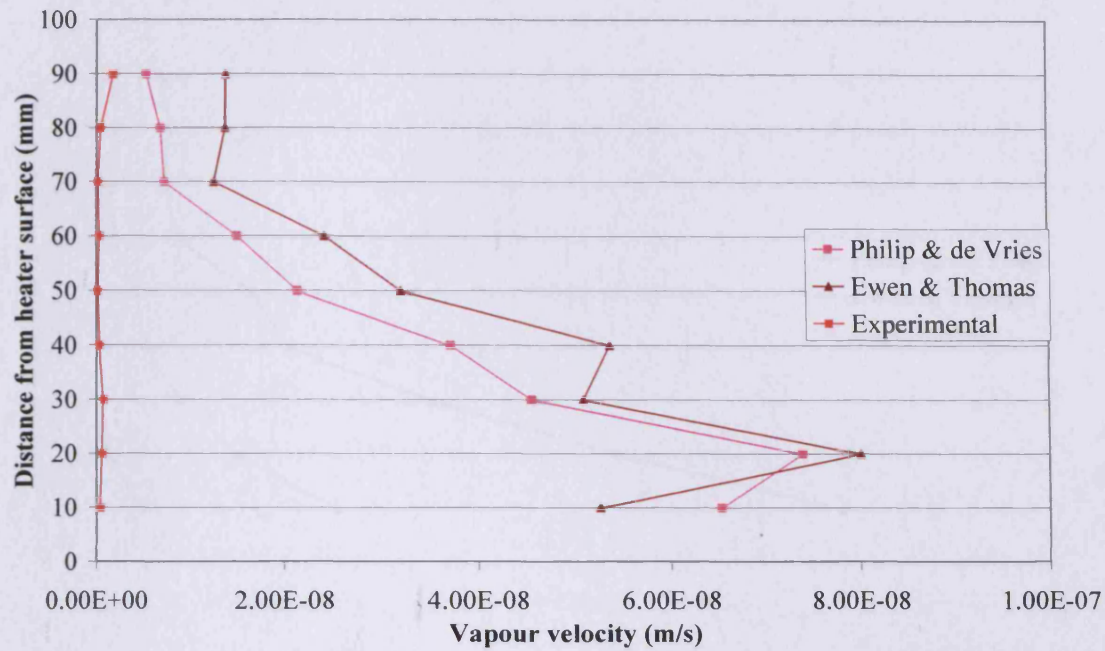
Figure 7.14 Vapour flux for the dry sample of MX-80 bentonite during 15 to 30 day thermal test
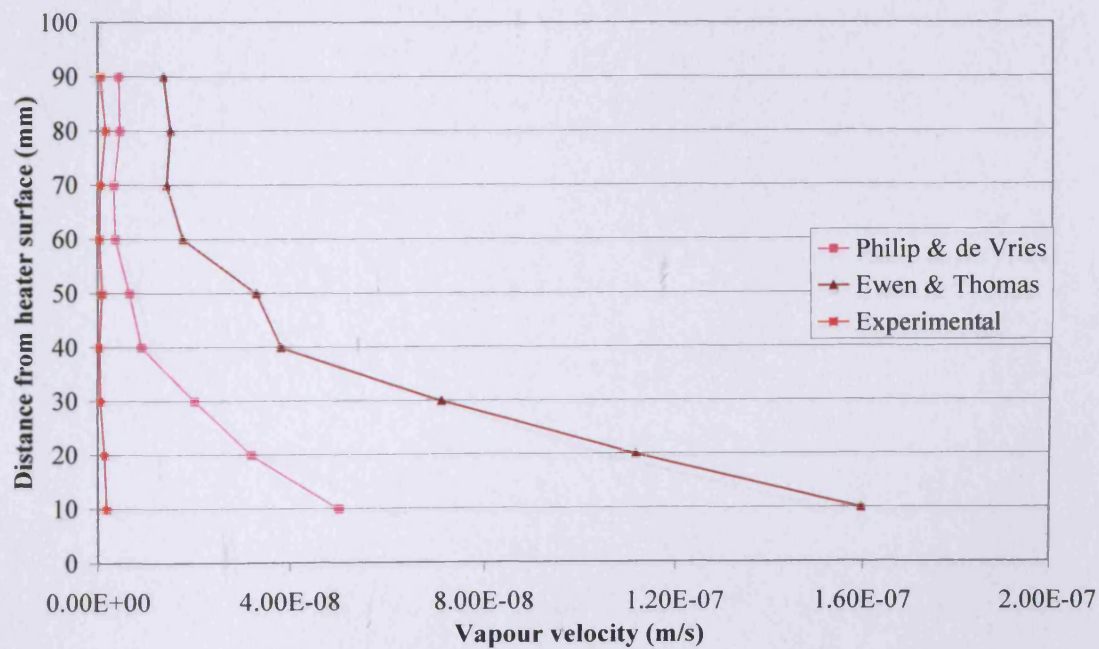
Figure 7.15 Vapour flux for the wet sample of MX-80 bentonite during 1 day thermal test
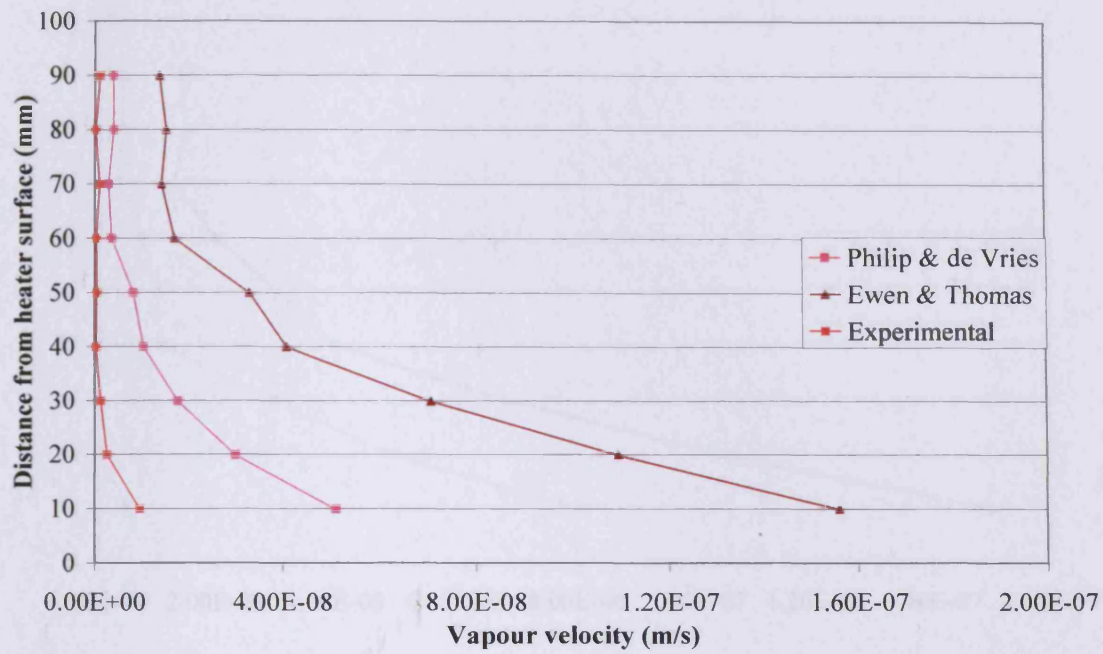
Figure 7.16 Vapour flux for the wet sample of MX-80 bentonite during 1 to 3 day thermal test
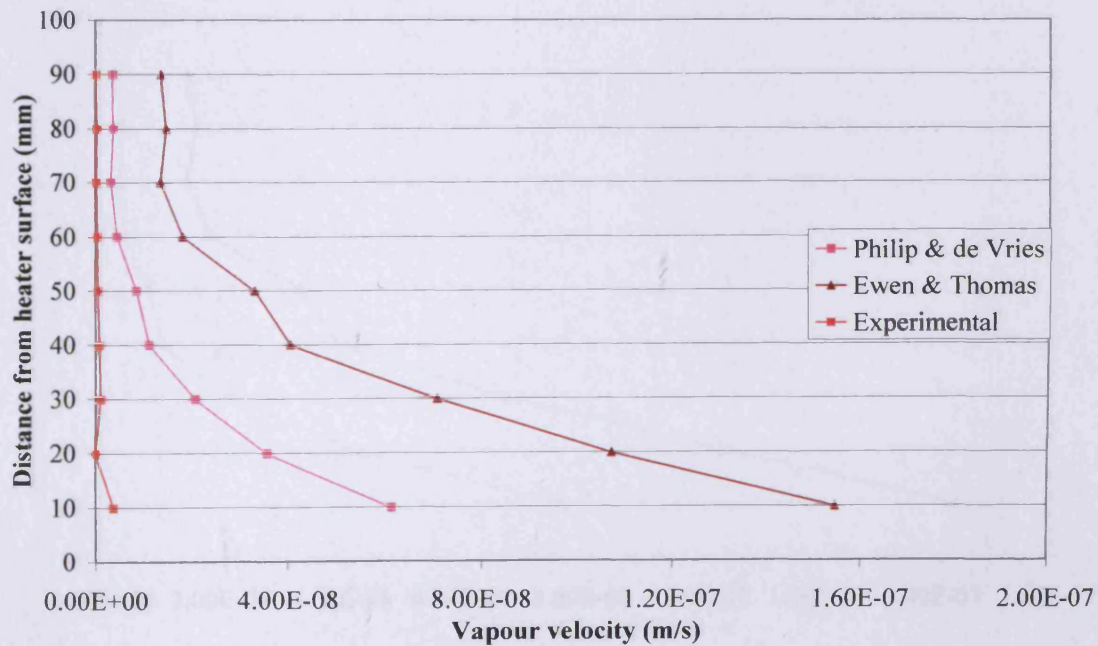
Figure 7.17 Vapour flux for the wet sample of MX-80 bentonite during 3 to 7 day thermal test
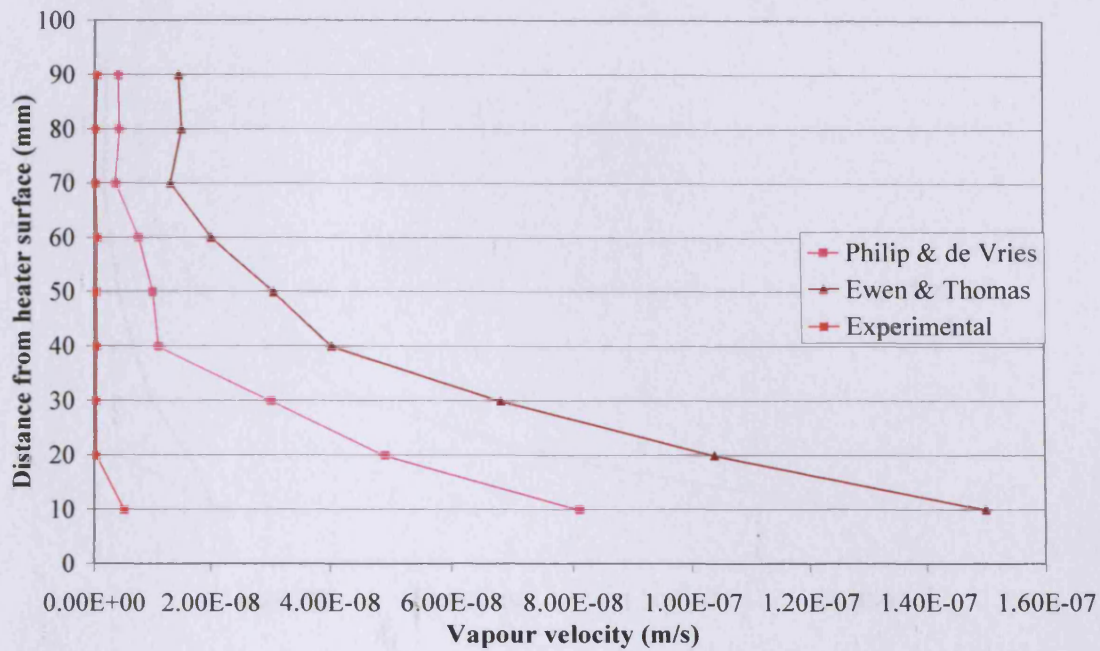
Figure 7.18 Vapour flux for the wet sample of MX-80 bentonite during 7 to 15 day thermal test
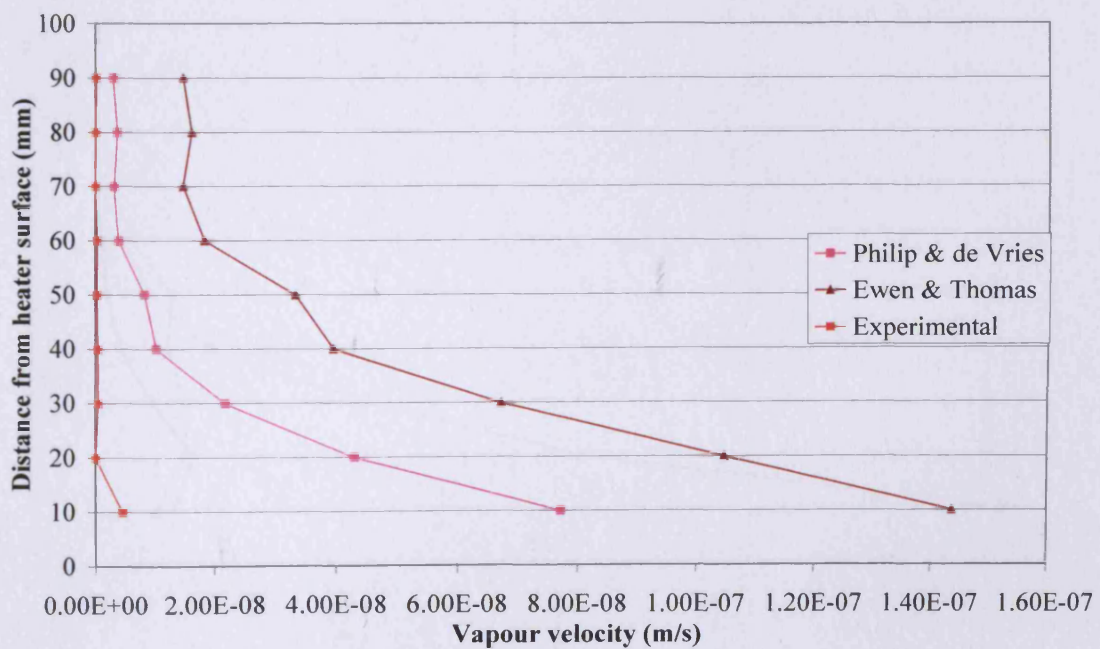
Figure 7.19 Vapour flux for the wet sample of MX-80 bentonite during 15 to 30 day thermal test
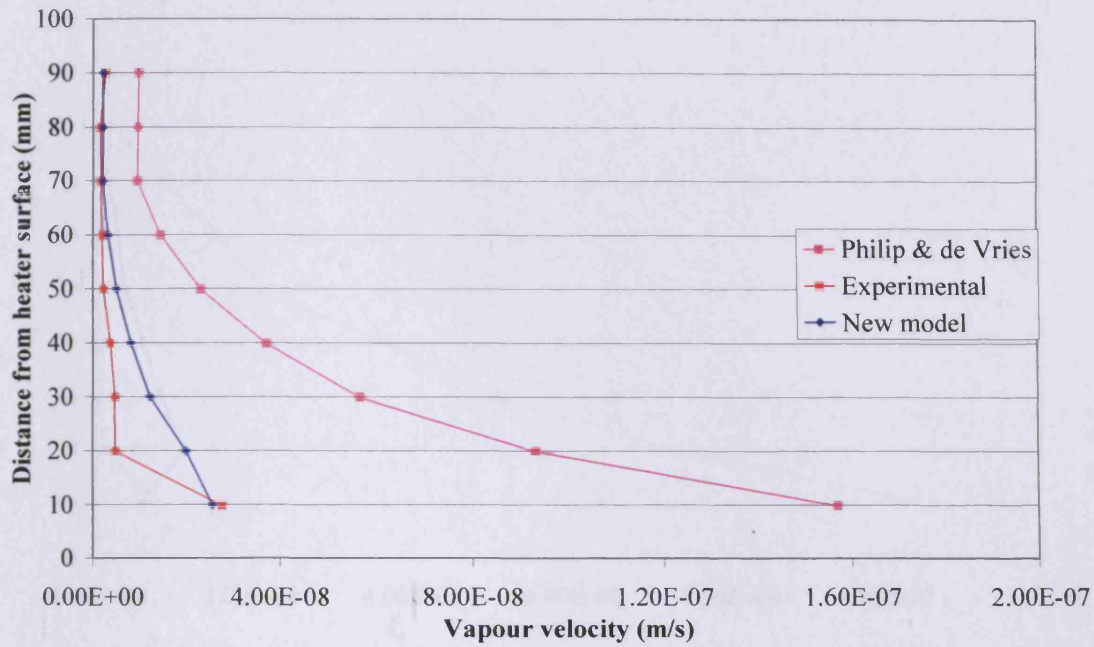
Figure 7.20 Vapour fluxes obtained from new vapour flux model for dry sample of Speswhite kaolin
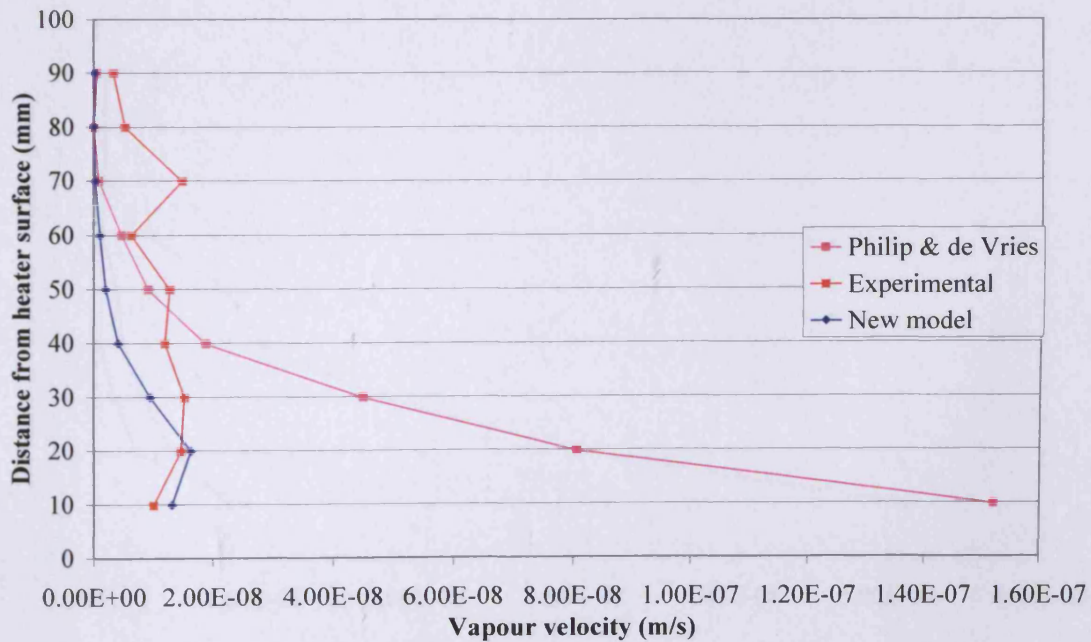
Figure 7.21 Vapour fluxes obtained from new vapour flux model for wet sample of Speswhite kaolin
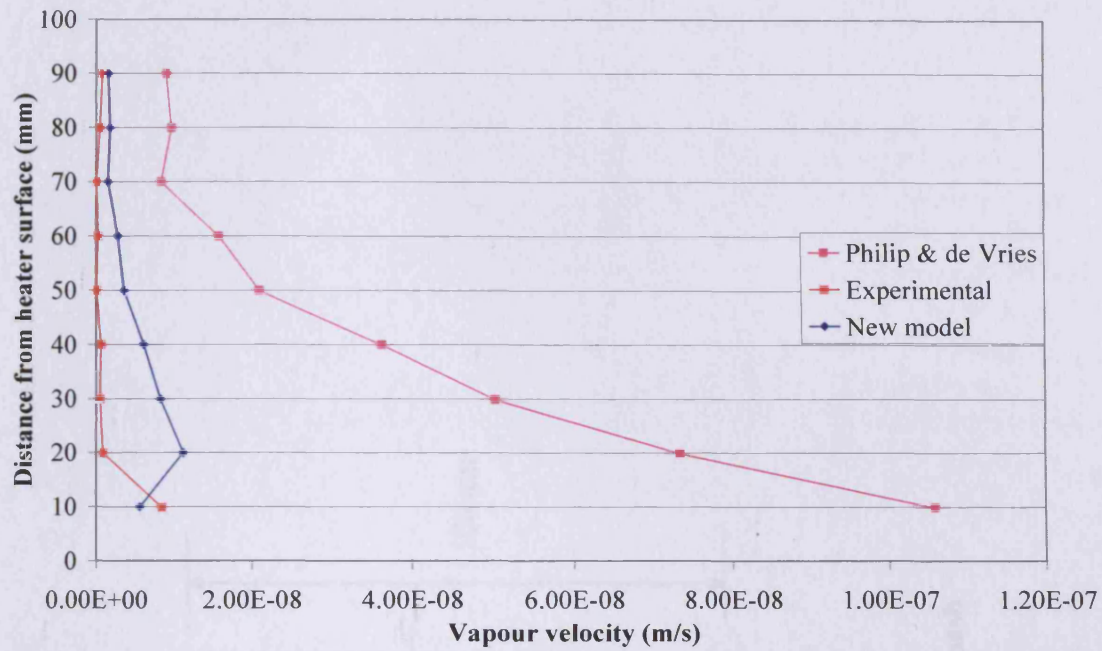
Figure 7.22 Vapour fluxes obtained from new vapour flux model for dry sample of MX-80 bentonite
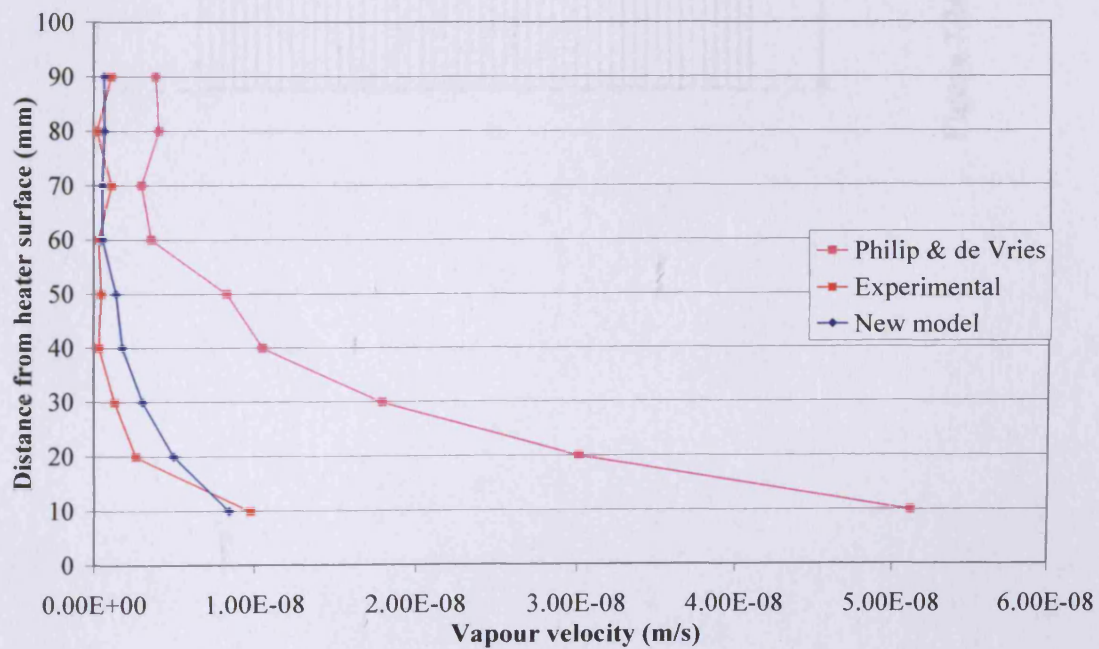
Figure 7.23 Vapour fluxes obtained from new vapour flux model for wet sample of MX-80 bentonite
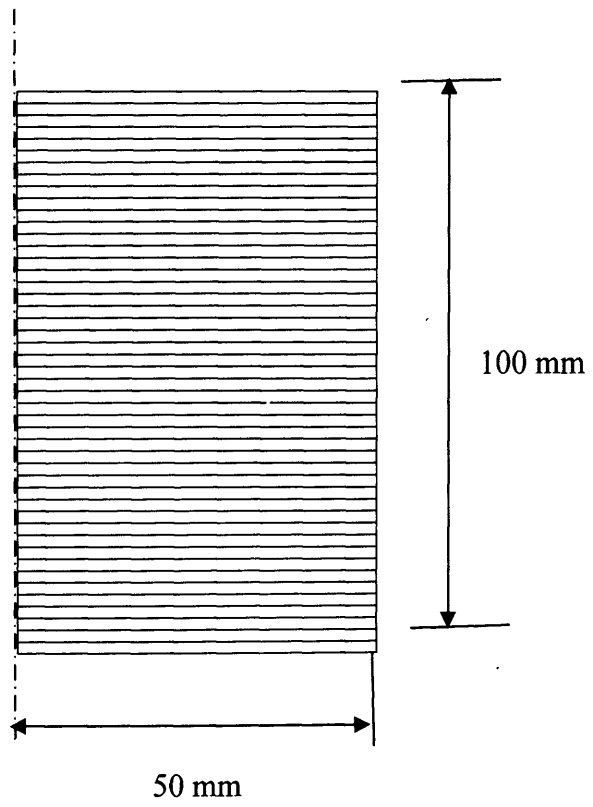
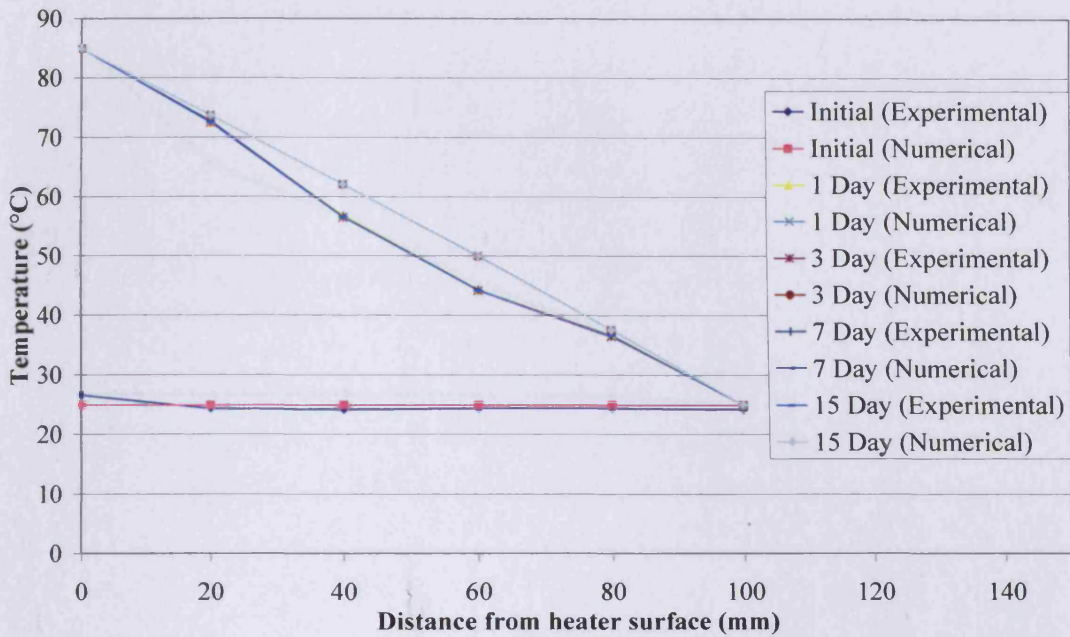**Figure 7.24 1D axisymmetric mesh**
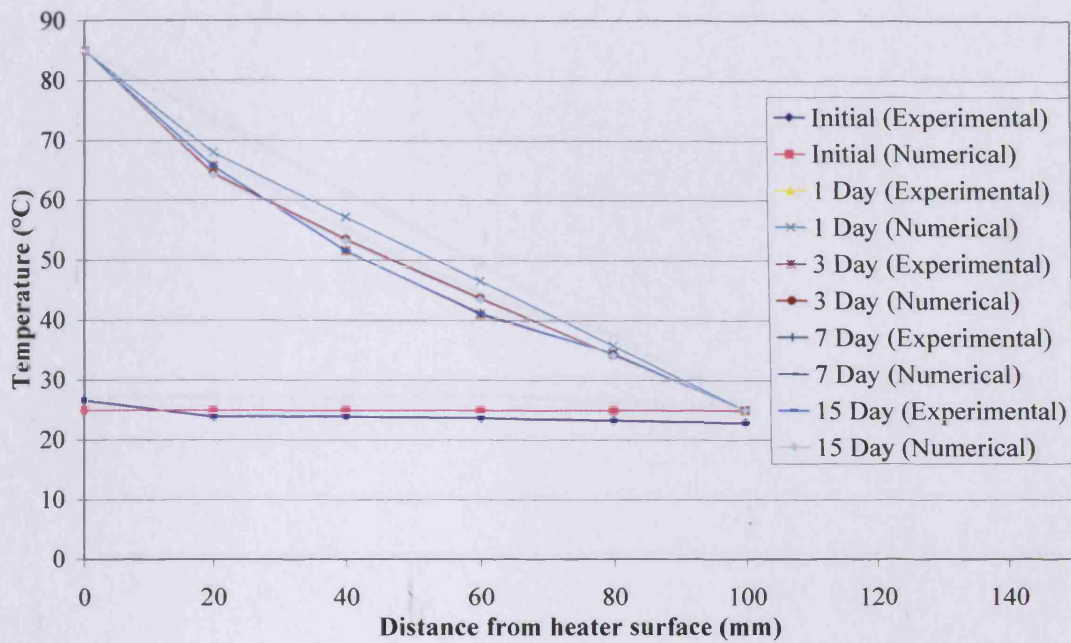
Figure 7.25 Thermal profile for the dry sample of Speswhite kaolin subjected to thermal test
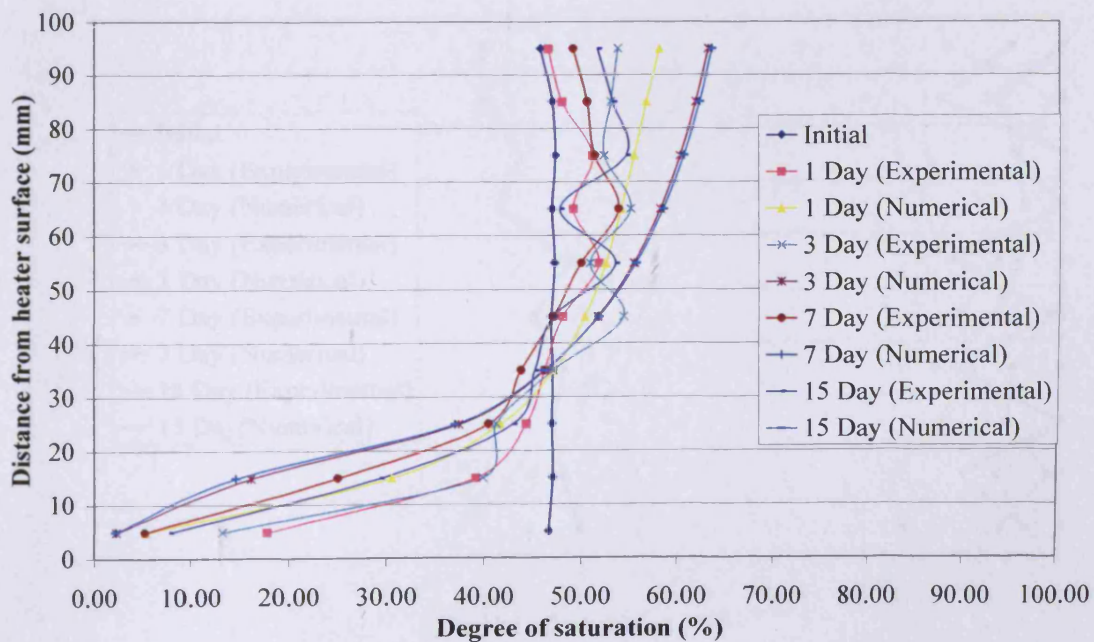
Figure 7.26 Degree of saturation for the dry sample of Speswhite kaolin subjected to thermal test
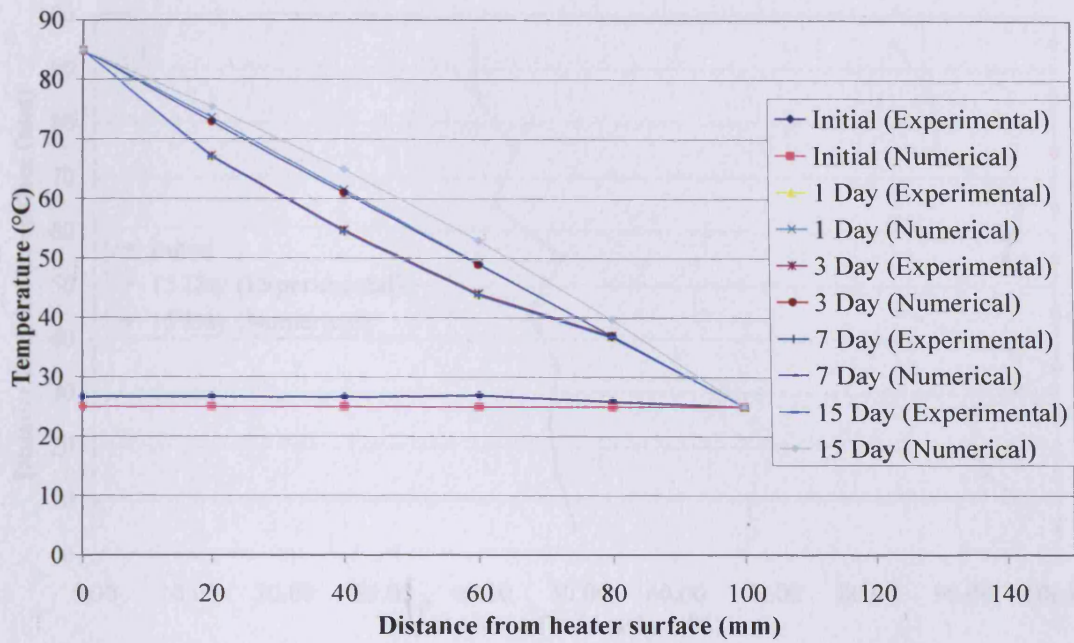
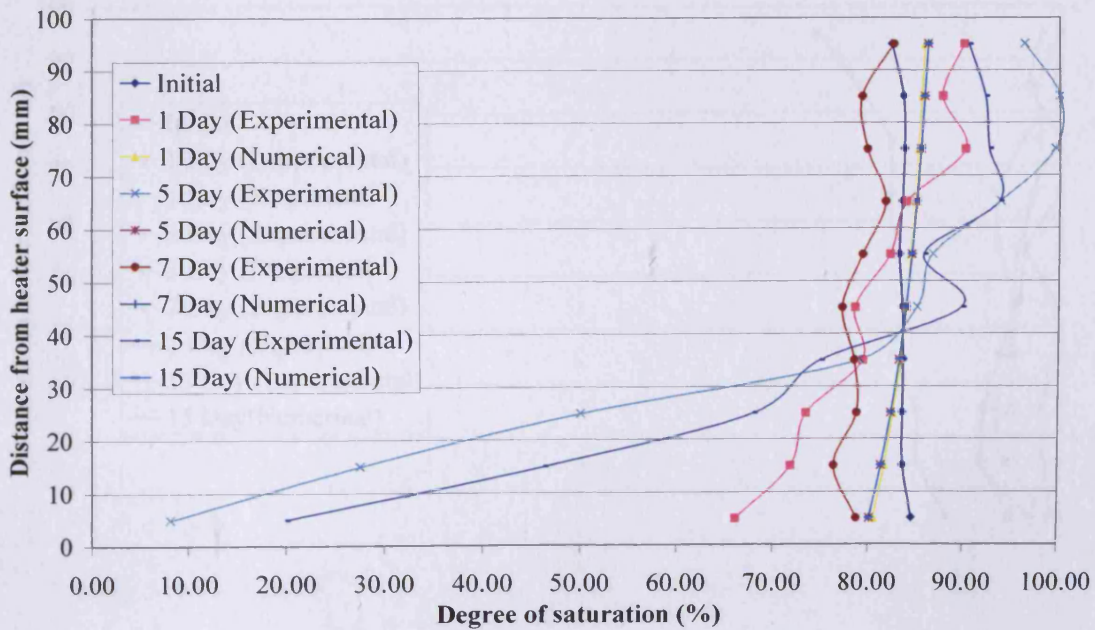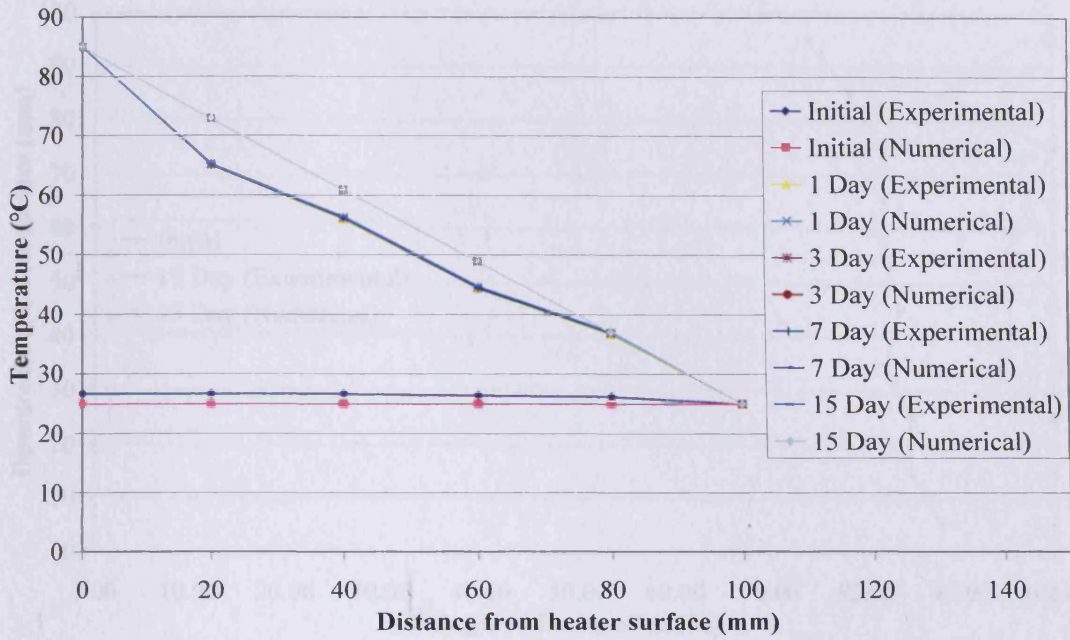**Figure 7.27 Thermal profile for the dry sample of Speswhite kaolin subjected to thermo-hydraulic test**
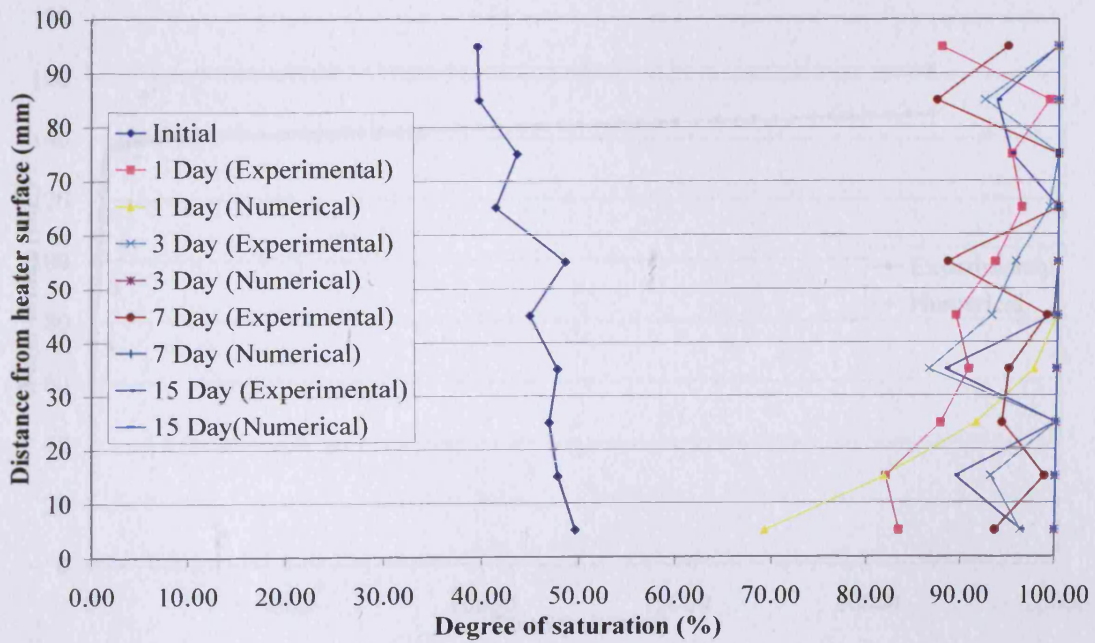
Figure 7.28 Degree of saturation for the dry sample of Speswhite kaolin subjected to thermo-hydraulic test
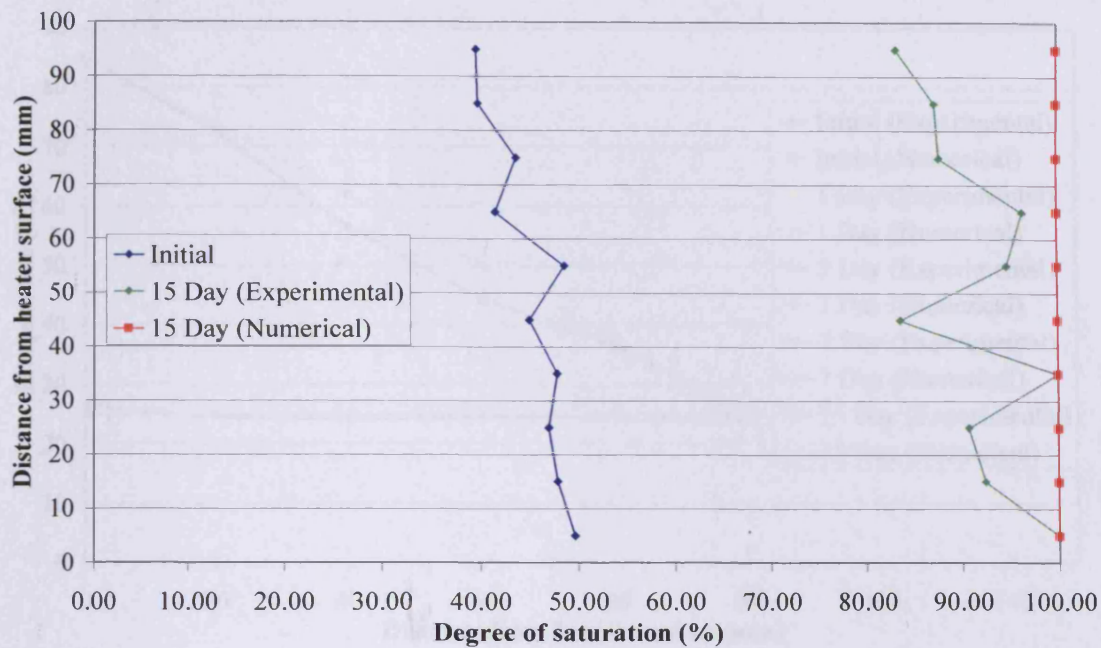
Figure 7.29 Degree of saturation for the dry sample of Speswhite kaolin subjected to isothermal test
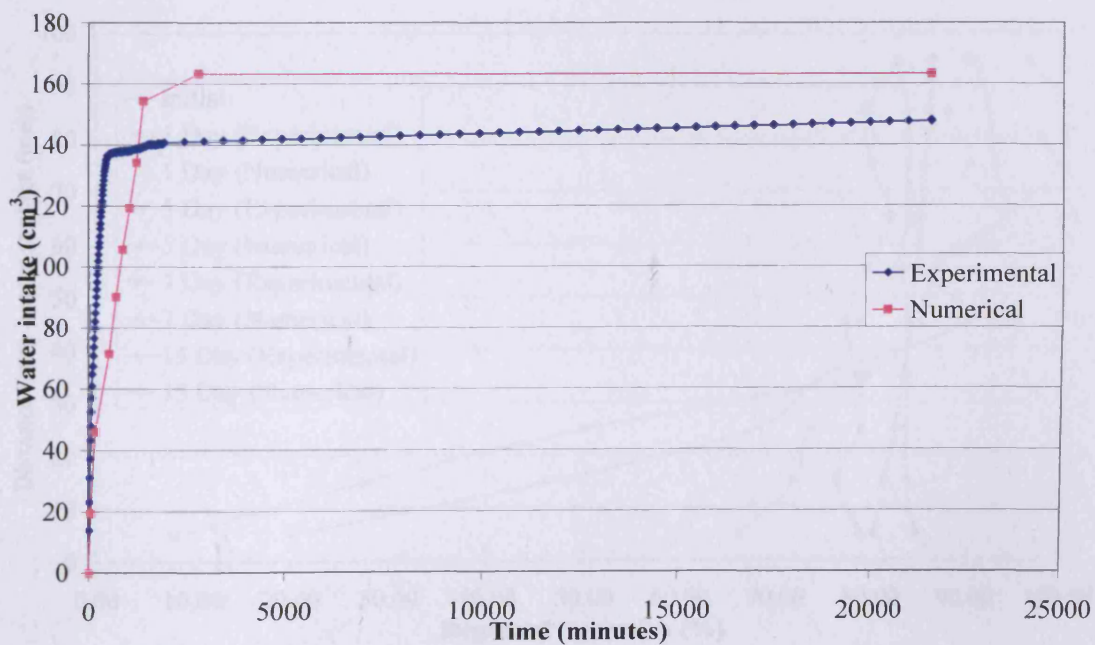
Figure 7.30 Water intake for the dry sample of Speswhite kaolin subjected to isothermal test

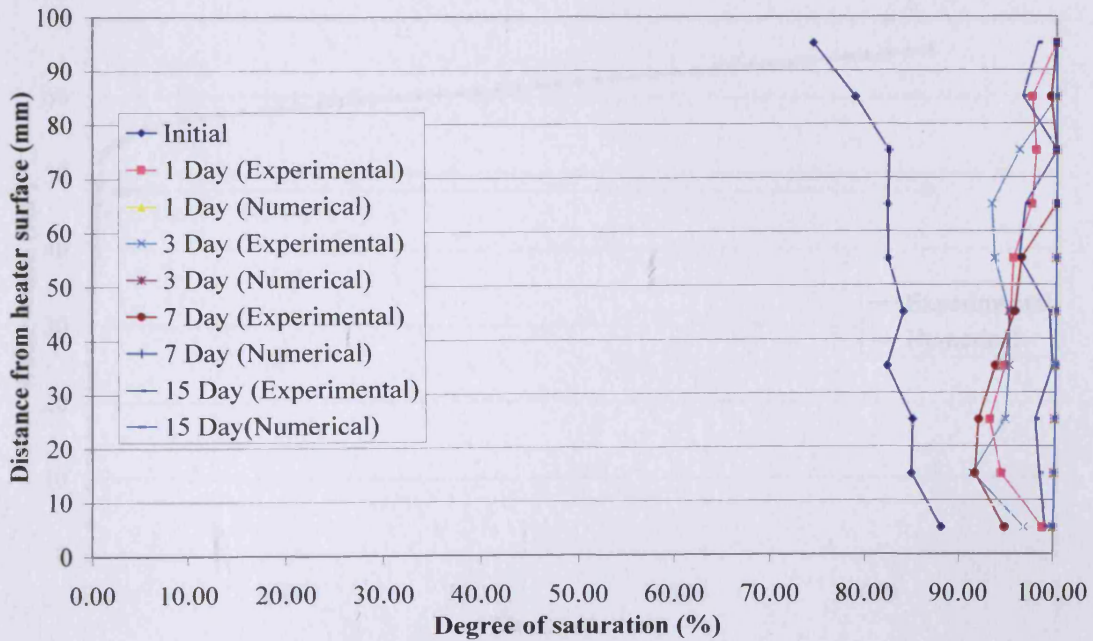**Figure 7.31 Thermal profile for the wet sample of Speswhite kaolin subjected to thermal test**

Figure 7.32 Degree of saturation for the wet sample of Speswhite kaolin subjected to thermal test

Figure 7.33 Thermal profile for the wet sample of Speswhite kaolin subjected to thermo-hydraulic test

Figure 7.34 Degree of saturation for the wet sample of Speswhite kaolin subjected to thermo-hydraulic test
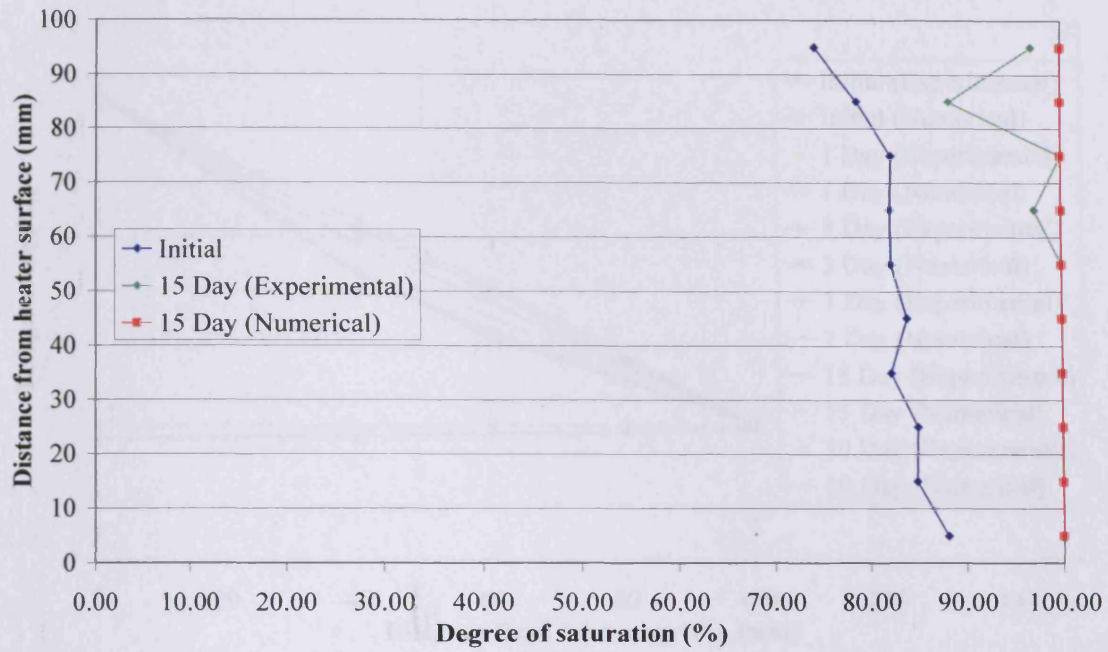
Figure 7.35 Degree of saturation for the wet sample of Speswhite kaolin subjected to isothermal test
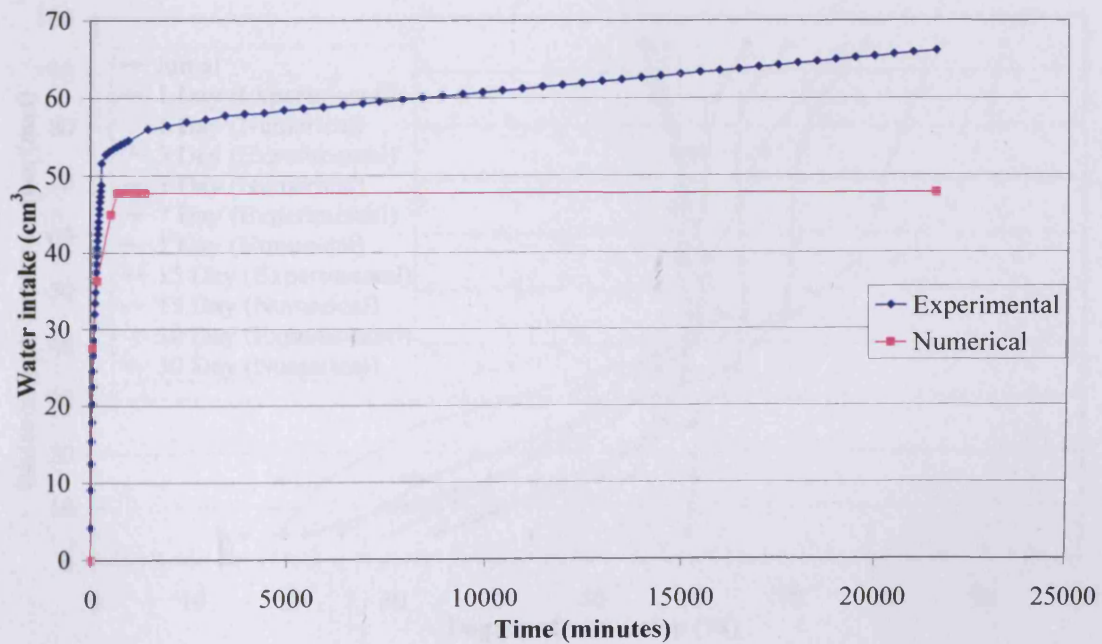

Figure 7.36 Water intake for the wet sample of Speswhite kaolin subjected to isothermal test
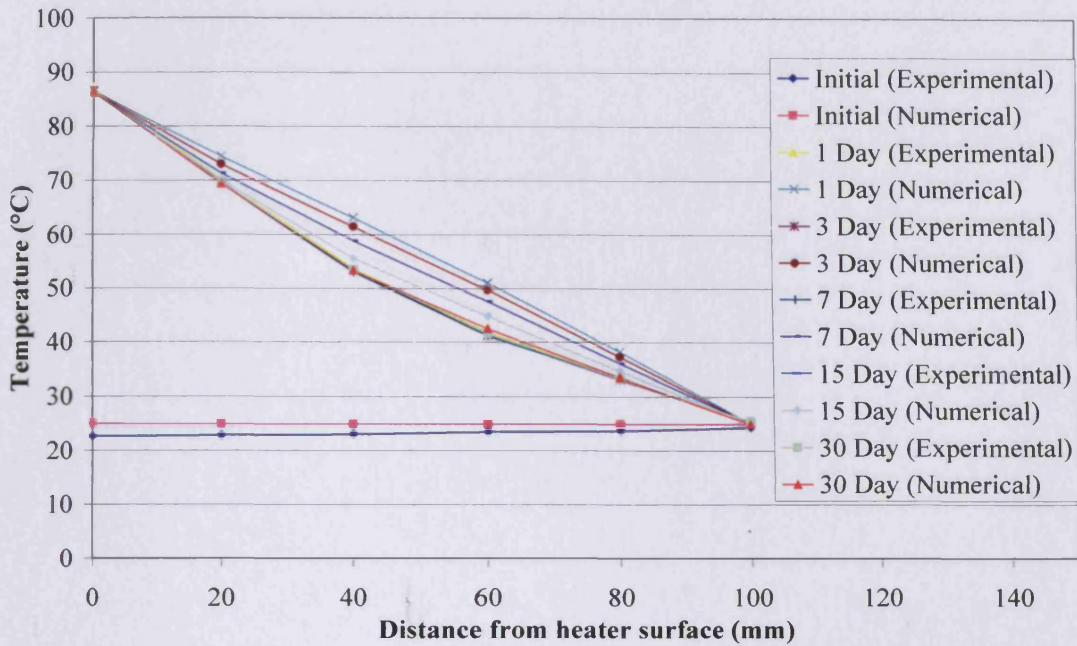
Figure 7.37 Thermal profile for the dry sample of MX-80 bentonite subjected to thermal test
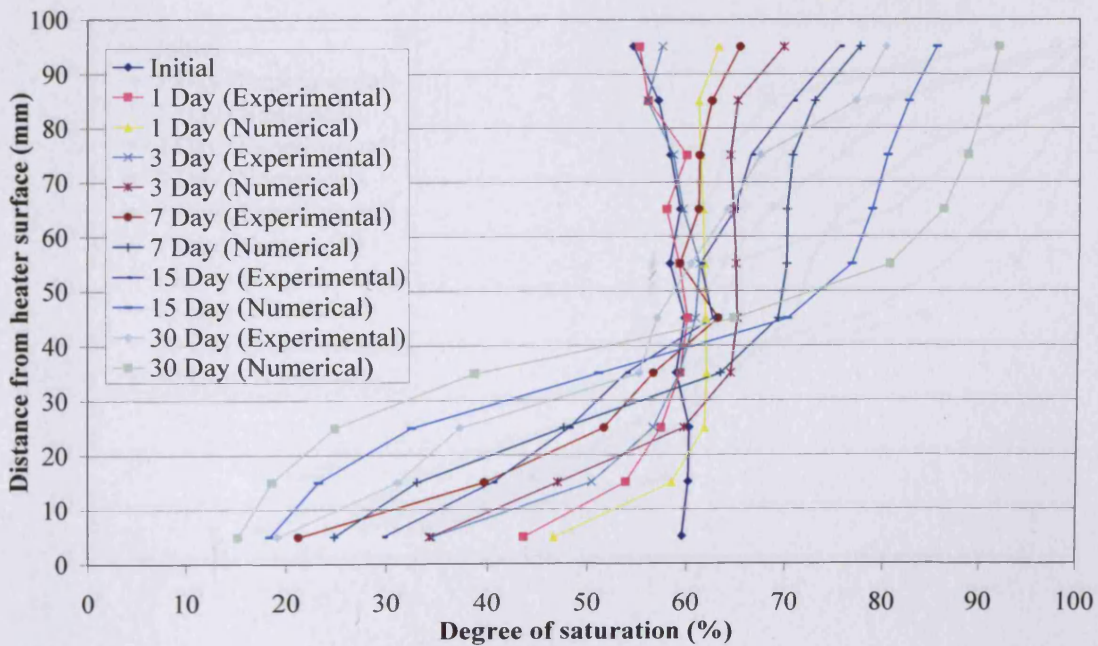

Figure 7.38 Degree of saturation for the dry sample of MX-80 bentonite subjected to thermal test
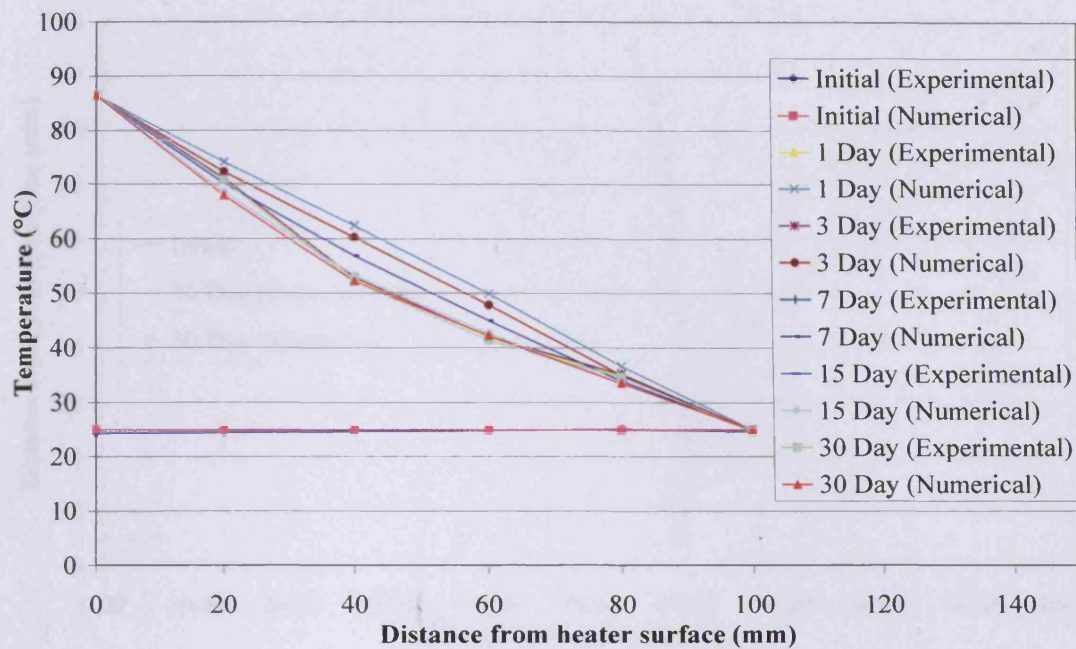
Figure 7.39 Thermal profile for the dry sample of MX-80 bentonite subjected to thermo-hydraulic test
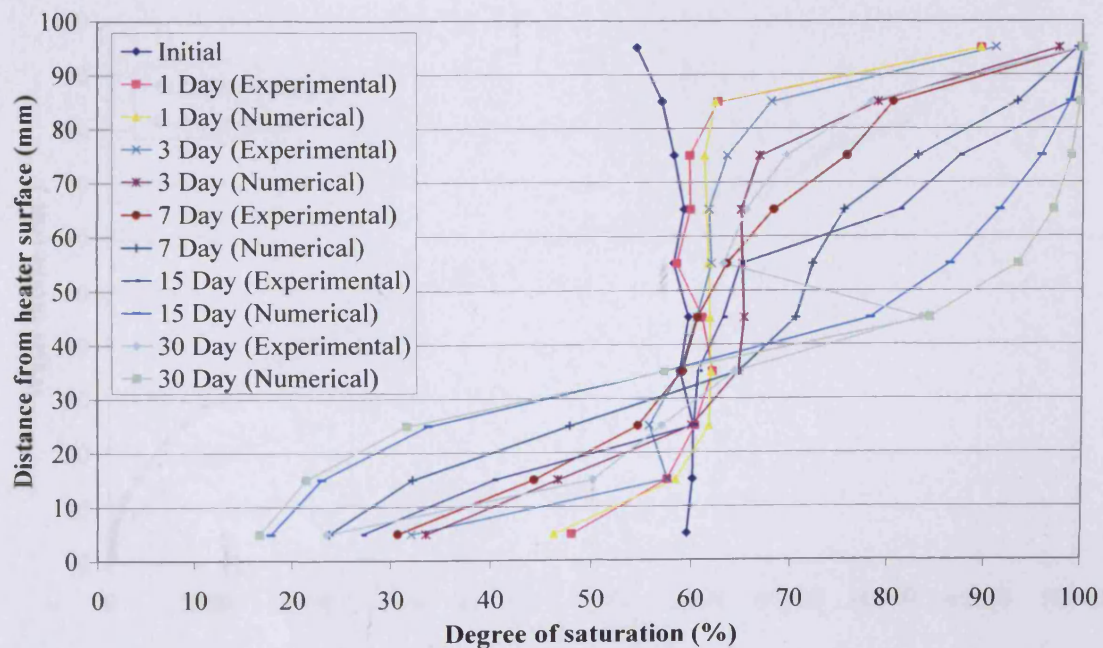

Figure 7.40 Degree of saturation for the dry sample of MX-80 bentonite subjected to thermo-hydraulic test

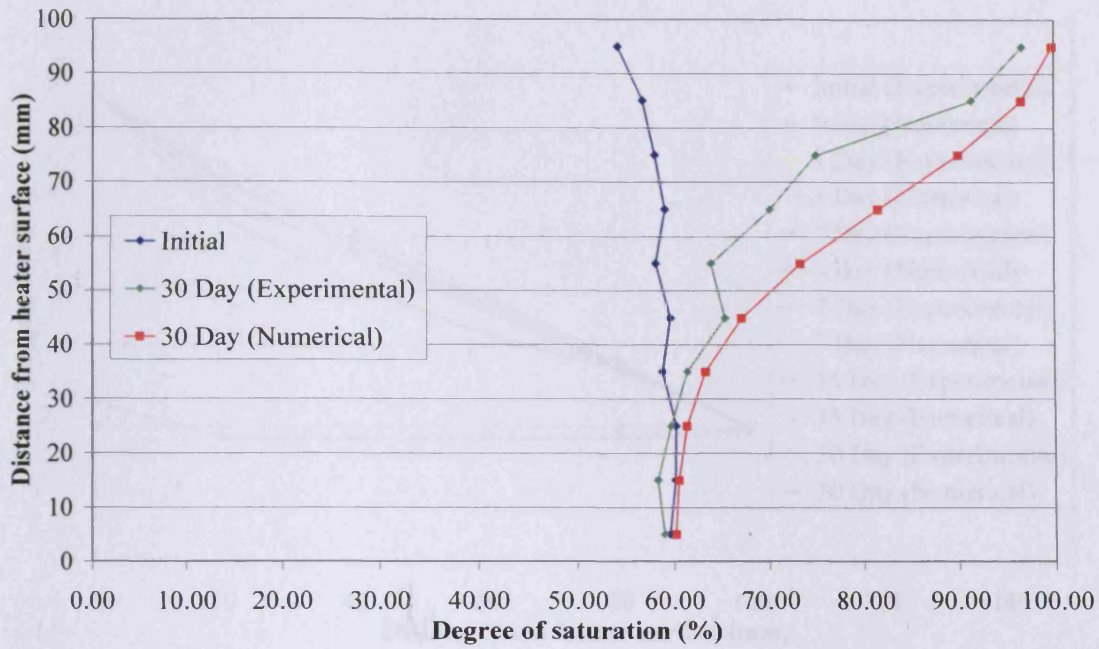**Figure 7.41 Degree of saturation for the dry sample of MX-80 bentonite subjected to isothermal test**

Figure 7.42 Water intake for the dry sample of MX-80 bentonite subjected to isothermal test
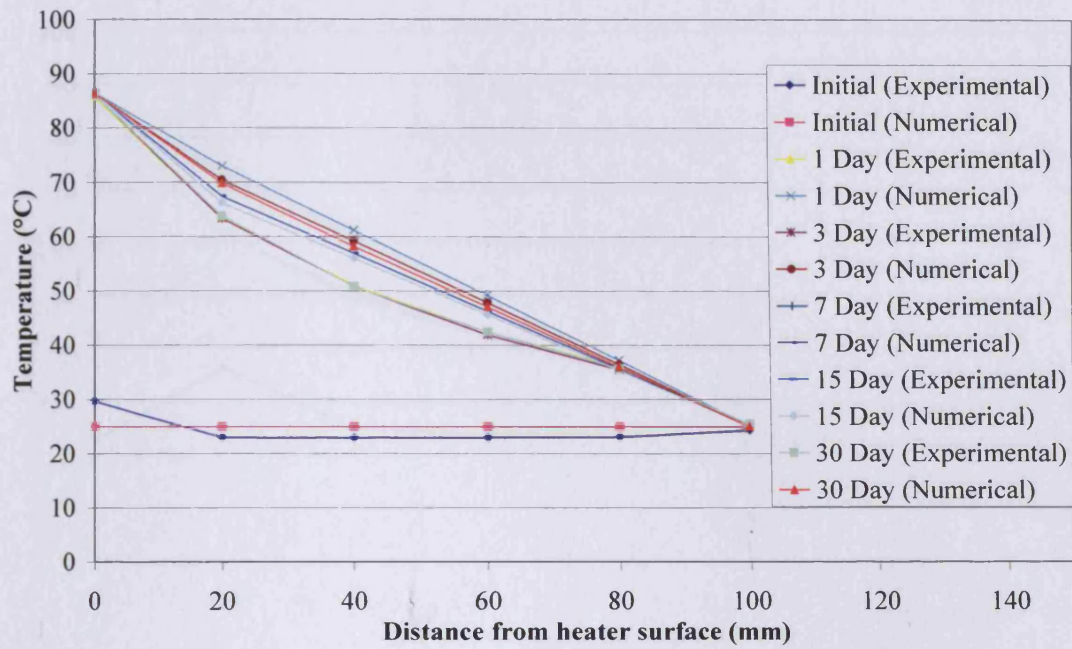
Figure 7.43 Thermal profile for the wet sample of MX-80 bentonite subjected to thermal test

Figure 7.44 Degree of saturation for the wet sample of MX-80 bentonite subjected to thermal test

Figure 7.45 Thermal profile for the wet sample of MX-80 bentonite subjected to thermo-hydraulic test

Figure 7.46 Degree of saturation for the wet sample of MX-80 bentonite subjected to thermo-hydraulic test

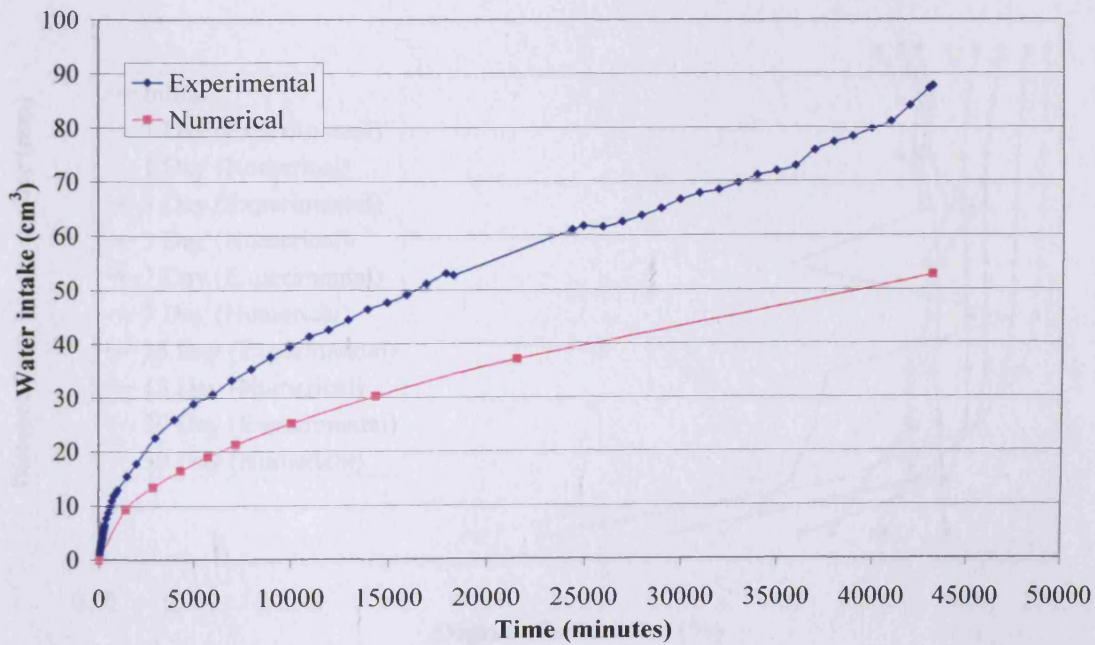**Figure 7.47 Degree of saturation for the wet sample of MX-80 bentonite subjected to isothermal test**
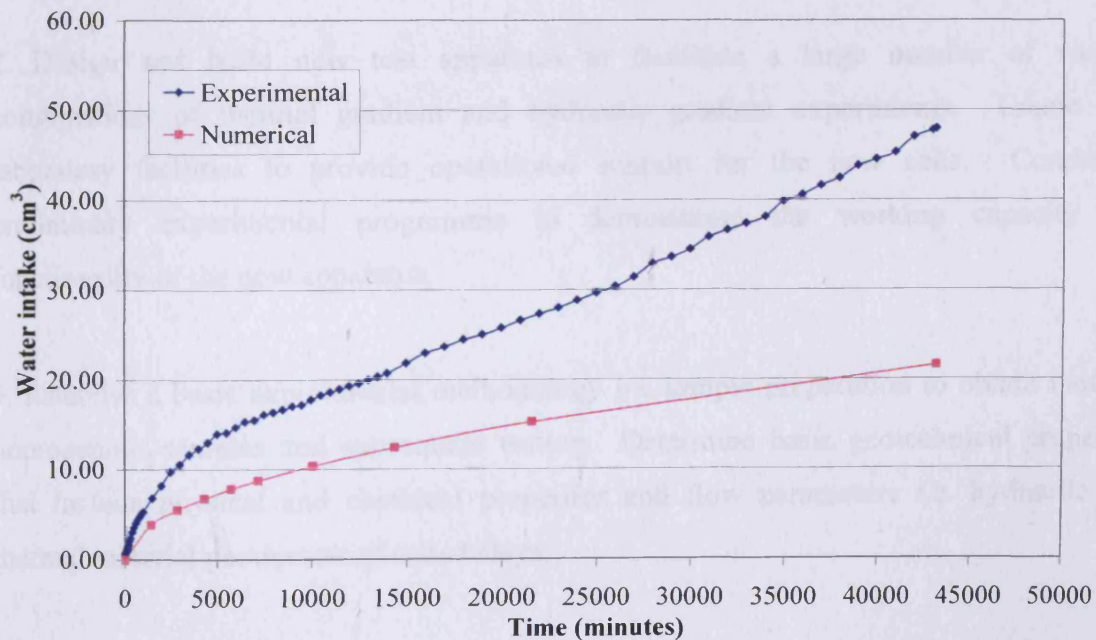
Figure 7.48 Water intake for the wet sample of MX-80 bentonite subjected to isothermal test
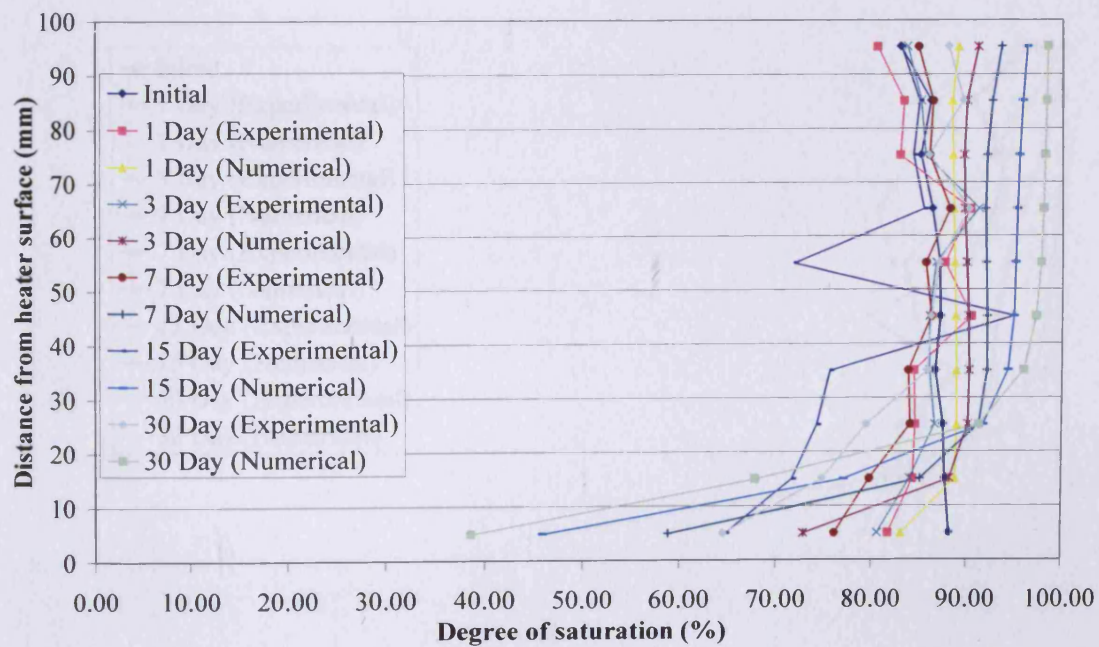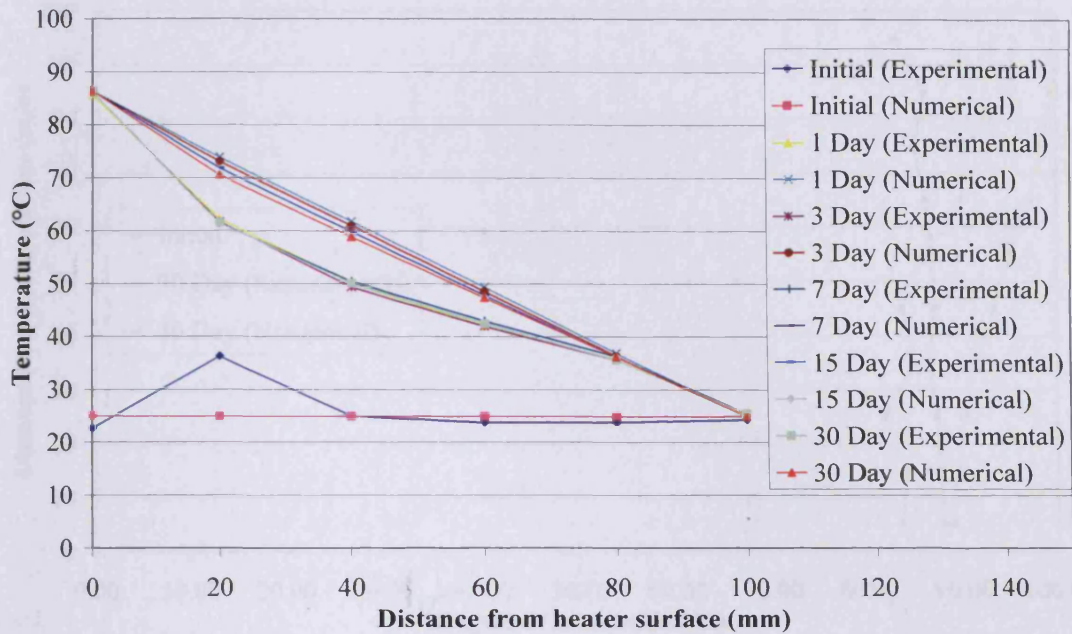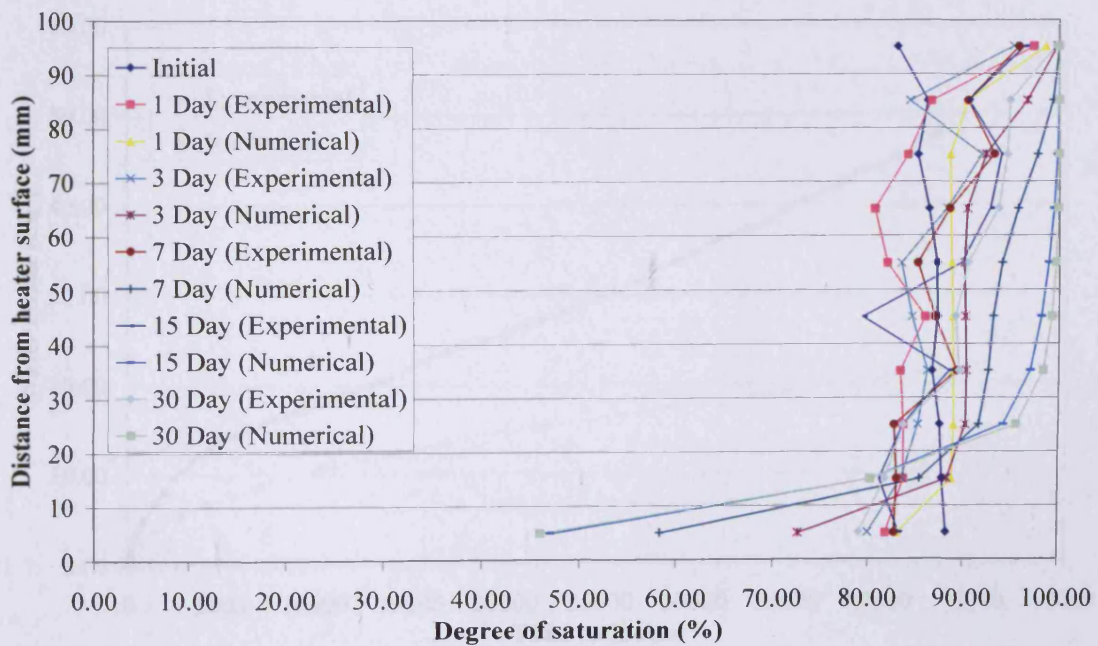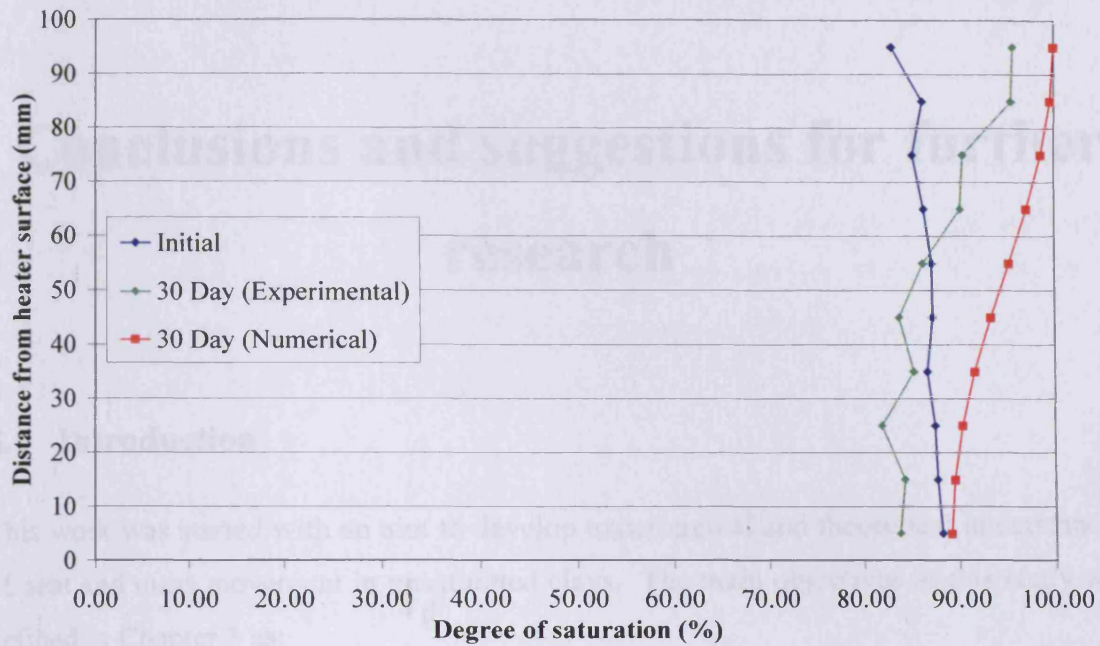
Chapter 8

Conclusions and suggestions for further research

8.1 Introduction

This work was started with an aim to develop experimental and theoretical understanding of heat and mass movement in unsaturated clays. The main objectives of this study were defined in Chapter 1 as:

1. Provide a state-of-the-art review of the review of development of theories and experimental work related to heat transfer and moisture movement in liquid and vapour phases in unsaturated soils from the beginning of 19th century to date.

2. Design and build new test apparatus to facilitate a large number of various combinations of thermal gradient and hydraulic gradient experiments. Create new laboratory facilities to provide operational support for the new cells. Conduct a preliminary experimental programme to demonstrate the working capacity and functionality of the new apparatus.

3. Establish a basic experimental methodology for sample preparation to obtain uniform homogenous samples and subsequent testing. Determine basic geotechnical properties that include physical and chemical properties and flow parameters i.e. hydraulic and thermal material parameters of tested clays.

4. Perform thermal gradient, thermo-hydraulic gradient and isothermo-hydraulic gradient tests to investigate the heat, liquid moisture and vapour moisture movement in clays with different initial degree of saturation but same dry density.

5. Develop an empirical method to calculate the vapour flux using the conservative ion (especially chloride ion) movement. Develop a new vapour flux model for swelling or non-swelling clays and integrate it with in an existing transient finite element model. Verify and validate the new vapour flux model against the results obtained from the heat and mass experiments performed in this study.

It is claimed that each one of these objectives has been achieved and completed successfully. The following sections detail the main conclusions drawn from this work, and suggestions are made for further research.

8.2 Current state of the art

A review of the theoretical and experimental developments in the field of heat and moisture movement in unsaturated soils was made. Existing theories of heat and mass movement are generally based on a rigid matrix and do not take into account the swelling and shrinking nature of expansive clays. Especially the vapour moisture flow has not been studied in past in same detail as liquid moisture flow and the relevant theories are not as well developed. The heat transfer theories are more or less well established and predict the evolution of temperature in swelling clays quite accurately.

The flow parameters (i.e. thermal and hydraulic material parameters) are the essential parameters to predict the heat and mass flow correctly. The accuracy of the theoretical models depends upon the accurate value of heat and moisture flow material parameters. The flow parameters and their experimental determination techniques were presented.

The experimental development in the area of heat and moisture movement studies starting from 19th century till date was presented in detail. However, it was found that in spite of

the significant experimental work that has been done to date there is still a clear shortage of reliable experimental data.

8.3 Experimental design and methodology

Chapter 3 presented the design and construction of the thermo-hydraulic (TH) cells to facilitate the study of heat and moisture movement, which is the main objective of the present research work. Design, fabrication and calibration of the three new TH cells, with each of the defined design criteria met, have been carried out successfully in-house. The TH cell is capable of measuring the transient temperature, relative humidity, volume flow rate of incoming water. The cell also facilitates the determination of moisture content, dry density and chemical composition of the soil samples at the end of the tests. However, safety constraints limit the maximum cell temperature to 100 °C and working pressure to 1.5 MPa.

The experimental approach developed and defined includes the soil preparation, compaction, assembling, dismantling, sectioning, and various soil properties determination with chemical composition. A chemical analysis methodology that includes anion determination using ion chromatography (IC) and cation determination using inductively coupled plasma mass spectroscopy (ICP-MS) was presented. Also an experimental methodology has been developed to perform the thermal, thermo-hydraulic and isothermal tests. The preliminary trial tests included thermal and thermo-hydraulic tests calibrated the test cells and verified the experimental approach.

8.4 Material characterisation and flow parameters

The investigation has been carried out on two types of clays, a non-swelling clay Speswhite kaolin and highly swelling clay MX-80 bentonite. Both clays have been characterised by determining their various geotechnical properties including physical and chemical properties. The basic geotechnical properties were determined via standard experimental techniques outlined in BS 1377. The hydraulic and thermal material parameters, which are very important for correct evaluation of heat and mass movement

in unsaturated soils, have been reported. The hydraulic parameters include the moisture retention curve, saturated hydraulic and unsaturated hydraulic conductivity while thermal parameters include thermal conductivity and specific heat capacity. The hydraulic parameters were measured and determined experimentally while thermal parameters were taken from the available work of other researchers.

A static compaction technique was established to achieve uniform high dry density and uniform water content along the length of the soil samples. The dry density of 1.63 Mg/m^3 was selected with 50 % and 85 % degree of saturation corresponding to 11 % and 19 % water contents respectively as initial conditions for the testing programme for Speswhite kaolin. For MX-80, the dry density of 1.63 Mg/m^3 was chosen with 60 % and 88 % degree of saturation which relate to initial water contents of 16% and 22% respectively as initial conditions.

8.5 Thermal, thermo-hydraulic and isothermal tests on Speswhite kaolin

The results of the thermal, thermo-hydraulic and isothermal tests undertaken were presented. It was found that the temperature distribution depends upon the initial conditions, the end conditions and the type of test. The different temperature values at steady state condition for the wet and dry samples indicate the thermal material parameters (e.g. thermal conductivity and specific heat capacity) rely upon the initial amount of water.

The moisture distribution results show the moisture movement within the sample but the chemical analysis of the samples give more insight in the actual process of liquid and vapour moisture movement. The accumulation of ions near the heater surface during the thermal test indicates that liquid moisture moved from the cold end to the hot end. This fact can not be observed solely from the moisture distribution results. Finally, T test results show that there is a cycle of vapour and liquid moisture movement within the sample, vapour moves from the hot end to the cold and condenses to liquid at the cold end and liquid moisture moves to the hot end.

The relative humidity results are almost same for the dry and wet samples irrespective of type of test. The relative humidity reaches to 100 % value very quickly and the total suction must reach to zero. The relative humidity values indicate the macroscopic level response but at microscopic level suction exists and causes moisture movement.

The moisture mass balance accuracy lies within ± 0.35 % for most of the test. This indicates the new test cell, TH cell, is working and functioning correctly and does not allow any moisture escape. The chemical mass balance was achieved in the T test but not in the TH test due to escape of ions to the hydration source during the TH tests.

8.6 Thermal, thermo-hydraulic and isothermal tests on MX-80 bentonite

Results of the thermal, thermo-hydraulic and isothermal test performed on MX-80 bentonite have been presented. The temperature distribution depends upon the initial conditions. The steady state temperature is higher for the dry samples due to less thermal conductivity and low heat dissipations resulted in higher temperature for the dry samples at corresponding points.

The gravimetric moisture content is decreasing near the hot end when the temperature gradient is applied due to moisture movement in vapour phase away from the hot region to the cold region. The amount of drying depends upon the initial moisture content. The dry sample has higher drying compared to the wet sample. The accumulation of salts (like chloride, nitrate and sulphate) near the cold end indicates that the liquid moisture moves towards the hot end from the colder region. The salts specially chloride ions are a good indicator of the liquid moisture movement and are used in chapter 7 to calculate the liquid and vapour moisture quantities.

8.7 Assessment of vapour movement

The new empirical method of predicting and calculating the vapour flux by using the chloride ions concentration distribution is presented. The empirical vapour flux values for both kaolin and bentonite clays are quite small compared to that calculated by Philip and de Vries (1957) theory and Ewen and Thomas (1989) theory. The existing theories are applicable to rigid matrix and needed to be changed. Hence, the new vapour flux model has been developed by introducing the factors to thermal diffusivity and isothermal diffusivity terms of Philp and de Vries (1957). The new vapour flux model has been introduced in the finite element code COMPASS and numerical analyses have been carried out.

The thermal and moisture regime is generally well captured by numerical analysis for both clays subjected to various end conditions. The water intake profiles determined numerically are not matching exactly due to the volume measurement error in the automatic volume change apparatus and the uniform average porosity used for numerical analysis not always reflecting the experiment condition. Overall the introduction of new vapour flux model improves the numerical analysis capability of finite element code.

The numerical results are very sensitive to hydraulic and thermal material parameters. There is a need to determine the material parameters in the same conditions as used in the numerical analysis. The factors applied to the diffusivity terms in the vapour flux equation are constant but the vapour flux reduces with the time. It would be interesting to investigate the dependency of the factors on the rates of drying and wetting. It is recognised that due to the time constraints in this study the new modified vapour model was applied to only for heat and mass problem. Further investigation is required to include the deformation and chemical species movement.

8.8 Overall conclusions

An experimental and numerical investigation of heat and mass movement in clays has been presented. Experimental study included the development and construction of the

new apparatus (TH cell) and later on performing thermal gradient, thermo-hydraulic gradient and isothermo-hydraulic gradient tests on Speswhite kaolin (non-swelling clay) and MX-80 bentonite (highly swelling clay) in it for various time intervals. At the end of the each test, the clay samples were analysed for moisture content, degree of saturation, dry density, porosity and anions and cations concentration. The transient temperature, transient relative humidity, transient swelling pressure and transient volume of water intake have been observed during the tests.

The new cell (TH cell) and other accessories have been working and functioning correctly except the miniature pressure transducer for swelling measurement which could not measure the overall transient swelling pressure of the soil sample.

The test results of both tested clays showed that the temperature field depends upon the thermal properties (thermal conductivity and specific heat capacity). It was found that the liquid moisture moves away from the hot end in vapour phase, condenses at the cold region and comes back in liquid form to the hot end. This fact has been confirmed by the chloride ions concentration variation along the sample height.

The chloride ions concentration has been used to develop the empirical method to calculate the amount of vapour fluxes across the clay sample. The empirically calculated vapour fluxes were compared with the existing vapour theories and found to be very less than that predicted by existing theories. Therofore, new vapour model has been developed by modifying the existing Philip and de Vries (1957) vapour theory and integrated with the transient finite element code to simulate the experimental results of various thermal, thermo-hydraulic and isothermal tests performed in this study. The numerically simulated thermal and moisture field results match with experimental results reasonably well. Hence, the numerical model captures the heat and mass movement in unsaturated clays quite well. Due to time constraints the deformation behaviour and chemical movement have not been investigated in this study. In conclusion, the simulation of the heating and hydration experiment on the clays gave confidence in the model's ability to solve coupled thermo-hydraulic problems.

8.9 Suggestions for further research

From the experimental results it is evident that the TH cells can achieve the objectives outlined as the start of this project. Further work is now necessary to investigate the influence of an extended range of temperatures and suctions. The proposed new vapour model is capable of predicting the TH behaviour of unsaturated swelling and non-swelling clays. However, prior to further work, several improvements to the experimental and numerical study are suggested below:

In this study the minimum temperature of 25 °C and maximum temperature of 85 °C was used. It is suggested to investigate the other temperature ranges and different thermal gradients across the soil samples. The different initial conditions e.g. initial dry density and initial moisture content can be varied in future studies. The soil preparation and compaction technique could be improved to achieve uniform and homogeneous soil samples especially at low moisture content.

The maximum number of test duration used in this study was 30 days. Kaolin has faster moisture movement and bentonite has slower moisture movement. Future studies could investigate heat and mass movement for long duration especially in bentonitic clays.

It was found that the miniature pressure transducer measures the local swelling pressure only. Therefore it is suggested to use a load cell or bigger size pressure transducer to measure the swelling pressure and stresses. The small diameter relative humidity probes are required to measure relative humidity at microscopic level. The future studies can combine geotechnical and instrumentation aspects to design and construct miniature size probes.

In this study only advection of chloride ions is considered. It is recommended to consider the effect of diffusion in future studies. The numerical modelling work carried out in this study was limited to thermo-hydraulic behaviour only and should be extended to include deformation behaviour and chemical species movement.

The proposed vapour model needs to be validated against large scale experiments. Exploring the predictive capabilities of the transport model on a field scale and under real field conditions is an area that needs to be addressed. Although hysteresis has been observed to occur in drying and wetting, it was not included in this study. Therefore the inclusion of this phenomenon is recommended.

The overall conclusions drawn indicate that the present work is an encouraging area for further research.

Appendix 1

Design of thermo-hydraulic cell

A1.   Stresses

Consider the thermo-hydraulic cell is a cylindrical pressure vessel with radius, r, and wall thickness, t, subjected to an internal swelling pressure, p. The cell will be subjected to longitudinal stress, σ_l, in longitudinal direction and hoop stress, σ_h, in hoop direction as shown in Figure A1.1 below.
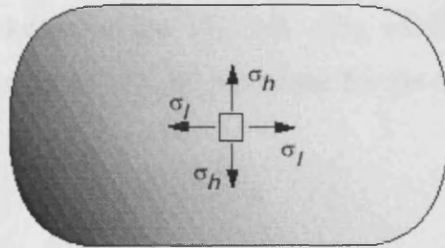

Figure A1.1 Stresses in the TH cell

The minimum wall thickness required for the TH cell to sustain the maximum swelling pressure of the soil sample can be determine by considering above two types of stress failure criteria i.e longitudinal stress and hoop stress.

A2.   Longitudinal stress criterion

To determine the longitudinal stress, σ_l, lets make a cut across the cylinder. The free body, shown in Figure A1.2, is in static equilibrium and the longitudinal stress around the wall take the internal swelling pressure of soil sample and can be written as:

$$\sigma_l.t.2r = p.\pi r^2 \tag{A1.1}$$

Simplifying the above equation (A1.1) yields:

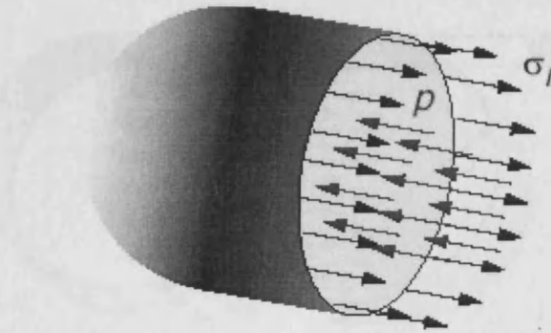$$t = \frac{pr}{2\sigma_l} \qquad\qquad\qquad (A1.2)$$

Figure A1.2 Longitudinal stresses in equilibrium with swelling pressure of soil

Now substitute the following values of variables in the above equation (A1.2) to determine the wall thickness of the TH cell. The swelling pressure is considered twice the actual swelling pressure of MX-80 bentonite for the safety of the cell.

p = 2 x 1.67 = 3.34 MPa

r = 62 mm

σ_l = yield strength (at 0.2 % proof stress) of stainless steel grade 316 L = 170 MPa

After substituting the values of variables the minimum wall thickness of the TH cell comes out to be 0.61 mm.

A3.   Hoop stress criterion

To find out hoop stress, σ_h, lets make a cut along the longitudinal axis of the cell. The free body is in static equilibrium as presented in Figure A1.3. The hoop stress can be written as:

$$2.\sigma_h.t.dx = p.2r.dx \qquad\qquad\qquad (A1.3)$$

Simplifying the above equation (A1.3) yields:

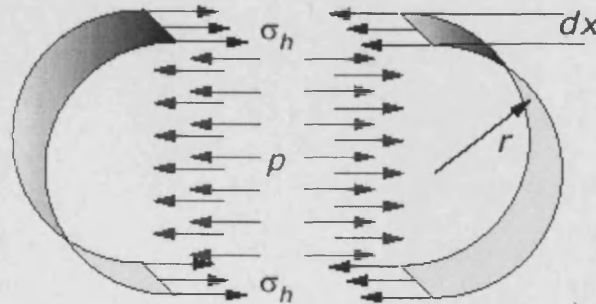$$t = \frac{pr}{\sigma_h}$$ (A1.4)

Figure A1.3 Hoop stresses in equilibrium with swelling pressure of soil

Now substitute the following values of variables in the above equation (A1.3) to determine the wall thickness of the TH cell.

p = 2 x 1.67 = 3.34 MPa

r = 62 mm

σ_h = yield strength (at 0.2 % proof stress) of stainless steel grade 316 L = 170 MPa

After substituting the values of the variables the minimum wall thickness required for the TH cell comes out to be 1.22 mm.

A4.   Design wall thickness of the cell

The longitudinal stress failure criterion gives the minimum wall thickness equals to 0.61 mm while the hoop stress failure criterion gives the minimum wall thickness of 1.22 mm. Therefore, the design wall thickness of the TH cell must be more than 1.22 mm. In this study the wall thickness of 10 mm is selected for the safety of the TH cell against any stress failure.